ISSN 2542-1565

Vol. 13 2020 No. 04

GEOGRAPHY ENVIRONMENT SUSTAINABILITY

«The journal GEOGRAPHY, ENVIRONMENT, SUSTAINABILITY was founded in 2008 by Russian Geographical Society, the Lomonosov Moscow State University Geography Department, and the Russian Academy of Sciences Institute of Geography. Since that time the journal publishes **4 issues per year**, containing original research papers and reviews. The journal issues are open source and distributed through subscriptions, library exchanges of leading universities, and via the website through the world»

FOUNDERS OF THE JOURNAL: Russian Geographical Society, Faculty of Geography, Lomonosov Moscow State University and Institute of Geography of the Russian Academy of Sciences

The journal is published with financial support of the Russian Geographical Society.

The journal is registered in Federal service on supervision of observance of the legislation in sphere of mass communications and protection of a cultural heritage. The certificate of registration: ПИ № ФС77-67752, 2016, December 21.

PUBLISHER
Russian Geographical Society
Moscow, 109012 Russia
Novaya ploshchad, 10, korp. 2
Phone 8-800-700-18-45
E-mail: press@rgo.ru
www.rgo.ru/en

EDITORIAL OFFICE
Lomonosov Moscow State University
Moscow 119991 Russia
Leninskie Gory, 1,
Faculty of Geography, 1806a
Phone 7-495-9391552
Fax 7-495-9391552
E-mail: ges-journal@geogr.msu.ru
www.ges.rgo.ru

DESIGN
Layout designer: Tereshkin Anton
Moscow, 115088,
26 Simonovsky Val str., bldg. One
Phone: +7 (903) 108-04-44
E-mail: smile.tai@gmail.com

DOI prefix: 10.24057

Format A4 (210x297mm)

"GEOGRAPHY, ENVIRONMENT, SUSTAINABILITY" is the only original English-language journal in the field of geography and environmental sciences published in Russia. It is supposed to be an outlet from the Russian-speaking countries to Europe and an inlet from Europe to the Russian-speaking countries regarding environmental and Earth sciences, geography and sustainability. The main sections of the journal are the theory of geography and ecology, the theory of sustainable development, use of natural resources, natural resources assessment, global and regional changes of environment and climate, social-economical geography, ecological regional planning, sustainable regional development, applied aspects of geography and ecology, geoinformatics and ecological cartography, ecological problems of oil and gas sector, nature conservations, health and environment, and education for sustainable development.

OPEN ACCESS POLICY. "GEOGRAPHY, ENVIRONMENT, SUSTAINABILITY" is an open access journal. All articles are made freely available to readers immediately upon publication. Our open access policy is in accordance with the Budapest Open Access Initiative (BOAI) definition - it means that articles have free availability on the public internet, permitting any users to read, download, copy, distribute, print, search, or link to the full texts of these articles, crawl them for indexing, pass them as data to software, or use them for any other lawful purpose, without financial, legal, or technical barriers other than those inseparable from gaining access to the internet itself.

Date of publication: December 31st, 2020.

EDITORIAL BOARD

EDITORIAL OFFICE

CONTENTS

ges.rgo.ru/jour/

ISSN 2542-1565 (Online)

REVIEW PAPER

ENVIRONMENTAL VARIABILITY OF THE PONTO-CASPIAN AND MEDITERRANEAN BASINS DURING THE LAST CLIMATIC MACROCYCLE

Tamara A. Yanina
Lomonosov Moscow State University, Leninskie Gory, 119991, Moscow, Russia
***Corresponding author:** paleo@inbox.ru
Received: July 1th, 2020 / Accepted: November 20th, 2020 / Published: December 31st, 2020
https://DOI-10.24057/2071-9388-2020-120

ABSTRACT. This paper reviews reconstructions of the the evolution of the Ponto-Caspian basin system to certain parts of the Pontian-Mediterranean system in order to analyze their correlation and response of the systems to the global climate change. The Ponto–Caspian and Mediterranean basins belong to different types of water basins and evolved differently in the Late Pleistocene responding in different ways to the global climate change. The paleogeographic reconstructions and correlation analysis of the Late Pleistocene events (within the last climatic macrocycle) made it possible to view the evolution of the basins as parts of a single system allowing to identify certain specific features and patterns in their functioning. The study is based on the analysis and integration of the data published by numerous researchers including the author of the paper and numerous colleagues from many countries who have been studying the paleogeography of the Ponto-Caspian and Mediterranean regions in the Late Pleistocene.

KEY WORDS: Caspian Sea, Sea of Azov, Black Sea, Marmara Sea, Eastern Mediterranean, ancient passages, late Pleistocene, sea level change, climate change, paleoenvironmental reconstruction, correlation

CITATION: Tamara A. Yanina (2020). Environmental Variability Of The Ponto-Caspian And Mediterranean Basins During The Last Climatic Macrocycle. Geography, Environment, Sustainabilit,, Vol.13, No 4, p. 6-23 https://DOI-10.24057/2071-9388-2020-120

ACKNOWLEDGEMENTS: The paper summarizes the results of the work on the Russian Foundation for Basic Research (RFBR) project № 19-15-50012. The author used also her materials obtained during the surveys performed as a part of the RSF № 16-17-10103 (Ponto-Caspian region), RFBR № 18-00-00470 and № 20-39-70020 (Eastern Caspian region) and RFBR № 18-05-00296 (Strait of Kerch) projects. The author is thankful to all her colleagues who took part in the survey in the region.

Conflict of interests: The authors reported no potential conflict of interest.

INTRODUCTION

The Ponto-Caspian and Mediterranean basins represent a system of intracontinental water bodies, relicts of the Paratethys sea basin, different in their natural characteristics and paleogeographic evolution. The Ponto-Caspian part of the system includes an isolated basin of the Caspian Sea, the Azov–Black Sea basin, which at certain periods connects with the ocean, and the Manych Depression, which occasionally functions as a strait between the Caspian and the Pontian basins. The Mediterranean part of the system is composed of the eastern part of the Mediterranean Sea, permanently connected to the ocean; the Sea of Marmara, which forms a kind of a «gate» between the Black and Mediterranean seas and is at certain periods isolated from the adjacent sea basins, and the Bosporus and Dardanelles straits (Fig. 1).

Fig. 1. Ponto-Caspian and Mediterranean basins

The evolution of the described natural system is influenced by multiple factors. This review aims to reveal connections between the global and regional climate changes, as well as between sea level fluctuations in the Caspian Sea, Black and Azov seas and the basins of the Eastern Mediterranean and the evolution of their environments.

The paleogeographic analysis focuses on the last climatic macrocycle, which corresponds to the time interval from the last interglacial period (MIS 5e) to the present day (MIS 1), thus spanning the entire Late Pleistocene. The interval covers several global climatic events different in their magnitude and impact, including glacial and interglacial periods, their individual stages and phases in their development. The natural systems of the Caspian and Pontian sea basins and those of the Mediterranean significantly differ in their characteristics. As a result, their response to the changes in paleoclimate, correlation of their transgression and regression phases, periodicity of the connection between the basins, the exchange of water and the biological diversity development – all provide the historic basis for predictive estimates of the environmental conditions in the region under the climate change.

The history of the above listed basins and their environments in the Late Pleistocene has been studied for a long time (more than three centuries). The studies in the Caspian region were started by Pallas (1776), Eichwald (1824), continued by Mushketov (1895), Andrusov (1888, 1900), Bogachev (1903), Pravoslavlev (1908, 1926), and many others. Results of multidisciplinary investigations were summarized in a number of monographs (Fedorov 1957, 1978; Vasilyev 1961; Moskvitin 1962; Svitoch, Yanina 1997; Rychagov 1997; Yanina 2005, 2012; Svitoch 2014). The first paleogeographic reconstructions of the Black Sea basins were performed by Andrusov (1889, 1890, 1925, a.o.) and developed further by Pavlov (1925), Gubkin (1913), Arkhangelskiy and Strakhov (1938), and many others. The results of integrated studies are presented in monographs by Fedorov (1963), Nevesskaya (1965), Popov (1983), Mikhailesku (1990), Svitoch et al. (1998), Izmailov (2005). Many specialists studied the evolution of environments of the Mediterranean basins (Lamothe 1899; Gignoux 1913; Issel 1914; Blanc 1937; Shimkus 1981; Bruckner 1986; Keraudren and Sorel 1987; Castradori 1993; Cita et al. 1973; Çagatay et al. 2000, 2009; Kaminski et al. 2002; Mudie et al. 2002; Cecilia et al. 2008; Wegwertha et al. 2014; Büyükmeriç et al. 2016; Krijgsman et al. 2019; Casini et al. 2020 and many others).

Hundreds of papers concerning the aspects of the environmental development in individual basins and the region as a whole have been published by now. And yet most of the paleogeographic problems in every region are still debatable. Among them is the topic of correlation between the events within the Ponto-Caspian basin system and the individual parts of the Pontian-Mediterranean system, as well as the response of both systems to the changes in the global and regional climate. Also, the question regarding the correlation between the paleogeographic events within the region and on the adjacent territories has not been done answered yet. In the present paper, the author addresses the above-stated problems and proposes a possible answer to some of the discussed questions.

The study is based on the analysis and integration of the data published by numerous researchers including the author of the paper and numerous colleagues from many countries who have been studying the paleogeography of the Ponto-Caspian and Mediterranean regions in the Late Pleistocene. The recent decades are marked by a sharp increase in the amount of such research, which indicates a growing interest of the global scientific community in the history of those intracontinental basins. That interest may be attributed to a considerable role the basins have played in the past evolution of the continent environment and still play today.

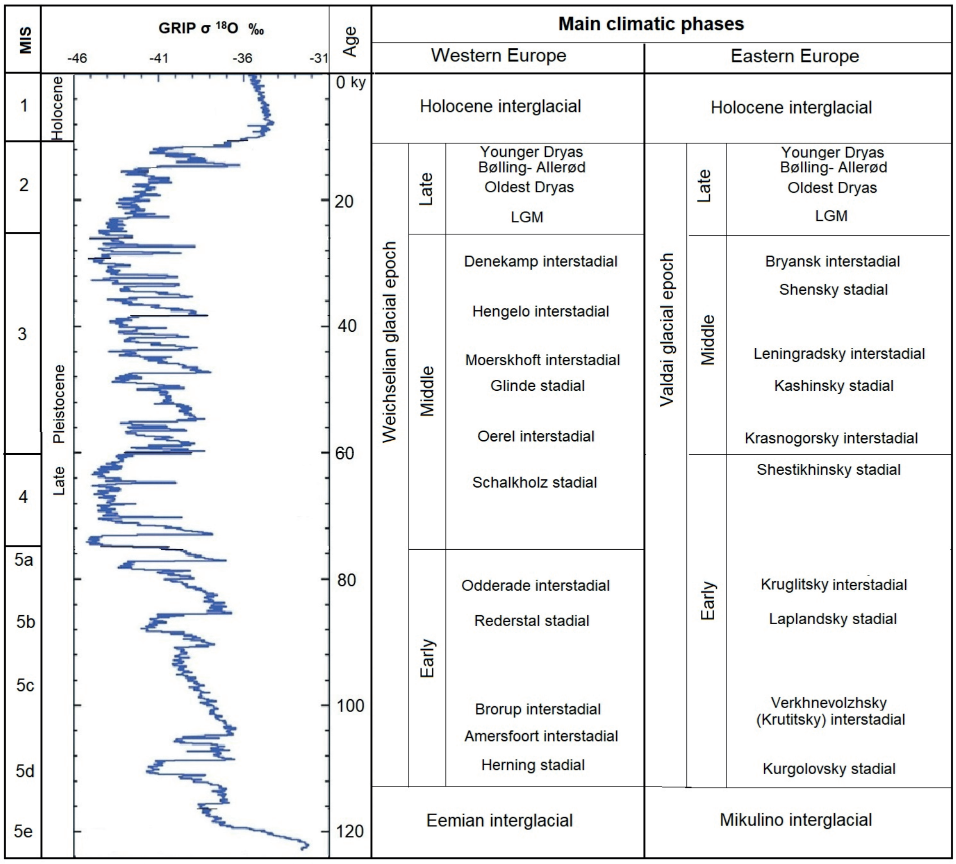

Fig. 2. The last climatic macrocycle and the climatostratigraphic scheme of Europe (Reprinted from Novenko 2016)

THE LAST CLIMATIC MACROCYCLE

Eemian (Mikulino) interglacial

The last interglacial period is thoroughly studied and described in scientific publications. In the climatostratigraphic scheme of European Russia it is denoted as Mikulino Interglacial (Fig. 2) (Dynamics… 2002; Shik 2014; Novenko 2016), and in the stratigraphic schemes of Western and Central Europe – as Eemian Interglacial (Kukla et al. 2002; Litt and Gibbard 2008; Brewer et al. 2008).

The position of the interglacial in the geochronological scheme and its time period is an important and still debatable question in the Pleistocene paleogeography. At present, the generally accepted approach to estimating the interglacial duration and its phases is based on the correlation of the oxygen isotope data in the deep-sea sediments and in the ice cores, which is an indication of the global climate changes (marine isotope stages – MIS) (Kukla et al. 2002; Berger et al. 1981; Imbrie et al. 1984). The majority of specialists agree that the Eemian (Mikulino) Interglacial corresponds to MIS 5e (Shackleton 1969). Its duration is estimated at 13 ka (128 to 115 ka BP) with the climatic optimum falling on ~125 ka BP. That geochronological position of the interglacial has been accepted by the International Commission on Stratigraphy (Litt and Gibbard 2008; Head 2020). Numerous dating results obtained using thorium and uranium technique (Kuznetsov et al. 2002; Gaigalas et al. 2005) and the OSL procedure (Degering and Krbetschek 2007; Boettger et al. 2009; Mania et al. 2010; Kurbanov et al. 2019) do not contradict the attribution of the last interglacial to that interval.

The ice cores obtained from deep drilling of the Greenland and Antarctic ice sheets present a natural archive, which can be used to study the natural environmental dynamics. As an example, the oxygen isotope data obtained from deep drilling in Greenland, conducted within the NGRIP (NorthGRIP Project members 2004) and NEEM (North Greenland Eemian Ice Drilling (NEEM) international project, 2007–2012) projects, provided a continuous record of the climate fluctuations over the last 123 and 130 ka, which allowed to estimate the chronological boundaries of the interglacial at 130-115 ka BP, with its thermal maximum falling on ~126 ka BP (NEEM Project members 2013; Turney et al. 2010).

Studies of marine deposits indicate a fast rise of the sea level at the beginning of the interglacial (Boreal transgression) related to the melting of the ice sheet (Zagwijn 1983, 1996; Forsström 2001; Kopp et al. 2010). The global sea level reached its current position around 127 ka BP, and exceeded it by 6-7.5 m (Kopp et al. 2010) or even by 7-9 m (Dutton and Lambeck 2012) at the peak of the transgression. Lowering of the sea level started around 116-118 ka BP (Kopp et al. 2013). The data on the dripstone calcite and stalagmites in the caves of southern Europe and the eastern Mediterranean indicate considerable warming that occurred around 129.7 – 125.8 ka BP (Drysdale et al. 2005; Wainer et al. 2011). The results of high-resolution analysis of the oxygen isotope composition and geochronological studies of Entrische Kirche cave (the Austrian Alps) allowed to date the upper boundary of the interglacial at approximately 118 ka BP (Meyer et al. 2008).

The age of the interglacial upper boundary (and, therefore, its duration) is still under discussion (Helmens 2014). Some authors include in the Eemian Interglacial not only MIS 5e but also 5d (Kukla et al. 2002; Brauer et al. 2007); others (Molodkov and Bolikhovskaya 2002, 2006) attribute the entire MIS 5 interval to the Mikulino Interglacial and distinguish periods with cold snaps within it. The interglacial duration is estimated at 75 ka. New data obtained every year is abundant, though not conclusive. Kukla et al. (1997) proposed to distinguish between the Eemian Interglacial *sensu stricto* (s.s.) – a warm period, identified in the deposits from Western Europe – and the Eemian Interglacial *sensu lato* (s.l.) – a period, when a thermophilic forest was present in southwestern and southern Europe.

Weichselian (Valday) Ice Age

Many specialists that consider the Eemian (Mikulino) Interglacial to correspond to MIS 5e attribute the next interval MIS 5d-a (complicated in structure regarding its climate) to the Vistulian (Valday) Ice Age. According to the stratigraphic schemes conventionally used for European Russia, the Late Pleistocene includes the Early Valday glaciation (MIS 5d-a and MIS 4), Middle Valday megainterstadial (MIS 3), and the Late Valday glaciation (MIS 2) (Fig. 2). MIS 5d-a interval includes the Kurgolovo cooling (5d stage), the Upper Volga (Krutitsa) interstadial (5c), Lapland cooling (5b), and Kruglitsa interstadial (5a) (Dynamics of... 2002; Paleoclimates… 2009). In Eastern and Central Europe several stages are identified within the Weichselian (Vistulian) Ice Age, namely, the early (MIS 5d-a), middle (MIS 4 – MIS 3) and late (MIS 2) stages (Mangerud 1989; Litt et al. 2007), while periods of warming and cooling are also distinguished within the stages.

The Late Pleistocene period corresponding to MIS 5 d-a lasted for 40 ka (115–75 ka BP). There is an opinion (Lavrushin et al. 2002; Shik 2014) that this interval should be considered as a separate stage under the name of, for example, Eovalday. In the author's opinion, it should be considered as a transitional (from interglacial to glacial) epoch. A deep and prolonged cooling corresponding to MIS 4 stage (75-60 ka BP) represents the Kalinin stage of the Valday glaciation. The Middle Valday epoch (MIS 3) is confined between 60 and 25 ka BP and includes a series of periods with relative cooling and warming; the period as a whole is characterized by a general decrease in the climate continentality (Paleoclimates… 2009). The late Valday (Ostashkov) glacial stage corresponds to MIS 2 (25-11.7 ka BP). The maximum cooling during the Valday glacial period is dated at 22 to 18 ka BP. At that time the entire boreal region of Europe not covered by the ice sheet represented a single hyperzone (Dynamics of… 2002) where the landscapes developed under a heavy influence of the cryogenesis. According to Rinterknecht et al. (2018), «local LGM» in the central part of the East European Plain is dated at 20 to 20.5 ka BP, while the deglaciation began around 17–15 ka BP.

The Late Glacial (14.7–11.7 ka BP) was characterized by short-term climate fluctuations. The time interval included distinct warming with two ineterstadials – Bølling (14.7–14.0 ka BP) and Allerød (13.6–12.9 ka BP), separated by a colder period known as Older Dryas (Walker et al. 2009; Merkt and Müller 1999; Dzieduszyńska and Forysiak 2019). A considerable cooling – Younger Dryas – occurred during 12.9–11.7 ka BP (Walker et al. 2009; NorthGRIP Project members 2004; EPICA community members 2004). The beginning of distinct warming immediately after the cold period is considered to be the lower boundary of the Holocene (Head 2019).

PONTO-CASPIAN AND MEDITERRANEAN SEA BASINS IN THE LATE PLEISTOCENE

Caspian Sea

The scheme of the Late Pleistocene events on the Caspian Sea includes the late Khazarian (late Khazarian and Hyrcanian transgressions) and Khvalynian (early and late Khvalynian) transgressive epochs separated by the

Atelian regression. Each of the above-named events was complicated by transgressive and regressive phases and oscillations, resulting from climate fluctuations and widely varying in their magnitude and direction.

Late Khazarian transgressive epoch

There are two transgressions (stages) distinguished within the late Khazarian epoch – the late Khazarian and the Hyrcanian. The level of late Khazarian transgressive basin reached about minus 10 meters at its maximum (Svitoch and Yanina 1997; Rychagov 1997; Yanina 2012). The sea expansion and its coast were described in a number of works (Leontyev et al. 1977; Rychagov 1977). The water was rather warm, as suggested by the composition of the mollusk assemblage dominated by crassoid Didacna (typically *D. nalivkini* and *D. surachanica*), which is characterized by large size and thick valves. The assumption is corroborated by the abundance of *Corbicula fluminalis* in the freshened water of the Northern Caspian at that time; currently, that species is encountered only in the south of the Caspian region (Yanina 2005; Bezrodnykh et al. 2015). The salinity was higher than at present – from 10–12‰ in the Northern Caspian to 14–15‰ in the Southern basin (Yanina 2012; Svitoch 2014). The pollen assemblages indicate a warm and dry climate (Abramova 1972; Yakhimovich et al. 1986). A distinctive feature of the sea was a predominance of depositional coasts (Leontyev et al. 1977) and a large volume of accumulative sand bodies, which might be an indicator of a prolonged stay of the sea at the same level, with only insignificant fluctuations.

The late Khazarian transgression was followed by sea level lowering. This is suggested by the gaps in marine sedimentation processes, that are distinguished in the sequences exposed in the coastal scarps (Fedorov 1957; Popov 1983; Rychagov 1997; Svitoch and Yanina 1997; Yanina 2005, 2012) and in the sedimentary series found in the Northern Caspian (Yanina et al. 2014; Bezrodnykh et al. 2015). At present, there is no data indicative of the scale of the sea level lowering.

The issue of the Hyrcanian transgressive sea basin has been a widely debated topic for many years (Yanina et al. 2014). The Hyrcanian transgressive stage was identified in the Caspian history by Goretsky (1957) and Popov (1967) based on the analysis of boreholes drilled in the northwest of the Caspian Lowland and the Vostochny (Eastern) Manych valley. Their position was subjected to a harsh criticism by many specialists (Vasilyev and Fedorov 1965; Fedorov 1978; Shkatova 2010; Svitoch et al. 1998), most of which rejected the idea of the Hyrcanian stage. Recently, however, the materials obtained from drilling in the Northern Caspian during the oil exploration allowed to return to that problem (Yanina et al. 2014; Sorokin et al. 2017). The drilling of the Upper Pleistocene series revealed the Caspian marine deposits corresponding to the Hyrcanian transgressive basin. The typical feature of its fauna is the joint occurrence of «Khvalynian-like» fauna (*Didacna subcatillus, D. cristata*) and rare late Khazarian mollusks. The sea basin was freshened and exceeded the late Khazarian basin in size. The pollen assemblages suggest a somewhat cooler and wetter climate (Yanina et al. 2014).

The late Khazarian transgressive epoch is attributed to the beginning of the Late Pleistocene. As has been shown by uranium series dating, the Late Khazarian transgressive stage corresponds to 127–122 ka BP (Shkatova 2010), while the entire Late Khazarian epoch is dated at 127–76 ka BP (Rychagov 1997; Shkatova 2010). Dating by the electron spin resonance technique (ESR) allowed to date the stage to the period from 140 to 85 ka BP (Molodkov and Bolikhovskaya 2006). The continental deposits exposed in the Srednyaya Akhtuba section in the lower reaches of the Volga correspond to the late Khazarian and Hyrcanian stages in the Caspian Sea evolution. Their age determined by the OSL (optically stimulated luminescence) technique corresponds to the entire MIS 5 stage (Yanina et al. 2017).

Atelian regression

The end of the Khazarian stage in the Caspian Sea evolution was marked by a deep regression. The estimates of the regression amplitude vary widely – from -43 m (Badyukova 2016), and -53 m (Leontyev et al. 1977), to -100 m (Bezrodnykh et al. 2017) and -140 м (Lokhin and Mayev 1990).

The estimates of the age and climate of the regressive stage also vary over a wide range. The deposits of the stage were first described by Pravoslavlev (1908, 1926), who attributed them to hot desert environments. A number of his colleagues – geologists Mazarovich (1927), Nikolayev (1941), Zhukov (1936) – shared the same opinion. Pavlov (1925) dated the Atelian continental deposits to the «beginning and culminating epoch of the Wurmian glaciation». That point of view was supported by Moskvitin (1962). Further on, the view of the Atelian epoch as a cold (glacial) interval was shared by the majority of researchers, though their opinions differed widely as to which particular cold interval it was. Vasilyev (1961) related the regression to the time of the Dnieper glacial period – Mikulino interglacial. In the opinion of Chepalyga (2004) and Lavrushin (Lavrushin et al. 2014) the regression coincided with the maximum of the last glaciation (Late Valday, Ostashkov) on the East European Plain. Some specialists (Fedorov 1978; Yakhimovich et al. 1986; Yanina 2012, 2014) correlate the Atelian regression with the Kalinin glacial epoch. There is also an opinion (Svitoch 2014; Svitoch et al… 1998) that the regression lasted longer and continued from the Kalinin glacial maximum to that of Ostashkov.

The Atelian continental deposits are widely spread in the north of the Caspian Lowland; quite often they form wedge-like structures penetrating deeply into underlying layers. Those wedges and frost fissures indicate severe climate conditions and occurrence of permafrost. Shells of freshwater and terrestrial mollusks found occasionally in the deposits are characterized by an oppressed appearance. Bone remains of mammals belonging to the «mammoth assemblage» indicate a cold climate of the Atelian time interval. That is supported by tundra-steppe pollen assemblages recovered from the Atelian deposits (Grichuk 1954; Moskvitin 1962).

In the depositional series of the Northern Caspian, the Atelian interval is represented by paleodepressions and erosional landforms, which are distinctly visible in the seismic stratigraphic profiles (Bezrodnykh et al. 2017). As appears from the composition of organic remains, the period was characterized by the presence of lakes with fresh or brackish water and wetlands. The pollen assemblages are indicative of rather diverse landscapes north of the Caspian Sea – from forests dominated by conifers to periglacial forest-steppe and tundra-forest-steppe (Bolikhovskaya et al. 2017).

The Atelian regression was dated by the TL method to the period 80–28 ka BP (Shakhovets and Shlyukov 1987). The age of its final phase was determined by the OSL method at 48.68±3.10 ka BP (Yanina et al. 2017); a few radiocarbon dating results fall into the interval of 44.40–41.80 ka BP, which corresponds to the first half of the intra-Valday interstadial warming. Well-developed cryogenic wedges found at the base of Atelian series deeply penetrating into the underlying deposits (dated to MIS 5) suggest that accumulation of the subaerial Atelian deposits began during the cold (glacial) epoch MIS 4 and the sea regression occurred in MIS 4 – the 1st half of MIS 3.

Khvalynian transgressive epoch

The Atelian regression was followed by a «great» Khvalynian transgression when the Caspian Sea reached its highest level over the entire Neopleistocene history. The Khvalynian basin left its traces on all the coasts and has been described in sufficient details (Leontyev et al. 1977; Rychagov 1997). Almost all the specialists agree that the Khvalynian transgression proceeded in two stages – the early and late Khvalynian, which were separated by Yenotayevka regression (Fedorov 1957, 1978; Rychagov 1977, and others). The sea level during the early Khvalynian transgressive stage reached 48–50 m a.s.l. at its maximum. The Lower Volga valley was enclosed by an extended estuary about 500 km long, the sediments of which are exposed in most of the sections (Fedorov 1957; Vasilyev 1961; Moskvitin 1962; Svitoch and Yanina 1997). One of the typical facies is the so-called «chocolate clays» – a distinctive kind of the Khvalynian basin deposits of the Caspian Sea (Makshaev and Svitoch 2016).

Traces of the ancient coastlines left by different stages of the early Khvalynian transgression are present in a form of erosional and depositional terraces on the coasts of Middle and Southern Caspian; in the Northern Caspian there are traces of incised deltas and other coastal landforms. The most distinct terraces are present at 34–36 m (Talginsksya terrace, Rychagov 1970), 20–22 m (Buynakskaya terrace, Fedorov 1956), 14–15 m (Turkmenian terrace, Fedorov 1957). The terrace development was probably related to the transgressive stages of the sea alternating with regressions (Rychagov 1970; Chepalyga 2006); others attribute the coastal landform development to temporary delays in the sea retreat during regressive phases (Fedorov 1957; Vasilyev 1961). A number of researchers (Britsyna 1954; Arkhipov 1958; Vasilyev 1961) studied the marine sediments in the Northern Caspian and came to a conclusion about two early Khvalynian transgressive phases separated with a regression (Eltonian regression, by Vasilyev (1961). This opinion is shared by Chepalyga (Chepalyga 2006).

The fauna inhabiting the sea basin was relatively poor and represented mostly by *Didacna parallella*, *D. protracta*, and *D. ebersini*, though crassoid didacnas were completely absent. The mollusks are characterized by thin shells, often small in size. The salinity is estimated at 11–12‰ at the main water body of the Early Khvalynian Caspian Sea and at 5–0.5‰ at the estuary (Kvasov 1975; Yanina 2012; Svitoch 2014). The small size of mollusks suggests rather low temperatures of water, which is confirmed by the pollen assemblages. For example, those recovered from the chocolate clays (in the lower reaches of the Volga) indicate the presence of periglacial landscapes (tundra-steppe, periglacial forest-steppe, periglacial open forests and parklands) (Bolikhovskaya and Makshayev 2020).

The end of the Early Khvalynian period was marked by the Yenotayevka regression with the sea level dropping, according to different estimates, to -43…-45 m (Rychagov 1997), -84 m (Varushchenko et al. 1987) or even to -110 m below sea level (Lokhin and Mayev 1990). Continental deposits occur in the Khvalynian sedimentary sequences (Brotskiy and Karandeeva 1953), though most often the regression may be traced by erosional landforms (Svitoch and Yanina 1997; Rychagov 1997). According to pollen data (Sorokin et al. 1983), the climate was dry and cool.

The sea level during the late Khvalynian transgression reached about 0 m at its maximum (Leontyev et al. 1977; Rychagov 1997). The Volga River divided into two channels near its mouth. The composition of late Khvalynian mollusk fauna was similar to that of the early Khvalynian; the only exception was the dominance of *D. praetrigonoides*, which occupied only insignificant biotopes in the early Khvalynian basin. The mollusk fauna composition suggests the salinity of about 10-12‰ (Yanina 2005). The abundance of mollusks with larger and more massive shells may be a result of a higher water temperature than in the early Khvalynian. Palynological data also indicates general warming in the region (Abramova 1972; Vronskiy 1976; Yakhimovich et al. 1986).

The lowering of the late Khvalynian sea level proceeded irregularly; periods of a slowdown are marked by the coastlines detected at altitudes of -10 to -12 m (Sartass stage) and -16 to -18 m (Dagestan stage) (Leontyev and Fedorov 1953). The time of the Dagestan stage proved to correspond to the Holocene epoch (New Caspian basin) (Rychagov 1997). New data obtained by Svitoch (2011) confirmed it to be an independent Holocene transgression, which was followed by regression as the climate became more arid (Abramova 1972).

The age of the Khvalynian transgression, as well as that of its individual stages, is still debatable. The early Khvalynian stage was dated by the TL to the period 70-40 ka BP, and the late Khvalynian – to 20-10 ka BP (Rychagov 1997). According to 14C and 230Th/234U data, the Khvalynian transgression may be dated to 19-8 ka (Kvasov 1975; Svitoch and Yanina 1997; Leonov et al. 2002; Tudryn et al. 2013; Arslanov et al. 2016). Values close to the radiocarbon (14C) ones were obtained using the OSL technique (Yanina et al. 2017).

Another transgressive basin has been recently uncovered by drilling in the Northern Caspian, which is the earliest Khvalynian basin (Bezrodnykh et al. 2014, 2015; Yanina et al. 2017; Sorokin et al. 2018), with mollusk fauna including *Didacna subcatillus, D. zhukovi, D. parallella*. Judging from the mollusk habitus, the sea was moderately warm. From numerous radiocarbon dates the period of its existence is estimated to span from 37 ka BP (the 2nd half of the MIS 3 interstadial) to LGM (MIS 2) (Bezrodnykh et al. 2014, 2015). That transgressive series is covered by a regressive layer dated by radiocarbon to 22–20 ka BP and corresponding to LGM. The overlying sedimentary series (repeatedly dated by radiocarbon) preserves traces of several transgressive and regressive phases of the Khvalynian basin evolution chronologically corresponding to the main phases of the degradation of the late Valday glaciation (Yanina et al. 2017).

It may be concluded from the above that the Late Pleistocene paleogeographic events in the Caspian region are closely related to the changes in the global climate (Fig. 3). The late Khazarian «little» transgression developed during the Mikulino (Eemian) Interglacial (MIS 5e). The Hyrcanian transgression that was characterized by a higher sea level developed during the transitional stage from the interglacial towards the Valday glaciation. As the maximum of the early Valday (Kalinin glaciation) approached, the Hyrcanian basin retreated under the conditions of cold and dry climate. The Atelian regression corresponded to the Kalinin glacial epoch and the first stage of the interstadial warming (MIS 3). At the 2nd half of the interstadial, the early stage of the Khvalynian transgression started. The transgressive changes of the sea level were interrupted by a regression during the period of the maximum cooling and drying of the late Valday (MIS 2, LGM).

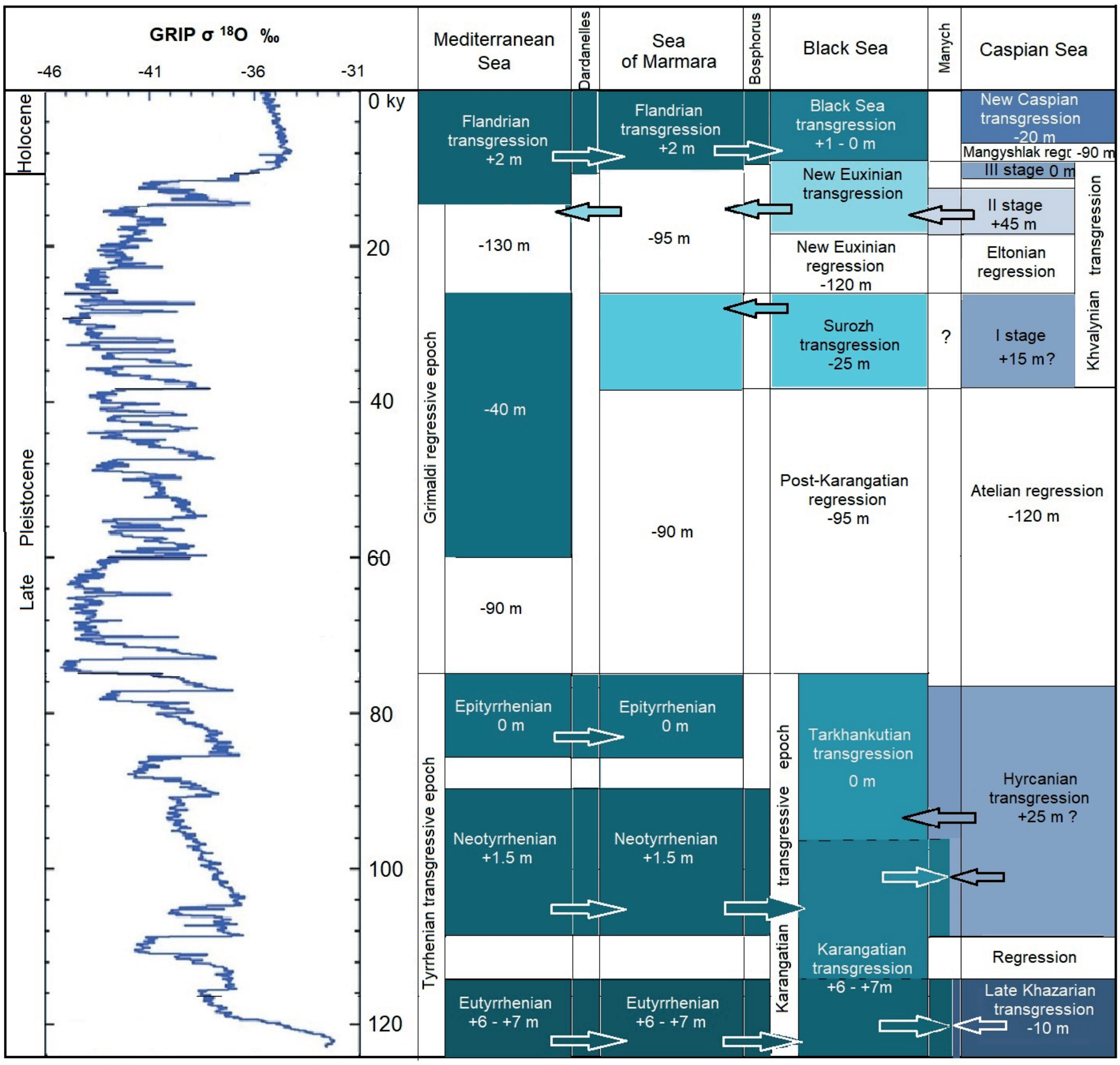

Fig. 3. Ponto-Caspian and Mediterranean basins during the late Pleistocene and their correlation More saturated shade of color shows higher salinity of the basin. Arrows indicate the water inflow and migration of fauna

The transgression resumed during the period of deglaciation. The most notable events of the Late Glacial – warming phases of Bølling and Allerød – activated the melting of the ice sheet and degradation of the permafrost within the drainage basin; those processes contributed to the further development of the Khvalynian basin transgression. That period was marked by the «chocolate clay» accumulation in the Volga estuary and in the pre-Khvalynian depressions in the Northern Caspian. The phases of considerable cooling known as Oldest Dryas, Older Dryas, and Younger Dryas resulted in a reduced runoff from the drainage area and regression of the Caspian Sea. The most significant regression corresponded to the Younger Dryas. The final phase of the Khvalynian transgression corresponds to the abrupt warming, which is considered as the Pleistocene / Holocene boundary. The decrease in sea level ended with the Mangyshlak regression, which developed under the conditions of a continental climate in the Boreal period of the Holocene.

Pont

The Pontian basin (including the Sea of Azov and the Black Sea) occupied an intermediate position between the Caspian and Mediterranean seas and therefore was influenced by both. Its Late Pleistocene history was marked by an alternation of marine and brackish-water basins. In the Late Pleistocene, the only marine basin was Karangatian which developed as a result of the Mediterranean water inflow. The next marine transgression occurred in the Holocene. The post-Karangatian, Surozh and New Euxinian basins were also characterized by brackish water.

Karangatian transgressive epoch

The fore-Karangatian drop of the sea level gave way to the Karangatian transgression at the beginning of the Late Pleistocene. Its deposits are widespread and the basin paleogeography has been studied in details (Andrusov 1904, 1925; Arkhangelskiy and Strakhov 1938; Nevesskaya 1965; Dimitrov and Govberg 1979; Božilova and Djankova 1976; Zubakov et al. 1982; Krystev et al. 1990; Markova and Mikhailesku 1990; Yanko et al. 1990; Nesmeyanov and Izmailov 1995; Svitoch et al. 1998; Dodonov et al. 2006; Sorokin 2011; Filipova-Marinova et al. 2012; Shumilovskikh et al. 2013a.b; Wegwerth et al. 2014; Krijgsman et al. 2019; Kurbanov et al. 2019).

The Karangatian period was marked by a large interglacial transgression that exceeded the present-day sea level by 6-7 m, while the water salinity reached up to 30 ‰. There are two stages distinguished in the transgression development – the Karangatian and Tarkhankutian, each of them characterized by faunal assemblages with different proportions of stenohaline and euryhaline groups of mollusks. Two phases are also noted in the Karangatian stage. The earlier – Tobechik phase (Nevesskaya 1965) was marked by a wide distribution of species typical of the sea up to the present days (*Cerastoderma glaucum, Abra ovata* and others). The sea level in the basin was below that of today. The second phase (Karangatian) was characterized by the dominance of the halophilic species including those that are currently absent from the basin (*Cardium tuberculatum,* et al.). High salinity was observed in the southern part of the Sea of Azov as well. Another distinctive feature of the transgression was a higher water temperature, which is suggested by the malacofauna composition as well as the presence of thermophilic subtropical species of diatoms and pollen assemblages (Zhuse et al. 1980; Vronskiy 1976).

A series of the U/Th dates obtained for the transgression fall within the period of 140–70 ka BP (Arslanov et al. 1975, 1983; Dynamics… 2002). The ESR (electronic spin resonance) dates fall into the period of 127-121 ka BP (Dynamics… 2002). According to the OSL data, the earlier stage of the transgression developed around 131–120 ka BP, and the later one – around 120–100 ka BP (Kurbanov et al. 2019).

The Tarkhankut stage deposits yielded faunal assemblage, that included impoverished Mediterranean mollusk fauna, barren of halophilic elements and dominated by *Cerastoderma glaucum* and *Abra ovata*. The entire basin was confined within the present-day outlines of the Black Sea coasts and the salinity did not exceed 14-15‰. There were some Caspian species – *Didacna cristata, D. subcatillus, D.* ex gr. *protracta*, in the Tarkhankut basin, but mostly confined to limited area sites (Yanina 2012; Sorokin et al. 2019).

Post-Karangatian regression

The sea level during the regression dropped to around -80 … -100 m (Fedorov 1978; History of the geological evolution … 1988). I.P. Balabanov and Ya.A. Izmailov (1988) recorded the presence of *Didacna* sp. shells in the deposits. Judging from the diatom species composition, the water in the basin was cold and characterized by low mineralization (History of the geological evolution… 1988). A considerable cooling of the climate is indicated by the pollen assemblages mostly corresponding to dry and cool steppes on the Black Sea coasts (Shcherbakov et al. 1979).

Surozh transgression

Not all the specialists studying the Late Pleistocene history of the Pontian basins accept the Surozh transgression. It was established by Popov (1955), later Goretskiy (1957) applied to it the term 'Alanian'. The highest level of the basin is estimated at -25 …-20 m abs. The deposits of that transgressive basin are found on the Black Sea shelf (History of the geological evolution… 1988; Kuprin and Sorokin 1982; Shcherbakov 1982). The pollen assemblages recovered from the cores suggest a climate warming (Shcherbakov et al. 1979) and the period, corresponding to the Surozh basin, is estimated at 40-25 ka BP (Shcherbakov 1982).

New Euxinian epoch of regression and transgression

The New Euxinian stage in the Pontian basin development began with a significant regression. The basin level at its minimum was estimated at -80 m (Shcherbakov et al. 1977); -90 m (Fedorov 1978), at -100 to -110 m (Ostrovskiy et al. 1977); and at about -140 to -150 м (Rayan 1997; Winguth et al. 2000). Most of the specialists believe that the New Euxinian basin represented a completely isolated lake. According to the data obtained by Sholten (1974), the bottom of the Bosporus Strait is located at a depth of 100 m, which suggests either a constant one-way discharge of water from the New Euxinian basin or isolation of the latter. The extent of this significantly freshened basin covered the area of deep water, continental slope, and the lower part of the shelf. It was inhabited by mollusk fauna of freshwater (*Viviparus duboisianus, Lithoglyphus naticoides, Valvata piscinalis* etc.) and freshened brackish-water (*Monodacna, Dreissena rostriformis, Dr. polymorpha*) species, dominated by dreissenas.

During the period of regression, a low coastal plain existed in place of the Azov Sea, with the Don River flowing across it (Kaplin and Shcherbakov 1986). The Don mouth was located ~50 km south of the Strait of Kerch. The mouths of the rivers Dnieper, Dniester, and Danube joined together and formed a great canyon and a joint delta. The diatom flora (Zabelina and Shcherbakov 1975) indicates a considerable cooling. The pollen assemblages also suggest a cold and dry climate (Vronskiy 1976; Mudie et al. 2007; Filipova-Marinova et al. 2012). The emerged shelf and low coastal plains were dominated by the landscape similar to periglacial ones. As follows from the available data (Shimkus et al. 1977; Degens and Ross 1972; Briceag et al. 2019), the cooling in the region reached its maximum at 22–23 ka BP.

The existence of the regressive basin is dated to 22-17(16) ka BP (Shcherbakov et al. 1977; Balabanov and Izmailov 1989); 25-22 ka BP (Degens and Ross 1972). Some other specialists dated the regression maximum to a later time – 14-12 ka BP (Ostrovskiy et al. 1977).

Many researchers noted complex transgressive and regressive patterns in the New Euxinian basin dynamics (Balabanov and Izmailov 1988; Balabanov 2006; Murdmaa et al. 2006). The sea level was rising from 16 to 12.5 ka BP (Balabanov and Izmailov 1989) and reached -45 m (Varushchenko 1975). The final transgressive phase of the New Euxinian stage when the sea level reached -25 m is dated to 9.8 ka BP (Kovalyukh et al. 1977; Balabanov 2006). In addition, Murdmaa and his colleagues (Murdmaa et al. 2006) identified another basin – Antian with the water level reaching -30 m around 13 ka BP.

The New Euxinian transgressive basin was inhabited by brackish-water fauna dominated by mollusks that prefer very low salinity and belong mostly to *Monodacna, Adacna* and *Dreissena* genera. Typically euryhaline Mediterranean species are completely absent (Nevesskaya 1965; Popov 1983; Fedorov 1978). Shells of an early Khvalynian *Didacna ebersini* (Fedorov 1978) are occasionally encountered and some Khvalynian ostracods (Popov and Suprunova 1977) have been identified. The inflow of Mediterranean water into the New Euxinian basin first occurred around 9.8-9.5 ka BP (Jones and Gagnon 1994) when the Holocene Black Sea transgression began in the Pontian region.

Caspian mollusks in the Late Pleistocene Black Sea

The presence of the Caspian Sea mollusks in the Azov – Black Sea basins is of primary importance for the correlation of events in the Pontian and Caspian basins as it proves the functioning of the paleo-straits between the basins. The Caspian mollusk fauna consists of species autochthonous for the Caspian Sea and endemic to the Pontian-Caspian basin. In the Neopleistocene the Caspian mollusks occasionally migrated through the Manych Strait into the Black Sea basin and evolved there.

As follows from the analysis of the Late Pleistocene malacofauna of the Pont (Yanina 2005), brackish-water didacnas persisted in isolated (freshened) water areas throughout the Karangatian epoch. Two groups of mollusks, different in origin, are identified: (1) Euxinian-Uzunlarian species (*Didacna pontocaspia, D. borisphenica*), that survived the period of increased salinity in the freshened parts of the basin; (2) Caspian species (*Didacna cristata, D. subprotracta, D. subcatillus*), which most likely penetrated into the retreating Karangatian basin with the Hyrcanian water and settled within a few limited areas of the Tarkhankut basin.

During the period of the New Euxinian regression, when the basin was noticeably freshened, all the didacnas became extinct. The New Euxinian transgressive basin was dominated by semifreshwater Caspian species (*Monodacna, Adacna, Hypanis, Dreissena*), with occasional *Didacna moribunda* (Andrusov 1926; Fedorov 1963; Semenenko and Sidenko 1979), identical to *Didacna ebersini* which is an index species of the Khvalynian fauna (early Khvalynian assemblage) of the Caspian Sea.

The presence of the Caspian assemblage members (Hyrcanian and early Khvalynian species) in the Tarkhankut and New Euxinian (Pontian) basins suggests the Caspian water inflow into the Black Sea during that period, most likely, via the Manych Strait.

Some researchers (Arkhangelskiy and Strakhov 1938; Dimitrov and Govberg 1979) believe that the faunal elements of the Old Euxinian basin could have survived during the marine Karangatian transgression in the freshened limans and then spread out over the New Euxinian basin. Others (Shnyukov et al. 1981) believe that the brackish-water New Euxinian species migrated from the Caspian Sea to the Surozh basin; they could have survived in the most freshened areas and then – at the New Euxinian time – expanded widely. As has been stated by zoologists (Mordukhay-Boltovskoy 1960) who have studied the Caspian fauna in the Azov-Black Sea basins, if the relicts of the Old Euxinian fauna persisted in the modern basin, the species composition of the Caspian fauna in the two basins (the Caspian and the Azov-Black Sea) would be quite different. The isolation is a powerful factor of species formation. The fact that the species of the two isolated basins are similar, means that the Caspian fauna existing now in the Azov-Black Sea basin persists seemingly since the end of the Pleistocene.

It can be concluded that the paleogeographic events that took place in the Pontian basin in the Late Pleistocene were closely connected with the global climate change (Fig. 3). The global warming at MIS 5e and the rise of the sea level forced the Mediterranean water to enter the Black Sea depression which resulted in the Karangatian transgression. The global cooling during the transition to the Valday glacial epoch initiated a drop of the Karangatian sea level that followed the global sea-level lowering. Separately from the Karangatian sea, the Hyrcanian basin of the Caspian Sea under similar conditions transgressed and a part of its water was transferred to the Tarkhankut basin (the 2nd stage of the Karangatian epoch). The early Valday ice age (Kalinin, MIS 4) was marked by the presence of the post-Karangatian regressive basin. Its level became somewhat higher (transgressed) during the interstadial warming (MIS 3), though still remained below zero mean sea level. The late Valday glacial epoch (Ostashkov glaciation, MIS 2) resulted in the most distinct sea level drop (at the LGM) and caused a deep New Euxinian regression of the Pontian basin. When the continental ice sheets and the permafrost degraded, the New Euxinian basin transgressed, though sea level was still negative. At that time water of the early Khvalynian transgression of the Caspian basin was partly discharged through the Manych into the Pontian basin. In the Holocene the global interglacial warming resulted in the inflow of the Mediterranean Sea water into the Black Sea basin and development of transgression.

Manych

The analysis of the Manych Strait functioning based on the Quaternary series studies in natural exposures and cores plays an important part in correlating the events and understanding the connection and interaction between the Caspian and Pontian basins in the Late Pleistocene.

Judging from the stratigraphic position and malacofauna recovered from the Manych valley deposits, there was an ingressive bay there at beginning of the Late Pleistocene (the Karangatian transgression maximum) which penetrated as far east as the Caspian – Black Sea water divide (Fedorov 1978; Popov 1983; Yanina 2014; Kurbanov et al. 2018). The presence of the Karangatian fauna in its deposits (*Cerastoderma glaucum, Chione gallina, Chlamys glabra, Ostrea edulis*) suggests a rather high salinity in the central part of the bay (~18–20‰). The head of the bay was close to the Kalaus River mouth. A wide distribution of *Cerastoderma glaucum* and disappearance of more halophilic species indicates considerably freshened water (up to 10‰) (Popov 1983).

Popov (1983) identified two stages in the Karangatian Sea ingression, the second marked by an increased ingression range. It can safely be assumed that the earlier stage corresponded chronologically to the development of an inlet of the late Khazarian basin with a lower water level (Yanina 2012). The 2nd stage of the ingression correlates with the Hyrcanian transgression with a bay deeply penetrating westward via the Eastern Manych valley. When the level of the Karangatian basin dropped and the ingressive inlet shrank, the Caspian (Hyrcanian) water penetrated into the strait bringing mollusks *Didacna cristata, D. parallella, D. subcatillus, Monodacna caspia, Dreissena polymorpha*. The salinity in the strait (judging from the malacofauna) was about 8–10‰, the water was notably freshened by the inflowing streams.

The Hyrcanian deposits in the central part of the Manych depression are dated using OSL at 107±7 ka BP (Kurbanov et al. 2018). It supports the earlier conclusion about the Karangatian sea level lowering (Tarkhankut stage) and the inflow of the Hyrcanian water during the cooling at the transition from the Milulino Interglacial to the Valday glaciation. At the end of the Hyrcanian a lake appeared in the Manych valley – Burtass lake, which, according to Goretskiy (1953) chronologically correlates with MIS 4 (Popov 1983; Kurbanov et al. 2018).

The next strait opening occurred during the Early Khvalynian epoch when the Caspian level reached about 50 m a.s.l. This follows from the geomorphological structure of the Manych depression and is substantiated by the paleontological findings recovered from its deposits (Popov 1983; Svitoch et al. 2010; Yanina 2012). The first stage in the strait development was marked by erosion processes. The early Khvalynian water reached the Manych threshold and flowed towards the Black Sea basin cutting through the Burtass lake sediments and subaerial deposits above them. That stage in the strait development is expressed in the linear hollows and ridges in the Manych depression (Svitoch et al. 2010) and Abeskun deposits that contain the early Khvalynian species *Didacna ebersini* (Goretskiy 1953; Popov 1983). That stage is dated using radiocarbon at 17–16 ka BP (Yanina 2012)

The next stage in the strait evolution was apparently depositional and was marked by the formation of fine deposits between the ridges and development of a ~22 m high terrace. Among the mollusks there were *Didacna ebersini, D. protracta, D. subcatillus, Monodacna caspia, Adacna laeviuscula, Hypanis plicatus, Dreissena polymorpha, Dreissena* *rostriformis distincta* present. The geological structure of the deposits suggests an ingressive type of the strait, with water penetrating the eroded valley and the stream increasing gradually in capacity (Svitoch et al. 2010). The strait of that type could have developed during the transgressive stage of the early Khvalynian basin when the sea level reached ~22 m. The sedimentary sequence and mollusk assemblages recovered from it indicate a unidirectional migration of the mollusk fauna from the Caspian Sea into the Pontian New Euxinian basin (Svitoch and Yanina 2001; Yanina 2005, 2006; Chepalyga 2004, 2006; Svitoch 2006, 2007). That stage, the last one in the strait development in the Pleistocene, is dated at 14.8–14.3 ka BP (Svitoch et al. 2010).

It can be concluded that during the Late Pleistocene the Manych Strait with a one-way flow of the Caspian water to the Pontian basin was open three times, namely once in the Hyrcanian and twice in the early Khvalynian intervals of the Caspian history. An ingressive bay that existed in the Manych valley during the Karangatian interglacial transgression of the Pont reached as far east as the Caspian–Black Sea water divide (Fig. 3).

Mediterranean Sea

The Late Pleistocene regime of the Mediterranean Sea depended on the global sea-level fluctuations due to continuous connection between the sea and the Atlantic Ocean through the Strait of Gibraltar.

Tyrrhenian transgressive epoch

The Tyrrhenian epoch represents a complicated and prolonged transgressive-regressive period in the Mediterranean Sea history. It was the most prominent interval in the Neopleistocene paleogeography, marked by a wide distribution of the tropical malacofauna of the Senegalese type, with its most characteristic type Strombus bubonius. It has been found that the penetration of tropical malacofauna elements started as early as the Middle Neopleistocene and persisted during at least a part of the Late Neopleistocene (Cita et al. 1973; Paskoff and Sanlaville 1980; Zazo and Goy 1984; Zubakov 1986; Svitoch et al. 1998; a.o.). There are as many as four marine terraces with Tyrrhenian malacofauna known on various coasts of the Mediterranean.

Three stages can be distinguished in the Tyrrhenian Sea level rise during the Late Pleistocene – Eutyrrhenian, Neotyrrhenian and Epityrrhenian, corresponding to climatic substages MIS 5e, 5c and 5a (Zubakov 1986; Svitoch et al. 1998). The main peak of transgression with the sea level ~4-6 m above present sea level corresponded to the climatic optimum of the Eemian Interglacial (MIS 5e), characterized by warmer and wetter climate compared to the current conditions. The 2nd transgressive rise of the sea level exceeded the present level by 1.5 m and occurred under the climate conditions similar to the present days. The 3rd sea level rise corresponding to MIS 5a was insignificant and did not rise above the modern level of the Mediterranean (Çağatay et al. 2009).

Grimaldi regressive epoch

The Tyrrhenian transgression was followed by a prolonged interval of decreased sea level (MIS 4-2). The process was rather irregular. During the glacial epoch (MIS 4) the Tyrrhenian sea level dropped by 60 - 90 m (Blanc 1937; Shimkus 1981; Svitoch et al. 1998; Çağatay et al. 2009). The deep-sea deposits attributed to that time are distinguished by alternating layers with warm-water and cold-water foraminifera indicative of insignificant warming and cooling of the climate. Pollen assemblages recovered from the deposits and dated to the interstadial warming (MIS 3) display also an alternation of the subtropical and sub-boreal (boreal) vegetation. The layers also differ in the proportion of the thermophilic planktonic foraminifera. At that time the level of the regressive post-Tyrrhenian basin increased up to (though no more than) -40 m abs. The Mediterranean deep-sea sediments dated to the last glacial epoch (MIS 2) are dominated by cold-tolerant foraminifera; the pollen assemblages abound in birch, pine, and Artemisia (Shimkus 1981). Numerous data sources indicate a sharp and deep drop of the sea level at the LGM with the estimates varying from 100 to 300 m (Keraudren and Sorel 1987; Zubakov 1986; Bruckner 1986; Svitoch et al. 1998; Çağatay et al. 2009; a.o.).

Flandrian transgression

In the Mediterranean region the post-glacial glacio-eustatic rise of the sea level is known as Versilian or Flandrian transgression. Its beginning is dated to the early post-glacial time (~17–15 ka BP), and further development has been thoroughly studied in various Mediterranean regions (Keraudren and Sorel 1987; Aksu et al. 1999; Badertscher et al. 2011; Cecilia et al. 2008; a.o.). The transgression began with a large volume inflow of the North-Atlantic water into the Mediterranean Sea and resulted in a wide distribution of the modern-type mollusk fauna of relatively thermophilic species represented by Mediterranean-Lusitanian and Mediterranean-Canarian forms (*Chlamys glabra, Mytilaster lineatus, Corbula mediterranea, Pitar rudis*, a.o.), moderately thermophilic Keltian (*Mytilus galloprovincialis, Cardium paucicostatum, Donax venustus*) and rather cold-loving Keltian forms (*Nucula nucleus, Ostrea edulis, Cerastoderma glaucum, Chione gallina, Solen vagina*). The amplitude of the sea level rise 10–9 ka BP is almost universally adopted to be up to -30 m abs.

Therefore, it may be safe to assume that the evolution of the Mediterranean basins through the Late Pleistocene was controlled by fluctuations of the World Ocean level, which in turn had been initiated by the global climate changes.

The Sea of Marmara

The Sea of Marmara, which is called the «gate» from the Mediterranean to the Black Sea, is a paleogeographically important element of the system under consideration that presents evidence of the interaction between the two sea basins in the past.

It has been established that the Late Pleistocene history of the Marmara Sea presented an alternation of marine and lacustrine stages. A marine basin existed in the Marmara Sea basin at the beginning of the Late Pleistocene (Eemian Interglacial, MIS 5e). The marine conditions developed as a result of the sea water invasion when the Mediterranean Sea level rose above the Dardanelles Strait threshold (at present its altitude -65 m). The sapropel layers rich in organic matter mark those events in the sedimentary record. The malacofauna was similar to that of Tyrrhenian age in composition: it included numerous Mediterranean species, mostly from euryhaline to moderately stenohaline; the stenohaline marine species are less common, which suggests the salinity about 28-30 ‰ (Çağatay et al. 2009; Büyükmeriç et al. 2016; Meriç et al. 2018; Krijgsman et al. 2019). Three marine stages are recognized in the Late Pleistocene history of the Marmara Sea – during the interglacial (MIS 5e) and during the warm intervals of the transitional period (MIS 5c and MIS 5a). The most significant influx of marine water occurred during the Eemian Interglacial period. The 4th marine stage began at the very end of the Pleistocene and continued during the Holocene Interglacial.

When the sea level dropped below the Dardanelles threshold, the marine environments were replaced with lacustrine ones. This was recorded in the Upper Pleistocene sedimentary series by the accelerated erosion, formation of rills, and the lacustrine deposition. The Sea of Marmara turned to a freshened brackish-water lake during the cooling phases of the transitional period (MIS 5d and MIS 5b), and in the glacial epochs (MIS 4 and MIS 2). The lacustrine environments persisted during the interstadial warming (MIS 3) when the ocean level rose. Evidently, the threshold in the Dardanelles was higher at that time and therefore prevented the marine water inflow into the Sea of Marmara basin. Some authors (Meriç et al. 2017) consider a possibility of the water discharge from the Surozh (Pontian) basin.

The lowest stand of the lake level (-85 to -95 m) was observed during the last glacial maximum (LGM) when it was completely isolated from the ocean (Çagatay et al. 2000; Algan et al. 2001; Aksu et al. 2002; Hiscott et al. 2002; Badertscher et al. 2011). The Marmara Sea turned to a freshened brackish-water lake of the «Caspian» type, with the salinity varying from 1 to 7‰. The seasonal contrasts were sharp. Such climatic and hydrological conditions persisted approximately till 20 cal ka BP. The first wave of the warming occurred between 20 and 18 cal ka BP; it was followed by a considerable increase of the melted water inflow. The lake was almost completely devoid of fauna except for occasional representatives of *Dreissena* and *Theodoxus* mollusk genera. Flora of brackish-water and freshwater diatoms was rather scarce. The coasts were mostly treeless (Filipova-Marinova et al. 2004; Mudie et al. 2001, 2007), which resulted in intensive erosion and transportation of the abundant clastic material into the lake.

An episode of a considerable inflow of the freshened water from the Black Sea was recorded in the interval between ~18 to 15 cal ka BP (Aksu et al. 1999, 2002; Çagatay et al. 2000; Bahr et al. 2005; Major et al. 2006; Herrle et al. 2018). Probably, it was a result of the Black Sea level rising above the Bosporus threshold at the time of the New Euxinian transgression in the Black Sea basin. The Bølling-Allerød interstadial brought warm conditions to the Marmara Lake, which is reflected in the sediments, fauna, and flora of the lacustrine facies. Brackish-water and freshwater diatoms and woody material became less abundant just before the marine incursion. Once having reached the Dardanelles threshold, the Mediterranean water began to gradually fill the Sea of Marmara depression.

A considerable cooling during the Younger Dryas period resulted in lowering of the Marmara Sea level and water inflow from the Black Sea, the intensity of the process is still open to discussion (Çagatay et al. 2000; Algan et al. 2001; Hiscott et al. 2002). Judging from the pollen assemblages, the Younger Dryas was the most arid interval of the last ice age in the Eastern Mediterranean (Filipova-Marinova et al. 2012; Mudie et al. 2002, 2007). The Mediterranean water inflow repeated in a rather short time, less than ~1.5 ka later as estimated by Reichel and Halbach (2007). The isotope analysis results revealed the following pattern: when the marine water enters the lake, it becomes saline in a rather short time (1 or 2 ka); when the marine water is outflowing through the Dardanelles Strait, its freshening proceeds slowly taking 3 to 5 ka (Reichel and Halbach 2007). The marine regime established in the Sea of Marmara basin by 9.3-9.0 ka BP (Büyükmeriç et al. 2016).

It can be safely concluded that the Marmara Sea development in the Late Pleistocene was mostly controlled by the level fluctuations in the Black Sea and the Mediterranean, which in turn resulted from the global changes of the climate. An interconnection between the basins depended also on the altitude of thresholds in the Bosporus and Dardanelles straits.

CORRELATION AND INTERRELATIONS OF THE EVENTS

The paleogeographic analysis of the basins forming the system of the Pontian–Caspian–Mediterranean seas (subsequently referred to as the System) allows to analyze the correlation between transgressive and regressive events in individual parts of the System and to reconstruct the functioning of the entire System under the conditions of global climate change (Fig. 4).

In the Caspian Sea, the beginning of Late Pleistocene was marked by a «little» late Khazarian transgression that occurred during the interglacial epoch (MIS 5e). The sea level rise resulted from the climate conditions characterized by a high humidity at the Mikulino (Eemian) Interglacial optimum. At the same time, in the context of the interglacial transgression of the global sea level that reached 6-7 m above the current level, all the sea basins connected to the ocean experienced a transgressive rise of the level: the Tyrrhenian transgression in the Mediterranean, and Karangatian in the Pontian basins. All the straits between the sea basins were functioning. The Karangatian water penetrated deeply into the Manych depression forming an ingression bay, though the Manych threshold prevented its discharge into the late Khazarian basin. The transgression of the marine basins reached its maximum during Neopleistocene, while the transgressive basin during the late Khazarian was isolated from the seas and its level stayed below present mean sea level (Fig. 4a).

The Tyrrhenian transgression proceeded in three stages, two of which were marked by the water penetrating into the Pontian basins and causing the two-stage Karangatian transgression. The 2nd Karangatian stage (Tarkhankut) developed together with the Hyrcanian basin of the Caspian Sea. Its water penetrated deeply into the Eastern Manych valley forming a bay. Another ingressive bay – Karangatian – existed from the Pontian side. The global cooling and the onset of the Valday (Weichselian) glaciation initiated a regressive trend in all the marine basins following the global sea level drop. The drop of the Karangatian sea level led to a gradual reduction of the Manych bay length and finally to its complete disappearance. The same climatic conditions favored the Hyrcanian lake basin transgression by increasing the positive constituent of its water balance. The basin level rose above the Manych threshold, and its water flowed towards the Pont, which resulted in a slight rise of the sea level and a decrease in salinity. Such correlation of the events is corroborated by the presence of Hyrcanian malacofauna in Manych and in the Tarkhankut Pontian basin (Fig. 4 b).

The long-lasting and structurally complicated Tyrrhenian transgression in the Mediterranean, as well as the two-stage Karangatian transgression in the Pontian basin and the Khazarian transgressive epoch, also two-stage, in the Caspian Sea – all of them developed within the period corresponding to MIS 5 – Eemian Interglacial *sensu lato* (s.l.), or Eemian Interglacial (MIS 5e), and the period transitional to the glacial period (MIS 5d-a). It should be noted that the transgressions developed in different basins for various reasons. The marine

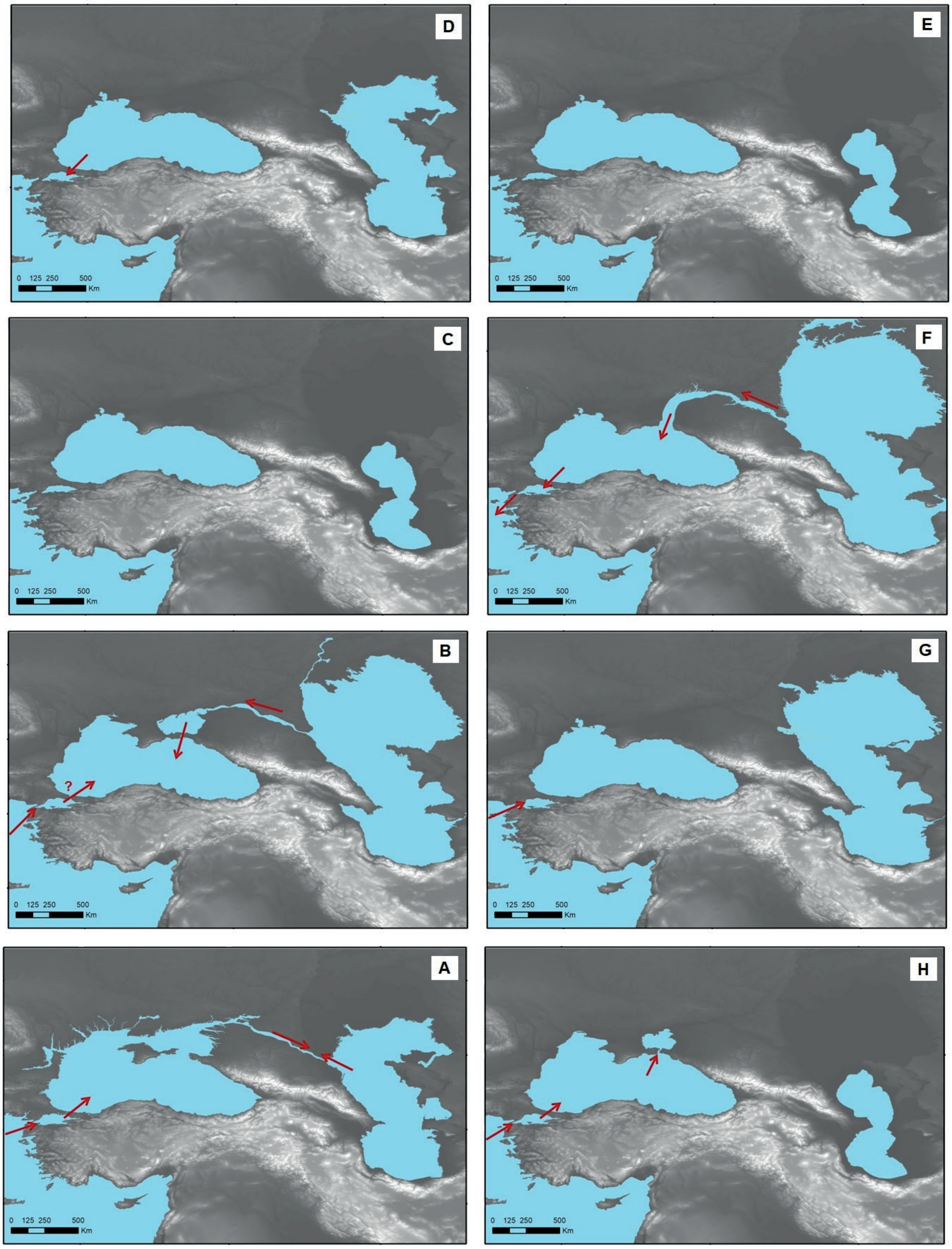

Fig. 4. The Pontian – Caspian – Mediterranean system functioning under conditions of the global climate changes

A - Mikulino - Eemian interglacial (MIS 5e): Tyrrhenian transgression in the Maditerranenan and Marmara seas, Krangatian marine transgression in the Pont (with ingression into the Manych valley) and the Late Khazarian lake transgression in the Caspian Sea;
B - Transition from interglacial to glacial (MIS 5 d-a): Tyrrhenian transgression in the Maditerranenan and Marmara seas, Tarkhankutian basin in the Pont and Hyrcanian transgression in the Caspian, Hyrcanian passage in the Manych Valley;
C - Early Valdai – Early Weichselian glaciation (MIS 4), Glacial maximum: Grimaldi regression in the Mediterranena and Marmara seas, Post-Karangatian regression in the Pont and Atelian regression in the Caspian;
D - Interstadial warming (MIS 3, second half): Inter-Grimaldi transgression in the Mediterranean Sea, lake transgression in the Sea of Marmara, Surozh transgression in the Pont and beginning of the Khvalynian transgression in the Caspian;
E - Late Valdai – Late Weichselian glaciation (MIS 2), Glacial maximum: the Grimaldi regression in the Mediterranean and Marmara seas, the Neoeuxinian regression in the Pont and regression (Eltonian?) in the Khvalynian (Caspian) basin;
F - Degradation of Glaciation (MIS 2): the Grimaldi basin in the Mediterranean and Marmara seas, the Neoeuxinian transgression in the Pont and maximum of the Khvalynian transgression in the Caspian; cascade of basins;
G - Glacial degradation (MIS 2): beginning of the Flandrian transgression in the Mediterranean and Marmara seas, the Neoeuxinian transgression in the Pont and Late Khvalynian transgression in the Caspian;
H – Holocene (MIS 1, beginning): the Flandrian transgression in the Mediterranean and Marmara seas, the Chernomorean (Black Sea) transgression in the Pont and the Mangyshlak regression in the Caspian Sea.
Arrows indicate the water inflow and migration of fauna.

transgressions resulted from the rise of the global sea level above the thresholds in straits connecting individual seas in the System. The Caspian transgressions resulted primarily from the positive water balance in the drainage basin. The discharge through the Manych and the strait functioning depended on the sea level rise above the Manych threshold.

During the glacial time (MIS 4) all the basins in the considered System were at a regressive state: the Roman regression in the Mediterranean, post-Karangatian regression in the Pontian basin and Atelian regression of the Caspian Sea. Lake basins existed in the depressions of the Marmara Sea, the Black Sea, and the Caspian Sea, a lacustrine plain of the Pre-Don occupied the area of the Sea of Azov, and none of the straits was functioning (Fig. 4c). Marine basins connected to the ocean followed its regression (the glacial regression). The Caspian regression resulted from the negative water balance under the conditions of glacial climate.

The rise of the Mediterranean Sea level began during the 1st half of the interstadial warming (MIS 3) following the interstadial rise of the global sea level. The straits were closed, and isolated lakes persisted in the depressions in places of the Marmara Sea, the Black Sea and the Caspian Sea.

The transgressive rise of the level in the Mediterranean Sea continued during the 2nd half of the interstadial warming (MIS 3). The Dardanelles Strait was closed. A lake regime persisted in the Marmara Sea depression, though the basin level has increased due to the increasing water inflow. The same reason has led to the post-Karangatian regression changing to a small-scale Surozh transgression (with sea level not reaching 0 m abs). It had been speculated that a part of its water was flowing into the Sea of Marmara. The Mediterranean water did not flow to the Marmara, or to the Pontian basins. The Manych Strait was closed (Fig. 4d). The Mediterranean Sea transgression was induced by the global sea level rise during the interstadial period. The sea level, however, was below the Dardanelles Strait threshold. The development of the lake basins in the Marmara Sea, Pontian basin, and the Caspian Sea depended on the relationship between the inflow and outflow constituents of the water balance in each of them.

During the glacial epoch (MIS 2) all the basins in the System have experienced regression. The Last Glacial Maximum (LGM) was marked by a deep regression of the global ocean which was followed by regression (Grimaldi) of the Mediterranean Sea. In the isolated basins of the Marmara Sea, Pontian and Caspian seas the LGM was marked by cold and dry conditions, which resulted in a considerable drop of the water level (Grimaldi, New Euxinian and Elton regressions) (Fig. 4e).

The deglaciation epoch led to the water level rise in all the basins under consideration. The Mediterranean Sea, closely related to the ocean in its evolution, transgressed gradually, though irregularly. The «Great» Khvalynian transgression developed in the Caspian Sea due to the sharp increase of the water inflow into that lake. One of the reasons for the high level of the Khvalynian basin was a high threshold of the Manych depression. After it was exceeded, the Khvalynian water started flowing into the New Euxinian (Pontian) lake basin. There were two stages distinguished in the Khvalynian water discharge corresponding to the transgression reaching 45-50 m a.s.l. (initial phase of the warming) and 22-20 m a.s.l. (Bølling warming). The Pontian basin and the Marmara Sea levels depended heavily on the levels of the Caspian and Mediterranean seas. The Mediterranian did not exert any influence onto the New Euxinian basin of the Pont till the Holocene. However, it was twice subjected to the impact of the Caspian due to the Manych Strait opening, which led to the increase of the New Euxinian basin level. Because of the low threshold in the Bosporus, the New Euxinian basin turned to a flow-through (drained) lake: it received the water from the Khvalynian basin of the Caspian, and when the lake level exceeded the Bosporus threshold it started flowing from the New Euxnian basin into the lake located in the Marmora Sea basin. Supposedly, the water could flow further, through the Dardanelles Strait into the eastern part of the Mediterranean (Grimaldi) Sea. So, a system of flow-through lakes developed as follows: Khvalynian basin of the Caspian Sea – New Euxinian (Pontian) basin – Grimaldi basin of Mediterranean (Fig. 4f).

Under the conditions of the ongoing deglaciation, the transgressing Mediterranean Sea reached the Dardanelles Strait threshold, the strait opened and marine water entered the Sea of Marmara, which gradually transformed into a marine basin. Another episode of the New Euxinian water outflow into the Marmara Sea occurred at the end of the Late Pleistocene, in the Younger Dryas. During the beginning of the Holocene, the marine regime stabilized. The sea level reached the Bosporus threshold, and the marine water started to fill the New Euxinian (Pontian) basin, which gradually turned into the modern Black Sea and the Sea of Azov (Fig. 4g). In the Caspian Sea, the cold and dry climate of the Younger Dryas led to a lowered level of the Khvalynian basin (Enotayevka regression). The subsequent sudden warming induced a transgressive rise of the sea level during the Late Khvalynian stage. The Khvalynian epoch in the Caspian Sea evolution ended with the Mangyshlak regression under conditions of a strongly continental climate in the Boreal period of the Holocene.

CONCLUSION. THE PONTIAN – CASPIAN – MEDITERRANEAN SYSTEM FUNCTIONING UNDER THE CONDITIONS OF THE GLOBAL CLIMATE CHANGE

The Pontian–Caspian and Mediterranean basins belonged to different types of water basins and evolved differently in the Late Pleistocene responding in different ways to the changes in global climate. Paleogeographic reconstructions and correlation analysis of the Late Pleistocene events (within the last climatic macrocycle) made it possible to view the evolution of the basins as parts of a single system allowing to identify certain specific features and patterns in their functioning.

The interglacial epoch (MIS 5e) was marked by transgression in all the basins in the System, which could be attributed to different reasons. Marine transgressions resulted from the rise of the global sea level and the opening of the straits (as the sea level exceeded the strait threshold) between the elements of the System. The Caspian lake transgression resulted from the positive water balance of the basin. The marine transgression reached its highest level, while the Caspian transgressive basin stayed below present mean sea level.

During the transition to the glacial period (MIS 5d-a), the Mediterranean Sea level was unstable: its development was interrupted twice (MIS 5d and 5b) by the level drop below the Dardanelles Strait threshold. Those events also affected the Marmara Sea, where marine transgression developed in two stages. During the first stage (MIS 5c) the level exceeded the Bosporus threshold, which led to the rise of the Black Sea level. In the Caspian Sea, the climatic conditions of the transitional period resulted in positive water balance, which caused transgressive evolution of the Caspian basin. The Caspian water flowing through the Manych into the Pontian basin and opening of the strait towards the Mediterranean resulted from the Caspian Sea level rising above the Manych threshold elevation.

During the peaks of the glacial epochs (MIS 4 and MIS 2) all the basins of the System were at regressive stages. None of the straits was functioning. The sea basins that have a connection with the ocean followed its regression; the Caspian Sea, however, regressed due to negative water balance under the conditions of the glacial climate. The colder and dryer conditions of the LGM resulted in even deeper regression.

The interstadial warming (MIS 3) was marked by a small increase in the sea level (not exceeding 0 m abs.). In the Mediterranean Sea, the transgressive level rise resulted from the global sea level increase. In contrast to that, the Marmara, Black and Caspian seas were isolated from the ocean during the glacial period, and their levels depended on the water balance conditions in their drainage basins.

The degradation of the last glaciation (MIS 2) and transition to the Holocene interglacial resulted in the level rise in all the basins (though different in magnitude), which was interrupted by the cold climate phases (Oldest, Older and Younger Dryas). The Mediterranean Sea was constantly connected to the ocean and transgressed accordingly. The highest level rise was observed in the Caspian Sea, which can be attributed to a considerable increase of the water input. The maximum sea level was controlled by the height of the Manych threshold, once that level was exceeded, the Caspian water started flowing into the Pontian basin, the level of which was then located below the present mean sea level. In total there were two instances of the outflow. The input of the Caspian water into the Pont led to the level rise and a discharge of water through the strait into the Sea of Marmara and further into the Mediterranean, thus forming a system of drainage lakes.

The marine regime in the Mediterranean – Pontian part of the system stabilized at the beginning of the Holocene, during the period of the interglacial transgression of the ocean. The Caspian Sea continued its development as a lake basin with high sensitivity to the climate fluctuations.

REFERENCES

Abramova T.A. (1972). Results of paleobotanic studying of Quarternary deposits of the western coast of the Caspian Sea. In: O.K.Leontiev ed. Complex researches of the Caspian Sea. Moscow, Moscow University Publ. House, 3, 134-146 (in Russian).

Aksu A.E., Hiscott R.N., Kaminski M.A., Mudie P.J., Gillespie H., Abrajano T., Yasar D. (2002). Last glacial–Holocene paleoceanography of the Black Sea and Marmara Sea: stable isotopic, foraminiferal and coccolith evidence. Marine Geology, 190 (1-2), 119-149.

Aksu A.E., Hiscott R.N., Yasar D. (1999). Oscillating Quaternary water levels of the Marmara Sea and vigorous outflow into the Aegean Sea from the Marmara Sea–Black Sea drainage corridor. Marine Geology, 153, 275-302.

Allen J.R.M., Brandt U., Brauer A., Hubberten H.W., Huntley B., Keller J., Kraml M., Mackensen A., Mingram J., Negendank J.F.W., Nowaczyk N.R., Oberha¨nsli H., Watts W.A., Wulf S., Zolitschka B. (1999). Rapid environmental changes in southern Europe during the last glacial period. Nature, 400, 740-743.

Andrusov N.I. (1884). Geological researches on the Kerch Peninsula. Notes of the Novorossiysk Society of scientists, 9(2), 1-198 (in Russian).

Andrusov N.I. (1888). Essay of history of development of the Caspian Sea and its inhabitants. Izvestiya Russkogo Geograficheskogo Obshestva, 24(1-2), 91-114 (in Russian).

Andrusov N.I. (1890). Preliminary report on participation in the Black Sea deep-measured expedition. Izvestiya Russkogo Geograficheskogo Obshestva, 26(2), 380-409 (in Russian).

Andrusov N.I. (1900). About ancient coastlines of the Caspian Sea. The Year-book on geology and mineralogy of Russia, 4(1-2), 3-16 (in Russian).

Andrusov N.I. (1925). A Posttertiary Tirrenian terrace in the Black Sea area. Bull. Intern. Acad. Sci. Boheme, 165-176 (in Russian).

Andrusov N.I. (1926). Geological structure and history of the Kerch Strait. Bulletin of the Moscow Society of investigators of the nature, Geology, 4(3-4), 294-332 (in Russian).

Ankindinova O., Aksu A.E., Hiscott R.N. (2019). Oxygen and carbon isotopes and trace-element/ca ratios in late Quaternary ostracods Loxoconcha lepida and Palmoconcha agilis from the Black Sea: paleoclimatic and paleoceanographic implications. Palaeogeography, Palaeoclimatology, Palaeoecology, 533, 109-227.

Arkhangelskiy A.D., Strakhov N.M. (1938). Geological structure and history of development of the Black Sea. Moscow-Leningrad, Academy of Sciences of the USSR Publishing House, 226. (in Russian).

Arkhipov S.A. (1958). To litologo-facial characteristic of the Khvalynian chocolate clays and to conditions of their accumulation. Bulletin of the Commission on Studying of the Quaternary Period, 22, 63-72 (in Russian).

Arslanov H.A., Balabanov I.P., Gey N.A. (1983). About age and climatic conditions of formation of late Pleistocene deposits of marine terraces of the coast of the Kerch Strait. Bulletin of the Leningrad University, 12, 69-79 (in Russian).

Arslanov H.A., Gerasimova S.A., Izmaylov Ya.A. (1975). About age of the Holocene and the late Pleistocene deposits of the Black Sea coast of the Caucasus and Kerch-Taman area. Bulletin of the Commission on Studying of the Quaternary Period, 44, 107-110 (in Russian).

Arslanov Kh.A., Yanina T.A., Chepalyga A.L., Svitoch A.A., Makshaev R.R., Makshaev R.R., Maksimov F.E, Chernov S.B., Tertychniy N.I., Starikova A.A. (2016). On the age of the Khvalynian deposits of the Caspian Sea coasts according to 14c and 230th/234u methods. Quaternary International, 409, 81-87.

Badertscher S., Fleitmann D., Cheng H., Edwards R.L., Gokturk O.M., Zumbuhl A., Leuenberger M., Tuysuz O. (2011). Pleistocene water intrusions from the Mediterranean and Caspian seas into the Black Sea. Nat. Geoscience, 4, 236-239.

Badyukova E.N. (2015). History of fluctuations of the Caspian Sea level during the Pleistocene (Whether there was a Great Khvalynian transgression?). Bulletin of the Commission on Studying of the Quaternary Period, 74, 111-120 (in Russian).

Balabanov I.P. (2006). Holocene sea-level changes in the Northern Black Sea. In: V. Yanko-Hombach et al. eds. Second Plenary meeting and field trip of Project IGCP-521 Black Sea – Mediterranean Corridor during the last 30 ky: sea level change and human adaptation. Odessa, Astroprint, 21-23.

Balabanov I.P., Izmaylov Ya.A. (1988). Change of the level and hydrochemical mode of the Black and Azov seas for the last 20 thousand years. Water resources, 6, 54-63 (in Russian).

Balabanov I.P., Izmaylov Ya.A. (1992). New synthesis of data on chronology of the late Pleistocene and Holocene of the Azov-Black Sea basin. In: V. Murzaeva et al. eds. Geochronology of the Quaternary period. Moscow, Nauka, 42-43.

Berger A., Guiot J., Kukla G., Pestiaux P. (1981). Long-term variations of monthly insolation as related to climatic changes. Geologisches Rundschau, 70, 748-758.

Bezrodnykh Yu.P., Deliya S.V., Romanyuk B.F., Sorokin V.M., Yanina T.A. (2015). New data on the Upper Quaternary stratigraphy of the North Caspian Sea. Doklady Earth Sciences, 462(1), 479-483.

Bezrodnykh Yu.P., Romanyuk B.F., Sorokin V.M., Yanina T.A. (2017). First data on the radiocarbon age of the Atelian deposits in the North Caspian region. Doklady Earth Sciences, 473(1), 277-280.

Bezrodnykh Yu.P., Romanyuk B.F., Sorokin V.M., Yanina T.A. (2019). Stratigraphy of the upper Quaternary deposits of the site of the Taman shelf. In: A. Lisitsyn ed. Geology of seas and oceans. Materials of the XXIII International scientific conference (School) on sea geology, 1. Moscow, IO RAS, 29-33 (in Russian).

Bezrodnykh Yu.P., Yanina T.A., Sorokin V.M., Romanyuk B.F. (2020). The Northern Caspian Sea: Consequences of climate change for level fluctuations during the Holocene. Quaternary International, 540, 68-77.

Blanc A. (1937). Levels of the Mediterranean sea during the Pleistocene glaciation. J. Geol. Soc. London, 93(1-4), 621-651.

Boettger T., Novenko E.Yu., Velichko A.A. et al. (2009). Instability of climate and vegetation dynamics in Central and Eastern Europe during the final stage of the Last In-terglacial (Eemian, Mikulino) and Early Glaciation. Quaternary International, 207, 137-144.

Bogachyov V.V. (1903). The geological observations in the Manych valley made in the summer of 1903. Izvestia of the Geological Committee, 22(9) (in Russian).

Bolikhovskaya N.S., Makshaev R.R. (2020). The Early Khvalynian stage in the Caspian Sea evolution: pollen records, palynofloras and reconstructions of paleoenvironments. Quaternary International, 540, 10-21.

Bolikhovskaya N.S., Yanina T.A., Sorokin V.M. (2017). Environment of the Atelian epoch (on tha data of palinology). Vestnik Moskovskogo Universiteta, Seriya Geografiya, 6, 96-101 (in Russian).

Božilova E., Djankova M. (1976). Vegetation development during the Eemian in the North Black Sea Region. Phytology, 4, 25-32.

Brauer A., Allen R.M., Mingram J., et al. (2007). Evidence for last interglacial chronology and environmental change from Southern Europe. PNAS, 104(2), 450-455.

Brewer S., Guiot J., Saŕnchez-Gon M.F., Klotz S. (2008). The climate in Europe during the Eemian: a multi-method approach using pollen data. Quaternary Science Reviews, 27, 2303-2315.

Briceag A., Melinte-Dobrinescu M.C., Yanchilina A., Ryan W.B.F., Stoica M. (2019). Late Pleistocene to Holocene paleoenvironmental changes in the NW Black Sea. Journal of Quaternary Science, 34(2), 87-100.

Britsina M.I. (1954). Distribution of the Kvalynian chocolate clays and some questions of paleogeography of the Northern Pre-Caspian. Trudy of the Institute of geography of Ac. Sci. of the USSR, (in Russian).

Broecker W.S. (2000). Abrupt climate change: causal constraints provided by the paleoclimate record. Earth-Science Reviews, 51, 137-154.

Brotskiy Yu.Z., Karandeeva M.V. (1953). The Western Pre-Caspian development during Quarternary time. Vestnik Moskovskogo Universiteta, Seriya physical-matem. and natural sciences, 2, 139-146 (in Russian).

Bruckner H. (1986). Stratigraphy, evolution and age of quaternary marine terraces in Marocco and Spain. Z. Geomorph. N.F., 62, 83-101.

Büyükmeriç Y., Wesselingh F., Alçiçek M. (2016). Middle-late Pleistocene marine molluscs from Izmit Bay area (eastern Marmara Sea, Turkey) and the nature of Marmara – Black Sea Corridors. Quaternary International, 401, 153-161.

Çağatay M.N. Eriş K., Ryan W.B.F., Sancar Ü., Polonia A., Akçer S., Biltekin D., Gasperini L., Görür N., Lericolais G., Bard E. (2009). Late Pleistocene–Holocene evolution of the northern shelf of the Sea of Marmara. Marine Geology, 265, 87-100.

Çagatay M.N., Görür N., Algan A., Eastoe C.J., Tchapalyga A., Ongan D., Kuhn T., Kuscu I. (2000). Late Glacial–Holocene palaeoceanography of the Sea of Marmara timing of connections with the Mediterranean and the black Sea. Marine Geology, 167, 191-206.

Casini L., Andreucci S., Sechi D., Pascucci V. (2020). Luminescence dating of Late Pleistocene faults as evidence of uplift and active tectonics in Sardinia, W Mediterranean. Terra Nova, DOI: 10.1111/ter.12458.

Castradori D. (1993). Calcareous nannofossil biostratigraphy and biochronology in eastern Mediterranean deep-sea cores. It. Paleont. Strat., 99, 107-126.

Chepalyga A.L. (2004). Late glacial flood in the Ponto-Caspian Basin as the Flood prototype. In: Yu. Lavrushin ed. Ecology of the Anthropogene and the Present: nature and man. SPb, Gumanistika, 83-88 (in Russian).

Chepalyga A.L. (2006). Epoch of extreme floodings in an arid zone of the Northern Eurasia. In: G. Matishov ed. Late Cainozoic geological history of the north of arid zone. Rostov-on-Don, 166-171 (in Russian).

Cita M.B., Chierici M.A., Ciampo G. et al. (1973). Quaternary record in Ionian and Tyrrhenian basins of Mediterranean Sea. Init. Rept. Deep-Sea Drill. Proj., 13, 1263-1340.

Dansgaard W., Johnsen S.J., Clausen H.B., Dahl J.D., Gundestrup N.S., Hammer C.U., Hvidberg C.S., Steffensen J.P., Sveinbjornsdottir A.E., Jouzel J., Bond G. (1993). Evidence for general instability of past climate from a 250-kyr ice-core record. Nature, 364, 218-220.

Degens E.T., Paluska A. (1979). Tectonic and climatic pulses recorded in Quaternary sediments of the Caspian – Black Sea region. Sediment. Geology, 23(1), 149-163.

Degens E.T., Ross D.A. (1972). Chronology of the Black Sea over the last 25 000 years. Chem. Geol., 10(1), 1-16.

Degering D., Krbetschek M.R. (2007). Dating of interglacial sediments by luminescence methods. In: F. Sirocko et al. eds. The Climate of Past Interglacials. Developments in Quaternary Science. Amsterdam, Elsevier, 157-172.

Dimitrov P.S., Govberg L.I. (1979). New data about the Pleistocene terraces and paleogeography of the Bulgarian shelf of the Black Sea. Geomorphology, 2, 81-89 (in Russian).

Drysdale R.N., Zanchetta G., Hellstrom J.C., et al. (2005). Stalagmite evidence for the on-set of the Last Interglacial in southern Europe at 129±1 ka. Geophysical Research Letters, 32(24), 1-4.

Dutton A, Lambeck K. (2012). Ice Volume and Sea Level During the Last Interglacial. Science, 337, 216-219.

Dynamics of landscape components and internal sea basins of the Northern Eurasia for the last 130000 years. (2002). A. Velichko ed. Moscow, GEOS, 232. (in Russian).

Dzieduszyńska D.A., Forysiak J. (2019). Chronostratigraphy of the late Vistulian in Central Poland and the correlation with Vistulian glacial phases. Studia Quaternaria, 36(2), 137-145.

Eichwald E. (1824). Introductio in historiam naturalem Caspii maris. Casani, 59.

Fedorov P.V. (1957). Stratigraphy of Quarternary deposits and history of development of the Caspian Sea. Moscow, Publishing house of Academy of Sciences of the USSR, 308 (in Russian).

Fedorov P.V. (1963). Stratigraphy of Quarternary deposits of the Crimean-Caucasian coast and some questions of geological history of the Black Sea. Moscow, Nauka, 157 (in Russian).

Fedorov P.V. (1978). Pleistocene of the Ponto-Caspian area. Moscow, Nauka, 165 (in Russian).

Filipova-Marinova M., Pavlov D., Coolen M., Giosan L. (2013). First high-resolution marinopalynological stratigraphy of Late Quaternary sediments from the central part of the Bulgarian Black Sea area. Quaternary International, 293, 170-193.

Forsström L. (2001). Duration of interglacials: a controversial question. Quaternary Sci-ence Reviews, 20, 1577-1586.

Forsström L., Punkari M. (1997). Initiation of the Last Glaciation in Northern Europe. Quaternary Science Reviews, 16, 1197-1215.

Gaigalas A., Arslanov Kh. A., Maksimov F. E. et al. (2005). Results of uranium-thorium isochron dating of Netiesos section peatbog in South Lithuania. Geologija, 51, 29-38.

Geological history of the Black Sea on rezuls of deep-water drilling. (1980). E. Neprochnov ed. Moscow, Nauka, 212 (in Russian).

Gignoux M. (1913). Les formations marines pliocènes et quaternaires de l'Italie du Sud et de la Sicilie. Ann. Université de Lyon. Nouvelle serie, 1(36).

Goretski G.I. (1957a). About a correlation of marine and continental sediments in Pre-Azov, Pre-Manych and the Lower Don region. Trudy of the Commission on Studying of the Quaternary Period, XIII, 36-54 (in Russian).

Goretski G.I. (1957b). About a Hyrcanian stage in the history of Pre-Caspian area. News of the oil equipment, 6 (in Russian).

Goretskiy G.I. (1953). About paleogeography of Pre-Azov and Western Pre-Manych areas during Uzunlar-Hyrcanian and Burtass centuries. Questions of Geography, 33, 190-221 (in Russian).

Grichuk V.P. (1954). Materials to paleobotanic characteristic of Quarternary and Pliocene deposits of the northwest part of the Pre-Caspian Depression. Materials on geomorphology and paleogeography of the USSR, 11. Moscow, Academy of Sciences of the USSR publishing house, 5-79 (in Russian).

Gubkin I.M. (1913). Review of geological formation of the Taman Peninsula. Izvestiya of the Geological Committee, 32(8), 803-859 (in Russian).

Head M.J. (2019). Formal subdivision of the Quaternary System/Period: Present status and future directions. Quaternary International, 500, 32-51.

Helmens K.F. (2014). The Last Interglacial-Glacial cycle (MIS 5-2) re-examined based on long proxy records from central and northern Europe. Quaternary Science Reviews, 86, 115-143.

Herrle J.O., Gebühr C., Sheward R.M., Giesenberg A., Bollmann J., Schulz H. (2018). Black Sea outflow response to Holocene meltwater events. Scientific Reports, 8(1), 4081.

History of geological development of the continental outskirts of the western part of the Black Sea. (1988). P.N. Kuprin ed. Moscow, Moscow University publ. house, 312 (in Russian).

Imbrie J., Hays J.D., McIntyre A. et al. (1984). The orbital theory of Pleistocene climate: support from a revised chronology of the marine δ18O record. In: A. Berger t al., eds. Milankovitch and Climate. Reidel, Boston, 269–305.

Issel A. (1914). Lembi fossiliferi quaternari e recente osservati nella Sardegna meridionali. R.C. Acad. Lincei. 5 ser., XXIII, 759-770.

Izmaylov Ya.A. (2005). Evolutionary geography of the Azov and Black Sea coasts. Book 1. Anapa Spit. Sochi: Lazarevskaya polygraphiya, 176 (in Russian).

Jones G.A., Gagnon A.R. (1994). Radiocarbon chronology of Black Sea sediments. Deep Sea Research Part I: Oceanographic Research Papers, 41(3), 531-557.

Kaminski M.A., Aksu A., Box M., Hiscott R.N., Filipescu S., Al-Salameen M. (2002). Late Glacial to Holocene benthic foraminifer in the Marmara Sea: implications for Black Sea–Mediterranean Sea connections following the last deglaciation. Marine Geology, 19, 165-202.

Kaplin P.A., Scherbakov F.A. (1986). Reconstruction of the paleogeographic situations on the shelf during late Quarternary time. Oceanology, 26(6), 976-980 (in Russian).

Keraudren B., Sorel D. (1987). The terraces of Corinth (Greece) – A detailed record of eustatic sea-level variations during the Last 500 000 years. Marine Geology, 77(1-2), 99-107.

Klotz S., Muller U., Mosbrugger V., de Beaulieu J.-L., Reille M. (2004). Eemian to early Wurmian climate dynamics: history and pattern of changes in Central Europe. Palaeogeography, Palaeoclimatology, Palaeoecology, 211, 107-126.

Kopp R.E., Mitrovica J.X., Griffies S.M. et al. (2010). The impact of Greenland melt on local sea levels: a partially coupled analysis of dynamic and static equilibrium effects in idealized water-hosing experiments. Climate Change, 103, 619-625.

Kopp R.E., Simons F.J., Mitrovica J.X. et al. (2013). A probabilistic assessment of sea level variations within the last interglacial stage. Geophysical Journal International, 21, 1-6.

Kovalyukh N.N., Mitropolskiy A.Yu., Sobotovich E.V. (1977). A radio-carbon method in marine geology. Kiev, Naukova dumka, 74. (in Russian).

Krijgsman W., Tesakov A., Yanina T., Lazarev S., Danukalova G., Van Baak C.G.C, Agustí J., Alçiçek M.C., Aliyeva E., Bista D., Bruch A., Büyükmeriç Y., Bukhsianidze M., Flecker R., Frolov P., Hoyle T.M., Jorissen E.L., Kirscher U., Koriche S.A., Kroonenberg S.B., Lordkipanidze D., Oms O., Rausch L., Singarayer J., Stoica M., van de Velde S., Titov V.V., Wesselingh F.P. (2019). Quaternary time scales for the Pontocaspian domain: interbasinal connectivity and faunal evolution. Earth-Science Reviews, 188, 1-40.

Krystev T.I., Svitoch A.A., Gunova V.S. (1990). New data on the Karangatian terrace near Varna (Bulgaria). In: T Krystev ed. Geological evolution of the western part of the Black Sea during the Neogene – Quarternary time. Sofia, 106-113 (in Russian).

Kukla G. (2000). The last interglacial. Science, 287, 987-989.

Kukla G., Bender M., de Beaulieu J.-L. et al. (2002). Last Interglacial Climates. Quaternary Research, 58, 2-13.

Kukla G., McManus J.F., Rousseau D.D., Chuine I. (1997). How long was the last interglacial. Quaternary Science Reviews, 16, 605-612.

Kuprin P.N., Sorokin V.M. (1982). Reflection of the Black Sea level changes in the Quarternary deposits. P. Kaplin ed. Sea level change. Moscow, Moscow University publishing house, 221-226 (in Russian).

Kurbanov R.N., Yanina T.A., Murray A., Borisova O.K. (2018). Hyrcanian stage in the late Pleistocene history of the Manych depression. Vestnik Moskovskogo Universiteta, Seriya Geografiya, 3, 77-88 (in Russian).

Kurbanov R.N., Yanina T.A., Murray A., Semikolennyh D.V., Svistunov M.I., Shtyrkova E.I. (2019). Age of the Karangatian transgression (late Pleistocene) of the Black Sea. Vestnik Moskovskogo Universiteta, Seriya Geografiya, 6, 29-40 (in Russian).

Kuznetsov V.Yu., Arslanov H.A., Kozlov V.B. (2002). Absolute age of buried peat from stratotype section Mikulino and prarastratotype Nizhnyaya Boyarshchina according to uranium-thorium dating. Materials of the III All-Russian meeting on studying the Quaternary Period. 1. Smolensk, Oykumena, 135-136 (in Russian).

Kvasov D.D. (1975). Late Quarternary history of large lakes and inland seas of Eastern Europe. Leningrad, Nauka, 278 (in Russian).

Lamothe L.J. (1899). Note sur les anciennes plages et terraces du bassin de J'Isser (department d'Alger) et de quelquesantres bassins de la cote algerienne. Bull. Soc. Geol. France. 3-me ser. Paris.

Lavrushin Yu.A., Spiridonova E.A., Holmovoy G.V. (2002). Calendar-event stratigraphy of the late Neopleistocene. Materials of the Third All-Russian meeting on studying the Quaternary Period, 1. Smolensk, Oykumena, 143-145 (in Russian).

Lavrushin Yu.A., Spiridonova E.A., Tudryn A., Shali F., Antipov M.P., Kuralenko N.P., Kurina E.E., Tukholka P. (2014). The Caspian Sea: Hydrological events of late Quarter. Bulletin of the Commission on studying the Quaternary Period, 73, 19-51 (in Russian).

Leonov Yu.G., Lavrushin Yu.A., Antipov M.P., Spiridonova E.A., Kuzmin Ya.V. (2002). New data on age of deposits of the transgressive phase of the Early Khvalynian transgression. Doklady Earth Sciences, 386(2), 229-233.

Leontyev O.K., Fedorov P.V. (1953). To history of the Caspian Sea during late- and after Khvalynian time. Izvstiya of Academy of Sciences of the USSR, series Geography, 4, 64-74 (in Russian).

Leontyev O.K., Mayev E.G., Rychagov G.I. (1977). Geomorfology of coast and bottom of the Caspian Sea. Moscow, Moscow Yniversity publ. house, 210 (in Russian).

Litt T., Behre K.-E., Meyer K.-D., Stephan H.-J., Wansa S. (2007). Stratigraphical Terms for the Quaternary of the Northern German Glaciation Area. Quaternary Science Journal, 56 (1/2), 7-65.

Litt T., Gibbard P. (2008). Definition of a Global Stratotype Section and Point (GSSP) for the base of the Upper (Late) Pleistocene Subseries (Quaternary System/Period). Episodes, 31(2), 260-263.

Lokhin M.Yu., Mayev E.G. (1990). Late Pleistocene deltas on the shelf of a northern part of the Middle Caspian Sea. Vestnik Moskovskogo Universiteta, Seriya Geografiya, 3, 34-40 (in Russian).

Major C.O., Ryan W., Lercolais G., Hajdas I. (2002). Constraints on Black Sea outflow to the Sea of Marmara during the last glacial–interglacial transition. Marine Geology, 190, 19-34.

Makshaev R.R., Svitoch A.A. (2016). Chocolate clays of the northern Caspian Sea region: Distribution, structure, and origin. Quaternary International, 409, 44-49.

Mangerud J. (1989). Correlation of the Eemian and the Weichselian with deep sea oxygen isotope stratigraphy. Quaternary International, 3-4, 1-4.

Mangerud J., Sonstegaard E., Sejrup H.-P. (1979). Correlation of Eemian (interglacial) stage and the deep-sea oxygen-isotope stratigraphy. Nature, 277, 189-192.

Markova A.K., Mikhaylesku K.D. (1990). New section with terio- and malakofauna in the Mikulino deposits of Lower Danube. Bulletin of the Commission on studying the Quaternary Period, 59, 94-101 (in Russian).

Mazarovich A.N. (1927). From the field of geomorphology and history of a relief of Lower Volga area. Zemlevedenie, 1927, 29(3-4) (in Russian).

McHugh C.M.G., Gurung D., Giosan L., Ryan W.B.F., Mart Y., Sancar U., Burckle L., Çagatay N. (2008). The last reconnection of the Marmara Sea (Turkey) to the World Ocean: A paleoceanographic and paleoclimatic perspective. Marine Geology, 255, 64-82.

Meriç E., Nazik A., Avşar N., Yümün Z., Büyükmeriç Y., Yildiz A., Sagular E.K., Koral H., Gökaşan E. (2018). Fauna and flora of drilling and core data from the Iznik lake: the Marmara and the Black Sea connection. Quaternary International, 486, 156-184.

Merkt J., Müller H. (1999). Varve chronology and palynology of the Lateglacial in Northwest Germany from lacustrine sediments of Hämelsee in Lower Saxony. Quaternary International, 61, 41-59.

Meyer M., Spötl C., Mangini A. (2008). The demise of the Last Interglacial recorded in isotopically dated speleothems from the Alps. Quaternary Science Reviews, 27, 476-496.

Mikhaylesku K.D. (1990). Origin of estuaries of the Danube Delta. Chisinau, Shtiintsa, 161 (in Russian).

Molodkov A.N., Bolikhovskaya N.S. (2002). Eustatic sea-level and climate changes over the last 600 ka as derived from mollusc-based ESR-chronostratigraphy and pollen evidence in Northern Eurasia. Sedimentary Geology, 150, 185-201.

Molodkov A., Bolikhovskaya N. (2006). Long-term palaeoenvironmental changes recorded in palynologically studied loess-palaeosol and ESR-dated marine deposits of Northern Eurasia: implication for sea-land correlation. Quaternary International, 152-153, 48-58.

Mordukhay-Boltovskoy F.D. (1960). The Caspian fauna in the Azov-Black Sea basin. Moscow-Leningrad, Academy of Sciences of the USSR publishing house, 287 (in Russian).

Moskvitin A.I. (1962). Pleistocene of Lower Volga area. Moscow, Academy of Sciences of the USSR publishing house, 263 (in Russian).

Mudie P.J., Marret F., Aksu A.E., Hiscott R.N., Gillespie H. (2007). Palynological evidence for climatic change, anthropogenic activity and outflow of Black Sea water during the late Pleistocene and Holocene: centennial- to decadal-scale records from the Black and Marmara Seas. Quaternary International, 167-168, 73-90.

Mudie P.J., Rochon A., Aksu A.E. (2002). Pollen stratigraphy of Late Quaternary cores from Marmara Sea: land–sea correlation and paleoclimatic history. Marine Geology, 190, 233-260.

Murdmaa I., Ivanova E., Chepalyga A., et al. (2006). Paleoenvironments on the North Caucasian Black Sea shelf since the LGM. In: V. Yanko-Hombach et al. eds. Second Plenary meeting and field trip of Project IGCP-521 Black Sea – Mediterranean Corridor during the last 30 ky: sea level change and human adaptation. Odessa, Astroprint, 127-129.

Mushketov I.V. (1895). Geological researches in the Kalmyk steppe. Trudy of the Geological Comitte, XIY(1), 168 (in Russian).

NEEM community members. (2013). Eemian interglacial reconstructed from Greenland folded NEEM ice core strata. Nature, 493, 489-494.

Nesmeyanov S.A., Izmaylov Ya.A. (1995). Tectonic deformations of the Black Sea terraces of the Caucasian coast of Russia. Moscow, PNIIS, 237 (in Russian).

Nevesskaya L.A. (1965). Late Quarternary mollusks of the Black Sea, their systematization and ecology. Moscow, Academy of Sciences of the USSR publishing house, 392 p. (in Russian).

Nikolaev N.I. (1941). Geology and hydrogeology of the Southern Zavolzhye. Moscow — Leningrad, Gosstoptekhizdat (in Russian).

North Greenland Ice Core Project members. (2004). High-resolution record of Northern Hemisphere climate extending into the last interglacial period. Nature, 431, 147-151.

Novenko E.Yu. (2016). Changes of vegetation and climate of Central and Eastern Europe in the late Pleistocene and Holocene during interglacial and transitional stages of climatic macrocycles. Moscow, GEOS, 228 (in Russian).

Ostrovskiy A.B., Izmaylov Ya.A., Balabanov I.P. (1977a). New data on the paleohydrological mode of the Black Sea during the upper Pleistocene and the Holocene. In: P. Kaplin ed. Paleogeography and deposits of the Pleistocene of the southern seas of the USSR. Moscow, Nauka, 131-140 (in Russian).

Ostrovskiy A.B., Izmaylov Ya.A., Shcheglov A.P. (1977b). New data on a stratigraphy and geochronology of the Pleistocene marine terraces of the Black Sea coast of the Caucasus and Kerch-Taman region. In: P. Kaplin ed. Paleogeography and deposits of the Pleistocene of the southern seas of the USSR. Moscow, Nauka, 61-68 (in Russian).

Paleoclimates and paleolandscapes of extra tropical space of Northern Eurasia. Late Pleistocene – Holocene. The atlas – monograph. (2009). A.A. Velichko ed. Moscow, GEOS, 120 (in Russian).

Pallas P.S. Reise durch verschiedene Provinzen des Russischen Reichs in den Jahren 1768–1774. SPb., 1771–1776, 1-3.

Pavlov A.P. (1925). Neogene and posttertiary deposits of Southern and Eastern Europe. Memoirs of Society of fans of natural sciences, anthropology and ethnography, 5, 217 (in Russian).

Popov G.I. (1955). History of Manych Straits in connection with a stratigraphy of the Black Sea and Caspian deposits. Bulletin of the Moscow society of the ivestigators of the nature, Dep. Geology, 20(2), 31-49 (in Russian).

Popov G.I. (1967). Hyrcanian transgression in the Northern Pre-Caspian area. Bulletin of the Commission on studying the Quaternary Period, 33, 77-86 (in Russian).

Popov G.I. (1983). Pleistocene of the Black Sea – Caspian passages. Moscow, Nauka, 216 (in Russian).

Popov G.I., Suprunova N.I. (1977). Stratigraphy of Quaternary deposits of the Kerch Strait bottom. Doklady of the Academy of Sciences of the USSR, 237(5) (in Russian).

Pravoslavlev P.A. (1908). Materials for knowledge of the Lower Volga Caspian deposits. Warsaw, 467 (in Russian).

Pravoslavlev P.A. (1926). The Caspian sediments in Lower Volga area. // Izvestiya Center. Hydromet-bureau, 6, 2-77 (in Russian).

Reichel T., Halbach P. (2007). An authigenic calcite layer in the sediments of the Sea of Marmara – A geochemical marker horizon with paleoceanographic significance. Deep Sea Research Part II Topical Studies in Oceanography, 54(11), 1201-1215.

Rinterknecht V., Hang T., Gorlach A., et al. (2018). The Last Glacial Maximum extent of the Scandinavian Ice Sheet in the Valday Heights, western Russia: Evidence from cosmogenic surface exposure dating using 10Be. Quaternary Science Reviews, 200, 106-113.

Ryan W.B.F., Pitman W.C., Major C.O., Shimkus K., Moskalenko V., Jones G.A., Dimitrov P., Gorür N., Sakinç M., Yüce H. (1997). An abrupt drowning of the Black Sea shelf. Marine Geology, 138, 119-126.

Rychagov G.I. (1970). Quarternary rhythms of the Caspian Sea. Questions of Geography, 79, 121-132 (in Russian).

Rychagov G.I. (1997). Pleistocene history of the Caspian Sea. Moscow, Publishing house of the Moscow University, 267. (in Russian).

Scherbakov F.A. (1982). Reflection of sea level changes in the late Quarternary marine deposits. In: P.A. Kaplin et al. ed. Fluctuations of level of the seas and oceans during 15000 years. Moscow, Nauka, 112-120 (in Russian).

Scherbakov F.A., Koreneva E.V., Zabelina E.K. (1979). Stratigraphy of late Quaternary deposits of the Black Sea. In: D. Gershanovich ed. Late Quaternary history and sedimentation in suburban and inland seas. Moscow, Nauka, 46-51 (in Russian).

Scherbakov F.A., Kuprin P.N., Zabelina E.K. (1977). Paleogeography of Azov-Black Sea Coast in the late Pleistocene and the Holocene. In: In: P. Kaplin ed. Paleogeography and deposits of the Pleistocene of the southern seas of the USSR. Moscow, Nauka, 51-60 (in Russian).

Semenenko V.N., Sidenko O.G. (1979). Reflection of deep structures in marine Quaternary deposits of the central part of the Sea of Azov. In: D. Gershanovich ed. Late quaternary history and sedimentation in suburban and inland seas. Moscow, Nauka, 87-99 (in Russian).

Shackleton N.J. (1969). The last interglacial in the marine and terrestreal records. Proceedings of the Royal Society. London, 174, 135-154.

Shackleton N.J. (1987). Oxygen isotopes, ice volume and sea level. Quaternary Science Reviews, 6, 183-190.

Shackleton N.J., Chapman M., Sanchez Goni M.F., Pailler D., Lancelot Y. (2002). The classic marine isotope substage 5e. Quaternary Research, 58, 14-16.

Shakhovets S.A., Shlyukov A.I. (1987). Thermoluminescent dating of deposits of the Lower Volga (new methodical approach). In: O.M. Petrov ed. New data on geochronology of the Quaternary Period. Moscow, Nauka, 197-204 (in Russian).

Shik S.M. (2014). Neopleistocene of the center of the European Russia: modern ideas of a stratigraphy and paleogeography. Stratigraphy and Geological correlation, 22(2), 108-120.

Shimkus K.M. (1981). Sedimentation in the Mediterranean Sea during the late Quarternary time. Moscow, Nauka, 239. (in Russian).

Shkatova V.K. (2010). Paleogeography of the late Pleistocene Caspian basins: Geochronometry, paleomagnetism, paleotemperature, paleosalinity and oxygen isotopes. Quaternary International, 225, 221-229.

Shnyukov E.F., Alenkin V.M., Inozemtsev Yu.I., Naumenko P.I., Put A.L., Skiba S.I. (1981). Geology of the shelf of the Ukrainian SSR. Kerch Strait. Kiev, Naukova Dumka, 160 (in Russian).

Sholten R. (1974). Role of the Bosherus in Black Sea chemistry and sedimentation. The Black Sea Geology, Chemistry, and Biology. Mem. Amer. Assoc. Publish. Geol. Tulsa, Okla, 20.

Shumilovskikh L., Arz H., Wegwerth A., Fleitmann D., Marret F., Nowaczyk N., Tarasov P., Behling H. (2013). Vegetation and environmental changes in Northern Anatolia between 134 and 119 ka recorded in Black Sea sediments. Quaternary Research, 80, 349-360.

Shumilovskikh L.S., Marret F., Fleitmann D., Arz H.W., Nowaczyk N., Behling H. (2013). Eemian and Holocene sea-surface conditions in the southern Black Sea: organicwalled dinoflagellate cyst record from core 22-GC3. Marine Micropaleontology, 101, 146-160.

Sorokin V.M. (2011). Correlation of upper Quaternary deposits and paleogeography of the Black and Caspian seas. Stratigraphy and Geological Correlation, 19(5), 563-578.

Sorokin V.M., Yanina T.A., Bezrodnykh Yu.P., Romanyuk B.F. (2018). Identification and age of submarine Girkanian sediment beds (upper Pleistocene) in the Caspian Sea. Quaternary International, 465(A), 152-157.

Svitoch A.A. (2011). Holocene history of the Caspian Sea and other basins of the European Russia: comparative analysis. Vestnik Moskovskogo Universiteta, Seriya Geografiya, 2, 28-38 (in Russian).

Svitoch A.A. (2014). Big Caspian Sea: structure and history of development. Moscow, Publishing house of the Moscow University, 272 (in Russian).

Svitoch A.A., Makshayev R.R. (2017). Interrelations of the paleogeographic events in the Pont-Manych-Caspian system during the late Pleistocene – the Holocene. Vestnik Moskovskogo Universiteta, Seriya Geografiya, 2, 24-32 (in Russian).

Svitoch A.A., Selivanov A.O., Yanina T.A. (1998). Paleogeographic events of the Pleistocene of the Ponto-Caspian and the Mediterranean seas (materials on reconstruction and correlation). Moscow, Publishing house of the Russian Academy of Agrarian Sciences, 288. (in Russian).

Svitoch A.A., Yanina T.A. (1997). Quarternary deposits of coasts of the Caspian Sea. Moscow, Publishing house of the Russian Academy of Agrarian Sciences, 268 (in Russian).

The Black Sea Flood Question: Changes in Coastline, Climate, and Human Settlement. Dordrecht, Springer, 2006, 971.

Tudryn A., Tucholka P., Chalie F., Lavrushin Yu.A., Antipov M.P., Lavrushin V.Yu., Spiridonova E.A., Leroy S.A.G. (2013). Late Quaternary Caspian Sea environment: Late Khazarian and early Khvalynian transgressions from the lower reaches of the Volga River. Quaternary International, 292, 193-204.

Turney C.S.M., Jones R.T. (2010). Does the Agulhas Current amplify global temperatures during superinterglacials? Journal of Quaternary Science, 25, 839-843.

Varushchenko S.I. (1975). Analysis of the late Pleistocene and Holocene history of development of the environment of the northwest shelf of the Black Sea. G. Kalinin et al. eds. Fluctuation of global sea level and questions of marine geomorphology. Moscow, Nauka, 50-62 (in Russian).

Varushchenko S.I., Varushchenko A.N., Klige R.K. (1987). Change of the level of the Caspian Sea and drainless basins in paleotime. Moscow, Nauka, 256.

Vasilyev Yu.M. (1961). Anthropohene of the Southern Zavolzhye. Moscow, Academy of Sciences of the USSR publishing house, 128 (in Russian).

Vasilyev Yu.M., Fedorov P.V. (1965). About stratigraphic position of the upper Khazarian deposits of the Lower Volga area in the uniform scale of the Caspian region. Izvestiya of the Academy of Sciences of the USSR, Geology, 12 (in Russian).

Vronskiy V.A. (1976). Marinopalinology of the southern seas. Rostov-on-Don, Rostov Univesity publishing house, 200.

Wainer K., Genty D., Blamart D. et al. (2011). Speleothem record of the last 180 ka in Villars cave (SW France): Investigation of a large d18O shift between MIS6 and MIS5. Quaternary Science Reviews, 30, 130-146.

Walker M., Johnsen,S., Rasmussen S.O. et al. (2009). Formal definition and dating of the GSSP (Global Stratotype Section and Point) for the base of the Holocene using the Greenland NGRIP ice core, and selected auxiliary records. Journal of Quaternary Science, 24(1), 3-17.

Wegwerth A., Dellwig O., Kaiser J., Ménot G., Bard E., Shumilovskikh L., Schnetger B., Kleinhanns I., Willee M., Arza H. (2014). Meltwater events and the Mediterranean reconnection at the Saalian–Eemian transition in the Black Sea. Earth and Planetary Science Letters, 404, 124-135.

Winguth C., Wong H.k., Panin N. et al. (2000). Upper Quaternary water level history and sedimentation in the northwestern Black Sea. Marine Geology, 167, 127-146.

Yakhimovich V.L., Nemkova V.K., Dorofeyev P.I., Popova-Lvova M.G., Suleymanova F.I., Khabibulina G.A., Alimbekova L.I., Latypova E.K. (1986). Pleistocene of the lower current of the Urals River. Ufa, BFAN USSR, 135 (in Russian).

Yanina T.A. (2005). Didacna of the Ponto-Caspian region. Smolensk: Madzhenta, 2005, 300 (in Russian).

Yanina T.A. (2006). Manych depression as the field of migrations of the Ponto-Caspian fauna during the Pleistocene. Geomorphology, 4, 97-106 (in Russian).

Yanina T.A. (2012). Neopleistocene of the Ponto-Caspian region: biostratigraphy, paleogeography, correlation. Moscow, Moscow University Publ. house, 264 (in Russian).

Yanina T.A. (2012). Correlation of the late Pleistocene paleogeographical events of the Caspian Sea and Russian plain. Quaternary International, 271, 120-129.

Yanina T., Sorokin V., Bezrodnykh Yu., Romanyuk B. (2018). Late Pleistocene climatic events reflected in the Caspian Sea geological history (based on drilling data). Quaternary International, 465 (A), 130-141.

Yanina T.A., Sorokin V.M., Bezrodnykh Yu.P., Romaniuk B.F. (2014). The Girkan stage in the Pleistocene history of the Caspian Sea. Vestnik Moskovskogo Universiteta, Seriya Geografiya, 3, 3-9 (in Russian).

Yanina T.A., Svitoch A.A., Kurbanov R.N., Murray A.S., Tkach N.T., Sychev N.V. (2017). Experience of dating o the Pleistocene deposits of the Lower Volga area by method of optically stimulated luminescence. Vestnik Moskovskogo Universiteta, Seriya Geografiya, 5, 21-29 (in Russian).

Yanko V.V., Frolov V.T., Motnenko I.V. (1990). Foraminifera and lithology of the stratotype horizon (Anthropogene of the Kerch peninsula). Bulletin of the Moscow Society of investigators of the nature, Geology, 3, 85-97 (in Russian).

Zabelina E.K., Scherbakov F.A. (1975). To stratigraphy of the upper Quaternary deposits of the Black Sea on the base of diatomic seaweed. Doklady of the Academy of Sciences of the USSR, 221(4) (in Russian).

Zagwijn W.H. (1983). Sea-level changes in the Netherlands during the Eemian. Geologie en Mijnbouw, 62, 437-450.

Zagwijn W.H. (1996). An analysis of Eemian climate in western and central Europe. Quaternary Science Reviews, 15, 451-469.

Zazo C., Goy J.L., Agnirre E. (1984). Did strombus surrive the Last Interglacial in the Western Mediterranean Sea? Mediterranea, Ser. geol., 3, 131-137.

Zhukov M.M. (1936). Quarternary deposits of the Lover Volga region. Trudy of the Moscow prospecting institute, 1 (in Russian).

Zubakov V.A. (1986). Global climatic events of the Pleistocene. Leningrad, Hydrometeoizdat, 288 (in Russian).

Zubakov V.A., Bogatkina N.V., Pisarevskiy S.A. (1982). Detailed subdivision, stratigraphic volume and age of the Karangatian horizon of the Black Sea Coast. Doklady of the Academy of Sciences of the USSR, 267(2), 426-428 (in Russian).

RESEARCH PAPER

IMPACT OF MOZHAYSK DAM ON THE MOSCOW RIVER SEDIMENT TRANSPORT

Dmitriy I. Sokolov[1], Oxana N. Erina[1*], Maria A. Tereshina[1], Valeriy V. Puklakov[1]
[1]Lomonosov Moscow State University, GSP-1, Leninskie gory, Moscow, 119991, Russia
***Corresponding author:** oxana.erina@geogr.msu.ru
Received: November 21th, 2019 / Accepted: November 20th, 2020 / Published: December 31st, 2020
https://DOI-10.24057/2071-9388-2019-150

ABSTRACT. Sediments are an essential part of the aquatic environment that define its transformation and development. The construction of dams results in severe changes in sediment fluxes. This study aims to assess how the sediment load of the upper Moskva River is affected by the Mozhaysk Dam flow regulation and to estimate its dynamics over the years of the reservoir's existence. Our analysis of the 1968, 2012 and 2016 detailed field data shows a 20-40% decrease in the proportion of the spring flood in the annual sediment load into the reservoir, which is caused by changes in the streamflow regime of the inflowing rivers. The peak suspended sediment concentrations have decreased 5- to 10-fold, likely due to a significant decline in the watershed's cultivated land area, which caused a decrease in the erosion rate. In the Moskva River below the dam, the seasonal dynamics of the suspended sediment concentration no longer corresponds to the natural regime. The annual suspended load of the Moskva River below the Mozhaysk Reservoir decreased up to 9-fold. The sediment retention in the reservoir has dropped from 90% to 70-85% and is to some extent restored by an outflow of the particulate organic matter produced in the reservoir. We also described the relationships between water turbidity and suspended sediment concentration of the reservoir's tributaries, which allow for the first time to estimate the sediment load with higher accuracy than was previously possible.

KEY WORDS: Mozhaysk Dam, sediment load, suspended sediment concentration, reservoir

CITATION: Sokolov D. I., Erina O. N., Tereshina M. A., Puklakov V. V. (2020). Impact Of Mozhaysk Dam On The Moscow River Sediment Transport. Geography, Environment, Sustainability, Vol.13, No 4, p. 24-31 https://DOI-10.24057/2071-9388-2019-150

ACKNOWLEDGEMENTS: This study was supported by the Russian Science Foundation (project no. 19-77-30004) with regard to calculations and methodology. Data collection was supported by the Russian Foundation for Basic Research (project no. 19-05-00087 a). Sediment balance of the reservoir was estimated with support of the Russian Geographical Society (project "The Moscow River from the headwaters to the mouth").

Conflict of interests: The authors reported no potential conflict of interest.

INTRODUCTION

Sediment is an essential part of a river ecosystem that defines its transformation and development (Vanmaercke et al. 2011; Wang et al. 2016). The erosion rate may vary under the influence of a great range of watershed processes, including climate change and various human activities (Syvitski et al. 2005). Soil erosion determines the chemical composition of the river water and its nutrient supply. Solid particles also act as a means of pollution transport due to their high sorption capacity for heavy metals and organic contaminants, such as pesticides, insecticides, etc.

At the same time, erosion, sediment transport, and deposition in the river system control the patterns of the spatial distribution of the riparian biomes. The macrophyte growth increases the self-purification capacity of a river and its resilience to human pressure; floodplain sediments act as a spawning and nursery zone for freshwater fish. Many aquatic organisms are sensitive to water turbidity and bedload properties (Shields 2009). This dictates the need to study the sediment flow in rivers as a necessary step towards understanding and predicting the dynamics of freshwater ecosystems, and preserving the habitat for indigenous species.

The construction of dams results in severe changes in both water and sediment fluxes (Kondolf et al. 2014; Kovacs et al. 2012; Snoussi et al. 2002; Yang et al. 2006). The disruption of the ecological integrity of a river leads to an increase in bank erosion rates at the downstream reaches (Grimshaw and Lewin 1980; Wright and Schoellhamer 2004), causing degradation and loss of river-floodplain habitats (Ligon et al. 1995). The peak sediment load in dammed rivers is separated in time from the maximum water flow (Dang et al. 2010; Topping et al. 2000). Moreover, the balance between inorganic and organic sediment is disrupted. The predominately mineral particles from the river are deposited in the bottom sediments, and increased biological production rates cause the suspended load of the reservoir outflow to be largely composed of the organic matter of the aquatic organisms.

Reservoirs interrupt the transit of suspended sediment with river runoff, trapping up to 50-90% and more of the incoming sediment flux and altering the distribution between particles of different sizes (Hojan and Rurek 2017; Berkovich 2012; Le et al. 2020; Piqué et al. 2017; Suif et al. 2017; Van Binh et al. 2020). This effect is particularly evident in cascades of reservoirs and in large reservoirs located in mouth zones of rivers, where the sediment retention rate may reach 100% (Guo et al. 2020; Huang et al. 2018; Ibàhez et al. 1996), although in the case of rivers with large sediment loads cascade reservoirs have lesser retention potential (Wu et al. 2018). In arid and semiarid regions of many countries (Mexico, Spain, Italy, Iran, and China), check dams are constructed as an effective measure for reducing the sediment load, allowing to intercept from 7% to 100% (50-90% on average) of the river sediment (Díaz-Gutiérrez et al. 2019; Tang et al. 2020).

The study of the long-term variability of the river sediment budget under the influence of flow regulation is not only relevant from the ecosystem dynamics point of view; it also has implications in reservoir design and management (Nagle et al. 1999; Zhao et al. 2017). Reservoir siltation reduces the water storage capacity and limits the operation performance of the dam (Anselmetti et al. 2007; Nagle et al. 1999; Palmeiri et al. 2001). In reservoirs with high siltation rates, especially in arid regions with highly cultivated watersheds, flushing is used to control rapid sediment deposition. Although flushing is highly efficient for restoring the water storage capacity, it causes significant deformation of the bottom sediment in both the reservoir and its downstream reaches (Maneux et al. 2001).

High interannual variation of the suspended load causes instability in the assessments of the reservoir siltation rates (Krasa et al. 2009; López et al. 2016). It is, therefore, necessary to overview long-term dynamics of the suspended sediment flux in the river system and its deposition in the reservoir to develop an efficient watershed management strategy (Jansson and Erlingsson 2000). In mountain watersheds, climatic changes become the primary driver for the changes in the suspended sediment load (Anselmetti et al. 2007; Chalov 2017; Valero-Garcés et al. 1999). In lowland reservoir watersheds, soil erosion rates are mostly controlled by agricultural development; its dynamics over the years can lead to a manifold increase or decrease in the reservoir siltation rates (Gellis et al. 2006; Thothong et al. 2011).

Over the last 35 years, social and economic factors have led to many changes in the land-use management of the watersheds in Russia (Kurganova et al. 2014; Oltchev et al. 2002; Walker et al. 2011). The major changes include the decrease of the cultivated land area and land afforestation, which led to a reduced soil erosion rate (Ivanov 2018; Sieber et al. 2013). The decline in the suspended sediment load is further enhanced by the climatic and hydrological changes, the key ones being the changing patterns of the spring flood and the increasing role of rain floods in the water budget. All this results in a significant shift in the sediment budget of reservoirs and alters the effect of dams on sediment transport.

For the Russian reservoirs, an accurate evaluation of the long-term sediment load dynamics is often hampered by the lack or insufficiency of monitoring data in the reservoir watersheds, and especially in their downstream reaches. An adequate assessment of the annual sediment load is also dependent on frequent measurements of the suspended sediment concentration (SSC) during peak discharge, rising and falling limbs of each flood, especially during the spring flood, which carries up to 75% of the total sediment load (The Mozhaysk… 1979; Sokolov 2015), as the SSC value may increase or decrease by several times in a very short time during high-flow periods.

For smaller reservoirs, determining the long-term variation of the sediment load is most crucial. All of the drinking water reservoirs in the Moscow Region have a low water storage capacity but play an essential role in supplying the drinking water for the 17-million population of Moscow city. One of the major parts of this water supply system is the Moskva River watershed, which in 2018 contributed to 78% of the total drinking water for the city; its water runoff, dissolved and particulate load is significantly affected by the Mozhaysk Dam on the Moskva River (Moscow City…).

The first detailed observations of the suspended sediment load that illustrate the Mozhaysk Reservoir's impact on the suspended sediment transport in the Moskva River were carried out in 1968 (Vinogradova 1970; The Mozhaysk… 1979), but until recently, no new studies have been conducted. In 2012 and 2016, we carried out two field programs with a similar level of detail. The objectives of this study are: a) to assess how the sediment load of the upper Moskva River is affected by the flow regulation by the Mozhaysk Dam and b) to estimate its dynamics over the years of the dam operating.

MATERIALS AND METHODS

Site description

The Mozhaysk Reservoir (55°35′ N, 35°50′ E) is located in the western part of the Moscow Region (Fig. 1). It was created in 1960 and serves as a part of the Moscow city water supply system. The reservoir has a drainage area of 1,360 km^2, covering a total surface area of 30.7 km^2 and has a storage capacity of 235 million m^3 at a normal pool level. Three rivers – The Moskva, Lusyanka, and Koloch (catchment areas F = 755 km^2, 170 km^2, and 279 km^2 respectively) – cover 91% of the reservoir's watershed; their combined flow accounts for 83% of the total water inflow to the reservoir (The Mozhaysk… 1979).

There are two discharge gauging stations operated by the Russian Federal Service for Hydrometeorology and Environment Monitoring (Roshydromet): Barsuki on the Moskva River and Cherniki on the Lusyanka River; both can be considered outlet stations as they are situated closely upstream from the backwater zones that form where the rivers reach the reservoir.

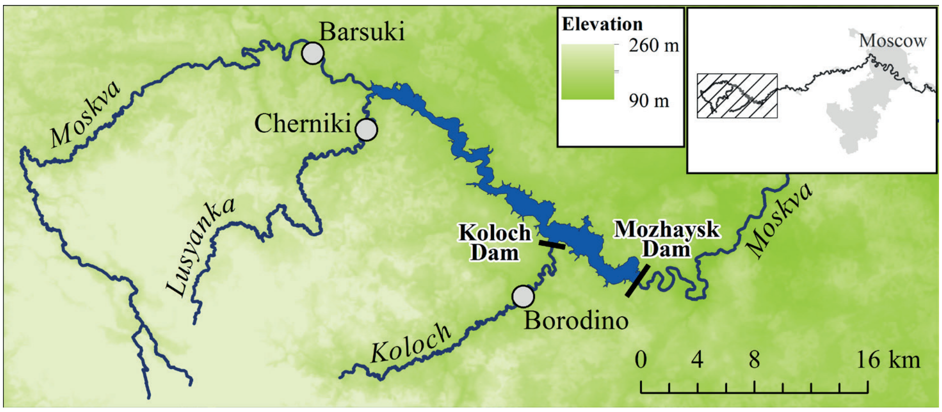

Fig. 1. The Mozhaysk Reservoir and its main tributaries

The Koloch River inflow is controlled by a pumping station that regulates the water flow between the Mozhaysk Reservoir and the smaller Koloch Reservoir.

Data collection

In an average-flow water year, 1968 (total inflow ΣIN = 245 million m^3), suspended sediment concentration was determined in 220 samples taken from the reservoir tributaries and the Moskva River below the dam (40-63 samples from each of the 4 designated stations). During the spring flood, samples were taken once every 1-2 days, in summer and autumn – about once a week, and in winter – once every 10 days (Vinogradova 1970).

In a high-water year, 2012 (ΣIN = 360 million m^3) we carried out a similar, though less detailed study (Sokolov 2015), with a total of 182 samples taken on the rivers (34-38 samples from each of the 5 stations). The samples were taken once every 2-4 days during the spring flood, once every 1-2 weeks in summer and fall, and once every 2-3 weeks in winter.

In another average-water year between March 2016 and March 2017 (ΣIN = 287 million m^3), we conducted another, more comprehensive study of the suspended load transport in the Mozhaysk Reservoir system (Sokolov et al. 2018). A total of 224 samples were taken from the rivers (56 samples at each of the 4 stations): once every 1-2 days during the spring flood and separate rain floods, and once every 10 days the rest of the year.

In 1968, observations on the Moskva River were carried out 1-2 km downstream from the Barsuki station (and 7-8 km downstream during winter due to a reduced extent of backwater zone). In 2012 and 2016, the observations made on the Moskva River were made directly at the gauging station.

Sampling of the Lusyanka River was carried out 1.5 km upstream from the Cherniki station in all 3 years.

In 1968, water samples from the Koloch Reservoir were taken directly from the pipe during periods of active pumping (Vinogradova 1970). In 2012, samples were taken near the dam, and at a free-flow part of the Koloch river at Borodino (9-10 km upstream from the Koloch dam, 3-4 km upstream from the backwater zone, F = 266 km^2, or 95% of the total watershed area). In 2016, samples were only taken at Borodino.

Sampling on the Moskva River below the reservoir was carried out 0.5 km downstream from the dam from a spillway during all three research years.

Measurement and analysis methods

The conventional method for estimating the concentration of suspended solids in water is gravimetric analysis, which is based on the determination of the total mass of the sediment and the subsequent calculation of its mass concentration SSC, mg/l. In 1968, membrane filters with a pore diameter of 0.90 µm were used to separate the sediment (Vinogradova 1970), and in 2016 0.45 µm membrane filters were used (Sokolov et al. 2018).

Since the gravimetric method is time-consuming, indirect methods for defining suspended sediment concentration are widely used; the most popular one being the optic measurement of water turbidity T, NTU (nephelometric turbidity units), which can indicate the presence of suspended solids, microorganisms, etc. In 2012 and 2016, we used a HACH 2100P portable turbidimeter to measure water turbidity with ±2% precision.

Water runoff data is also crucial for suspended sediment load estimation. Complete data series on the water discharges from the Mozhaysk Dam and the Koloch pumping station are present in the Mozhaysk Reservoir hydrological reports. Daily water discharges from Roshydromet gauging stations at Moskva and Lusyanka were published in official hydrological bulletins until the 1990s. After that, only water level data is available. Water discharges (Q) can be calculated from water levels (H) using a *Q = f(H)* rating curve. However, this relationship needs to be regularly updated, whereas the most recent official rating curves for the Moskva and Lusyanka were published in 1996. These calculations also include sets of adjustment coefficients k_Q, which help to account for ice and vegetation at different times of the year. These coefficients can also vary greatly over time, and demand detailed observations of the channel state, which is unavailable for these rivers.

Because of these difficulties, we used data on the daily net inflow into the Mozhaysk Reservoir, also published in hydrological reports, to recreate daily discharges of the Moskva and Lusyanka Rivers. The percentage of each river in the total inflow was proportional to the shares of their watershed areas in the reservoir's total drainage area.

To assess the impact of the Mozhaysk Reservoir on the sediment transport in the Moskva River, we estimated the annual sediment load of the three of the reservoir's main tributaries and compared it to the sediment load of the Moskva River below the dam. The annual sediment load (ASL, t/year) was calculated as a sum of daily sediment loads (DSL, t/day). Daily sediment loads were estimated by multiplying the daily water discharge volumes by the suspended sediment concentrations:

$$ASL = \Sigma DSL = \Sigma(Q \times 86{,}400 \times SSC \times 10^{-6}) \quad (1)$$

where Q is the mean daily water discharge (m^3/s), 86,400 is the number of seconds in a day.

Regular field observations and increased frequency of sampling during the spring flood allowed us to use linear interpolation between the data points to get reliable daily values of suspended sediment concentration.

Given that in 2016 we only collected data on the suspended flow of the free-flow part of the Koloch River, but a significant part of the sediment is retained in the Koloch Reservoir and does not reach the Mozhaysk Reservoir, to estimate the sediment load from the Koloch watershed we used the retention rate of the Koloch Reservoir, which we calculated based on the data of 2012 when suspended sediment concentration was determined both at the Borodino station and at the Koloch Dam.

RESULTS AND DISCUSSION

Sediment load calculations

To assess the sediment load, it is necessary to convert turbidity units *(T, NTU)* into *SSC, mg/l*. This conversion is often hampered by the fact that the empirical dependences *SSC = f (T)* usually vary across different regions (Belozerova and Chalov, 2013). For the water of the Mozhaysk Reservoir itself we have used before (Sokolov et al. 2011) the equation:

$$SSC = T \quad (2)$$

This equation (r = 0.97 on sample size n = 219) closely matches the one that is recommended for small and medium rivers of the European part of Russia (Belozerova and Chalov, 2013), so we have also used it in an attempt to quantify the sediment load into the reservoir in 2012 (Sokolov 2015). However, despite the high statistical significance of both links, it is obvious that their applicability to specific rivers requires additional justification.

Regular coupled measurements of the suspended sediment concentration and water turbidity in 2016 allowed us to obtain the hitherto first-ever *SSC = f(T)* relationships (Sokolov et al. 2018) for the tributaries of the Mozhaysk Reservoir (Fig. 2):

$$\begin{cases} \text{SSC (the Moskva, Barsuki)} = 1.1\text{T} + 1.6 \\ \text{SSC (the Moskva, below the dam)} = 0.8\text{T} + 1.4 \\ \text{SSC (the Lusyanka)} = 1.7\text{T} - 4.3 \\ \text{SSC (the Koloch)} = 1.6\text{T} - 0.7 \end{cases} \quad (3)$$

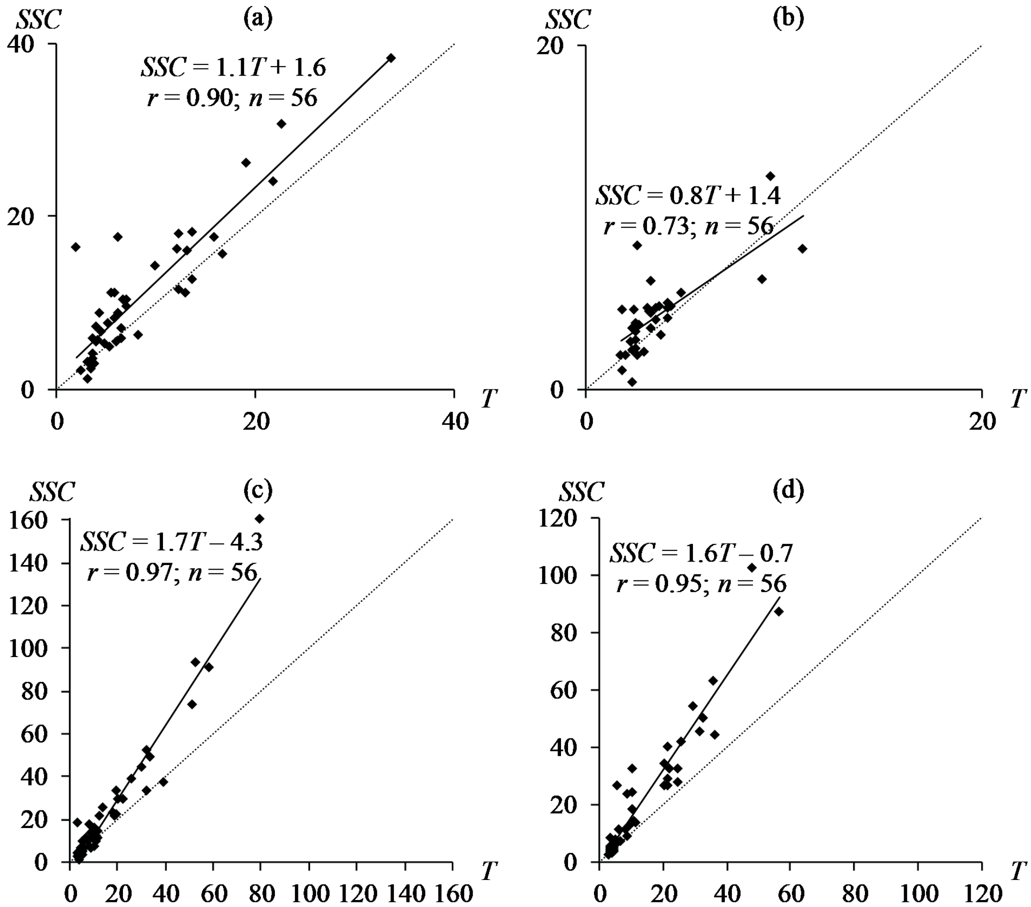

Fig. 2. Relationships (Eq. 3) between suspended sediment concentration *(SSC, mg/l)* and water turbidity (*T*, NTU) in the Moskva River upstream (a) and downstream (b) from the Mozhaysk Reservoir, and in the Lusyanka (c) and Koloch (d) based on 2016-2017 data. The dotted line represents the *SSC* = *T* (Eq. 2) relation for the Mozhaysk Reservoir water

According to (Belozerova and Chalov 2013), river-specific values of regression coefficients in the *SSC* = *kT* + *b* equation depend on geographical patterns of the water and sediment runoff, the extent of anthropogenic impact on the watershed, hydrological seasons, the sediment's genesis and composition, its natural variability and the streamflow parameters. For instance, the value of the k constant varies quite widely (0.65-4.85) and is proportional to the mean diameter of the suspended particles. The Lusyanka (*k* = 1.7) and Koloch (*k* = 1.6) have steeper stream profiles and higher banks, and on average have a bigger sediment particle size compared to the Moskva River at Barsuki (*k* = 1.1), and even more so compared to the Moskva river below the dam (*k* = 0.8), which receives the finer fraction of sediment from the reservoir.

Table 1 contains our estimates of the annual sediment load of the main tributaries of the Mozhaysk Reservoir and the Moskva River downstream from the reservoir in 1968, 2012, and 2016. Several assessments were made for

Table 1. Estimated suspended sediment inflow, outflow and retention in the Mozhaysk Reservoir in 1968, 2012 and 2016

ar	Method for SSC assessment	Annual sediment load, tons				Total income ASL^{+}, tons	Annual sediment load from the dam ASL^{-}, tons	Sediment retention $1-\frac{ASL^{-}}{ASL^{+}}$
		Moskva	Lusyanka	Koloch	Other inflows			
1968	gravimetric	11.510	4.540	1.750	4.450	22.250	2.250	90%
2012	Eq. 2	3.204	1.443	1.043	1.324	7.014	1.426	80%
	Eq. 3	3.847	2.277	1.691	2.089	9.904	1.600	84%
2016	gravimetric	1.870	840	561	771	4.042	1.160	71%
	Eq. 2	1.440	590	353	541	2.924	970	67%
	Eq. 3	1.860	880	534	808	4.081	1.140	72%

each river using different methods of defining the sediment concentration: using measured suspended sediment concentrations and based on the older (Eq. 2) or updated (Eq. 3) relationships between the sediment concentration and water turbidity. The sediment influx via other streams and non-streamflow runoff in 1968 was set using the data of (Vinogradova 1970), and in 2012 and 2016 was calculated by extrapolating the specific sediment yield of the Lusyanka watershed to ungauged areas.

The results presented in Table 1 suggest high convergence of the annual sediment loads in 2016 calculated using the measured suspended sediment concentrations, (which should be considered the most reliable method), with those derived from turbidity values and converted using the Eq. 3 (the error does not exceed ±5% for each river and 1% for total annual influx into the reservoir). The application of the older relationship (Eq. 2), which was based on the Mozhaysk Reservoir data, results in a significant underestimation of the annual sediment load of all of the rivers (22-34% for the tributaries and 15% for the Moskva River downstream from the reservoir).

Comparison of the $SSC = kT + b$ formulae that we suggested for the Mozhaysk Reservoir itself (Eq. 2) and its tributaries (Eq. 3) and the data presented in Table 1 allow concluding that the choice of a particular calculation method significantly affects the estimates of the suspended load. Regularly updated and catchment-specific SSC-turbidity relationships allow for more accurate assessments (as shown by the high convergence of ASL values calculated from direct SSC measurements and recent relationships in 2016).

Hydrological regime

The spring flood hydrographs and dam operation regimes varied greatly between the years covered by this research (Fig. 3). In 2012, the spring flood was the latest, the shortest, and had the highest peak discharge. In 2016, it started the earliest, had a low peak discharge with two separate peaks, and lasted the longest.

In 1968, the water discharge below the Mozhaysk Dam during the rising of the spring flood did not exceed the environmental flow (1.5 m^3/s) and increased up to 50 m^3/s after the peak. In the spring of 2012, the discharge was over 9-12 m^3/s and reached 124 m^3/s at maximum flow. During the entire reservoir filling in 2016, the discharge below the dam did not exceed 1.5 m^3/s.

Suspended sediment dynamics

In the winter of 1968, the suspended sediment concentration in the rivers ranged from 1 to 9 mg/l, reaching 12-16 mg/l during thaws (Fig. 3). During spring, the concentration rose from 9 mg/l to 100 mg/l and more in the Moskva River, and from 7 to over 300 mg/l in the Lusyanka. During the peak flow, maximum suspended sediment concentration reached 500 mg/l in the Moskva, over 300 mg/l in the Lusyanka, and 90 mg/l in the water pumped from the Koloch River. After the peak of the spring flood, the concentrations dropped sharply to 6-10 mg/l, increasing to 30-40 mg/l during rainy periods. During the summer and fall, low flows the sediment concentration

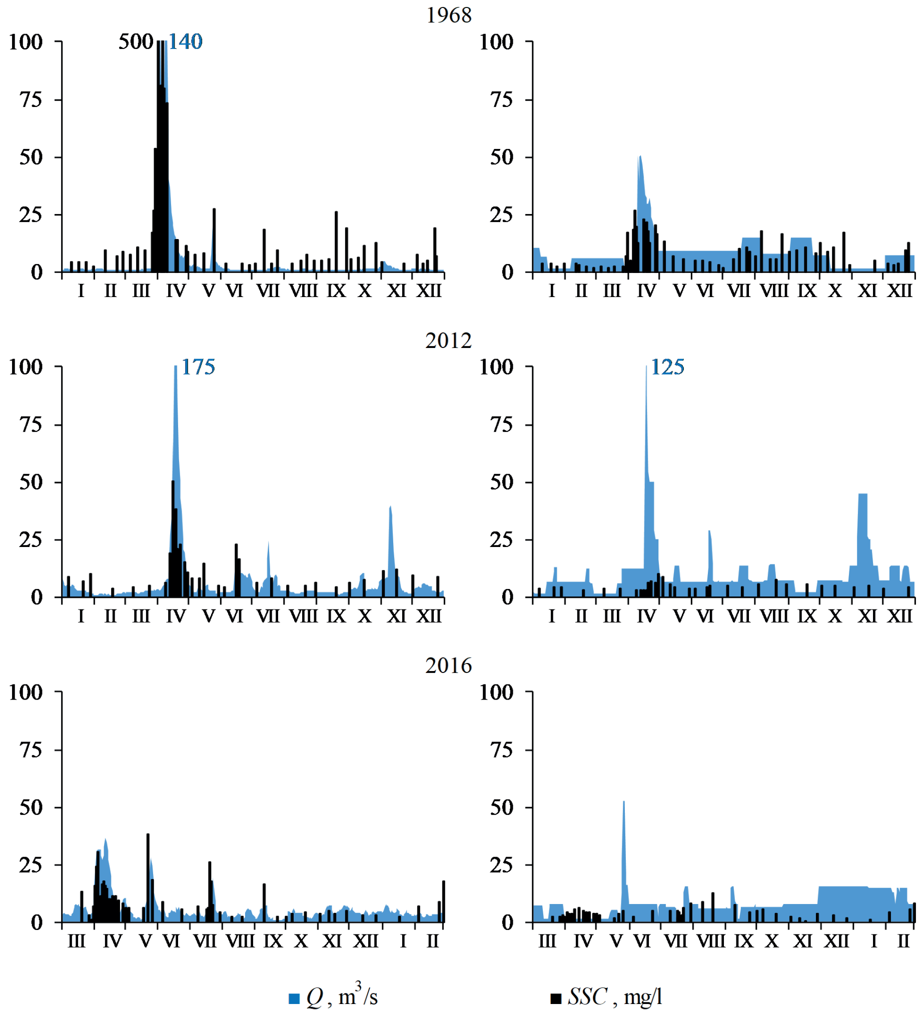

Fig. 3. Water discharge Q, m^3/s and suspended sediment concentration SSC, mg/l in the Moskva River upstream (left) and downstream (right) from the Mozhaysk Reservoir in 1968, 2012 and 2016 (SSC values for 2012 were calculated from measured NTU using Eq. 2, in 1968 and 2016 – directly measured; interpolated daily values are not shown)

varied greatly from 2-9 mg/l to 10-25 mg/l during rainwater inflow (Vinogradova 1970).

In the Moskva River below the dam, the suspended sediment concentration ranged from 1.4 to 3.8 mg/l during the ice-covered period of 1968. When the spring flood began, the concentration rose quickly to 20 mg/l. During the summer and fall of 1968, the sediment concentration varied from 1.4 to 16.8 mg/l with maximum values achieved during phytoplankton blooms and in periods of strong wind mixing (Vinogradova 1970).

In winter of 2012, the turbidity of the Mozhaysk Reservoir's tributaries ranged from 2 to 9 NTU (which corresponds to SSC values of 3-12 mg/l when using Eq. 3) and reached 7-13 NTU (9-18 mg/l) during thaws. During the spring, flood turbidity increased to 33-45 NTU (38-50 mg/l) in Moskva River and Koloch Reservoir and to 70-80 NTU (110-130 mg/l) in Lusyanka and Koloch Rivers. Similar to 1968, by the end of the spring flood, the turbidity in the rivers fell sharply to 6-13 NTU (8-18 mg/l). During summer and fall, the sediment load into the reservoir with river flow steadily declined, reaching minimum values in August-September at 2-4 NTU (2-6 mg/l). During rain floods, the turbidity reached 30-50 NTU (35-80 mg/l) in summer and 9-26 NTU (12-41 mg/l) in autumn.

In the winter of 2012, the water turbidity downstream from the dam ranged from 2.3 to 5.6 NTU (3.2-5.9 mg/l with Eq. 3). The lowest value (1.7-2.2 NTU, or 2.8-3.2 mg/l) was observed at the beginning of the reservoir's fill during the spring flood. The turbidity increased as the reservoir filled up, but less significantly than in 1968 – up to 9-11 NTU (9-10 mg/l). During summer and fall water turbidity below the reservoir varied from 3 to 8 NTU (4-8 mg/l).

In the winter of 2016, suspended sediment concentration in the reservoir's tributaries was 2-9 mg/l, and water turbidity ranged from 3 to 5 NTU. Because of a low double-peaked spring flood (Fig. 3), during the spring, the suspended sediment concentration in the Moskva River upstream from the reservoir did not exceed 31 mg/l, and turbidity – 23 NTU. In the Lusyanka and Koloch, however, during the rise of the spring flood these values reached 100-160 mg/l and 60-80 NTU. During low-flow periods of the summer and fall, the suspended sediment concentration ranged between 2-9 mg/l. During the summer rain floods, the sediment concentration reached 20-40 mg/l (20-30 NTU) in the Moskva River, 70-90 mg/l (50-60 NTU) in the Lusyanka and 30-45 mg/l (20-30 NTU) in the Koloch. During the fall rain floods, the suspended sediment concentration increased up to 15-20 mg/l in the Lusyanka and Koloch and did not change in the Moskva River.

In 2016, the suspended sediment concentration downstream from the reservoir stayed within 1-6 mg/l (2-7 NTU) throughout the year, except for August, when it reached 8-12 mg/l (7-11 NTU) during a phytoplankton bloom in the reservoir.

The highest suspended sediment concentration and total suspended load are observed during the spring flood. As stated in (Vinogradova 1970; The Mozhaysk… 1979), in 1968 over 90% of the annual suspended sediment load passed in April and May. Our data of 2012 (Sokolov 2015) show the share of the spring flood in the annual sediment load to be around 75%, in 2016 – less than 50%. This decline in the spring sediment load over the decades is caused by the modern changes in the streamflow regime – decreasing spring flow and the increasing importance of the summer and fall rain floods and winter thaws (Kireeva et al. 2019).

Downstream from the Mozhaysk Dam, the seasonal variability of the sediment concentration is reduced compared to that of the reservoir's tributaries (the coefficient of variation C_V is reduced by half – from 0.8–1.2 to 0.4–0.6).

Long-term sediment load dynamics

Even considering high possible errors (up to 100-150%) in our estimates of the suspended load caused by short observation periods (Vanmaercke et al. 2012), it is hard to ignore the manifold decrease in the suspended sediment concentration and the annual suspended load of the Mozhaysk Reservoir tributaries that occurred over the past half-century.

Peak suspended sediment concentration of the spring flood in the Moskva, and Lusyanka has decreased by almost 10 times – from 300-500 mg/l to 45-80 mg/l (see Fig. 3). Annual values decreased by 3-7 times: in the Moskva River – from 70 mg/l in the average-water 1968 to 18 mg/l in the high-water 2012 and to 10 mg/l in the average-water 2016; in Lusyanka – from 130 mg/l to 48 and 21 mg/l, respectively. Such significant changes cannot be dismissed as a calculation inaccuracy, especially since the results of 1968 were more likely to be underestimated and not overestimated, due to the use of filters with pore diameter twice bigger than that of the filters used in 2012. The changes in the sediment load of the Koloch River can only be roughly estimated, as the data of the three study years are not completely compatible. Our estimates do not suggest any significant changes in the suspended sediment outflow from the Koloch Dam. This is likely caused by the sediment retention by the small Koloch Reservoir, which, much like the Mozhaysk Reservoir itself, accumulates some part of the Koloch River sediment load and lessens its seasonal variation.

Below the Mozhaysk Dam, the suspended sediment concentration has been reduced approximately by half between 1968 and 2012-2016 (see Fig. 3). The peak suspended sediment concentration, for one, dropped from 20 to 11 mg/l.

The annual sediment load has changed correspondingly (see Table 1). According to (Vinogradova 1970; The Mozhaysk… 1979), the total sediment load of the three major tributaries (the Moskva, Lusyanka, and Koloch) varied over the first 10 years of the reservoir's operation from 8,100 tons in the low-flow 1964 to 68,000 tons in the high-flow 1962. The annual sediment inflow into the reservoir decreased by almost 9 times between the two of high-water years – 1962 and 2012, and by over 5 times between two average-water years – 1968 and 2016.

The total sediment outflow from the reservoir in the 1960s has varied from 1,150 tons in 1964 to 10,000 tons in 1962 (Vinogradova 1970; The Mozhaysk… 1979). Thus, the suspended load of the Moskva River downstream from the dam has decreased by 6 times for high-water years and halved for the average-water years.

We attribute these trends to an effect of the land-use changes that occurred on the reservoir's watershed: after the 1980s–90s, there was a significant decline in agricultural activities and a noted decrease in cultivated land area (Koronkevich and Melnik 2015).

In 1968, the annual sediment outflow from the Mozhaysk dam was equivalent to 20% of the annual suspended load of the Moskva River, 13% of the combined sediment load of the Moskva, Lusyanka, and Koloch, and to 10% of the total sediment load from the reservoir's watershed. In 2012, the annual suspended load of the Moskva River below the dam amounted to 42% of the suspended load of the Moskva River at Barsuki, 20% of the total sediment load of the three major tributaries, and 16% of the total sediment inflow to the reservoir. In 2016, these percentages were 62%, 35% and 29%, respectively.

It can be concluded that the manifold decrease of the suspended loading of the Mozhaysk Reservoir is paralleled by a decline of its sediment retention capacity, which was reduced from 90% in 1968 to 84% in 2012, and to 71% in 2016 (see Table 1).

CONCLUSIONS

In this study, we have assessed the effect of the Mozhaysk Dam on the suspended sediment transport in the Moskva River and addressed the dynamics of its sediment load over the past 50 years.

The major part of the annual suspended load into the Mozhaysk Reservoir is received during the spring flood, but its share decreased from 90% to 50-75% over the past half-century, likely due to the transformation of the river flow regime confirmed by various authors. Downstream from the dam, the seasonal dynamics of the suspended sediment content is less pronounced, and its variability is reduced by half compared to the reservoir's tributaries.

Peak suspended sediment concentrations, and annual sediment inflow into the reservoir have decreased 5- to 10-fold over the 50 years, sediment concentration and suspended load of the Moskva in downstream reaches decreased by 2-6 times. It is most likely caused by the significant decline in the cultivated land area on the watershed.

Although the larger part of the sediment inflow is accumulated in the reservoir, its sediment retention capacity over the half-century has dropped from 90% to 70-85%. Such trap efficiencies are common for most lowland reservoirs (Berkovich 2012; Le et al. 2020; Piqué et al. 2017; Suif et al. 2017; Van Binh et al. 2020). We attribute this to the progressing siltation of the reservoir, combined with an increased production of autochtonous particulate organic matter and its subsequent outflow from the reservoir due to its continuous eutrophication (Datsenko et al. 2017), which creates additional biogenic sediment flux.

REFERENCES

Anselmetti F., Bühler R., Finger D., Girardclos S., Lancini A., Rellstab C., and Sturm M. (2007). Effects of Alpine hydropower dams on particle transport and lacustrine sedimentation. Aquatic Sciences, 69(2), 179-198, DOI: 10.1007/s00027-007-0875-4.

Belozerova E.V. and Chalov S.R. (2013). Assessment of river water turbidity using the optic methods. Moscow University Bulletin. Series 5, Geography. 6, 39-45 (in Russian with English summary).

Berkovich K.M. (2012). Riverbed processes in rivers influenced by reservoirs. Moscow: Faculty of Geography, MSU (in Russian with English summary).

Chalov S. (2017). Hydroclimatic development and anthropogenic impact on sediment loads in the Selenga catchment. Geography and Tourism, 5(2), 27-39, DOI: 10.5281/zenodo.1118161.

Dang T., Coynel A., Orange D., Blanc G., Etcheber H. and Le L. (2010). Long-term monitoring (1960–2008) of the river-sediment transport in the Red River Watershed (Vietnam): Temporal variability and dam-reservoir impact. Science of the Total Environment, 408(20), 4654-4664, DOI: 10.1016/j.scitotenv.2010.07.007.

Datsenko Yu.S., Puklakov V.V. and Edelstein K.K. (2017) Analysis of the influence of abiotic factors on phytoplankton growth in a low-flow stratified storage reservoir. Transactions of KarRC RAS, 10, 73-85, (in Russian with English summary). DOI: 10.17076/lim611

Díaz-Gutiérrez V., Mongil-Manso J., Navarro-Hevia J. and Ramos-Díez I. (2019). Check dams and sediment control: final results of a case study in the upper Corneja River (Central Spain). Journal of Soils and Sediments, 19, 451-466, DOI: 10.1007/s11368-018-2042-z.

Gellis A., Webb R., McIntyre S. and Wolfe W. (2006). Land-use effects on erosion, sediment yields, and reservoir sedimentation: A case study in the Lago Loíza Basin, Puerto Rico. Physical Geography, 27(1), 39-69, DOI: 10.2747/0272-3646.27.1.39.

Grimshaw D. and Lewin J. (1980). Reservoir effects on sediment yield. Journal of Hydrology, 47(1-2), 163-171, DOI: 10.1016/0022-1694(80)90054-2.

Guo C., Jin Z., Guo L., Lu J., Ren S. and Zhou Y. (2020). On the cumulative dam impact in the upper Changjiang River: Streamflow and sediment load changes. Catena, 184, 104250, DOI: 10.1016/j.catena.2019.104250.

Hojan M. and Rurek M. (2017). Particle-size distribution of channel bars of the lower Vistula between Bobrowniki and Bydgoszcz-Fordon. Geography and Tourism, 15(2), 97-104, DOI: 10.5281/zenodo.1118185.

Huang X.R., Gao L.Y., Yang P.P. and Xi Y.Y. (2018). Cumulative impact of dam constructions on streamflow and sediment regime in lower reaches of the Jinsha River, China. Journal of Mountain Science, 15(12), DOI: 10.1007/s11629-018-4924-3.

Ibàhez C., Prat N. and Canicio A. (1996). Changes in the hydrology and sediment transport produced by large dams on the lower Ebro River and its estuary. Regulated Rivers: Research & Management, 1996, 12, 51-62, DOI: 10.1002/(SICI)1099-1646(199601)12:1<51::AID-RRR376>3.0.CO;2-I.

Ivanov M. (2018). Changes of cropland area in the river basins of the European part of Russia for the period 1985-2015 years, as a factor of soil erosion dynamics. IOP Conference Series: Earth and Environmental Science, 107, DOI: 10.1088/1755-1315/107/1/012010.

Jansson M. and Erlingsson U. (2000). Measurement and quantification of a sedimentation budget for a reservoir with regular flushing. Regulated Rivers: Research and Management, 16(3), 279-306, DOI: 10.1002/(SICI)1099-1646(200005/06)16:3<279::AID-RRR586>3.0.CO;2-S.

Kireeva M., Frolova N., Rets E., Samsonov T., Entin A., Kharlamov M., … Povalishnikova E. (2019). Evaluating climate and water regime transformation in the european part of russia using observation and reanalysis data for the 1945-2015 period. International Journal of River Basin Management, 1-12, DOI: 10.1080/15715124.2019.1695258.

Kondolf G., Rubin Z. and Minear J. (2014). Dams on the Mekong: Cumulative sediment starvation. Water Resources Research, 50(6), 5158-5169, DOI: 10.1002/2013WR014651.

Kovacs A., Fulop B. and Honti M. (2012). Detection of hot spots of soil erosion and reservoir siltation in ungauged Mediterranean catchments. Energy Procedia. 18, 934-943, DOI: 10.1016/j.egypro.2012.05.108.

Koronkevich N. and Melnik K.S. (2015). Runoff transformation under the effect of landscape changes in the Moskva R. basin and in the territory of Moscow City. Water Resources, 42(2), 159-169, DOI: 10.1134/S0097807815020062.

Krasa J., Dostal, T., Vrana K. and Plocek J. (2009). Predicting spatial patterns of sediment delivery and impacts of land-use scenarios on sediment transport in Czech catchments. Land Degradation & Development, 21(4), 367-375, DOI: 10.1002/ldr.959.

Kurganova I., Lopes de Gerenyu V., Six J. and Kuzyakov Y. (2014). Carbon cost of collective farming collapse in Russia. Global Change Biology, 20(3), 938-947, DOI: 10.1111/gcb.12379.

Le N.D., Le T.P.Q., Phung T.X.B., Duong T.T. and Didier O. (2020). Impact of hydropower dam on total suspended sediment and total organic nitrogen fluxes of the Red River (Vietnam), Proceedings of the International Association of Hydrological Sciences, 383, 367-374, DOI: 10.5194/piahs-383-367-2020.

Ligon F., Dietrich W. and Trush W. (1995). Downstream Ecological Effects of Dams. BioScience, 45(3), 183-192, DOI: 10.2307/1312557.

López P., López-Tarazón J., Casas-Ruiz J., Pompeo M., Ordoñez J. and Muñoz I. (2016). Sediment size distribution and composition in a reservoir affected by severe water level fluctuations. Science of the Total Environment, 540, 158-167, DOI: 10.1016/j.scitotenv.2015.06.033.

Maneux E., Probst J., Veyssy E. and Etcheber H. (2001). Assessment of dam trapping efficiency from water residence time: Application to fluvial sediment transport in the Adour, Dordogne, and Garonne River basins (France). Water Resources Research, 37(3), 801-811, DOI: 10.1029/2000WR900195.

Moscow City water supply and sewerage plan to the year 2025 [online] (in Russian). Availible at: https://www.mos.ru/dgkh/documents/skhemy/view/41896220 [Accessed 26 Jul. 2020].

Nagle G.N., Fahey T.J. and Lassoie J.P. (1999). Management of sedimentation in tropical watersheds. Environmental Management, 23(4), 441-452, DOI: 10.1007/s002679900199.

Oltchev A., Cermak J., Gurtz J., Tishenko A., Kiely G., Nadezhdina N., … Gravenhorst G. (2002). The response of the water fluxes of the boreal forest region at the Volga's source area to climatic and land-use changes. Physics and Chemistry of the Earth, 27(9-10), 675-690, DOI: 10.1016/S1474-7065(02)00052-9.

Palmeiri A., Shah F. and Dinar A. (2001) Economic reservoir sedimentation and the sustainable management of dams. Journal of Environmental Management, 61, 149-163, DOI: 10.1006/jema.2000.0392.

Piqué G., Batalla R.J., López R., Sabater S. (2017). The fluvial sediment budget of a dammed river (upper Muga, southern Pyrenees). Geomorphology, 293, A, 211-226, DOI: 10.1016/j.geomorph.2017.05.018.

Shields F. (2009). Do we know enough about controlling sediment to mitigate damage to stream ecosystems? Ecological Engineering, 35(12), 1727-1733, DOI: 10.1016/j.ecoleng.2009.07.004.

Sieber A., Kuemmerle T., Prishchepov A., Wendland K., Baumann M., Radeloff V., … Hostert P. (2013). Landsat-based mapping of post-Soviet land-use change to assess the effectiveness of the Oksky and Mordovsky protected areas in European Russia. Remote Sensing of Environment, 133, 38-51, DOI: 10.1016/j.rse.2013.01.021.

Snoussi M., Haida S. and Imassi S. (2002). Effects of the construction of dams on the water and sediment fluxes of the Moulouya and the Sebou rivers, Morocco. Journal of Material Cycles and Waste Management, 3(1-3), 5-12, DOI: 10.1007/s10113-001-0035-7.

Sokolov D.I. (2015). Water turbidity regime of the Mozhaysk Reservoir In: Contemporary issues of reservoirs and their watersheds. Proceedings of the International academic and applied science conference. Perm: PSU Publishing, 153-157 (in Russian with English summary).

Sokolov D.I., Erina O.N., Tereshina M.A. (2018). Relationship between water turbidity and suspended sediment concentration in the tributaries of the Mozhaysk Reservoir In: N.N. Mitin, ed., Water resources, ecology, hydrological security. Proceedings of the XI International Scientific Conference for Young Scientists and Talented Students. Moscow: IWP, 112-114 (in Russian with English summary).

Sokolov D.I., Kremenetskaya E.R., Lomova D.V., Arakelyants A.D., Filippova P.S. (2011). Profile of the water turbidity regime in a lowland reservoir during low water level. Moscow University Vestnik. Series 5. Geography. 3, 27-32 (in Russian with English summary).

Suif Z., Yoshimura C., Saavedra O., Ahmad N. and Hul S. (2017). Suspended sediment dynamics changes in Mekong River basin: possible impacts of dams and climate change. International Journal of Geomate, 12(34), 140-145, DOI: 10.21660/2017.34.2688.

Syvitski J.P.M., Vörösmarty C.J., Kettner A.J. and Green P. (2005). Impact of humans on the flux of terrestrial sediment to the global coastal ocean. Science 308, 376-380, DOI: 10.1126/science.1109454.

Tang H., Pan H. and Ran Q (2020). Impacts of Filled Check Dams with Different Deployment Strategies on the Flood and Sediment Transport Processes in a Loess Plateau Catchment. Water, 12, 1319, DOI: 10.3390/w12051319.

The Mozhaysk Reservoir (1979). Moscow: LMSU Publishing (in Russian with English summary).

Thothong W., Huon S., Janeau J., Boonsaner A., de Rouw A., Planchon O., … Parkpian P. (2011). Impact of land use change and rainfall on sediment and carbon accumulation in a water reservoir of North Thailand. Agriculture, Ecosystems and Environment, 140(3-4), 521-533, DOI: 10.1016/j.agee.2011.02.006.

Topping D., Rubin D. and Vierra L. (2000). Colorado River sediment transport 1. Natural sediment supply limitation and the influence of Glen Canyon Dam. Water Resources Research, 36(2), 515-542, DOI: 10.1029/1999WR900285.

Valero-Garcés B., Navas A., Machín J. and Walling D. (1999). Sediment sources and siltation in mountain reservoirs: A case study from the Central Spanish Pyrenees. Geomorphology, 28(1-2), 23-41, DOI: 10.1016/S0169-555X(98)00096-8.

Van Binh D., Kantoush S. and Sumi T. (2020) Changes to long-term discharge and sediment loads in the Vietnamese Mekong Delta caused by upstream dams. Geomorphology, 353, 107011, DOI: 10.1016/j.geomorph.2019.107011.

Vanmaercke M., Poesen J., Verstraeten G., de Vente J. and Ocakoglu F. (2011). Sediment yield in Europe: Spatial patterns and scale dependency. Geomorphology, 130(3-4), 142-161, DOI: 10.1016/j.geomorph.2011.03.010.

Vanmaercke M., Poesen J., Radoane M., Govers G., Ocakoglu F. and Arabkhedri M. (2012). How long should we measure? An exploration of factors controlling the inter-annual variation of catchment sediment yield. Journal of Soils and Sediments, 12, 603-619, DOI: 10.1007/s11368-012-0475-3.

Vinogradova N.N. (1970). Features of suspended sediment production and dynamics in small reservoirs on the Moskva River (on the case of the Mozhaysk Reservoir). Candidate of Sciences dissertation. (in Russian).

Walker D., Forbes B., Leibman M., Epstein H., Bhatt U., Comiso J., … Yu Q. (2011). Cumulative effects of rapid land-cover and land-use changes on the Yamal Peninsula, Russia. In: G. Gutman and A. Reissell., eds., Eurasian Arctic Land Cover and Land Use in a Changing Climate. Dordrecht: Springer Netherlands, 207-236, DOI: 10.1007/978-90-481-9118-5_9.

Wang S., Fu B., Piao S., Lü Y., Ciais P., Feng X., and Wang Y. (2016). Reduced sediment transport in the Yellow River due to anthropogenic changes. Nature Geoscience, 9(1), 38-41, DOI: 10.1038/ngeo2602.

Wright S. and Schoellhamer D. (2004). Trends in the Sediment Yield of the Sacramento River, California, 1957–2001. San Francisco Estuary and Watershed Science, 2(2), DOI: 10.15447/sfews.2004v2iss2art2.

Wu X., Xiang X., Chen X., Zhang X. and Wenjuan H. (2018). Effects of cascade reservoir dams on the streamflow and sediment transport in the Wujiang River basin of the Yangtze River, China. Inland Waters, 8, 1-13. DOI: 10.1080/20442041.2018.1457850.

Yang Z., Wang H., Saito Y., Milliman J.D., Xu K., Qiao S. and Shi G. (2006). Dam impacts on the Changjiang (Yangtze) River sediment discharge to the sea: the past 55 years and after the Three Gorges Dam. Water Resources Research. 42(4), DOI: 10.1029/2005WR003970.

Zhao G., Kondolf G., Mu X., Han M., He Z., Rubin Z., … Sun W. (2017). Sediment yield reduction associated with land use changes and check dams in a catchment of the Loess Plateau, China. Catena, 148, 126-137, DOI: 10.1016/j.catena.2016.05.010.

RESEARCH PAPER

THE ROLE OF ARTIFICIAL IMPOUNDMENTS IN IMPROVING AGRICULTURAL PRODUCTION IN THE SEMI-ARID REGIONS OF NORTHERN MOROCCO

Mustapha Hmamou[1*], Boujemaa Bounakaya[1]
[1]Faculty of letters and humanities, Abdelmalek Essaadi University, BP 210 Avenue Hassan II, Martil 93150, Morocco.
***Corresponding author:** stoph249@gmail.com
Received: March 2th, 2019 / Accepted: November 20th, 2020 / Published: December 31st, 2020
https://DOI-10.24057/2071-9388-2020-46

ABSTRACT. At the end of the last century, the Rif mountains of Morocco have experienced significant changes in the level of agricultural activity, especially it concerns the increase in cannabis cultivation, which is characterized by high water requirements. For that reason, a number of Artificial Impoundments (AIs) have been constructed in the Tangier-Tetouan-Al Hoceima (TTA) region, where by August 2017 there were more than 1400 of such structures. This requires to a study the efficiency and potential negative effects of such noticeable development. It has been shown that these hydraulic structures have provided additional positive value to the agricultural sector, especially to the proscribed industry of cannabis cultivation. Regarding other effects, the present study has found that their impact on the hydraulic and hydrographic aspects at the moment is very limited and that the only major constraint for their application is related to the issue of security, which arises from the fragile geological structure that is observed in the majority of the region.

KEY WORDS: Rif Mountains, the Tangier-Tetouan-Al Hoceima region, hydro-agricultural development, Artificial Impoundments, cannabis

CITATION: Mustapha Hmamou, Boujemaa Bounakaya (2020). The Role Of Artificial Impoundments In Improving Agricultural Production In The Semi-Arid Regions Of Northern Morocco. Geography, Environment, Sustainability, Vol.13, No 4, p. 32-42
https://DOI-10.24057/2071-9388-2020-46

Conflict of interests: The authors reported no potential conflict of interest.

INTRODUCTION

The construction of dams is considered among the many water practices of ancient times. It is spread in different parts of the world. The total actual volume of the water impoundment in the world's artificial reservoirs today is 10,800 km^3 (Chao and Li 2008; Chao 1988). Also, their types vary between large dams (Buttress Dam, Embankment Dam, Storage Dam...) and small ones like AIs. The latter kind (also called artificial ponds), which constitute the subject matter of the present study, are considered among the many artificial hydraulic structures that are built separately from the hydraulic networks and are refilled with water during the periods of precipitation through surface runoff (Ministère de l'écologie, du développement durable des transports et du logement 2012) and/or from the groundwater or rivers in order to be used during the summer season (Directions Régionales de l'Environnement, de l'aménagement et du logemen 2012). The functions of these AIs are numerous as they are used to breed fish (Keshavanath et al. 2001), for recreation and aesthetic purposes (Callihan 2013), for extinguishing fires and so on. Along with that, the irrigation of farmlands in the Mediterranean region is considered to be the most important function of these AIs (Casas et al. 2011). It also helps to improve landscape amenity in highly anthropized horticultural areas (Bonachela et al. 2013).

The growing propagation of AIs has made it necessary to frame it legally to avoid all deficiencies that are likely to be caused. In France, for example, the first laws to control these AIs date back to 1968. Since 2007, new rules have appeared via the water law that founded a much more secure system for declaration and permission (Dunglas 2014). But as far as Morocco is concerned, the water law number 36-15 (fourth chapter, article 62), which concerns the pricing and use of rainwater, is considered among the clearest provisions in the law about the AIs since «the owners, users and the estate possessors have the legal right to collect, use and price rainwater that falls on their estates...and the technical conditions are determined by an organising text to establish, manage and maintain the edifices for collecting and storing rainwater» (la loi n°36-15 relative à l'eau promulguée par Dahir n°1-16-113 du 10 Août 2016).

These AIs provide a lot of benefits as they help to irrigate reasonable surfaces of farmlands. However, the problem is that these AIs are costly both at the financial and property levels. Regarding the financial level, the establishment of such AIs requires large sums of money and only those whose incomes are high can afford them. And as far as the property level is concerned, the Rif Mountains are known to have small agricultural holdings. This problem is found also at the global level as the AIs are estimated to occupy between 0.1% and 6% of farm area worldwide (Downing et al. 2011). Hence, despite the beneficial aspect of these AIs, they will without doubt make the problem bigger. On the other hand, we should not forget that they may have negative social, environmental and ecological effects since they will inevitably disrupt the equilibrium that is specific to the management of water. Also, these AIs are constructed haphazardly and over geological structures generally characterized by their fragility (the risk of collapsing). The problem gets much more complicated as these AIs are constructed in most of the cases, especially in the Chefchaouen province, to irrigate the cannabis fields, which in itself represents a problem/constraint that even the state has not been able to deal with. In general, this study aims to describe, interpret and analyse the spatial distribution of these AIs in relation to the geological, topographical and hydrological characteristics as well as administrative divisions to show the scope of their effectiveness in terms of irrigation water security and also demonstrate the negative effects that accompany them in the TTA region. In order to find a temporary interpretation to this problematic, we hypothesize that these AIs are considered to be good and beneficial water projects and that their current impact on the capacity of the large dams and the sustenance of the groundwater is minor.

MATERIALS AND METHODS

Study Area

The area of study (Fig. 1) is the TTA region, which is located in northern Morocco, bordered from the north by the Mediterranean Sea, from the south by the Rabat-Sale-Kenitra and Fes-Meknes regions, from the east by the Oriental region and from the west by the Atlantic Ocean. It is one of the twelve regions of Morocco. The TTA region includes six provinces and two prefectures whose population is about 3,556,729 inhabitants according to RGPH 2014, 40.20% among them are rural. Despite the mountainous topographic relief, the rural area of this region depends mainly on the agrarian economy. It is worth mentioning that in the last few years the Rif has witnessed great change concerning the types of the adopted agriculture that has been accompanied by an obvious change in the adoption of irrigation sources for the lands, as some farmers resorted to the technique of collecting water from many sources in the basin (AIs).

Materials and Methods

For this study, we have used a scientific method, which includes description, interpretation, analysis and statistics. Testing of the hypothesis was conducted using the mapping technique, which allowed to localize the studied AIs, register their distinguishing properties such as area and depth as well as estimate the quantity of the water stored. Moreover, to cover the research problem a bit further, it was also necessary to go to the field to take some photos and review the available literature on the topic. It should be noted, that there have been many previous studies, especially in the European countries. To digitize the AIs, we used The Map-Tools application that offers several utilities under Google Maps (http://tool-online.com/index.php) such as import-export text, DXF, KML files. The coordinates and the surface area of AIs were identified using the website indicated. These data were then exported to GIS (ArcGIS 10.2) to build a database comprising the subsequent columns: FID (the name primarily used in shapefiles), surface area, bottom area, maximum depth, minimum depth, average depth, maximum volume, minimum volume, average volume.

To estimate the volume of the water in these AIs, it is necessary to know the depth and the area of the top and the bottom. The area of the top is very easy to determine, unlike the bottom area and the depth of the AI. For this reason, we have worked on a sample of 50 cases conducting interviews with the owners of these water projects. Then by generalizing the calculations about the other AIs, we have finally achieved a result presented in Table 1. As for the volume of water that can be stored in these AIs, it was calculated using simple equation (Volume = length *width * height) and since the area of the top is always different from that of the bottom, they were added to each other to obtain the average.

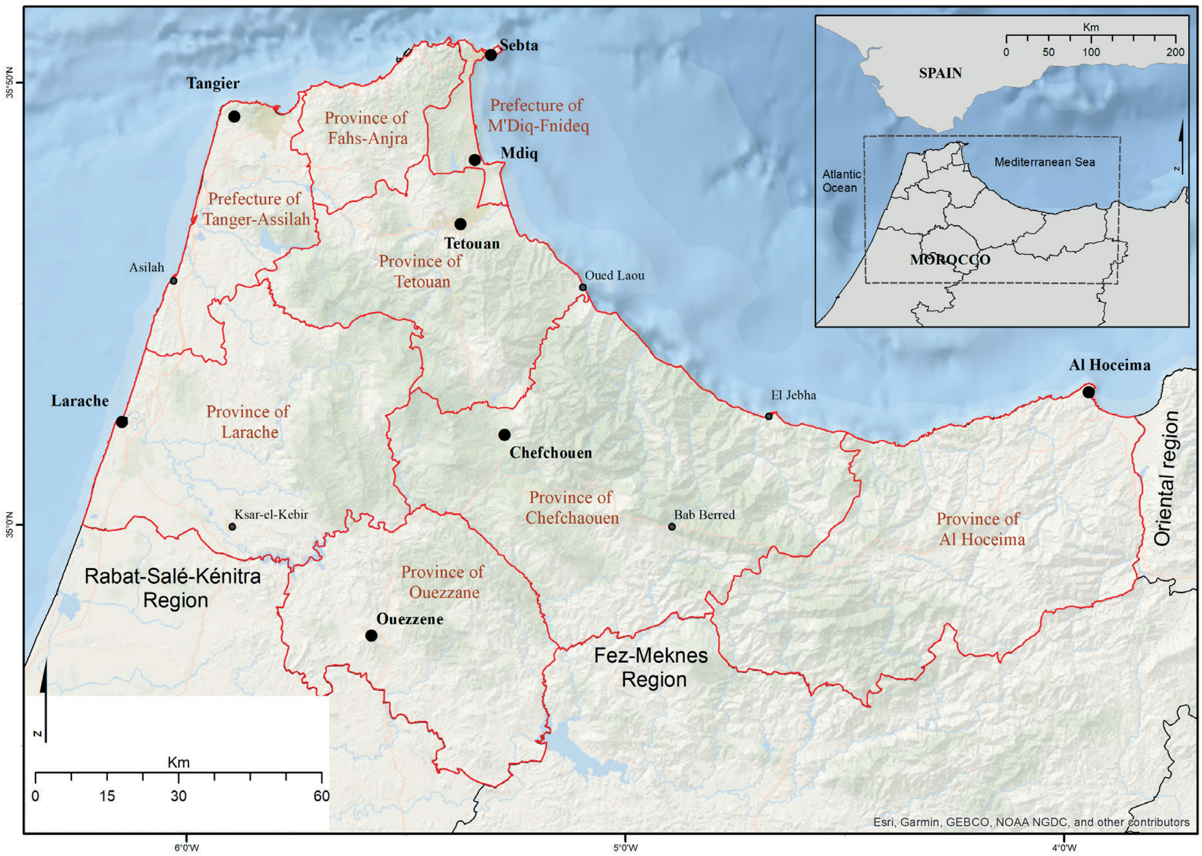

Fig. 1. Study area location
(Source: the official maps available through the website (ANCFCC: https://www.ancfcc.gov.ma/))

Table 1. Relative Risk of the spatiotemporal clusters of cardiovascular mortality

Area* (m^2)		Depth (m)		
Top	Bottom	Average	Minimum	Maximum
> 10000	> 2500	18	15	21
8000–9999	2000–2499	14	13	15
7000–7999	1750–1999	12.5	12	13
6000–6999	1500–1749	11.5	11	12
5000–5999	1250–1499	10.5	10	11
4000–4999	1000–1249	9.5	9	10
3000–3999	750–999	8.5	8	9
2000–2999	500–749	7.5	7	8
1500–1999	375–499	6.5	6	7
1000–1499	250–374	5.5	5	6
900–999	225–249	4.5	4	5
800–899	200–224	4	3.5	4.5
700–799	175–199	3.5	3	4
< 600	< 150	2.5	2	3

* The bottom area of 84% AIs (The survey sample) nearly equal a quarter of its top area.

Source: the field survey, August 2017

RESULTS

Spatial Relationship Between the AIs and Structural Units

The geological conditions are an issue of great importance for the study of dams. Geologically, the Rif area is characterized by its torsions, creepy folds and overlays. According to many geologists, the Rif may be divided into three principal regions: the internal Rif, the flysch unit and the external Rif.

The internal Rif includes three small units: Ghomarids, Sebtids and the «*Dorsal Calcaire*», which in total occupy about 13% of the geological area of the region (Fig. 2). The first two units are characterized by the metamorphic rocks that date back to the Paleozoic and Mesozoic Era (Azzouz et al. 2002). Their rocky formations are marked by very poor water permeability and their immense sensitivity to erosion. As for the «*Dorsal Calcaire*», it constitutes from limestone and dolomite formations with the occasional inclusion of marl. Regarding the hydrological behaviour, these units are characterized by their high water permeability.

It is generally noticed that this region is marked by a semi-complete absence of the AIs (1% of the AIs in the TTA region) (Fig. 2 & Fig. 3). This can be explained by the hydrological factor: there is an abundance of water resources flowing from the «*Dorsal Calcaire*» springs, which are converged towards downstream into the *Ouad Lou* and *Elkanar* rivers and provide an important source of water for irrigation of a large agricultural area.

The flysch unit (Early Cretaceous to Earliest Miocene) represents about 22.67% of the total area of the study region (Fig. 2). This field is considered by Durand-Delga and others (2000) as turbiditic deposits that consist of calcareous clay and sandstone (Nold et al. 1981). This geological unit in terms of hydrological behaviour is characterized by its little permeability. Also, the sensitivity to erosion differs according to the degree of rock resistance, which weakens when the marl prevails and increases in the presence of the sandstone. A great number of AIs (238) have been constructed within this unit, which constitutes 16. 95% of all the AIs in the region, with a density that reaches 0.07 AIs/km^2.

The external Rif (Middle-Upper Triassic to Upper Eocene) occupies a large area of the Rif's chain territory, representing 43.33% of the total area of the region (Fig. 2). This unit includes various types of rock such as marl with the presence of limestone, schistose, sandstone and quartzite formation, which are characterized by the little water absorption and increased exposure to different kinds of erosion. This unit includes the largest number of AIs constructed in the region (594), which corresponds to 42.30% (Fig. 2 & Fig. 3). As for the distribution of the AIs within these geological units, it is related to hydrological, socio-economic and historical factors which will be clarified later.

In addition to these principal geological units, formations that go back to the Pliocene Epoch can be found in the study area. Besides, we also find Quaternary deposits which are formed of clay and sand of red colour (El Ouahabi et al. 2014). These formations are mainly present in the Loukkos area, which in its turn is characterized by a large propagation of AIs (544), that corresponds to 38.74% of the total number of AIs in the region with the highest density (0.2 AIs/km^2) (Fig. 2 & Fig. 3). The prominent presence of such water projects may be caused by the fact that despite the Loukkos area has been developed since the year 1970 within the framework of the national policy of hydro-agricultural managements (El Kellouti 2004), the traditional water sources of the area (Ouad El Makhazin dam, the groundwater of the R'mel aquifer and the Dradar...) are not sufficient to satisfy the irrigation and other needs within the cultivated farming lands most of which are characterized by a flat and vast area.

Distribution of the AIs According to the Relief

The topographical analysis, especially in mountains, is without a doubt extremely important when studying the water structures, particularly those located at the slope and altitude. The division of

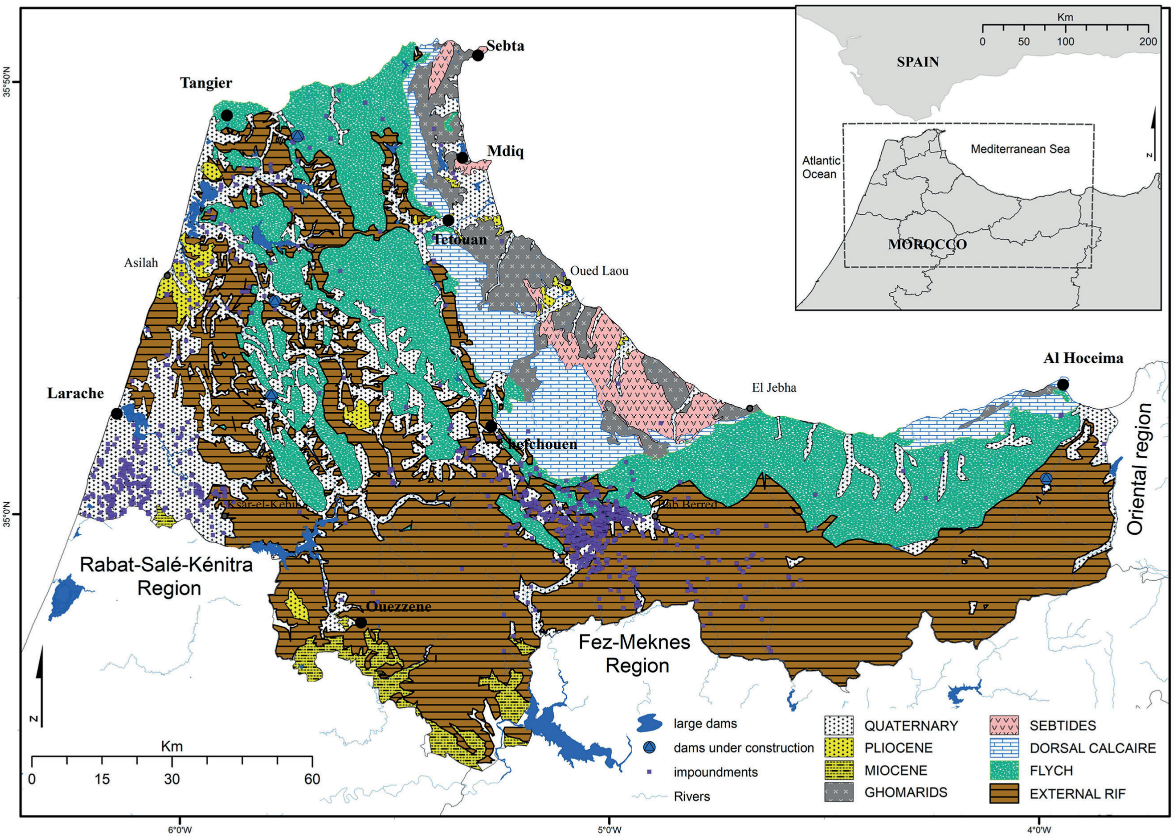

Fig. 2. Structural units and location of AIs
(Source: Modified from geological map of Rif (1/500 000))

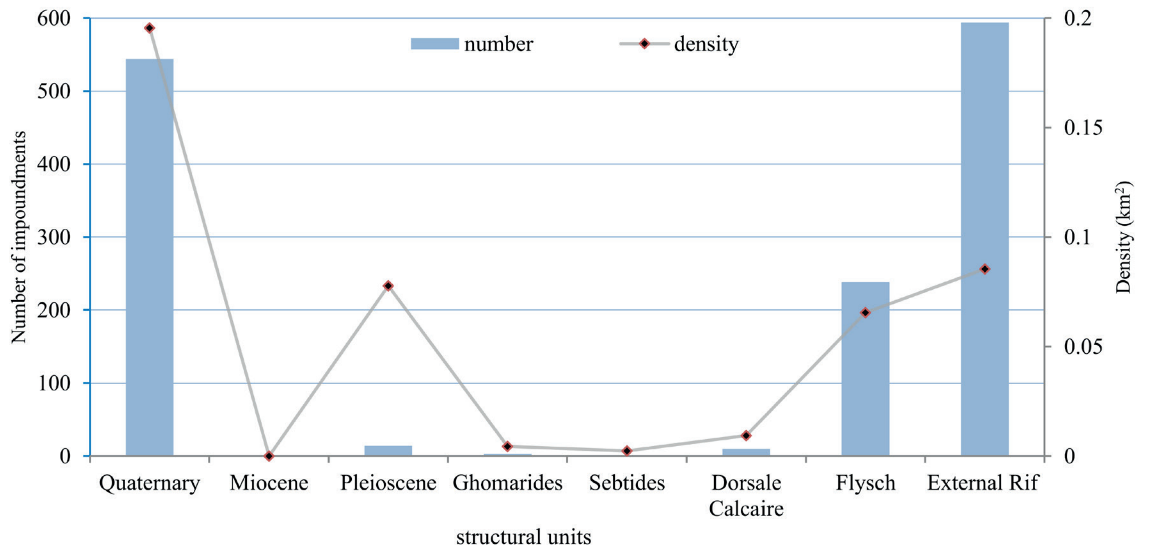

Fig. 3. Number and density of AIs according to the structural units
(Source: Compilation based on the map's database – Fig. 2)

the study area according to the altitude categories has shown that the elevation of half of the TTA region area exceeds 400 metres above sea level and in more than one third it exceeds 800 metres (Fig. 4). In general, the elevation increases from the west to the east. Comparing the distribution of AIs with the altitude classes it can be seen that more than one third of the AIs in the region were constructed at an altitude between 800 and 1200 metres with a density that reaches 0.12 AI/km^2 and that more than one fourth is found at an altitude which does not exceed 200 metres with a density estimated at 0.15 AI/km2 (Fig. 5).

Regarding the slope (Fig. 6), in more than half of the territory of the region (54%) it exceeds 5% and in one fifth of the area the steepness exceeds 10%. The Fig. 7 reveals that some peasants constructed the AIs on steep slopes exceeding 15% (5 AIs). 60 AIs were built on slopes ranging between 10% and 15%, meanwhile, the highest presence of such water projects in their number and density corresponds to the slope of less than 5%. This is normal if we consider the absence of the farmlands and its narrowness on one hand, and the danger that construction of the AIs within the area with steep terrain may cause on the other hand, especially given that the majority of the studied region formations are fragile and unstable and that their surface is extremely broken up as a result of the erosion of the rivers.

Distribution of the AIs according to the watersheds

It is impossible to study the effect of the hydrological factor on the distribution of AIs without taking into consideration

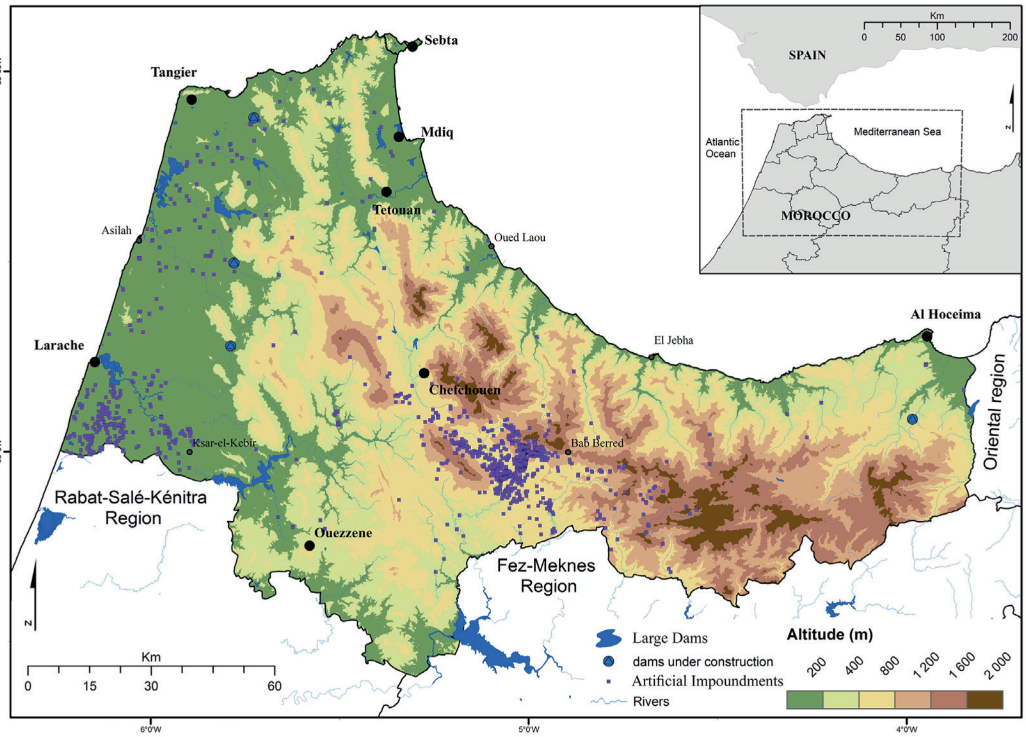

Fig. 4. Elevation and location of AIs

(Source: Modified from SRTM elevation data at 90 m resolution)

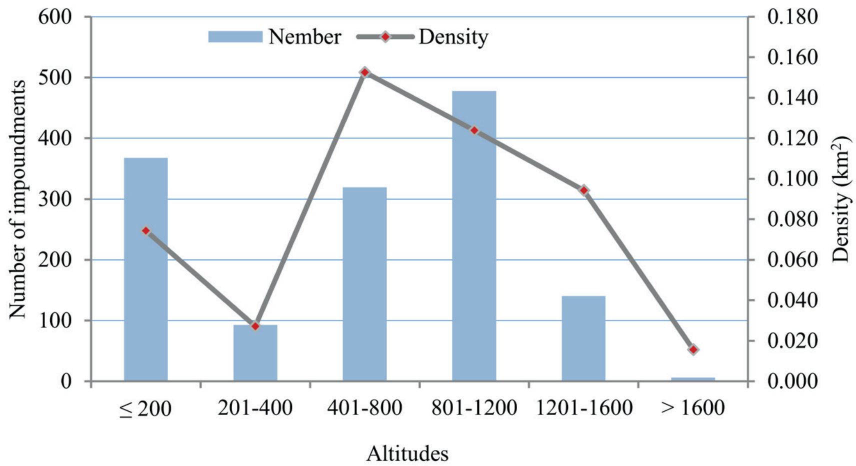

Fig. 5. Number and density of AIs according to the altitude

(Source: Compilation based on the map's database – Fig. 4)

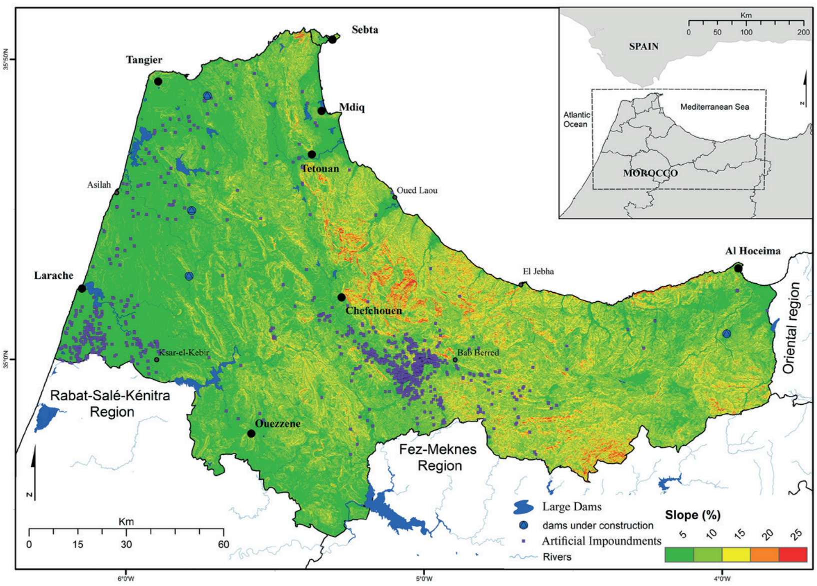

Fig. 6. Slope and location of AIs

(Source: Modified from SRTM elevation data at 90 m resolution)

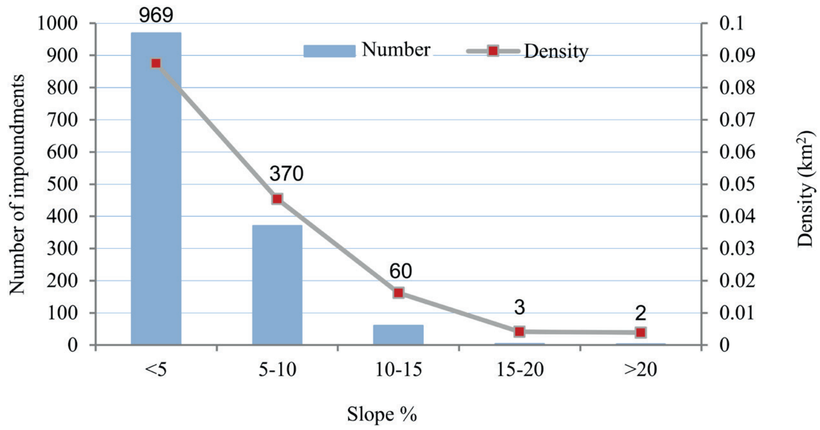

Fig. 7. Number and density of AIs according to the slope

(Source: Compilation based on the map's database – Fig. 6)

both climatic factors, particularly the factor of rain and snow precipitations, and hydrological factors. Concerning the climatic factors, the amount of rainfall in the TTA region varies significantly since precipitation generally decreases from west to east and registers its highest level (more than 1000 millimetres per year) in the centre (the province of Chechaouen) (Salhi et al. 2019) due to the exposure of foothills to the Atlantic influences, which also coincides with the wide development of the AIs. Meanwhile, considering hydrological factors, the geological and geomorphological evolution has contributed to the extension of some groundwater aquifers, the most prominent of which are: *«Dorsal Calcaire», R'Mel, Martil-Alila, Oued Lou, Ghiss-Nkkor, Sherf Elaqab*. 250 AIs, about 17.80% of the total number of AIs in the region, were constructed on these geological formations, which are mostly water absorbent and permeable. Among these formations, the majority of these AIs (233) corresponds to the *R'Mel* aquifer, which is because this is predominantly an agricultural area. However, the water stored in this aquifer and obtained from other sources is not sufficient to satisfy the increasing irrigation needs, particularly within the recurring dry periods in the last few years. In general, these figures indicate that more than 8 out of 10 AIs were built on geological formations impervious to water. In other words, they were built mainly in areas depending mostly on surface water resources.

In TTA region there are 5 large watersheds (Fig. 8) but all of them except for the Tangérois watershed are shared with the other regions: the Sebou watershed, for example, is shared with the regions of Fes-Meknes and Rabat-Sale-Kenitra.

The comparison of the area of these watersheds with the distribution of the constructed AIs has shown that 2/3 of them were built within the Sebou watershed, which is followed by the Loukkos watershed with 17.09%. However, regarding the density of the AIs, as it is shown in Fig. 9, the Dradar Sweer watershed is characterized by the highest density with an average of 0.36 AIs/km², which is followed by Sebou with 0.60 AIs/km^2. Hence, the question is whether the difference in the distribution of these AIs regarding their number and density is related to the hydrological properties of the region watersheds.

There is no doubt that the hydrological factor is present and controls the distribution of AIs in the study region. The main reason is that the areas that are characterized by the absence of underground water tables, as it has been mentioned previously, are the ones that are marked by a large proliferation of these water

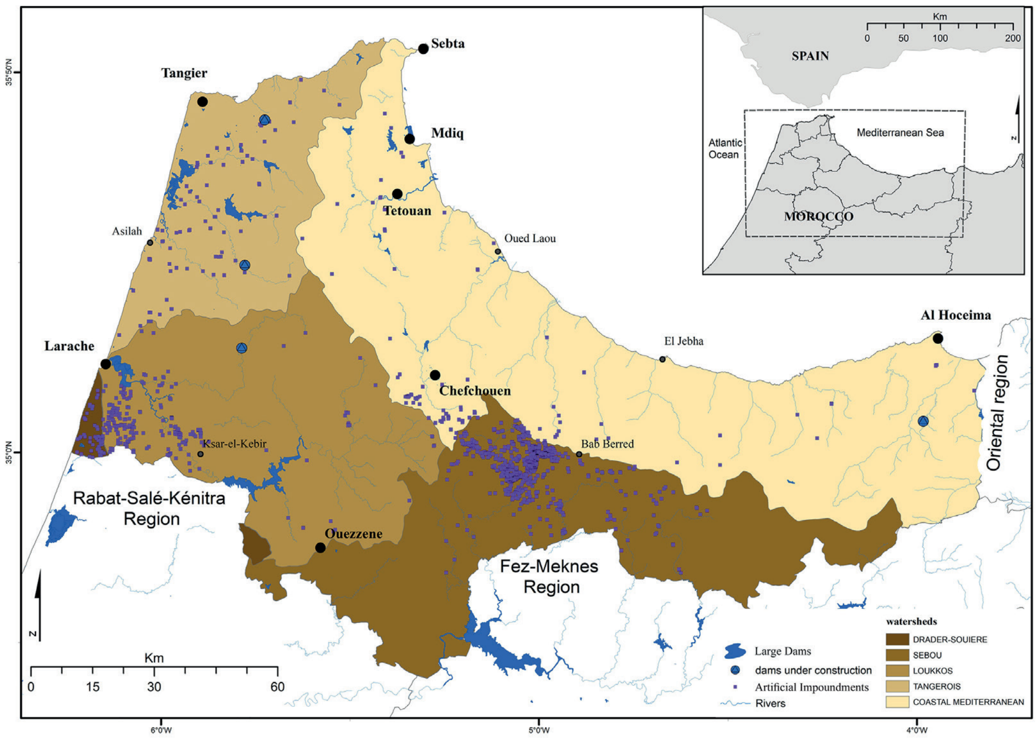

Fig. 8. Watersheds and location of AIs

(Source: Modified from SRTM elevation data at 90 m resolution)

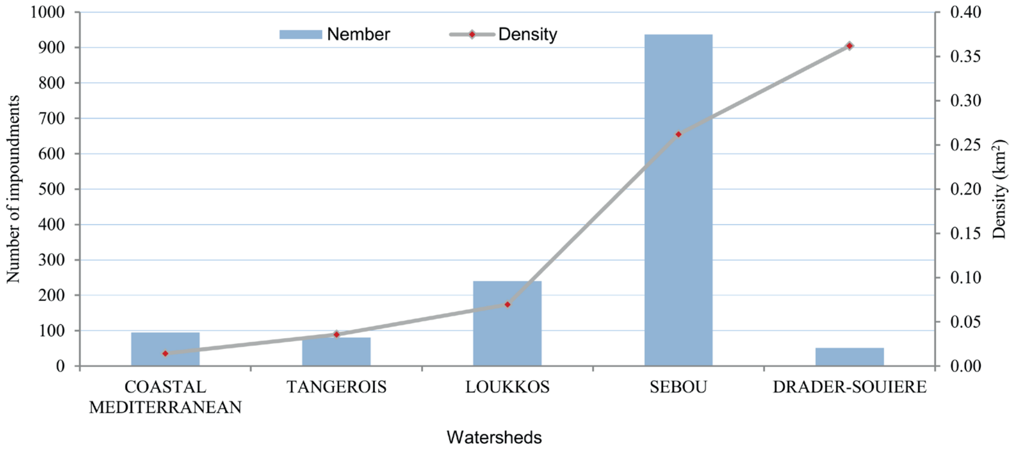

Fig. 9. Number and density of AIs in different watersheds
(Source: Compilation based on the map's database – Fig. 8)

projects. These areas are characterized by a high surface runoff discharge during the rain periods (the wet season) and an almost complete depletion in the dry seasons, which forces peasants to resort to the construction of AIs to remedy the deficit during the dry periods. However, from the maps of the distribution of AIs, it can be observed that they are present in some areas but not in the others even if they are similar in the climatic and hydrological conditions. This means that the hydrological factor is not the only controlling one but there is a combination of some other natural and human (historical and socio-economic) factors as it will be subsequently clarified.

Distribution of the AIs according to administrative division

The two provinces combined, Chefchaouen and Larache, have the largest share of the AIs in the region (9/10 of the AIs) (Fig. 10), the highest number and density of AIs is observed in the first province with a percentage of 70.08%, which is followed by the second one with 20.44%. However, besides the differences between the provinces, there is also variation present within the provinces themselves and as we found out that about 8/10 of the AIs were built in just four out of 28 rural communes in the province of Chefchouen: Bni Salh (368 AIs), Bab Bered (197 AIs), Ouad Elmelha (107 AIs), Bab Taza (104 AIs). These communes are also marked by the highest density of the Ais with 3 AIs/km² in the Bni Salah commune, which rises to about 5 AIs/km² in some areas such as Bni Aammar village (rural commune of Bni Salah). As for the province of Larache, half of its water projects are exclusive to the Ouamra commune (149 AIs) which has the highest density of 0.45 AI/km², followed by Oulad Ouchih commune 0.35 AI/km².

The dominance of the two provinces of Chfchaouen and Larache can be primarily explained by their great dependence on the agricultural economy from two different perspectives: in the first province, the prohibited agricultural activities (cultivation of cannabis) is widely practiced while in the second province there is a predominance of different kinds of allowed agricultural products like bananas, citrus fruits and sugar cane. All these agricultural products require a significant amount of water. However, if the conclusion about the importance of the water projects in the province of Larache is really significant because it is the only province that includes several large investments in different agricultural activities, the proliferation of AIs in the Chefchaouen Province due to cultivation of cannabis is questionable because there are other provinces where this forbidden agricultural product is practised. Still, as it has been mentioned previously, in the province of Chefchaouen these hydraulic structures are concentrated within particular areas, which means that there were factors that have contributed to their creation, namely the absence of water resources and more specifically groundwater, which has led to the necessity to look for adaptable methods to deal with the shortage of water. However, the implementation of these adaptable procedures, particularly the AIs, require great financial resources and this is what can distinguish some of these regions over others as the cultivation of cannabis, agriculturally and commercially, for a long time has contributed to the accumulation of significant financial resources that made it possible for their owners to invest in such

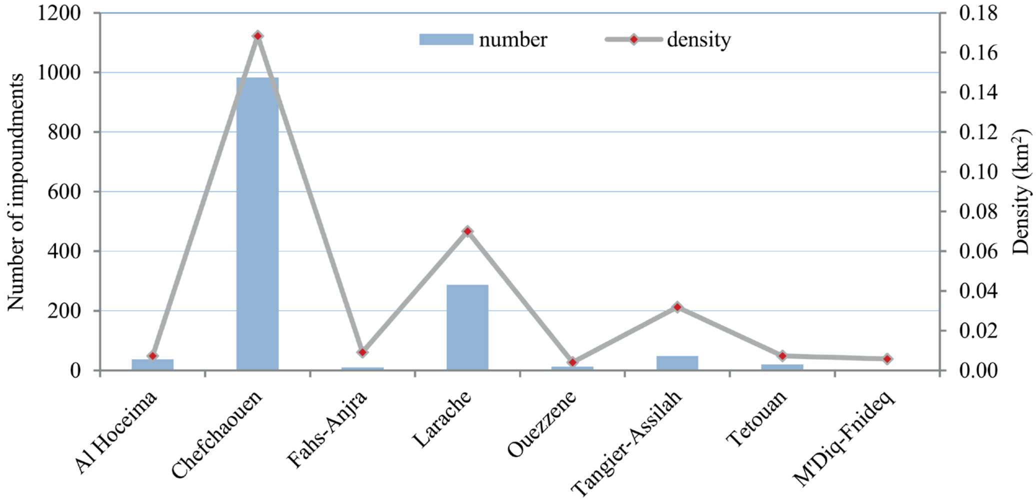

Fig. 10. Number and density of impoundments according to the prefectures and provinces
(Source: Compilation based on the map's database – Fig. 1)

hydro-agricultural projects. In connection with this, the AIs are always based in some particular areas and we can point out that the Al Anassar village (rural commune of Bab berred) was the first to practice these water techniques. This is due to the fact that this area for a long time depended on a small dam upstream of the village which was used communally, but its collapse in the last few years made the population to continue the irrigation of their lands relying on dams, but this time independently. For this reason, this practice has spread noticeably, changing the geographical landscape in the region as it is illustrated in the photo (Fig. 11).

DISCUSSION

The capacity of the AIs in the TTA region exceeds 7 million m³ (Table 2). There is a clear dominance of the AIs in the Sebou watershed, in which store 2/3 of the total volume of water in the AIs is stored. Then there are the AIs of the Loukkos watershed with a volume that exceeds 1.3 million m³. This results from the high number of these water projects in the two watersheds compared with the rest. In comparison, the volume of water in these AIs combined exceed the capacity of many large dams such as Nahkla (4.33 million m³), Aljomoua (5.05 million m³), Sidi Driss

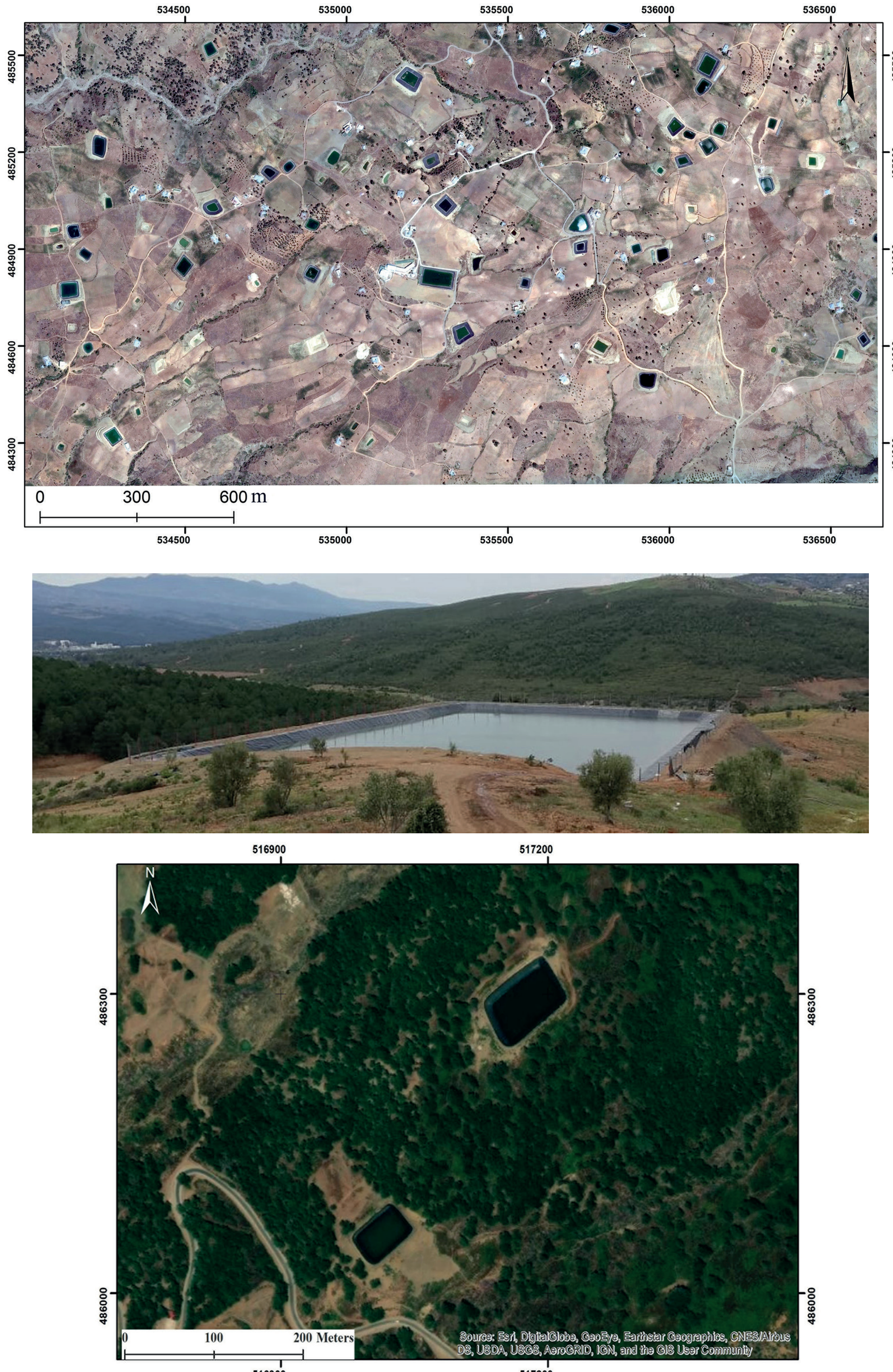

Fig. 11. Examples of AIs in the Tangier-Tetouan-Al Hoceima region

a - Al Anassar village (rural commune of Bab berred)
b - Ben zid village (rural commune of Bab taza)
c - the north of Fifi center

(Source: A and C – Bing Map hybrid, 2017, B – shootin 02-04-2019 by Mustapha Hmamou) dam (2.2 million m³), considering that the majority of these AIs are refilled with water twice a year, the volume of stored water in them also exceeds the volume of Asmir dam in August 2017 (11.4 million m³), the regular capacity of which reaches 40.7 million m³ (Royaume du maroc, Ministère de l'Equipement, du Transport de la Logistique et de l'eau 2017).

While the large dams integrate numerous functions, including irrigation of the farmlands, providing the cities and villages with drinkable water and producing hydroelectric energy, the functionality of the AIs is limited to irrigation of the agricultural land. As many studies have found out, one hectare of agricultural land needs an average of 5836 m3 of water per year (Aahd et al. 2009). This means that these AIs if we take into consideration the effect of evaporation, which is between 1000 and 1400 millimetres per year (Lahlou 2000), can on average irrigate more than 1370 hectares, which is more than 2/3 of the Chefchaouen province area. Also, it is necessary to point out that the number of AIs capable of irrigating more than one hectare has reached 364, 3/4 of which are located in the Chefchaouen province. Regarding the cost-effectiveness, one irrigated hectare yields more than five tons of raw cannabis.

Besides the contribution AIs make to the development of the local agricultural product, they can also have other positive roles, they can be resorted to in case of a fire outbreak and also they contribute to the diminution of the water flow hostility during the periods of rainfall. They also have other positive effects on the local

Table 2. Distribution of AIs according to the watersheds and its volume of water

Watersheds	Numbers of AIs	Capacity (one thousand m³)		
		Average	Minimum	Maximum
COASTAL MEDITERRANEAN	95	241	212	270
TANGEROIS	81	656	603	709
LOUKKOS	240	1585	1393	1777
SEBOU	937	6059	5494	6624
DRADER-SOUIERE	51	131	116	147
Total	1404	8672	7817	9527

Source: the field survey, August 2017

Table 3. The impacts of AIs on the capacity of the large dams

Large dams	C (M/m³)	V. S m³	AIs				I-LD %
			N	A.V (K/m³)	Min. V (K/m³)	Max. V (K/m³)	
Ibn Battouta	29.1	13					0.000
9 April	300	131.8	2	9.6	8.6	10.5	0.003
The Tanger Mediterranean	22.1	19.7					0.000
Hassan Ben El Mehdi	28.8	4.7					0.000
Smir	40.7	11.4					0.000
Nakhla	4.32	2.86	1	1.6	1.4	1.9	0.037
Moulay Bouchta	11.6	11.6	1	0.2	0.1	0.6	0.004
El Jomaâ	5.05	2.72					0.000
Moh.Ben Abde krim Al Khattbi	11.6	1,8					0.000
O. El Makhazine	672.9	385.3	21	76.96	69.1	84.9	0.011
Al Wahda *	3522.5	1790.6	943	6403.5	5780.9	7026.1	0.182
Kharroub**	185		2	12.8	11.7	13.8	0.007
Oued Martil**	120		2	0.9	0.9	1.0	0.001
Dar Khrofa**	480		2	35.7	33.4	37.9	0.007
Total	5433.67	2375.48	974	6541.0	5906.1	7176.7	0.120

C (M/m³): Capacity (million m³), V. S m³: the volume of the stored water in August 2017 (million m³)
Number: N
A.V: The Average volume:
Min. V: The minimum volume
Max. V: The maximum volume
K/m³: 1000 m³
I-LD: Impacts on large dams %
*- dam outside the Tangier-Tetouan-Al Hoceima region
**- dam under construction

Source: Compilation based on the mapping database of this research animal and plant environment (the amphibians and the birds) (Fang et al. 2009; Casas et al. 2012; Ferreira and Beja 2013) and can produce beautiful landscapes. However, they can also have different negative effects that should be taken into consideration, namely concerning the environmental and socio-economic aspects (Fuentes-Rodriguez et al. 2013; Casas et al. 2015). Thes AIs may provide new habitats for macroinvertebrates (Abellán et al. 2006), change the geographical landscape (Montginoul and Erdlenbruch 2009), along with their negative effect on the security of people and animals (the recurrent cases of drowning accidents) and the construction of the AIs in forests (Fig.11-c). However, the most dangerous negative impact is related to their quantitative and qualitative effect on the hydraulic and hydrographic features of the watersheds. These AIs divert and delay downstream water flow and modify the groundwater interaction (Smith et al. 2002). Moreover, the consumption of water will increase in the presence of these hydro-agricultural structures and thus, its saving will not be possible (Loubier et al. 2011).

There are ten large dams in the TTA region with a retaining capacity that reaches 1.1 billion m³, by August 2017 the refilled volume has reached 584 million m3 (Royaume du maroc, Ministère de l'Equipement, du Transport de la Logistique et de l'eau 2017). Along with that, there are some dams that are in the process of construction and also dams located outside the region which are refilled from its river basins such as the *Wahda* dam.

As for the effects of the AIs on the large dams, the *Wahda* dam comes in the first place with 943 AIs built in the upstream watershed. They can store about 6.4 million m3, which is the equivalent of 0.18% of the reservoir capacity of the dam (3.5 billion m3) and 0.35% of the volume of water stored during the year 2017. It is followed by the *Ouad El Makhazine* dam in the upstream of which 20 AIs were constructed with a load capacity around 77 thousand m3, 0.01% of the reservoir capacity of the dam and 0.02% of its stored volume in August 2017. As for the other remaining large dams that are either already built or currently under construction, only very few AIs have been constructed by August 2017 (Table 3).

From these figures, we can conclude that the effect of the AIs on the capacity of large reservoirs is meagre/ insignificant as it does not exceed 0.12% of their total storage capacity. Thus, the factors that cause a decline in the filling of these large reservoirs are related to the recurrence of the periods of droughts. On the other hand, it is worth pointing out that the surface water is still not fully exploited as it ought to be, especially within the Mediterranean watershed. Especially given the fact that the volume of the reservoirs in this area does not exceed 90 million m^3, while the average annual runoff from the Mediterranean watersheds is about 1.8 billion m^3. Considering that the volume of water discharged from these watersheds exceeds 40% of the annual rainfall (Royaume du Maroc, Agence du bassın hydraulıque du loukkos 2007), the share of water stored in these reservoirs remains low (less than 15%).

CONCLUSIONS

Taking into account all discussed above, it is clear that the AIs can be considered to be useful water projects for the mountainous areas both economically and socially. The water discharged from the mountains and particularly from the dams in the form of drinkable or industrial water or water for irrigation or producing electricity does not benefit fairly these mountainous areas (Boujrouf 2002). Besides, their impact on the retaining capacity of the large dams is low, especially considering that the Rif mountains are among the rainiest areas at the national level, even despite the fluctuations in the rainfall temporal distribution, as the volume currently stored within the AIs does not exceed 0.12% of the retaining capacity of the large dams. In addition to that, their effect on the groundwater recharge in the TTA region is considerably limited as most of the rocks in the study area are impermeable.

This kind of private hydro agricultural structures can be considered an ideal solution to maintain the population's stability due to the absence of the large dams in the upstream watersheds. Generally speaking, these solutions, despite their high costs, are less harmful from both the environmental and social perspectives, especially compared to the solutions that include drillings, which have spread greatly in the region during the last few years. On the other hand, we should not forget that the studied water projects are highly dependent on the climatic conditions, particularly rainfall and snow, as refilling of these AIs is determined by the surface water runoff. Thus, in the case of recurring droughts, pumping of groundwater still has to be used, which can consequently create conflicts within the population. In addition to that, the complexity of the administrative procedures at the level of granting construction permits leads to the illegal propagation of these AIs, which means that their effects will not remain minor.

REFERENCES

Aahd A., Simonneaux V., Sadik E., Brahim B. and Fathallah S. (2009). Estimation des volumes d'eau pompés dans la nappe pour l'irrigation (plaine du Haouz, Marrakech, Maroc). Comparaison d'une méthode statistique et d'une méthode basée sur l'utilisation de la télédétection. Revue des sciences de l'eau / Journal of Water Science, 22(1), 1-13, DOI: 10.7202/019820ar.

Abellán P., Sanchéz-Fernández D., Millán A., Botella F., Sánchez-Zapata J.A. and Giménez A. (2006). Irrigation pools as macroinvertebrate habitat in a semi-arid agricultural landscape (SE Spain). Journal of Arid Environments, 67(2), 255-269, DOI: 10.1016/j.jaridenv.2006.02.009.

Azzouz O., El Fellah B. and Chalouan A. (2002). Processus de glissement dans le Massif de Bokoya (Rif interne, Maroc): exemple de Cala Bonita. Bulletin de l'Institut scientifique, Rabat, section Sciences de la Terre, 24, 33-40. [online]. Available at: http://www.israbat.ac.ma/wp-content/uploads/2015/03/04-%20Azzouz%20et%20al.%20(33-40).pdf. [Accessed 28 Sep. 2017].

Boujrouf S. (2002). Innovation et recomposition territoriale au Maroc. Une mise en perspective géo–historique. In Rencontres scientifiques franco-Sud-Africaines de l'innovation territoriale, Grenoble – Avignon, France, 01-01 2002, 14.

Bonachela S., Juan M., Casas J.J., Fuentes-Rodríguez F., Gallego I. and Elorrieta M.A. (2013). Pond management and water quality for drip irrigation in Mediterranean intensive horticultural systems. [journal article]. Irrigation science, 31(4), 769-780, DOI: 10.1007/s00271-012-0361-1.

Chao B.F. (1988). Excitation of the Earth's Polar Motion due to Mass Variations in Major Hydrological Reservoirs. Journal of Geophysical Research: Solid Earth, 93(B11), 13811-13819, DOI: 10.1029/JB093iB11p13811.

Chao B.F., Wu Y.H. and Li Y.S. (2008). Impact of Artificial Reservoir Water Impoundment on Global Sea Level. Science, 320(5873), 212-214, DOI: 10.1126/science.1154580.

Callihan R.A. (2013). Distribution, Proliferation and Significance of Small Impoundments in Kansas. Thesis, University of Kansas, Kansas. [online]. Available at: https://kuscholarworks.ku.edu/bitstream/handle/1808/12980/Callihan_ku_0099M_13190_DATA_1.pdf?sequence=1&isAllowed=y. [Accessed 22 Aug. 2017].

Casas J., Toja J., Bonachela S., Fuentes F., Gallego I., Juan M., et al. (2011). Artificial ponds in a Mediterranean region (Andalusia, southern Spain): agricultural and environmental issues. Water and Environment Journal, 25(3), 308-317, DOI: 10.1111/j.1747-6593.2010.00221.x.

Casas J.J., Toja J., Peñalver P., Juan M., León D., Fuentes-Rodríguez F., et al. (2012). Farm Ponds as Potential Complementary Habitats to Natural Wetlands in a Mediterranean Region. [journal article]. Wetlands, 32(1), 161-174, DOI: 10.1007/s13157-011-0265-5.

Casas J.J., Bonachela S., Moyano F.J., Fenoy E. and Hernández J. (2015). Chapter 3 – Agricultural Practices in the Mediterranean: A Case Study in Southern Spain. In V. R. Preedy, & R. R. Watson (Eds.), The Mediterranean Diet (23-36). San Diego: Academic Press, DOI: 10.1016/B978-0-12-407849-9.00003-8.

Directions Régionales de l'Environnement de l'environnement, de l'aménagement et du logemen (2012). Zoom sur les retenues artificielles. [online]. Available at: http://www.pays-de-la-loire.developpement-durable.gouv.fr/IMG/pdf/Outils_et_reperes_21_-_Fiche_retenues_artificielles.pdf. [Accessed 23 Aug. 2017].

Downing J.A., Prairie Y.T., Cole J.J., Duarte C.M., Tranvik L.J., Striegl R.G., et al. (2006). The global abundance and size distribution of lakes, ponds, and impoundments. Limnology and Oceanography, 51(5), 2388-2397, DOI: 10.4319/lo.2006.51.5.2388.

Dunglas J. (2014). Stockage de l'eau : quel avenir pour les retenues collinaires? [online]. Available at: https://www.agri-mutuel.com/wp-content/uploads/2018/02/stockage-de-l-eau.pdf. [Accessed 23 Aug. 2017].

El Kellouti M. (2004). Modernisation de la gestion de l'irrigation dans le périmètre du Loukkos (Maroc). In Séminaire sur la modernisation de l'agriculture irriguée, Rabat, Morocco, 2004, 10: IAV Hassan II.

El Ouahabi M., Daoudi L. and Fagel N. (2014). Mineralogical and geotechnical characterization of clays from northern Morocco for their potential use in the ceramic industry. Clay Minerals, 49(1), 35-51, DOI: 10.1180/claymin.2014.049.1.04.

Fang W.-T., Chu H.-J. & Cheng B.-Y. (2009). Modeling waterbird diversity in irrigation ponds of Taoyuan, Taiwan using an artificial neural network approach. [journal article]. Paddy and Water Environment, 7(3), 209-216, DOI: 10.1007/s10333-009-0164-z.

Ferreira M. and Beja P. (2013). Mediterranean amphibians and the loss of temporary ponds: Are there alternative breeding habitats? Biological Conservation, 165, 179-186, DOI: 10.1016/j.biocon.2013.05.029.

Fuentes-Rodriguez F., Juan M., GALLEGO I., Lusi M., Fenoy E., León D., et al. (2013). Diversity in Mediterranean farm ponds: trade-offs and synergies between irrigation modernisation and biodiversity conservation. Freshwater Biology, 58(1), 63-78, DOI: 10.1111/fwb.12038.

Keshavanath P., Gangadhar B., Ramesh T.J., Van Rooij J.M., Beveridge M.C.M., Baird D.J., et al. (2001). Use of artificial substrates to enhance production of freshwater herbivorous fish in pond culture. Aquaculture Research, 32(3), 189-197, DOI: 10.1046/j.1365-2109.2001.00544.x.

Lahlou A. (2000). Quel environnement pour l'Afrique du nord? : Rabat, Dar al Qalam.

Law No. 36-15 on water promulgated by Dahir No. 1-16-113 of August 10, 2016, , B.0 nº 6494: August, 25th, 2016.

Loubier S., Poussin J.-C., Gleyses G., Le Mat O. and Garin P. (2011). Faut-il subventionner la création de réserves d'eau pour l'irrigation? [aide à la décision; analyse microéconomique; irrigation ; réservoir d'eau ; subvention]. 2011, 20(1-2), DOI: 10.1684/agr.2011.0484.

Ministère de l'écologie, du développement durable des transports et du logement (2012). Guide juridique construction de retenues. [online]. Available at: https://www.ecologique-solidaire.gouv.fr/sites/default/files/2012_03%20guide%20juridique_construction%20retenues.pdf. [Accessed 14 Dec. 2017].

Montginoul M. and Erdlenbruch K. (2009). Les réserves de substitution sont-elles une solution à la pénurie d'eau. Ingénieries, (59-60), 131-136. [online]. Available at: http://katrin.erdlenbruch.free.fr/MontginoulErdlenbruch2009IEAT.pdf. [Accessed 12 Dec. 2017].

Nold M., Uttinger J. and Wildi W. (1981). Géologie de la dorsale calcaire entre Tétouan et Assifane (Rif interne, Maroc). Notes et Mémoires du Service géologique du Maroc, 233, 1-233.

Royaume du Maroc, Agence du bassın hydraulıque du loukkos (2007). Mission 1: Analyse et synthèse des connaissances actuelles dans le domaine des ressources en eau – évaluation et prévision des besoins et des demandes en eau, Ressources en Eau superficielles. [online]. Available at: http://www.abhloukkos.ma. [Accessed 20 Aug. 2017].

Royaume du maroc, Ministère de l'Equipement, du Transport de la Logistique et de l'eau (2017). Situation journalière des principaux grands barrages. [online]. Available at: http://www.equipement.gov.ma. [Accessed 25 Sep. 2017].

Salhi A., Martin-Vide J., Benhamrouche A., Benabdelouahab S., Himi M., Benabdelouahab T., et al. (2019). Rainfall distribution and trends of the daily precipitation concentration index in northern Morocco: a need for an adaptive environmental policy. [journal article]. SN Applied Sciences, 1(3), 277, DOI: 10.1007/s42452-019-0290-1.

Smith S.V., Renwick W.H., Bartley J.D. and Buddemeier R.W. (2002). Distribution and significance of small, artificial water bodies across the United States landscape. Science of the Total Environment, 299(1), 21-36, DOI: 10.1016/S0048-9697(02)00222-X.

RESEARCH PAPER

LAND USE/LAND COVER CHANGE WITH IMPACT ON LAND SURFACE TEMPERATURE: A CASE STUDY OF MKDA PLANNING AREA, WEST BENGAL, INDIA

Samrin Fatema[1*], Dr. Abhisek Chakrabarty[1]
[1]Vidyasgar University, Remote Sensing & GIS Department, Midnapore, 721102, India
*Corresponding author: asamrin1@gmail.com
Received: March 31th, 2019 / Accepted: November 20th, 2020 / Published: December 31st, 2020
https://DOI-10.24057/2071-9388-2020-62

ABSTRACT. The type of surface influences the temperature of a surface. If it is made of concrete or another hard material, the temperature will be higher. Hence it is essential to study the land surface temperature (LST) of urban areas. The LST is an important parameter in the estimation of radiation budgets and heat balance and is a controlling factor of dynamic climate changes. In this work, we made an effort to identify the LST of the Midnapore Kharagpur Development Authority planning region. Multi-temporal images acquired by Landsat 7 ETM+, Landsat 5 TM and Landsat 8 using OLI sensors on 3 May 2001, 7 May 2011 and 29 May 2019, respectively, were corrected for radiometric and geometric errors and processed to extract LULC classes and LST. Thermal remote sensing can be used to monitor the temperature and local climate of urban areas. This study has shown that the temperature varies across the surface according to land use. It was found that the urbanized area increased from 6.79% (40.39 sq. km) to 11.6% (69.2 sq. km) between 2001 and 2011 and from 11.6% (69.2 sq. km) to 17.22 % (102.79 sq. km) between 2011 and 2019. The LST study has shown that there has been a tremendous change in the spatial pattern of the temperature between 2001 and 2019. Whereas in 2001 the highest temperature did not exceed 34°C, by 2019 it had increased by nearly 8°C, reaching 41.29°C. So, the findings of this study are significant.

KEY WORDS: LULC, Change detection, LST, Thermal Remote sensing, GIS

CITATION: Samrin Fatema, Dr. Abhisek Chakrabarty (2020). Land Use/Land Cover Change With Impact On Land Surface Temperature: A Case Study Of Mkda Planning Area, West Bengal, India. Geography, Environment, Sustainability, Vol.13, No 4, p. 43-53 https://DOI-10.24057/2071-9388-2020-62

ACKNOWLEDGEMENTS: The authors would like to thank the Department of Remote Sensing and GIS, Vidyasagar University for providing the necessary infrastructural facility to carry out the research.

Conflict of interests: The authors reported no potential conflict of interest.

INTRODUCTION

The land surface temperature (LST) is the temperature of the earth's surface. The LST varies with Land Use Land Cover (LULC) type. It is a result of the energy and water balance of the earth's surface at the global and regional levels (Rozenstein et al. 2014). It gives information about the surface energy changes with time. This is an important parameter for monitoring vegetation, global warming and changes in built-up area. Currently, the LST is a significant environmental issue (Kayet et al. 2016). The temperature is increasing across the world daily because of the greenhouse gas effect, the ozone hole, etc. Scientists need to concentrate on studying the LST to reduce the impacts of global climate change. Hence, more research is required in this field. Various studies have been carried out on estimating the LST using thermal remote sensing (Southworth 2004). The first remotely sensed thermal images were obtained in 1960 from the NOAA satellite TIROS II with a very low resolution. In 1984, NASA launched the first operational satellite mission with a thermal camera (Landsat 4 TM), which covered the 10.5–12.5 µm spectrum with a resolution of 60–120 m. In 2013, NASA launched Landsat 8, with an enhanced thermal infrared (TIRS) camera. This had two bands (bands 10 and 11), covering the thermal spectrum (10.6–12.5 µm). Atmospheric correction was carried out using the split-window technique (Reuter et al. 2015). Landsat is still the only mission with more than 30 years of archived imagery, including thermal infrared imagery (Wan & Li 2010). Kustas & Anderson, 2009 utilized thermal infrared remote sensing to model land surfaces. Remote sensing and GIS techniques can be used to detect land use change and its impact on the LST (Latif S. 2014). Fu & Weng (2016) and Lv & Zhou (2011) used the Landsat thermal band to estimate the surface energy of an urban area and generate a land use change map. Alavipanah et al. (2007) used remote sensing techniques and Landsat thermal data to produce a temperature map of the Yardang region of the Lut Desert (Iran). Satiprasad (2013) created a methodology to determine the activity of land use change in the surface temperature in Howrah city. Heat islands are formed in the air above urban areas due to the heat absorbed and discharged by buildings, concrete structures and other impervious surfaces, which act as inactive vaults (Renssen et al. 2005). The LST is a vital climate variable related to climate change and is an exponent of the energy balance at the surface. It plays a key role in the physics of the land surface processes (James &

Mundia 2014). Saradjian and Jouybari-Moghaddam (2019) developed a method to retrieve the land surface emissivity (LSE) and LST simultaneously from Landsat 8 images. Li and Jiang (2018) estimated the LST using a generalized split-window (GSW) algorithm and validated it using the MOD11_L2 V6 product. Nguyen et al. (2019) derived the LST from Landsat 8 data using the split-window method. Their results showed that the LST is much higher than in the early part of the dry season. The LST and vegetation are strongly related. Temperature–vegetation plots reveal the chronological trajectory of pixels from low-temperature–high-vegetation conditions to high-temperature–low-vegetation conditions (Amiri et al. 2009). A study carried out in an urban area showed that an increase in the built-up area was accompanied by a decrease in vegetation, resulting in urban microclimatic changes (Buyadi et al. 2013). Another study revealed that the LST and vegetation are closely related. Different vegetation indices show an excess of vegetation, such as fractional vegetation cover and the normalized vegetation index (NDVI) (Amiri et al. 2009). A negative relation was found between the LST and NDVI. Green area affected the temperature (Jiang & Tian 2010) through soil moisture variations, LSE, albedo and vegetation type with dense vegetation reducing the temperature (Chen et al. 2000). Both the LST and surface imperviousness (SI) can be derived from satellite imagery. The temperatures of non-urban areas are lower than those of urban areas (White-newsome et al. 2013).

In this study, we attempted to calculate changes in the LST using thermal remote sensing and GIS. As we all know, the use of remote sensing and GIS is a powerful technique for acquiring temporal and spatial information within a narrow time span. This methodology allows to detect LULC change. Two major urban patches and a suburban-rural area were studied. The primary objectives of this study were (1) to extract and calculate the LST of the present study area during three timespans and (2) to analyse the LULC changes in relation to the changes in the LST.

STUDY AREA

The area under the Midnapore Kharagpur Development Authority (Fig.1) is situated in Paschim Medinipur District of West Bengal, India. It was formed in 2003 with the basic aim of controlling land use and development by preventing haphazard growth within the planning area. The authority has a total planning area of 596.76 sq. km, consisting of 464 mouzas (cadastre). The area consists of 14 gram-panchayats (GP) of Medinipur, Kharagpur-I, Kharagpur-II, Salboni Block and 54 wards of Kharagpur and Medinipur municipal areas. The study area extends between 87º09´00´´E and 87º28´00´´E and between 22º14´00´´N and 23º34´00´´N, it has several stretches of agricultural land and many industries that are situated in the Kharagpur Municipality (Fatema, & Chakrabarty 2017). The Kangsabati is the only perennial river of the study area. It flows almost in the middle of the Midnapore Kharagpur Development Authority area. Besides, there is an important stream within the Midnapore town, known as the 'Dari Bandh Khal', which has a south-easterly course. It joins the river Kasai and contributes to the system's internal drainage. The elevation of the study area varies between 20 m and 60 m above mean sea level.

MATERIALS AND METHODS

Three sets of remotely sensed data for path 139, row 44, 45 (WRS-2) were downloaded from the USGS portal, including data from Landsat 5, Landsat 7 and Landsat 8. The surface reflectance and brightness temperature data of these sets were processed by the Landsat Ecosystem Disturbance Adaptive Processing System (Fu & Weng 2016). Details of the dataset are provided in Table 1. Since the satellite images may still contain noisy pixels, all the images were subjected to geometric, radiometric and atmospheric correction. Also, a mosaic operation was performed to obtain the study area and the Normalized Difference Vegetation Index (NDVI) was derived from the surface reflectance.

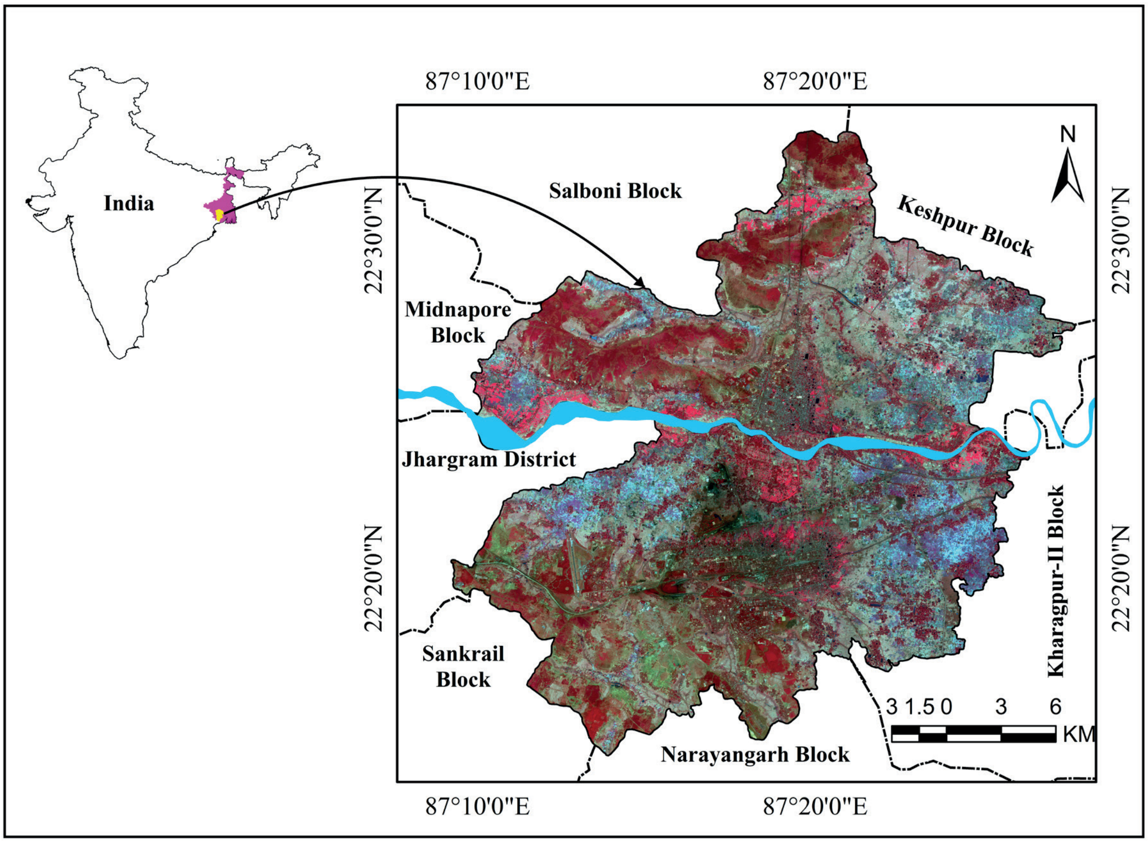

Fig. 1. Location map of the study area

LULC classification

We attempted to determine the land use land cover (Fig. 2) of our study area using remote sensing and GIS techniques. The supervised classification (maximum likelihood algorithm) method was used for identifying the LULC categories from the satellite images and the toposheet. The LULC classes (2001, 2011 & 2019) included agricultural fallow, fallow land, cultivated land, forest, river, sand, settlement, vegetation, water body and industry. The areas corresponding to different LULC classes were calculated using the pixel grid cell method (15 m×15 m) (Kayet et al. 2016). The LULC feature category was identified based on visual interpretation of the satellite imagery and the information on the actual LULC. The LULC nomenclature is presented in Table 2.

Maximum likelihood classification

A lot of research has been conducted in the field of satellite image classification, both parametric and nonparametric. We chose the maximum likelihood classifier, which uses a parametric method. This is the most popular method used to classify satellite images. It essentially uses Bayes' theorem. It is based on the use of a discriminant function to fix the pixel that belongs to the highest likelihood class (Ahmad & Quegan 2012). Maximum likelihood classification was performed using Equation 1. The accuracy (Kappa coefficient) of a classification process is usually assessed by comparing the results of classification against data obtained from field visits, high-spatial-resolution images or toposheets (Bokaie et al. 2016).

Table 1. Data used of the present study

Data	Sensor	Date	Band	Resolution (Thermal)	Path/Row
Landsat 7	ETM	3rd May 2001	6	60 (30)	139/44,45
Landsat 5	TM	7th May 2011	6	120 (30)	139/44,45
Landsat 8	OLI TIRS	29th May 2019	10/11	100	139/44

Table 2. Land use and land cover (LULC) nomenclature

LULC Classes	Land Use Included in This Class
Agriculture Fallow (AF)	Non-irrigated lands
Fallow land (FL)	Ready for construction, real-estate plots, open area
Cultivated Land (CL)	Irrigated lands
Forest	Open Forest, Dense Forest, Protected forest
River	River
Sand	Sand
Settlement (Sett)	Built-up area
Vegetation (Veg)	Plantation and Shrub
Water Body (WB)	Reservoir, Ponds, Open water
Industry (Indus)	Industrial area

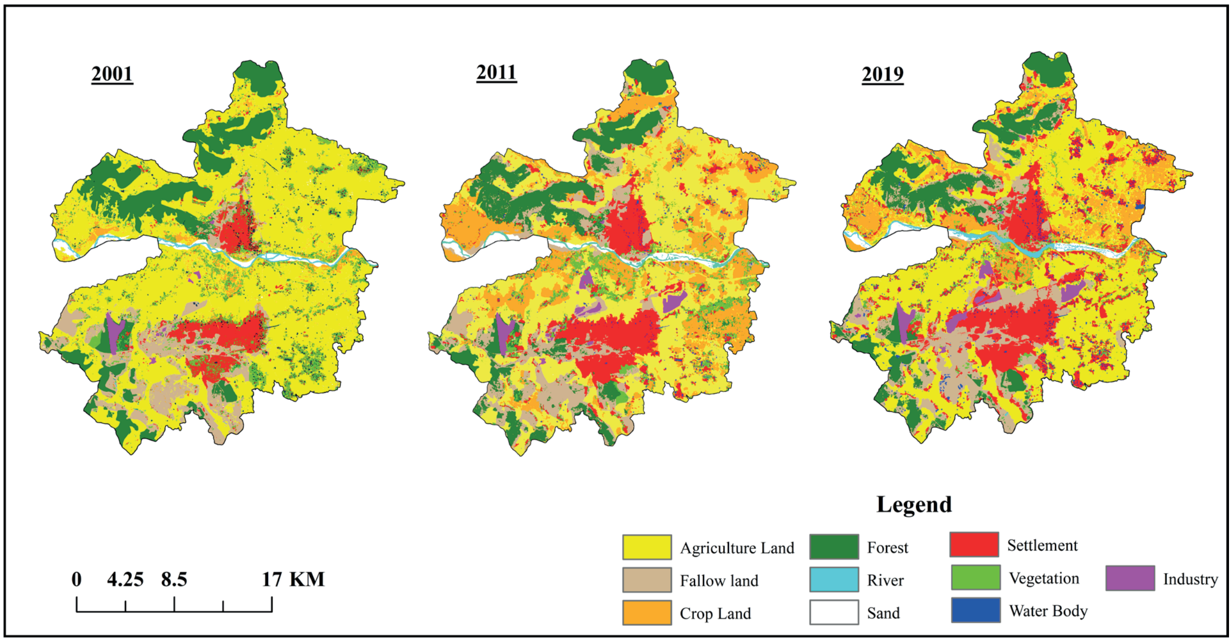

Fig. 2. Spatio-temporal pattern of land transformation

$$Lk(X) = \frac{1}{(2\pi)^{\frac{n}{2}}|\Sigma_k|^{\frac{1}{2}}} \exp\left(-\frac{1}{2}(X-\mu_k)\Sigma_k^{-1}(X-\mu_k)^t\right) \quad (1)$$

where
n is the number of bands,
X is the image data of bands n,
Lk (X) is the likelihood of X belonging to class k,
μk is the mean vector of class k,
∑k defines the variance-covariance matrix of class k and
|Σk| is the determinat of Σk.

Determination of kappa coefficient

An accuracy assessment plays a significant role in the analysis of the resultant classes after the classification process. The Kappa index (Table 5) is a method that is used widely to measure the accuracy of the assessment of a remotely sensed image (Conglaton, 1991). The Kappa coefficient is considered to be more robust than the simple overall accuracy because it takes into account the proportion of pixels that have been classified correctly merely by chance. A confusion (error) matrix was used to represent the accuracy assessment (Lillesand et al. 1994) using random sampling methods. The Kappa coefficient was computed as follows (Conglaton 1991):

$$KA = \frac{na - s}{n^2 - s} \quad (2)$$

where
KA = Kappa coefficient,
n = number of ground points in the error matrix (the sum of all r individual cell values),
a = sum of diagonal segments and
s = sum of row and column.

Determination of land surface temperature

The TIR band (band 6 of Landsat 5 and 7 and band 10/11 of Landsat 8 OLI) records the radiation with the spectral range between 10.4 μm and 12.5 μm, which is emitted by the surface of the earth (Buyadi et al. 2013). The LST plays a vital role in environmental processes and provides basic information on the earth surface biophysical properties and climate. For example, Landsat 7 ETM+ data can be used to estimate radiation budgets in heat balance studies and as a control for climate models (Mallick, Kant and Bharath 2008). In most of the research, the LST is generated using digital image processing software and GIS software. In this study, the ArcGIS 10.3 and ERDAS Imagine software packages were used to generate LST maps. The methodology developed for the LST mapping is shown in Fig. 3.

Thermal map generation

The remotely sensed data were acquired and stored in a binary format. The values ranged between 0 and 255. Thermal remote sensing can convert the data from digital numbers to radiance values. The thermal energy responses of various landforms reveal the variations in the temperatures of different surfaces. In this study, the surface temperature was extracted from the thermal bands 6, 6.1, 10 and 11 of Landsat ETM+, TM, and OLI_TIRS data.

Computation of the NDVI

The NDVI is widely used in LST studies because it is less sensitive to changes in atmospheric conditions compared with other indices. The NDVI is a numerical indicator of live green vegetation. It is derived from the near-infrared and visible bands of the electromagnetic spectrum. The range of NDVI values is from -1 to 1. In this study, the NDVI was used to represent the relationship between the vegetation and LST. The NDVI can be obtained using the following equation:

$$NDVI = \frac{NIR -}{NIR +} \quad (3)$$

The NIR and red bands of Landsat 5–7 {(Band 4 – Band 3)/(Band 4 + Band 3)} and Landsat 8 {(Band 5 – Band 4)/(Band 5 + Band 4)} were used in this study. NDVI maps were generated using the ERDAS Imagine software package (Version 14).

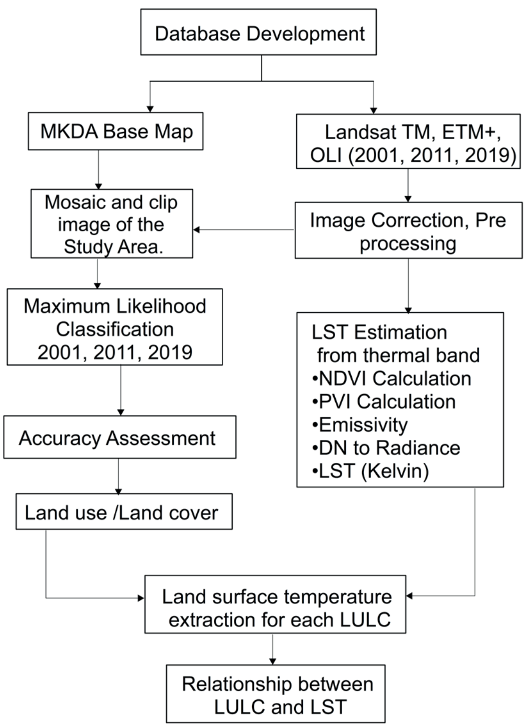

Fig. 3. Methodology flow diagram of the study

Computation of land surface temperature LST

The thermal infrared bands of the Landsat images (band 6 of Landsat 5 and 7, bands 10 and 11 of Landsat 8 OLI, with spatial resolution of 30 m) were used to calculate the LST of the MKDA planning area. The LST was derived as described in the following sections.

Calculation NDVI and Proportional Vegetation Index

The land surface emissivity (LSE) was derived from the NDVI. The PVI value was calculated as:

$$Pv = \left(\frac{NDVI - NDVImin}{NDVImax - NDVImin} \right) 2 \quad (4)$$

where Pv is the proportion of vegetation.

Calculation of Emissivity

The NDVI threshold can be used to calculate the emissivity using the following formula (Guha, Govil and Diwan 2020) & (Baba 2016):

$$\varepsilon = 0.004 * Pv + 0.986 \quad (5)$$

The value of NDVI ranges between -1 and 1. When the NDVI value crossed this range (-1 to 1), the corresponding LSE value was used (Anandababu D et al. 2018).

DN to Radiance

The digital numbers (DN) of the Landsat 7 and 5 data for 2001 and 2011 were converted to spectral radiance (L) values (USGS, 2001) using Equation 6. Similarly, Equation 7 was used for the Landsat 8 OLI_TRS data of 2019. The values obtained using these equations are presented in Table 3.

Landsat 5/7
Landsat 8

$$L\lambda = \frac{L_{max} - L_{min}}{Qcal_{max} - Qcal_{min}} * \left(Qcal - Qcal_{min} \right) + L_{min} \quad (6)$$

$$L\lambda = M_L Q_{cal} + A_L \quad (7)$$

where
Lλ = spectral radiance,
Qcal = quantized and calibrated standard product pixel value (DN),
L_{min} = spectral radiance scaled to Qcalmin,
L_{max} = spectral radiance scaled to Qcalmax,
$Qcal_{min}$ = minimum quantized calibrated pixel value,
$Qcal_{max}$ = maximum quantized calibrated pixel value,
M_L = band specification multiplicative rescale factor (Radiance _Add_Band_X) and
A_L = band specification additive rescale factor (Radiance _ Add_Band_X) (USGS, 2001).

Compute Land Surface Temperature (Kelvin)

The spectral radiance (Lλ) values of Landsat 7 and 5 of the years 2001 and 2011 were converted to the temperatures (in Kelvin) (USGS, 2001) using Equation 8. Similarly, the Landsat 8 OLI_TRS data for the year 2019 were converted using Equations 8 and 9. The values obtained using these equations are presented in Table 4.

Landsat 5/7

$$BT = \frac{K2}{\left(\frac{k1}{L\lambda} + 1 \right)} \quad (8)$$

Landsat 8

$$T = \frac{BT}{\left[1 + \left(\lambda * BT / c2 \right) * \ln(e) \right]} \quad (9)$$

where
BT = at-satellite brightness temperature (K),
T = Brightness temperature to land surface temperature (K),
λ = wavelength of emitted radiance (Landsat 8 Band 10 = 10.60 – 11.19, Band 11 = 11.50 – 12.51),
Lλ = DN-to-radiance conversion value,
K1 = band-specific thermal conversation constant (K1_ Constant _Band_x),
K2 = band-specific thermal conversation constant (K2_ Constant _Band_x),
c2 = h*c/s = 1.4388* 10-2 m K = 14388 μm,
e = emission,
h = Planck's constant = 6.626176*10-34 J s,
s = Boltzmann constant =1.38*10-23 J/K and
c = velocity of light = 2.998*108 m/s.

Converted Kelvin to Centigrade

The temperature in Kelvin was converted to the temperature in Celsius [19] using Equation 10

Temperature (°C) = Temperature (Kelvin) - 273.15 (10)

RESULTS

Spatio-temporal land use land cover change detection (2001, 2011 and 2019)

Several techniques are available for assessing spatio-temporal changes in the land use land cover of any

Table 3. Related value for DN to radiance conversion

Data	L_{max}	L_{min}	$Qcal_{max}$	$Qcal_{min}$	M_L	A_L
Landsat7	17.040	0.00	255	1	-	-
Landsat5	15.303	1.23	255	1	-	-
Landsat8	-	-	65535	1	3.3420E-04	0.10000

Table 4. Related value for Spectral radiance (Lλ) to temperature conversion

Data	Date	Constant 1-K1	Constant 2-K2
Landsat 7	3rd May 2001	666.09	1282.71
Landsat 5	7th May 2011	607.76	1260.56
Landsat 8	29th May 2019	774.8853 / 480.89	1321.0789 / 1201.14

area and a useful post-classification change detection technique was selected for the present study. The easiest technique was selected. Multi-sensor or multi-temporal images provide better results after reducing the atmospheric, sensor and environmental impacts (Hussain et al. 2013). In this study, reclassified fractional images of three years (2001, 2011 and 2019) were used to monitor the spatial changes in the MKDA planning area. Supervised classification method was used to generate land use land cover maps (with accuracy assessment), as shown in Table 5. The total extent of the study area was 596.76 sq. km. The proportion of agricultural land was 55% and that of active agricultural land was 11%, as indicated by the classification. Both agricultural land and active agricultural land were widely distributed throughout the planning area (Table 6). The extent of the urbanized area has increased from 6.79% (40.39 sq. km) to 11.6% (69.2 sq. km) between 2001 and 2011 and between 2011 to 2019 it has further increased up to 17.22% (102.79 sq. km). Also, the vegetation cover has decreased from 6.72% (40.08 sq. km) to 3.29% (19.63 sq. km) between the years 2001 and 2019. This is the clearest cause of the increased LST.

Retrieval of Land Surface temperature (LST)

The remote sensing technique can be used to assess and map the LST of any study area. The LST maps of May show that there has been a tremendous change in the spatial pattern of the temperature from 2001 to 2019 (Fig. 4). The details of the temperature ranges (2001, 2011 and 2019) of the area are provided in Table 7 and Fig. 5. The lowest temperatures (<25°C) in 2001 were mainly confined to the central and northern parts of the study area, adjacent to the river and forested areas. In the year 2011, the lowest temperature increased by almost 1°C. This temperature was mainly confined to the north-eastern part of the study area. In 2019, the minimum temperature increased by nearly 4°C (to 28.13°C) and surpassed the

Table 5. Result of the accuracy assessment of land use/land cover classification

LULC Classes	3rd May 2001		7th May 2011		29th May 2019	
	User's	Producer's	User's	Producer's	User's	Producer's
AF	81.72	96.20	67.62	86.67	67.68	95.71
FL	83.33	47.62	60.00	78.33	100	54.76
CL	66.67	50.00	57.50	50.00	89.66	54.17
Forest	94.12	94.12	83.33	100	92.00	95.83
River	0.00	0.00	100	79.87	100	100
Sand	100	100	92.31	80.00	100	75.00
Set	88.89	80.00	81.25	86.67	84.00	100
Veg	71.43	62.50	84.62	73.33	85.71	100
WB	100	50.00	100	80.00	100	100
Indus	0.00	0.00	88.24	100	100	100
Overall accuracy (%)	83.33		81.48		81.60	
Kappa Index	0.7394		0.7185		0.7718	

Table 6. Area distribution of land use/land cover classification of the study area

Class Name	2001 (sq.km)	Area %	2011 (sq.km)	Area %	2019 (sq.km)	Area %
AF	328.91	55.12	207.08	34.70	225.93	37.86
FL	62.46	10.47	70.73	11.85	80.4	13.47
CL	23.98	4.02	119.35	20.00	71.14	11.92
Forest	76.39	12.80	75.56	12.66	65.35	10.95
River	4.84	0.81	3.73	0.63	5.01	0.84
Sand	7.36	1.23	8.29	1.39	7.07	1.18
Set	40.39	6.77	69.2	11.60	102.79	17.22
Veg	40.08	6.72	29.38	4.92	19.63	3.29
WB	8.67	1.45	5.76	0.97	10.04	1.68
Indus	3.68	0.62	7.68	1.29	9.4	1.58
Total	596.76	100	596.76	100	596.76	100

highest temperature of 2001 and 2011. The LST map of May 2019 (Fig.4) shows the temperature increase in the north-eastern, south-western and western parts. The highest temperature of 2019 was not confined to built-up or urban land (Midnapore and Kharagpur municipalities). Instead, it was observed in seasonal agricultural fallow land, fallow land, industrial land and riverside sand areas. There is a remarkable similarity between the patterns of the areas where the temperature was relatively high and the areas where the surface was impervious. The low-temperature areas mainly corresponded to vegetated land. The different temperatures of the built-up area and the semi-urban regions indicate the effect of the urban heat island.

Inter-relationship between LST and each LULC classes

The present study shows that Midnapore and Kharagpur municipalities and their peripheral areas experienced rapid change during 2001–2019. The growth of urban areas was found to be closely related to LULC changes. The primary cause of these changes was the increasing population density, especially in the peri-urban areas. This change played an important role in controlling the micro-climate of the study area. The expansion of the industrial area and the built-up area affected the summer temperature, which aggravated the greenhouse effect.

It was found that that there is a trend in the LST changes over time in the study area and that it is related to the land

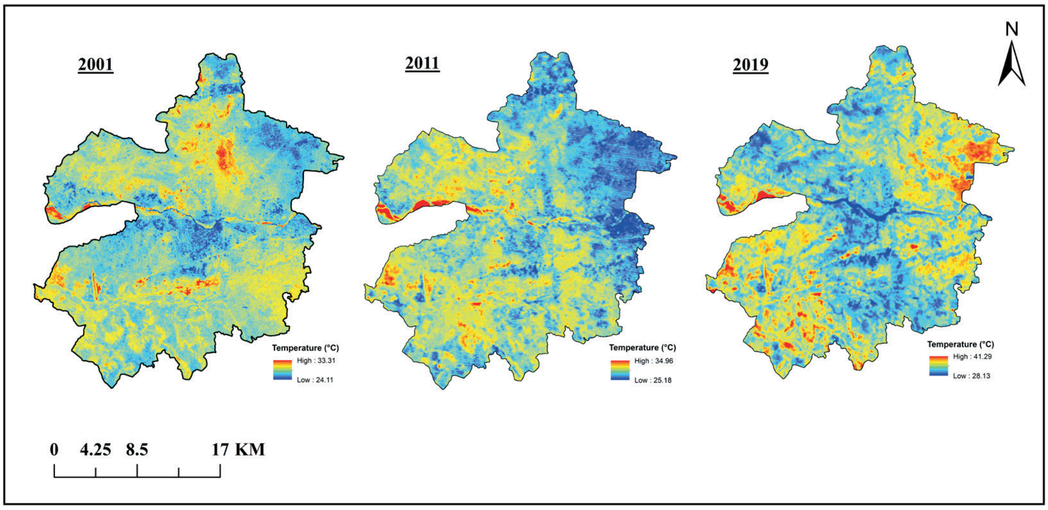

Fig. 4. Spatio-temporal pattern of LST 2001, 2011 & 2019

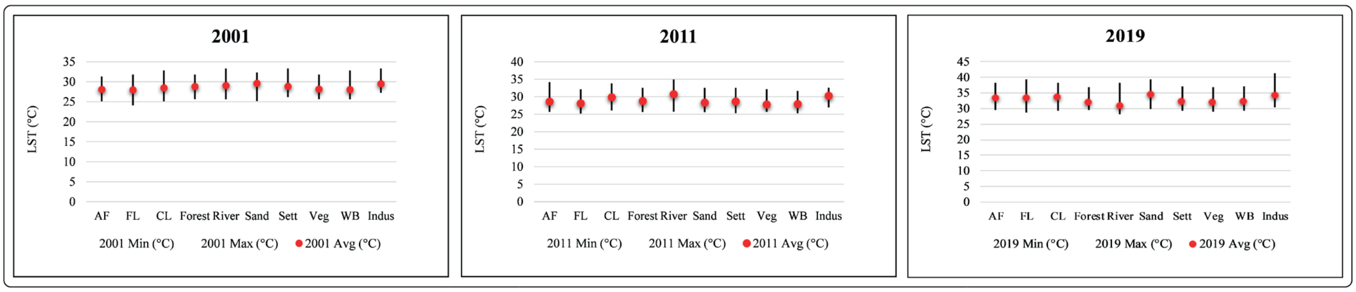

Fig. 5. LULC and the LST range 2001, 2011 & 2019

Table 7. LST for each LULC category

Class Name	3rd May 2001		7th May 2011		29th May 2019	
	Min (°C)	Max (°C)	Min (°C)	Max (°C)	Min (°C)	Max (°C)
AF	25.12	31.31	25.68	34.20	29.65	38.29
FL	24.11	31.82	25.18	32.10	28.76	39.36
CL	25.09	32.82	26.06	33.80	29.33	38.26
Forest	25.64	31.82	25.63	32.52	29.58	36.97
River	25.16	32.32	25.61	32.51	28.13	38.31
Sand	25.63	33.31	25.72	34.96	29.93	39.24
Set	26.15	33.31	25.29	32.51	29.16	37.08
Veg	25.64	31.81	25.68	32.14	29.04	36.95
WB	25.61	32.81	25.27	31.68	29.21	37.23
Indus	27.21	33.4	26.97	32.57	30.35	41.29

use and land cover categories (Fig. 6). The relationship between LULC category and LST was analyzed to identify the role of the surface type in the micro-climate. Some areas of interest (AOI) (Fig. 7) were selected to identify the relation between the LST and LULC changes. It was found that the changes in LULC from 2001 to 2019 affected the LST. The temperatures of the settlement, sand, fallow land and other categories increased gradually. The increasing trend of LST is shown in Fig. 8. It can be seen that the extent of the built-up surface (Fig. AOI 1) increased gradually, from 0.38 sq. km (2001) to 1.79 sq. km (2019). Similarly, the LST of the built-up area increased from 30.69°C (2001) to 39.31°C (2019). From Fig.8 (AOI 2) it can be seen that in 2001 in the outer part of Midnapore Municipality only small part of the area (0.72 sq. km) corresponded to settlements, but it has rapidly increased to 1.83 sq. km in 2019, while the LST also increased from 27.88°C to 39.89°C within 8 years.

In Fig. 8 (AOI 3), the most important industrial zone of the MKDA planning area is presented. In 2001 there was agricultural fallow land, but it turned into the industrial zone in 2011 (2.08 sq. km), the extent of which has gradually increased (2.14 sq. km in 2019). Similarly, the changes in the agricultural fallow land to industrial area caused the LST to change from 28.53°C (2001) to 38.52°C (2019).

Correlation between LST and NDVI

Random points were generated to show the relationship between the LST and NDVI. A negative correlation was found between LST and NDVI (Fig. 9), with R^2 = 0.1173,

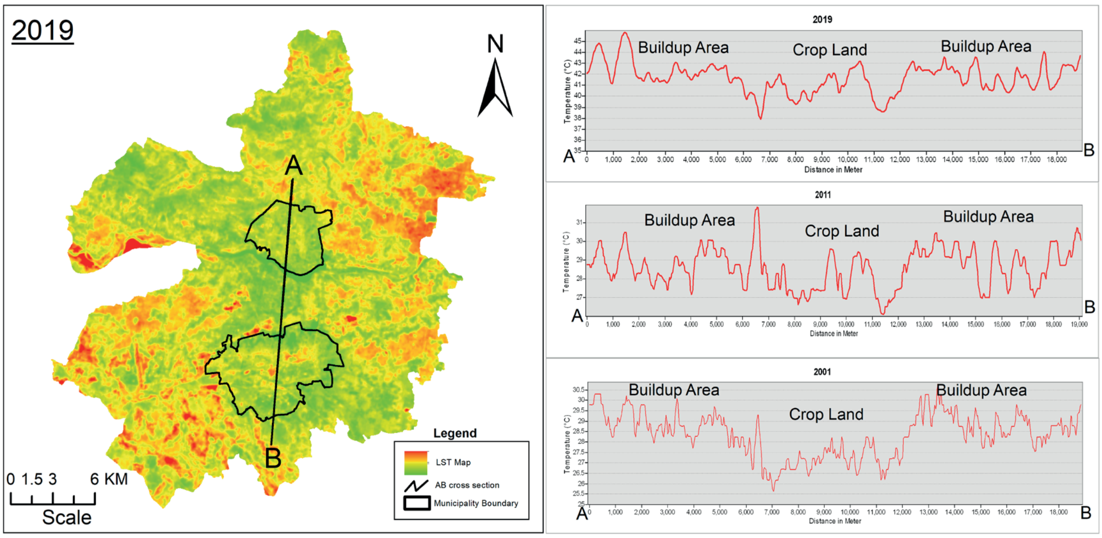

Fig. 6. LST profile of 2001, 2011 & 2019

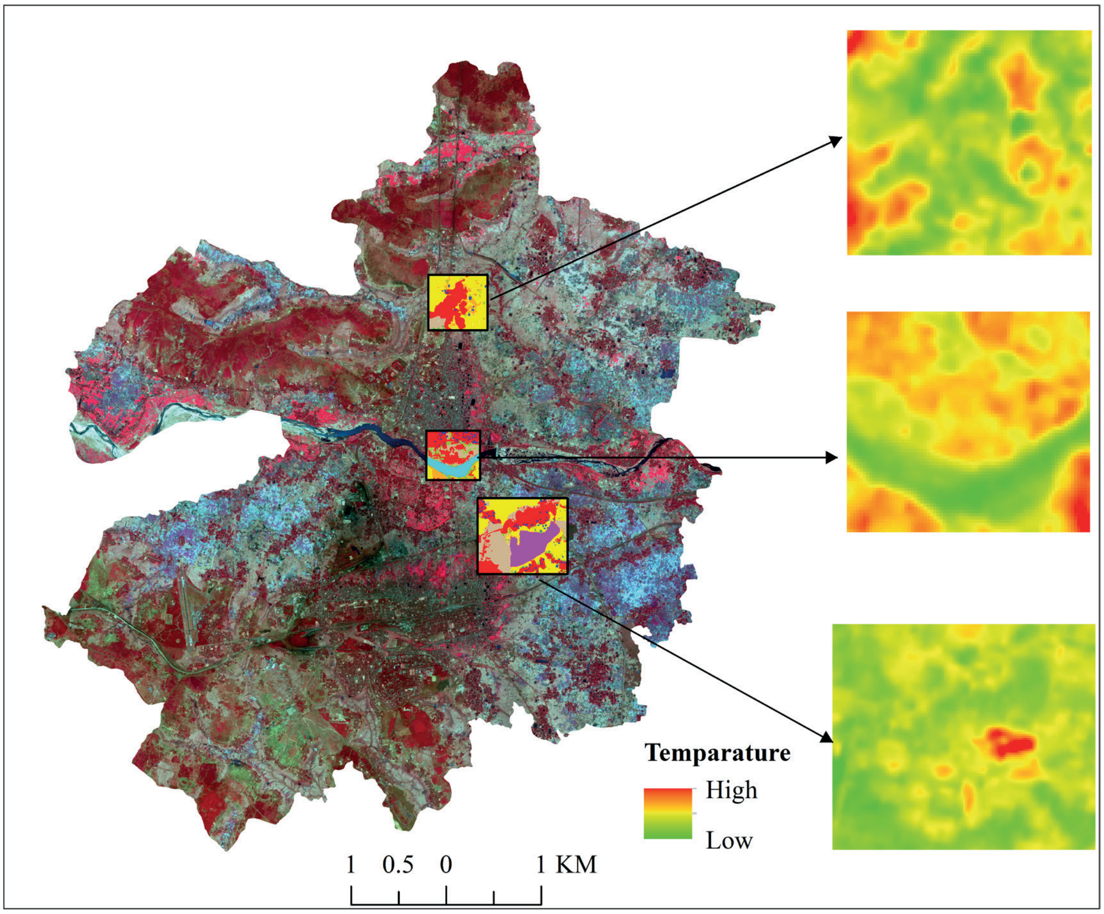

Fig. 7. Selection of the Areas of Interest

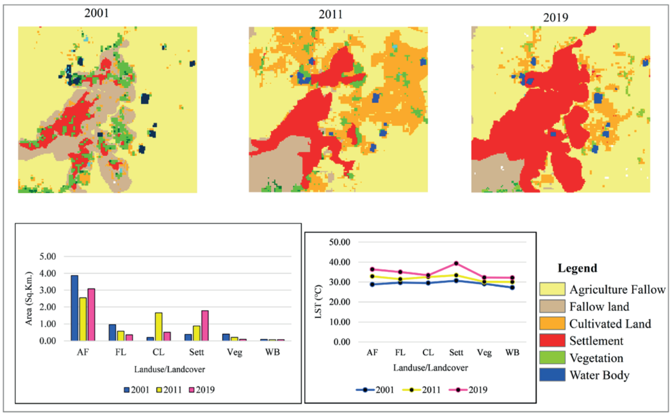

Fig. AOI 1

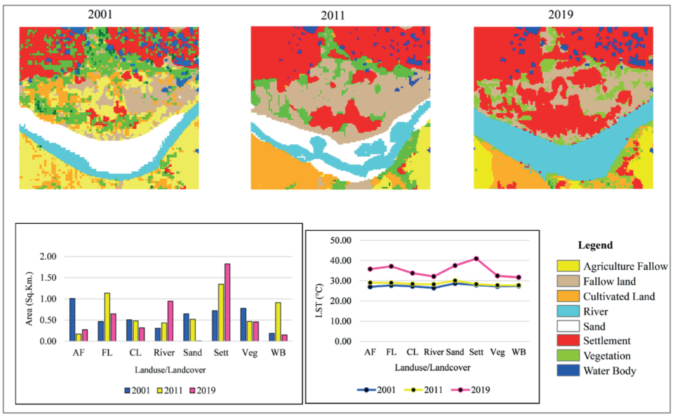

Fig. AOI 2

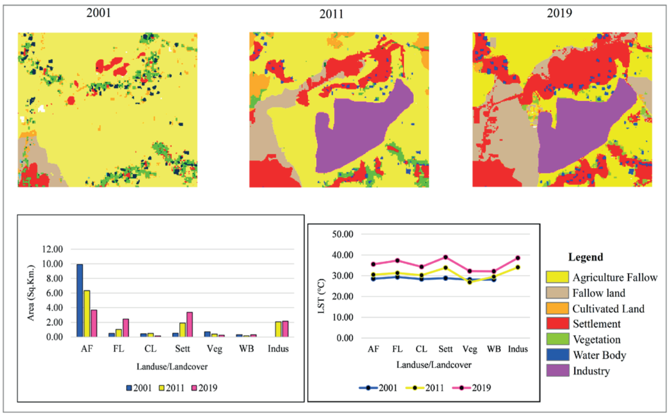

Fig. AOI 3

Fig. 8. Temporal increase of temperature in different areas over time 2001, 2011 & 2019

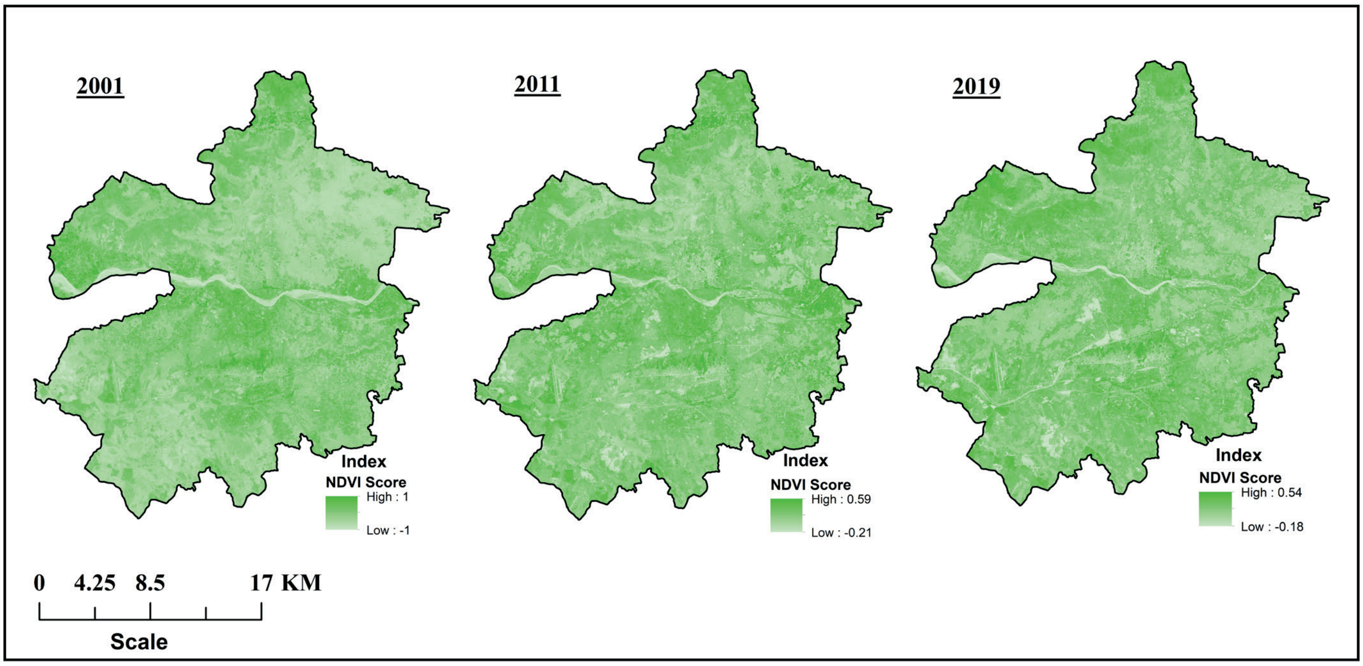

Fig. 9. NDVI classes of 2001, 2011 & 2019

0.1955 and 0.3635 in 2001, 2011 and 2019, respectively (Fig.10). The lower LST corresponded to the higher NDVI values. In 2001, the NDVI score varied between -1 and 1; in 2011 the score ranged between -0.21 and 0.59 and in 2019 it increased and ranged between -0.18 and 0.54. So, it can be said that the LST increased in the urban area over time. The results indicate that the relation between NDVI and LST is negative, with the R2 value of 0.1173 in 2001, which increased to 0.3635 in 2019.

CONCLUSIONS

Remote sensing techniques were used in this study to identify the spatio-temporal pattern of the LULC change and how this pattern impacts the LST in the MKDA planning region. It was found that the MKDA planning area experienced significant changes between 2001 and 2019. The research area was classified into ten categories: Agriculture Fallow, Fallow Land, Cultivated Land, Forest, River, Sand, Settlement, Vegetation, Water Body and Industry. The percentage of the built-up or settlement

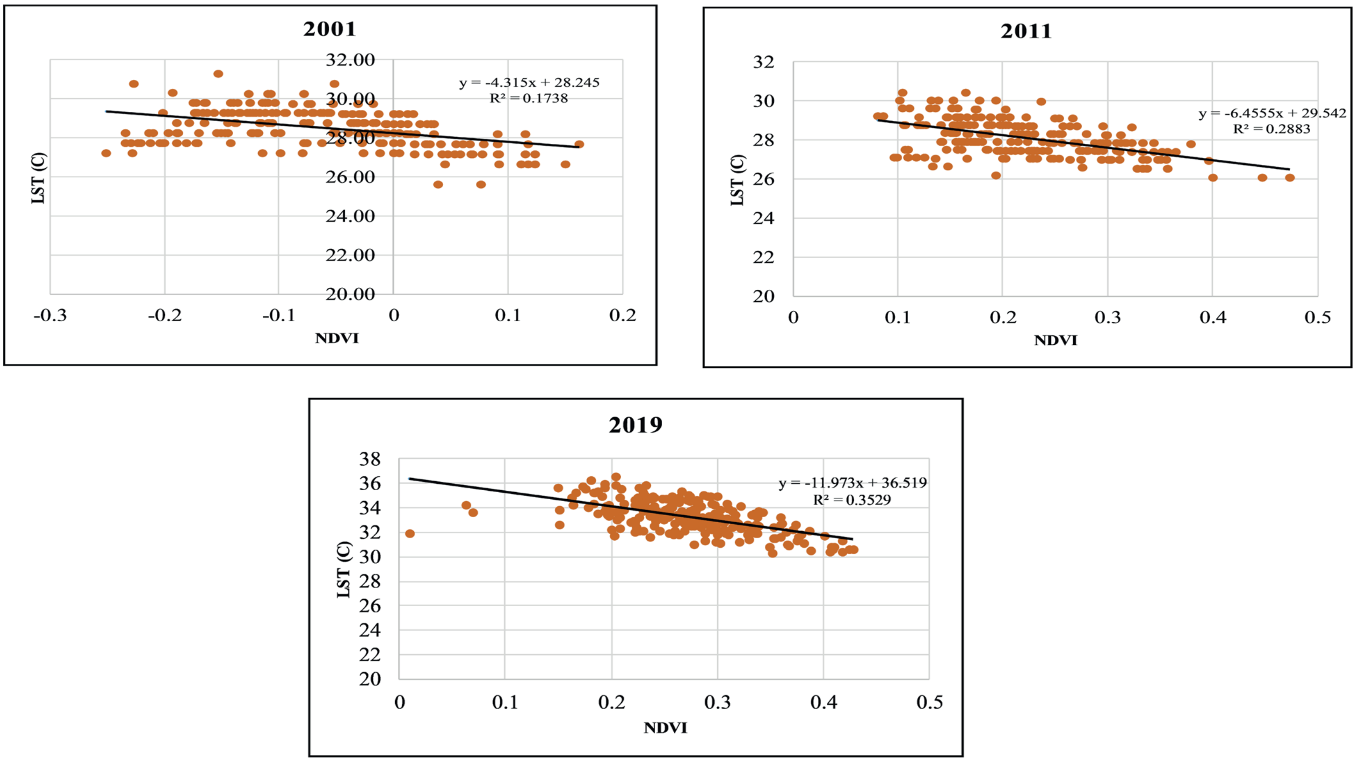

Fig. 10. Changing influence of NDVI on LST in 2001, 2011 & 2019

area increased almost three times, from 6.77% to 17.22% between 2001 to 2019. The area under this category grew particularly in the periphery of Midnapore and Kharagpur municipalities through the conversion of low-density built-up area, agricultural fallow, fallow land, etc. The extent of the industrial area and fallow land has also increased (from 0.62% to 1.58% and from 10.47% to 13.47%, respectively) through the transformation of agricultural fallow land. The extent of the forest areas and vegetation decreased by 1.85% and 3.43%, respectively. There is a strong relationship between the LULC and LST. This study found that the LST value varies depending on the LULC category. The radiant temperature in fallow land, sand and built-up areas has increased. The temperatures were higher not only in settlement or built-up areas but also in industrial areas and on riverside sand. From 2001 to 2019, the mean LST of the whole study area increased remarkably. This increasing trend of the LST can be explained by the growth of the built-up area, especially in the regions around Kharagpur and Midnapore municipalities.

REFERENCES

Ahmad A. and Quegan S. (2016). Analysis of Maximum Likelihood Classification on Multispectral Data, (January 2012).

Alavipanah S.K. et al. (2007). Land Surface Temperature in the Yardang Region of Lut Desert (Iran) Based on Field Measurements and Landsat Thermal Data, Journal Agriculture Science Technology, 9, 287-303.

Amiri R. et al. (2009). Spatial-temporal dynamics of land surface temperature in relation to fractional vegetation cover and land use/cover in the Tabriz urban area, Iran, Remote Sensing of Environment. Elsevier Inc., 113(12), 2606-2617, DOI: 10.1016/j.rse.2009.07.021.

Anandababu D., Purushothaman B. M. and Dr. S. Suresh Babu (2018). Estimation of Land Surface Temperature using LANDSAT 8 Data, INTERNATIONAL JOURNAL OF ADVANCE RESEARCH, IDEAS AND INNOVATIONS IN TECHNOLOGY, 4(2), 177-186.

Baba I.I. (2016). ESTIMATION OF LAND SURFACE TEMPERATURE OF KADUNA METROPOLIS, NIGERIA USING LANDSAT IMAGES, 11(3), 36-42.

Bokaie M. et al. (2016). Assessment of Urban Heat Island based on the relationship between land surface temperature and Land Use/Land Cover in Tehran, Sustainable Cities and Society. Elsevier B.V., 23, 94-104, DOI: 10.1016/j.scs.2016.03.009.

Buyadi S.N.A., Mohd W.M.N.W. and Misni A. (2013). Impact of Land Use Changes on the Surface Temperature Distribution of Area Surrounding the National Botanic Garden, Shah Alam, Procedia – Social and Behavioral Sciences. Elsevier B.V., 101, 516-525, DOI: 10.1016/j.sbspro.2013.07.225.

Chen S.P., Zeng S. and Xie C.G. (2000). Remote sensing and GIS for urban growth analysis in China, Photogrammetric Engineering and Remote Sensing, 66(5), 593-598, DOI: 10.1007/978-94-007-4698-5.

Congalton R.G. (1991). A Review of Assessing the Accuracy of Classifications of Remotely Sensed Data, 46 (October 1990), 35-46.

Congalton R.G. (1991). A Review of Assessing the Accuracy of Classifications of Remotely Sensed Data, 46(October 1990), 35-46.

Fatema S. and Chakrabarty A. (2020). Accident Hotspot Identification on the Midnapore Kharagpur Development Authority Planning Area, (2), 169-174, DOI: 10.35940/ijrte.B3351.079220.

Fu P. and Weng Q. (2016). A time series analysis of urbanization induced land use and land cover change and its impact on land surface temperature with Landsat imagery, Remote Sensing of Environment. Elsevier Inc., 175, 205-214, DOI: 10.1016/j.rse.2015.12.040.

Ghulam A. and Louis S. (2010). Calculating surface temperature using Landsat thermal imagery, 1-9.

Guha S., Govil H. and Diwan P. (2020). Monitoring LST-NDVI Relationship Using Premonsoon Landsat Datasets, 2020(1).

Hussain M. et al. (2013). ISPRS Journal of Photogrammetry and Remote Sensing Change detection from remotely sensed images: From pixel-based to object-based approaches, ISPRS Journal of Photogrammetry and Remote Sensing. International Society for Photogrammetry and Remote Sensing, Inc. (ISPRS), 80, 91-106, DOI: 10.1016/j.isprsjprs.2013.03.006.

James M.M. and Mundia C.N. (2014). Dynamism of land use changes on surface temperature in Kenya: a case study of Nairobi City. International Journal of Science and Research, 3(4), 38-41.

Jiang J. and Tian G. (2010). Analysis of the impact of Land use/Land cover change on Land Surface Temperature with Remote Sensing, Procedia Environmental Sciences, 2(5), 571-575, DOI: 10.1016/j.proenv.2010.10.062.

Kayet N. et al. (2016). Spatial impact of land use / land cover change on surface temperature distribution in Saranda Forest, Jharkhand, Modeling Earth Systems and Environment. Springer International Publishing, 2(3), 1-10, DOI: 10.1007/s40808-016-0159-x.

Kustas W. and Anderson M. (2009). Agricultural and Forest Meteorology Advances in thermal infrared remote sensing for land surface modeling, 149, 2071-2081, DOI: 10.1016/j.agrformet.2009.05.016.

Latif S. (2014). Land Surface Temperature Retrival of Landsat-8 Data Using Split Window Algorithm – A Case Study of Ranchi District, 2(4), 3840-3849.

Li S. and Jiang G.M. (2018). Land Surface Temperature Retrieval from Landsat-8 Data with the Generalized Split-Window Algorithm, IEEE Access. IEEE, 6, 18149-18162, DOI: 10.1109/ACCESS.2018.2818741.

Lillesand T., Kiefer R.W. and Chipman J. (2015). Remote sensing and image interpretation. John Wiley & Sons.

Lv Z. Q. and Zhou Q.G. (2011). Utility of Landsat image in the study of land cover and land surface temperature change, Procedia Environmental Sciences, 10(PART B), 1287-1292, DOI: 10.1016/j.proenv.2011.09.206.

Mallick J., Kant Y. and Bharath B.D. (2008). Estimation of land surface temperature over Delhi using Landsat-7 ETM +, (August).

Nguyen Q.K., et al. (2019). Land Surface Temperature Dynamics In Dry Season 2015-2016 According To Landsat 8 Data In The South-East Region of Vietnam, Geography, Environment, Sustainability, 12(1), 75-87, DOI: 10.24057/2071-9388-2018-06.

Renssen H., et al. (2005). Simulating the Holocene climate evolution at northern high latitudes using a coupled atmosphere-sea ice-ocean-vegetation model, 23-43, DOI: 10.1007/s00382-004-0485-y.

Reuter D.C., et al. (2015). The thermal infrared sensor (tirs) on landsat 8: Design overview and pre-launch characterization, Remote Sensing, 7(1), 1135-1153, DOI: 10.3390/rs70101135.

Rozenstein O., et al. (2014). Derivation of Land Surface Temperature for Landsat-8 TIRS Using a Split Window Algorithm, 5768-5780, DOI: 10.3390/s140405768.

Saradjian M.R. and Jouybari-Moghaddam Y. (2019). Land Surface Emissivity and temperature retrieval from Landsat-8 satellite data using Support Vector Regression and weighted least squares approach, Remote Sensing Letters. Taylor & Francis, 10(5), 439-448, DOI: 10.1080/2150704X.2019.1569273.

Satiprasad S. (2013). Monitoring urban Land use land cover change by Multi-Temporal remote sensing information in Howrah city, India, International Research Journal of Earth Sciences, 1(5), 1-6.

Southworth J. (2010). An assessment of Landsat TM band 6 thermal data for analysing land cover in tropical dry forest regions, 1161, DOI: 10.1080/0143116031000139917.

USGS (2001). Landsat 7 Science Data Users handbooks.

Wan Z. and Li Z. L. (2010). Radiance – based validation of the V5 MODIS land – surface temperature product, 1161, DOI: 10.1080/01431160802036565.

White-Newsome J.L., et al. (2013). Measurements: A Public Health Perspective, 121(8), 925-931.

RESEARCH PAPER

CALIBRATION OF REGIONAL VULNERABILITY FUNCTIONS BY APPLYING EARTHQUAKE EVENTS DATABASE

Nina I. Frolova[1*], Valery I. Larionov[1,4], Jean Bonnin[2], Sergey P. Sushchev[3], Alexander N. Ugarov[4]
[1]Institute of Environmental Geosciences, Russian Academy of Sciences, Ulansky per. 13, Moscow, 101000, Russia
[2]Institut de Physique du Globe, University of Strasbourg, Strasbourg F-67084, France
[3]Extreme Situations Research Center, Vyatskaya str. 35, Moscow, 127015, Russia
[4]Bauman Moscow State Technical University, 2-nd Baumanskaya, 5, Moscow, 105005, Russia
*Corresponding author: frolovanina7@gmail.com
Received: May 21th, 2019 / Accepted: November 20th, 2020 / Published: December 31st, 2020
https://DOI-10.24057/2071-9388-2020-97

ABSTRACT. The paper describes the structure and content of the Information System database containing information on earthquake events, which is developed and supported within the framework of computer support for the EMERCOM of the Russian Federation. The database is assigned to provide analytical support for decision making in case of an emergency situation, including tools for mathematical simulation of hazardous excitation, the response of elements at risk to excitation and loss generation. The calibration procedure of the earthquake vulnerability functions for buildings and structures using the database with descriptions of events is presented. The calibrated functions of earthquake vulnerability for buildings of different types are applied to provide an acceptable accuracy of situational assessments for the case of a strong earthquake. The examples of earthquake damage estimations for the test site in Siberia showed that region-specific parameters in the vulnerability functions yield more reliable results to estimate possible damage and losses due to a large earthquake. For Irkutsk City, the estimates of the numbers of heavily damaged and completely collapsed buildings obtained when using different sets of parameters for vulnerability functions differ by 30%. Such difference in damage estimates can significantly affect the plans for rescue and recovery operations. The conclusion is made about the advantage of the calibrated functions application for near real-time damage and loss assessment due to strong earthquakes in order to ensure population safety and territory sustainable development.

KEY WORDS: earthquakes, reliability of near real time loss estimates, impact database, calibration of mathematical models for vulnerability of buildings and structures

CITATION: Nina I. Frolova, Valery I. Larionov, Jean Bonnin, Sergey P. Sushchev, Alexander N. Ugarov (2020). Calibration Of Regional Vulnerability Functions By Applying Earthquake Events Database. Geography, Environment, Sustainability, Vol.13, No 4, p. 54-64 https://DOI-10.24057/2071-9388-2020-97

ACKNOWLEDGEMENTS: The research was carried out for the state projects No. AAAA-A19-119021190077-6 and No. 175-11-2019-087 dated 18.12.2019 (Resolution № 218 of 09.04.2010, the Ministry of science and higher education).

The authors thank the editor and the anonymous reviewer who read the paper and provided helpful comments for improvements. We thank our colleagues for continuous support and discussion of different steps of EMERCOM IS database development and its application for the calibration of Extremum System mathematical models. Special thanks are extended to the staff of Extreme Situations Research Center for their contribution to the development of GIS environment and colleagues in Institute of the Earth Crust of RAS for fruitful cooperation. Also, we wish to acknowledge the helpful comments by Dr. A. Petrosyan

Conflict of interests: The authors reported no potential conflict of interest.

INTRODUCTION

In Russia, as in the world in general, great attention is paid to the protection of people from natural and manmade disasters within the framework of the Sendai Framework for Disaster Risk Reduction 2015–2030 (https://www.unisdr.org/files/43291.pdf). Earthquakes, their secondary environmental effects (https://www.isprambiente.gov.it/files/progetti/inqua/esi-eee-volume-april-2012.pdf) and manmade phenomena are the most frequent factor to cause casualties and considerable economic losses. According to the statistical data supplied by international agencies and reinsurance companies, there is a growing number of natural disasters and increasing associated economic and social impact due to uncontrollable urbanization of territories and an insufficient amount of prevention measures. According to the data supplied by the Centre for Research on the Epidemiology of Disasters (http://www.emdat.be), the years 1900–2015 saw an increasing rate of earthquake disasters and associated social and economic losses. The rate of casualties varies over the years in a periodic manner, peaking at the earthquakes in China (1976), Indonesia (2004), and in Haiti (2010). Earthquakes and associated manmade accidents and environmental effects continue to be the leading events in terms of casualties.

The world statistics of casualties and injured due to strong earthquakes shows that more than a half of all people under collapsed buildings (55%) died during the first three days (Goncharov et al. 2009). The first six hours are fatal for 60% of those who have suffered heavy injuries critical for survival. The number of casualties can be considerably reduced by timely and appropriate measures by rescuers (Aleksandrov et al. 2019). Fast and reliable information on a situation is necessary for making proper decisions about search-and-rescue operations and measures to be taken to provide humanitarian aid during the first hours following an event. In Russia, as in many other countries worldwide, a near real-time reliable forecasting of losses is based on the use of information systems (IS) such as the Automated Information Management System of the Russian Unified Emergency Prevention and Response System, the Russian abbreviation to be used in what follows being AIUS RSChS (Izmalkov 2017a, b; Kachanov et al. 2011; 2014). The efficiency of an IS is supported by high reliability in the fast prediction of the current situation based on data contained in the AIUS RSChS database of events. These data are used to calibrate the software that is employed in the assessments of situations, including models for the behavior of various buildings under seismic excitation. It is supposed that timely and reliable estimates of possible losses accelerate the response of decision making and reduce the time people stay in the hit zone, which allows to reduce the losses.

We provide a brief description of the structure and contents of database on events as recorded by the Ministry of the Russian Federation for Civil Defence, Emergencies and Elimination of Consequences of Natural Disasters (EMERCOM) using the AIUS RSChS. The procedure for applying the database to calibration of an earthquake vulnerability model and examples to illustrate the enhancement of earthquake-related loss assessment based on calibrated models are given.

A BRIEF DESCRIPTION OF THE DATABASE ON EVENTS RECORDED BY AIUS RSCHS

The database that stores descriptions of events is part of the AIUS RSChS data storage that is developed and supported within the framework of computer support for the EMERCOM of the Russian Federation. For instance, for earthquakes, the information includes magnitude, epicenter coordinates, source depth, seismic intensity, macroseismic data, as well as resources and forces used for the response. In addition to the data storage, the AIUS RSChS also includes software that consists of numerous units and interfaces. The development of this system relied on using Web-technology from Microsoft, in particular «.NETCORE and C #» (https://docs.microsoft.com/ru-ru/dotnet/core) (Izmalkov 2017a, b).

The database application fields are the following:

• storage and structuring of the documented data on disaster sources and elements at risk, for instance, information about residential buildings inventory;

• data support for forecasting the level of hazard and risk, as well as for preparing warnings, including those disseminated by mass media;

• storage of data acquired from recording the events that have been classified as emergency situations;

• data provision for the analytical support of decision making in case of an emergency situation, including tools of mathematical simulation of hazardous excitation, the response of elements at risk to excitation and loss generation;

• data provision for risk assessment and identification of risk zones;

• data provision for preparing reports on the situation, weather conditions, forces and equipment involved, as well as losses.

The generalized AIUS RSChS block diagram (Fig. 1) includes principle functional units, the data storage, and a user interface, as described in detail by Kachanov et al. (2011; 2014). The principle units are «Inventory», «Analytics» and «Operational management». The names of the units display their functions; description of units is supplemented by input and output information.

The «Analytics» unit contains mathematical models for the main types of technological accidents and natural hazards, including earthquakes and secondary processes. In the case of earthquakes, the software of the unit allows to simulate shaking intensity distribution, behavior of buildings and population, resources and forces needed for rescue and other urgent operations. The computations may be made just after the event, as well as for expected future «scenarios». The models are specific in that they are required to have high response speeds to input the data and the forecasting results have to be protected from the influence of possible considerable uncertainties. The uncertainties in input data arise from the estimation of parameters, their measurement, and transmission (Frolova et al. 2018).

An acceptable accuracy for the simulation results is achieved by calibrating the mathematical models in the «Analytics» unit specifically to a location of interest. Areas are mapped, and for each area there is a specific set of calibration parameters in the mathematical models. For example, for the shaking intensity

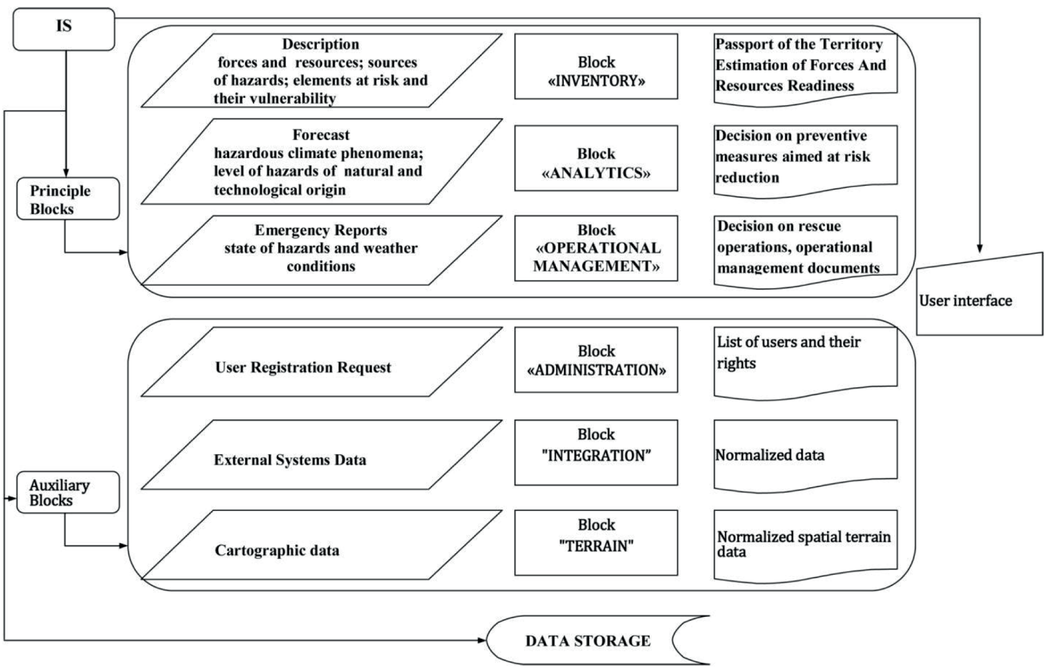

Fig. 1. Structure of EMERCOM Information System

simulation model these parameters are: regional coefficients in the Shebalin macroseismic field equation (Shebalin 1977); the orientation of the elliptic isoseist axes; the ratio k of the major and minor axes of macroseismic field ellipse (Frolova et al. 2019). The calibration of this kind satisfactory mimics learning processes for artificial intelligence systems. After calibration, any mathematical model that is implemented as a software module first determines the area of its calibration and retrieves the values of area-specific calibration parameters. The next step is the assessment itself.

All area-specific calibration parameters specific to areas and software modules are stored in the AIUS RSChS storage. Figure 2 shows the structure of the storage and the locations of the tables that contain calibration data in this structure.

The thicker line in Fig. 2 indicates the «Database with descriptions of events» and databases with «Zones with stable calibration parameters of mathematical models». These zones are formed during the calibration of the mathematical models. Each zone has its own mathematical model and its own set of calibration parameters.

It should be noted that the description of seismic events has some features that are important for calibrating simulation models used to assess earthquake-related losses during different phases of the simulation following the SP 322.1325800.2017 «Buildings and structures in seismic region. Rules of inspection of consequences of the earthquake» approved by the Ministry of Construction of Russia (https://files.stroyinf.ru/Index2/1/4293739/4293739217.htm).

The structure of the tables with descriptions of seismic events is displayed in Fig. 3. A structured description of a seismic event can be accompanied by various appended unstructured information like maps, tables, photographs, and other documents. The calibration of a mathematical model for predicting the behavior of various buildings is based on data related to observed damage (Berzhinski et al. 2008, 2009; Berzhinskaya et al. 2009) in the form of damage tables.

When a strong earthquake is in question, the records in the damage table (Fig. 3) can be supplemented with the following materials of field observations and their analyses:

A map of observed macroseismic effects where the isoseismals show the area subject to shaking of intensity 6, 7, 8 or greater on the MMSK-86 scale (Shebalin et al. 1986);

photographs of damage inflicted to buildings of various types;

summarized tables of macroseismic effects at population centers based on a variety of factors, including the behavior of buildings, human response, and the state of household objects;

updated information on the condition of residential buildings, on the numbers of residents in buildings of various types (type of building, total and residential area, number of residents, construction year, the degree of wear, and so on) (Berzhinski et al. 2008, 2009).

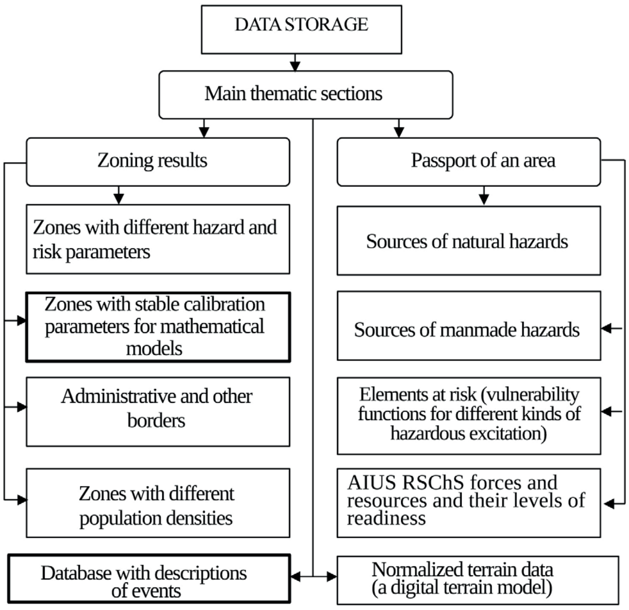

Fig. 2. The structure of the AIUS RSChS storage

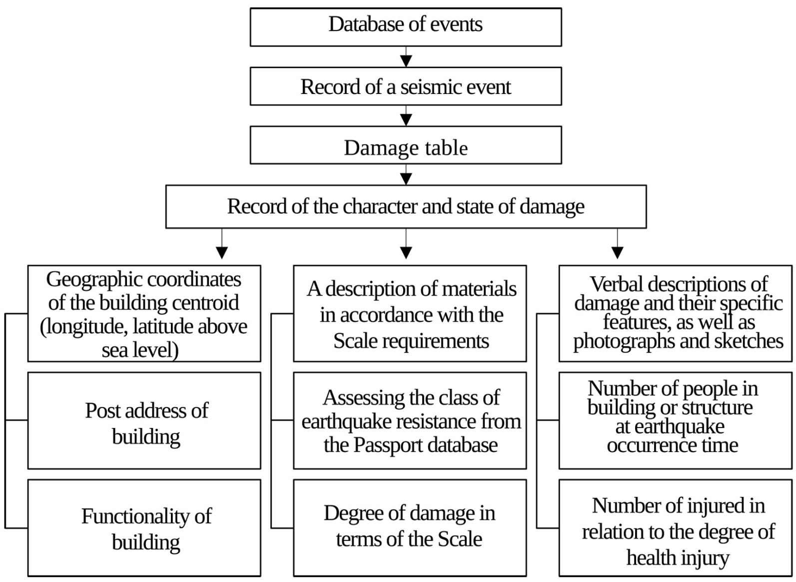

Fig. 3. The structure of tables with descriptions of events in the data base of events

CALIBRATION PROCEDURE OF THE EARTHQUAKE VULNERABILITY FUNCTIONS FOR RESIDENTIAL BUILDINGS

In this section, we discuss the calibration procedure for the earthquake vulnerability functions of buildings and structures using the database with descriptions of events. This procedure requires specifying the form of mathematical vulnerability model (function) used in a computer simulation.

The last decades saw great effort devoted to the development of earthquake vulnerability models. One of the key papers reviewing the methodologies over the last 30 years was written by Calvi et al. (2006). The number of types and forms for the representation of these functions as reported in the literature is steadily growing. The earliest study that proposed vulnerability matrices was (Martel 1964). These were later modified by Whitman (1973). Boore et al. (1993) specified a vulnerability function for discrete values of earthquake intensity I. All works usually adopt intensity I as a parameter to be related to damage d using a variety of approaches. This is also the case in later publications, e.g., (Braga et al. 1982; Spence et al. 1992; Di Pasquale et al. 2005). Work, done for national and international projects resulted in the development of an earthquake vulnerability model in which the state of damage is a function of both intensity and dynamic and spectral ground motion parameters (Lumantarna et al. 2014; Martinis et al. 2018; Yepes-Estrada et al. 2014; Xin et al. 2019). Taking into account the dynamic and spectral parameters of ground motion when constructing a vulnerability model allows to avoid the contradiction in the fact that the same measure, namely the observed effect, is used both for cause and consequences. Nevertheless, the use of vulnerability functions with MMSK-86 intensity I as input and the state of damage d as output based on the same scale remains rather popular today (Berzhinski et al. 2008; 2009a; 2009b; Zaalishvili et al. 2019). The difference between the input and the output is that the input is found by simulating the macroseismic field based on the laws that govern the propagation of ground motion, while the output quantity is found from physical laws that govern the excitation of buildings and structures due to ground motion. It should be noted that the measure in both of these cases is a scale, a table consisting of two columns, with the one being intensity grade I and the other the observed impact, including the reported descriptions of various state of damage d for buildings (objects) and structures. The scales consider combining buildings (objects) according to parameters that affect the vulnerability to produce vulnerability classes. This combination of objects of different designs into classes is convenient for large scale assessments of earthquake impact. The combination results in individual properties of objects being replaced with averaged values that characterize a class, while the deviations from the average are random. This allows to reduce the number of vulnerability functions, making it equal to the number of classes. The parameters that vulnerability functions involve vary from class to class, as well as from one area to another. The sets of vulnerability functions chosen to serve for specific regions are referred to here as regional families characterized by sets of regional parameters. The use of regional parameters considerably reduces the deviation of properties for each object from the value that is typical of the appropriate class, thus enhancing the accuracy of the damage assessment.

An analysis of various ways to describe the relationship between felt intensity and the corresponding response of elements at risk has yielded main features of the vulnerability model. Each set of same-type elements has a corresponding unique vulnerability model of its own.
These elements and the relationship between them are displayed in Fig. 4.

In the analysis of this procedure, the main factors that generate the various vulnerability functions are the following: the type of input data; the manner in which the functional relationship is specified; and the form in which the result is displayed. Objects or elements at risk are generally combined into classes based on similarities among the properties that characterize their vulnerability. In that case, each individual object, assuming that it does belong to a certain class, is assigned by the vulnerability properties of that class. Descriptions of vulnerability classes can

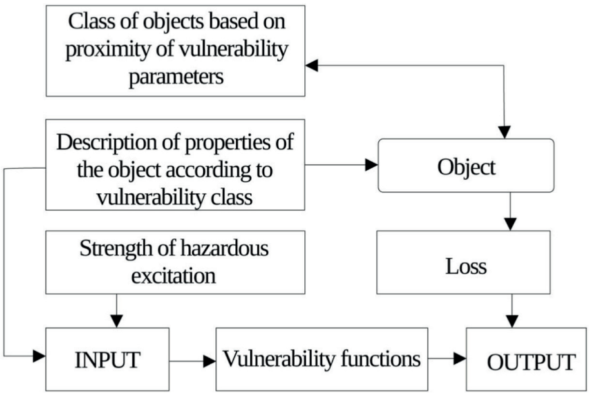

Fig. 4. The elements of the vulnerability model

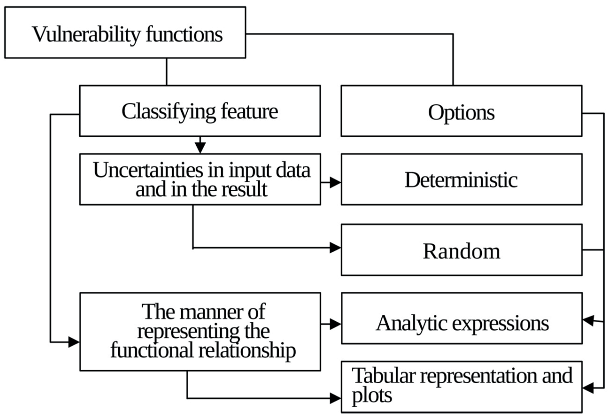

Fig. 5. The main classification parameters for vulnerability functions

be found in the scales due to (Shebalin et al. 1986; European… 1993; Sherman et al. 2003). The observed damage to a building may be expressed in different terms, but more often it is classified according to the rules specified by seismic intensity scales.

Figure 5 shows classification parameters for the vulnerability functions that are most frequently encountered in the literature.

Figure 5 shows the two main classification parameters that include the degree of uncertainty in input and output data, as well as the way the functional relationship is specified. It should be noted that random functions are used more frequently. The analytical and tabular forms of presentation are equally frequent.

The main difference between vulnerability functions consists in the way we represent the intensity-loss relationship. Vulnerability functions may be deterministic ones that use average values of the arguments, or probabilistic functions where, given values of the argument and function, we specify and/or calculate the parameters of the distribution law of random variables.

Arguments of a vulnerability function and the results can both be random. Random variables can be represented as either discrete or continuous values. Each individual case has its own distribution functions to describe the properties of discrete and continuous random variables. The probabilities of discrete random variables are usually specified in tabular form, while the probabilities of continuous random variables are specified in analytical form, with the Gauss distribution as one of the most frequent options (Aleksandrov et al. 2019).

The AIUS RSChS system contains a function of earthquake vulnerability for objects, which uses random intensity as input. The vulnerability function may be presented as a table with two fields of input. The table defines the relationship between the probability for an object to receive a certain state of damage d and an intensity I. The intensity I resulting in a state of damage d is interpreted as a continuous random variable that obeys the Gauss distribution with specified mean and variance. The intensity I for the location of an object found from Shebalin's formula (Shebalin 1968) is received by the vulnerability function as the mean and by the table where the second input is the class of vulnerability for the object. The output consists of pairs of values, characterizing the state of damage d and its probability. The first step in the calculation uses a list of pairs with all possible states of damage d and their probabilities. The pair with the highest probability is selected from the list. The state of damage d is used as the expected damage in subsequent calculations. In case the object is a block of buildings or a residential area of a population center with a uniform density of urban development rather than an individual building, the state of damage d is interpreted as the proportion of the buildings that have suffered the associated state of damage.

The calibration of a vulnerability function is limited by calculation of the mean and variance for the intensity I, which provides the most realistic estimate of the expected state of damage d for buildings that have been classified to a certain vulnerability class. The mean and variance are estimated using maximum likelihood method in relation to computed values and the data contained in the AIUS RSChS data base.

The calibration of a mathematical vulnerability model is made taking into account the relationship between the parameters in the Gauss distribution and the geographic area, as well as the boundaries to the zones where the same calibration parameters are used.

The calibration procedure is as follows. At the first step, the boundary of the area is specified depending on the properties of the used construction materials and the designs of structures, which are determined by the geographic location of the area, the level of earthquake hazard, and the level of its economic development. Next, the data related to the engineering impacts of earthquakes is collected. For each area it is necessary to have samples of estimated states of damage d with specified values of earthquake resistance of buildings and earthquake intensity I. The samples must be representative to ensure an unbiased estimate of the parameters in the Gauss distribution. This method requires that the sample mean is used as an estimate of the mathematical expectation, while the variance is determined using an unbiased estimator of the sampling values.

It can thus be said that in order to calibrate the mathematical model of earthquake vulnerability it is first necessary to obtain sufficient statistical material, which should include a number of records, which can be considered representative for the number of buildings and structures in the area subject to earthquake impact.

The more diverse are the structures in an area, and the higher the level of earthquake hazard, the greater will be the number of records required for the damage tables. The number of records on same-type buildings belonging to a certain vulnerability class affects the accuracy of the parameter estimates in a family of earthquake vulnerability functions. Nevertheless, the analysis of data on the impacts of strong earthquakes in Russia and worldwide has shown that, in spite of considerable economic and social losses, for some regions there is no exhaustive information on high states of damage d. When such cases are encountered, it becomes necessary to search for analogous regions where the impact of disastrous earthquakes has been recorded and stored with a high level of detail. The AIUS RSChS includes the possibility of record the events and produce the damage tables for any location worldwide.

In the next section, we are going to show how a database containing calibration parameters can be used in the calculating module to simulate the behavior of buildings in order to provide acceptable accuracy in situational assessments in case of a strong earthquake.

USING REGIONAL VULNERABILITY FUNCTIONS TO ENHANCE ACCURACY FOR BETTER LOSS ASSESSMENT

This section presents the results of a comparison between the earthquake impacts based on two sets of vulnerability functions; the first set was obtained through calibration, which was done following the rules given in the preceding section, while the second set consisted of generalized vulnerability functions based on extensive data on the engineering impact of earthquakes in a number of countries. The first set was applied to the test region, while the other can be used for any location in the seismic regions worldwide (Frolova et al. 2011).

The test region covers the seismic region of Baikal and Transbaikalia, which includes the large social and industrial facilities of Irkutsk Oblast, the Republic of Buryatia and adjacent areas (Fig. 6). From the calibration results the values of the regional parameters for vulnerability functions were obtained in accordance with the regional scale (Sherman et al. 2003). The scale incorporates seismological, engineering-geological, and climate-controlled construction features of the region (Berzhinski 2001). In terms of seismic zonation, the test region includes the Baikal Rift Zone which is characterized by the highest level of seismic activity; Transbaikalia with moderate seismic activity and with «transient» earthquakes emanating from the Baikal Rift Zone and Mongolia; and the southern Siberian Platform, which is practically aseismic with merely some «transient» earthquakes emanating from the Baikal Rift Zone (Berzhinski 2001). According to the review seismic zoning of the Russian Federation territory OSR-97 (Ulomov et al. 1999) the seismic intensity I which may occur in a given area within a 50-year time interval with the probability of exceedance equal to 10% (OSR-97A), 5% (OSR-97B) and 1% (OSR-97C) varies from I = V up to I = IX. Fig. 6 shows the fragment of OSR-97B map for the study area.

According to the studies of the Institute of the Earth Crust of the RAS Siberian Branch (Khromovskikh et al. 1996; Radziminovich 2003) there are few zones, which can be a possible source of a hazardous earthquake for the Irkutsk City. Their names and characteristics are given in Table 1. The value of the hypocenter depth h is estimated to be the same for all zones and equal to 15-20 km.

For the scenario earthquake, an earthquake with the epicenter located at φ= 51.7° and λ=103.6° in the East Sayan source area extending along the Main Sayan Fault was chosen. The maximum magnitude M_{max} for this zone is estimated at 8.0, with hypocentral depth h = 20 km. The impact of the scenario earthquake was calculated using the AIUS RSChS software (Extremum System) (Larionov et al. 2000; Larionov et al. 2003a; 2003b; Sushchev et al. 2010; Larionov et al. 2017).

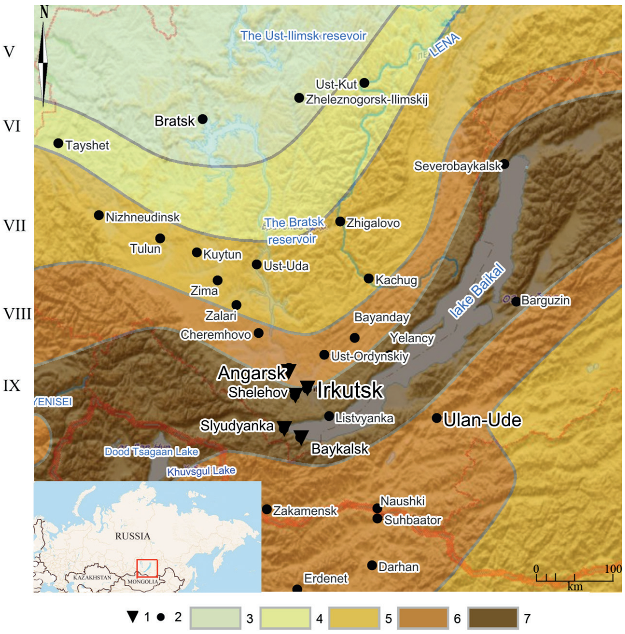

Fig. 6. The boundary of the test region modified after (Berzhinski, 2001)

1. settlements with representative buildings for vulnerability study; 2. industrial centers and transport hubs; 3. OSR-B zone with I=V; 4. OSR-B zone with I=VI; 5. OSR-B zone with I=VII; 6. OSR-B zone with I=VIII; 7. OSR-B zone with I=IX

State of damage d calculations were based on regional calibration parameters that determine earthquake vulnerability functions in accordance with the regional seismic intensity scale (Berzhinski 2001) (Table 2) and generalized vulnerability function parameters used in the AIUS RSChS for «default» calculations in any region worldwide in case no regional functions are available (Table 3). The generalized parameters were derived by processing an empirical data set on earthquake impact observations for earthquakes of intensity I greater than VI MMSK-86 grades that have occurred since the 1960s in Russia, Moldavia, Georgia, Armenia, Turkmenia, Uzbekistan, and other countries.

The impact of the scenario earthquake for the test region was found by calculating the refined parameters of N.V. Shebalin's macroseismic field model I=1.5M-3.44lg(r)+3.13 that was previously reported in (Frolova et al. 2019). The anisotropy of the macroseismic field was incorporated by using a compression ratio k equal to 1.5 and by arranging the greater axis of the isoseismal ellipse along the fault field.

The rms deviation of the intensity σ_I = 0.5 was used for buildings of all vulnerability classes and for all observed degrees of damage in order to obtain the interval estimates (Aleksandrov et al. 2019).

The results of the scenario earthquake impact calculations are presented as tables, which show estimated proportion of buildings in the settlement that have received a certain state of damage d, as well as the average damage state for the town d_{aver}. The average state of damage d_{aver} is also shown on thematic maps in Figs. 7 and 8.

In these figures, the size of symbols indicates the number of inhabitants on the settlement and the color of a symbol shows the average state of damage inflicted on the structures.

Figure 9 shows the percentage of cities, in which buildings have suffered different average degrees of damage when using two considered vulnerability functions.

Tables 4 and 5 show the proportion of buildings in the larger settlements that have received a certain state of damage d and average states of damage d_{aver} for the buildings in a settlement as a whole.

Comparison of Figs. 7 and 8 shows a systematic overestimation of the damage, calculated based on parameters of the generalized vulnerability functions (Table 3) compared to the simulation results, obtained using parameters of the regional vulnerability functions (Table 2). Figure 8 shows, that most of the settlements are characterized by the average state of damage between d_{aver} =3 and d_{aver} =5. When the regional vulnerability functions are used, the number of settlements that have suffered a high level of damage is considerably reduced. The number of settlements with average damage state d_{aver}=5 is reduced by a factor of three and that with d_{aver}=4 almost by a

Table 1. The most hazardous possible earthquake source zones for Irkutsk City

Possible source zone names	Minimum distance to Irkutsk City, km	M_{max}	Calculated intensity I in Irkutsk City, MMSK-86 grades
East Sayan	70	8.0	8.6
Tunkinskaya	140	7.5	6.6
Primorskaya sublatitudinal	70	7.5	8.8
Primorskaya southern	75	7.0	7.9
Marine	150	7.5	8.1

Table 2. The regional parameters of vulnerability functions in accordance with the regional scale of (Berzhinski 2001; Sherman et al. 2003)

Building types according to the regional scale	Buildings damage state d				
	Light d=1	Moderate d=2	Heavy d=3	Partially destroyed d=4	Completely collapsed d=5
	Mathematical expectation of the intensity I which results in a certain damage state of a building				
A, E5	6.2	7.0	7.8	8.6	9.4
B, E6	6.4	7.4	8.4	9.4	10.4
C, E7	6.7	8.0	9.1	10.1	11.0
E8	7.3	8.7	9.8	10.7	11.3
E9	8.3	9.5	10.4	11.2	11.5

Table 3. The default parameters of generalized vulnerability functions used in the Extremum System (Larionov et al. 2003a)

Building types according to MMSK-86 scale	Buildings damage state d				
	Light d=1	Moderate d=2	Heavy d=3	Partially destroyed d=4	Completely collapsed d=5
	Mathematical expectation of the intensity I which results in a certain damage state of a building				
A1, A2	6.0	6.5	7.0	7.5	8.0
B1, B2	6.5	7.0	7.5	8.0	8.5
C1, C2	7.0	7.5	8.0	8.5	9.0
E7	7.5	8.0	8.5	9.0	9.5
E8	8.0	8.5	9.0	9.5	10.0
E9	8.5	9.0	9.5	10.0	10.5

The rms deviation of the intensity σI = 0.5 for all types of buildings.

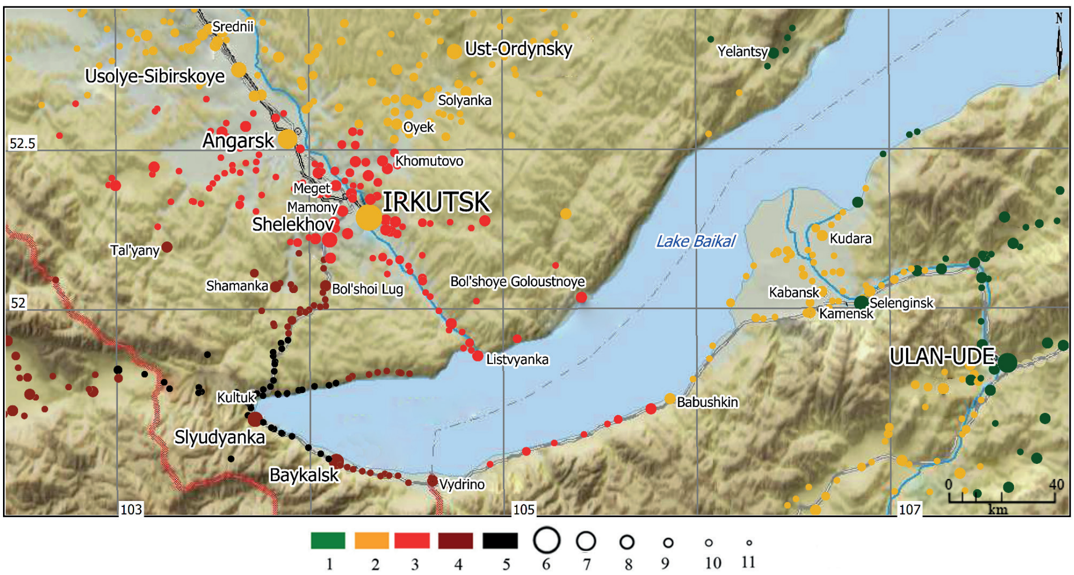

Fig. 7. The theoretical impact of the scenario earthquake in the East Sayan seismic source zone obtained using calibrated regional parameters of the vulnerability functions (shown in Table 2)

Average state of damage d_{aver}: 1-1; 2- 2; 3- 3; 4- 4; 5- 5; Number of inhabitants: 6 – 500,000 and more; 7 - 100,000 up to 500,000; 8 – 10,000 up to 100,000; 9 – 5,000 up to 10,000; 10 – 500 up to 5,000; 11 - less than 500.

factor of two (Fig. 9). Towns with the average state of damage d_{aver} =1 and d_{aver} =2 can also be found on the map, presented in Fig. 7. Overall, the difference between the average state of damage calculated using different approaches varies between 0.5 and 1.5 (Fig. 10).

According to Table 5, when the city of Irkutsk experiences the impact of the scenario earthquake, the fraction of buildings that can receive heavy damage or completely collapse is approximately 30%. Meanwhile, according to Table 4, there will be no cases of heavy damage or complete building collapse and over 50% of all buildings in the city can be moderately damaged (d_2).

Thus, the use of calibrated parameters of vulnerability functions in accordance with the regional seismic scale for the Baikal Region and Transbaikalia provides evidence of the importance of incorporating region-specific structural features.

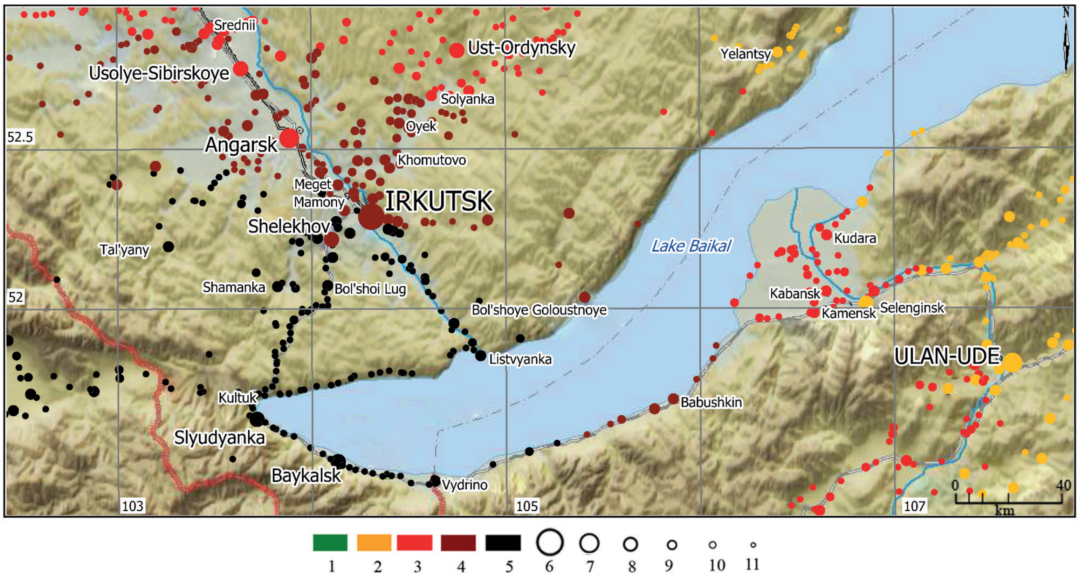

Fig. 8. The theoretical impact of the scenario earthquake obtained by using parameters of the generalized vulnerability functions (shown in Table 3)

Average state of damage d_{aver} : 1-1; 2- 2; 3- 3; 4- 4; 5- 5; Number of inhabitants: 6 – 500,000 and more; 7 - 100,000 up to 500,000; 8 – 10,000 up to 100,000; 9 – 5,000 up to 10,000; 10 – 500 up to 5,000; 11 - less than 500.

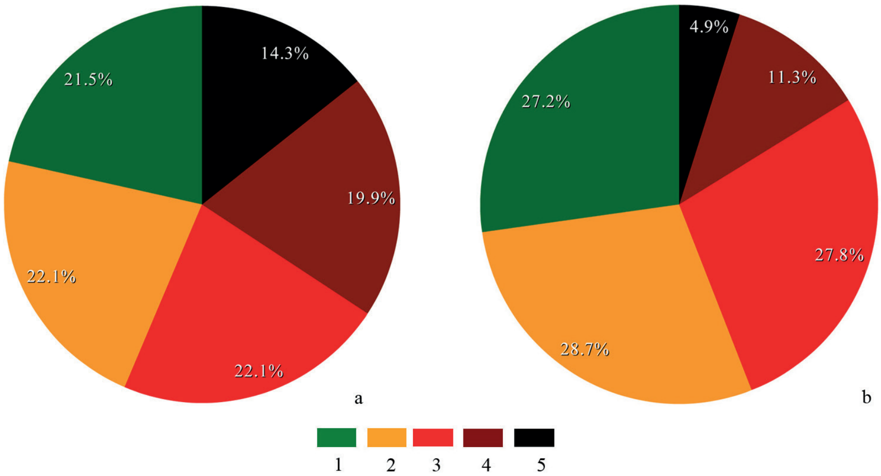

Fig. 9. Distribution of settlements with different damage grades; a - when using parameters of the generalized vulnerability functions; b - when using parameters of the regional vulnerability functions

Table 4. The estimated proportion of buildings that have received a certain state of damage d due to the scenario earthquake obtained using parameters in the regional vulnerability functions presented in Table 2

Settlement	Fraction of buildings with a certain state of damage					d_{aver}
	d_1	d_2	d_3	d_4	d_5	
Irkutsk	0.133	0.521	0.287	0.055	0.003	2.27
Shelekhov	0.064	0.465	0.365	0.097	0.008	2.518
Angarsk	0.254	0.525	0.195	0.023	0	1.979
Usol'e -Sibirskoe	0.405	0.464	0.111	0.008	0	1.697
Bajkalsk	0	0.069	0.422	0.355	0.149	3.571
Slyudyanka	0	0	0.083	0.412	0.504	4.418
Utulik	0	0.007	0.067	0.248	0.678	4.596
Kultuk	0.039	0.333	0.513	0.112	0	2.692

Table 5. The estimated proportion of buildings that have received a certain state of damage d due to the scenario earthquake obtained using parameters in the generalized vulnerability functions presented in Table 3

Settlement	Fraction of buildings with a certain state of damage					d_{aver}
	d_1	d_2	d_3	d_4	d_5	
Irkutsk	0.03	0.134	0.248	0.285	0.298	3.673
Shelekhov	0.012	0.078	0.191	0.284	0.435	4.051
Angarsk	0.076	0.211	0.286	0.248	0.17	3.196
Usol'e -Sibirskoe	0.149	0.274	0.28	0.181	0.079	2.656
Bajkalsk	0	0.001	0.012	0.064	0.922	4.905
Slyudyanka	0	0	0	0.001	0.998	4.997
Utulik	0	0	0.003	0.013	0.983	4.977
Kultuk	0.009	0.037	0.141	0.326	0.485	4.232

DISCUSSION OF THE RESULTS

The present paper focuses on the AIUS RSChS database, which contains descriptions of the earthquake events; the database allows for subsequent improvements to the entire Extremum System by incorporation of the collected and systematized data from assessments of the situation in a disaster zone. The results of field surveys covering both the observed impact and a description of the location, time, seismic intensity, and type of the damaging excitation at various sites are recorded in the database. During calibration, the expected states of damage obtained by modeling are compared with the results of field surveys in the disaster zone. The goal of this comparison is to minimize the discrepancies, which is necessary for calibration of the mathematical models for vulnerability of buildings. A result that differs from the observed value by no more than 30% is generally considered to be acceptable.

When dealing with seismic events that involve damage and destruction of buildings, the database enables successive calibration of the vulnerability models. The first step includes classification of the buildings, defining the boundary of the region where the construction code, structural solutions, and construction materials are similar. The next step consists of adjusting the parameters of the vulnerability functions in order to minimize the discrepancies between the modeling results and observations. In the considered case, we adjusted the mean intensity I and the rms deviation of the intensity σ so that the buildings arranged over different building types or vulnerability classes receive a certain average damage state. The procedure assumes that intensity I is a continuous random variable and that considered building belongs to a single building type or vulnerability class. This procedure is commonly used when developing regional seismic intensity scales. One such seismic intensity scale for the Siberian region of Russia is presented in the current paper. The use of this scale to simulate the impact of a scenario earthquake occurring in the earthquake generation zone of the greatest hazard for Irkutsk City has enhanced the accuracy of the simulation results, including the degrees of damage to buildings.

The example (Table 2, Table 3, Figure 7, and Figure 8) compares the results of modeling the impact of a seismic event with all equal parameters, except for the parameters of the vulnerability functions. The example shows that the use of generalized parameters considerably increases the errors in assessing the consequences of an earthquake compared with the case when the regional parameters were used. From this example it can be seen that the use of generalized data on vulnerability for assessing earthquake impact was a matter of necessity for users of the Extremum System. It can also be concluded from the example that all seismic events should be recorded with subsequent incorporation of the survey results in the database, thus enabling refinement of the regional scales and calibration of the system in order to enhance the accuracy of near real-time damage and loss estimates.

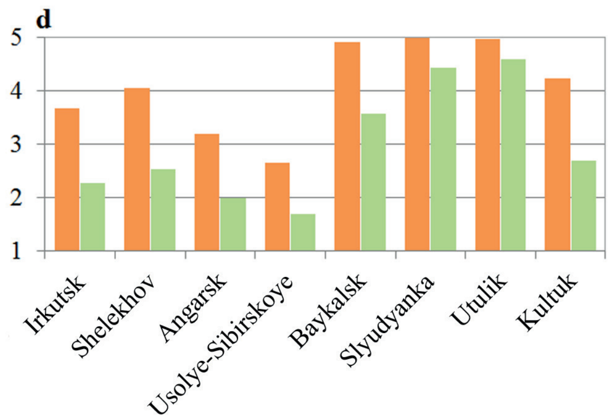

Fig. 10. The distribution of the average state of damage in a town as a result of the scenario earthquake obtained using regional and generalized vulnerability functions for the structures in the region: orange – values of d_{aver} from Table 5; green – values of d_{aver} from Table 4.

CONCLUSIONS

1. The studies have shown that the use of a database with descriptions of seismic events for calibrating a seismic vulnerability model yields a noticeable effect that provides acceptable accuracy for the near real-time simulation of a possible earthquake scenario.
2. Calibration can have positive effect on the results if the following conditions are met:
• A special AIUS RSChS database receives detailed information on the level of damage to buildings due to each seismic event. The structure of a record has special sections for storing formalized data on the location of the study object (coordinates and address), a description of its structural design and construction materials, an assessment of earthquake resistance carried out when the object was subjected to inventory, damage suffered due to the seismic excitation of a certain intensity.
• interconnection is established between the records with descriptions of events and their impacts.
• the database used for calibration contains information on the boundary of the region where the same calibration parameters are used. For all seismic events that fall in a selected region, the same set of vulnerability functions will be used; the functions are characterized by the mean and rms deviation of the intensity;
• there is an indication of the seismic intensity scale, which is used to classify the buildings within the region.
3. The goal of the calibration process is to minimize the discrepancies between the degrees of damage that were obtained by modeling and those reported after the field survey. The calibration is performed by adjusting the mean and rms deviation that characterize each vulnerability function. This can only be done with a fixed seismic intensity scale that provides a detailed description of the vulnerability classes.
4. The structure of the AIUS RSChS data depository has been adjusted in the optimal way to provide the storage of the calibration data. The data are collected by the survey specialists from the sites and are revised in subsequent reports of engineering seismologists and structural designers, as well as in scientific publications that contain analyses of the observations.
5. After revision of the records or input of additional data, a second calibration is carried out to improve (by self-learning processes) those blocks in the System which are responsible for the simulation of possible earthquake scenarios.
6. The example given in the paper illustrates the influence of vulnerability functions on the damage simulation results and demonstrates the importance of taking the regional characteristics into account. Modeling of the impact of the scenario earthquake with the epicenter in the East Sayany source zone has shown that the use of region-specific parameters in the vulnerability functions yields more reliable estimates of potential damage and losses due to a large earthquake. For Irkutsk City, the estimated number of heavily damaged and completely collapsed buildings obtained using different sets of parameters for vulnerability functions differs by 30%, which can significantly affect the plans for rescue and recovery operations.

REFERENCES

Aleksandrov A., Larionov V., Sushchev S. (2019). Technological and natural risk analysis and management. Manuel. Moscow: Bauman Press Publ (in Russian).

Berzhinski Yu. (2001). A regional macroseismic scale for the Baikal area. An abstract of the dissertation for candidate of geological and mineralogical sciences. Irkutsk (in Russian).

Berzhinski Yu., Berzhinskaya L., Ivankina L., Ordynskaya A., Radziminovich Ya. and Chernykh E. (2008). Monitoring the Condition of Natural and Technical Systems. The Baikal Earthquake of August 27, 2008. Earthquake Resistant Design. Safety of Structures, 6, 53-57 (in Russian).

Berzhinskaya L. and Berzhinski Yu. (2009). Methods for inventory of buildings in seismic regions. Voprosy Inzhenernoi Seismologii. ISSN 0132-2826. 36(2), 57-69 (in Russian).

Berzhinski Yu., Ordynskaya A., Gladkov A., Lunina O., Berzhinskaya L., Radziminovich N., Radziminovich Ya., Imaev V., Smekalin O. and Chipizubov A. (2009). An experience in the use of the ESI 2007 scale for estimating the intensity of shaking due to the Kultuk earthquake of August 27, 2008 in the southern Baikal region. Voprosy Inzhenernoi Seismologii, 36(3), 5-26 (in Russian).

Braga F., Dolce M. and Liberatore D. (1982). A statistical study on damaged buildings and an ensuing review of the MSK-76 scale. In: Proc. of the Seventh European Conference on Earthquake Engineering, Athens, Greece, 431-450.

Boore D., Joyner W. and Fumal T. (1993). Estimation of response spectra and peak accelerations from western North American earthquakes: an interim report. U.S. Geological Open-file Report, 93-509.

Calvi G., Pinho R., Magenes G., Bommer J., Restrepo-Vélez L. and Crowley H. (2006). Development of seismic vulnerability assessment methodologies over the past 30 years. ISET Journal of Earthquake Technology, 43(3), 75-104.

Di Pasquale G., Orsini G. and Romeo R. (2005). New developments in seismic risk assessment in Italy. Bulletin of Earthquake Engineering 3(1), 101-128.

European Macroseismic Scale 1992: (up-dated MSKscale). (1993). Cahier du Centre Europeen de Geodynamique et de Seismologie, vol. 7, G.Grunthal (Ed.).

Frolova N., Larionov V., Bonnin J. (2011). Earthquake casualties estimations in emergency mode. In: Spence R. et al (eds) Human casualties in earthquakes: progress in modelling and mitigation, advances in natural and technological hazards research, 29. Springer, 107-123, DOI: 10.1007/978-90-481-9455-1_8.

Frolova N., Ugarov A. (2018). Knowledge base about past earthquakes consequences as a tool to increase the reliability of near real time loss estimation. Geoekologiya, 37, 3-20, DOI: 10.1134/S0869780318060017-37.

Frolova N., Gabsatarova I., Petrova N., Ugarov A., and Malaeva N. (2019). Influence of shaking intensity attenuation peculiarities on reliability of earthquake loss estimation in emergency mode. Geoekologiya, 37, 23–37, DOI: 10.31857/S0869-78092019523-37.

Frolova N., Larionov V., Bonnin J., Suchshev S., Ugarov A., and Malaeva N. (2020). Impact database application for natural and technological risk management. Nat. Hazards Earth Syst. Sci., 20, 95-106, DOI: 10.5194/nhess-20-95-2020.

Goncharov S., Frolova N. (2011). Casualty Estimation due to Earthquakes: Injury Structure and Dynamics. In: Spence R et al (eds) Human casualties in earthquakes: progress in modelling and mitigation, advances in natural and technological hazards research, 29. Springer, 142-149, DOI: 10.1007/978-90-481-9455-1_10.

Izmalkov V. (2017a). Development of AIUS RSCHS as a dynamic automated system. Civ. Secur. Technol., 14, 26-31.

Izmalkov V. (2017b). Automated Information Management System of The Russian Unified Emergency Prevention and Response System AIUS RSCHS-2030: Analysis of its Operating Experience and Further Development Priorities. Civ. Secur. Technol., 14, 38-42.

Kachanov S., Nekhoroshev S. and Popov A. (2011). Decision support information technology in the case of emergencies: AIUS RSCHS: yesterday, today, tomorrow. Moscow: Delovoj Ekspress Publ., ISBN 978-5-93970-064-1, 400.

Kachanov S., Ageev S., Kovtun O., Belyaeva I., Lukina Y. and Chernov V. (2014). Automated Control System of a Unified System of Professional Training for the Russian Emergencies Ministry. Civ. Secur. Technol., 11, 16-21.

Khromovskikh V., Delyanskiy E., Smekalin O. (1996). Paleoseismogeology at a new stage of development. Geophysical research in Eastern Siberia at the turn of the XXI century. Novosibirsk: Nauka, 99-101 (in Russian).

Larionov V., Frolova N., Ugarov A. (2000). Methodological Approaches for Seismic Vulnerability Assessment and their Application for Near Real Time Loss Assessment due to Strong Earthquakes In: Proc. of All-Russian Conference «RISK-2000», Moscow: Publishing House «Ankil», 132-135.

Larionov V., Frolova N. (2003a). Peculiarities of seismic vulnerability estimations. In book: Natural Hazards in Russia, volume 6: Natural Risks Assessment and Management, Moscow: Publishing House «Kruk», 120-131.

Larionov V., Sushchev S., Ugarov A., Frolova N. (2003b). Seismic risk assessment with GIS-technology application. In book: Natural Hazards in Russia, volume 6: Natural Risks Assessment and Management, Moscow: Publishing House «Kruk», 209-231.

Larionov V., Frolova N., Ugarov A., Sushchev S., Kozlov M., Malaeva N., Barskaya T. (2017). Seismic Risk Assessment. Geoekologiya, 2, 11-26 (in Russian).

Lumantarna E., Lam N., Tsang H., Wilson J., Gad E., and Goldsworthy Y. (2014). Review of Methodologies for Seismic Vulnerability Assessment of Buildings. In: Proc. Of Australian Earthquake Engineering Society Conference, 21-23, Lorne, Victoria.

Martel R. (1964). Earthquake damage to type III buildings in Long Beach, 1933. Earthquake Investigations in the western United States, 1931–1964, Publication 41-2, U.S. Department of Commerce, Coast and Geodetic Survey, Washington, DC.

Martins L., Silva V. (2018). A global database of vulnerability models for seismic risk assessment. In: Proc. Of 16th European conference on Earthquake Engineering, Thessaloniki, https://www.researchgate.net/publication/327905554

Radziminovich Ya. (2003). Assessment of seismic risk in Irkutsk City. Dissertation. Irkutsk: IZK, 25.00.10, 160.

Shebalin N. (1968). Procedures of engineering seismological data application for seismic zoning. In: Seismic zoning of the USSR, Moscow: Nauka, 95-121 (in Russian).

Shebalin, N. (1977). Reference earthquakes and macroseismic field equations. In: New catalogue of strong earthquakes for the USSR territory from ancient times till 1975. Moscow: Nauka, 20-30 (in Russian).

Shebalin N., Ershov I., Gekhman A., and Shestoperov G. (1986). Development of improved version of seismic intensity scale (MMSK-86) on the bases of MSK-64 scale and scale of Joint Council on Seismology and Earthquake Engineering – 73. Report on scientific research study within the Federal Program 0.74.03, number of state registration 01814003271, Joint Council on Seismology and Earthquake Engineering, Academy of Sciences of the USSR, Moscow, Russian Federation.

Sherman S., Berzhinski Yu., Pavlenov V. and Aptikaev F. (2003). Regional scales of seismic intensity. Novosibirsk: SO RAN, filial «Geo».

Spence R., Coburn A.W., Pomonis A. (1992). Correlation of ground motion with building damage: The Definition of a New Damage-Based Seismic Intensity Scale. In: Proc. of the Tenth World Conference on Earthquake Engineering, Madrid, Spain, 1, 551-556.

Sushchev S., Larionov V., Frolova N. (2010). Seismic Risk Assessment and Management with Extremum System Application. In: Proc. Of XV international conference «Problems of population and territory protection against emergencies». Moscow: VNII GOChS, 327-345.

Ulomov V., Shumilina L. (1999). Set of maps OSR-97-A, B, C of review seismic zoning of the Russian Federation territory – OSR-97. Scale 1:8 000 000. Explanatory note and list of cities and settlements located in earthquake prone areas. Moscow: OIFZ Publ., 57 (in Russian).

Xin D., Daniell J., Wenzel F. (2019). Review of fragility analyses for major building types in China with new implications for intensity-PGA relation development. Natural Hazards and Earth System Sciences, DOI: 10.5194/nhess-2019-195.

Whitman R. (1973). Damage probability matrices for prototype buildings, Department of Civil Engineering Research Report R73 – 57, Massachusetts Institute of Technology, Cambridge Massachusetts.

Yepes-Estrada C., Silva V., Crowley H. (2014). GEM Vulnerability Database for the Openquakeplatform. In: Proc. of the Second European conference on Earthquake Engineering and Seismology, Istanbul.

Zaalishvili V., Burdzieva O., Kanukov A. and Melkov D. (2019). Seismic Risk of Modern City. The Open Construction & Building Technology Journal, 13, 308-318, DOI: 10.2174/1874836801913010308.

https://files.stroyinf.ru/Index2/1/4293739/4293739217.htm (2019). SP 322.1325800.2017 Buildings and structures in seismic region. Rules of inspection of consequences of the earthquake, in force since May 4, 2018 (in Russian).

https://www.isprambiente.gov.it/files/progetti/inqua/esi-eee-volume-april-2012.pdf. (2012). Earthquake Environmental Effects, intensity and seismic hazard assessment: the ESI intensity scale and the EEE Catalogue.

RESEARCH PAPER

RURAL POPULATION DYNAMICS IN THE RUSSIAN EXTREME NORTH IN 1989–2019: A CASE OF SAKHA REPUBLIC (YAKUTIA)

Tamara V. Litvinenko[1*], Kazuhiro Kumo[2], Antonina N. Savvinova[3], Viktoriia V. Filippova[4]

[1]Institute of Geography, Russian Academy of Sciences, 29 Staromonetny pereulok, 119017, Moscow, Russian Federation

[2]Hitotsubashi University, Institute of Economic Research, Naka 2-1, Kunitachi, Tokyo 186-8603, Japan

[3]M. K. Ammosov North-Eastern Federal University, 58 Belinskogo str., Yakutsk, 677007, Russian Federation

[4]The Institute for Humanities Research and Indigenous Studies of the North, Siberian branch, Russian Academy of Sciences, Petrovskogo str. 1, 677027, Yakutsk, Russian Federation

***Corresponding author:** tamaralit@bk.ru

Received: August 20th, 2020 / Accepted: November 20th, 2020 / Published: December 31st, 2020

https://DOI-10.24057/2071-9388-2020-137

ABSTRACT. In this study, the specific characteristics of Yakutia's rural population dynamics in 1989-2019 in comparison with other Extreme North regions are identified along with geographical differences in the population dynamics of the republic's rural districts. The research results are based on the analysis of the official statistical data and field trip observations in rural areas of Yakutia. Sakha has witnessed a relatively small decline in total rural population compared to other regions, which can be explained by the high proportion of the indigenous population that has a historical preference for living in rural areas and higher birth rates as well as by the regional rural support measures. Despite the common overall trend in the rural population dynamics, significant intraregional differences have been identified. In the regions characterized by more central location and a larger share of the indigenous people, the population growth due to migration and the natural increase was observed, while in more remote northern locations with poor transport accessibility to the region's centre population decreased due to migration outflow. A shift in rural population took place in the districts of Central Yakutia, historical settlement area of Yakuts, who are engaged in livestock and horse breeding, which are the traditional types of economic activities for this territory. The largest population decrease due to migration outflow was observed in Momsky and Zhigansky ulus, which are characterized by their northern location, poor transport accessibility and a smaller share of indigenous people.

KEY WORDS: rural population dynamics, Russian Extreme North, Republic of Sakha (Yakutia), indigenous people, Namsky ulus, Anabarsky ulus

CITATION: Tamara V. Litvinenko, Kazuhiro Kumo, Antonina N. Savvinova, Viktoriia V. Filippova (2020). Rural Population Dynamics in the Russian Extreme North IN 1989–2019: A Case OF SAKHA Republic (Yakutia). Geography, Environment, Sustainability, Vol.13, No 4, p. 65-71 https://DOI-10.24057/2071-9388-2020-137

ACKNOWLEDGEMENTS: The study of Tamara V. Litvinenko was carried out as part of the State Assignment of the Institute of Geography of the Russian Academy of Sciences (No. 0148-2019-0008 'Problems and Prospects for the Territorial Development of Russia in the Conditions of Its Unevenness and Global Instability') and supported by the Russian Foundation for Basic Research (Grant No. 19-05-00822).

The study of Kazuhiro Kumo was financially supported by the research grant (B) (19H01478) of the Ministry of Education, Science, Culture and Sports of Japan and a scholarship from the Japan Securities Fund.

The study of Antonina N. Savvinova was financially supported by a grant of the Research Council for the Humanities and Social Sciences of Canada (Project 'The Rights of Indigenous Minorities of the North in the Russian Federation in the Area of Land Use for the Last Quarter of a Century') and was implemented within the research project of Laboratory of Electronic Cartography Systems North-Eastern Federal University «Sustainable development of the territories of traditional nature management of Yakutia in terms of global challenges in the Arctic: cartographic support».

The study of Viktoriia V. Filippova was carried out as part of the State Assignment of the Institute for Humanities Reserach and Indigenous Studies of the North of the SB RAS (№XII.186.4.6) and financially supported by the Russian Foundation for Basic Research (Grant №20-09-00257A).

Conflict of interests: The authors reported no potential conflict of interest.

INTRODUCTION

The Russian Extreme North[1] is mostly located north of the Arctic Circle and has recently attracted a lot of attention due to its rapid population decline (Arctic…2014; Orttung 2017; Khoreva et al. 2018; etc.). Certain Far East regions, such as Chukotka and Magadan, have experienced a severe population outflow. However, there is a region that can be considered an exception, where demographic stability and even a slight increase in the rural population are observed. That is the Republic of Yakutia, which suggests that its approach to the use of resources and population allocation has a positive impact on its demographic trends and the conclusions that can be drawn from the experience of Yakutia may provide important knowledge for understanding the demographics of other regions.

Thus, the purpose of this study is to identify region-specific characteristics, intraregional and local differences in rural population dynamics in Sakha Republic, as well as its determining factors. Issues of population dynamics and demographic development of Yakutia were reviewed in the publications of several researchers (Fedorova 1998; Sukneva and Mostakhova 2002; Sukneva 2010; Savvinova and Filippova 2016; Sukneva et al. 2017). Detailed analysis of the dynamics of rural settlements, their population size and functions in the post-Soviet period was carried out by G.A. Ponomareva and V.I. Bubyakin (2013) and T.S. Mostakhova (2015). Spatial distribution of' the economic activities of the population was investigated by M. Yu. Prisyazhniy (2011). Our studies complement the above works by establishing specific characteristics of Yakutia's rural population dynamics in 1989–2019 in comparison with other Russian Extreme North regions and identifying geographical variation in the population dynamics of the republic's rural districts in relation to their location, ethnic composition and the dominant type of economic activity.

MATERIALS AND METHODS

The research was carried out using statistical, geographical, cartographic and field study methods. The primary source of material for research at all spatial levels were the census data and current population records. Population dynamics in Anabarsky and Namsky uluses (districts) were analysed based on data presented in their socio-economic development programmes available at the official municipalities' websites. The authors also used the results of their surveys of rural settlements conducted during field research in 2017 in Namsky ulus (all authors), and in Amginsky, Gorny, Verkhnevilyuisky, Oleneksky, Suntarsky, Churapchinsky, Ust-Aldansky and Eveno-Bytantaysky uluses in 2008–2018 (A.N. Savvinova, V.V. Filippova).

The application of an integrated approach resulted in a study, which was divided into several stages. At the first stage, common trends and regional differences in rural population dynamics of the Russian Extreme North were established. At the second stage, the factors of a relatively small decline in Yakutia's rural population compared to other regions were identified. During the third stage, the differences in Yakutia's rural population trends in various post-Soviet years (periods) were analysed and the intraregional differences in rural population dynamics of districts (uluses) were identified in relation to their geographical location, ethnic composition and the dominant type of economic activity. The fourth stage consisted of identification of local characteristics of rural population dynamics and its major driving factors on the example of Anabarsky and Namsky uluses.

The choice of the Arctic Anabarsky ulus and the Namsky ulus, located in Central Yakutia, as the key areas was determined by the differences in their geographic location, ethnic composition of the population, the prevailing type of economic activity, population size and population density.

Results and Discussion

Rural population dynamics in the Russian Extreme North

Looking at the Russian Extreme North in general, it can be seen that the total population has been decreasing continuously since the collapse of the Soviet Union (Fig. 1). The volume of urban population has stabilized in the first half of the 2000s but, as shown in Fig. 1, rural population demonstrates an apparent decreasing trend even after that period and the rate of its decline remains approximately the same over the last 20 years.

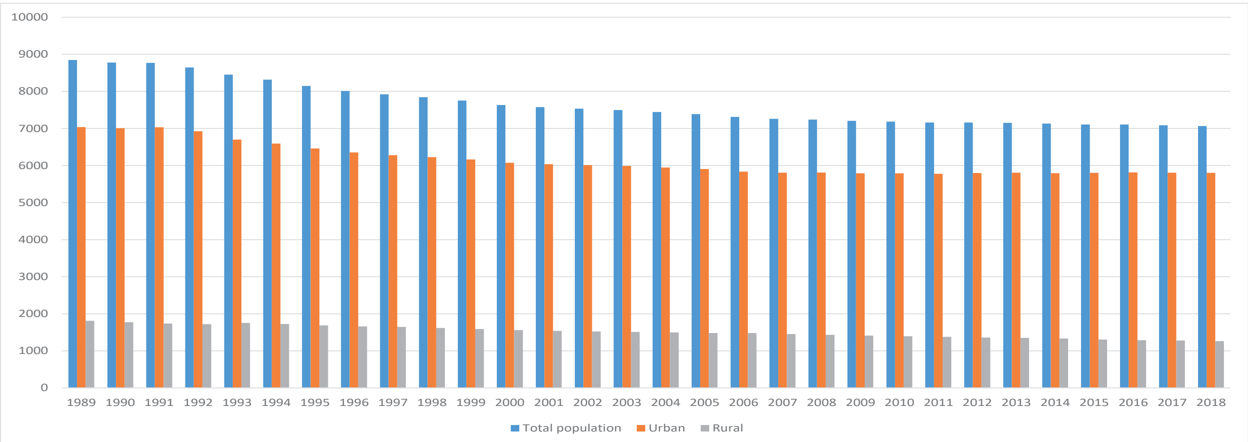

Fig. 1. Population dynamics in the Russian Extreme North, 1989–2018 (thousand people)

[1] «Extreme North» is a region defined by the Russian government. Largely it is located north of the Arctic Circle. Because of its harsh environment, the government offers higher wages or other benefits to the residents.
In this article and, particularly, in the figures 1-2, all the regions that are categorized as «the Extreme North» or «equivalent with the Extreme North» are included: namely, Republic of Karelia, Murmansk oblast, Arkhangelsk oblast, Republic of Komi, Yamalo-Nenets autonomous okrug, Khanty-Mansi autonomous okrug (Yugra), Taimyr raion, Evenki raion, Republic of Sakha (Yakutia), Magadan oblast, Kamchatka krai and Chukotka autonomous okrug. Although all the territories of Sakhalin oblast and Tyva republic are also defined as the Extreme North, they were excluded because of their southern location.

The trends in the rural population differ from region to region (Fig. 2). The biggest decline in rural population was observed in Magadan oblast and Chukotka autonomous okrug (Fig. 2) due to the abolishment of mining settlements populated predominantly by Russian people during 1990s (Litvinenko and Kumo 2017). The largest growth of rural population compared to 1989 is observed in Khanty-Mansi autonomous okrug (109.9% in 2018), Sakha republic is the second region in this aspect as its population in 2018 equals 91.6% of that in 1989, then it is followed by Evenki raion (88.2%), Karelia republic (82.3%) and Yamalo-Nenets autonomous okrug (81.4%).

These observations are essential when studying the factors which contribute to stabilization or even growth of the rural population in the regions of Extreme North. The rural population in Khanty-Mansi autonomous okrug, where the share of the indigenous population is fairly low (Fig. 2), showed continuously increasing trend as a result of its economic growth due to export of hydrocarbon resources. The share of the rural population in the region though is only about 8%, which the smallest among all regions of the Extreme North. The relatively positive situation in Yamalo-Nenets autonomous okrug can be attributed to its huge deposits of natural gas. Such industry, however, may not be the factor that explains the stabilization of the rural population, the share of which in the region is around 15%. To account for that, other possible factors should also be examined. The one factor, which plays a significant role in the rural population dynamics of these regions, is the presence of ethnic (indigenous) people in the Russian Extreme North (Fig. 2). A notable example here is the small decrease in rural population observed in Evenki raion, which can be attributed to this ethnic factor. Some of the authors' papers were also devoted to the districts with relatively high share indigenous people in Chukotka autonomous region, which maintained their population (Litvinenko and Kumo 2017; Kumo and Litvinenko 2019).

Meanwhile, the Republic of Sakha is characterized by the combined effect of both factors described above. Namely, on the one hand, Yakutia has a huge endowment of natural resources such as diamond, coal, non-ferrous metals, oil and gas, which might have positively affected the urban population dynamics in Sakha. On the other hand, Sakha is famous for its indigenous people, who engage in pastoralism, reindeer herding or other traditional natural resource use, which might have contributed to the relatively small decrease in the rural population of the region.

The authors believe that the main factor which prevented a greater decline in the rural population in Yakutia was the high (the highest among all Far North regions) proportion of the indigenous population, which traditionally a has higher birth rate and historically lives in rural areas. This proportion increased from 35% according to the 1989 census to slightly more than half of the total population according to the 2010 census (Fig. 3). A certain positive contribution was made by the growth of the region's revenues from export-oriented diamond and coal mining industries in the post-Soviet period, and in recent years also from oil and gas production, which allowed the regional authorities to implement support measures targeting rural residents, particularly young families. Nevertheless, the regional government has admitted that the measures implemented to promote sustainable development of rural areas have been insufficient to ensure comprehensive and effective use of rural areas' potential and improvement of villagers' quality of life[2].

Rural population dynamics in the Republic of Sakha

Throughout the Soviet period, the share of the rural population in the total population was decreasing, reaching 33% in 1989. After the collapse of the USSR, over the intercensal period of 1989–2002, it increased by two percent and has only been changing slightly thereafter. The share of the indigenous population also declined during the Soviet period, but less than the share of the rural population, and between the censuses of 1989 and 2010, as it was noted above, it has increased significantly (Fig. 3).

During the Soviet period, between the censuses of 1959 and 1989, Yakutia's total rural population increased by a factor of 1.4 and by the end of the Soviet period it exceeded the 360,000. During the economic crisis that

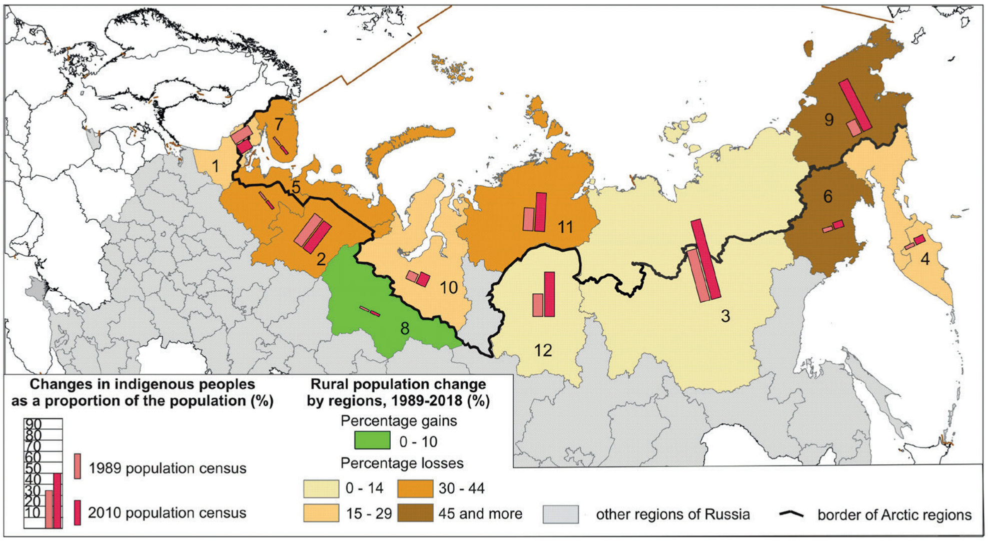

Number of regions

1 Republic of Karelia
2 Republic of Komi
3 Republic of Sakha (Yakutia)
4 Kamchatka krai
5 Arkhangelsk oblast (including Nenets autonomous okrug)
6 Magadan oblast
7 Murmansk oblast
8 Khanty-Mansi Autonomous okrug – Yugra
9 Chukotka autonomous okrug
10 Yamal-Nenets autonomous okrug
11 Taimyr raion of Krasnoyarskiy krai
12 Evenki raion of Krasnoyarskiy krai

Fig. 2. Rural population dynamics in the Russian Extreme North by regions, 1989–2018 (%)

[2]A comprehensive programme of the Republic of Sakha (Yakutia) «Sustainable development of rural territories of the Republic of Sakha (Yakutia) in 2013-2016 and for the period until 2020», approved by Ordinance No 421 of the Government of the Republic of Sakha (Yakutia) of December 9, 2013. https://www.sakha.gov.ru/files/front/download/id/1232325

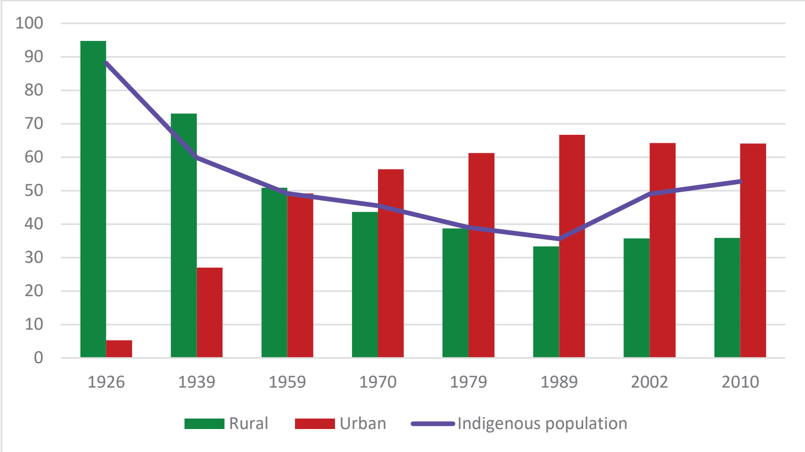

Fig. 3. The share of urban, rural and indigenous populations in the total population of Sakha republic

Source: census data

followed the collapse of the USSR, rural population of Yakutia (Fig. 4) and most of its uluses continued growing until 1994, while total and urban population started decreasing from 1992. Faced with the closure of many industrial enterprises and loss of income, part of the urban population, seeking means to feed their families, returned to villages to run their private subsidiary plots and engage in cattle, horses and pigs breeding and vegetable gardening. Despite the intensifying intraregional migration from rural to urban settlements in the intercensal period of 2002–2010, rural population in 2010 has increased by 1.4% compared to 2002 due to the natural increase as well as the recategorization of several urban-type settlements (Tabaga, Magan, Bolshoi Nimnir, Yllymakh, Zarechny) into rural settlements.

Between 1995 and 2019, with the exception of some years, a slight gradual decrease in rural population was observed (Fig. 4) due to internal migration from villages to urban settlements, particularly to the region's capital. The region's rural and urban population trends diverged in 2004 (Fig. 4), whereas the total population has been slightly growing, primarily due to the growing population of the city of Yakutsk.

In order to identify what caused the trends presented above, more detailed data on the region was used. Along with the overall trends observed at the regional level, significant intraregional differences in the rural population dynamics were identified. Out of Yakutia's 35 uluses, only 13 have a rural population (Fig. 5). The share of the indigenous population in such uluses varies from 82% in Zhigansky to 99% in Ust-Aldansky ulus. Rural uluses vary by the ethnic composition of their population and the prevailing type of economic activities. The prevailing economic activity in the mostly Yakut-populated Western and Central Yakutia is agriculture (nomadic cattle and horse breeding); in the northwestern regions populated by the small indigenous peoples of the North (Dolgans, Evenks, Evens) the dominant activities are reindeer-herding, hunting and fishing, and Momsky ulus, which has predominantly Yakut population but also a large share of Evens, is dominated by agriculture, reindeer-herding, hunting and fishing (Prisyazhnyy 2011). Rural uluses of Central Yakutia are characterized by greater population size and density, while those located to the north have smaller population size (Fig. 5) and density. The largest population decline (over 20%) was observed in Zhigansky ulus in the north-west and Momsky ulus in the north-east. They are both characterised by a northern location, reindeer-herding, hunting and fishing as their major types of economic activities and a smaller, less than 90%, share of the indigenous population compared to other rural districts (Fig. 5).

A decrease of 19% or less occurred in the Arctic reindeer-herding-type Anabarsky ulus and agrarian uluses – the western Suntarsky ulus and the central Ust-Aldansky ulus (Fig. 5). They differ from districts with a larger population decline by a higher proportion of the indigenous population (ranging from 92% in Suntarsky to 99% in Ust-Aldansky ulus) and from districts with an increasing population by their remote location relative to the regional centre (Anabarsky and Suntarsky uluses) and poor transport accessibility to the capital compared to other districts in Central Yakutia (Ust-Aldansky ulus).

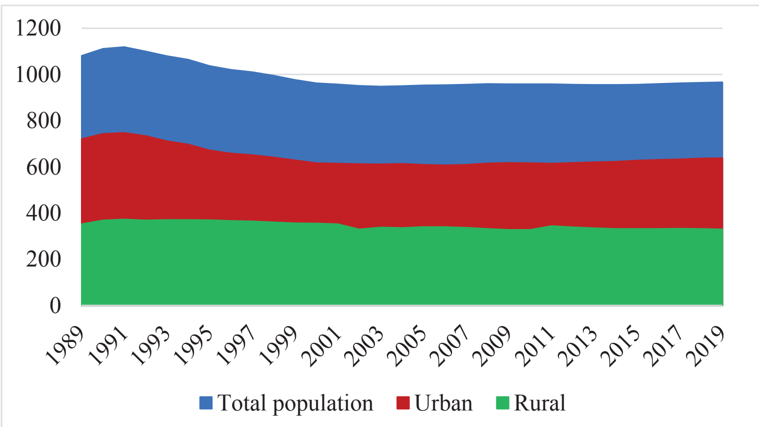

Fig. 4. Dynamics of the rural population in comparison with the urban and the total population in the Republic of Sakha in 1989–2019, thousand people

Source: current population records and 1989, 2002 and 2010 census data

In 7 out of the 13 rural districts, the population increased by less than 20% – from 1% in Verkhnevilyuisky to 19% in Gorny ulus (Fig. 5). The common characteristic of these districts is a high, more than 96%, share of the indigenous population, except for Amginsky ulus (93%). At the same time, they differ in their ethnic composition, type of prevailing economic activities and geographic location, as represented by the reindeer-herding, hunting and fishing-type Oleneksky and Eveno-Bytantaysky uluses located far from the region's centre in contrast to some agrarian districts of Central Yakutia. The largest (over 20%) population growth was observed in the central agrarian Namsky ulus with a 96% share of the indigenous population. It is characterized by its proximity to the region's centre and the best transport accessibility to Yakutsk.

The reindeer-herding, hunting and fishing-type districts compared to the agrarian ones are characterized by larger decrease and lower growth of population, ranging from an 8% growth in Eveno-Bytantaysky ulus to a 26% decrease in Zhigansky ulus. In the agrarian districts, the increase was larger, and the decline was smaller, ranging from an increase of 35% in Namsky ulus to a decline of 10% in Suntarsky ulus. Population only grew in districts that have a proportion of the indigenous population of 93% or more. In districts like Suntarsky, Zhigansky and Momsky, where it was lower, the population decreased by 10% or more. Thus, the post-Soviet dynamics of the population in rural districts was determined by their geographic location, the prevailing type of economic activity, ethnic composition of the population, and the share of the indigenous population in the total.

Local-specific characteristics and differences

Geographic and ethnic differences between Anabarsky and Namsky key districts defined their overall population trends in 1989–2019, explaining the highest growth among all the rural districts in Namsky and a decline in Anabarsky ulus.

Located beyond the Arctic Circle, the Anabarsky ethnic (Dolgan-Evenk) ulus is sparsely populated (population density is less than 0.1 person per sq. km) and has the

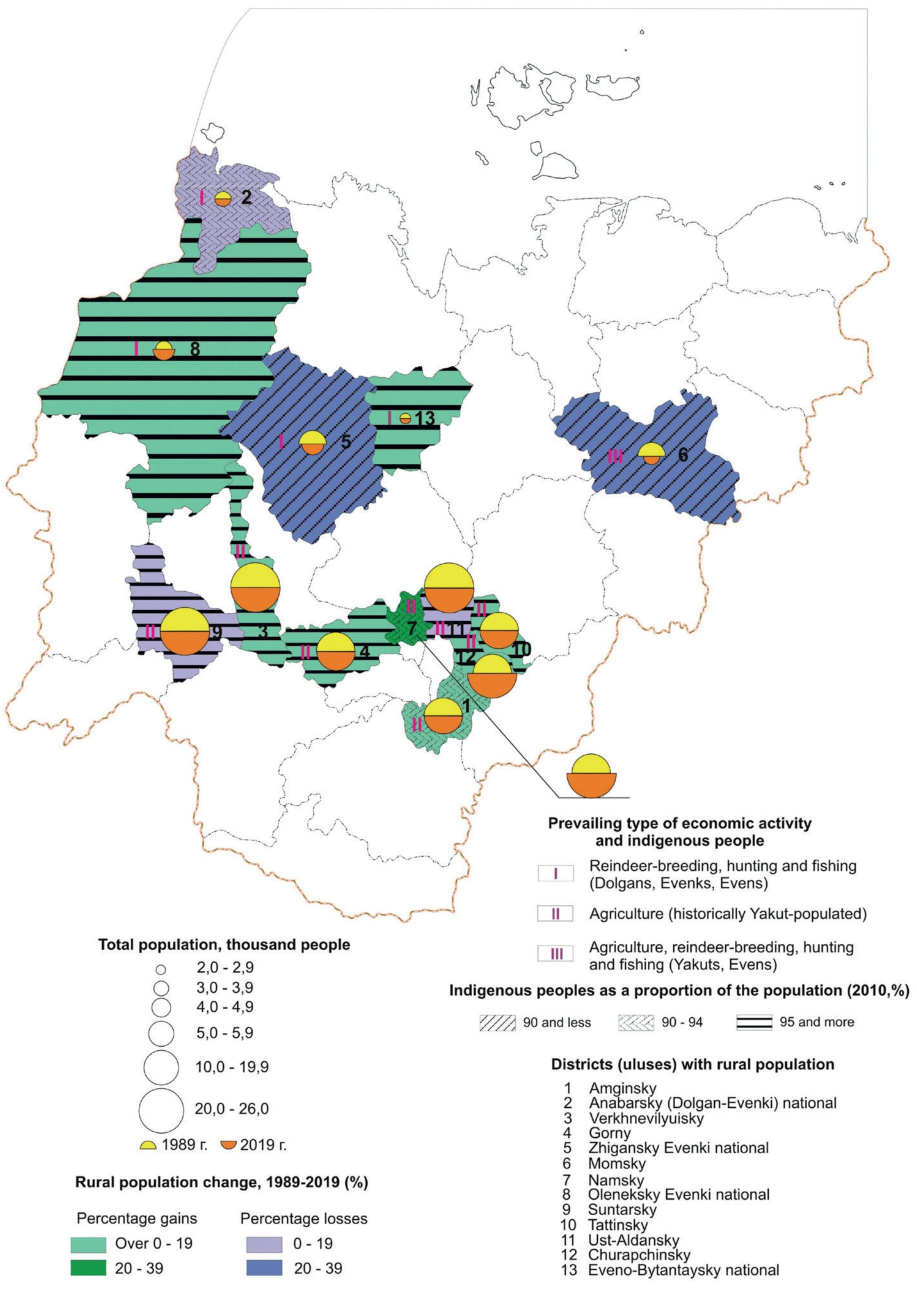

Fig. 5. Population dynamics in rural districts of the Republic of Sakha (Yakutia), 1989–2019 (%)

Source: compiled by the authors based on statistical data smallest, except for Eveno-Bytantaysky ulus, population among the rural districts (3.5-4.0 thousand in the post-Soviet period) (Fig. 5). According to the 2010 census, its indigenous population is dominated by Dolgans with a share of 42.4%, while Evenks comprise 22.7%, Yakuts – 21.6%, Evens – 6.4%. In addition to the traditional types of economic activities of the indigenous people living in the tundra zone, such as reindeer-herding, fishing and hunting, the diamond-mining industry has been actively developing in recent decades. This rural population-dominated district has become an industrial area, occupying a leading position in diamond mining among the republic's northern districts. Production bases, not including mining areas, of large diamond-mining enterprises such as «Almazy Anabara» JSC and «Nizhne-Lenskoye» JSC cover 30.3% of the district's entire area[3].

During the reviewed period, the population of ulus decreased in 1992–1994, 2007 and 2009–2012, while in other years it did not change or increased slightly. The net population decrease of 7.9% in 1989–2019 was primarily due to migration outflow partially offset by natural population growth. Abolishment of the previously engaged in geological exploration and diamond mining rural settlements (the villages of Amakinsky and Ebelyakh) in 1999 and 2011, respectively, contributed significantly to the negative net migration. The abolishment of Ebelyakh village with a population of just under one thousand people due to the closure of Anabarsky mining and processing plant which operated in the village in 1999–2007 resulted in a significant migration loss in 2008–2014. According to local experts, a larger migration outflow from Anabarsky ulus was avoided due to the remote location of the district relative to the region's centre and the high cost of relocating to Yakutsk or nearby areas.

Namsky ulus, located in the Central Yakutian Lowlands 84 km from the city of Yakutsk, is distinguished by the most favourable geographical location and transport accessibility to the region's centre via an asphalt road. The district is located in Yakuts' historical homeland and is characterized by a relatively large population size (Fig. 5), as well as high density of settlements and population. Its population density exceeds that of Anabarsky ulus more than 20 times, and its total population –4-5 times. Availability of fertile grasslands and pastures in the Lena river valley has historically contributed to the development of livestock and horse breeding[4]. This ulus is the republic's only district where, despite the post-Soviet crisis, the population has been increasing, with an exception of just a few years. This can be explained by the migration inflow and high birth rate, combined with the population's young age structure[5]. Such a significant and unusual growth for a rural area (more than 30% in 1989–2019) was due to a combination of factors positively affecting population dynamics: the ethnic factor (Yakuts comprise 96.7% of the population according to the 2010 census), the historical factor (the district is located in Yakuts' historical homeland with higher populated settlements and higher population density), natural resources (availability of sufficient renewable resources for traditional agriculture) and the geographic location factor. The importance of the latter has increased and played a key role in the migration inflow from more northern and remotely located uluses that have poorer transportation access from the republic's capital. The highest growth, just over 50% in 1989–2019, was observed in the district centre – the village of Namtsy. In addition to the above-mentioned factors, this largest rural settlement with a population of over 10,000 people in 2019, attracted residents of other uluses by its relatively well-developed social infrastructure, availability of a pedagogical college, new sports facilities, opportunities for self-employment or employment in proximity to the region's centre. During the field research, changes in the appearance of the village due to the positive population dynamics and income growth were observed including new buildings and facilities, burgeoning individual housing construction activities, and the construction of an apartment building.

CONCLUSION

Similar to other Extreme North regions located north of 55ºN, with the exception of Yugra, the Republic of Sakha (Yakutia) has witnessed a decline in the total rural population in 1989–2019. However, this decline was relatively small due to the high proportion of the indigenous population which has historical preferences for living in rural areas, as well as higher birth rates. A certain positive role was played by regional rural support measures that became possible due to significant budget inflows resulting from the development of profitable export-oriented industries.

Differences in the Republic of Sakha rural population dynamics can be observed in certain periods and years. Whereas at the beginning of the 1990s rural areas were preferred for survival purposes, in subsequent years there was a general trend of migration outflow to district centres, towns and the capital city of Yakutsk. Despite migration outflow recorded in the 2002–2010 intercensal period and in 2003–2005 according to current population records, the rural population increased due to the recategorization of former urban-type settlements into rural settlements.

Despite the overall trend in the rural population dynamics, significant intraregional differences have been identified. In rural districts, differences ranging from a decrease of over 20% in the northern Momsky and Zhigansky uluses to an increase exceeding 30% in the central Namsky ulus were observed. A more central location and a larger share of the indigenous population contributed to the population growth due to migration and natural increase, while a more northerly location, remoteness and poor transport accessibility to the region's centre contributed to a decrease due to migration outflow.

A shift in rural population took place in Namsky, Churapchinsky and Gorny uluses, where statistics show more than a 10% growth over three decades. The common characteristic of these districts is their location in Central Yakutia in the Central Yakutian Lowlands – the historical homeland of the Yakuts, who are engaged in livestock and horse breeding, which are the traditional types of economic activities for this territory. These are relatively densely populated districts, with larger population of settlements and a share of the indigenous population of over 96%. Their district centres are located 185 km or less from the regional centre; federal highways pass through two uluses (Gorny and Churapchinsky). Namsky

[3]A comprehensive socio-economic development programme of the «Anabarsky ethnic (Dolgan-Evenk) ulus (district)» municipality in 2017-2019. «Anabarsky ethnic (Dolgan-Evenk) ulus (district)» municipal district's official website. Electronic access: https://mr-anabarskij.sakha.gov.ru

[4]Ulus's history. «Namsky ulus (district)» municipal district's official website. Electronic access: https://mr-namskij.sakha.gov.ru/mo-namskij-ulus/istorija-ulusa

[5]A comprehensive socio-economic development program of the «Lensky nasleg (village)» municipality in 2020-2024. Namtsy village, 2019. Electronic access: https://nam.sakha.gov.ru/files/front/download/id/2248234

and Churapchinsky districts have an additional advantage of operating higher education facilities, which is contributing to the migration influx of young people.

Research in the districts selected for case studies has identified influences of other factors on population dynamics as well. Abolishment of villages due to suspension of geological exploration and diamond mining stimulated migration outflow of non-indigenous population from Anabarsky ulus. Construction of new education and sports-related buildings and facilities as well as burgeoning housing construction boosted the migration attractiveness of Namsky ulus and its centre.

The impact of the ethnic factor (the share of the indigenous population, which historically lives mainly in rural areas and is characterized by higher birth rate, in the total population) on rural population dynamics was observed at all spatial levels, from regional to local. Zonal differences between the more northern reindeer-herding, hunting and fishing-type districts, where the growth was smaller and the decline was larger, and the central agrarian districts, where the trends were the opposite, demonstrate the influence of geographic location factor in combination with the type of economic activity. At the intraregional and local level, a very strong influence of accessibility to the region's centre can be noted; the better it is, the smaller was the observed decline, or even population growth was recorded. While population growth took place in rural districts of various total population and settlements sizes, the largest (over 20%) decline was only noted in districts with a total population of less than 6 thousand.

The influence of socio-economic factors on rural population dynamics was observed at the interregional level but is more difficult to reveal at lower spatial levels. ■

REFERENCES

Arctic Human Development Report: Regional Processes and Global Linkages (2014). Copenhagen: Nordic Council of Ministers.

Khoreva O., Konchakov R., Leonard C.S., Tamitskiy A. (2018). Attracting skilled labour to the North: Migration loss and policy implications across Russia's diverse Arctic regions, Polar Record, 5-6(54), 324-338.

Kumo K. and Litvinenko T. (2019). Post-soviet population dynamics in the Russian Extreme north: A case of Chukotka. Polar Science, 21, 58-67, DOI:10.1016/j.polar.2018.11.002.

Litvinenko T. and Kumo K. (2017). Post-soviet period changes in resource utilization and their impact on population dynamics in Chukotka autonomous okrug (Russia). Geography, Environment, Sustainability, 11(3), 66-86, DOI: 10.24057/2071-9388-2017-11-3-66-86.

Mostakhova T. (2015). Demographic aspects of rural development in the Republic of Sakha (Yakutia). ECO, 4(45), 138-143 (in Russian).

Mostakhova T. (2016). Geographical aspects of population development in the Republic of Sakha (Yakutia): problems of territorial concentration and settlement. Natural resources of the Arctic and Subarctic, 2, 65-71 (in Russian with English summary).

Orttung R.W. ed. (2017). Sustaining Russia's Arctic cities: resource politics, migration, and climate change. New York: Berghahn Books.

Ponomareva G. and Bubyakin V. (2013). Typology of rural settlements of the Republic of Sakha (Yakutia) by the size of the number of inhabitants (population). Economic analysis: theory and practice, 31(334), 56-62 (in Russian).

Prisyazhnyy M. (2011) Territorial organization of the economy of Yakutia. Spatial economics, 2, 33-53 (in Russian).

Sukneva S. and Mostakhova T. (2002). Demographic development of the region: assessment, forecast, policy. Novosibirsk: Science (in Russian).

Sukneva S. (2010). Demographic development potential of the population of the Northern region. Novosibirsk: Science (in Russian).

Sukneva S., Mostakhova T., Barashkova S., Tumanova D., Elshina I. (2017). Demographic processes in the Republic of Sakha (Yakutia): territorial aspect. Yakutsk: Sakhaada (in Russian).

Fedorova E. (1998). Population of Yakutia: Past and present (geodemographic study). Novosibirsk: Science (in Russian).

Savvinova A. and Filippova V. (2016). Historical mapping of traditional rural settlements of the indigenous peoples of the North from the 20th century to the beginning of 21st century (the case of Yakutia). Berichte Geographie und Landeskunde, 90(4), 327-338.

RESEARCH PAPER

THE INFLUENCE OF VEGETATION ON REFLECTED SOLAR RADIATION IN ARID AND EXTRA-ARID ZONE OF MONGOLIAN GOBI

Viktor P. Dedkov[1], Elena V. Danzhalova[2], Sergey N .Tkachenko[1], Khadbaatar S.[3], Ariunbold E.[4] Peter D. Gunin[2], Sergey N. Bazha[2*]

[1]Immanuel Kant Baltic Federal University, 14, A. Nevskogo ul., Kaliningrad, 236036, Russia

[2]A.N. Severtsov Institute of Ecology and Evolution, Russian Academy of Sciences, 33, Leninsky Prospekt, Moscow, 119071, Russia

[3]Mongolian National University of Education, 14, Baga toiruu, Ulaanbaatar-48, 210648, Mongolia

[4]Botanical Garden – Institute, Mongolian Academy of Sciences, 77 – Jukov avenue-77, Ulaanbaatar – 51, 13330, Mongolia

*Corresponding author: sbazha@inbox.ru

Received: May 12th, 2020 / Accepted: November 20th, 2020 / Published: December 31st, 2020

https://DOI-10.24057/2071-9388-2020-91

ABSTRACT. Vegetation cover has a noticeable effect on surface reflectivity and local microclimate in arid areas of Mongolian Gobi. Over the past decades, various shrub species (*Haloxylon ammodendron* and *Calligonum mongolicum*) have appeared on the previously unvegetated hamada. The climatic consequences of bush encroachment are still poorly understood. Using the experimental data, this article estimates the reflectance of plants dominating in Mongolia's dry steppe, desert-steppe, and desert ecosystems. The average values of the total reflection coefficient at visible and infrared wavelengths range from 19.7% ± 1.4% to 20.1% ± 1.7% in plants growing in desert-steppe ecosystems, and from 25.0% ± 0.9% to 24.8% ± 1.5% on the bare surface. The difference between the reflectance of vegetated and unvegetated surfaces reaches 5%. Therefore, in daylight hours, the vegetated day surface loses less solar energy than the non-vegetated surface does. This phenomenon may be defined as a quasi- or secondary greenhouse effect – in daylight hours, solar energy is retained on the surface by vegetation and this contributes to the temperature increase. Such an impulse, which seems to be insignificantly small at first glance, triggers a series of climatic variations leading to a change in the structure of the radiation and heat balance as well as the climate not only in the desert-steppe and desert ecosystems but also in Central Asia as a whole. All this may explain the 1.2-2.3°C increase in air temperatures in the Gobi observed over the last 25 years.

KEY WORDS: Mongolia, Gobi desert, desert-steppe, plant cover, solar radiation, reflectance, surface temperature

CITATION: Viktor P. Dedkov, Elena V. Danzhalova, Sergey N .Tkachenko, Khadbaatar S., Ariunbold E., Peter D. Gunin, Sergey N. Bazha (2020). The Influence Of Vegetation On Reflected Solar Radiation In Arid And Extra-Arid Zone Of Mongolian Gobi. Geography, Environment, Sustainability, Vol.13, No 4, p. 72-80
https://DOI-10.24057/2071-9388-2020-91

Conflict of interests: The authors reported no potential conflict of interest.

INTRODUCTION

The surface of the Earth is not uniform and climatic zones have different functions in the biosphere. Eurasia's desert-steppe zone, which occupies approximately 4 b ha (Zalibekov and Novikova 2016), is a special type of landscape that is characterised by accelerated development. In deserts, successive evolutionary changes occur much more rapidly than they do in other landscapes. Many millions of years ago, the early evolution of deserts was affected primarily by the physiographical factors – high solar radiation intensity, winds, dryness of air and soils, scarcity of precipitation, and others. The later stages of evolution were shaped by not only the physiographical but also the biotic factor – namely, the emergence of the vegetation cover and fauna. The latter had a corrective effect on ecological regimes and the trajectory of climate change (Gunin et a1. 1980; Dedkov et al. 2017).

This phenomenon has been observed in some deserts of Central Asia including the Gobi desert (Karthe et al., 2019; Gradel et al., 2019). Our data suggets that the unvegetated areas of the Gobi desert have reduced over the last 35-40 years. The desert land cover on the inter-gully areas (hamada) in Trans-Altai Gobi, which had a dark shade in the 1970s, looks pale-yellowish today, which is explained by the accumulation of sandy material. Large amounts of sandy material are found in the wind shadow of *Haloxylon ammodendron*[1], *Calligonum mongolicum*, *Nitraria sphaerocarpa*, and *Reaumuria soongarica*. The formation of sand ridges and a porous crust horizon under plants results in the emergence of biotopes that differ from gullies and inter-gully areas in terms of environmental conditions.

Over the past decades, various shrub species (*Haloxylon ammodendron* and *Calligonum mongolicum*)

[1]Latin names of plants are given by The Plant List (http://www.theplantlist.org/)

have appeared on the previously unvegetated hamada (Slemnev et al. 1994; Gunin et al. 1999). The depth of gullies below the surface of inter-gully areas has decreased as a result of the accumulation of sand and gravel material. Unlike previous decades, the process taking place in gullies is accompanied by an increase in the number of shrubs and semi-shrubs characterised by a large phytomass and significant projective cover (*Haloxylon ammodendron, Ajania fruticulosa*, and *Salsola arbuscula)*, as well as in the number of perennial grasses (*Arnebia fimbriata*, *Zygophyllum potaninii*, etc.).

In 1952–2013, plant communities developed and expanded in inter-gully areas, in gullies, on dunes and mountain slopes. The number of rodent colonies rose and the volume of, and area occupied by shed vegetative parts increased. A progressive expansion of *Ephedra sinica* and *Allium polyrhizum* was observed (Gunin et al. 2012; Bazha et al. 2015). Areas of low temperatures emerged and expanded above the surface of plants as well as regions of very high temperatures above the surfaces of shed vegetative parts in the mountains, on hamadas, in gullies, and on dunes. The ensuing fragmentation of biotopes increased the extremeness, dispersion, and diurnal amplitude of temperatures (Dedkov 2016). Over 60 years (1952–2013), the proportion of such degradation indicator species as *Artemisia adamsii, A. frigida, Leymus chinensis, Carex duriuscula, Sibbaldianthe bifurca, Polygonum angustifolium, and others rose in the communities of Gobi's dry* and desert steppes. (Bazha et al. 2012). At the same time, a good condition of typical desert steppe dominants – *Allium polyrhizum, Cleistogenes songorica, Stipa tianschanica*, and *S. caucasica* was observed alongside an increase in the number of plant species (in some places by 100%), the projective cover, and especially the total aboveground phytomass (Kazantseva 2009; Kazantseva et al. 2015).

Animal husbandry has been Mongolia's economic specialisation since ancient period. Natural pastures account for about 70% of the country's territory or approximately 112.4 m ha, according to FAOSTAT, 2014. In 2016, the National Statistical Agency of Mongolia estimated the national livestock at 62 million animals (http://www.en.nso.mn/). This cannot but affect the structure of vegetation cover, surface reflectance, microclimate, and the radiation balance. A major area of vegetation cover studies is the application of remote methods based on satellite and aerial imagery of vast areas. Such studies include an assessment of plant biomass (Zhao et al. 2014, Sibanda et al. 2017); leaf area index monitoring (Rusli and Majid 2014, Kappas and Propastin 2012); analysing temporal dynamics of vegetation given phenological phases (Marstona et al. 2016); classifying plant communities (Chopping et al. 2008); assessing the quality of fodder and pasture productivity (Ali et al. 2016), and other research. The analysed parameters include various vegetative indices (Karnieli et al. 2013).

It was found that vegetation cover can have a noticeable effect on surface reflectivity and local temperatures (Bonan 2008; Brovkin et al. 2013; Collatz et al. 2000; Heck et al. 2001). At the same time, there is an opinion that in arid landscapes, the influence of vegetation on the reflectivity is insignificant due to its scarcity and strong sparseness (Curadeau et al., 2016). However, due to the active process of shrubbery in ecosystems of arid and semi-arid landscapes, which occurs in different regions of the planet (North and South America, Africa, Australia), researchers start to notice various consequences of this process, mainly concerning the changes in the soil and vegetation cover (Van Auken 2000; Knapp et al. 2008; Buffington and Herbel 1965; Cyrus et al. 2017., Archer et al. 2017). In particular, it was found that overgrowth in the Chihuahua Desert in North America leads to a change in the microclimate, namely, an increase in soil temperature and night air temperature is noted (D'Odorico et al. 2010). It should be noted that the climatic consequences of bush encroachment are still poorly understood.

It is well known, that certain applied research issues cannot be solved solely using remote methods. The value of NDVI obtained remotely depends on the species composition, vegetation density and condition, exposure and angle of inclination of the surface, the colour of the soil under sparse vegetation. Besides, the NDVI is sensitive to changes in the soil background when the projective vegetation cover is below 30% (Cherepanov, Druzhinina 2009), which is typical for most of the studied areas.

Alongside general information on the condition of the vegetation cover, it is important to have an idea about the effect of certain plants on the transformation of surface reflectance. Studying the spectral properties of plants and plant communities is important for analysing the surface radiation balance, identifying the current causes of climate change, modelling the energy-mass exchange processes, and solving other research problems. Another urgent objective is estimating the contribution of invasive plant species to the changes in the radiation balance and microclimate structure. This data is necessary for monitoring the state of ecosystems affected by both anthropogenic factors and natural processes.

This work aims to examine the reflectance of plants in Mongolia's arid and extra-arid zone in order to study their properties and characteristics and to analyse the influence of their reflectance on climate processes and the component structure of the radiation balance. The authors analysed the reflectance of solar radiation not only for the plants under natural conditions but also for those affected by grazing. The analysis took into account weather and climate characteristics, phenological states, biotope ecology, etc. Another objective was to measure the integrated spectra of steppe and desert communities (averaged a certain area) for its later use in classifying Landsat ETM and MODIS data.

METHODOLOGY AND MATERIALS PROCESSING

The fieldwork was carried out in August – September 2013, as part of a Joint Russian-Mongolian Complex Biological Expedition (JRMCBE) – a collaboration between the Russian Academy of Sciences and the Mongolian Academy of Sciences. We worked during the maximum vegetation period, therefore, we can assume that the influence of vegetation on the surface reflectance during this period will also the highest. The sampling sites (key plots) included dry steppe communities in the Dundgovi aimag (the Delgertsogt sum), mountain steppe, desert steppe and middle desert in the Ömnögovi aimag (the Bulgan and Gurvantes sums), middle desert, true desert and extra-arid desert in the Bayankhongor aimag (the Shinejinst sum) of Mongolian Gobi (Table 1, Fig. 1).

The research team used ASD FieldSpec II UV/VNIR handheld field spectroradiometer (Malvern Instruments, UK) to measure the intensity of solar radiation reflected from the surface of plants in the range of 325-1075 nm (at ultraviolet, visible, and near-infrared wavelengths). The measurement accuracy reached +/- 1.0 nm, the resolution – 3 nm. Measurements were possible at a viewing angle of 1-25 degrees. Due to the complex geometry of plants, the

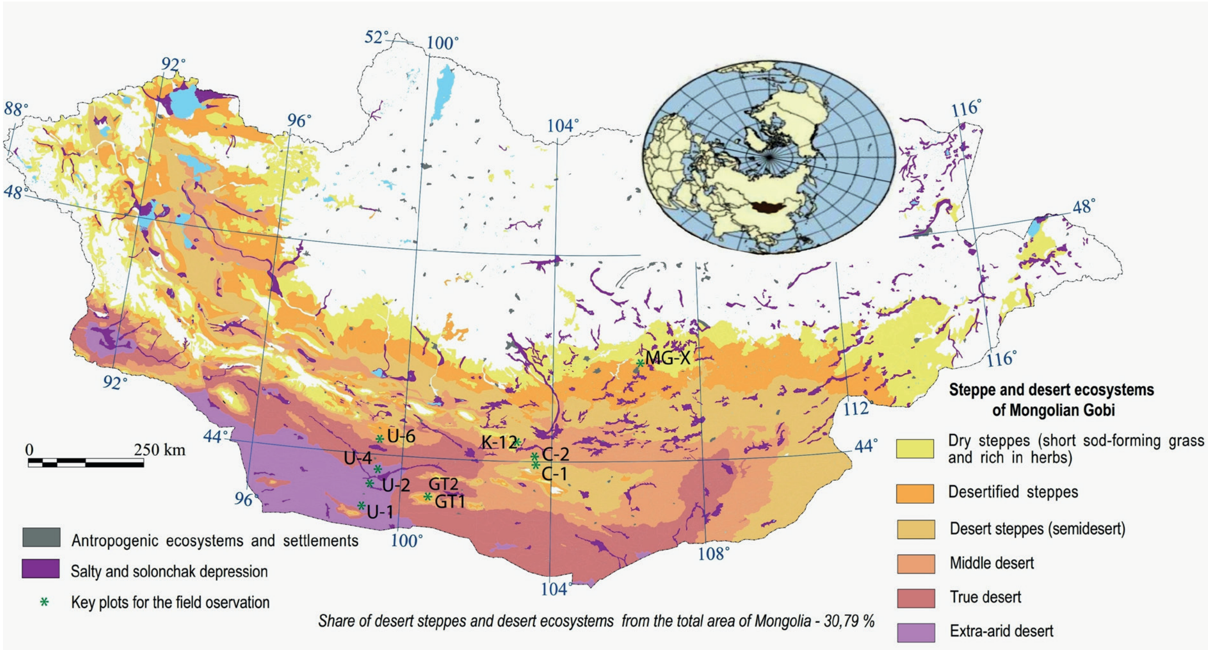

Fig. 1. Location of key plots on the Distribution Map of Subzonal Vegetation of the Mongolian Gobi (Gunin and Saandar 2019)

solar radiation reflected by plants consists of the radiation reflected by green and non-green fractions and the radiation transformed by plants. Thus, the level of the reflected signal depends on the solar elevation angle, weather conditions, phenology, the composition of plants and plant communities, and the optical properties of plants, shoots, and other vegetative and non-vegetative plant components.

Most measurements were performed at noon at a solar elevation angle of 45-55 degrees, and a viewing angle of 1 degree, the solar disc was open. White calibration was performed before each measurement. At the first stage, the spectra of the radiation reflected both by individual species and the unvegetated surface were measured. The integral spectra of the steppe and desert plant communities were measured within 30 by 30 m squares. In the first case, the instrument was placed in a vertical position to prevent soil reflectance at a viewing angle of 1 degree.

In the second case, the instrument was placed at an angle of 45 degrees to the surface to measure the radiation reflected by vegetation communities. Areal measurements using the 'envelope method' were performed alongside point ones. Within 30 by 30 m areas, measurements were performed from one corner to the opposite and then from the next corner to the opposite.

During the fieldwork, 142 spectra of reflected radiation were obtained, including 20 of steppe plant species, 65 of desert plants species, 35 of non-vegetated open areas, and 22 of plant communities.

The reflected radiation spectra were processed as follows: the 325-1075 nm range was divided into three parts (Shulgin 1973) – from 325 to 380 nm (UV wavelengths), 380-780 nm (visible wavelengths), and 780-1075 (near-infrared wavelengths). The total reflection coefficient was calculated for each of the three ranges. The coefficient corresponds to the total quantity of solar energy reflected by the object within each range, expressed as a percentage of the initial incident solar energy or of the energy reflected from an ideal dispersion surface of radiation within the same wavelength range.

Thus, three total coefficients characterising the reflectance of a certain plant or a 30*30 m area within a relevant wavelength range were obtained for each spectrum.

RESULTS AND DISCUSSION

The analysis of the data on the reflected short-wave solar radiation spectra in the plant communities of Gobi shows that the amount of radiation does not only depend

Table 1. Spectra of solar radiation reflection (SRR) by vegetation community dominants in the arid and extra-arid zone of Gobi, acquired on August 21 – September 03, 2013

Date/ Index	Subzone / plant community	Coordinates, Elevation, m	Time /Solar elevation	Plant species	Plant life-form	Reflected solar radiation spectra (%)			
						Total	UV	V	IR
21.08.13/ MG-X	Dry steppe / [Caragana leucophloea]-Allium polyrhizum	46°08'32"N 106°30'46,9"E H 1363	12.05-12.40/ 55.1°	*A. polyrhizum*	Herbaceous perennial succulent	25	4	23	30
				Control	-	29	4	26	36
				Scorzonera divaricata	Herbaceous perennial	25	4	24	29
				Control	-	28	4	27	32
				Artemisia scoparia	Herbaceous biennial	16	3	16	18
				Control	-	25	5	26	28

24.08.13/ C-2	Desert steppe / *Stipa tianschanica+Allium polyrhizum*	44°00'43.1"N, 103°33'34.8"E H 1434	11.42-12.04/ 53.9°	*Kraschenninnikovia ceratoides*	True dwarf shrub	15	4	17	14
				Control	-	19	6	21	20
25.08.13/ K-12	Middle desert / *Salsola passerina+Bracha nthemum gobicum*	44°14'21.2" N, 103°31 '05.3"E H 1081	12.15-12.29/ 54.8°	*Salsola passerina*	Succulent dwarf shrub	15	7	17	15
				Reaumuria soongarica	True dwarf shrub	26	11	30	26
				Control	-	31	12	35	30
28.08.13/ GT-1	Mountain steppe / *Ephedra sinica +Ajania fruticulosa +Allium polyrhizum*	43º11'54,4"N 100°42'26,4"E H 2093	09.55-10.23/ 37.2°	*E. sinica*	Dwarf shrub	14	5	16	14
				Control	-	20	5	19	25
28.08.13/ GT-2	Mountain steppe / *Ephedra sinica* (in the gorge close to GT-1)	-	10.56-11.12/ 45.7°	*E. sinica* (parent individual)	-	13	2	11	17
				Kraschenninnikovia ceratoides	True dwarf shrub	9	3	11	7
				Control	-	18	6	23	15
29.08.13/ U-1	Extra-arid desert / *Haloxylon ammodendron+ Ephedra przewalskii*	43°11'08.1"N 98°55'56.0"E H 1108	11.32-11.45/ 49.1°	*E. przewalskii*	Shrub	19	3	21	20
				H. ammodendron	Shrub	26	6	30	25
				Control	-	16	6	20	12
30.08.13/ U-2	Extra-arid desert / *Iljinia regelii*	43°22'29.5"N 99° 07'00.4"E H 763	10.49-11.15/ 48.8°	*I. regelii (on hamada)*	Dwarf shrub	12	6	15	9
				H. ammodendron (on hamada)	Shrub	15	7	19	11
				Control	-	14	7	18	10
				I. regelii (on gully)	-	7	2	6	8
				Control	-	19	8	24	14
02.09.13/ U-4	True desert / *Haloxylon ammodendron*	43°57'23.0"N, 99°13'41.8"E H 1264	13.54-14.28/ 52.5°	*H. ammodendron* (vegetative plant)	-	12	4	14	11
				H. ammodendron (drying plant)	-	20	6	24	18
				Control	-	28	7	34	25
03.09.13/ U-6	Middle desert / *Anabasis brevifolia*	44°15'29.8"N, 99°21'34.6"E, H 1253	10.43-10.58/ 40.8°	*Zygophyllum xanthoxylon*	Shrub	5	2	5	5
				Control (on hamada)	-	19	7	21	18
				Control (on gully)	-	10	3	10	11

on the geographical coordinates of the biotope, the absolute elevation, the phenological and physiological characteristics of plants, the structure of the crown, the feature of the surface, and the weather conditions but is also species-specific. The analysis of the data presented in table 1 (Index MG-X) suggests that, at noon, at a 4-6 tenths cloud cover (cumulus humilis), *Artemisia scoparia* reflects less shortwave solar radiation in the visible and infrared ranges than the other species dominating the *[Caragana leucophloea]-Allium polyrhizum* community in a dry steppe do.

The maximum reflected solar radiation was observed in the visible range of 525-625 nm. The quantity of reflected solar radiation at visible wavelengths was decreasing in the 625-725 nm range and increasing in the near-infrared range. In the nature of changes, the signal reflected from the surface of *Allium polyrhizum* is similar to that observed in *Artemisia scoparia*. However, the magnitude of reflectance at visible and infrared wavelengths was much higher. The reflection of solar radiation from the soil surface, which was used as a control, changes similarly to the reflection from the surfaces of plants. The only difference is that, at infrared wavelengths, the magnitude of reflection from the soil surface is higher than that from plant surfaces.

The species of the *Salsola passerina+Brachanthemum gobicum* community reflected more solar radiation at visible wavelengths than dry steppe plants did (Tab.1, Index K-12).

The maximum reflected radiation (up to 60%) at visible wavelengths (525-625 nm) was observed in *Zygophyllum xanthoxylon* and the minimum (below 30%) in *Salsola passerina*. A significant difference between these species was detected at infrared wavelengths. *Reaumuria soongarica* and *Anabasis brevifolia* were characterised by average reflected radiation values.

In an extremely arid desert (Table 1, Index U-1; U-2), the reflected solar radiation spectrum data is mainly similar to that of plants growing in dry steppes and desert steppes. The maximum solar radiation reflected from plant surfaces at visible wavelengths was detected in the aphyllous shrub *Haloxylon ammodendron*, and the minimum in *Ephedra przewalskii*. At near-infrared wavelengths, the situation did not differ from that described above. The maximum infrared solar radiation was observed in *Haloxylon ammodendron* and the minimum in the shrub *Calligonum mongolicum*.

As it was shown above, the Gobi desert is undergoing a rapid change in the species composition accompanied by the expansion of the vegetation cover – both human-induced and natural. Earlier publications have emphasised that the expansion of vegetation communities leads to changes in the surface temperature and increasing biotope fragmentation (Dedkov et al. 2017). It is reasonable to assume that the emergence of plants and the expansion of vegetated areas will affect the reflectance, the structure of the radiation and heat balance as well as climate processes. For this purpose, quasi-synchronic observations were performed. They included measuring the radiation reflected from the surfaces of plants and the unvegetated surface (Table 1).

The data presented in table 1 suggests that the dominant plants in different vegetation communities of Gobi reflect much less shortwave solar radiation – both visible and infrared – than the unvegetated surface. At visible wavelengths, in approximately 73% of all cases, plants reflected less shortwave solar radiation than the unvegetated surface. This difference varied from biotope to biotope, ranging from -1 to -20% (Fig. 2).

Clustering made it possible to identify the centroids as points and calculate the distances to all centroids. Each object is assigned to the nearest cluster by distance. Straight lines were used as central axes of a cluster. Objects were assigned to a cluster based on the distance to these lines. The boundary conditions were as follows – the root-mean-square error (RMSE) → min within each cluster, the R-squared value (R^2) > 0.6, the total squared error → min, and the number of clusters → min.

As fig. 2 shows, based on the visible wavelengths, plants can be divided into five groups depending on the correlation between the total reflection coefficients of the unvegetated surface and the plant. Groups 1, 2, and 3 comprise species characterised by an intensity of SRR that is lower than that of the unvegetated surface. Most of the studied plants belong to one of these three groups. In group 1, which brings together *Haloxylon ammodendron, Salsola passerina*, and *Iljinia regelii*, the difference between the total coefficient of plants and the surface is very significant at visible wavelengths. In group 3, which comprises *Zygophyllum rosowii* and *Ephedra przewalskii*, this difference is rather negligible. Group 2 is characterised by a moderate difference. There is a distinct boundary between groups 1 and 2 – the distance between the nearest points assigned to groups 1 and 2 is very significant and comparable to the size of the clusters. An indirect indication of correct clustering is the approximate equality of the linear trend slopes for each cluster.

Group 4 (*Haloxylon ammodendron* and *Stipa caucasica*) and group 5 (*Haloxylon ammodendron* and *Zygophyllum xanthoxylon*) bring together plants that demonstrate a higher total reflection coefficient at visible wavelengths than the unvegetated surface. These groups are rather small in comparison to groups 1-3.

Similar results were obtained for SRR at infrared wavelengths. Over 72% of plants reflected infrared radiation less intensively that the unvegetated surface did. However, the difference between the plant surfaces and control was more significant than in the case of visible radiation, reaching 33% (Fig. 3).

According to fig. 3, the plants can be divided into three groups based on the correlation between the unvegetated surface/plant total reflection coefficients. These groups can be described as follows. Group 1 (*Allium polyrhizum, Haloxylon ammodendron*, and *Salsola passerina*) comprises plants, whose reflection intensity is much lower than that of the adjacent unvegetated area. This is the largest group. Group 2 (*Haloxylon ammodendron, Iljinia regelii*, and *Krascheninnikovia ceratoides*)

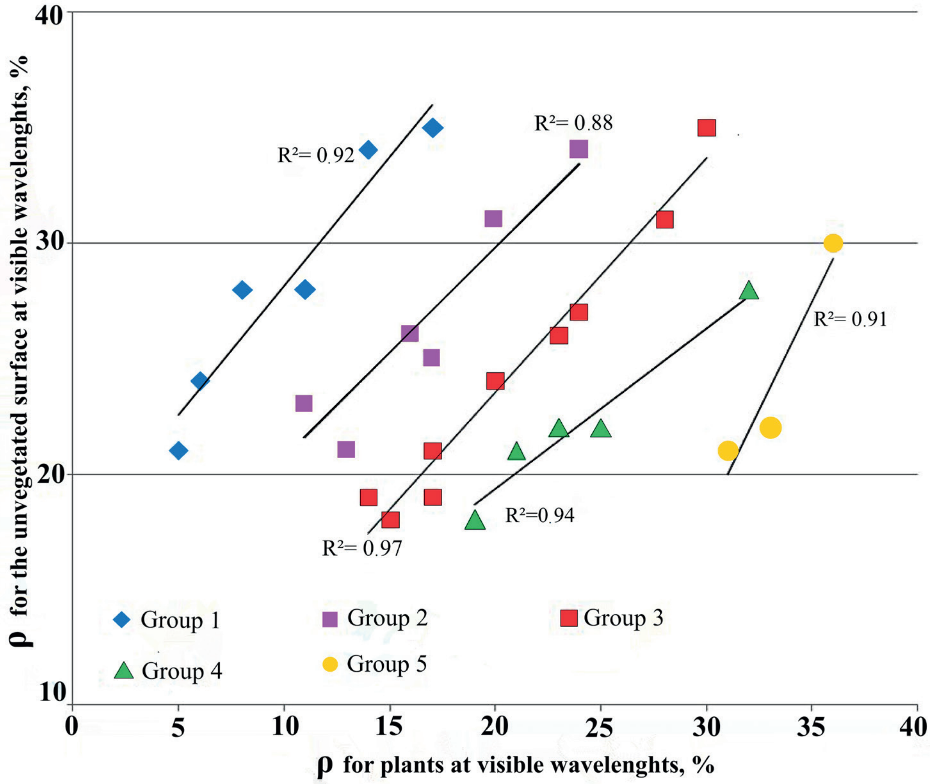

Fig. 2. The correlation between the total reflection coefficient of plants and adjacent unvegetated areas at visible wavelengths for 32 dominant species in different communities of Gobi. k-means clustering was performed using the obtained data (MacQueen 1967)

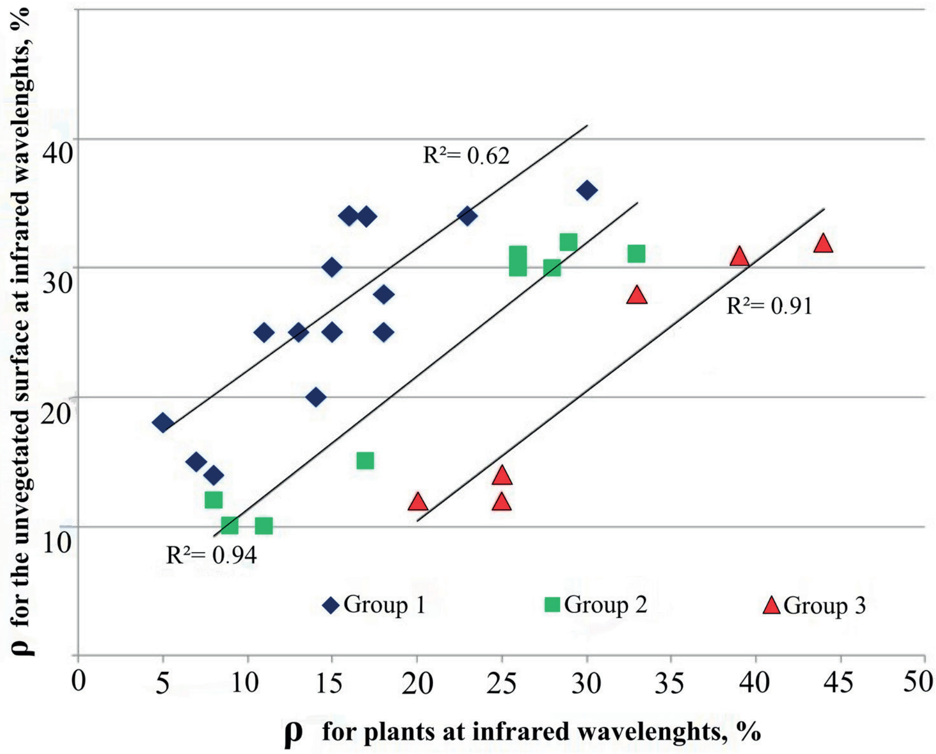

Fig. 3. The relationship between the total plants and unvegetated surface reflection coefficient at infrared wavelengths for 32 dominant plant species in different communities of Gobi. *k*-means clustering of the objects was performed

is characterised by roughly equal total plant and unvegetated surface coefficients (the difference is not more 5 %). Group 3 (*Haloxylon ammodendron, Ephedra sinica*, and *Zygophyllum xanthoxylon*) brings together plants, whose reflection intensity significantly exceeds that of the unvegetated surface. This group is the smallest.

It is impossible to identify plants characteristic of a certain group, since some of the species may belong to several groups, which is the case for *Haloxylon ammodendron*. This can be indicative of a complex interdependence between the reflectance of plants and the adjacent surface.

The most intensive absorption of solar radiation by plants was observed in the morning and at noon. However, when measuring the solar radiation reflected by *Haloxylon ammodendron, Ephedra sinica* and *Zygophyllum xanthoxylon*, the opposite phenomenon was detected – plants reflected more solar radiation at visible and infrared wavelengths than the unvegetated surface. These anomalous results may be explained by the structure of tree crowns, the phenological and physiological state of plants, as well as the weather conditions.

In the desert steppe of the Northern Gobi (C-1, C-2), measurements of reflected radiation were carried out on pasture under grazing and in enclosed areas. In the pasture area dominated by *Stipa tianschanica+Convolvulus ammannii* community, the projective cover did not exceed 10% and the height of plants was less than 10 cm, due to the livestock impact. In the non-pasture area dominated by a *Stipa tianschanica+Allium polyrhizum* community, the projective cover reached 15% and the plant height 15-20 cm. Vegetation was of darker colour in the pasture and of lighter colour in the non-pasture area. Observations were performed in clear and windless weather in the morning on August 24, 2013.

It was found that the intensity of solar radiation reflected from the surface was minimum in the non-pasture (enclosed) area and maximum in the pasture (Fig. 4). The most significant differences were observed at visible wavelengths. In the non-pasture areas, the quantity of solar radiation at 525-625 nm wavelengths did not exceed 20%, whereas, in the pasture areas, it was almost twice that level. At infrared wavelengths, SRR was more intense in the pasture than in the non-pasture area.

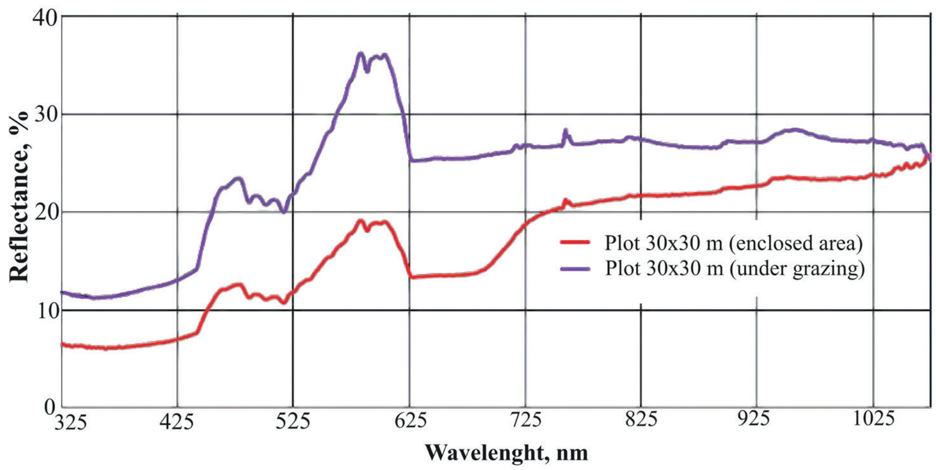

Fig. 4. Spectra of solar radiation reflectance in a desert steppe: in the non-pasture (enclosed) and pasture (under grazing) areas (24.08.2013; 10:00-10:22 a.m.)

This data is consistent with the measurements of surface temperature in the pasture and enclosed areas. Observations were performed in clear and windless weather over 24 hours on August 24-25, 2013. The maximum soil surface temperature was 56.4°C in the non-pasture area and did not exceed 54°C in the pasture area. The frequency of occurrence of temperatures above 50°C was six in the pasture and almost 2.5 times that (15) in the non-pasture area. Average temperatures also differed. The average of 30 measurements reached 50.8°C in the non-pasture area and 48.1°C in the pasture. The difference between the soil surface temperature measured at night and in the morning in the pasture and non-pasture areas was negligible. The absolute minimum was observed at 7 a.m. local time (12.5°C) in the pasture on August 25, 2013. The non-pasture absolute minimum was 13.5°C (Dedkov et al. 2017).

Thus, it was experimentally confirmed that the reflectance from a vegetated surface is lower than from an unvegetated surface. The total reflection coefficient of a large number of plants is lower than that of the unvegetated surface at visible and infrared wavelengths.

To prove this hypothesis, the average total plant and surface reflection coefficients (ATRC) were calculated for the considered wavelengths (a total of 32 plants). Table 2 shows the obtained values. The data are presented in the form $\bar{x} \pm \sigma_{\bar{x}}$, where $\bar{x} = \frac{1}{n}\sum_{i=1}^{n} x_i$ is the average value, $\sigma_{\bar{x}} = \sqrt{\frac{\sum_{1=1}^{n}(x_i - \bar{x})^2}{n(n-1)}}$ – root-mean-square error of the average value, and n the number of elements in the sample.

The data shown in table 3 suggest that the projective cover has increased by 3-18% in the steppe and desert vegetation communities of Mongolian Gobi over the past 50 years. The average increase is 10%, which is comparable to the data obtained by other researchers (Donohue et al. 2013).

CONCLUSIONS

The collected data was used to obtain a first approximation the contribution of the vegetation cover to the reduction in solar radiation from the day surface across the arid territories of Central Asia. According to Petrov (1973), the area of Central Asian deserts is 16.5 m km^2. Approximately 10% of the desert area is covered with plants. The amount of solar radiation reflected from the surface of the Gobi

Table 2. Average values of the total reflection coefficient of plants and unvegetated surfaces

Wavelengths	ATRC of plants, %	ATRC of surfaces, %
Visible	19.7±1.4	25.0±0.9
Infrared	20.1±1.7	24.8±1.5

Table 3. Multidecadal changes in the projective cover in the desert and steppe zones of the Gobi, 1972–2013

Subzone/ Index	Year /Total PC (%)	Year /Total PC (%)	Plant community	Plant species	Year / Total PC (%)	Year /Total PC (%)
Middle desert / K-12	1972/ 10.2	2003/ 15.8	*[Zygophyllum xanthoxylon, Nitraria sibirica] – Brachanthemum gobicum + Reaumuria soongarica*		1972	2003
				B. gobicum	5.0	5.4
				R. soongarica	2.0	1.9
Desert steppe / C-2	1972/ 9.0	2003/ 11.8	*[Haloxylon ammodendron + Zygophyllum xanthoxylon] – Reaumuria soongarica + Brachanthemum gobicum*		1972	2003
				R. soongarica	3.0	3.4
				B. gobicum	0.8	0.8
				Z. xanthoxylon	1.3	0.5
				H. ammodendron	0.2	1.3
Mountain steppe/ GT-1	1993/ 15.5	2013/ 18.8	*Ephedra sinica + Ajania fruticulosa + Allium polyrhizum*		1993	2013
				E. sinica	7.0	12.0
				A. fruticulosa	1.8	2.2
				A. polyrhizum	1.5	2.5
Extra- arid desert/ U-1, U-2	1978/ 3.5	1993/ 22.6	*Haloxylon ammodendron + Ephedra przewalskii*		1978	1993
				H. ammodendron	3.0	22.0
				E. przewalskii	0.5	0.6
Middle desert/ U-6	1978/ 3.2	1993/ 7.6	Anabasis brevifolia + Stipa caucasica + Allium polyrhizum		1978	2013
				A. brevifolia	2.5	No data
				A. polyrhizum	0.3	
				S. caucasica	0.4	

Desert in the summer months reaches 4 MJ/m^2/day (Gunin et al. 1980). Plants reduce solar radiation reflectance by 5%. In the absence of vegetation and under normal conditions, the bare surface of the Central Asian deserts would reflect 66·1013 MJ/day. A 10% projective cover accounts for a 5% change in reflectance and retains 3.3·1011 MJ/day or 0.5% of the total amount of energy reflected daily from the total day surface of the Central Asian deserts. In the Gobi Desert – given the same projective cover parameters – the amount of plant-retained energy will amount to 3.0·1010 MJ/day.

Thus, the overgrowth of deserts by plants increases not only the leaf surface area, projective cover, and biomass but also the amount of solar radiation retained at the surface, which affects the structure of the radiation and heat balance and the air temperature. According to the Choir, Sainshand, and Zamyn-Uud weather stations, the temperature increased by 1.2-2.3°C in the east of the Gobi desert over 25 years from 1989 to 2015. The projective cover, the leaf surface area, and biomass depend on precipitation, the amount of which differs from year to year. It can be assumed that the amount of solar radiation reflected by the vegetation cover on arid territories will differ under various weather conditions. Probably, deserts have a stronger effect on the reduction in solar radiation reflectance by the surface than other natural ecosystems do. Thus, they affect the structure of the radiation and heat balance as well as air temperature.

The accumulation of solar radiation by plants growing on arid territories was proven experimentally. The difference in reflection from the vegetated and unvegetated surfaces is 5%, according to our estimates. Therefore, during daylight hours, the vegetated day surface releases less solar energy than the unvegetated surface does. This effect may be defined as a quasi- or secondary greenhouse effect – in the daytime, a portion of solar energy is not released from the surface but is rather retained by vegetation. This impulse, which seems to be insignificantly small at first glance, may trigger a series of climatic variations leading to a change in the structure of the radiation and heat balance as well as the climate of the desert-steppe and desert ecosystems in the Gobi.

REFERENCES

Archer S.R., Andersen E.M., Predick K.I., Schwinning S., Steidl R.J., Woods S.R. (2017). Woody Plant Encroachment: Causes and Consequences. In: Briske D. (eds) Rangeland Systems. Springer Series on Environmental Management. Springer, Cham, DOI: 10.1007/978-3-319-46709-2_2.

Bazha S.N., Gunin P.D., Danzhalova E.V., Drobyshev Yu.I., Kazantseva T.I., Ariunbold E., Myagmarsuren D., Khadbaatar S., Tserenkhand G. (2015). Invasive successions as an indicator of desertification of dry steppe by way of example of Central Mongolia. Russian Journal of Biological Invasion., [online] Available at: https://www.pleiades.online/cgi-perl/search.pl?type=abstract&name=bioinv&number=4&year=15&page=223. 6(4), 223-237, DOI: 10.1134/S2075111715040025.

Bonan G.B. Forests and climate change: forcings, feedbacks, and the climate benefits of forests. (2008). Science 320, 1444-1449.

Brovkin V. et al. (2013). Evaluation of vegetation cover and land-surface albedo in MPI-ESM CMIP5 simulations. J. Adv. Model. Earth Syst. 5, 48-57.

Buffington L. C. and C.H. Herbel (1965). Vegetational changes on a semidesert grassland range from 1858 to 1963. Ecological Monographs. 35 (2), 139-164.

Cherepanov A., Druzhinina E. (2009). Spectral characteristics of vegetation and vegetation indexes // Geomatics. [online] Available at: https://elibrary.ru/item.asp?id=22298135. 3, 28-32 (In Russian).

Collatz G.J., Bounoua L., Los S.O., Randall D.A., Fung I.Y. & Sellers P.J. (2000). A mechanism for the influence of vegetation on the response of the diurnal temperature range to changing climate. Geophysical Research Letters, 27, 3381-3384.

Cyrus M. Kavwele, Johnstone K. Kimanzi, Mwangi J. Kinyanjui (2017). Impacts of Bush Encroachment on Wildlife Species Diversity, Composition, and Habitat Preference in Ol Pejeta Conservancy, Laikipia, Kenya. International Journal of Ecology, vol., Article ID 5620125, 6.

Dedkov V.P. (1989). The ecological niche and water balance of desert phytocenoses dominants. Leningrad State University Press: Leningrad, 264 (In Russian).

Dedkov V.P. (2016). On the influence of biotisation of Central Asian deserts on the changes in the surface temperature and the Earth's climate. In: Natural and anthropogenic changes in arid ecosystems and the struggle to combat desertification. Alef: Makhachkala. [online] Available at: https://elibrary.ru/item.asp?id=2751178346-49 (In Russian).

Dedkov V.P., Gunin P.D., Kazantseva T.I., Drobyshev Yu. I. (2017). The temperature of underlying surface in the arid zone of Mongolia ecosystems and the role of biota in its change. Russian Journal of Ecology. 48(1), 32-37, DOI: 10.1134/S1067413617010052.

D'Odorico P., Fuentes J.D., Pockman W.T., Collins S.L., He Y., Medeiros J.S., Litvak M.E. (2010). Positive feedback between microclimate and shrub encroachment in the northern Chihuahuan desert. Ecosphere, 1(6), art. 17, DOI: 10.1890/ES10-00073.1.

Donohue R.J., Roderick M.L., McVicar T.R., and Farquhar G.D. (2013). Impact of CO2 fertilisation on maximum foliage cover across the globe's warm, arid environments, Geophys. Res. Lett. 40(12), 3031-3035, DOI: 10.1002/grl.50563.

Fen Zhao, Bin Xu, Xiuchun Yang, Yunxiang Jin, Jinya Li, Lang Xia, Shi Chen and Hailong Ma. (2014). Remote Sensing Estimates of Grassland Aboveground Biomass Based on MODIS Net Primary Productivity (NPP): A Case Study in the Xilingol Grassland of Northern China. Remote Sens. [online] Available at: https://www.mdpi.com/2072-4292/6/6/5368. 6, 5368-5386.

Food and agriculture organization of the United Nation: [e-resource]. Available at: http://www.fao.org/home [Accessed 19 Sep. 2019].

Gradel A., Sukhbaatar G., Karthe D., Kang H. (2019). Forest Management In Mongolia – A Review Of Challenges And Lessons Learned With Special Reference To Degradation And Deforestation.GEOGRAPHY, ENVIRONMENT, SUSTAINABILITY, 12(3), 133-166, DOI: 10.24057/2071-9388-2019-102

Gunin P.D. & Saandar M. Eds. (2019). Ecosystems of Mongolia Atlas. ADMON Print: Ulaanbaatar, 264.

Gunin P.D. (1990). The ecology of arid ecosystem desertification. VASKHNIL: Moscow, 354 (in Russian).

Gunin P.D., Bazha S.N., Danzhalova E.V., Dmitriev I.A., Drobyshev Yu.I., Kazantseva T.I., Miklyaeva I.M., Ogureeva G.N., Slemnev N.N. (2012). Expansion of Ephedra sinica Stapf. in the arid steppe ecosystems of eastern and central Mongolia. Arid Ecosystems. 2(1), 18-33, DOI: 10.1134/S2079096112010052.

Gunin P.D., Dedkov V.P. (1978). Ecological regimes of desert biogecenoses. Nauka: Moscow, 228 (in Russian).

Gunin P.D., Vostokova E.A., Dorofeyuk N.I., Tarasov P.E., Black C. (1999). Vegetation Dynamics of Mongolia. Kluwer Acad. Publ., 238.

Heck P., Lüthi D., Wernli H., Schär Ch. (2001). Climate impacts of European scale anthropogenic vegetation changes: A sensitivity study using a regional climate model. Journal of Geophysical Research: Atmospheres. 106. Issue D8., 7817-7835.

Iftikhar Ali, Fiona Cawkwell, Edward Dwyer, Brian Barrett and Stuart Green. (2016). Satellite remote sensing of grasslands: from observation to management. Journal of Plant Ecology. 9(6), 649-671, DOI: 10.1093/jpe/rtw005.

Kappas M.W., Propastin P.A. (2012). Review of Available Products of Leaf Area Index and Their Suitability over the Formerly Soviet Central Asia. Journal of Sensors. 2012, (ID 582159). 11, DOI: 10.1155/2012/582159.

Karnieli A., Bayarjargal Y., Bayasgalan M., Mandakh B., Dugarjav Ch., Burgheimer J., Khudulmur S., Bazha S.N. and Gunin P.D. (2013). Do vegetation indices provide a reliable indication of vegetation degradation? A case study in Mongolian pastures. International Journal of Remote Sensing. 34(17), 6243-6262.

Karthe D., Chalov S., Gradel A., Kusbach A. (2019). Special issue «Environment change on the Mongolian plateau: atmosphere, forests, soils and water». GEOGRAPHY, ENVIRONMENT, SUSTAINABILITY, 12(3), 60-65, DOI: 10.24057/2071-9388-2019-1411

Kazantseva T.I. (2009). Productivity of the zonal vegetation community of steppes and deserts in the Gobi part of Mongolia. Moscow: Nauka. 336 (in Russian with English summary).

Kazantseva T.I., Bazha S.N., Gunin P.D., Danzhalova E.V., Dedkov V.P., Drobyshev Yu.N., Dugarzhav Ch., Khadbaatar S. (2015). Long-term dynamics in the vegetation communities of desert steppes of Central Mongolia: The case of the Övörkhangai aimag. // Botanical Journal. 100(3), 249-270, DOI: 10.1134/ S0006813615030047 (in Russian with English summary).

Knapp A.K., Briggs J.M., Collins S.L., Archer S.R., Bret-Harte M.S., Ewers B.E., Peters D.P., Young D.R., Shaver G.R., Pendalland E., Cleary M.B. (2008). Shrub encroachment in North American grasslands: shifts in growth form dominance rapidly alters control of ecosystem carbon inputs. Global Change Biology. 14, 615-623, DOI: 10.1111/j.1365-2486.2007.01512.x.

MacQueen J. (1967). Some methods for classification and analysis of multivariate observations. Proc. 5th Berkeley Symp. on Math. Statistics and Probability. Univ. of Calif. Press. 281-297. [online] Available at: https://projecteuclid.org/euclid.bsmsp/1200512992. [Accessed 11 Jul. 2019].

Mark Chopping, Lihong Su, Albert Rango, John V. Martonchik, Debra P.C. Peters, Andrea Laliberte. (2008). Remote sensing of woody shrub cover in desert grasslands using MISR with a geometric-optical canopy reflectance model. Remote Sensing of Environment. 112(1), 19-34, DOI: 10.1016/j.rse.2006.04.023.

Petrov M.P. (1973). Deserts of the Earth. Nauka: Leningrad, 435 (In Russian).

Rusli N. & Majid M.R. (2014). Monitoring and mapping leaf area index of rubber and oil palm in small watershed area. In: IOP Conference Series: Earth and Environmental Science. V. 18. [012036] Institute of Physics Publishing. [online] Available at: https://iopscience.iop.org/article/10.1088/1755-1315/18/1/012036, DOI: 10.1088/1755-1315/18/1/012036.

Shulgin I.A. (1973). Plants and the Sun. Gidrometeoizdat: Leningrad, 251 (in Russian).

Sibanda M., Mutanga O., Mathieu Rouget M. and Kumar L. (2017). Estimating Biomass of Native Grass Grown under Complex Management Treatments Using WorldView-3 Spectral Derivatives. Remote Sens. 9(1), 55, 1-21. [online] Available at: https://www.mdpi.com/2072-4292/9/1/55, DOI: 10.3390/rs9010055.

Slemnev N.N., Gunin P.D., Kazantseva T.I. (1994). On the natural seed regeneration of dominant plants in the ecosystems of Mongolia's deserts. Plant resources. 30(4), 1-5 (in Russian with English summary).

The Plant List // http://www.theplantlist.org/ [Accessed 1 May. 2020].

Van Auken O.W. (2000). Shrub invasions of North American semiarid grasslands. nnual Review of Ecological Systems. 31, 197-215. [online] Available at: https://www.jstor.org/stable/221730?seq=1.

Zalibekov Z.G., Novikova N.M. (2016). Research and applied framework for a planetary strategy for combating desertification./in: Natural and anthropogenic changes in arid ecosystems and the struggle to combat desertification. Alef: Makhachkala, 31-37. [online] Available at: https://elibrary.ru/item.asp?id=27511780.

RESEARCH PAPER

ASSESSING LONG-TERM DEFORESTATION IN NAM SAN WATERSHED, LOEI PROVINCE, THAILAND USING A DYNA-CLUE MODEL

Katawut Waiyasusri[1]*, Parichat Wetchayont[2]
[1]Geography and Geo-Informatics Program, Faculty of Humanities and Social Sciences, Suan Suandha Rajabhat University, 1 U-Thong Nok Road, Dusit, Bangkok 10300 Thailand
[2]Department of Geography, Faculty of Social Science, Srinakharinwirot University, 114 Sukhumvit 23, Khlong Toei Nuea, Wattana District, Bangkok, Thailand
***Corresponding author:** katawut.wa@ssru.ac.th
Received: January 23th, 2020 / Accepted: November 20th, 2020 / Published: December 31st, 2020
https://DOI-10.24057/2071-9388-2020-14

ABSTRACT. This research analyzed land-use changes (LUC) in the Nam San Watershed (NSW) by applying geoinformatics methods and land-use modeling approach to explore LUC in the past. Landsat satellite images from years 2002, 2007 and 2013 were classified using a maximum likelihood algorithm to create land-use maps. For assessing future LUC over a period of twenty years (2014–2033), land-use simulations were conducted using a dynamic LUC model (Dyna-CLUE model) in two land management scenarios: Scenario 1 is a simple projection of the LUC trend without reservation area, while Scenario 2 projects the LUC trend with reservation area in future periods. NSW land-use maps for 2002–2013 were analyzed using geoinformatics technology. The results revealed that the amount of forested area within the NSW has reduced drastically, from 380.40 km^2 to 267.23 km^2, changing to fields and perennial crops, which the logistic regression identified as being influenced by a slope factor. These data was used as a reference for LUC detection with the model simulation in two scenarios. Model results have shown that by 2033, Scenario 1 predicts a significant decrease in the overall forest area, from 72.21 km^2 to 41.55 km^2 in Phu Ruea district, and from 107.31 km^2 to 45.62 km^2 in Phu Luang district. Whereas Scenario 2 predicts slightly decreasing forest area within the reservation area, but rapid decrease, from 177.86 km^2 to 28.54 km^2 outside the reservation area, where the distance to village factor is the main influencer. These findings highlight the importance and the potential of model predictions for planning activities to protect forested areas.

KEY WORDS: Land-Use Change, Dyna-Clue Model, Deforestation, Nam San Watershed, Loei Province

CITATION: Katawut Waiyasusri, Parichat Wetchayont (2020). Assessing Long-Term Deforestation In Nam San Watershed, Loei Province, Thailand Using A Dyna-Clue Model. Geography, Environment, Sustainability, Vol.13, No 4, p. 81-97
https://DOI-10.24057/2071-9388-2020-14

ACKNOWLEDGEMENTS: Acknowledgements to Tom Veldkamp, Louise Fresco and Peter Verburg from the Institute for Environmental Studies (IVM), VU University, Amsterdam for providing the Dyna-CLUE model, and the U.S. Geological Survey (EarthExplorer Homepage: https://earthexplorer.usgs.gov/) for providing their Landsat imagery.

Conflict of interests: The authors reported no potential conflict of interest.

INTRODUCTION

Over the last several decades, South East Asian ecosystems have been altered substantially as a result of the socio-economic change (Mallinis et al. 2011; Moreira et al. 2001), while future changes are also expected to occur (Islam et al. 2018; Lambin 1997). Thailand is only one of the countries in Southeast Asia facing this problem. As mentioned previously, from 1961 to 1993 Thailand's forest area decreased by an average rate of 4,368 km^2 per year, with a high tendency to continue declining, especially in Loei province in the NSW area. Even though there was a royal act to dismiss the concession forest or control the boundary of Phu Ruea National Park and Phu Luang Wildlife Sanctuary, decreasing forested areas are still found periodically (Royal Forest Department 2016). This leads to problems such as soil erosion, and cause repetitious natural disasters, i.e. landslides and floods in the monsoon season from June to October every year (Yumuang 2001), and water deficiency for agriculture in the dry season (Santiphop et al. 2012), which results in loss of agricultural production and affects public utility systems in communities in mountainous areas (Gilani et al. 2015; Lambin 1997). Generally, research related to LUC dynamics in mountainous regions of Southeast Asia has found that the push factors affecting LUC are usually of a socio-economic context in each watershed area (Geist and Lambin 2002; Luo et al. 2010; Turner II et al. 2007). For instance, in the study area of the NSW is characterized by complex mountainous geography with abundant forest resources, wild animals and seedlings, which is a unique terrain in Thailand (Department of Mineral Resources 2009). Nowadays, this watershed area has been affected by human activities (Klongvessa et al. 2018; Satika B. and Chotpantarat 2014; Satika B and Chotpantarat 2018;

Waiyasusri and Chotpantarat 2020), not only by the growing population but also by conversion of forested areas for agricultural use. The area is characterized by the presence of low plains between valleys, which bring about the ease of access to the area (Benítez-López et al. 2017; Clements et al. 2014; Consiglio et al. 2006), causing a rapid expansion of agricultural areas (Santiphop et al. 2012; Trisurat et al. 2019) and construction, leading to an increase in the economic status of the local communities and population (Hooke et al. 2012; Lagrosa IV et al. 2018; Sadler et al. 2011). This has directly affected the land-use, as agricultural areas became replaced by recreational areas, hotels, accommodations and other structures, the number of which has increased in the NSW. Geoinformatics methods can be applied to analyze the patterns of land-use change dynamics using both quantitative and qualitative approach.

The Dyna-CLUE Model (Peng et al. 2016; Verburg and Overmars 2009; Verburg and Veldkamp 2004; Verburg et al. 1999; Zhang et al. 2018) brings land-use pattern of the past to work relating to spatial data with the grid of the proper land allocations by defining top-down policy conditions, for instance, specifying reserved areas (Guang et al. 2017; Verburg et al. 2002). Specifying conditions was done for various land-uses, according to spatial demand from the people in the area (bottom-up) from the characteristics of each appropriate location for various types of land-use (Verburg and Overmars 2009). The physical and socio-economic factors are ones of the most significant factors, used to process spatial data as the grid of the proper land allocation to acquire land-use pattern for the future (Jia Z. et al. 2018). This information is complicated data that is variable all the time during the period and in study area (Verburg and Veldkamp 2004). The mentioned model utilized a logistic regression model (Gobin et al. 2002; Zhang et al. 2018), integrated with the Dyna-CLUE model analyze and effectively forecast future LUC for empirical data to make decisions in land-use planning in the NSW area, a mountainous area, in order to develop the area and allocate limited natural resources for the highest sustainable benefit and improve people's life quality in the watershed.

In this research, the pattern of LUC dynamics was analysed over the period 2002–2013 and then the Dyna-CLUE Model was applied to simulate land-use patterns in the future period covering 2014–2033 in order to detect the direction of change in the forest area and plan sustainable land-use in the NSW area, Loei Province, Thailand. Moreover, analysis of the spatio-temporal dynamics of land-use type development was conducted under the conditions of two dynamic scenarios, namely, a scenario without a reservation area, and a scenario with a reservation area, such as Phu Luang Wildlife Sanctuary and Phu Ruea National Park, to assess the direction of land-use dynamics under the 2 mentioned scenarios. The results of this paper provide important information for local land-use management by assessing the impact of LUC.

MATERIALS AND METHODS

Study Area

The NSW area located in Loei Province, Northeast Thailand (Fig. 1), is a part of the watershed area of the Khong River. The total study area is approximately 852 km^2 under coverage path 129, row 48 of LANDSAT-8 satellite (OLI/TIRS). The elevation ranges from 300 to 1600 m above mean sea level (amsl). The topography surrounding the NSW mostly consists of complex mountain ranges. Phu Luang is the highest mountain at a height of 1,571 meters located in the southeast region of the NSW. The mountain ranges are aligned from north to south and are characterized by huge sedimentary rock and mesa morphology in the southeast of the NSW. In the south of the NSW Tableland and Double Cuesta ridge morphology appears (Department of Mineral Resources 2009). At the bottom of the cliffs, there are lowlands in between narrow valleys formed by rill and gully

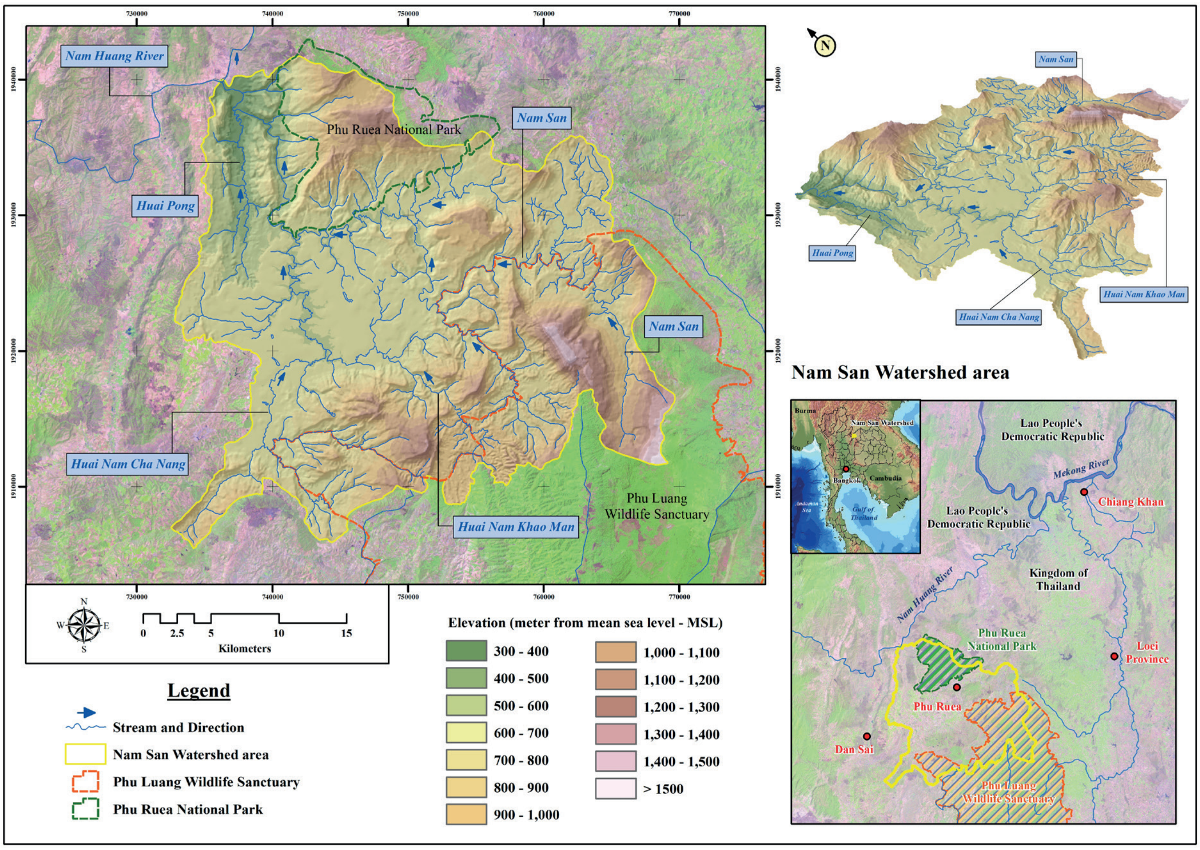

Fig. 1. Geographic map and topography in three-dimensional digital terrain of the study area NSW, Loei Province

erosion (Department of Mineral Resources 2007). The NSW includes four major watercourses: Huai Nam San stream, Huai Nam Khaw Man stream, Huai Nam Cha Nang stream and Huai Pong. Following the orientation of the mountain range, the flow of the watercourses is directed from south to north and discharges into down to the Huang river and Khong river. Moreover, the catchment includes several conservation areas such as Phu Luang Wildlife Sanctuary and Phu Ruea National Park located in the southeast and north regions of the NSW, respectively.

Data

Satellite images recorded by Landsat 5 TM, Landsat 7 ETM+ and Landsat 8 OLI/TIRS. for the years 2002, 2007 and 2013 were used in this research. The satellite images were downloaded from the U.S. Geological Survey to analyze land-use changes using Erdas Imagine 8.7 software. Table 1 contains a summary of the satellite data used for Geospatial information analysis. In addition, land-use data from the Land Development Department (LDD) was used as a land-use reference for examining the spatial land-use changes and accuracy for each year before processing the data in the next step. Table 2 shows land characteristics and socio-economic factors in the NSW, Loei Province, which are statistically processed and displayed in the form of maps. The LUC driving factors in the NSW, such as elevation, slope, soil suitability, distance to stream, distance to road, distance to a village, population density and poverty level are displayed in Fig. 2, along with information on Phu Luang Wildlife Sanctuary and Phu Ruea National Park boundaries.

Method

The research process consists of the following steps, as shown in Fig. 3 (1): Geoinformatic approach, (2) Dyna-CLUE model approach and (3) Dynamic Annual Change of LUC analysis. The details of each step are briefly explained below.

Table 1. Satellite Image Data over the NSW for LUC Analysis

Image type	Path/row	Band (R:G:B)[a]	Acquisition date	Original		
				Format	Resolution	Source[b]
Landsat 5 TM	129/048	5:4:3	2002-03-29	TIFF	25 m	USGS
Landsat 7 ETM+	129/048	5:4:3	2007-01-14	TIFF	25 m	USGS
Landsat 8 OLI/TIRS	129/048	6:5:4	2013-04-20	TIFF	25 m	USGS

[a] R:G:B red:green:blue
[b] USGS United States Geological Survey

Table 2. Description of Geo-spatial Data (Physical Factors and Socio-economic Factors) Selected for Logistic Regression Analysis

Driving Factor	Variable (Theme)	Year	Data preparation methodology	Source
Land characteristics factor	Elevation	2007	Topo to raster on spatial analyst	Royal Thai Survey Department (RTSD) topographic map sheet series L7018
	Slope	2007	Slope on spatial analyst	Derived from the DEM
	Soil Suitability	2013	Feature to raster on spatial analyst	Land Development Department (LDD), Thailand
	Distance to stream	2013	Interpolated grid theme contains a Euclidean distance from the drainage system on spatial analyst	Department of Water Resource, Thailand
Socio-economic factors	Distance to road	2013	Interpolated grid theme contains a Euclidean distance from the highway and road on spatial analyst	Department of Public Works and Town & Country Planning
	Distance to village	2013	Interpolated grid theme contains a Euclidean distance from the village in NSW on spatial analyst	Royal Thai Survey Department (RTSD)
	Population density	2002–2013	Feature to raster on spatial analyst	National Statistical Office of Thailand
	Percentage of poverty	2002–2013	Feature to raster on spatial analyst	National Statistical Office of Thailand
etc.	National park and wildlife sanctuaries area	2000	Feature to raster on spatial analyst	the Department of National Parks, Wildlife and Plant Conservation, Thailand

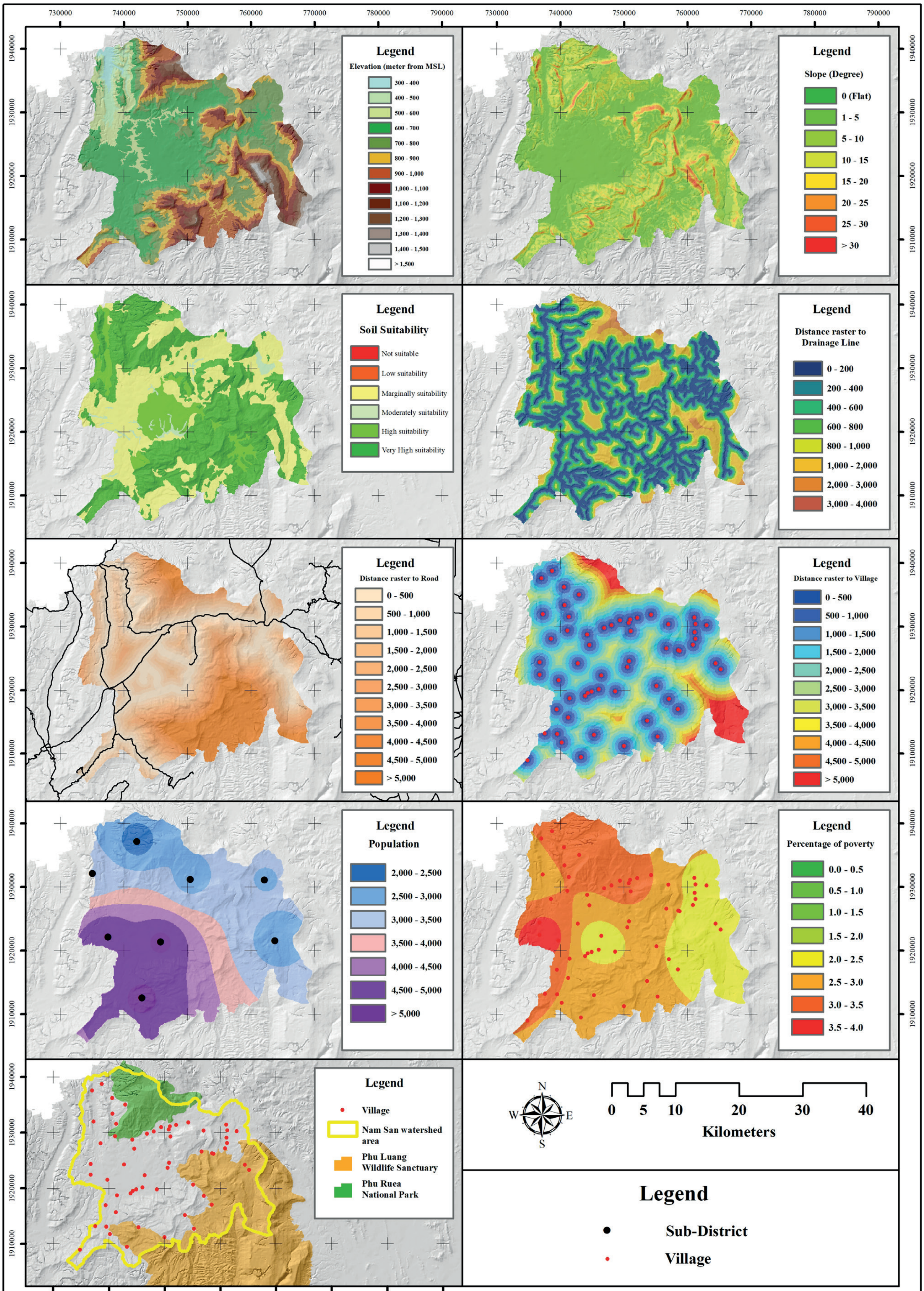

Fig. 2. Driving factors of LUC in the NSW area. a) elevation, b) slope, c) soil suitability, d) distance to stream, e) distance to road, f) distance to village, g) population density, h) income data and severity of population poverty, and i) National Park and Wildlife Sanctuary boundaries in the NSW area

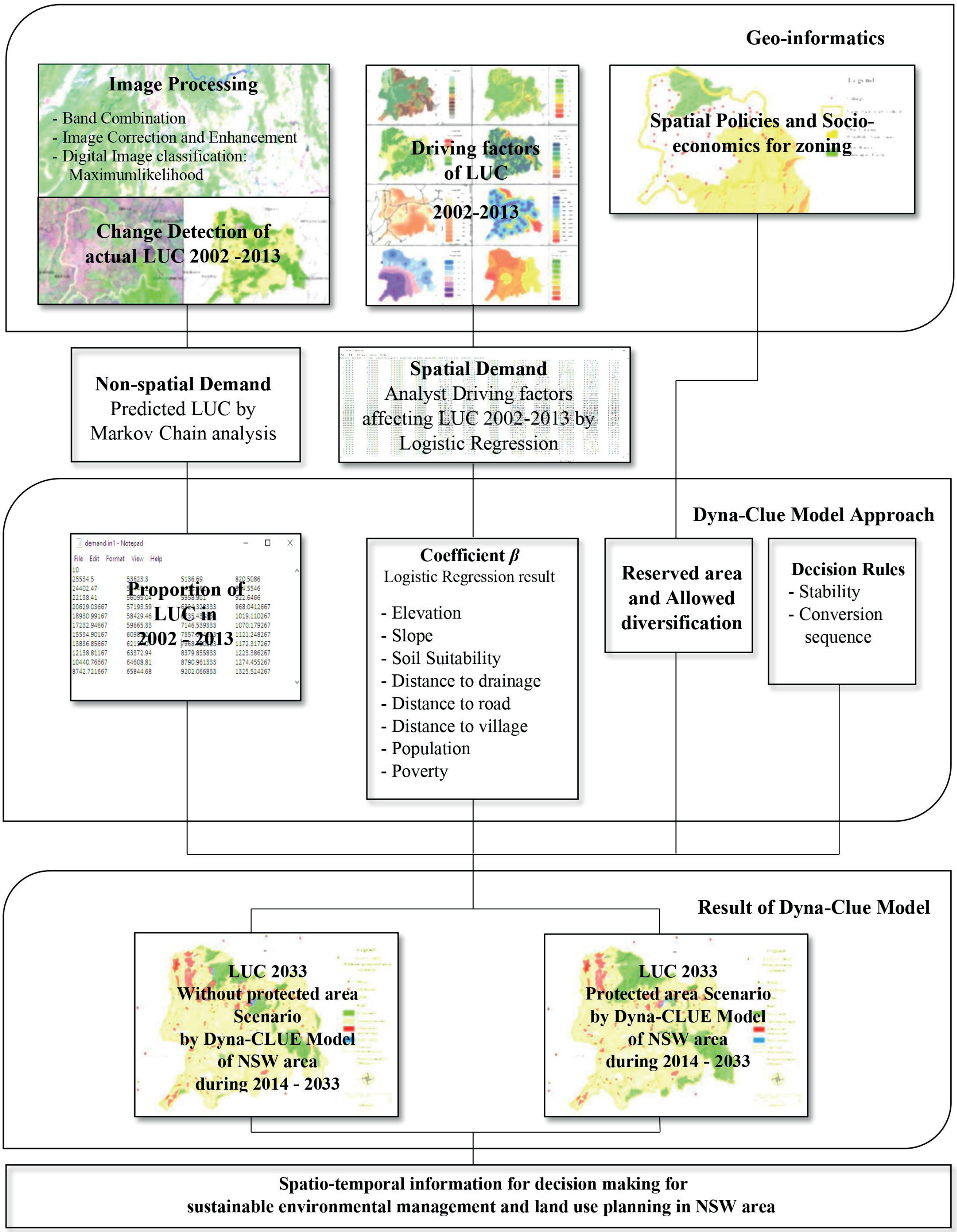

Fig. 3. Flowchart of the main methodology used in this research

Geoinformatics approach

Data in different bands from each of the Landsat satellite images were combined in three-channels red, green and blue (R:G:B). Band combination 543 corresponds to the R:G:B for Landsat 5 TM and Landsat 7 ETM+, where red is band 5 (short-wavelength infrared), green is band 4 (near-infrared), and blue is band 3. Similarly, band combination 654 including band 6 (short-wavelength infrared), band 5 (near-infrared), and band 4 was used for Landsat 8 OLI/TIRS as the R:G:B. Both band combinations 543 and 654 clearly demonstrate the extent of forest area, agricultural area and urban/built-up area (Barsi et al. 2014; U.S. Geological Survey 2014). Landsat images received enhanced contrast using a histogram equalization approach for further interpretation of the land-use. Then, the land-use map in the study area as well as field-survey data were used to verify the accuracy of LUC, the researcher collected data in several sampling points to use in the next steps for an accuracy assessment of the land-use classifications.

For image classification, a maximum likelihood algorithm (MLA) (Bakr et al. 2010; Foody and Mathur 2004; Richards and Jia 2006; Shalaby and Tateishi 2007; Waiyasusri et al. 2016) was applied to categorize the study area into four classes,

Table 3. Overall Accuracy Value and Kappa Coefficient (KHAT) for Accuracy of the Land-use Classification

KHAT Coefficient	Level of Accuracy
< 0	Unacceptable
0.01 – 0.40	Fair
0.41 – 0.60	Moderate
0.61 – 0.80	Good
0.81 – 1.00	Substantial

including agricultural (A), forest (F), water bodies (W) and urban/built up areas (U). This method used the training points from both the Landsat images and field surveys during the GPS-assisted field campaigns. First, 250 sampling ground control points were selected from all the classes (80 points from each of the A, F and U classes, and 10 points from W class) by choosing the regions of interest (ROIs) using ArcMap version 10.2 software, which contained the true samples that represent these classes. Then the study area was classified into four classes using the MLA to produce a land-use map for each Landsat image in the NSW area. In this study, Overall Accuracy values and Kappa coefficients (KHAT) were used to assess the accuracy of classification for each class, as shown in Table 3 (Jensen and Kiefer 2007; Poursanidis et al. 2015).

Dyna-CLUE model approach

The Dynamic land-use change model (Dyna-CLUE model) (Verburg and Overmars 2009; Verburg et al. 2002) is effective in eventual land-use modeling to determine LUC and affecting factors in the future which can apply to the mountainous areas (Cheng et al. 2019). In this research, the Dyna-CLUE Model has been simulated with two scenarios for the next 20 years: without (Scenario 1) and with (Scenario 2) a reservation area for land-use monitoring, in order to project the effect of urbanization and the direction of land-use dynamics into the future. The reference case scenario was based on the socio-economic trends from the past period (2002-2013). The forecasting case was based on the two simulation scenarios for the future period (2014-2033). There are two important modules in the Dyna-CLUE model: a non-spatial demand module and a spatially explicit allocation module (Fig. 4). For non-spatial demand, we used Markov chain analysis, which is a random process explaining certain types of conditions that change in sequential steps through the land-use geospatial dataset. The Markov chain can bring up a dynamic ratio of the past to the present year of the study, and then calculate it into a table matrix to determine the demand of LUC in the future. The results represent the proportion of land-use types in the future according to the study period (Guan et al. 2011). The likelihood of change from class i to class j in t time moment is shown as Equations 1 and 2.

$$P_{i,j} \times i_t = i_{t+1} \tag{1}$$

$$\begin{pmatrix} P_{UU}P_{UA}P_{UW} \\ P_{AU}P_{AA}P_{AW} \\ P_{WU}P_{WA}P_{WW} \\ P_{FU}P_{FA}P_{FW} \end{pmatrix} \begin{bmatrix} U_t \\ A_t \\ W_t \\ F_t \end{bmatrix} = \begin{bmatrix} U_{t+1} \\ A_{t+1} \\ W_{t+1} \\ F_{t+1} \end{bmatrix} \tag{2}$$

where

t : Time (Year)

$P_{i,j}$: Transition Probability Matrix (TPM) of the land-use class i change to class j

$_i$ and $_j$: the land-use class in the first year and the second year, respectively

The results of the demand module were used as input for the spatial allocation module of the Dyna-CLUE model (Verburg and Overmars 2009). Then, the Markov chain analysis was used to determine the demand for the probability of each land-use pattern, where the probability of transition (Pi, j) is given for every ordered set of conditions. In a Markov chain with a limited number of conditions, such as j, a new transition probability matrix is bounded, as in Equation 3 (Waiyasusri et al. 2016).

$$V_j \times P_{ij} = [V_1, V_2, V_3, \ldots V_n,] \begin{bmatrix} P_{1,1}P_{1,2}P_{1,3}\ldots P_{1,n} \\ P_{2,1}P_{2,2}P_{2,3}\ldots P_{2,n} \\ P_{3,1}P_{3,2}P_{3,3}\ldots P_{3,n} \\ \ldots\ \ldots\ \ldots\ \ \ldots \\ P_{n,1}P_{n,2}P_{n,3}\ldots P_{n,n} \end{bmatrix} \tag{3}$$

Where

$V_j \times P_{jk}$: Proportion of land-use in the second year

$P_{j,k}$: Land-use activity (f) derived from the TPM

V_j : Proportion of land-use in the first year

The Markov chain model is a tool that can quickly and

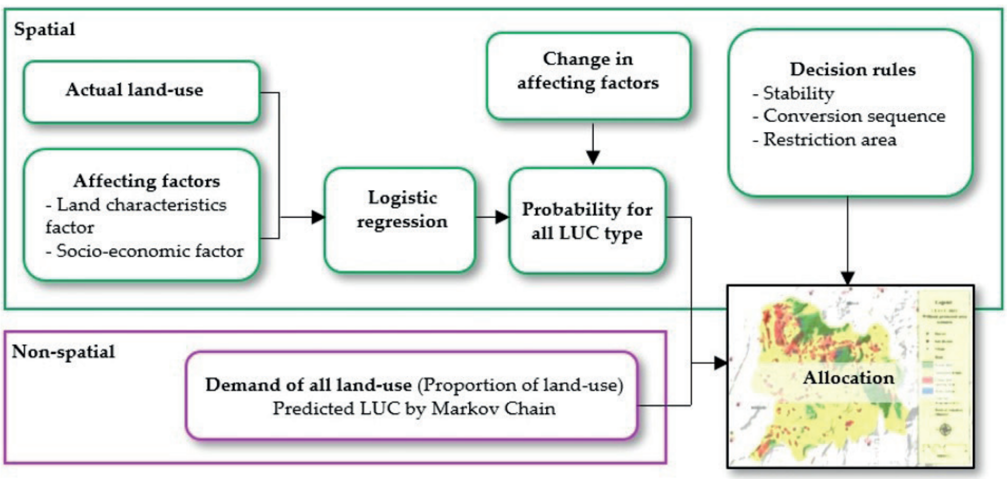

Fig. 4. The Dyna-CLUE model structure. (Adapted from (Verburg et al. 2002))

efficiently analyze land-use ratios in the future. The highlight of this model is that it uses land-use ratios for the reference year to predict the potential distribution of the land use types in the study area which may occur in the future.

Even though the Markov chain model itself can forecast the dynamic of LUC in the future, it has some restrictions, particularly in its ability to provide accurate spatial analysis or identify factors affecting land-use (Guang et al. 2017). Thus, it requires another empirical model like the Dyna-CLUE model to calculate future land-use demand. The Dyna-CLUE model was developed to include different factors affecting land-use change into the analysis. Generally, the main factors affecting LUC are physical factors (Elevation, Slope, Soil Suitability, Distance to stream) and socio-economic factors (Distance to road, Distance to village, population density, income data and population poverty) (Geist and Lambin 2002; Lambin and Meyfroidt 2010). The selection of factors was made based on Lambin and Meyfroidt (2010) study which concluded that these 8 factors that directly affect changes in land use in tropical rainforests, where also the NSW is located. The Dyna-CLUE model runs based on statistical analysis and logistic regression analysis of the factors affecting LUC on a pixel per pixel level for both future reservation area scenarios (Liu et al. 2014; Trisurat et al. 2010). The location preferences of the different land-use types were quantified by the Dyna-CLUE model based on logistic regression models. The relation between the occurrence of a land-use type and the physical and socio-economic factors of a specific location indicate the preference for a specific type of land-use by logit models. The distribution of land-use types is expressed using a binary numeral system with labels 0 (no transition) and 1 (with transition). Equation 4 is a stepwise logistic regression which was used to evaluate the relationship between the land-use and its affecting factors.

$$Log\left(\frac{P_i}{1-P_i}\right)=\beta_0+\beta_1 x_{1,i}+\beta_2 x_{2,1}+\ldots+\beta_n x_{n,i} \quad (4)$$

where

P_i : The land-use change probability

x_i : Independent factors

ß : Coefficient value of each independent factor

The relation between the factors affecting each type of LUC was also obtained, moreover, its accuracy was assessed using Relative Operating Characteristic (ROC) (Pontius and Schneider 2001). The ROC value was used to obtain the reliability of the logistic regression results. ROC values vary between 0 and 1: ROC values between 0.5 and 0.7 indicate that the forecasting results are of low accuracy; ROC values between 0.7 and 0.9, indicate that the forecasting results are excellent; with ROC value > 0.9, the model has high precision. In the Dyna-CLUE model, after the land-use change probability, coefficient and relative elasticity are assigned, LUC is assessed through the determination of ROC for all grid cells. The total probability (TPROPi,u) is calculated for each grid cell i and each of the land-use types u, as shown in the equation below (Verburg et al. 1999).

$$TPROPi,u=Pi,u+ELASu=ITERu \quad (5)$$

Where

ITERu : Iteration variable of a specific land-use

ELASu : Relative elasticity for change specified in the decision rules and is only given a value if grid cell i is already under land-use type u in the year considered.

Dynamic Annual Change of LUC

Dynamic LUC in the NSW area in 2002, 2007 and 2013 was analyzed using the Supervised Classification technique and by reclassifying the land-use data in a raster format to obtain the results. Using a spatial analysis method of classified and tabulated data in the NSW area, the results are obtained for the period from 2002 to 2013 using a cross-classification application. Estimation of LUC was used for specifying the transition among land-use classes and for quantifying the different rates and magnitudes of these changes. Equation 6 is used for evaluating the annual change in land-use (Jia K. et al. 2014).

$$\Delta=\frac{\left(\frac{A_2-A_1}{A_1}\times 100\right)}{\left(T_2-T_1\right)} \quad (6)$$

where

D : Average annual rate of change (%)

A_1 : Amount of a land-use type at time 1 (T1)

A_2 : Amount of a land-use type at time 2 (T2).

RESULTS

Dynamics of LUC in the NSW area

The image classification analysis for 2002, 2007 and 2013 were reclassified into four classes (100x100 raster grid resolution), as displayed in Fig. 5. Table 4 shows the quantitative data for each land-use class for each year. The overall accuracy assessment was at 84.3, 76.5 and 75.9% for 2013, 2007 and 2002, respectively, with a kappa coefficient (KHAT) of 0.81, 0.73 and 0.71, respectively. The total area with observed land-use change in the NSW from 2002 to 2013 was equal to 258.52 km² (30.37% of the total area). Table 5 illustrates a matrix of the various LUC classes in the NSW from years 2002 to 2013. The results reveal that forests have suffered the highest loss, at 113.17 km^2. Even though there is a new-growth forest of 23.04 km^2 under a public awareness campaign, the forest decline has continued throughout the past ten years (Royal Forest Department Resources 2016). Fig. 6 shows LUC from 2002 to 2013, which confirms deforestation in the NSW, while the area of urban/build-up, agricultural land and water bodies has increased by 92.36, 16.04 and 4.77 km^2, respectively.

Factors that caused LUC in the NSW area

All 8 factors (physical and socio-economic) affecting the land-use patterns were analyzed one cell at a time to find the most important parameter for the LUC using a statistical regression equation. The results were classified into four land-use classes and displayed with a value of β coefficient in logistic regression analysis (Table 6). A positive value of the β coefficient indicates a positive correlation, whereas a negative value of the β coefficient indicates a negative correlation. We used the ROC to indicate the reliability of the affecting factors resulting from the Dyna-CLUE model. To demonstrate a probability level of %ROC, a comparison between the results and the observed values was performed. ROC above 0.5 was better than random (Pontius and Schneider 2001). As shown in Table 6, we obtained ROC values of 0.827 (forest), 0.791 (agricultural), 0.873 (urban/built-up lands) and 0.773 (water bodies). In all classes, the ROC value was more than 0.7, which indicates that the spatial distribution of all classes of land-use was explained well by the selected affecting factors.

All variables are significant at $p < 0.01$ entry and $p > 0.02$ removal levels, except for those marked * (not statistically significant). ROC is a relative operating characteristic.

The β coefficient value in Table 6 shows that the forest area is mainly affected by soil suitability and slope. When

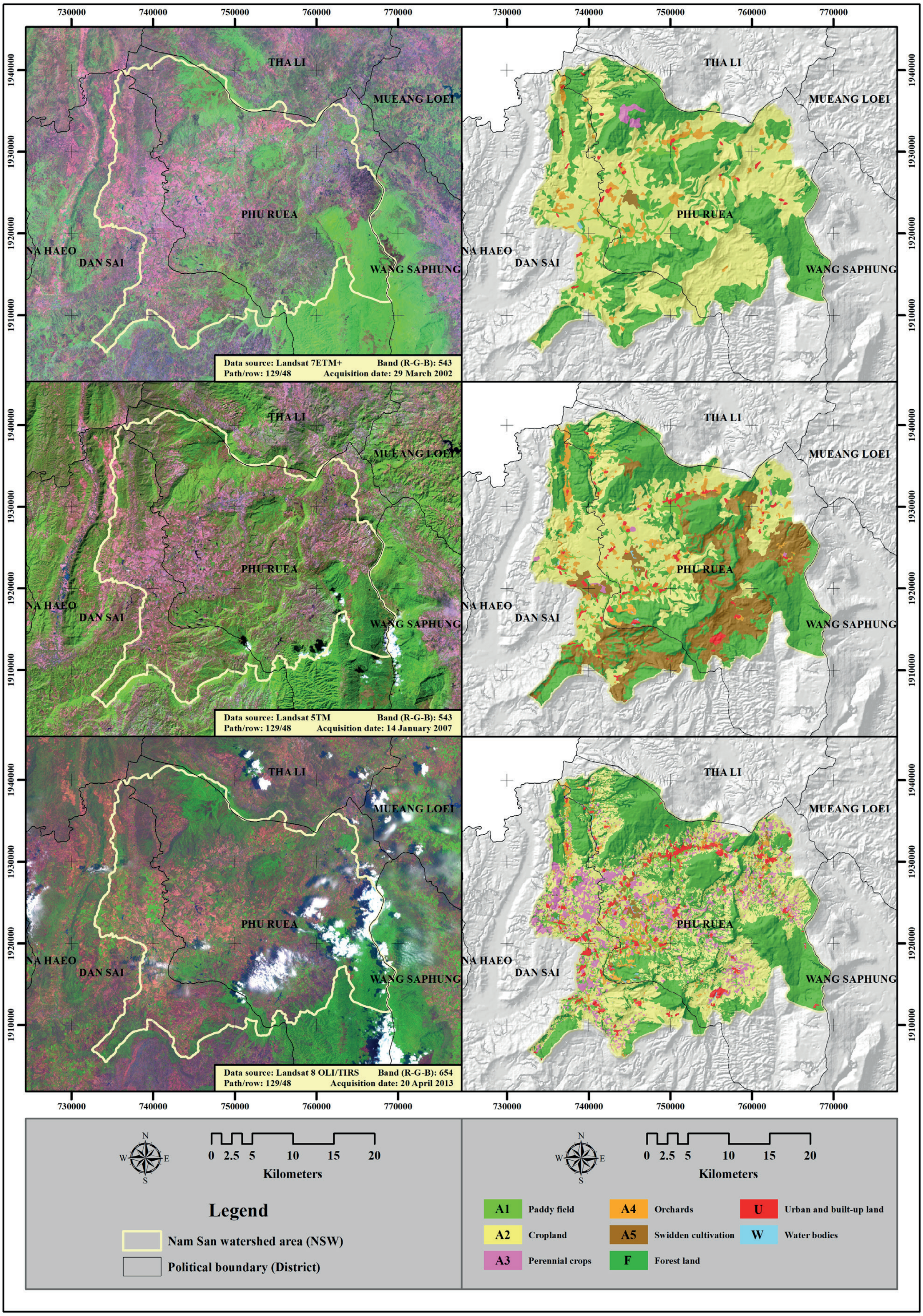

Fig. 5. Land-use pattern and Landsat 5TM (band combination 543), Landsat 7ETM+ (band combination 543), and Landsat 8OLI/TIRS (band combination 654) satellite image of the NSW area for (a, b) 2002, (c, d) 2007 and (e, f) 2013; (a, c, e) shows land-use patterns and (b, d, f) shows satellite images. Land-use codes as shown in Table 4

Table 4. Comparison of land-use in the NSW area, as derived from the Landsat 5TM, Landsat 7ETM+ and Landsat 8 OLI/TIRS satellite images in 2002, 2007 and 2013

Land-use (code)		2002		2007		2013	
Level I	Level II	km^2	%	km^2	%	km^2	%
Agricultural (A)	Paddy field (A1)	26.40	3.10	27.61	3.24	31.92	3.75
	Field crops (A2)	406.54	47.76	339.93	39.94	303.02	35.60
	Perennial crops (A3)	4.87	0.57	63.96	7.51	86.14	10.12
	Orchards (A4)	25.49	2.99	33.91	3.98	33.15	3.89
	Horticultural (A5)	2.74	0.32	9.49	1.11	7.85	0.92
	Total	466.04	54.74	474.90	55.78	462.08	54.28
Forest (F)		380.40	44.69	353.33	41.51	357.23	41.97
Water bodies (W)		0.37	0.04	4.81	0.57	5.14	0.06
Urban/built up (U)		4.34	0.51	18.11	2.13	26.70	3.14
Total		851.15	100.00	851.15	100.00	851.15	100.00

Table 5. Matrix of land-use changes in the NSW area, 2002–2013 (km^2)

		2013					Changing areas
	Land-use	Forest land	Agricultural land	Urban/built-up land	Water bodies	Total	
2002	Forest land	244.19	130.77	3.92	1.52	380.40	-113.17
	Agricultural land	22.24	348.00	92.27	3.53	446.04	+16.04
	Urban/built-up land	0.75	3.06	0.44	0.09	4.34	+92.36
	Water bodies	0.05	0.25	0.07	0.00	0.37	+4.77
	Total	267.23	482.08	96.70	5.14	851.15	

Table 6. Logistic regression analysis of the land-use patterns and affecting factors

Variable	Land-use pattern			
	β Forest	β Agricultural	β Urban/ built-up	β Water bodies
Elevation	0.0025	-0.0036	*	-0.0002
Slope	-0.1172	0.0881	-0.1591	0.2727
Soil Suitability	0.1364	0.2891	*	*
Distance to drainage	0.0018	-0.0017	*	0.0004
Distance to road	-0.1009	0.0008	0.8113	*
Distance village	-0.0008	0.1005	0.0028	*
Population	-0.0004	0.0009	0.0061	*
Poverty	-0.0007	-0.0965	0.7035	*
Constant	-4.8052	4.443	-2.758	-3.768
ROC value	0.827	0.791	0.873	0.773

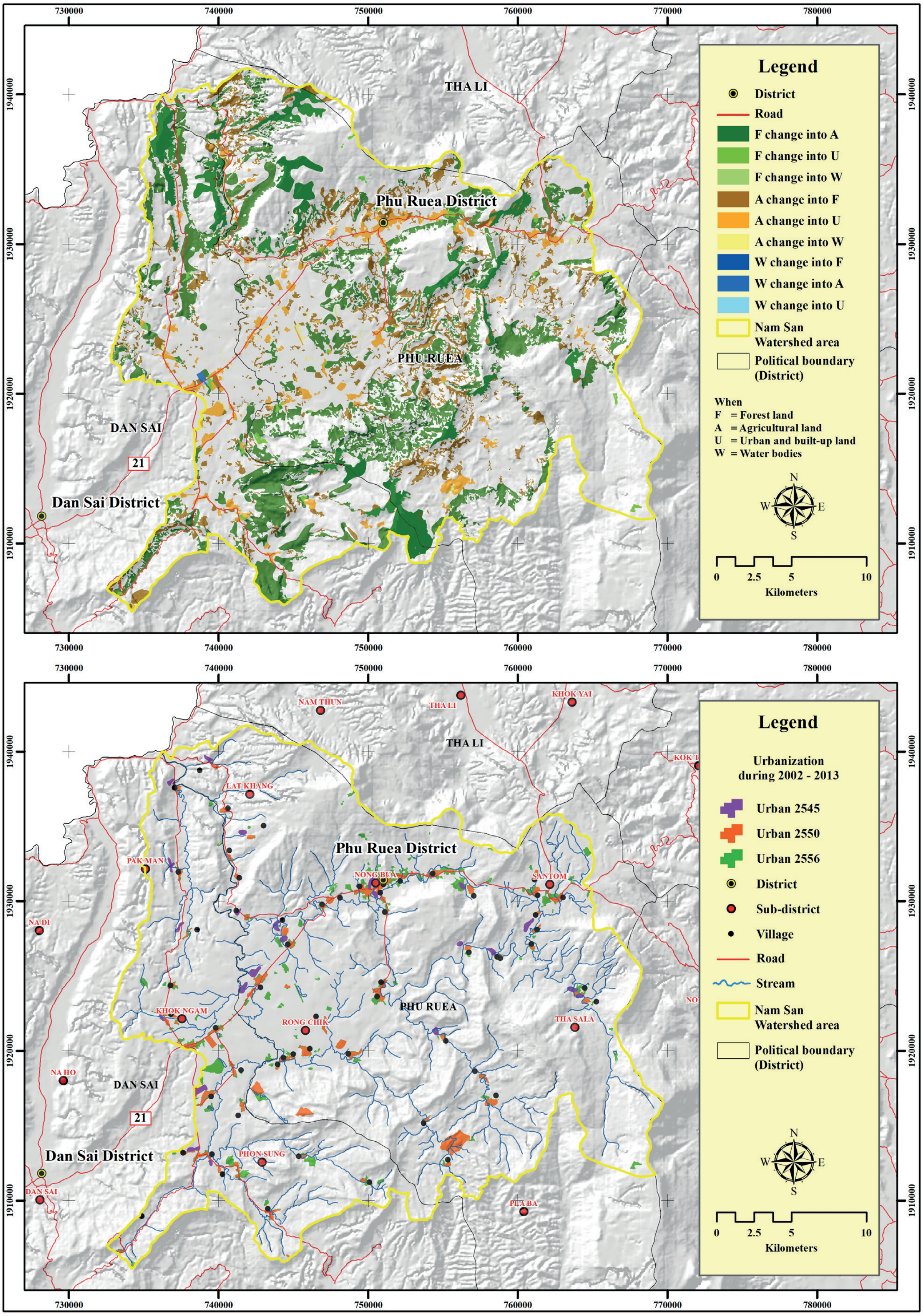

Fig. 6. Map of the land-use change dynamics from 2002 to 2013 in the NSW area, Loei Province (6a). Urbanization expansion map during 2002–2013 in the NSW area, Loei Province (6b)

soil suitability adds a one-unit change, the probability of forest area change increases by 13.64%. Soil suitability is secondary data from the analysis of soil taxonomy method (Boonsompopphan et al. 2008) obtained from the Department of Land Development, it has been analyzed and accepted at the national level. Therefore, it can be considered as an effective parameter for the model and one of the most important factors that affect the expansion of forest areas with a probability of up to 13.64%. Whereas, if slope adds a one-unit change, the probability of a forest area change decreases by 11.72%. This indicates that forest areas are characterized by abundant soil and high steepness topography. For agricultural areas, the factor of soil suitability was also found to affect its expansion by 28.91%, and the effect of distance to village factor was at 10.05%. Moreover, this indicates that factors affecting agricultural areas and forested areas tend to go in the opposite direction, which correlates with Table 6 presenting how most of the NSW area has changed into an agricultural area. For urban/built up areas, the most important factors were distance to a road and poverty factors; distance to a road influences an increase of urban/built up land with a probability of 81.13%, the second factor was poverty, affecting 70.35%. These indicate that urban development and facilities have expanded along transportation routes, and poverty has had a tendency to decrease through all previous 20 years, resulting in a higher income of inhabitants of the watershed. This has led to changes in the way of life for some families, who switched from agricultural occupations to tourism and service businesses such as opening their own shops.

Table 7. Demand area of future land-use (km²)

Year	Land-use			
	Forest land	Agricultural land	Urban/ built up land	Water bodies
2014	265.91	483.32	96.44	5.48
2015	264.59	483.56	97.18	5.82
2016	263.27	484.46	97.26	6.16
2017	261.95	485.20	97.50	6.50
2018	260.63	485.94	97.74	6.84
2019	259.31	486.68	97.98	7.18
2020	257.99	487.42	98.22	7.52
2021	256.67	488.16	98.46	7.86
2022	255.35	488.90	98.70	8.21
2023	254.02	489.64	98.94	8.55
2024	252.70	490.38	99.18	8.89
2025	251.38	491.12	99.42	9.23
2026	250.06	491.86	99.66	9.57
2027	248.74	492.60	99.90	9.91
2028	247.42	493.33	100.14	10.25
2029	246.10	494.07	100.39	10.59
2030	244.78	494.81	100.63	10.93
2031	243.46	495.55	100.87	11.27
2032	242.14	496.29	101.11	11.61
2033	240.82	497.03	101.35	11.95

Table 8. Forecasting future deforestation using the Dyna-CLUE model, inside and outside reservation areas

Location	Forest area in 2013	Deforestation			
		Without a reservation area scenario 2033		Reservation area scenario 2033	
		km²	Decrease	km²	Decrease
Phu Ruea National Park	72.21	41.55	-30.66 (-42.46 %)	72.12	-0.09 (-0.13 %)
Phu Luang Wildlife Sanctuary	107.31	45.62	-61.69 (-57.49 %)	106.37	-0.94 (-0.88 %)
Outside reservation area	177.86	46.29	-131.57 (-73.98 %)	28.54	-149.32 (-83.96 %)

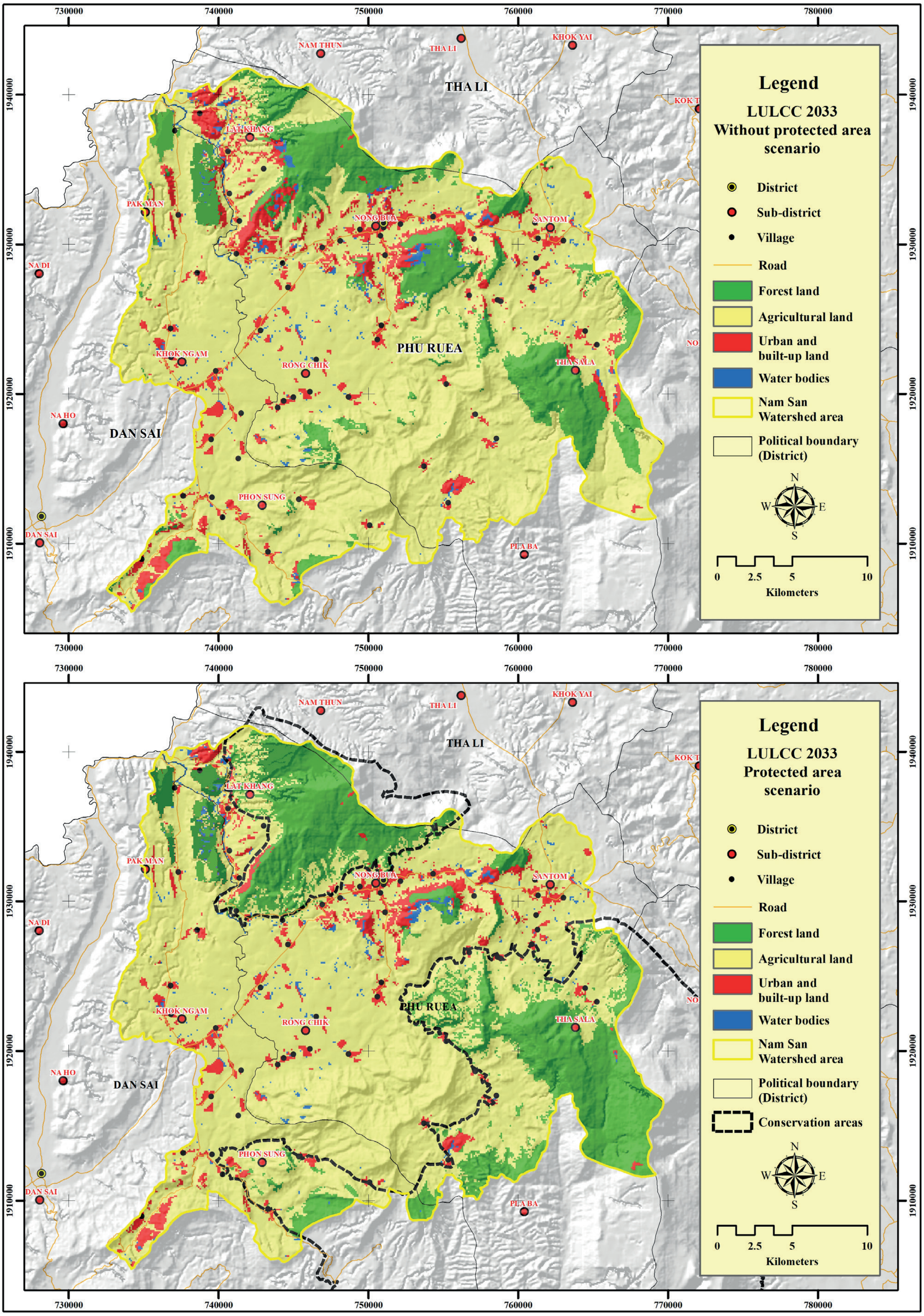

Fig. 7. Simulation results from the Dyna-CLUE model for the year 2020: without reservation area scenario (upper) and with reservation area scenario (lower)

Anyhow, the logistic regression analysis demonstrated the affecting factors of LUC indicating by the β coefficient value which are used as spatial information in the next topic.

Forecasting future land-use conditions to estimate possible land-use patterns in the NSW area

The Dyna-CLUE model has been used to simulate land-use in the future under 2 simulation scenarios: with, and without, a reservation area in the NSW from the year 2014 to 2033, as shown in Fig. 7. In addition, Markov chain analysis found the proportion of land-use change (Demand of all land-use) for 2014–2033; when inputting models with the results in Table 7. We found the tendency of the forest area ratio to decrease by 0.546% on average, while the ratio of water bodies, urban and agricultural areas tended to increase by 0.045%, 0.025% and 0.001%, respectively.

Scenario 1: without reservation area

Results of the land-use simulation in Scenario 1: without a reservation area in 2033, was compared with the land-use in 2013. The comparison showed that the north region of the NSW area is sensitive to the change in the proportion of the land-use types, as the forest area reduces from 31.47% to 28.30% due to agricultural expansion, which covers 58.40% of all the watershed area. This is especially true for the forests in Phu Luang Wildlife Sanctuary and Phu Ruea National Park, which have rapidly decreased from 107.31 km^2 to 45.62 km2, and from 72.21 km2 to 41.55 km^2, respectively (Table 8). Moreover, urbanization also occurs as the area of urban/built-up land expands from 11.36% in 2013 to 11.91% in 2033. Concerning the affecting factors (Table 6), induced agricultural and urbanization expansion occurs in Nong Bua Sub-district, Khok Ngam Sub-district, and Lat Khang Sub-district, but especially in Nong Bua Sub-district with the highest rate of urban expansion being observed in Phu Ruea district. This results from the role it has as a trading, services and tourism center due to its location near recreation areas such as Phu Luang Wildlife Sanctuary and Phu Ruea National Park and their businesses of tourism, hotels and resorts.

Scenario 2: with reservation area

In Scenario 2: with reservation area, the obvious restriction of the national park and wildlife sanctuary border in the watershed was set into the Dyna-CLUE model. The results of the model indicate that forested areas in the national park and wildlife sanctuary are well-protected (Table 8). On the other hand, for the land outside the reservation area the model shows a decrease of forest area by 83.96% in the middle of the watershed, from 177.86 km^2 in 2013 to 28.54 km^2 in 2033. The results indicate that distance to the village and steepness of the mountain range are major and minor affecting factors of forest decline. The areas with high steep mountains, mainly around cuesta mountain, and tableland are the dominant types of topography in the southeast section of the NSW.

Finally, evaluation of the model results was done by comparing the simulated map from the Dyna-CLUE model with the actual map derived from the LDD that was surveyed in 2016 to obtain the overall accuracy and the kappa coefficient value. We found that results from the spatio-temporal model in Scenario 1 had overall accuracy of 0.8421, and a kappa coefficient value at level 0.8178. Whereas, the result of the spatio-temporal model in Scenario 2 had an overall accuracy of 0.8368 and a kappa coefficient value of 0.8073. This indicates that simulations of both scenarios are in substantial agreement. In addition, simulation of LUC using this model allows to make a long-term projection, such as for the next 20 years (2014-2033), as shown in Fig. 8. The simulation results could be essential information for making decisions on land-use planning and monitoring deforestation in the NSW.

DISSCUSSION

Deforestation in the NSW area during 2002–2013

There were LUC in the NSW from 2002 to 2013, the results show a decrease of the southern forest area in a corridor pattern near the Dan Sai district, Loei Province, in an area characterized by piedmont topography and flatland valleys. Urban and agricultural land also expanded into the eastern forest and some of the reservation areas in a patchy pattern near Phu Luang Wildlife Sanctuary, around San Tom Sub-district, Tha Sala Sub-district, and Rong Chik Sub-district, as well as near Phu Ruea National Park, around Nong Bua Sub-district and Lat Khang Sub-district. Because that area is characterized by cuesta mountains, there is a higher population density, which has contributed to a loss of forest area at a higher rate. In winter, there are commercial crops such as corn, rubber and others, which are found in the eastern part of the NSW area. Moreover, urban expansion is found in particular in the regions of the road network growth, especially along the highway no. 21, which connects Dan Sai district and Phu Ruea district. Regarding the support of tourism businesses, land development includes new community areas, built-up hotels and resorts. In the NSW, the rapid expansion of urban areas and agriculture has taken place over the last 10 years. This result is in contrast to a study of LUC in Bhutan during 1990–2010 (Gilani et al. 2015), which found that overall forest area increased with an average annual rate of 59 km^2/year (0.22%) within the reservation areas and biological corridors as well as outside of those territories. Moreover, their results showed that the forest changed to another type of land-use when urban area expanded around a reservation area. This can be found all over Thailand and Southeast Asia where there is a valley landform (Geist and Lambin 2002; Trisurat et al. 2019; Verburg and Veldkamp 2004). It is possible that all 3 types of land-use can be transformed into forest areas. Due to the NSW watershed campaign to create teak plantations, the agricultural area has been transformed into a protected forest area (Komaki et al. 2012) and forest areas near the national park and wildlife sanctuaries are being restored due to the forest fires, replacing the water resources, communities, and agricultural areas. There is a forest fire prevention, reforestation and development project for community forest conservation (Konpian et al. 2020), which however only slightly affects the NSW area, only 22.24 km^2.

Driving factors of deforestation and LUC in the NSW

Deforestation within the NSW area was caused by the expansion of agricultural land and urban expansion. The results indicate that slope and distance to a road are important factors driving agricultural and urban expansion. The study of β coefficient value shows that forest area is mainly affected by the slope factor that diminishes (Royal Forest Department, 2007) The most sensitive area for change often corresponds to the watershed classification class 1, 2 and 3 respectively, especially watershed classes 2 and 3 with only 35-50% and 25-35% slopes (Chunkao 2008), which are sensitive to changes in forest areas in the NSW watershed, where land-use patterns are changed to rubber, corn and

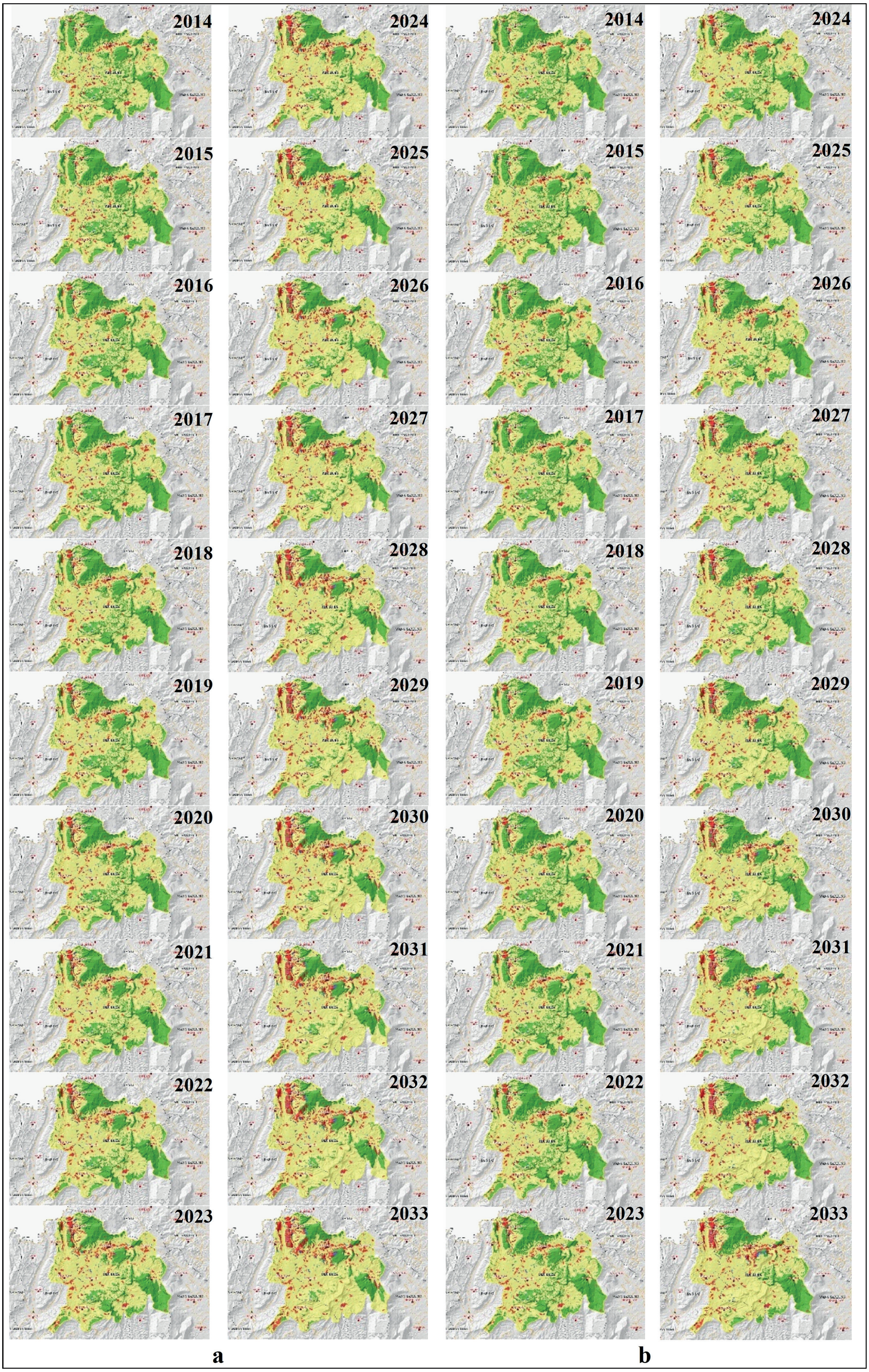

Fig. 8. Spatial allocation maps from 2013–2032 with a reservation area scenario (a) and without a reservation area scenario (b) by Dyna-CLUE model for decision-making on land-use planning and sustainable development in the NSW area

orchards. Meanwhile, Waiyasusri et al. (2016) found LUC in Huai Thap Salao Watershed area, Uthaithani Province, Thailand trend towards an increase in the forest area driven by the slope factor, which can be explained by the geology and topography of the area as it includes a granite mountain with high slopes. The NSW, however, contains sandstone mountains with cuesta mountain formations and lower slopes, which makes it easier for agricultural and urban areas to expand. This deforestation characteristic can be found in the east and northern regions of Thailand, particularly Chiang Mai and Chiang Rai (Tabor et al. 2018). A secondary driving factor is a distance from a village, which has a direct effect on agricultural land change because most communities in NSW are farmers. The area close to the community is, therefore, an agricultural ground, with most of the land being planted with rice and corn. Today, however, the expansion of agricultural land is observed closer to the park area, which is mostly occupied by rubber because it is an commercial plant. This results in an increasing deforestation rate. Similarly, results by Trisurat et al. (2010) found that in north Thailand LUC is driven by slope, distance to a road and distance to a village, especially along the highway no. 21, where mixed forest and deciduous dipterocarp forest has rapidly been decimated, which was shown in a report by Royal Forest Department (2016). Additionally, rock and topography types are minor driving factors, particularly in the NSW where sedimentary rock is mostly found in lowlands and alluvial landforms. Since suitability of the soil in the NSW is only at a moderate level due to winter crop farming. The forested areas' decreasing trend is growing every year due to the replacement of forests by agricultural fields with cultures like corn, cassava and sugar cane. In contrast to a study by Santiphop et al. (2012), it was found that most cash crops are grown in the upland areas rather than in the lowland areas as there do not get submerged.

Sensitivity of reservation area to deforestation in the future

Continuous deforestation over the past few decades has caused rapid LUC in the NSW. Most of the reservation areas in Thailand has changed to agricultural fields, which are used to grow rubber trees and winter crops (Trisurat et al. 2019). Regarding the study area, deforestation has dominated in the central and southern parts of the NSW where the upstream forest is located. Therefore, the Dyna-CLUE model employed two land-use scenarios in this study to test the sensitivity of reservation areas to deforestation patterns in the NSW over the next twenty years. Different deforestation patterns under two scenarios were shown, the results of Scenario 1 indicated large forest area loss spreading throughout the NSW due to the extension of city areas, which was observed mostly along the edge of forested areas (hotels and resorts in Thailand are often built there because of the good location and low land prices) (Clements et al. 2014). On the other hand, Scenario 2 showed a forest area loss of 83.96 % outside the reservation area, but inside the reservation area, the forest was preserved. Regarding the results, the edge of forest areas should be the first point of concern (Gilani et al. 2015). It is important for policy makers to know how future deforestation will happen, and what actions need to be taken to restrict future LUC in the NSW by enforcing local laws and regulations, following the Thai government's strategy to encourage an increase in forest area by 15% overall in Thailand, especially in reservation areas (Royal Forest Department Resources 2007; Royal Forest Department Resources 2016). However, the spatial and socio-economic factors that affect forest area changes in NSW also affect temperature changes in that region, it is estimated that the mean temperature in Thailand would rise by 2.0. – 5.5 ° C under the HadCM3 A2 scenario (IPCC 2007). Under the current climate change situation, National Mitigation/Adaptation Plans and Policies should be implemented in watershed planning by the local authorities throughout the assessment, policy making, and implementation steps (Dastgerdi et al. 2020) to deal with disasters that may occur in the NSW.

This research shows the sensitivity of the reservation area to future deforestation in the NSW and reveals the importance of providing the biological reservation area to ensure environmental resilience. In addition, Dastgerdi et al. (2020) laid out constructive strategic guidelines for sustainable environmental management in the Umbria Region in Italy which solve the environmental problems by cooperation between local community networks such as local residents, concerned government agencies, and stakeholders. The relevant departments will develop skills and find support markets to add value to agricultural products. This will enable farmers living near the reservation area to have a better life in harmony with nature by cooperating to protect the forest area and sustainably reducing forest encroachment. They also highlight that sustainable management requires the integration of an inclusive effort in the social, economic, and environmental policies with regional plans.

CONCLUSIONS

The NSW is located in northeastern Thailand near the Thai-Laos border crossing point which is abundant with natural and environmental resources. The public authority has defined 2 conservation areas, Phu Ruea National Park and Phu Luang Wildlife Sanctuary. Over the years, forest area has decreased by 70.25% and was mostly replaced by agricultural area such as cropland (corn or sugar cane) and perennial plants such as rubber trees. Moreover, the local government authorities have improved transportation routes to allow more efficient access in order to support agricultural industries and transportation of agricultural products. This has continuously decreased the value of the slope and distance to a road factor.

Results from the 2 model scenarios - with, and without, reservation area, describe the context of what could happen in the future in the NSW area. Various factors affecting the area are taken into account, which allows to effectively indicate sensitive areas of dynamic land-use. This allows to describe the agricultural expansion and urbanization in the areas of Lat Khang sub-district, Khok Ngam sub-district and Nong Bua sub-district all along the road, especially in Lat Khang sub-district where expansion is happening continuously. The expansion of local villages is appeared in the downstream area, with a piedmont topography characterized by lowland between valleys. Besides this subdistrict, there is a compromising point at the border where the people of 2 countries can enter and do trade. This can also easily affect the expansion of building areas in the future. For deforestation and agricultural expansion occurring by 2033, or throughout the next 20 years, we found that in the south of Lat Khang sub-district and the south of Nong Bua sub-district, in the scenario without a reservation area, forests occupied a wider area than in the scenario of reservation area. In other words, in the scenario without a reservation area, the expansion of urbanization and agriculture into Phu Ruea National Park is observed over a wider area up to the slope of sandstone mountains because of the low steepness of the area and its good accessibility via connected roads. The results of two model scenarios occurring in Nam San Watershed show that what is happening there should be a cause of great concern.

The results of the Dyna-CLUE model shown for the spatio-temporal dynamics land type were analyzed for the overall accuracy and kappa coefficient by comparing them with the data on actual land-use from 2016. The results show that for the scenario without a reservation area the criteria values of 0.8421 and 0.8178, and 0.8368 and 0.8073 for the reservation area scenario. This validation results confirm the good accuracy of the model. Besides, Dyna-CLUE model can show the future of land use patterns every year that are forecasted, which is a strong point of the model: simulation images through the study period spanning the next 20 years (2014–2033), as shown in Fig. 8. However, this research only shows validation of the model for the year 2016 because of a limitation of available validation data at the Land Development Department, which in the present is only collected once every 2 years. However, studying land-use requires continuous monitoring of the LUC information in this study area, as well as greater frequency of study and more validation to ensure the accuracy of the model to examine the trends of land-use change. Availability of the observations in the actual area and understanding the context of each watershed, especially regarding factors that determine physical characteristics of the watershed and socio-economic factors, before bringing the model in is also very significant. Regarding this study, the analysis of the LUC is necessary to understand the context of the physical change of the watershed. These results revealed the guidelines and conclusions on the future land use predictions that can be applied to other sub-watershed studies at both local and regional levels. Future approaches should study additional sub-watersheds in order to monitor areas sensitive to changes in deforestation that may occur in other watersheds. Because watershed areas are extremely important and affecting watershed systems might lead to the more frequent disaster events, it is necessary to define reservation areas to be concrete and create an empirical database for the conservation of watershed areas in the future. ■

REFERENCES

Bakr N., Weindorf D.C., Bahnassyb M.H., Mareib S.M., and El-Badawi M.M. (2010). Monitoring land cover changes in a newly reclaimed area of Egypt using multi-temporal Landsat data. Applied Geography, 30, 59, DOI: 10.1016/j.apgeog.2009.10.008.

Barsi J.A., Lee K., Kvaran G., Markham B.L. and Pedelty J.A. (2014). The Spectral Response of the Landsat-8 Operational Land Imagery. Remote Sensing, 6, 20, DOI: 10.3390/rs61010232.

Benítez-López A., Alkemade R., Schipper A.M., Ingram D.J., Verweij P.A., Eikelboom J.A.J. and Huijbregts M.A.J. (2017). The impact of hunting on tropical mammal and bird populations. Science, 356, 4, DOI: 10.1126/science.aaj1891.

Boonsompopphan B., Vearasilp T., Yost R.S. and Attanandana T. (2008). Field Identification of Soil Series Enabling Thai Farmers Share Experiences and Knowledge. Soil Science, 173(10), 736-744, DOI: 10.1097/SS.0b013e31818939cf.

Cheng L., Sun H., Zhang Y. and Zhen S. (2019). Spatial structure optimization of mountainous abandoned mine land reuse based on system dynamics model and CLUE-S model. International Journal of Coal Science & Technology, 6(1), 13, DOI: 10.1007/s40789-019-0241-x.

Chunkao K., (2008). Principles of watershed management. Kasetsart University Publishers, Bangkok, Thailand.

Clements G.R., Lynam A.J., Gaveau D., Yap W.L., Lhota S., Goosem M., . . . Laurance W.F. (2014). Where and How Are Roads Endangering Mammals in Southeast Asia's Forests? PLOS ONE, 9(e115376), DOI: 10.1371/journal.pone.0115376.

Consiglio T., Schatz G.E., McPherson G., Lowry P.P., Rabenantoandro J., Rogers Z. S., Rabehevitra. D. (2006). Deforestation and plant diversity of Madagascar's littoral forests. Conservation Biology, 20, 5.

Dastgerdi A.S., Sargolini M., Pierantoni I., and Stimilli F. (2020). Toward An Innovative Strategic Approach For Sustainable Management Of Natural Protected Areas In Italy. Geography, Environment, Sustainability, 13(3), 68-75, DOI: 10.24057/2071-9388-2019-143.

Department of Mineral Resources D. (2007). Geology of Thailand. Retrieved from Bangkok, Thailand.

Department of Mineral Resources D. (2009). The Geological Classification for Geological and Mineral Resources Management, Loei. Retrieved from Bangkok, Thailand.

Foody G.M. and Mathur A. (2004). Toward intelligent training of supervised image classifications: directing training data acquisition for SVM classification. Remote Sensing of Environment, 93, 11, DOI: 10.1016/j.rse.2004.06.017.

Geist H.J. and Lambin E.F. (2002). Proximate causes and underlying driving forces of tropical deforestation. Bioscience, 52, 8.

Gilani H., Shrestha H.L., Murthy M.S.R., Phuntso P., Pradhan S., Bajracharya B. and Shrestha B. (2015). Decadal land cover change dynamics in Bhutan. Journal of Environmental Management, 148, 10, DOI: 10.1016/j.jenvman.2014.02.014.

Gobin A., Campling P. and Feyen J. (2002). Logistic modelling to derive agricultural land use determinants: A case study from southeastern Nigeria. Agriculture Ecosystems & Environment, 89(3), 16, DOI: 10.1016/S0167-8809(01)00163-3.

Guan D., Li H., Inohae T., Su W., Nagaie T. and Hokao K. (2011). Modeling urban land use change by the integration of cellular automaton and Markov model. Ecological Modelling, 222, 13, DOI: 10.1016/j.ecolmodel.2011.09.009.

Guang L., Jin Q., Li J., Li L., He C., Huang Y. and Yao Y. (2017). Policy factors impact analysis based on remote sensing data and the CLUE-S model in the Lijiang River Basin. China. Catena, 158, 12, DOI: 10.1016/j.catena.2017.07.003.

Hooke R.L., J. F. Martín-Duque and Pedraza J. (2012). Land transformation by humans. A review. GSA Today, 22, 7.

IPCC (2007). Climate Change 2007: Synthesis Report. Contribution of Working Groups I, II and III to the Fourth Assessment Report of the Intergovernmental Panel on Climate Change, IPCC, Geneva, Switzerland, 104.

Islam K., Jashimuddin M., Nath B. and Kumar T. N. (2018). Land use classification and change detection by using multi-temporal remotely sensed imagery: The case of Chunati wildlife sanctuary, Bangladesh. The Egyptian Journal of Remote Sensing and Space Sciences, 21, 17, DOI: 10.1016/j.ejrs.2016.12.005.

Jensen J.R. and Kiefer R.W. (2007). Remote sensing of the environment. New Jersey: Pearson Prentice Hall.

Jia K., Liang S., Zhang L., Wei X., Yao Y. and Xie X. (2014). Forest cover classification using Landsat ETM+ data and time series MODIS NDVI data. International Journal of Applied Earth Observation and Geoinformation, 33, 7, DOI: 10.1016/j.jag.2014.04.015.

Jia Z., Ma B., Zhang J. and Zeng W. (2018). Simulating Spatial-Temporal Changes of Land-Use Based on Ecological Redline Restrictions and Landscape Driving Factors: A Case Study in Beijing. Sustainability, 10, DOI: 10.3390/su10041299.

Klongvessa P., Lu M. and Chotpantarat S. (2018). Response of the flood peak to the spatial distribution of rainfall in the Yom River basin, Thailand. Stochastic Environmental Research and Risk Assessment, 32(10), 17.

Komaki T., Noda I., Furuya N., Yokota Y., Himmapan W. and Pusudsavang A. (2012). The present circumstances of teak wood processing, marketing and future prospects in Northeast Thailand. JIRCAS Working Report, 74, 64-68.

Konpian S., Som-ard J., Jitsukka W. and Suwanlee S. R. (2019). Assessment of Forest Recovery at Conservation Areas in Loei Province Using Landsat Imagery in Time Series. Thai Science and Technology Journal, 28(7), 1185-1201.

Lagrosa IV J.J., Zippwerer W.C. and Andreu M.G. (2018). Projecting Land-Use and Land Cover Change in a Subtropical Urban Watershed. Urban Science, 2(1)(11), 23, DOI: 10.3390/urbansci2010011.

Lambin E.F. (1997). Modelling and monitoring land-cover change processes in tropical regions. Progress in Physical Geograph, 21, 9.

Lambin E.F. and Meyfroidt P. (2010). Land use transitions: socio-ecological feedback versus socio-economic change. Land Use Policy, 27, 11, DOI: 10.1016/j.landusepol.2009.09.003.

Liu Y., Huang X., Yang H. and Zhong T. (2014). Environmental effects of land-use/cover change caused by urbanization and policies in Southwest China Karst area e A case study of Guiyang. Habitat International, 44, 10.

Luo G., Yin C., Chen X., Xu W. and Lu L. (2010). Combining system dynamic model and CLUE-S model to improve land use scenario analyses at regional scale: A case study of Sangong watershed in Xinjiang, China. Ecological Complexity, 7, 10, DOI: 10.1016/j.ecocom.2010.02.001.

Mallinis G., Emmanoloudis D., Giannakopoulos V., Maris F. and Koutsias N. (2011). Mapping and interpreting historical land cover/land use changes in a Natura 2000 site using earth observational data: The case of Nestos delta, Greece. Applied Geography, 31, 9, DOI: 10.1016/j.apgeog.2010.07.002.

Moreira F., Rego F. C. and Ferreira P. G. (2001). Temporal (1958-1995) pattern of change in a cultural landscape of northwestern Portugal: implications for fire occurrence. Landscape Ecology, 16(6), 11.

National Statistical Office. (2019). Household Income & Expenditure. [online] Available at: http://web.nso.go.th/en/stat_theme_socpop.html [Accessed 15 January 2019].

Peng L., Chen T. and Liu S. (2016). Spatiotemporal Dynamics and Drivers of Farmland Changes in Panxi Mountainous Region, China. Sustainability, 8(11), DOI: 10.3390/su8111209.

Pontius R. G. and Schneider L.C. (2001). Land-cover change model validation by an ROC method for the Ipswich watershed, Massachusetts, USA. Agriculture, Ecosystems & Environment, 85(1-3), 10, DOI: 10.1016/S0167-8809(01)00187-6

Poursanidis D., Chrysoulakis N. and Mitraka Z. (2015). Landsat 8 vs. Landsat 5: A comparison based on urban and peri-urban land cover mapping. International Journal of Applied Earth Observation and Geoinformation, 35, 11, DOI: 10.1016/j.jag.2014.09.010.

Richards J. A. and Jia X. (2006). An introduction. In Remote sensing digital image analysis: Springer.

Royal Forest Department Resources. (2007). Forestry Statistics Year 2006. Royal Forest Department, Ministry of Natural Resources and Environment, Bangkok, Thailand.

Royal Forest Department Resources. (2016). Forestry Statistics Year 2016. Royal Forest Department, Ministry of Natural Resources and Environment, Bangkok, Thailand.

Sadler J., Bates A., Donovan R. and Bodnar S. (2011). Building for biodiversity: Accommodating people and wildlife in cities. In In Urban Ecology. Patterns, Processes and Applications (12). Oxford, UK: Oxford University Press.

Santiphop T., Shrestha R. P. and Hazarika M. K. (2012). An analysis of factors affecting agricultural land use patterns and livelihood strategies of farm households in Kanchanaburi Province, Thailand. Journal of Land Use Science, 7, 8, DOI: 10.1080/1747423X.2011.587208.

Satika B. and Chotpantarat S. (2014). Simulation of nitrate concentration affected from land use changes in the lower part of Yom river basin, Thailand: a preliminary study. Advanced Materials Research, 931-932, 6.

Satika B. and Chotpantarat S. (2018). Impacts of land-use changes on watershed discharge and water quality in a large intensive agricultural area in Thailand. Hydrological Sciences Journal, 63(9), 12, DOI: 10.1080/02626667.2018.1506128.

Shalaby A. and Tateishi R. (2007). Remote sensing and GIS for mapping and monitoring land cover and land-use changes in the Northwestern coastal zone of Egypt. Applied Geography, 27(1), 4.

Shirvani D.A., Sargolini M., Broussard A.S., Chatrchyan A. and De Luca G. (2020). Climate Change and Sustaining Heritage Resources: A Framework for Boosting Cultural and Natural Heritage Conservation in Central Italy. Climate. 2020, 8(2), 26, DOI: 10.3390/cli8020026.

Tabor K., Hewson J., Tien H., González-Roglich M., Hole D. and Williams J.W. (2018). Tropical Protected Areas Under Increasing Threats from Climate Change and Deforestation. Land, 7(3), 90, DOI: 10.3390/land7030090.

Trisurat Y., Alkemade R. and Verburg P. H. (2010). Projecting land-use change and its consequences for biodiversity in Northern Thailand. Environmental Earth Sciences, 45, 14, DOI: 10.1007/s00267-010-9438-x.

Trisurat Y., Shirakawa H. and Johnston J. M. (2019). Land-Use/Land-Cover Change from Socio-Economic Drivers and Their Impact on Biodiversity in Nan Province, Thailand. Sustainability, 11, DOI: 10.3390/su11030649.

Turner II B. L., Lambin E. and Reenberg A. (2007). The emergence of land change science for global environmental change and sustainability. Paper presented at the The National Academy of Sciences (PNAS).

U.S. Geological Survey. (2014). Landsat Bands. United States Department of the Interior, Virginia. Retrieved from https://landsat.usgs.gov/what-are-band-designations-landsat-satellites

Verburg P.H. and Overmars K.P. (2009). Combining top–down and bottom– up dynamics in land use modeling: exploring the future of abandoned farmlands in Europe with the Dyna-CLUE model. Landscape Ecology, 24, 5, DOI: 10.1007/s10980-009-9355-7.

Verburg P.H., Soepboer W., Limpiada R., Espaldon M.V.O., Sharifa M. and Veldkamp A. (2002). Land use change modelling at the regional scale: The CLUE-S model. Environmental Management, 30, 15.

Verburg P. H. and Veldkamp. (2004). A Projecting land use transitions at forest fringes in the Philippines at two spatial scales. Landscape Ecology, 19, 12.

Verburg P.H., Veldkamp A. and Fresco L.O. (1999). Simulation of changes in the spatial pattern of land use in China. Applied Geography, 19, 22.

Waiyasusri K. and Chotpantarat S. (2020). Watershed Prioritization of Kaeng Lawa Sub-Watershed, Khon Kaen Province Using the Morphometric and Land-Use Analysis: A Case Study of Heavy Flooding Caused by Tropical Storm Podul. Water, 12(6), 1570, DOI: 10.3390/w12061570.

Waiyasusri K., Yumuang S. and Chotpantarat S. (2016). Monitoring and predicting land use changes in the Huai Thap Salao Watershed area, Uthaithani Province, Thailand, using the CLUE-s model. Environmental Earth Sciences, 75, 17, DOI: 10.1007/s12665-016-5322-1.

Yumuang S. (2001). Debris flow and debris flood in Nam Ko area, Phetchabun province, central Thailand. Environ Geology, 2006(51), 18.

Zhang L., Cao M., Xing A., Sun Z. and Huang Y. (2018). Modelling the Spatial Expansion of Green Manure Considering Land Productivity and Implementing Strategies. Sustainability, 10, DOI: 10.3390/su10010225.

RESEARCH PAPER

IMPACT ASSESSMENT AND STOCHASTIC MODELING OF MORPHOMETRIC PARAMETERS OF THERMOKARST HAZARD FOR UNPAVED ROADS

Timofey V. Orlov[1*], Aleksey S. Victorov[1], Maria V. Arkhipova[1], Andrey V. Zverev[2]
[1]Sergeev Institute of Environmental Geoscience RAS (IEG RAS), Ulansky per., 13/2, Moscow, 101000, Russia.
[2]Moscow State University of Geodesy and Cartography (MIIGAiK), Gorokhovskiy per., 4, Moscow, 105064, Russia.
***Corresponding author:** tim.orlov@gmail.com
Received: March12th, 2020 / Accepted: November 20th, 2020 / Published: December 31st, 2020
https://DOI-10.24057/2071-9388-2020-54

ABSTRACT. Active construction of new roads and other linear structures requires new techniques for the natural hazard assessment. These techniques can involve both stochastic modeling and remote sensing data (RSD). First, the dynamics of thermokarst appearance along an unpaved road (winter road) was analyzed. Then a probabilistic model of the thermokarst morphological pattern was developed for the area in the vicinity of a linear structure, a road in particular. The model operates with initial assumptions based on the physical parameters of thermokarst development and includes relations for estimating the distribution of morphometric dimensions of thermokarst depressions (ponds). The model was empirically tested for the study area, which represented a site with an unpaved road located in West Siberia region. To verify the model, we calculated the correlation coefficient values for the length of the focus projections on the linear structure and the perpendicular axis and compared the empirical distribution of the projections with the theoretical lognormal distribution using the Pearson's criterion. The proposed model assumptions appeared to be valid for the study area, which makes it possible to proceed to the problem of probabilistic impact risk assessment to a linear structure by foci of human-induced thermokarst.

KEY WORDS: Stochastic modeling; Pearson's criterion; remote sensing; mathematical morphology of landscapes; roads; human-induced thermokarst

CITATION: Timofey V. Orlov, Aleksey S. Victorov, Maria V. Arkhipova, Andrey V. Zverev (2020). Impact Assessment And Stochastic Modeling Of Morphometric Parameters Of Thermokarst Hazard For Unpaved Roads. Geography, Environment, Sustainability, Vol.13, No 4, p. 98-106
https://DOI-10.24057/2071-9388-2020-54

ACKNOWLEDGEMENTS: The study was carried out under the state funding within the framework of a state assignment, scientific project No. AAAA–A19–119021190077–6 and the Russian Geographical Society and the Russian Foundation for Basic Research Grant # 17-05-41141 (modeling and testing).

Conflict of interests: The authors reported no potential conflict of interest.

INTRODUCTION

Construction of unpaved roads within the permafrost zone is a widespread practice in Russia (Ragozin 1997). Because of that, there is an urgent problem concerning modeling the thermokarst processes initiated by the impact of an engineering structure itself (Arenson 2017; Doré et al. 2016; Fel'dman 1984; Hjort et al. 2018; Mazhitova et al. 2004; Shiklomanov et al. 2013; Streletskiy et al. 2012). The majority of researches use the thermodynamic approach (Dvornikov et al. 2018; Ling et al. 2003; Ling et al. 2012; Romanovskii et al. 2001; Tumskoy 2002; Shur 1977) though it has major drawbacks resulting from the complexity of the models on one hand and a lack of information as well as high variability of many background parameters such as ice content, soil temperature and particle size distribution on the other hand. The complexity of the models results from taking into account the phase transitions as well as from their three-dimensional approach.

Our previous studies showed that central points of natural thermokarst lakes in a homogeneous environment fit the Poisson distribution, meaning that they appear independently of each other (Victorov et al. 2015). Moreover, the area of natural thermokarst lakes fits the lognormal distribution, which means that they expand due to the proportional heat transfer through the side surface (Victorov et al. 2015). These conclusions were empirically verified at several sites all over the Russian and Canadian permafrost areas.

We have also revealed that the projections of the centers of the emerged thermokarst ponds divided the road into sections, the length of which follows the exponential distribution. It proves that the thermokarst depressions appear independently of each other due to the heating influence of the road (Victorov et al. 2019).

The aim of the present research is to perform advanced stochastic modeling of human-induced thermokarst development along a road and assess the thermokarst hazard based on the stochastic approach and remote sensing data.

The general research procedure includes:
- analyzing the type and activity of thermokarst at different sites;

- formulating initial assumptions on the occurrence and development of human-induced thermokarst;
- mathematical implementation of these assumptions using the probability theory approach;
- transformation of the initial assumptions through mathematical analysis;
- obtaining the final equation and laws determining the thermokarst development process;
- empirical testing of the obtained laws for the study area;
- confirmation or refutation of the model assumptions and equations.

MATERIALS AND METHODS

The study area (Fig. 1) is located in the West Siberian lowland. It is an accumulative weakly dissected alluvial plain, covered by fluvioglacial sand with continuous permafrost of 100-300 m deep. The average annual temperature at the bottom of annual fluctuations zone is -1 – -3 C, in the unstable active layer it is 1 – -2 C. The plain is covered by the tundra forest vegetation. It is crossed by a perennial winter road, some parts of which are used in the summer also.

Our study area satisfies the following criteria:
- Morphological homogeneity of the site:
- Physiographic (geology and topography in particular) homogeneity of the site:
- High thermokarst dynamics.

The morphological homogeneity of the study area was confirmed from the interpretation of remote imagery. Physiographic homogeneity was proven by the analysis of geological and other field data together with the interpretation of remote imagery.

Our research involved two different approaches.

First, we followed the common practice, which includes direct determination of the thermokarst foci and statistical analysis of their development. We call it the «traditional approach».

The second approach was based on stochastic modeling.

Traditional approach

The traditional approach assesses the actual thermokarst impact on engineering structures (Cosford et al. 2014)*. Let us demonstrate its application.

The study area (2.42 sq. km) is crossed by a 6.6 km long section of the winter road Nadym-Salekhard (Russia). It is a part of the West Siberian plain (plate) bounded by the Poluy and Ob rivers, Russia (State geological map 2015; Savincev 2012; Shamilishvili et al. 2012).

For the analysis, we used the satellite imagery from 1968, before the winter road was built (Corona 2/pix), as well as more recent imagery from 2012 and 2016 (WorldView-2 и WorldView-3) provided by DigitalGlobe under a grant from the DigitalGlobe Foundation+, Arctic DEM++.

The study area was chosen based on the following criteria: morphological and physiographic uniformity of the area, presence of the linear structure, active thermokarst.

Using the traditional approach, it was revealed that all the thermokarst foci mostly appeared along the road, which operates at different times.

Then the territory was divided according to its thermokarst activity, which includes the appearance and development of the thermokarst foci. We compared the territory according to the number and area of the foci. Afterwards, a criterion was developed based on the ratio between the size of the foci and their area, which characterizes the technogenic pressure.

Stochastic approach: the advanced mathematical model of the human-induced thermokarst in the vicinity of linear structures

The advanced model, in particular, takes into account the basic model (Victorov et al. 2019) and the results of the previous research (Kapralova 2015; Victorov et al. 2015; Victorov A.S., Trapeznikova O.N. 2019; Gonikov T.V. 2019).

The proposed model is based on the following main assumptions and limitations. Let us consider an unpaved road built across a plain with homogenous geology. The construction of the road has changed the thermal regime and based on that three zones can be distinguished: under the road, near the road, and at a certain distance from the road. Change of the thermal regime leads to the thermokarst development, including the emergence of thermokarst depressions (ponds). The stochastic modeling is applied for every zone of the thermal regime within the isotropic area.

It is evident that while the soil and permafrost properties somehow determine the development of the thermokarst depressions, these factors are the same for the entire study area.

During the first stage, the initial thermokarst depression represents a shallow puddle of an irregular shape, filled with water. Multiple researchers (Boike et al. 2015; Huang et al. 2019; Matell et al. 2013; Perl'shteyn et al. 2005; Shur 1977) have described this phase of the thermokarst development. During the second stage, which is longer, the thermokarst depressions become more isometric because of the ice melting (Methodical guidelines 1978). The proposed model deals with the second stage.

The model of the human-induced thermokarst has the following assumptions:

1. Thermokarst depressions emerge within a narrow band (with a width a) in the vicinity of a linear structure. They appear independently from each other, and the probability of their appearance within the given section depends only on its area Δ_s (thus, in small areas the probability for development of a single depression is much higher than that for several depressions) and the distance from the linear structure.

$$p(r,\Delta s)=\lambda(r)\Delta s+o(\Delta s) \tag{1}$$

where $\lambda(r)$ is a coefficient.

2. A focus of the human-induced thermokarst in the vicinity of a linear structure has an approximately elliptic shape with the ratio of the axes length ξ_i (where *i* is a year), which follows the uniform probabilistic distribution and independently changes from year to year:

$$\beta=\xi_i a \tag{2}$$

where α and β are the lengths of the semi-axes.

3. The growth of the linear dimensions of the thermokarst depressions (the semi-axes of the ellipse) due to thermo-abrasion (the low intensity of the thermos-abrasion is possible, at that, the process tends to the «classic thermokarst») occurs independently from each other; it is directly proportional to the density of heat loss through the side surface of the depressions below water level.

Thus, we analyze the scenario of a synchronous start when the primary depressions appear in a short period from the beginning of the linear structure construction. The first

*URL: https://earthexplorer.usgs.gov/
+URL: www.digitalglobefoundation.org
++URL: https://www.pgc.umn.edu/data/arcticdem/

assumption comes from the homogeneity of the area in question. It reflects the fact that any limited area contains a finite quantity of thermokarst depressions (their centers, to be precise). Besides, this assumption considers the nature of the disturbances, which cause thermokarst, including that of the soil, vegetation cover, microrelief and permafrost in the vicinity of the linear structure. They vary depending on the distance from the linear structure and generally do not change along the structure. Hence, the main direction of the thermokarst emergence variability is the direction perpendicular to the structure. The function λ(*r*) accounts for this variability, which depends on the distance from the structure.

The second assumption reflects the proportionality of the thermokarst focus growth rate to the average density of heat loss through a side surface below water level; at the same time, the growth depends on many random factors including average annual air temperature and ice content of the soil in the vicinity of the pond.

Fig. 1 shows a typical remote sensing image of the emerged thermokarst depressions along a linear structure and Fig. 2 represents a schematic depiction of the model parameters.

From the mathematical analysis of the assumptions, a set of conclusions can be made. For instance, the distribution of the number of thermokarst depressions (or their centers) within a given length of a linear structure (*L*) follows the Poisson law.

$$P0(k,L)=\frac{[YL]^k}{k!}e^{-YL} \quad (1)$$

where *Y* is an average linear density of the thermokarst centers.

The analysis of this equation allows us to obtain the distribution of distances between the centers of thermokarst depressions along the linear structure, which must, subject to the model's validity, correspond to the exponential distribution.

Let us determine the distribution for semi-axes length. If *V* is the volume of water in the depression, which resulted from the water concentration from the catchment area, evaporation, runoff and other processes of water balance formation, then the depth of the lower part filled with water, taking into account the equation for the area of the ellipse μ

$$\mu=\pi a\beta \quad (2)$$

and proportionality of the semi-axes α и β (assumption 2)

$$\beta=\xi_i a \quad (3)$$

in the year *j* is equal to

$$h_j=\frac{V}{\pi\xi_j u_j^2} \quad (4)$$

In that case, the side area covered with water is

$$S=\frac{V(\xi_j+1)}{\xi_j u_j} \quad (5)$$

where u_j is the length of the semi-axis *α* in the beginning of the year *j*.

Hence, the second assumption gives us the formula

$$\Delta u_j=\frac{ct^0V}{S}U_j^0 \quad (6)$$

Fig. 1. (a, b). A typical remote sensing image of emerged thermokarst depressions along a road: a) high-resolution remote sensing data, GeoEye image b) photo

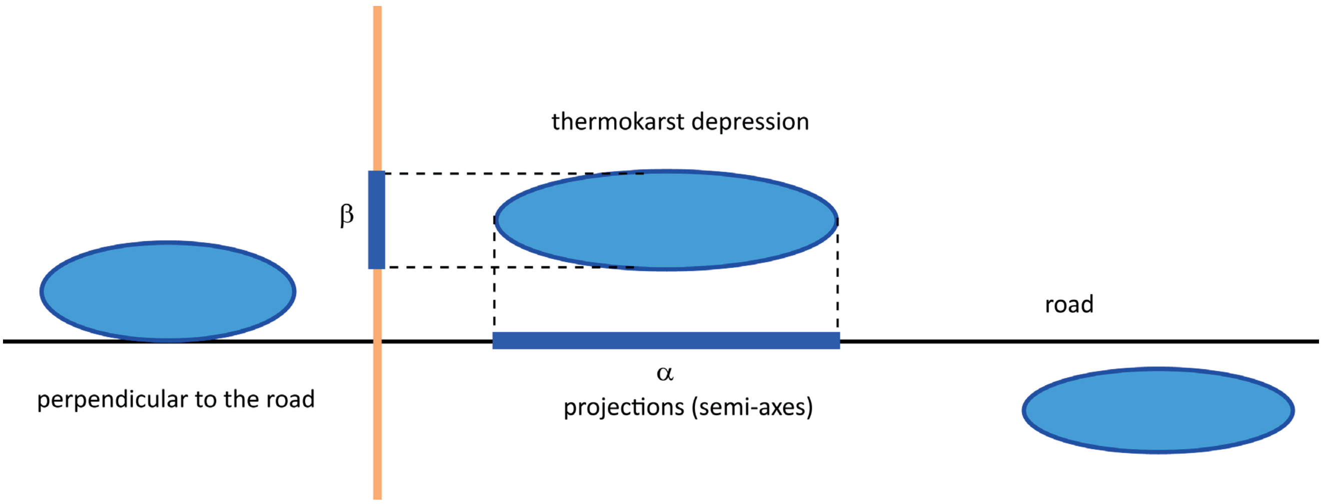

Fig. 2. A scheme of the model parameters

where Δuj is an increment the length of the axis a per year j, c is the specific heat capacity, t^0 is the average water temperature, u_j^0 is a random variable for episodic factors.

After the substitution of the area from the equation (5) and simplification, this equation takes the form

$$\Delta u_j = \frac{U_j \xi_j}{\xi_j + 1} u_j \tag{7}$$

Accordingly, the length of the semi-axis in successive years is described by the following relation:

$$u_{j+1} = \left[1 + \frac{U_j \xi_j}{\xi_j + 1} u_j \right] \tag{8}$$

So, if we take the diameter of the initial depression equal to 1, the length of the semi-axis in the year j can be determined from the equation:

$$u_j = \prod_{i=1}^{j} \left[1 + \frac{U_j \xi_j}{\xi_j + 1} \right] \tag{9}$$

or

$$\ln u_j = \sum_{i=1}^{j} \ln \left[1 + \frac{U_j \xi_j}{\xi_j + 1} \right] \tag{10}$$

The function u_j^0 in the right side of the equation is a random variable for the permafrost degradation over a certain year, which depends on summer and winter temperatures, snow thickness, rainout, soil temperature, rainfall characteristics, ice and ground content in the direction of the semiaxes. These parameters do not depend on each other from year to year but they all follow the same distribution.

Since, according to the central limit theorem, the sum of a large number of independent identically distributed random variables is normally distributed, then the logarithm of the semi-axis will be normally distributed as well. Hence the growth of the semi-axis of initiated thermokarst depressions with a large value of j we can approximately consider as a Markov random process with continuous-time and the transition function:

$$f_a(v,x,t) = \frac{1}{\sqrt{2\pi}\sigma x \sqrt{t}} e^{-\frac{\left(\ln\frac{x}{v} - at\right)^2}{2\sigma^2 t}} \tag{11}$$

where *a, a* are the distribution parameters, v is the initial length of the semi-axis of the thermokarst pond, x is the length of the semi-axis of the thermokarst pond after time t.

If we suppose that the functions of the right side are normally distributed then the same conclusion will hold for any period of the development (even a little one).

Let us simplify the model and assume that the primary thermokarst depressions at the moment of their occurrence have a unit axis length (this corresponds to normalization by the minimum value), then for any given time we should get the lognormal distribution of the axis length of the thermokarst ponds, i.e.

$$f_a^0(x,t) = \frac{1}{\sqrt{2\pi}\sigma x \sqrt{t}} e^{-\frac{(\ln x - at)^2}{2\sigma^2 t}} \tag{12}$$

where *a, a* are the distribution parameters and t is time since the beginning of the process.

Since the first semi-axis and the proportionality coefficient ξ_j follow the lognormal distribution and are independent, their product (the second semi-axis β) should then also follow the lognormal distribution, but with a slightly different value of the parameter a.

$$\mu_i = \pi \xi_i a^2 \tag{13}$$

Finally, taking into account the quadratic relationship between the area and the axis length

the area of the human-induced thermokarst pond should then also follow the lognormal distribution.

RESULTS

Initial thermokarst basic investigation

Situation at the study area in 1968 is shown in Fig 3.

The studied part of the winter road was divided into 14 sections using the satellite image from 2016 based on the relative uniformity of the distribution of thermokarst ponds, which allowed to identify the sections with the most significant anthropogenic load (Fig. 4).

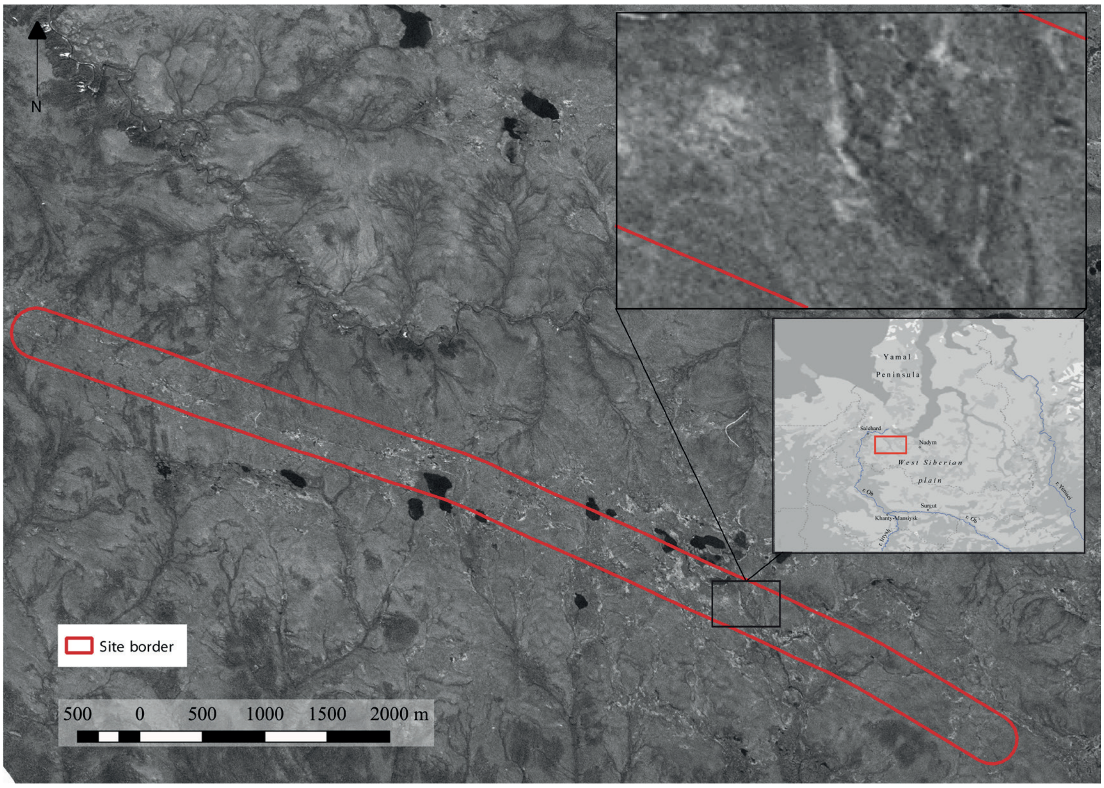

Fig. 3. A satellite image 1968, Corona

The winter road was absent in 1968, but by 2016 it has been functioning for many years, with many thermokarst ponds developed.

Fig. 5 shows the rate of depressions development.

As we can see from Fig. 5, the winter road affected the emergence of the thermokarst ponds, and their number increased significantly. Due to the active use in 2012–2016, for the winter road sections 7, 9, 11 an apparent accelerated increase in the depressions development can be observed, while sections 3, 5, 8, 14 demonstrate a decrease in their number. The average annual number of new thermokarst ponds during the construction period and moderate use of the winter road in 1968–2012 is relatively uniform along the entire road. At the present stage, during the period from 2012 to 2016, we see high dynamics of changes in their quantity; this indicates the thermokarst intensification during the period of active exploitation of the road. Fig. 6 shows the change in the area of ponds over the considered periods.

As we see in Fig. 6, there is an essential decrease in the area of ponds over the period 2012–2018 along the entire winter road. The negative values of the area change indicate drying out of the thermokarst ponds or their separation into smaller ones.

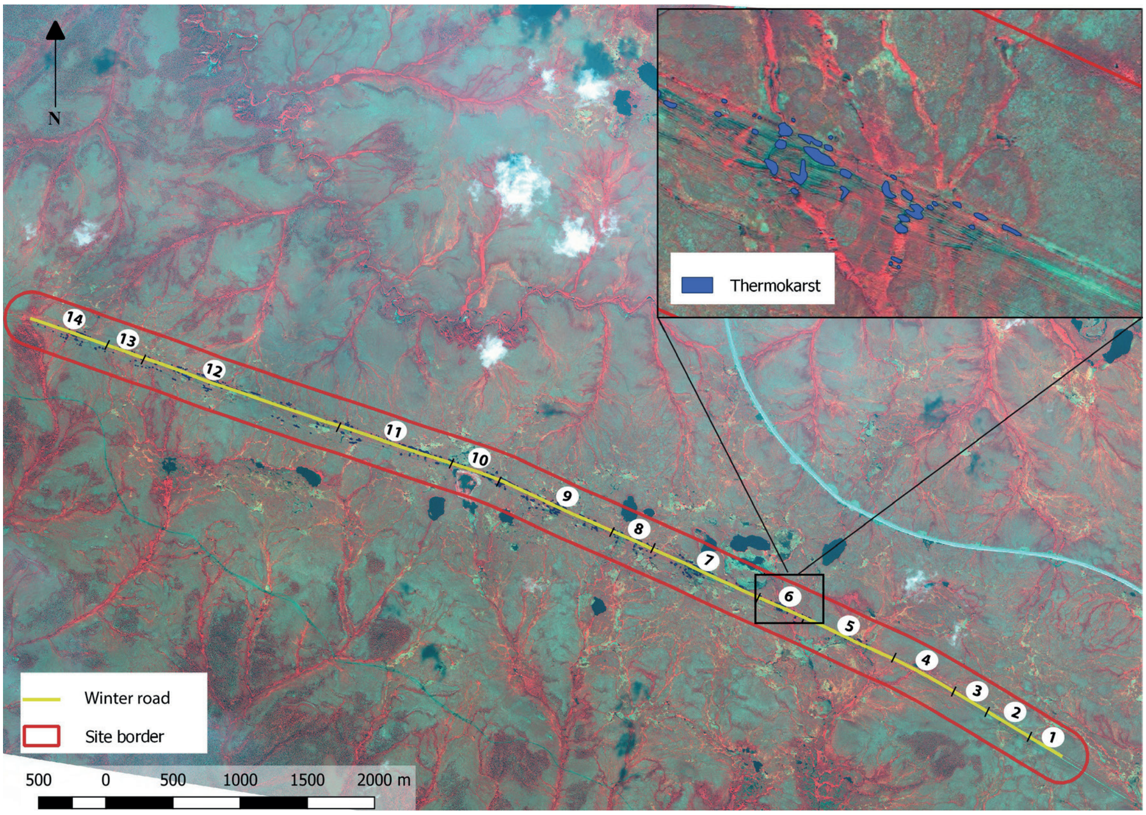

Fig. 4. A satellite image 2012, WorldView-2

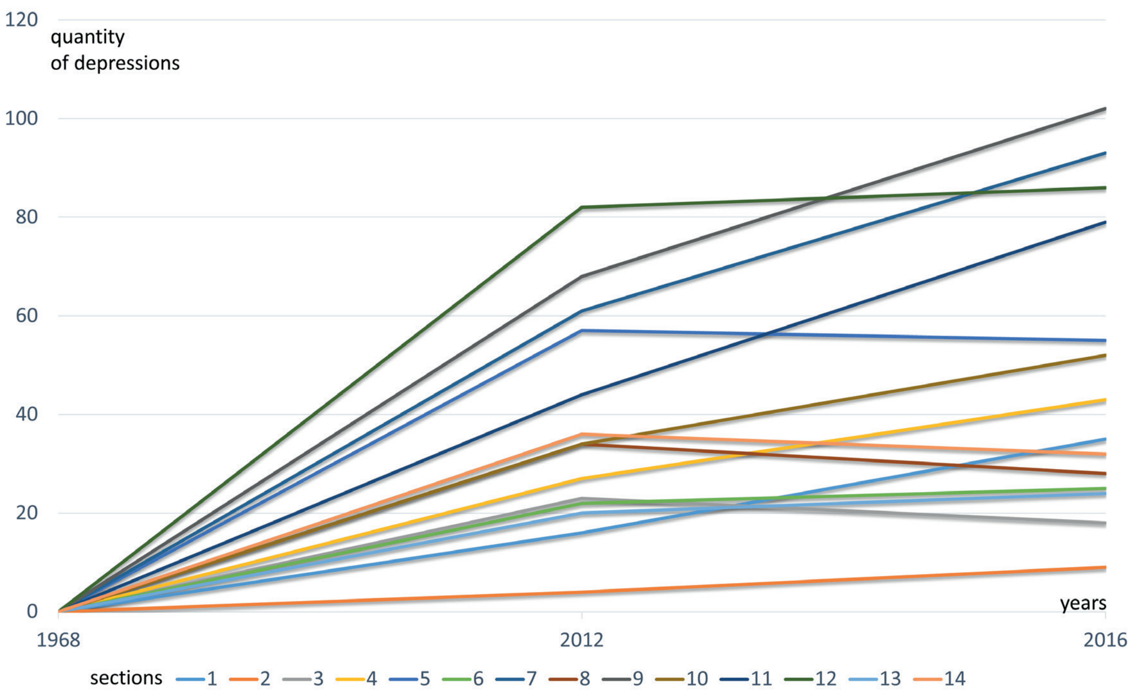

Fig. 5. The rate of depressions development over the periods 1968–2012 and 2012–2016

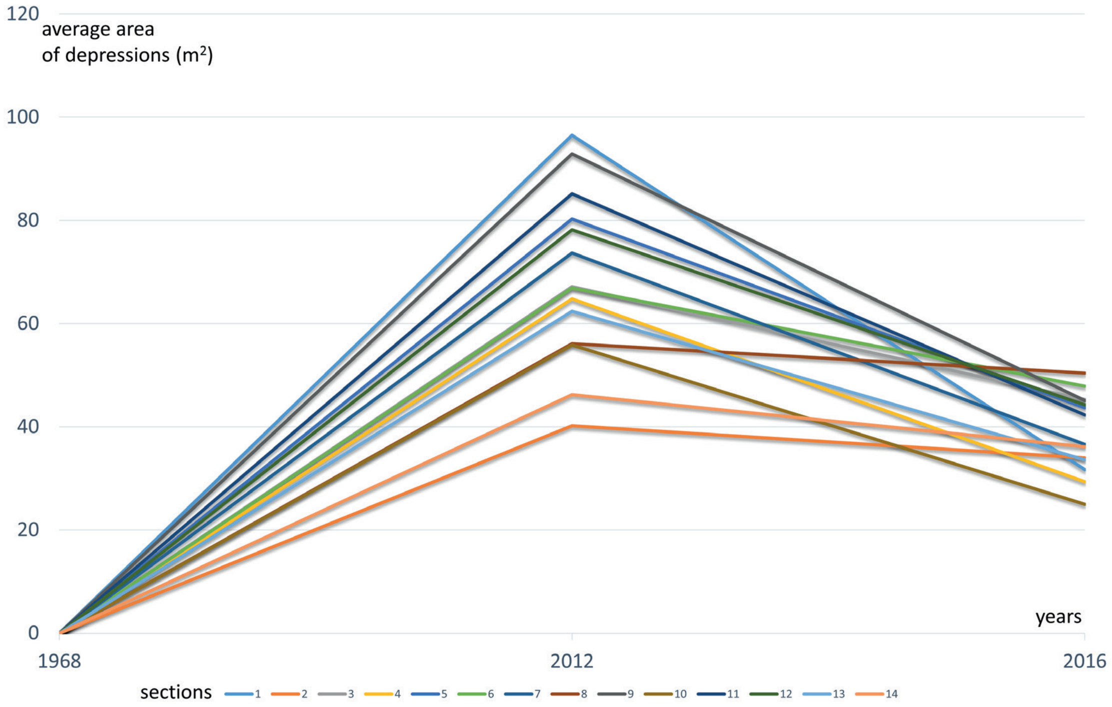

Fig. 6. Area of appearing of depressions per year over the periods 1968–2012 and 2012–2016

So, over the period 2012–2016, the number of thermokarst ponds along the winter road increased while their areas decreased.

We propose an evaluation criterion to assess the impact on the winter road: the ratio of the total area of the ponds to the length of the road section. Table 1 contains the results of the estimation. We chose the following classes: 1- negligible (less than 0.8); 2 – low (0.8-2.6); 3 – medium (2.6-3.4); 4 – high (3.4-4.2); 5 – critical (4.2-5.0) as it shown in Fig. 7.

So, the technogenic impact on the thermokarst development is negligible within section 12 (Fig. 7). The winter road influence on the thermokarst within sections 4,5,7,9,11 can be classified as low. Sections 10 and 14 have a medium technogenic impact. The high technogenic impact is found in sections 2 and 8, while sections 1, 3, 6, 13 are characterized by the critical load. Thus, the essential part of the road (23% or 1.485 km) is under either the high or critical impact. About twelve percent of the road belongs to the medium hazard class. It means that more than one-third of the road (35%) has dramatically changed due to the technogenic impact and the area of the winter road has changed over the period of its functioning.

Particular attention should be paid to the areas where many ponds have appeared to prevent further occurrence of the new thermokarst foci and the technology of construction and reconstruction of the winter road should be considered carefully.

Table 1. The ratio of the total area of the ponds to the length of the road section (2016)

Section	Length of a section, m	Total area, m^2	Ratio (m^2/ m)	Class of technogenic impact
1	223.84	1065.74	4.76	5
2	296.62	184.34	3.59	4
3	221.05	620.64	4.82	5
4	494.40	1249.99	2.16	2
5	572.37	2192.55	1.86	2
6	236.73	1052.60	4.50	5
7	707.80	3247.99	1.51	2
8	275.96	1409.49	3.86	4
9	730.37	4519.39	1.46	2
10	344.74	1284.99	3.09	3
11	707.18	3404.93	1.51	2
12	1248.99	3857.61	0.79	1
13	230.99	765.97	4.61	5
14	394.32	1052.71	2.70	3

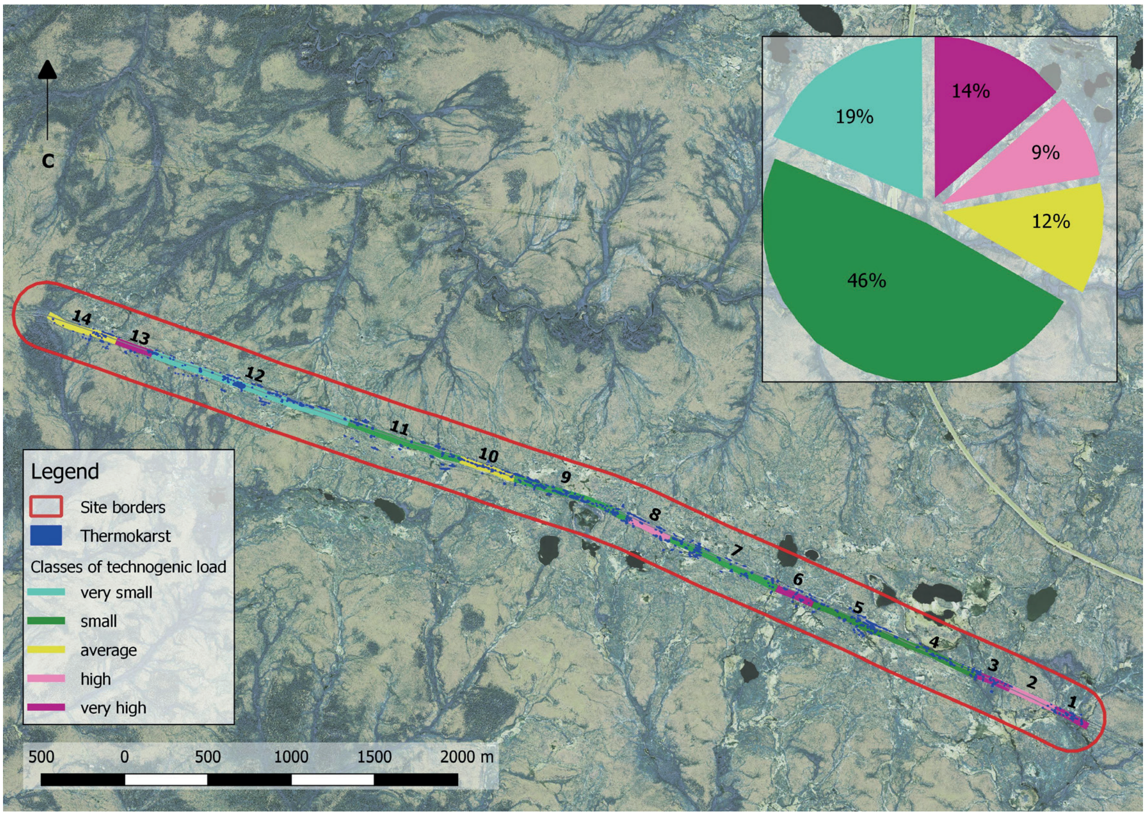

Fig. 7. A schematic map of the thermokarst impact on the winter road

DISCUSSION

We tested our stochastic model empirically. The empirical testing includes:
- Identifying human-induced thermokarst depressions (thermokarst ponds) using RSD,
- Measuring the length of the focus projections on the linear structure,
- Detecting the centers of the focus projections on the axis perpendicular to the linear structure,
- Estimating correlation coefficients for the length of the focus projections on the linear structure and the axis perpendicular to the linear structure,
- Comparison of the empirical distribution of the projections with the theoretical lognormal distribution using Pearson's criterion.

When identifying the thermokarst depressions, we always used archival Corona images taken before the construction of the linear structure (1960–1970). Thus, we are sure that all detected thermokarst depressions either appeared or radically changed due to the anthropogenic influence.

The model expects that the distribution of length for the projections of the depressions on the linear structure and the perpendicular axis should follow the lognormal distribution — table 2 contains the results of the comparison between the empirical and theoretical (lognormal) length distributions for the projections.

We used Pearson's chi-squared test to analyze the correspondence between the empirical and theoretical distributions. It is a statistical test applied to categorical datasets to evaluate how likely it is that any observed difference between the two sets arose by chance. It tests a null hypothesis stating that the frequency distribution of certain events observed in a sample is consistent with a particular theoretical distribution. The statistical significance was checked with p-value or probability value or asymptotic significance, which is the probability for a given statistical model that, when the null hypothesis is correct, the statistical summary (such as the sample mean or the difference between two compared groups) would be greater than or equal to the actual observed results. The analysis of table 2 shows that all samples of the length of the projections correspond to the lognormal distribution. According to the analysis of table 2, the initial hypothesis that the distributions of the length of the projections on the linear structure and the axis perpendicular to the linear structure are lognormal is confirmed for all the samples at a significance level of 0.99.

We have also analyzed the change of the ratio between the projections of the depressions on the linear structure and the perpendicular axis.
Table 3 contains the average ratio between the projections on the linear structure and its perpendicular axis (elongation coefficient), the correlation coefficient between the projections for each depression and the result of comparing the elongation coefficient distribution with the lognormal distribution.

For the study area, a significant positive correlation of

Table 2. Comparison between the empirical and theoretical lognormal distribution for the focus projections on the linear structure and the perpendicular axis

Study area	Projection	Sample size, (foci)	The average length of a projection, m	p*
Salekhard	Road	528	6.862	0.413
	perpendicular	528	12.590	0.187

p* – here and later p is additional to quantile value, corresponding the actual significance criterion; for example, the hypothesis is consistent with a probability of 0.99 if p is greater than or equal to 0.01.

Table 3. Elongation and correlation coefficients for the length of projections on the linear structure and its perpendicular axis and comparison between the elongation coefficient and the lognormal distribution

Study area	Average elongation coefficient	Correlation coefficient	p*
Salekhard	0.732	0.577	0.272

the length of projections on the linear structure and the perpendicular axis is observed. It confirms the validity of the second assumption of the model about a certain, though stochastic, proportionality between the semi-axes length.

Table 3 shows the correspondence between the distribution of the elongation coefficient and the lognormal distribution. In most cases, the testing results confirm the suggested model at the level of significance 0.99.

The obtained results seem to be useful as they show that we can study the patterns of thermokarst development even without advanced engineering geological descriptions. We plan the following steps for improving our approach. First, further empirical testing will be conducted for different environments. Second, we will search for relations between the field-measured ground and permafrost characteristics and the obtained statistical data. The further improvement of the approach can make it a good base for the thermokarst forecasting in the conditions of lacking field data.

CONCLUSION

1. We developed and empirically tested the advanced model of the human-induced thermokarst in the vicinity of built linear structures. This model is based on the reasonable assumptions that the thermokarst depressions appear in a narrow strip along a road and develop independently of each other. Their growth depends on the water volume in each of them.
2. This model is expected to be more promising than the basic investigation approach.
3. The assumptions of the model were written as mathematical equations, from which, using strict transformations, the following main conclusions are derived:
- the length of the projections on the road and the axis perpendicular to it must follow the lognormal distribution,
- the distribution of the centers of the projections of the depressions must follow the exponential distribution,
- the relation between the projections must be correlated and follow the lognormal distribution.
4. The empirical testing proved the validity of these laws for the study area.

REFERENCES

Arenson L., Matthias J. (2017). Permafrost-Related Geohazards and Infrastructure Construction in Mountainous Environments. Oxford Research Encyclopedia Natural Hazard Science.

Boike G., Kirillin C., Muster G., Abramova S., Fedorova K., Chetverova I., Grigoriev A., Bornemann M., Langer M. (2015). Thermal processes of thermokarst lakes in the continuous permafrost zone of northern Siberia—Observations and modeling (Lena River Delta, Siberia), Biogeosciences, 12.

Cosford J., Zeyl D., Penner L. (2014). Terrain analysis for pipeline design, construction, and operation. Journal of Pipeline Engineering. 13, 149-165.

Doré G., Fujun N., Brooks H. (2016). Adaptation Methods for Transportation Infrastructure Built on Degrading Permafrost. Permafrost and Periglacial Processes, 27.

Dvornikov Y., Leibman M., Heim B., Bartsch A., Herzschuh Ulrike., Skorospekhova T., Fedorova I., Khomutov A., Widhalm Barbara., Gubarkov A., Roessler S. (2018). Terrestrial CDOM in Lakes of Yamal Peninsula: Connection to Lake and Lake Catchment Properties. Remote Sensing, 10, 167.

Fel'dman G.M. (1984). Thermokarst and permafrost, Novosib., 360 (in Russian).

Gonikov T.V. (2019). Using earth remote sensing to study the parameters of the morphological structure of the ridge landscape in the north caspian region. Izvestiya – Atmospheric and Oceanic Physics. 55(9), 1346-1352

Hjort J., Karjalainen O., Aalto J., Westermann S., Romanovsky V., Nelson F., Etzelmüller B., Luoto Miska. (2018). Degrading permafrost puts Arctic infrastructure at risk by mid-century. Nature Communications, 9.

Huang W., Zhang J., Leppäranta M., Li Z., Cheng B., Lin Z. (2019). Thermal structure and water-ice heat transfer in a shallow ice–covered thermokarst lake in central Qinghai-Tibet Plateau. Journal of Hydrology. 124122.

Kapralova V.V. (2015). Implementation of Remote Sensing and Mathematical Modeling for Study of Risk Assessment to Linear Engineering Structures Due to Thermokarst Processes// G. Lollino et al. (eds.), Engineering Geology for Society and Territory – Volume 1, Springer International Publishing Switzerland, 267-270, DOI: 10.1007/978-3-319-09300-0_50

Ling F., Zhang T. (2003). Numerical simulation of permafrost thermal regime and talik development under shallow thaw lakes on the Alaskan Arctic Coastal Plain. J. Geophys. Res., 108, 4511.

Ling F., Wu Q., Zhang T. and Niu F. (2012). Modelling Open-Talik Formation and Permafrost Lateral Thaw under a Thermokarst Lake, Beiluhe Basin, Qinghai-Tibet Plateau Permafrost and Periglac. Process., 23(4), 312-321.

Matell N., Anderson R., Overeem I., Wobus C., Urban F., Clow G. (2013). Modeling the subsurface thermal impact of Arctic thaw lakes in a warming climate. Computers & Geosciences, 53, 69-79.

Mazhitova G., Karstkarel N., Oberman N., Romanovsky V., Kuhry P. (2004). Permafrost and Infrastructure in the Usa Basin (Northeast European Russia): Possible Impacts of Global Warming. Ambio, 33, 289-94, DOI: 10.1579/0044-7447-33.6.289.

Methodical guidelines for engineering-geological survey of a scale of 1: 200 000 (1: 100000-1: 500000) (1978). Moscow: Nedra, 391 (in Russian).

Perl'shteyn G.Z., Pavlov A.V., Levashov A.V., Sergeyev D.O. (2005). Non-temperature factors of heat exchange of the active layer with the atmosphere. Materials of the Third Conference of russian geocryologists, Moscow: MSU, 86-91 (in Russian).

Ragozin A. (1997). Basic theses of the theory of dangerous geological processes and risks. New ideas in the Earth Sciences: Abstracts, Moscow, 4, 115 (in Russian).

Romanovskii, N.N., Hubberten H.W. (2001). Results of permafrost modelling of the lowlands and shelf of the Laptev Sea Region/ Permafrost and Periglac. Process., 12(2), 191-202.

Tumskoy V. (2002). Thermokarst and its role in the development of the Laptev Sea region in the Late Pleistocene and Holocene. Author's Candidate's summery, Moscow (in Russian).

Savincev I. (2012). Engineering-geological conditions of the valley areas of the cryolithozone of Yanao (on the example of Salekhard and Nadym areas). Dissertation, Ekaterinburg (in Russian).

Shamilishvili G., Abakumov E., Pechkin A. (2016). Features of the soil cover of the Nadym region, JaNAO. – Scientific Bulletin of the Yamal-Nenets Autonomous Okrug, 3, 16-25 (in Russian).

Shiklomanov N., Nelson F. (2013). Thermokarst and Civil Infrastructure. In Treatise on Geomorphology, 8. Elsevier Inc. 354-373, DOI: 10.1016/B978-0-12-374739-6.00214-1.

Shur Y.U. (1977). Thermokarst (to the thermophysical foundations of the doctrine of the laws of the development of the process). Moscow: Nedra, 80 (in Russian).

State geological map RF scale 1:1 000 000 (tret'e pokolenie), West Siberian series, s. Q 43 – Novyj Urengoj (2015). S-Pb (in Russian).

Streletskiy D., Shiklomanov N., Nelson F. (2012). Permafrost, Infrastructure, and Climate Change: A GIS-Based Landscape Approach to Geotechnical Modeling, Arctic, Antarctic, and Alpine Research, 44:3, 368-380.

Victorov A.S., Kapralova V.N., Orlov T.V., Trapeznikova O.N., Arhipova M.V., Berezin P.V., Zverev A.V., Panchenko E.N., Sadkov S.A. (2015). An analysis of the morphological structure development of the thermokarst-lake plains on the base of the mathematical model. Geomorphology RAS (3), 3-13, DOI: 10.15356/0435-4281-2015-3-3-13.

Victorov A.S., Orlov T.V., Kapralova V.N., Trapeznikova O.N., Sadkov S.A., Zverev A.V. (2019). Stochastic Modeling of Human-Induced Thermokarst and Natural Risk Assessment for Existing and Planned Engineering Structures. Natural Hazards and Risk Research in Russia. Svalova V. (eds). Springer, Cham, 219-239.

Victorov A.S., Trapeznikova O.N. (2019). Stochastic Models Of Dynamic Balance State For The Morphological Patterns Of Cryolithozone Landscapes. GEOGRAPHY, ENVIRONMENT, SUSTAINABILITY; 12(3), 6-15, DOI: 10.24057/2071-9388-2018-68.

RESEARCH PAPER

THE DYNAMICS OF URBANIZATIONS AND CONCOMITANT LAND USE LAND COVER TRANSFORMATIONS IN PLANNED AND QUASI-PLANNED URBAN SETTLEMENTS OF PAKISTAN

Zaman M. Haq[1], Saqib Z.[1], Atif S. Bokhari[1,2*], Akhtar N.[1], Amir S.[1]

[1]GIS and Eco-Informatics Laboratory, Department of Environmental Science, International Islamic University, H-10, Islamabad, 44000, Pakistan

[2]Department of Geography, Government College, Asghar Mall, Rawalpindi, 46000, Pakistan

*Corresponding author: syedatifbokhari@gmail.com

Received: April 01th, 2020 / Accepted: August 9th, 2020 / Published: October 1st, 2020

https://DOI-10.24057/2071-9388-2020-64

ABSTRACT. An attempt has been made to compare the salient characteristics of LULC transformations in planned (Faisalabad) and quasi-planned (Jhang) urban settlements of Pakistan. The Landsat-5 TM, Landsat 7 EMT+ and Landsat-8 images of 1989, 1999, 2009 and 2019, respectively, were retrieved and processed through google earth engine. The dynamics of LULC critically analyzed for the three periods 1989–1999, 1999–2009 and 2009–2019. The LULC analyzed in terms of quantity of change, gains, losses, and persistence of the study area examined carefully. The study mainly focuses on the LULC transformations of the previous 30 years (1989–2019). These 30 years witnessed massive physical expansions and LULC convergences. During this time interval, the built-up areas in these cities expanded, and productive agricultural land substantially squeezed. The spatial-temporal analysis of LULC changes calls for improvised strategies for the resilience of land and environmental resources. The direct beneficiaries of this research are resource managers and regional planners as well as others scientific community.

KEY WORDS: Landsat images, LULC mapping, LULC dynamics, Planned Settlement, Quasi-planned settlement, Pakistan

CITATION: Zaman M. Haq, Saqib Z., Atif S. Bokhari, Akhtar N., Amir S. (2020). The Dynamics Of Urbanizations And Concomitant Land Use Land Cover Transformations In Planned And Quasi-Planned Urban Settlements Of Pakistan. Geography, Environment, Sustainability, Vol.13, No 4, p. 107-120 https://DOI-10.24057/2071-9388-2020-64

Conflict of interests: The authors reported no potential conflict of interest.

INTRODUCTION

Land resources are indispensable for the existence of life in all forms (Pimentel and Pimentel, 2003). Human beings are a product of the land environment and it is this very environment that provides man the wherewithal for survival (Davis et al. 2009; Goudie 2018). The intrusions in the lithospheric environment by them are, primarily, conceived for acquiring food and sustaining socio-economic progressions. The perception, action, and exchanges between human and land resources have witnessed many transformations. The phenomenon of permanent settlements stimulated man's role in changing the face of the earth (Metzger et al. 2006; Roberts 2013). The ensuing demographic transitions, also, have their peculiar imprints on the interrelationship between human and land resources. The advent of agriculture, the expansions in the permanent settlements, and socio-technological changes further redefine the orientation and magnitude of these exchanges (Larondelle et al. 2016; Seto et al. 2011). The resultant urbanization and associated lifestyle changes are now challenging the carrying capacity of the environment (Saarela and Rinne 2016; Elmqvist et al. 2013; Appiah et al. 2017; Cobbinah et al. 2015b; Cobbinah et al. 2015a).

The consequential implications produce different types of strains for city-based urbanization and in-situ urbanization. The city-based urbanization is a product of planned LULC modifications in natural landscapes, while, the in-situ urbanization are the gradual transformations of rural settlements into urban areas. It was during such conversions that the semi-planned or quasi-planned urban settlements evolved (Zhu et al. 2007; Iftikhar et al. 2018; Zhu 2002). The concomitant initiatives for developments in such quasi-planned (semi-planned) contextual settings blur the distinction between the urban and rural settlements (Zhu 2004; SUN et al. 2010).

Therefore, the planned and unplanned modifications in the urban land resources necessitate careful assessments. The Land Use Land Cover (LULC) assessments are a realistic option to quantify such transformations as are required for the resilience of land resources. The LULC is a combination of two distinctive terminologies, often used interchangeably, while, Land Cover (LC) describes the physical characteristics of land surface, Land Use (LU) focuses on the particular use of a certain land area. Hence, the term LU evaluates the functional utility of land from the perspective of its practical utility (Rawat and Kumar 2015).

Presently, the LULC changes are intensifying (Tian et al. 2014) to an extent that they are now compromising the resilience of the hydrosphere, the lithosphere, and the atmosphere at all possible spatial scales (Adhikari and Hartemink 2016). The resultant alterations, thus, characteristically impact the terrestrial and aquatic ecosystems (Du and Huang 2017; De Groot et al. 2002; Lambin et al. 2000; Briassoulis 2000; Cai et al. 2016; Aguilar et al. 2003; Hamad et al. 2017; Rimal et al. 2018). Therefore, scholars such as Gill et al. (2008), Du and Huang (2017) and Rimal et al. (2018) emphasize scrupulous assessments of land resources as a mean to ameliorate the stresses. Consequently, LULC change-detection is gaining focus in research. These inclinations are obligatory to enhance the productivity of land resources (El-Kawy et al. 2011; Shalaby and Tateishi 2007).

Schneider et al. (2015), Appiah et al. (2017) and Rimal et al. (2018) delved on the causes responsible for the reported urbanization in the developing countries. They assiduously tried to decipher the ensuing impacts in the form of LULC changes on the urban landscape. The findings infer that these resource-stricken regions are rapidly transforming under the influence of globalization. The lack of awareness, capacity building, inconsistencies in the land-use policies, and paucity of resources are exacerbating the urban environmental degradation in these regions (Atif et al. 2018a; Bokhari et al. 2018; Amir et al. 2020). Resultantly, the urban environmental dilapidation is more pronounced in these countries as compared to the developed ones (Ahern et al. 2014; Cohen 2006). Environmental degradation has corollary impacts on social dilapidations in these regions. The emerging scenario is, thus, posing challenges for life and livelihood in developing countries like Pakistan (Amir et al. 2020).

The phenomena of permanent settlement started thousands of years ago in the Indus valley located in Pakistan (Kenoyer 1998; Kenoyer et al. 2013; Danino 2008). The Indus valley civilization evolved in a depositional plain formed by the river Indus and its tributaries. The physiographic region is sub-divided into Upper and Lower Indus plains. The Upper Indus plain is the northern section formed by the Indus and its five eastern tributaries. The Lower Indus plain is the southern section and is solely developed by the Indus itself. The land area between the two adjoining streams in the Upper Indus plain is called a doab (river-interfluves). The upper Indus plain is subdivided in Sind Saghar; Chaj; Rechna and Bari doabs (Grewal 2004).These land areas offer fertile tract for abode and agriculture. Overtimes, a varied set of factors such as the canalization of Indus plains (Khan 1990) the migration (Valentine et al. 2015); the green revolution of 1960s in Pakistan (Ali et al. 2017; Byerlee and Siddiq 1994) and associated industrial and infrastructural developments stimulated population growth and urbanization in this geographical region (Farah et al. 2016). However, the expansion was not supported by the desired management initiatives and, thus, added to the misery of fragile urban ecological resources in these areas (Mayo, 2012).

Therefore, the LULC based impact assessments are incumbent for postulating preventive and curative measures to ensure socio-ecological and environmental resilience (El-Kawy et al. 2011; Shalaby and Tateishi 2007). It entails for reliable estimations and assessments based upon empirical findings. The advancements in the Remote Sensing (RS) and Geographic Information System (GIS) enable the measurements of all spatial-temporal LULC changes (La Rosa and Wiesmann 2013; Thapa 2012; Khalil 2017). Therefore, the reliance on RS and GIS is gaining recognition to ensure accurate estimation of land resource management (Naqvi et al. 2014; Rawat and Kumar 2015; Hegazy and Kaloop 2015).

The present study tries to compare the salient characteristics of LULC transformations in planned and quasi-planned urban settlements of Pakistan. The specific objectives of this study are 1) to compare the impacts of

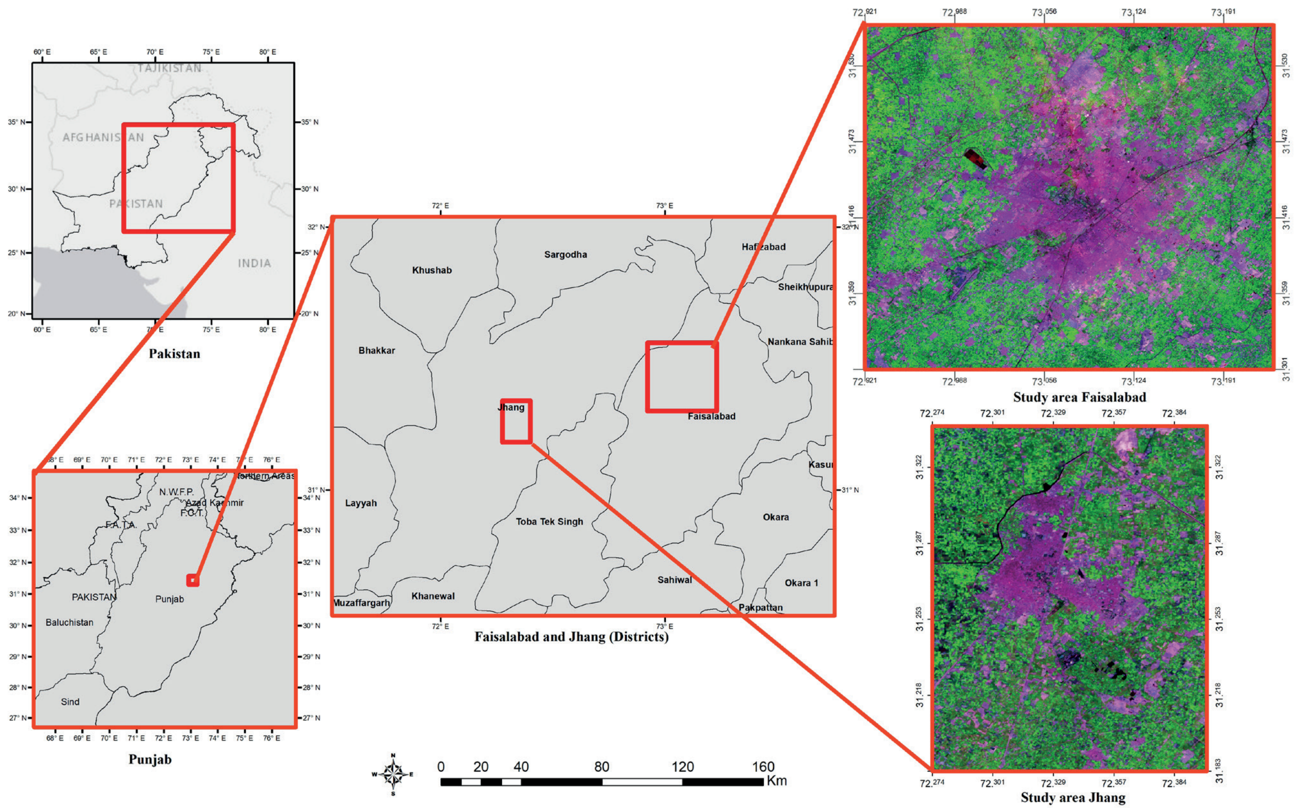

Fig. 1. Location map of study area

urbanization on the LULC changes in urban Faisalabad and Jhang from 1989 to 2019, and 2) to quantify the changes in the selected LULC categories of these urban centers for a similar time period (1989–2019).

MATERIALS AND METHODS

The study area

The current investigation evaluates the impacts of urbanization on LULC changes in the urban areas of Pakistan. The study was carried out in the contrasting contextual settings of the Faisalabad and Jhang cities (Fig. 1). Whereas, these urban settlements are located in a similar physical environment i.e. Rechna doab (river-interfluve) of the Indus plain but evolved differently to cater for different socio-economic needs.

Faisalabad city is ranked third amongst the big cities of Pakistan, after Karachi and Lahore (https://worldpopulationreview.com/world-cities/faisalabad-population). Faisalabad was conceived as a planned urban settlement. It was designed to serve as a trading centre for promoting agricultural activities during the colonial period (Stock and Chusid 2019). The subsequent industrialization and the accompanying demographic changes have their peculiar imprints on the LULC of this sprawling urban settlement. The urban area of Faisalabad stretches across an area of approximately 1163.60 km^2. It lies between 72° 55’15.041 E to 73°13’38.803 eastern longitudes and from 31°33’44.988 N to 31°18’9.275 northern latitudes.

Jhang is among the oldest districts of Punjab province (Steedman, 1882). While the Jhang city is a quasi-planned and agro-based urban settlement. It covers an area of approximately 287.64 km^2. The urban center is located between 72°16’24.521 E to 72°23’55.075 E and from 31°20’27.309 N to 31°11’0.647 N. The Jhang city is also expanding (https://worldpopulationreview.com/world-cities/jhang-population) but the speed and scale of urban sprawl in this city is slower than Faisalabad. Thus, the contextual settings of these cities enable us to comprehend the dynamics of LULC changes in the urban landscape of Pakistan.

Data acquisition and assessment approach

The spatial-temporal changes in the LULC of these cities were assessed through remotely sensed data. The selected satellite images span the complete study areas, i.e., Faisalabad (Path 150/Row 38) and Jhang (Path 150/ Row 39) cities. The images were retrieved through Landsat-5 TM, Landsat 7 EMT+ and Landsat-8 (Annexure. 1). The required images at 30-meter resolution for the selected time intervals (1989–2019) are available in the archives of USGS/EROS (U.S. Geological Survey/Earth Resources Observation and Science) (https://www.usgs.gov). The images were processed online in the Google Earth Engine (GEE) platform (https://earthengine.google.com).

Image normalization is carried out prior to change detection. The criterion at work here is the Landsat Ecosystem Disturbance Adaptive Processing System (LEDAPS). Therefore, Top Of Atmosphere (TOA) reflectance

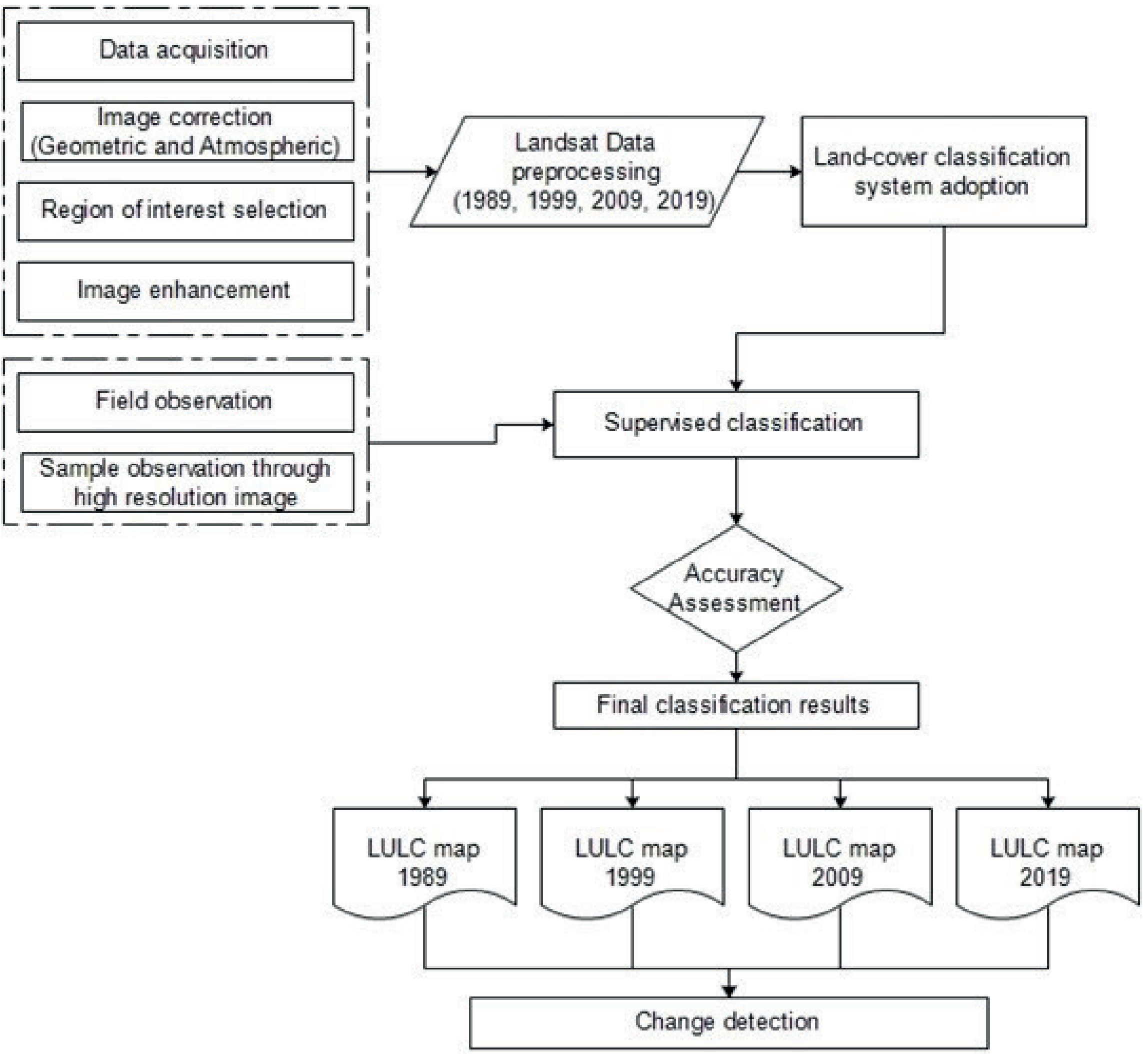

Fig. 2. The methodological framework for LULC change assessments

Table 1. LULC Classes considered for Classification

Class	Discerption
Agriculture	Planned crop land, Agriculture fallow land, herbaceous vegetation and crop, lands that are regularly used for hay and grazing
Barren	Areas of sparse vegetation cover that is likely to change or be converted to other uses in near future
Built-up	Areas covered by residential, commercial services, industrial, transportation, communications, industrial and commercial, mixed urban or buildup land, airports, parking lots, highways, housing societies.
Grasses	Characterized by high percentage of grasses, other herbaceous vegetation, city parks
Trees	Areas covered by dense trees with relatively darker green colors, inner recreational areas, river line plantation
Water	All areas of open water, generally with greater than 95% cover of water, including lakes, streams, and reservoirs.

itemized by the bands 1 to 5 and 7 were adjudged relevant. The reference dataset and selected land cover classes were corroborated. The merger enables a quantification of the spatial-temporal changes in the designated LULC categories. Subsequently, the data was ported in the GIS environment to analyze, assess and illustrate oscillations in the observed land cover classes. Figure 2 succinctly illustrates the measures and mechanism deployed for the assessments.

Land-Use/Land-Cover classification

The research was confined to six classifiable LULC surfaces in the study area (Table 1). The field observations from 600 locations were carried out for quantitative assessments. These sites were marked with the help of the Global Positioning System (GPS). Besides, 2095 sample plots were manually observed from 1989 to 2019 through higher resolution images. For this purpose, the training and validation samples of each year were separately uploaded and integrated with the Google Fusion Tables (GFT) via GEE. For this purpose the Supervised and Un-supervised Classification techniques are considered standards (Shetty 2019; Prasad et al. 2006; Lewis 2000), and were, therefore, used (Table 1). For the land cover maps, the Classification and Regression Tree (CART) classifier was used because it is based upon the supervised classification mechanism.

Accuracy assessment

The accuracy assessment is a key feature and is useful to authenticate findings (Ahmadizadeh, 2014). The LULC based maps were cross-validated and scrutinized on the criteria of the Kappa test (Annexure 2).

RESULTS

Spatial-temporal transformations in LULC

The spatial-temporal assessments of LULC changes divulge the trajectories of urban expansions regarding these settlements. Therefore, the absolute and proportionate changes in the selected LULC classes during (1989–2019) in Faisalabad (Annexure 3) and Jhang cities (Annexure 4) were analysed. The illustrations (Fig. 3 and Fig. 4) succinctly portray the orientation and magnitude of such transformations in these settlements. The findings formulate that the agricultural land cover is shrinking, and built-up areas are expanding in both cities. The comparisons are portrayed with the help of a uniform intensity line. The line succinctly portrays the differences in the rate of LULC conversions between/among different contextual settings (Mondal et al. 2015). The line of uniform intensity (Fig. 5) inferred that the speed and magnitude of such conversions is more pronounced in Faisalabad as compared to Jhang.

Besides this, the urban sprawl in these settlements was observed more inclined towards the lines of communications such as highways and motorways (Fig. 3 and Fig. 4). Resultantly, the arable land cover is transforming into a non-productive and a barren one (Fig. 8 and Fig. 9). However, the phenomena of urban densification is gaining momentum in recent times. Consequently, the resultant vertical growth is gaining impetus in these cities.

Quantitative assessments of LULC transformations

The oscillations in each specific land use category for Faisalabad (Fig. 6) and Jhang cities (Fig. 7) were computed. Subsequently, the relative changes and consistencies in the proportion of these land use categories were assessed. The assessments formulate a noticeable increase in the proportion of tree cover, grassy surfaces, barren lands, and water surfaces of these settlements during (1989–2019). However, the significant fluctuations in the shares of water surfaces and barren lands are also observed (Fig. 3 and Fig. 4).

Gross Gains, Losses and Persistence in LULC

The impacts of urbanization during (1989–2019) on the persistence, increases, or decreases in the share of a specific land category were quantified. The findings have been summarized (Fig. 8 and Fig. 9) to depict the orientation and magnitude of such transformations (Fig. 6) and (Fig. 7). The findings revealed that such transformations were more pronounced from 1999 to 2009 (Fig. 8 and Fig. 9). However, the speed and scale of such changes was stunted in the following decade (2009 to 2019).

The assessments formulate that the agricultural land considerably reduced (-17.38%) during (1989–2019) in Faisalabad (Fig. 8). Whereas, the percentage shares of all the other LULC categories remained stable or marginally enhanced during this time-frame. However, the most significant growth (16.05%) was observed in the built-up areas of Faisalabad.

The proportionate shares of agricultural land significantly reduced in (-8.93%) in Jhang city during (1989–2019). While, the proportions of tree covers (1.27%), water surfaces (0.09%), and grassy surfaces (0.03%) marginally enhanced. However, the chunks of barren land (3.10%) and built-up areas (4.44%) substantially inflated in this city during this time interval (Fig. 9).

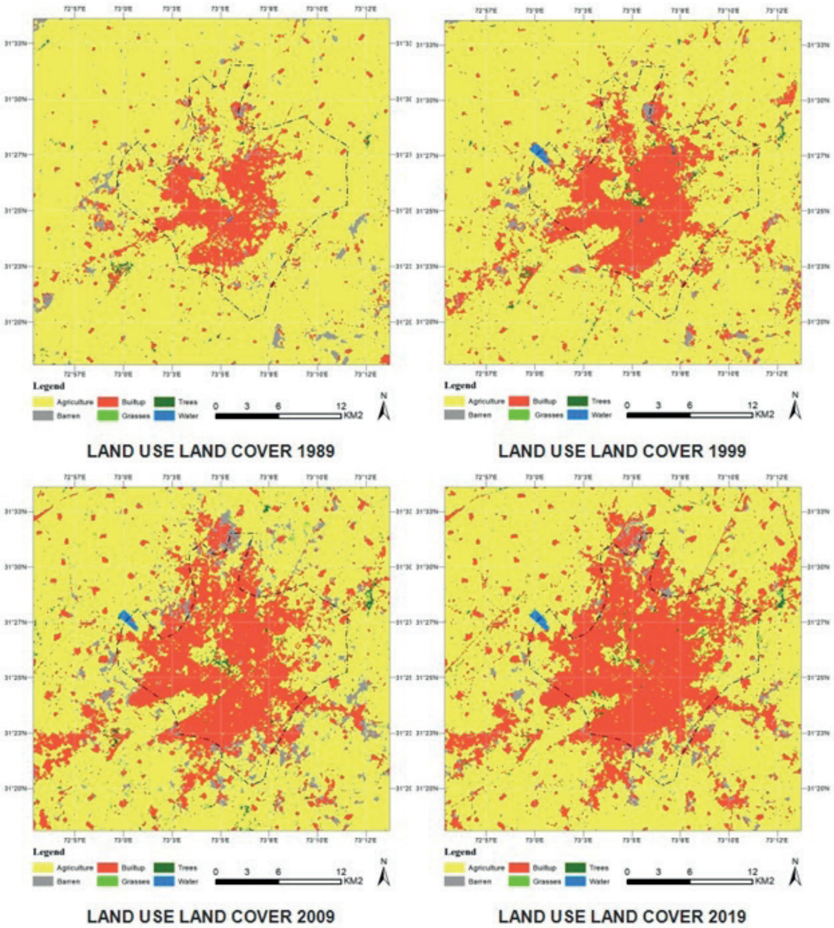

Fig. 3. Land use land cover classification maps of Faisalabad city

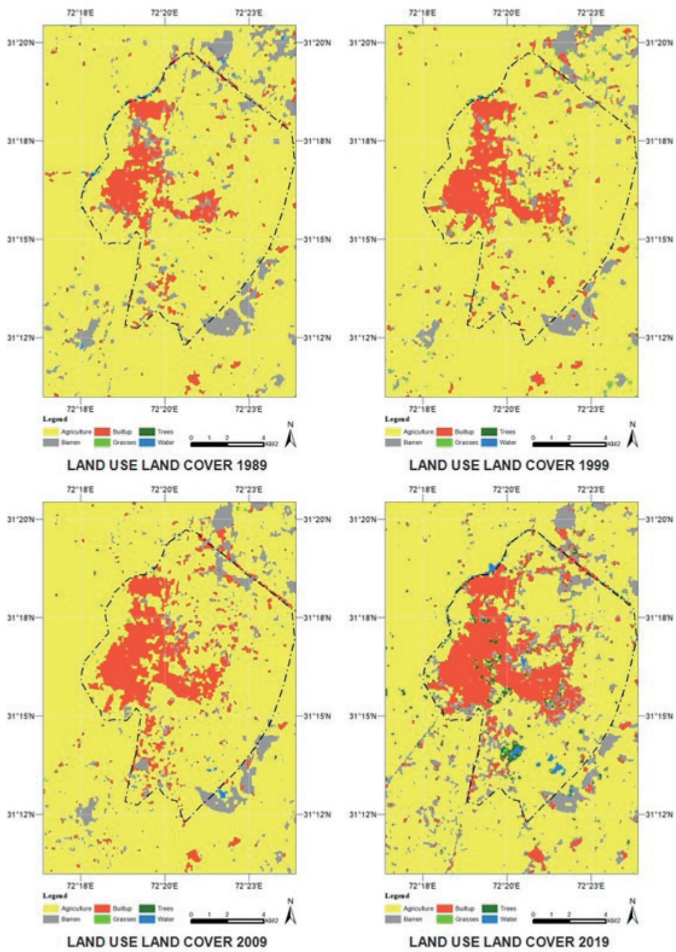

Fig. 4. Land use land cover classification maps of Jhang city

Uniform Intensity Line

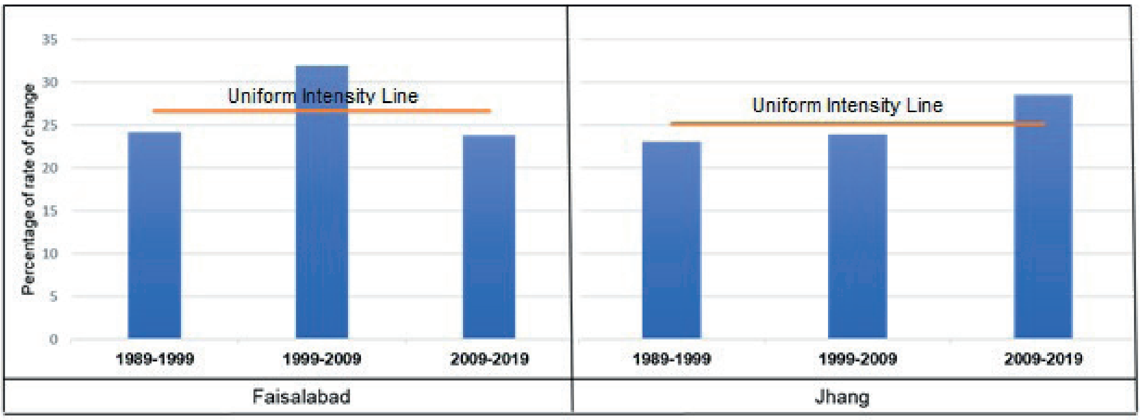

Fig. 5. The comparison of land conversion speed during the selected time intervals between Faisalabad and Jhang

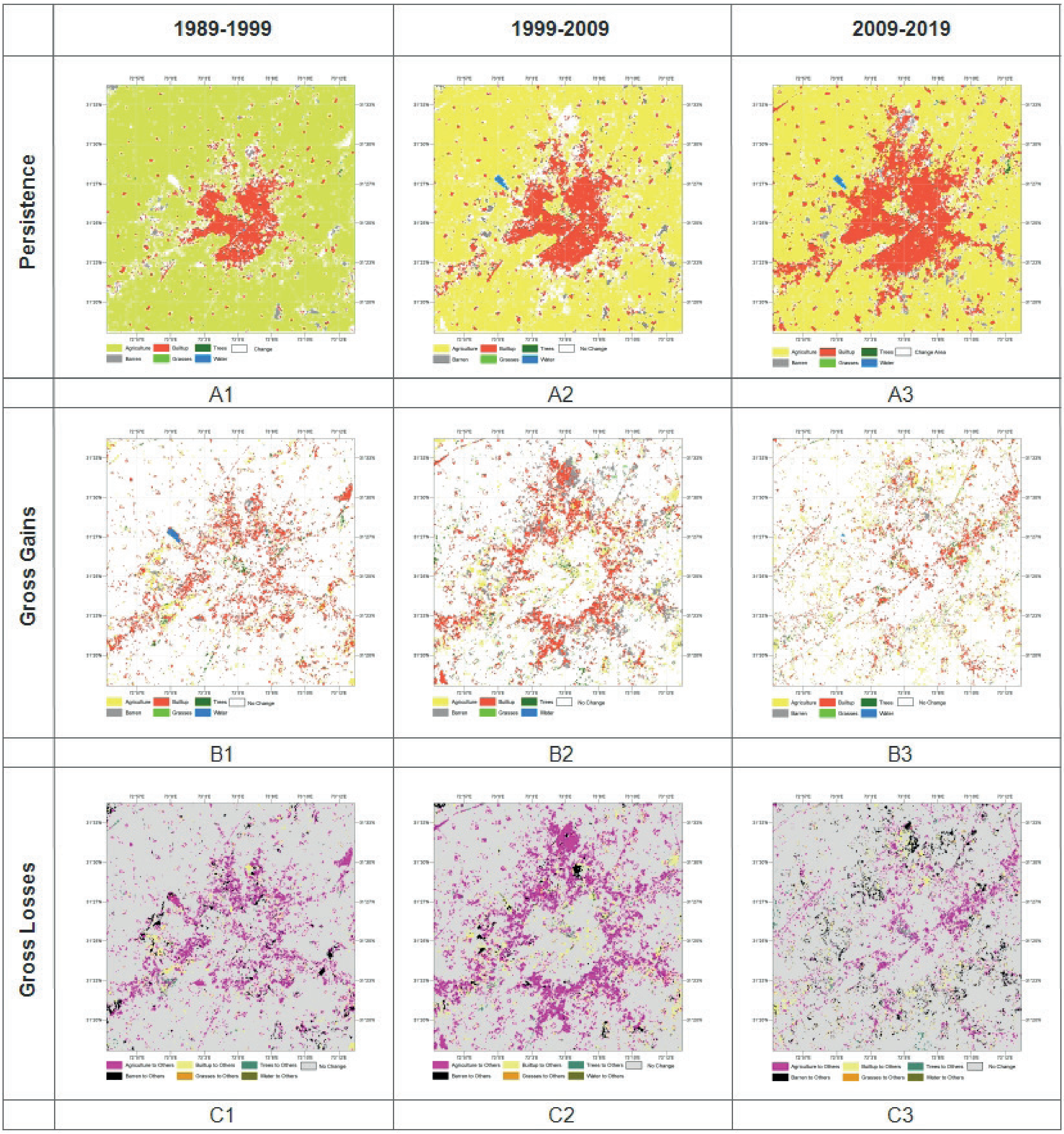

Fig. 6. Maps of persistence, gross gains and gross losses of urban center of Faisalabad

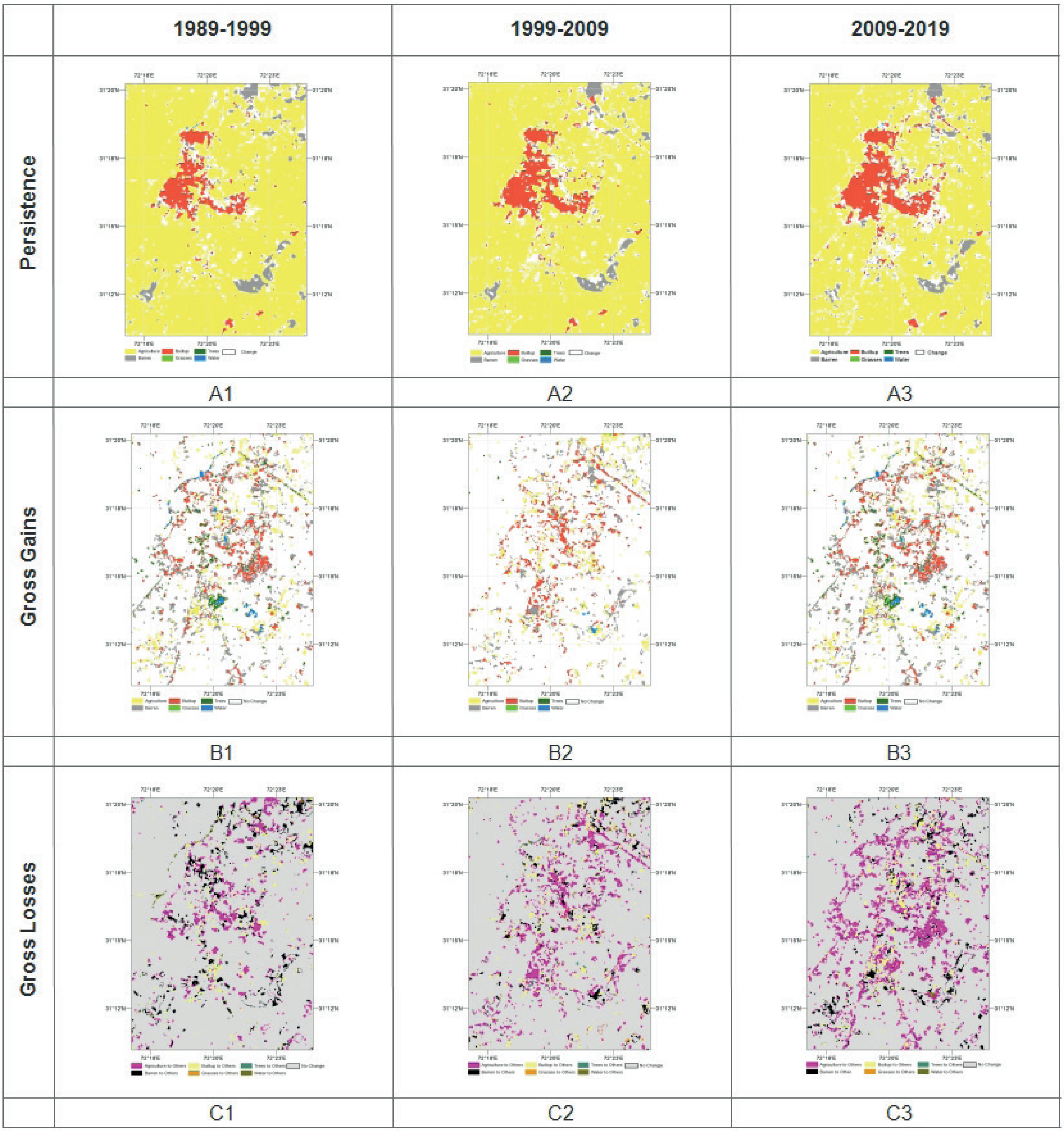

Fig. 7. Maps of persistence, gross gains and gross losses of urban center of Jhang

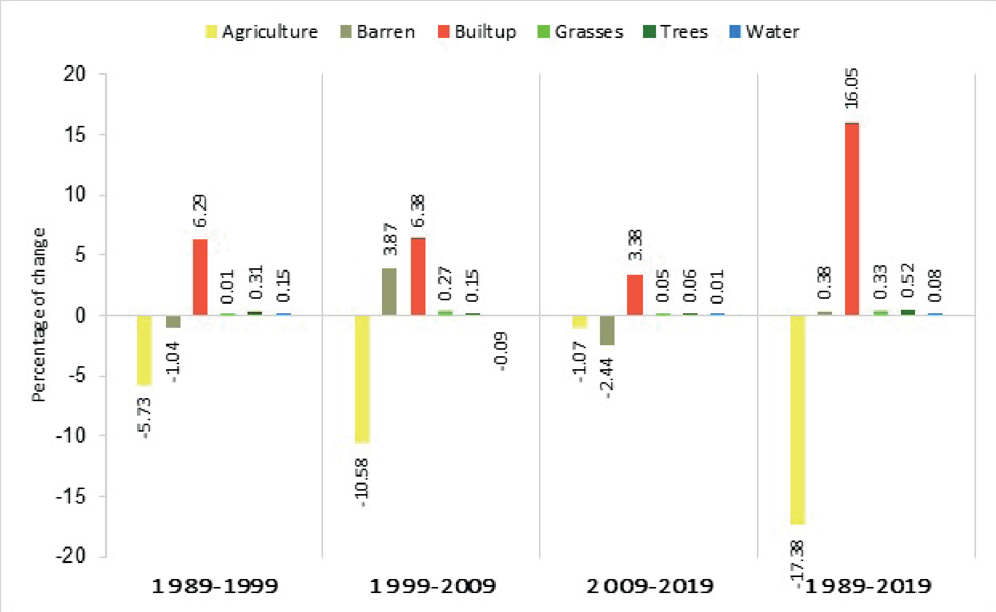

Fig. 8. Gains and losses in the LULC classes of Faisalabad (1989–2019)

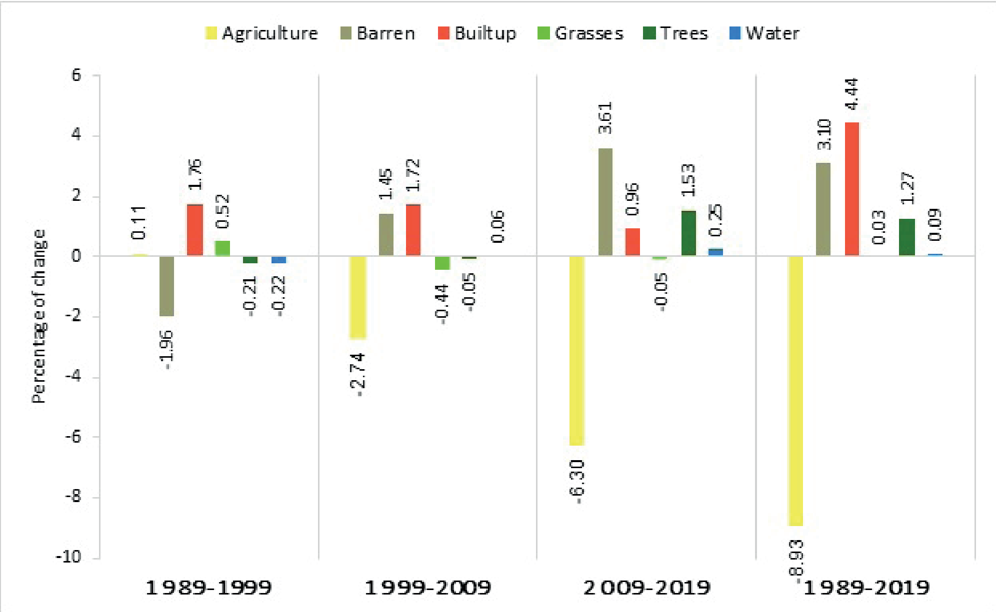

Fig. 9. Gains and losses in the lulc classes of Jhang (1989–2019)

DISCUSSION

Pakistan, like many other South Asian countries, has rapidly urbanized (Vasenev et al. 2019; Ouyang et al. 2016). The phenomenal increase in the rate and scale of urbanization in Pakistan (UNDP 2018; Shah et al. 2020) is attributed to the natural population growth (Kugelma, 2014) and rural-to-urban migration (Arif and Hami, 2009). This massive migration is attributable to the peculiar historic (Farooq et al. 2005; Farah et al. 2012; Safder and Babar 2019), social (Lopes and Farooq, 2020), economic (Chiesura and De Groot 2003; de Molina and Toledo 2014; Gilani et al. 2020), environmental (Shaheen et al. 2020) and geo-strategic (Shaheen et al. 2020) dynamics of this region.

The ensuing speed and impacts of urbanization in Pakistan (Nisar et al., 2013) are straining the urban land resources (Atif et al. 2018b; Atif et al. 2018a). It entails comprehending the dynamic and consequential impacts of the resultant changes in urban landscapes (Shao et al. 2005). The evolving scenario demands pragmatic responses based on empirical findings. Therefore, the research should be oriented more towards LULC assessments for the sustainability of urban land resources (Naqvi et al. 2014; Rawat and Kumar 2015; Hegazy and Kaloop 2015). The spatial-temporal analysis of LULC changes calls for improvised strategies for the resilience of land and environmental resources (Atif et al. 2018b).

The current study evaluates the spatial-temporal dimensions of the LULC changes regarding Faisalabad and Jhang cities (Annexure 3 and Annexure 4). The study mainly focuses on the LULC transformations of the previous 30 years (1989–2019). These 30 years witnessed massive physical expansions and LULC convergences (Fig. 3 and Fig. 4). During this time interval, the built-up areas in these cities expanded, and productive agricultural land substantially squeezed (Fig. 8 and Fig. 9). These observations substantiate the reported assertions that the accompanying processes of urbanization characteristically modify the LULC patterns (Butt et al. 2015; Ali et al. 2011; Ali and Malik 2010; Hassan et al. 2016). The findings of the study substantiate the notions that the reported population growth in these cities (Mazhar and Jamal 2011; Bukhari 1971; Farah et al. 2012; Ghalib et al. 2017) is stressing these urban centers

The chronological assessment of spatial expansions regarding Faisalabad formulates that the settlement was initially and intrinsically planned to serve as a market town. The area around Ghanta Ghar was designed to cater to the needs of the Central Business District (CBD). The initial extensions in the structure of Faisalabad city followed the pattern of the Concentric Zone Model (CZM). E. W. Burgess proposed it in 1923 (Brown and Holmes 1971). The model hypothesized that urban settlements expand outward from a central location like the water ripples in a pond. This urban settlement expanded outward from the CBD like the growth rings of a tree. The urban neighborhoods such as Jinnah Colony, Tata Bazaar, and Civil Lines developed during the early phases of urban expansion. The process of urban sprawl was expedited with the advent of canalization, and the subsequent industrial and manufacturing activities. However, the lateral growths in the city followed the orientation of road infrastructure. The demographic pressures, lacunas in the policies, and compromises over urban land management deter any possibility of a planned urban growth (Omwoma 2016). Besides this, the loose regulatory control encouraged unplanned and irregular LULC transformations in Faisalabad (Saeed et al. 2012; Shakeel et al. 2015). Resultantly, the unplanned and congested residential localities like Duglus Pura; Sant Nagar; Dhobi Ghaat; Islam Nagar emerged. These observations corroborate the notions that integrated management of urban environmental resources is a prerequisite for the socio-ecological resilience of urban life (Atif et al. 2018a).

While the historic city of Jhang is an autogenously developed human settlement it evolved without any formal planning. The embedded flaws of the earlier developments, still, haunt the process of urbanization in the Jhang city. The imprints of irregular growth are visible in such localities as Kot Akbar, Ludhan Shah, Loharan wali, Jalal Abad and Deewan wali. The provisioning of civic facilities is cumbersome in these unplanned, congested and irregular neighborhoods. The findings entail that a coordinated urban planning is obligatory for environmentally friendly urban growth. Therefore, the recent trends of urban expansion in Jhang city were adjudged more skewed towards organized and planned growth. These tendencies are quite visible in the form and structure of the recently developed Satellite town, Lal Zar Housing Schemes (Phase-1 and 2), Ali Garden and Al-Karam City etc. The planned orientations in these expansions are due to public pressures (Haaland and van Den Bosch 2015). These findings construe that consciousness about environmental issues is positively contributing to urban planning in Pakistan. Contrarily, the demographic and economic stresses are culpable for unintended urban sprawl.

The impacts of road infrastructure on the process of urbanization were also evaluated. The recent urban expansions were observed more tilted towards inter-city highways and motorways during (1989–2019). These observations corroborate the postulations of sector theory. The model was envisaged by Homer Hoyt (Beauregard 2007; Ju et al. 2016). It formulates that urban expansions intensify along the lines of communications i.e., roads and railway networks.

The findings of this study substantiate that the RS and GIS-based understandings facilitate in deciphering the spatial-temporal connotations of urbanization (La Rosa and Wiesmann 2013). The findings corroborate the reported notions such as (La Rosa and Wiesmann 2013; Thapa 2012; Khalil 2017) regarding the robustness of RS and GIS techniques. These resources were also found appropriate for detecting previous changes in the LULC (El-Kawy et al. 2011). Therefore, the reliance on such cost-effective resources is a pragmatic option for developing economies such as Pakistan.

CONCLUSIONS

The holistic assessments of this study imply that the people in developing countries move towards urban areas for economic opportunities. The resultant uncontrolled urbanization and concomitant LULC transformations are adversely impacting the urban infrastructures. Therefore, integrated measures are obligatory to regulate the speed and scale of such LULC conversions. Besides this, the inflow of people is promoting horizontal and vertical growth in the city structure. The resultant impacts stress the ecological and environmental resources of the cities and their peripheral zones. The emerging scenario is proving burdensome specifically for the resource stricken regions. The massive urban growth, due to migration is exacerbating the urban social life of these countries. The scenario entails for synchronization in policies and an integration of efforts for a more resilient urban development. The decentralization of power is a pragmatic option for countries such as Pakistan. It will productively contribute towards curtailing the inflow of migrants from rural hinterlands towards the more central places like Faisalabad and Jhang. The creation of employment opportunities in the rural hinterlands is another viable preference to ameliorate stresses on urban infrastructures. However, the findings affirm that population control is the most reliable measure to address such daunting challenges in countries like Pakistan (Heinke 1997; Simon 2019).

REFERENCES

Adhikari K. and Hartemink A.E. (2016). Linking soils to ecosystem services-A global review. Geoderma, 262, 101-111.

Aguilar A.G., Ward P.M. and Smith Sr C. (2003). Globalization, regional development, and mega-city expansion in Latin America: analyzing Mexico City's peri-urban hinterland. Cities, 20(1), 3-21.

Aher, J., Cilliers S. and Niemelä J. (2014). The concept of ecosystem services in adaptive urban planning and design: A framework for supporting innovation. Landscape and Urban Planning, 125, 254-259.

Ahmadizadeh S. (2014). Land use change detection using remote sensing and artificial neural network: Application to Birjand, Iran. Computational Ecology and Software, 4(4), 276.

Ali G., Ashraf A., Bashir M.K. and Cui S. (2017). Exploring environmental Kuznets curve (EKC) in relation to green revolution: a case study of Pakistan. Environmental Science & Policy, 77, 166-171.

Ali M., Khan S.J., Aslam I. and Khan Z. (2011). Simulation of the impacts of land-use change on surface runoff of Lai Nullah Basin in Islamabad, Pakistan. Landscape and Urban Planning, 102(4), 271-279.

Ali S.M. and Malik R.N. (2010). Vegetation communities of urban open spaces: Green belts and parks in Islamabad city. Pak. J. Bot, 42(2), 1031-1039.

Amir S., Saqib Z., Khan M.I., Khan M.A., Bokhari S.A., Zaman-Ul-Haq M. and Majid A. (2020). Farmers' perceptions and adaptation practices to climate change in rain-fed area: a case study from district Chakwal, Pakistan. Pakistan Journal of Agricultural Sciences, 57(2), 465-475.

Appiah, D. O., Forkuo E. K., Bugri J. T. and Apreku T. O. (2017). Geospatial Analysis of Land Use and Land Cover Transitions from 1986–2014 in a Peri-Urban Ghana. Geosciences, 7(4), 125.

Arif G. and Hamid S. (2009). Urbanization, city growth and quality of life in Pakistan. European Journal of Social Sciences, 10(2), 196-215.

Atif S., Saqib Z., Ali A. and Zaman M. (2018a). The impacts of socio-economic factors on the perception of residents about urban vegetation: a comparative study of planned versus semi-planned cities of Islamabad and Rawalpindi, Pakistan. Applied Ecology and Environmental Research, 16(4), 4265-4287.

Atif S., Saqib Z., Ali A., Zaman M., Akhtar N., Fatima H., Atif M. and Farooqi S. (2018b). Identification of key-trends and evaluation of contemporary research regarding urban ecosystem services: a path towards socio-ecological sustainability of urban areas. Applied Ecology and Environmental Research, 16(3), 3545-3581.

Beauregard R. (2007). More Than Sector Theory: Homer Hoyt's Contributions to Planning Knowledge. Journal of Planning History, 6(3), 248-271.

Bokhari S., Saqib Z., Ali A. and Zaman-Ul-Haq M. (2018). Perception of Residents about Urban Vegetation: A Comparative Study of Planned Versus Semi-Planned Cities of Islamabad and Rawalpindi, Pakistan. Journal of Ecosystem & Ecography, 8(251), 2.

Briassoulis H. (2000). Analysis of land use change: theoretical and modeling approaches. Regional Research Institute, West Virginia University Morgantown, WV.

Brown L.A. and Holmes J. (1971). Intra-urban migrant lifelines: a spatial view. Demography, 8(1), 103-122.

Bukhari M. (1971). Growth and development of Lyallpurcity. Pakistan Geographical Review, 26(2), 1-15.

Butt A., Shabbir R., Ahmad S. S. and Aziz N. (2015). Land use change mapping and analysis using Remote Sensing and GIS: A case study of Simly watershed, Islamabad, Pakistan. The Egyptian Journal of Remote Sensing and Space Science, 18(2), 251-259.

Byerlee D. and Siddiq A. (1994). Has the green revolution been sustained? The quantitative impact of the seed-fertilizer revolution in Pakistan revisited. World Development, 22(9), 1345-1361.

Cai Y.-B., Li H.-M., Ye X.-Y. and Zhang H. (2016). Analyzing three-decadal patterns of land use/land cover change and regional ecosystem services at the landscape level: Case study of two coastal metropolitan regions, eastern china. Sustainability, 8(8), 773.

Chiesura A. and De Groot R. (2003). Critical natural capital: a socio-cultural perspective. Ecological Economics, 44(2), 219-231.

Cobbinah P.B., Erdiaw-Kwasie M.O. and Amoateng P. (2015a). Africa's urbanisation: Implications for sustainable development. Cities, 47, 62-72.

Cobbinah P.B., Erdiaw-Kwasie M.O. and Amoateng P. (2015b). Rethinking sustainable development within the framework of poverty and urbanisation in developing countries. Environmental Development, 13, 18-32.

Cohen B. (2006). Urbanization in developing countries: Current trends, future projections, and key challenges for sustainability. Technology in society, 28(1-2), 63-80.

Danino M. (2008). New insights into Harappan town-planning, proportions, and units, with special reference to Dholavia. Man and Environment, 33(1), 66-79.

Davis J.L., Green J.D. and Reed A. (2009). Interdependence with the environment: Commitment, interconnectedness, and environmental behavior. Journal of environmental psychology, 29(2), 173-180.

De Groot R.S., Wilson M.A. and Boumans R.M. (2002). A typology for the classification, description and valuation of ecosystem functions, goods and services. Ecological economics, 41(3), 393-408.

De Molina M.G. and Toledo V.M. (2014). Social Metabolism at the Local Scale. The Social Metabolism. Springer.

Du X. and Huang Z. (2017). Ecological and environmental effects of land use change in rapid urbanization: The case of hangzhou, China. Ecological Indicators, 81243-251.

El-Kawy O.A., Rød J., Ismail H. and Suliman A. (2011). Land use and land cover change detection in the western Nile delta of Egypt using remote sensing data. Applied Geography, 31(2), 483-494.

Elmqvist T., Fragkias M., Goodness J., Güneralp B., Marcotullio P.J., Mcdonald R.I., Parnell S., Schewenius M., Sendstad M. and Seto K.C. (2013). Urbanization, biodiversity and ecosystem services: challenges and opportunities: a global assessment, Springer.

Farah N., Khan I.A., Manzoor A. and Shahbaz B. (2016). Changing Land Ownership Patterns and Agricultural Activities in the Context of Urban Expansion in Faisalabad, Pakistan. Pakistan Journal of Life & Social Sciences, 14(3).

Farah N., Zafar M.I. and Nawaz N. (2012). Socio-Economic and Cultural Factors Affecting Migration Behavior in District Faisalabad, Pakistan. Pakistan Journal of Life & Social Sciences, 10(1), 28-32.

Farooq M., Mateen A. and Cheema M. (2005). Determinants of migration in Punjab, Pakistan: A case study of Faisalabad metropolitan. Journal of Agriculture and Social Sciences (Pakistan).

Ghalib A., Qadir A. and Ahmad S. (2017). Evaluation of developmental progress in some cities of punjab, pakistan, using urban sustainability indicators. Sustainability, 9(8), 1473.

Gilani H., Ahmad S., Qazi W.A., Abubakar S.M. and Khalid M. (2020). Monitoring of Urban Landscape Ecology Dynamics of Islamabad Capital Territory (ICT), Pakistan, Over Four Decades (1976–2016). Land, 9(4), 123.

Gill S.E., Handley J.F., Ennos A.R., Pauleit S., Theuray N. and Lindley S.J. (2008). Characterising the urban environment of UK cities and towns: A template for landscape planning. Landscape and urban planning, 87(3), 210-222.

Goudie A.S. (2018). Human impact on the natural environment, John Wiley & Sons.

Grewal J. (2004). Historical geography of the Punjab. JPS, 11(1), 2.

Haaland C. and Van Den Bosch C.K. (2015). Challenges and strategies for urban green-space planning in cities undergoing densification: A review. Urban forestry & urban greening, 14(4), 760-771.

Hamad R., Balzter H. and Kolo K. (2017). Multi-criteria assessment of land cover dynamic changes in halgurd sakran national park (HSNP), kurdistan region of Iraq, using remote sensing and GIS. Land, 6(1), 18.

Hassan Z., Shabbir R., Ahmad S.S., Malik A. H., Aziz N., Butt A. and Erum S. (2016). Dynamics of land use and land cover change (LULCC) using geospatial techniques: a case study of Islamabad Pakistan. SpringerPlus, 5(1), 1-11.

Hegazy I.R. and Kaloop M.R. (2015). Monitoring urban growth and land use change detection with GIS and remote sensing techniques in Daqahlia governorate Egypt. International Journal of Sustainable Built Environment, 4(1), 117-124.

Heinke G.W. (1997). The challenge of urban growth and sustainable development for Asian cities in the 21st century. Environmental monitoring and assessment, 44(1-3), 155-171.

United Nations population estimates and projections of major Urban Agglomerations [Online]. Available: https://worldpopulationreview.com/world-cities/faisalabad-population [Accessed 30-07-2020].

United Nations population estimates and projections of major Urban Agglomerations [Online]. Available: https://worldpopulationreview.com/world-cities/jhang-population [Accessed 30-07-2020].

Iftikhar M.N., Ali S. and Sarzynski A. (2018). Community–government partnership for metered clean drinking water: A case study of Bhalwal, Pakistan. Climate Change in Cities. Springer.

J, C., Zhou X. and He Q. (2016). On the application of a concentric zone model (CZM) for classifying and extracting urban boundaries using night-time stable light data in Urumqi of Xinjiang, China. Remote sensing letters, 7(11), 1033-1042.

Kenoye J.M. (1998). Ancient cities of the Indus valley civilization, Oxford University Press Karachi.

Kenoye J.M., Price T.D. and Burton J.H. (2013). A new approach to tracking connections between the Indus Valley and Mesopotamia: initial results of strontium isotope analyses from Harappa and Ur. Journal of Archaeological Science, 40(5), 2286-2297.

Khali R. Z. (2017). InSAR coherence-based land cover classification of Okara, Pakistan. The Egyptian Journal of Remote Sensing and Space Science.

Kha M.S. (1990). The impact of human activities on the status and distribution of amphibians in Pakistan. Hamadryad, 15(1), 21-24.

Kugelma, M. (2014). Pakistan's Runaway Urbanization: What Can Be Done? Asia Program, Woodrow Wilson International Center for Scholars.

La Rosa D. and Wiesmann D. (2013). Land cover and impervious surface extraction using parametric and non-parametric algorithms from the open-source software R: An application to sustainable urban planning in Sicily. GIScience & remote sensing, 50(2), 231-250.

Lambin E.F., Rounsevell M. and Geist H. (2000). Are agricultural land-use models able to predict changes in land-use intensity? Agriculture, Ecosystems & Environment, 82(1-3), 321-331.

Larondelle, N., Frantzeskaki N. and Haase D. (2016). Mapping transition potential with stakeholder-and policy-driven scenarios in Rotterdam City. Ecological Indicators, 70, 630-643.

Lewis R.J. (2000). An introduction to classification and regression tree (CART) analysis. Annual meeting of the society for academic emergency medicine in San Francisco, California.

Lopes N.V.M. and Farooq S. (2020). Smart City Governance Model for Pakistan. Smart Governance for Cities: Perspectives and Experiences. Springer.

Mayo S.M. (2012). Determination of urban settlement pattern for optimal regional development in Punjab. University of Engineering and Technology Lahore-Pakistan.

Mazhar F. and Jamal T. (2011). Temporal population growth of Faisalabad city. Pakistan Journal of Science, 63(4), 249-251.

Metzger M., Rounsevell M., Acosta-Michlik L., Leemans R. and Schröter D. (2006). The vulnerability of ecosystem services to land use change. Agriculture, ecosystems & environment, 114(1), 69-85.

Mondal M., Sharma N., Kappas M. and Garg P. (2015). Critical assessment of land use land cover dynamics using multi-temporal satellite images. Environments, 2(1), 61-90.

Naqvi H. R., Siddiqui L., Devi L. M. and Siddiqui M. A. (2014). Landscape transformation analysis employing compound interest formula in the Nun Nadi Watershed, India. The Egyptian Journal of Remote Sensing and Space Science, 17(2), 149-157.

Nisar A., Akram A. and Hussain H. (2013). Determinants of internal migration in Pakistan. The Journal of Commerce, 5(3), 32.

Omwoma R.M. (2016). A Land-tenure Based Model for Guiding and Controlling Development on Freehold Land in Urban Areas: Exploring Possibilities for Management of Spatial Quality in Kenya.

Ouyang Z., Fan P. and Chen J. (2016). Urban built-up areas in transitional economies of Southeast Asia: Spatial extent and dynamics. Remote Sensing, 8(10), 819.

Pimentel D. and Pimentel M. (2003). World population, food, natural resources, and survival. World Futures: The Journal of General Evolution, 59(3-4), 145-167.

Prasad A.M., Iverson L.R. and Liaw A. (2006). Newer classification and regression tree techniques: bagging and random forests for ecological prediction. Ecosystems, 9(2), 181-199.

Rawat J. and Kumar M. (2015). Monitoring land use/cover change using remote sensing and GIS techniques: A case study of Hawalbagh block, district Almora, Uttarakhand, India. The Egyptian Journal of Remote Sensing and Space Science, 18(1), 77-84.

Rimal B., Zhang L., Stork N., Sloan S. and Rijal S. (2018). Urban Expansion Occurred at the Expense of Agricultural Lands in the Tarai Region of Nepal from 1989 to 2016. Sustainability (2071-1050), 10(5).

Roberts B. (2013). Landscapes of settlement: prehistory to the present, Routledge.

Saarela S.-R. and Rinne J. (2016). Knowledge brokering and boundary work for ecosystem service indicators. An urban case study in Finland. Ecological Indicators, 6149-62.

Saeed Q., Bhatti I., Ashraf A. and Ahmad B. (2012). Physiochemical Analysis of Drinking Water from Different Urban Areas of Faisalabad. International Journal of Basic & Applied Sciences IJBAS-IJENS, 12(6), 183-186.

Safder Q. and Babar U. (2019). Assessment of Urbanization and Urban Sprawl Analysis through Remote Sensing and GIS: A Case Study of Faisalabad, Punjab Pakistan. INTERNATIONAL JOURNAL OF ACADEMIC RESEARCH IN BUSINESS AND SOCIAL SCIENCES, 9(4).

Schneider A., Mertes C., Tatem A., Tan B., Sulla-Menashe D., Graves S., Patel N., Horton J., Gaughan A. and Rollo J. (2015). A new urban landscape in East–Southeast Asia, 2000–2010. Environmental Research Letters, 10(3), 034002.

Seto K.C., Fragkias M., Güneralp B. and Reilly M. K. (2011). A meta-analysis of global urban land expansion. PloS one, 6(8), e23777.

Shah S.A.R., Naqvi S.A.A. and Anwar S. (2020). Exploring the linkage among energy intensity, carbon emission and urbanization in Pakistan: fresh evidence from ecological modernization and environment transition theories. Environmental Science and Pollution Research, 1-23.

Shaheen A., Sheng J., Arshad S., Salam S. and Hafeez M. (2020). The Dynamic Linkage between Income, Energy Consumption, Urbanization and Carbon Emissions in Pakistan. Polish Journal of Environmental Studies, 29(1), 267-276.

Shakeel M., Khan A.U., Munir A.R. and Ahmed T. (2015). Spatial Variation in Urban Air Pollution: A GIS Based Approach in Faisalabad, Pakistan. Asian Journal of Natural & Applied Sciences, 4(3), 40-48.

Shalaby A. and Tateishi R. (2007). Remote sensing and GIS for mapping and monitoring land cover and land-use changes in the Northwestern coastal zone of Egypt. Applied Geography, 27(1), 28-41.

Shetty S. (2019). Analysis of Machine Learning Classifiers for LULC Classification on Google Earth Engine. University of Twente, Netherlands.

Simon J.L. (2019). The economics of population growth, Princeton University Press, New Jersey.

Steedman E.B. (1882). Report on the Revised Settlement of the Jhang District of the Punjab, 1874-1880, W. Ball.

Stock J.L. and Chusid J.M. (2019). Urbanizing India's frontier: Sriganganagar and canal-town planning on the Indus plains. Planning Perspectives, 1-24.

Sun Q., Xu J. and Chi X. (2010). A study of planning of commercial-net in quasi-urbanization area: taking luogang district in guangzhou as an example. Journal of South China Normal University (Natural Science Edition), (2), 27.

Thapa R.B. (2012). Monitoring landscape change in Kathmandu metropolitan region using multi-temporal satellite imagery. SPIE Asia-Pacific Remote Sensing, 85281-85281.

Tian H., Banger K., Bo T. and Dadhwal V. K. (2014). History of land use in India during 1880–2010: Large-scale land transformations reconstructed from satellite data and historical archives. Global and Planetary Change, 12178-88.

Undp (2018). «Human Development Reports». The 2016 Global Multidimensional Poverty Index (MPI).

Valentine B., Kamenov G.D., Kenoyer J.M., Shinde V., Mushrif-Tripathy V., Otarola-Castillo E. and Krigbaum J. (2015). Evidence for patterns of selective urban migration in the Greater Indus Valley (2600-1900 BC): a lead and strontium isotope mortuary analysis. PLoS One, 10(4), e0123103.

Vasenev V.I., Yaroslavtsev A.M., Vasenev I.I., Demina S.A. and Dovltetyarova E.A. (2019). Land-use change in new Moscow: First outcomes after five years of urbanization. Geography, Environment, Sustainability, 12(4), 24-34.

Zhu Y. (2002). Beyond large-city-centred urbanisation: in situ transformationof rural areas in Fujian Province. Asia pacific viewpoint, 43(1), 9-22.

Zhu Y. (2004). Changing urbanization processes and in situ rural-urban transformation: reflections on China's settlement definitions. New forms of urbanization: Beyond the urban-rural dichotomy. Ashgate Publishing Ltd.

Zhu Y., Qi X., Shao H. and He K. (2007). The evolution of in situ urbanization and quasi-urban populations and their planning and environmental implications in China: Case studies from Quanzhou Municipality. Centre for Population and Development Research, Fujian Normal University, China.

Appendix

Appendix 1. Satellite images characteristics

Path/Raw	Year	Satellite	Sensor	Data Acquired	Thermal Resolution	Radiometric Resolution	Bands Description		
							Name	Wavelength (μm)	Discerption
149/38	1989	Landsat 5	TM	1989-06-19	16 Days	8bit	B1	0.45-0.52	Blue
							B2	0.52-0.60	Green
							B3	0.63-0.69	Red
150/38				1989-04-11			B4	0.77-0.90	Near infrared
							B5	1.55-1.75	Shortwave infrared 1
							B7	2.08-2.35	Shortwave infrared 2
149/38	1999	Landsat 5	TM	1999-05-14	16 Days	8bit	B1	0.45-0.52	Blue
							B2	0.52-0.60	Green
							B3	0.63-0.69	Red
150/38				1999-04-24			B4	0.77-0.90	Near infrared
							B5	1.55-1.75	Shortwave infrared 1
							B7	2.08-2.35	Shortwave infrared 2
149/38	2009	Landsat 7	ETM+	2009-06-16	16 Days	8bit	B1	0.45-0.52	Blue
							B2	0.52-0.60	Green
							B3	0.63-0.69	Red
150/38				2009-05-23			B4	0.77-0.90	Near infrared
							B5	1.55-1.75	Shortwave infrared 1
							B7	2.08-2.35	Shortwave infrared 2
149/38	2019	Landsat 8	TOA	2019-06-01	16 Days	16bit	B2	0.45-0.51	Blue
							B3	0.53-0.59	Green
							B4	0.64-0.67	Red
							B5	0.85-0.88	Near infrared
150/38				2019-04-17			B7	2.11-2.29	Shortwave infrared 2
							B10	10.60-11.19	Thermal infrared 1
							B11	11.50-12.51	Thermal infrared 2

Appendix 2. Accuracy assessment for each classified image

Image (Path/Raw)	Year	Classified Image	Overall Classification accuracy	Overall Kappa Statistics
Urban Center of Faisalabad (149/38)	1989	Landsat 5 TM	81.73%	0.6863
	1999	Landsat 5 TM	86.42%	0.7478
	2009	Landsat 7 EMT+	83.93%	0.7068
	2019	Landsat 8 TOA	91.11%	0.9285
Urban Center of Jhang (150/38)	1989	Landsat 5 TM	82.33%	0.6923
	1999	Landsat 5 TM	87.23%	0.7631
	2009	Landsat 7 EMT+	81.53%	0.7958
	2019	Landsat 8 TOA	89.41%	0.9101

Appendix 3. Land Use Land Cover (LULC) area of Urban Center of Faisalabad

		1989		1999		2009		2019	
Sr. No	Class	Area (km^2)	Area (%)	Area (km^2)	Area (%)	Area (km^2)	Area (%)	Area (km^2)	Area (%)
1	Agriculture	1003.57	86.25	936.87	80.51	813.78	69.94	801.38	68.87
2	Barren	33.33	2.86	21.23	1.82	66.22	5.69	37.80	3.25
3	Buildup	121.60	10.45	194.80	16.74	269.07	23.12	308.39	26.50
4	Grasses	0.06	0.01	0.23	0.02	3.33	0.29	3.96	0.34
5	Trees	4.16	0.36	7.80	0.67	9.54	0.82	10.25	0.88
6	Water	0.87	0.07	2.66	0.23	1.65	0.14	1.82	0.16
Total		1163.60	100.00	1163.60	100.00	1163.60	100.00	1163.60	100.00

Appendix 4. Land Use Land Cover (LULC) area of Urban Center of Jhang

		1989		1999		2009		2019	
Sr. No	Class	Area (km^2)	Area (%)	Area (km^2)	Area (%)	Area (km^2)	Area (%)	Area (km^2)	Area (%)
1	Agriculture	244.96	85.16	245.27	85.27	237.39	82.53	219.28	76.23
2	Barren	21.35	7.42	15.73	5.47	19.89	6.91	30.26	10.52
3	Buildup	19.44	6.76	24.49	8.52	29.45	10.24	32.20	11.20
4	Grasses	0.05	0.02	1.54	0.54	0.27	0.09	0.14	0.05
5	Trees	1.05	0.36	0.44	0.15	0.29	0.10	4.70	1.63
6	Water	0.79	0.27	0.16	0.06	0.35	0.12	1.06	0.37
Total		287.64	100.00	287.64	100.00	287.64	100.00	287.64	100.00

RESEARCH PAPER

ASSESSMENT AND DETECTION OF LAND COVER CHANGES IN THE SOUTHERN FRINGE OF KOLKATA USING REMOTELY SENSED DATA

Sushobhan Majumdar
Former Research Fellow, Department of Geography, Jadavpur University, Kolkata, India
*Corresponding author: sushobhan91@gmail.com
Received: April 02th, 2020 / Accepted: August 9th, 2020 / Published: October 1st, 2020
https://DOI-10.24057/2071-9388-2020-65

ABSTRACT. Continual, historical, and precise information about the land use and land cover (LULC) changes of the Earth's surface is extremely important for any kind of sustainable development program, in which LULC serves as one of the major input criteria. In this study, a supervised classification was applied to five types of Landsat images collected over time (1980, 1990, 2000, 2010 and 2015) that provided recent and historical LULC conditions for the area. Four LULC categories were identified and mapped. Post-classification comparisons of the classified images indicated that the major change consisted of barren land changing into agricultural land. This analysis revealed that substantial growth of built-up areas in the south eastern part of Kolkata over the study period resulted in significant decrease in the area of water bodies, cultivated land, vegetation and wetlands. Urban land transformation has been largely driven by large number of population and high population growth rate with rapid economic and infrastructural development like the extension of metro railway, flyovers and hence huge real estate development.

KEY WORDS: Detection of Land Use and Land Cover Change, Sustainable Development, Urban Land Transformation, Substantial Growth

CITATION: Sushobhan Majumdar (2020). Assessment And Detection Of Land Cover Changes In The Southern Fringe Of Kolkata Using Remotely Sensed Data. Geography, Environment, Sustainability, Vol.13, No 4, p. 121-132
https://DOI-10.24057/2071-9388-2020-65

Conflict of interests: The authors reported no potential conflict of interest.

INTRODUCTION

Urbanization is an inexorable process due to economic development and rapid population growth of an area. Encroachment of urban development in the agricultural areas may pose dire consequences such as land degradation and desertification (Shalaby et al. 2004). Urban growth is the movement of residential areas or commercial areas to the semi urban or rural areas. It has long been considered a sign of regional economic sustainability. Its benefits are increasingly balanced against the ecosystem impacts, including degradation of air and water quality and loss of agricultural tracts and socio-economic effects of economic disparities as well as regional disparities, social fragmentation and the cost of infrastructure (Squires2002).

The rate of population growth is very high in developing countries rather than the developed countries. The population of urban areas is expected to exceed 60% by 2030, with 90% of the projected increase occurring in low income countries i.e. developing or under developed countries, which have urban settlements that are growing five times the rate of those in developed countries.The rapid changes of land use and cover, in the developing countries, are often characterized by rapid urban growth, land degradation, or the transformation of agricultural land to shrimp farming ensuing huge cost to the environment (Sankhala and Singh 2014). Land cover is dynamic and varies at different spatial and temporal scales (Cihlar 2000). Therefore, determining the trend and the rate of land cover conversion are necessary for the development and planning in order to develop rational land use policy. For this purpose, the temporal dynamics of remote sensing data can play an important role in monitoring and analyzing land cover changes.

Geographic Information Systems (GIS) and Remote Sensing (RS) are very powerful and cost-effective tools for assessing the spatial and temporal dynamics of LULC (Lambin, et al. 2003; Serra et al. 2008). In case of developing countries satellite data are particularly useful due to the cost and time associated with traditional survey methods (Dong et al. 1997), and these techniques have become viable alternatives to conventional survey and ground-based urban mapping methods (Jensen et al. 2004). It is also the most common data source for detection, quantification, and mapping of LULC patterns and changes because of its repetitive data acquisition, digital format suitable for computer processing, and accurate geo-referencing procedures (Chen et al. 2005; Jensen 1996; Lu et al. 2004). Satellite data provide valuable multi-temporal data on the processes and patterns of LULC change, and GIS is very much essential for mapping and analyzing the patterns of LULC (Zhang et al. 2002). Retrospective and consistent synoptic coverage from satellites is particularly useful in areas where changes have been rapid (Blodget et al. 1991).Pre and post-classification comparisons have been extensively used (Coppin et al. 2004; Singh 1989). In the pre classification approach, procedures such as image differencing (Toll et al. 1980; Cohen and

Fiorella1998); band rationing (Eastman et al. 2005), change vector analysis (Johnson andKasischke 1998); Lu et al. 2005) vegetation index differencing (Townshend and Justice 1995).Post-classification comparisons of derived thematic maps go beyond simple changedetection and attempt to quantify the different types of change. The degree of success depends upon the reliability of the maps made by image classification. Broadly speaking, large-scale changes such as widespread logging or major urban development might be mapped reasonably easily. Whereas evolutionary changes such as erosion, succession,colonization or degradation, the boundaries may be indistinct and class-labels uncertain (Foodyand Boyd 1999); Khorram et al.1999).

Change detection and monitoring by remote sensing involves the use of several multi-date images to evaluate the differences occurring in LULC between the acquisition dates of images that are due to various environmental conditions and human actions (Singh 1989). The successful use of satellite remote sensing for LULC change detection depends upon an adequate understanding of landscape features, imaging systems, and methodology employed in relation to the aim of analysis (Yang and Lo 2002). Many change detection techniques have been developed and used for monitoring changes in LULC from remotely sensed data. There are many techniques available to detect and record differences (e.g. imagedifferencing, ratios or correlation) and these might be attributable to change (Singh 1989;Stow et al. 1996; Yuan et al. 1999). However, the simpledetection of change is rarely sufficient in itself: information is generally required about theinitial and final land cover or types or land uses, the «from-to» analysis (Khorram et al.1999). Furthermore, the detection of image differences may be confused with problems inphenology and cropping, and such problems may be exacerbated by limited imageavailability and poor quality in temperate zones, and difficulties in calibrating poor images.

Change detection is useful in many applications related to land use and land cover (LULC) changes, such as shifting cultivation and landscape changes (Imbernon 1999; Serra et al. 2008), land degradation, land suitability and desertification (Adamoand Crews- Meyer 2006); Majumdar 2020); Gaoand Liu (2010), coastal change and urban sprawl (Shalaby and Tateishi 2007), urban landscape pattern change BatisaniandYarnal(2009); Dewanand Yamaguchi (2009); Long-qian et al. (2009), deforestation (Schulz et al. 2010; Wyman and Stein 2010), quarrying activities (Mouflis et al. 2008), and landscape and habitat fragmentation and other cumulative changes (Munroe et al. 2005; Nagendra et al. 2006).

Accurate and up-to-date land cover change information is necessary to understanding and assessing the environmental consequences of such changes (Giri et al. 2005). While remote sensing has the capability of capturing such changes, extracting the change information from satellite data requires effective and automated change detection techniques (Roy et al. 2002). Digital change detection is the process of determining or describing changes in land cover and land-use properties based on co-registered multi-temporal remote sensing data. The basic premise in using remote sensing data for change detection is that the process can identify change between two or more dates that is uncharacteristic of normal variation. Numerous researchers have addressed the problem of accurately monitoring land-cover and land-use change in a wide variety of environments (Chan et al. 2001;Muchoneyand Haack (1994); Singh 1989).

In this article remote sensing and GIS techniques was applied with the aim of answering the question how the land use and land cover has changed in RajpurSonarpurMunicpality from 1980 to 2015, 10 years interval.

STUDY AREA

RajpurSonarpur Municipality (Fig. 1) lies on the delta of the Hooghly River with a gentle slope. It is bounded in the north by the Kolkata Municipal Corporation, to the south by Baruipur Community Development (C.D.) Block, to the east and west by Sonarpur C.D. Block. This municipality is well connected with the head quarter of eastern railway of India (i.e. Sealdah station) by the different railway stations one of them (i.e. Sonarpur) is a junction station. Other important stations are Garia, Narendrapur, and Subhasgram. By these railway stations the commuters from south 24 parganas come to city for their daily work. This town is also well connected with the Eastern-Metropolitan By pass and it also provides easy connectivity from the NetajiSubhash International Airport. The Metro Railway line connects the municipality on the northern side through KaviSubhash metro station, which is also terminal station of the existing metro railway route at present time. RajpurSonarpur Municipal area is surrounded by five outfalls viz. Adi Ganga, Kurigachhi Irrigation Channel, Tolly'sNullah, Srinagar Panchanna Gram Drainage Channel, and Rania KeorapukurKhal.

Rajpur Sonarpur Municipality comprises of 37 mouzas namely Harinavi, Kodalia, Rajpur, Malancha, Mahinagar, Jagaddal, Dhamaitala, Mallikapur, Baikunthapur, Bansidharpur, Ellachi, Ukhila-Paikpara, Barhans-Fartabad, Kumrakhali, Nischintapur, Chak-Harinavi, Manikpur, Balia, Kandarpapur-Boalia, Tentulberia, Dhalua, Panchapota, Kusumba, Garagachha, Lashkarpur, Sripur-Bagher Ghola, Boral, Rania, Paschim-Nishintapur, Sonarpur, Ghasiara, Gorkhara, Kamrabad, Noapara, Tegharia, Chowhati, Jagannathpur. Total population of this municipality is 424368 comprising 35 wards with a growth rate of 26.03 between the years 2001–2011. In comparison with the Kolkata Metropolitan Area (KMA) the population growth rate of entire KMA is 10.30 according to Census 2011. This municipality is located in the suburbs of Kolkata city which has experienced very high growth rate i.e. 26.03 per centMajumdar and Sivaramakrishnan (2020). People from the surrounding areas migrate into this area which is the major cause of high growth rate of population. In order to provide better citizen services, amenities and infrastructural services for the inhabitants of this municipality, it has been divided (Table 1) into five local offices. Those are as listed below.

Table 1. Composition of Municipal Administration in RajpurSonarpur Municipality

Name of the Local Offices	Ward Number
Garia	1 to 7
Sonarpur	8to 15
Rajpur	16 to 26
Mahamayatala	27 to 31
Baral	32 to 35

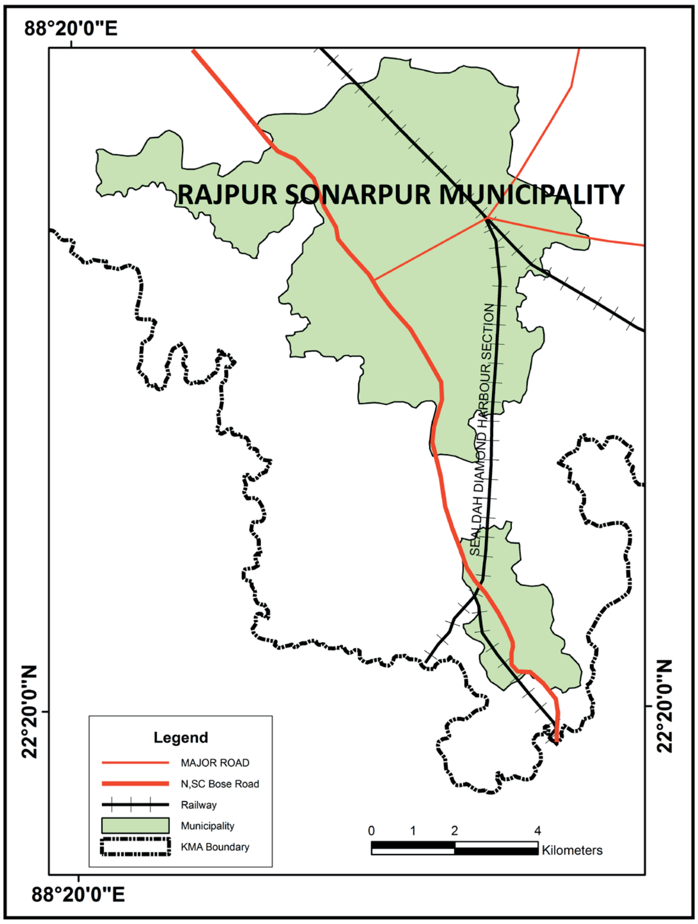

Fig. 1. Location Map of RajpurSonarpur Municipality

MATERIAL AND METHODS

The data set for this study is comprised of five Landsat images recorded from 1980 to 2015. Detailed description of those images discussed below (Table 2). The data has been chosen for 10 years interval because the Census of India is calculated in the interval of 10 years. By calculating 10 years interval time the researcher can easily correlate demographic characteristics (like population growth rate, density etc.) and land use land cover change of this area.

Five sets of landsat satellite images were used here. First, Landsat MSS, Landsat Thematic Mapper (TM) and Enhanced Thematic Mapper (ETM+) images and two sets of OLI 8 images (with path/row 138/45). At the time of layer stacking of those images thermal band was excluded. Digital maps published from the RajpurSonarpur Municipality, has been digitized and geo-referenced from digital topographic maps with scale of 1:50,000 which has been published by the Census of India in 2010 under the Government of India. This map has been used as a reference image only for the geometric correction and geo-referencing of the municipal area. It has also been used for geometric correction of those satellite images and to collect some ground truth information of that time period. Finally, ground information (for cross checking of the produced maps (like various types of land use and land cover information, number of water bodies or wetland in municipal area from 1980 to 2015) was collected between the years 1980 until 2015 to get land use/land cover information. Then supervised classification algorithm was used to scrutinize the land cover types.

Image Processing

The images were geometrically corrected and geo-referenced to the Universal Transverse Mercator (UTM) coordinate system by using a reference image which has been geo-referenced previously by the topographical sheets which were provided by the Survey of India (SOI). This minimum of 30 randomly distributed ground control points (GCPs) were selected from the topographical sheets for geo-referencing the image. Re-sampling technique was performed using a nearest neighbour algorithm technique. Image transformation technique was used with root mean square (RMS) error of 0.1 pixels indicating that the image was accurate to within one pixel.

Table 2. Detailed Information of Utilized Satellite Imagery

Satellite	Acquisition Date	Sensor	Spatial Resolution	Projection
Landsat 8	08-03-2015	OLI-TIRS	30m	WGS 84 UTM 45 N
Landsat 7	21-01-2010	TM	30m	
Landsat 7	17-11-2000	ETM+	30m	
Landsat 5	14-11-1990	TM	30m	
Landsat 3	21-02-1980	MSS	60m	

Source: US Geological Survey, 2015

Image Enhancement and Visual Interpretation

Image enhancement is basically the modification of image by improving clarity and visual interpretability of the remotely sensed image. The process of visually interpreting digitally enhanced imagery attempts to optimize the complementary abilities of the human mind and the computer. The mind is excellent at interpreting spatial attributes on an image and is capable of identifying obscure or subtle features. Generally these images are used for visual analysis while original images used for automated analysis. (Lillesandand Kiefer 1994); Eastman 2006). By the process of supervised classification five land use and land cover maps were produced. Some of the classes were spectrally confused in the image of 1980 because of very low resolution of image which is MSS imagery in nature. So it could not be separated well by supervised classification. For this reason visual interpretation technique has been used to separate them properly.

Image classification

Land cover classes are typically mapped from digital remotely sensed data through the process of a supervised digital image classification (Campbell 1987; Thomas et al. 1987). The overall objective of the image classification procedure is to automatically categorize all pixels in an image into land cover classes or themes (Lillesandand Kiefer 1994). The maximum likelihood classifier has been used because it quantitatively evaluates both the variance and covariance of the category spectral response patterns when classifying an unknown pixel so that it is considered to be one of the most accurate classifier since it is based on statistical parameters.

Supervised Classification

Researcher used ERDAS IMAGINE 2014 software for digital image processing and image classification of the Landsat images described above. Training samples were selected for each of the predetermined LULC types by delimiting polygons around representative sites with the help of feature space tool. Using those polygons the researcher derived spectral signatures for the respective land cover types which are recorded on the satellite images. A spectral signature is considered to be satisfactory when confusion among the land covers to be mapped [is] minimal' (Gaoand Liu 2010). After collecting spectral signatures image classification was done using maximum likelihood as a classification method.

Maximum livelihood algorithm is one of the common parametric classifiers used for especially in case of supervised classification. This algorithm is used for computing the weighted distance or likelihood (D) of unknown measurement vector (X) belonging to one of the known classes (Mc) which is based on the Bayesian equation(Mukhopadhyay et al. 2013).

$$D = In(a_c) - \left[0.5In(\mathrm{cov}_c)\right] - \left[0.5(X - M_c)T(\mathrm{cov}_e - 1)(X - M_e)\right]$$

The class is assigned with the unknown measurement vector in which it has the highest probability of belonging. The advantage of maximum livelihood algorithm is that it considers the variance covariance matrix with in the class distributions. In case of normally distributed data, this performs better than the other known parametric classifiers, though the results may be unsatisfactory for the data not having normal distributions (Mukhopadhyay et al. 2013). it may be of two types parametric and non-parametric. By the supervised classification a raster layer i.e. the classified image and a distance file originates. Both the thematic layer and the distance file were used for post-classification thresholding. Four initial LULC maps were produced. Because these are the major land use land cover types of this area (Table 3).

Classification Improvement

Some LULC classes were spectrally confused because of mixing of different colours of pixels. So it could not be properly separated by supervised classification especially in the images of 1980. For instance, confusion between the deep water bodies and wetland in some portions of the area. Because in areas of discontinuous free water bodies, significant numbers of pixels were misclassified to the fallow class due to the existence of aquatic plants which are hydrophytes in nature. To improve the level of accuracy of the classified image and to reduce misclassifications, the researcher integrated the initial LULC maps resulting from supervised classification with the maps resulting from visual interpretation. Visual interpretation was very important for increasing classification accuracy and, consequently, the quality of the LULC maps produced. In case of MSS Landsat images, due to the low resolution image correction techniques were used. Finally, the researcher produced accurate LULC maps which was also compared with the reference data (the archived data, historical maps, topographic maps, and ground control points).

Classification Accuracy Assessment

Accuracy assessment method is very useful for individual classification when resulting data are used for the change detection analysis (OwojoriandXie2005). Accuracy assessment technique was performed based on using a random sample method of more than 150 check points i.e. ground control points, old sketch maps, topographic maps as a referenced map in ERDAS Imagine 9.2 software to scrutinize theland use or land cover classes of the area.

Detection of LULC changes

Post Classification Comparison (PCC) method and change detection analysis were applied to compare and analyze the LULC maps resulting from the integration of the results of visual interpretation and supervised classification. PCC was employed to detect the differences between each pair of LULC maps (i.e., 1980 to 1990, 1990 to 2000, 2000 to 2010 and 2010 to 2015).

Fig.2. shows an overlay of RajpurSonarpur Municipality administrative boundaries in 1980,1990,2000,2010 and 2015. The total urban areas for the five respective periods were estimated at 8.21, 10.80, 15.92, 21.67 and 23.22 (Table 4). Analysis of annual rate of change between the four periods (1980–1990), (1990–2000), (2000–2010), (2010–2015) showed that the area expanded by 52.5%, 84.5%, 136.1%, 62.8% respectively, with an average rate of 84% for the whole study period, from 1980 to 2015.

Table 3. Identified Classes by Supervised Classification

No	Land Use Classes	Description
1	Built-up Area	Residential, Commercial, Industrial, Roads, Railway, mixed urban or built-up area
2	Vegetation	Vegetative areas, Agricultural areas
3	Water body	Pond, Canal, Reservoir
4	Fallow land	Waste land, Fallow land

Change detection

Following the classification of imagery from the individual years, a multi-date post-classification comparison change detection algorithm was used to determine changes in land use and land cover in four intervals, 1980–1990, 1990–2000, 2000–2010, and 2010–2015. This is perhaps the most common approach to change detection (Jensen 2004) and has been successfully used by (Yang 2002) to monitor land use changes in the Atlanta, Georgia area.

Change detection accuracy assessment

Change detection presents unique problems for accuracy assessment since it is difficult to sample areas that will change in the future before they change. A concern in change detection analysis is that both position and attribute errors can propagate through the number of multiple dates. This is especially true when more than the two dates are used in the analysis. The simplest method of accuracy assessment of change maps is to multiply the individual classification map accuracies to estimate the expected accuracy of the change map (Yuan et al. 1999). A more rigorous approach is to randomly sample areasclassified as change and no-change and determine whether they were correctly classified (Fuller et al. 2003).

Overall accuracy was calculated from the error matrix by dividing the sum of the entries that make major diagonal by the total number of examined pixels. Kappa co-efficient of agreement was also calculated by using following equations (Afify2011).

$$\hat{K} = p_o - p_c \div 1 - p_c$$

$$P_o = \sum_{i=1}^{r} P_{ii}$$

$$P_c = \sum_{i=1}^{r} P_i + P + i$$

Here,
r =The number of rows in the error matrix.
Pii=The proportion of pixels in row 'i' and column 'i'.
Pi+ =The proportion of the marginal total of row 'i'.
P+i = The proportion of the marginal total of column 'i'.

RESULTS

Land use pattern in 1980

To scrutinize the land use pattern in 1980, the researcher first tried to focus on the Landsat MSS imagery for the year 1980. Different land use categories had been identified and used as past reference for the year 1980. Those identified land use pattern was verified in the ground truth verification. Because Prior ground verification knowledge is crucial to recognize the pattern of land use classes during supervised image classification. By applying the ground truth knowledge the researcher identified the pixel along with their color tone, texture to verify each land use category during the classification of image. The land use pattern which were categorized into four classes for the year are listed in Table 3 and shown in Fig. 2A total of 49.26 Sq.km. of land area was estimated for this municipality after the supervised classification. From the identified land use categories, the highest category was vegetation (53% of the total land area) and it is followed by fallow land (16.93% of the total land area), built up area (16.67% of the total land area) and waterbody (12% of the total land area) shown in Table 4.

In figure 2a, brownish patches indicates built up area which was more prominent in this municipal areas. The yellow color indicates fallow land which was high in this time period. In the eastern side the percentage of fallow land is relatively high than the other areas (Fig. 2a).In this period the percentage of fallow land is relatively high than the other periods which is because of low resolution of the image.

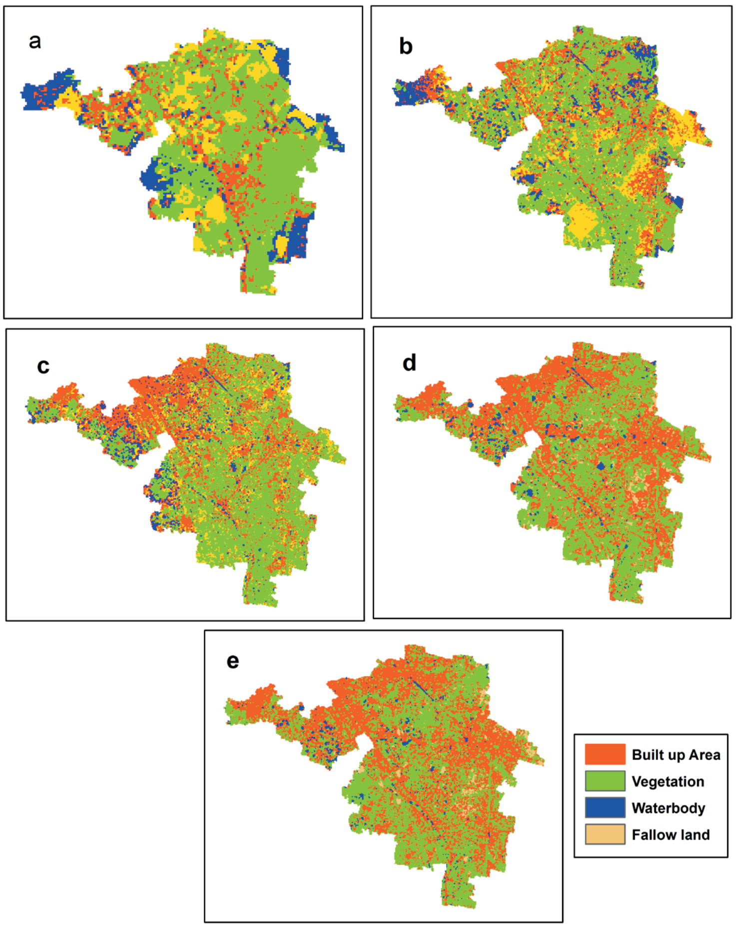

Fig. 2a. to 2e. LULC of RajpurSonarpur Municipality 1980–2015

Land use pattern in 1990

After 1990 land use classification, land use pattern of 1990 (Fig. 2b) was visually interpreted.A total of 4 land use categories were identified during 1990 image classification. Based on 1990 image classification results, the highest category was vegetation (24.72 sq.km. sharing 50% of total land area) followed by built up area, 10.80 sq.km. (22%) and fallow land 7.89 sq.km. (16%) and water body sharing 4.28 sq.km. (9%) respectively (Table 3 and 4).Advantageous location of the municipality, nearness to adjacent railway station i.e. Sonarpur and Subhasgram railway station, good market facility, both type of well-connected roads (Metalled and arterial roads) and good infrastructure facility were the main causes behind the growth of built up area.

Land use pattern in 2000

In 2000 (Fig 2c), built up area covered 32% of the study area, whereas vegetation, water bodies and fallow land accounted for 47%, 11% and 6% of the area respectively (Table 4). In this figurebuiltup area is high in the north west portion. It is relatively high than the other areas which are because of accessibility from the city core areas by the N.S.C. Bose road. Beside these factors metro railway is another factor behind the huge population density of the region.

After the year 1993 different mouzas were added under this municipality's jurisdiction. After the addition of those panchayats, it has seen that right side of the railway track is denser than the left side. Because left side portion of the railway track is already highly dense from the past years.

Land use pattern in 2010 and 2015

In 2010 (Fig. 2d), vegetation area accounted for 45.92% of the study area, whereas built up area, water bodies and fallow land covered 44.99%, 4.66% and 4.26% of the study area. But after the five years i.e. in the year 2015 (Fig. 2e), majority (47%) of the study area was categorized as built up area and it is followed by vegetation, water bodies and fallow land i.e. 44%, 2% and 3% respectively (Table 4).The observed difference of the LULC classes of RajpurSonarpur area as shown in Table 5.

Relative Changes in Land Use in RajpurSonarpur

Relative change in land uses (percentage) of this municipality was assessed based on data presented in Table 6. The relative changes showed some irregular pattern in this study area from 1980 to 2015. Land use change from 1980–2015 showed negative changes in most of the categories except the built up area.

Around6% of Natural vegetated area had decreased between 1990 to 2000 time period,while 30% of the wetlands or water bodies has been converted built up areas between these time period. Between the year 2000 to 2010 the percentage of Built up area has been increased into 36% while 55% of the wetlands or water bodies has been converted into fallow land or builtup area.In the year 2015, 32% of the fallow landhas been decreased due to urban growth. These are the consequences of huge urban growth in this area.

Classification and Change Detection Accuracy

Error matrices were used to assess classification accuracy and are summarized for all five years in Table 7a-7e. The overall accuracies for 1980, 1990, 2000, 2010 and 2015 were, respectively, 92.5%, 85%, 87.5%, 90% and 92.5%, with Kappa statistics of 87%, 77%, 78%, 81% and 86%. Users and producer's accuracies of individual classes were consistently high, ranging from 85% to 92%. Specially 1980, the resolution of the image was very low. To minimize the errors of the image, post classification comparison has been done among the classified images of 1990 and 1980.

Table 4. Trend of Land use and Land cover (sq.km.) in RajpurSonarpur Municipality

Year	1980	1990	2000	2010	2015
Built up area	8.21	10.80	15.92	21.67	23.22
Vegetation	26.02	24.72	23.23	22.62	21.86
Waterbody	6.14	4.28	2.96	1.31	1.21
Fallow land	8.34	7.89	5.67	2.10	1.42

Table 5. Trend of Land Use and Land Cover in RajpurSonarpur Municipality

Year	Percentage of Area in Sq.km					Changes of Area in Percentage			
	1980	1990	2000	2010	2015	1980–1990	1990–2000	2000–2010	2010–2015
Built up area	16.85	22.65	33.53	45.43	48.67	5.79	10.88	11.90	3.24
Vegetation	53.42	51.83	48.93	47.42	45.82	-1.58	-2.91	-1.50	-1.60
Waterbody	12.61	8.97	6.23	2.75	2.54	-3.63	-2.74	-3.49	-0.21
Fallow land	17.12	16.54	11.94	4.40	2.98	-0.58	-4.60	-7.54	-1.43

Table 6. Relative changes in the land use and land cover from 1980 to 2015

Land Use Categories	Changes in Area (Percentage)			
	1980–1990	1990–2000	2000–2010	2010–2015
Built up area	31.47	47.35	36.14	4.77
Vegetation	-4.99	-6.04	-2.61	-3.35
Water body	-30.37	-30.65	-55.59	-47.10
Fallow land	-5.42	-28.06	-62.86	-32.39

Table 7. Error matrix of LULC Classification

Sub-table 7a							
Error matrix showing accuracy and Kappa statistics of 1980 supervised land use classification							
Reference Data						PA (%)	UA (%)
Classified Data	Built up Area	Vegetation	Water Body	Fallow Land	Total		
Built up Area	9	0	0	0	9	100	100
Vegetation	0	22	0	0	22	100	80
Water Body	0	0	4	3	7	100	100
Fallow Land	0	0	0	0	0	40	100
Total	9	22	4	3	38		
Overall Accuracy = 92.50%, Kappa Statistics = 0.87							
Sub-table 7b							
Error matrix showing accuracy and Kappa statistics of 1990 supervised land use classification							
Reference Data						PA (%)	UA (%)
Classified Data	Built up Area	Vegetation	Water Body	Fallow Land	Total		
Built up Area	7	2	0	2	11	78	63
Vegetation	2	18	0	0	20	90	90
Water Body	0	0	3	0	3	100	100
Fallow Land	0	0	0	6	6	75	100
Total	9	20	3	8	40		
Overall Accuracy = 85%, Kappa Statistics = 0.77							
Sub-table 7c							
Error matrix showing accuracy and Kappa statistics of 2000 supervised land use classification							
Reference Data						PA (%)	UA (%)
Classified Data	Built up Area	Vegetation	Water Body	Fallow Land	Total		
Built up Area	0	0	0	2	2	87	87
Vegetation	13	0	0	1	14	100	87
Water Body	2	20	1	0	23	100	100
Fallow Land	0	0	0	1	1	25	100
Total	15	20	1	4	40		
Overall Accuracy = 87.50%, Kappa Statistics = 0.78							
Sub-table 7d							
Error matrix showing accuracy and Kappa statistics of 2010 supervised land use classification							
Reference Data						PA (%)	UA (%)
Classified Data	Built up Area	Vegetation	Water Body	Fallow Land	Total		
Built up Area	18	2	0	0	20	95	90
Vegetation	1	17	1	0	19	90	90
Water Body	0	0	0	0	0	-	-
Fallow Land	0	0	0	1	1	100	100
Total	19	19	1	1	40		
Overall Accuracy = 90%, Kappa Statistics = 0.81							
Sub-table 7e							
Error matrix showing accuracy and Kappa statistics of 2015 supervised land use classification							
Reference Data						PA (%)	UA (%)
Classified Data	Built up Area	Vegetation	Water Body	Fallow Land	Total		
Built up Area	0	3	0	0	3	100	87
Vegetation	19	17	0	0	36	85	100
Water Body	0	0	1	0	1	100	100
Fallow Land	0	0	0	0	0	-	0
Total	19	20	1	0	40		
Overall Accuracy = 92.50%, Kappa Statistics = 0.86							

Classification and Change Maps and Statistics

Change detection maps were generated for all five years (Fig. 3a to 3d) and the individual class area and change statistics for the five years are summarized in Table 4 and Table 5.

From 1980 to 2015, urban area increased approximately 15.01 Sq.km. while vegetation area decreased 4.17 Sq.km. (%), water body 4.93 Sq.km., and fallow landdecreased 6.92 Sq.km. Relatively, urban and developed areas increased 8.21 Sq.km. to 23.22 Sq.km. from 1980 to 2015, with the greatest increase occurring from 1990 to 2000 i.e. 47% of the total change, while vegetation, water bodies and wetland decreased, respectively, 6%, 30% and 28%.But changes in vegetation, water bodies and fallow land was intensive from the year 2000 to 2010 i.e. 1.50%, 3.49% and 7.54% respectively (Table 5). To reduce this error image correction techniques was used. To further evaluate the results of land cover conversions, matrices of land cover changes from 1980 to 1990, 1990 to 2000, 2000 to 2010, and 2010 to 2015 were created (Table 8a to 8d).In the table, unchanged pixels are located along the major diagonal of the matrix. Conversion values were sorted by area.These results indicate thatincreases in urban areas mainly came from conversion ofvegetated land and water bodies to urban uses during the twenty five year period,1980–2015(Table 8a to 8d).

From 2000 to 2010, 7.32 Sq.km. was converted fromvegetated area and 2.97 Sq.km. from fallow land. While in 2010 to 2015,5.26 sq.km area was converted into built up area from the vegetated area, while at the same time, some portionof urban area was converted to forest. These changes may seem tobe classification errors. But vegetated areas are among some of the most sought after areas for developing new housing. Roads and railway lines were generally classified as urban, but when urban trees along the streets grow and expand, the associated pixels may be classified as vegetation. The researcher note that the changes from urban to forest occurred almost entirely near city streets and railway. This same thing also happened in some cases of water body areas. Because some time it falls under the vegetation areas because of the cover by hydrophytes. Classification errors may also cause other unusual changes.

In Table 8the researcher examines more specifically the changes in cover type between 1980 and 2015 for the random sample of the correctly classified 200 change samples from the 300change sites evaluated. Maximum percentage of land use change was «vegetation to urban» and «water bodies to urban». These percentages of change are similar to the results of the change detection from the Landsat classifications of the entire area. Relatively rare and unlikely types of conversions, such as fallow land to water body, and then to urban areas and urban to vegetation, and then to urban area, totaling 5%, are assumed to largely be classification errors.

Table 8. Matrices of LULC changes from 1980–2015

Matrices of Land Cover and Changes (Sq.Km.) from 1980 to 1990					
a. 1980–1990 1990	1980				
	Built up Area	Vegetation	Water Body	Fallow Land	1990 Total
Built up Area	1.84	0	0.7	0.8	10.81
Vegetation	5.18	14.66	1.44	4.33	24.73
Water Body	1.55	1.93	1.41	0.91	4.28
Fallow Land	2.21	3.37	0.71	1.84	7.89
1980 Total	8.22	26.03	6.15	8.34	49.26
Matrices of Land Cover and Changes (Sq.Km.) from 1990 to 2000					
b. 1990–2000 2000	1990				
	Built up Area	Vegetation	Water Body	Fallow Land	2000 Total
Built up Area	5.42	3.55	0.33	1.44	15.92
Vegetation	5.9	15.25	1.23	2.21	23.24
Water Body	1.1	1.83	0.88	0.42	2.97
Fallow Land	2.4	3.75	0.12	1.57	5.68
1990 Total	10.81	24.73	4.28	7.89	49.26
Matrices of Land Cover and Changes (Sq.Km.) from 2000 to 2010					
c. 2000–2010 2010	2000				
	Built up Area	Vegetation	Water Body	Fallow Land	2010 Total
Built up Area	10.84	3.53	0.14	0.46	21.68
Vegetation	7.32	15.91	0.92	0.93	22.63
Water Body	0.55	1.27	0.76	0.03	1.32
Fallow Land	2.97	1.92	0.09	0.7	2.11
2000 Total	15.92	23.24	2.97	5.68	49.26

Matrices of Land Cover and Changes (Sq.Km.) from 2010 to 2015					
d. 2010–2015 2015	2010				
	Built up Area	Vegetation	Water Body	Fallow Land	2015 Total
Built up Area	16.9	4.19	0.19	0.39	23.23
Vegetation	5.26	16.34	0.39	0.64	21.87
Water Body	0.23	0.41	0.64	0.04	1.21
Fallow Land	0.83	0.93	0	0.35	1.42
1990 Total	21.68	22.63	1.32	2.11	49.26

DISCUSSION

Although similar statistics could be generated for other units such as county, township, or census tract, etc., the above change statistics shed little light on the question of where land use changes are occurring. However, by constructing a change detection map (Fig. 3a to 3d), the advantages of satellite remote sensing in spatially disaggregating the change statistics can be more fully appreciated. Fig. 3a to 3eshows a map of the major land cover types and the conversion from semi urban to urban uses. Built up area, vegetation and water bodies representing maximum percentage of the total area, are the three major land cover types in this municipality.Conversions involving these three classes also represent the most significant changes. Urban growth and the loss of vegetation land were the most important conversions in this area. Although Fig. 3a to 3eonly displays the changes from vegetation, water bodies and fallow land to urban, other changes can also be mapped. The urban growth occurred to the west (Harinavi area), towards eastern side (towards the railway station), and south (Subhashgram railway station area) directions. Whereas growth towards the northern side was limited by the influence of Kolkata Municipal Corporation (Fig. 1). The southward expansion and the westward expansion was the highest and is attributed to the presence of the Sonarpur and Subhashgram railway station and because of the availability of abundant flat vacant land which was suitable for housing construction. A major road named Eastern Metropolitan By pass connecting the airport with Kolkata city is also passing through the RajpurSonarpur Municipality in this area.

In summary, information from satellite remote sensing can play a significant role in quantifying and understanding the nature of changes in land cover and where they are occurring. Such information is essential to planning for urban growth and development.

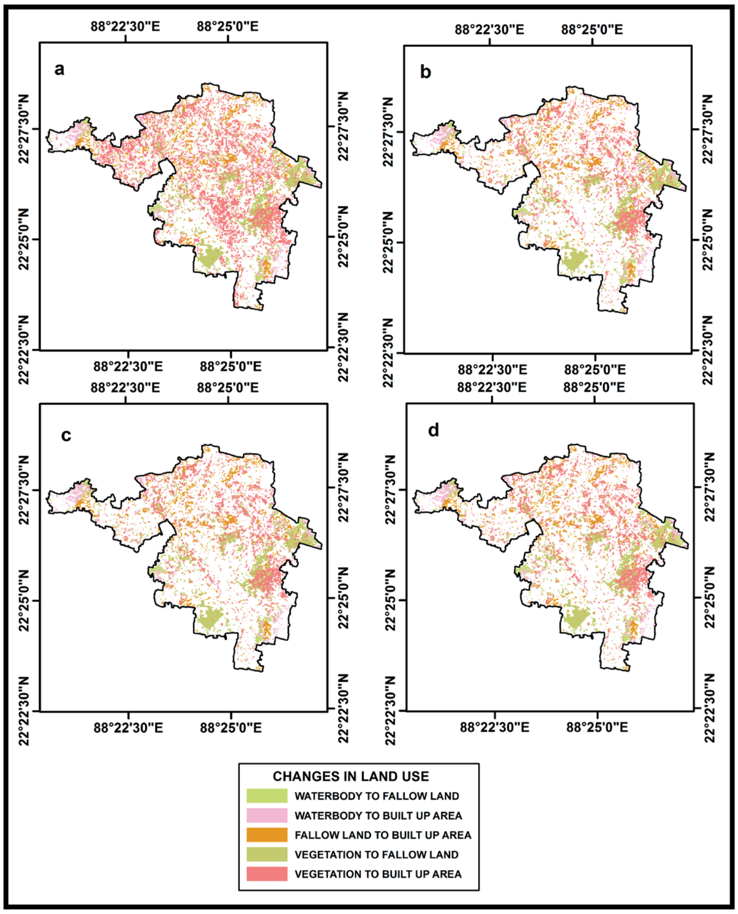

Fig. 3a. to 3d. showing changes in the LULC from 1980 to 2015; Fig. 3a showing the changes of land use between 1980 to 1990, Fig. 3b showing the changes of land use between 1990 to 2000, Fig. 3c showing the changes of land use between2000 to 2010, Fig. 3d showing the changes of land use between 2010 to 2015

Fig. 3a to 3d showing changes in the LULC from 1980 to 2015; Fig. 3a showing the changes of land use between 1980 to 1990, Fig. 3b showing the changes of land use between 1990 to 2000, Fig. 3c showing the changes of land use between2000 to 2010, Fig. 3d showing the changes of land use between 2010 to 2015.

CONCLUSION

The objective of the study were to provide multi-temporal land cover map and its change analysis in the last twenty five years.The study area has undergone a very severe land cover changes as a result of large residential projects and good infrastructural facilities. It leads into high population growth which results into the increases in built up areas. Due to this reason vegetation, wetland and fallow land decreases rapidly. This also demonstrates that supervised classifications of the landsat imageries can be used to produce accurate landscape change maps and future planning of the area. General patterns and trends of land use change in RajpurSonarpur Municipal Area were evaluated by: (1) classifying the land, it has been found that agricultural tracts, vegetation and wetland were converted into urban land during the periods from 1980 to 2015; (2) comparing the results of multi temporal Landsat-derived statistics to estimates from other inventories; (3) quantitatively assessing the accuracy of change detection maps by kappa statistics or khat statistics. By this study the changes and pattern of land use and land cover has been identified. After land use and land cover analysis, it has been found that most of the land use and land cover in this area has been transformed in to urban area or built up area in this time period which creates extreme pressure in the local land resources and ecosystem. This study will help to identify the major urban land use change patterns in relation to policy making and planning, transportation and population growth for the sustainable development of the area. The results quantify the land cover change patternsof this municipal area and demonstrate the potential of multi temporal Landsat data to provide an accurate, economical means to map and analyze changes in land cover over time that can be used as inputs to land management and policy decisions. ■

REFERENCES

Afify H.A. (2011). Evaluation of change detection techniques for monitoring landcoverchanges: a case study in new Burg El-Arab area. Alexandria Eng. J. 50, 187-195, DOI: 10.1016/j.aej.2011.06.001.

Adamo S.B. and Crews-Meyer K.A. (2006). Aridity and desertification: exploring environmental hazards in Jáchal, Argentina. Applied Geography, 26(1), 61-85.

Batisani N. and Yarnal B. (2009). Urban expansion in Centre County, Pennsylvania: spatial dynamics and landscape transformations. Applied Geography, 29(2), 235-249.

Blodget H., Taylor P. and Roark J. (1991). Shoreline changes along the Rosetta-NilePromontory: monitoring with satellite observations. Marine Geology, 99, 67-77.

Campbell J.B. (1987). Introduction to remote sensing. The Guilford Press.

Cihlar J. (2000). Land cover mapping of large areas from satellites: status andresearchpriorities. International Journal of Remote Sensing, 21, 1093-1114.

Chan J.C., Chan K.P. and Yeh A.G.O. (2001). Detecting the nature of change in an urbanenvironment: A comparison of machine learning algorithms. Photogrammetric Engineering and Remote Sensing, 67, 213-225.

Chen X., Vierling L. and Deering D. (2005). A simple and effective radiometric correctionmethod to improve landscape change detection across sensors and across time. Remote Sensing of Environment, 98(1), 63-79.

Cohen W.B., Fiorella M., Gray J., Helmer E., Anderson K. (1998). An efficient and accurate method for mapping forestclearcuts in the Pacific Northwest using Landsat imagery. Photogrammetric Engineering and Remote Sensing 64, 93-300.

Coppin P., Jonckheere I., Nackaerts K., Muys B. and Lambin E. (2004). Digital change detection methods inecosystem monitoring: a review. InternationalJournal of Remote Sensing, 25(9), 1565-1596.

Dewan A.M. and Yamaguchi Y. (2009). Land use and land cover change in Greater Dhaka, Bangladesh: using remote sensing to promote sustainable urbanization. Applied Geography, 29(3), 390-401.

Dong Y., Forster B. and Ticehurst C. (1997). Radar backscatter analysis for urban environments. International Journal of Remote Sensing, 18(6), 1351-1364.

Eastman J.R., McKendry J., Fulk M.A. (2005). Change and time series analysis. In: Explorations in Geographic Informations Systems Technology, United Nations Institute for Training and Research (UNITAR), Geneva.

Fuller R.M., Smith G.M. and Devereux B.J. (2003). The characterization and measurement of land cover change through remote sensing: Problems in operational applications. International Journal of Applied Earth Observation and Geoinformation, 4, 243-253.

Gao J. and Liu Y. (2010). Determination of land degradation causes in Tongyu County,NortheastChina via land cover change detection. International Journal of Applied Earth Observation and Geoinformation, 12(1), 9-16.

Giri C., Zhu Z. and Reed B. (2005). A comparative analysis of the Global Land Cover 2000 and MODIS landcover data sets. Remote Sensing of Environment, 94, 123-132.

Foody G.M. and Boyd D.S. (1999). Detection of partial land cover change associated with the migration ofinner-class transitional zones. International Journal of Remote Sensing, 20, 2723-2740.

IGBP. (1999). Land-Use and Land-Cover Change (LUCC) implementation strategy. IGBP Report No. 48/IHDP Report No 10. Stockholm (Sweden): International Geosphere-Biosphere Programme (IGBP) e International Human Dimension Programme on Global Environmental Change (IHDP).

Imbernon J. (1999). Changes in agricultural practice and landscape over a 60-yearperiod in North Lampung, Sumatra. Agriculture, Ecosystems and Environment, 76(1), 61-66.

Jensen J.R. (1996). Introductory digital image processing: A remote sensing perspective. Upper Saddle, NJ: Prentice-Hall.

Jensen J.R., Hodgson M.E., Tullis J.A. and Raber G.T. (2004). Remote sensing ofimpervious surfaces and building infrastructure. In R.R. Jensen, J.D. Gatrell (eds.). Geospatial Technologies in Urban Environments: Policy, Practice in Heidelberg, 5-20.

Johnson R.D., Kasischke E.S. (1998). Change vector analysis: a technique for the multispectral monitoring of land cover and condition. International Journal of Remote Sensing 19, 411-426.

Khorram S., Biging G.S., Chrisman N.R., Congalton R.G., Dobson J.E., Ferguson R.L. et al. (1999). Accuracy assessment of remote sensing-derived change detection. Bethesda: American Society of Photogrammetryand Remote Sensing.

Lambin E.F., Geist H. and Lepers E. (2003). Dynamics of land use and cover change I tropical regions. Annual Review of Environment and Resources, 28, 205-241.

Lenney M.P., Woodcock C.E., Collins J.B. and Hamdi H. (1996). The status of agricultural lands in Egypt: The use of multi temporal NDVI features derived from Landsat TM. Remote Sensing Environment, 56, 8-20.

Lillesand T.M. and Kiefer R.W. (1994). Remote sensing and image interpretation (4thed.) New York: Wiley.

Long-qian C., Li W. and Lin-shan Y. (2009). Analysis of urban landscape pattern change in Yanzhou city based on TM/ETM+ images. Procedia: Earth and Planetary Science, 1(1), 1191-1197.

Lu D., Mausel P., Brondizio E. and Moran E. (2004). Change detection techniques. InternationalJournal of Remote Sensing, 25(12), 2365-2407.

Lu D.S., Mausel P., Batistella M., Moran E. (2005). Land-cover binary change detection methods for use in the moist tropical region of the Amazon: a comparative study. International Journal of Remote Sensing 26, 101-114.

Majumdar S. (2020). Land Suitability Analysis for Peri-urban Agriculture Using Multi-criteria Decision Analysis Model and Crop Condition Monitoring Methods: A Case Study of Kolkata Metropolitan Area. In: Pattnaik P., Kumar R., Pal S., Panda S. (eds) IoT and Analytics for Agriculture. Studies in Big Data, 63, Springer, Singapore.

Majumdar S., Sivaramakrishnan L. (2020). Mapping of Urban Growth Dynamics in Kolkata Metropolitan Area: A Geospatial Approach. In: Bandyopadhyay S., Pathak C., Dentinho T. (eds) Urbanization and Regional Sustainability in South Asia. Contemporary South Asian Studies. Springer, Cham.

Mendoza J.E. and Etter R. (2002). Multi-temporal analysis (1940–1996) of land cover changes in the south western Bogota high plain (Colombia). Landscape and Urban Planning, 59(3), 147-158.

Mouflis G.D., Gitas I.Z., Iliadou S. and Mitri G.H. (2008). Assessment of the visual impact of marble quarry expansion (1984–2000) on the landscape of Thasos island, NE Greece. Landscape and Urban Planning, 86(1), 92-102.

Muchoney D.M. and Haack B. (1994). Change detection for monitoring forest defoliation. Photogrammetric Engineering and Remote Sensing, 60, 1243-1251.

Mukhopadhyay A., Mukherjee S., Garg R. and Ghosh T. (2013). Spatio-temporal analysis of land use-landcoverchanges in Delhi using remote sensing and GiS techniques.International Journal of Geomatics and Geosciences, 4(1), 213-223.

Munroe D.K., Croissant C. and York A.M. (2005). Land use policy and landscape fragmentation in an urbanizing region: assessing the impact of zoning. Applied Geography, 25(2), 121-141.

Nagendra H., Pareeth S. and Ghate R. (2006). People within parks-forest villages, land-cover change and landscape fragmentation in the TadobaAndhari Tiger Reserve, India. Applied Geography, 26(2), 96-112.

Owojori A. and Xie H. (2005). Landsat image-based LULC changes of San Antonio, Texas using Advanced atmospheric correction and Object-oriented image analysis Approaches. Paper presented at the 5th International Symposium on Remote Sensing of Urban Areas, Tempe, AZ.

Palmer A.R. and Van Rooyen A.F. (1998). Detecting vegetation change in the southern Kalahari using LandsatTM data. Journal of Arid Environments, 39, 143-153.

Ram B. and Kolarkar A.S. (1993). Remote sensing application in monitoring land-use changes in arid Rajasthan.International Journal of Remote Sensing, 14(17), 3191-3220.

Roy D.P., Lewis P.E. and Justice C.O. (2002). Burned area mapping using multi-temporal moderate spatial resolution data-a bi-directional reflectance model-based expectation approach. Remote Sensing of Environment, 83, 263-286.

Rembold F., Carnicelli S., Nori M. and Ferrari A. (2000). Use of aerial photographs, landsatTM imagery andmultidisciplinary field survey for land-cover change analysis in the lakes region (Ethiopia). InternationalJournal of Applied Earth Observation and Geoinformation, 2(3-4), 181-189.

Sadek S.H.A. (1993). Use of landsat imagery for monitoring agricultural expansion of East and West Nile Delta, Egypt. Egyptian Journal of Soil Sciences, 33(1), 23-24.

Sankhala S., Singh B. (2014). Evaluation of urban sprawl and land use land cover change using remote sensing and GIS techniques: a case study of Jaipur City, India. Int. J. Emerging Technol. Adv. Eng. 4(1), 66-72.

Schulz J.J., Cayuela L., Echeverria C., Salas J. and Rey Benayas J.M. (2010). Monitoring land cover change of the dryland forest landscape of Central Chile (1975–2008). Applied Geography, 30(3), 436-447.

Serra P., Pons X. and SauríD. (2008). Land-cover and land-use change in a Mediterraneanlandscape: a spatial analysis of driving forces integrating biophysical and human factors. Applied Geography, 28(3), 189-209.

Shalaby A., AboelGhar M. and Tateishi R. (2004). Desertification impact assessment in Egypt using low resolution satellite data and GIS. The International Journal of Environmental Studies, 61(4), 375-384.

Shalaby A. and Tateishi R. (2007). Remote sensing and GIS for mapping and monitoring landcover and land-use changes in the North western coastal zone of Egypt. Applied Geography, 27(1), 28-41.

Singh A. (1989). Digital change detection techniques using remotely sensed data. International Journal of RemoteSensing, 10, 989-1003.

Squires G.D. (2002). Urban Sprawl and the Uneven Development of Metropolitan America. In Gregory D. Squires (Ed.), Urban sprawl: Causes, consequences, and policy responses, Washington, D.C.:Urban Institute Press, 1-22.

Stow D.A., Chen D.M. and Parrott R. (1996). Enhancement, identification and quantification of land cover change. In Morain S.A. and Lopez Barose S.V. (Eds.), Raster imagery in geographical information systems. Santa Fe: One Word, 307-312.

Thomas I.L., Benning V.M. and Ching N.P. (1987). Classification of remotely sensed images. Bristol: Adam Hilger.

Toll D.L., Royal J. and Davis J.B. (1980). Urban areas update procedures using Landsat data. In Proceedings ofAmerican Society of Photogrammetry. Falls Church, VA: American Society of Photogrammetry.

Townshend J.R.G. and Justice C.O. (1995). Spatial variability of images and the monitoring of changes in the normalized difference vegetation index.International Journal of Remote Sensing, 16, 2187-2195.

Yang X. and Lo C. (2002). Using a time series of satellite imagery to detect land use and land cover changes in the Atlanta, Georgia metropolitan area. InternationalJournalof Remote Sensing, 23(9), 1775-1798.

Yuan D., Elvidge C.D. and Lunetta R.S. (1999). Survey of multi-spectral methods for land cover changeanalysis. In R.S. Lunettaand C.D. Elvidge (Eds.), Remote sensing change detection: Environmental monitoringmethods and applications. London: Taylor and Francis, 21-39.

Wyman M.S. and Stein T.V. (2010). Modeling social and land-use/land-cover change data to assess drivers of smallholder deforestation in Belize. Applied Geography, 30(3), 329-342.

Zhang B.P., Yao Y.H., Cheng W.M., Zhou C H., Lu Z. and Chen X.D. (2002). Human induced changes to biodiversity and alpine pastureland in the Bayanbulak Region of the East Tianshan Mountains. Mountain Research and Development, 22, 1-7.

RESEARCH PAPER

COMMUNICATIONAL TIES BETWEEN THE REPUBLIC OF BASHKORTOSTAN AND OTHER RUSSIAN REGIONS BASED ON VOICE CELL PHONE DATA

Valeriy V. Yumaguzin[1], Maria V. Vinnik[1]
[1]National Research University Higher School of Economics (HSE), Moscow, Russia.
*Corresponding author: vyumaguzin@hse.ru
Received: May 24th, 2020 / Accepted: August 9th, 2020 / Published: October 1st, 2020
https://DOI-10.24057/2071-9388-2020-98

ABSTRACT. The article aims to present social ties of the Republic of Bashkortostan based on voice cell phone data, which covers 12 million calls from and to the region during the first five days of March 2020. About 96% of calls are made within the republic and only 4% of them are interregional. The people of the Republic of Bashkortostan have close connections with those who live in neighboring regions (Orenburg, Sverdlovsk oblast, the Republic of Tatarstan and especially Chelyabinsk oblast). Being a part of the Ural Economic Region, the Volga Federal District and Volga-Ural Macro Region, the republic has turned mostly towards Ural regions. We also found that the republic has close social ties with Moscow and Moscow region, St. Petersburg and Leningrad oblast, as well as Krasnodar kray, Samara oblast and two Autonomous Districts: Khanty-Mansi and Yamalo-Nenets. We estimated the number of persons who possessed Bashkir SIM-card and were outside the republic during the research period – 183 thousand; the most of them were in the abovementioned regions. While conversation between residents lasts 50 seconds, which is among the smallest values, the calls to and from republics of Altai, Tyva, Khakassia, Sakha and Magadan oblast are 5-8 times longer. Overall, the communication pattern reflects migration flows and economic relations between regions. The results of this study can be utilized by researchers and Bashkir government to explore spatial interaction patterns between regions and may help to guide transportation planning and other potential applications, e.g. infrastructure construction projects. In conclusion, we postulate that cell phone data can be exploited as a source of social ties data, however, the strengthening communication shift into Internet space is diminishing information on the directional features of the ties.

KEY WORDS: cell phone data, social ties, Bashkortostan, Chelyabinsk oblast, migration, communication, digital demography, regional relations, Ural Economic Region

CITATION: Valeriy V. Yumaguzin, Maria V.Vinnik (2020). Communicational ties between the Republic of Bashkortostan and other Russian regions based on voice cell phone data. Geography, Environment, Sustainability, Vol.13, No 4, p. 133-139
https://DOI-10.24057/2071-9388-2020-98

ACKNOWLEDGEMENTS: This article is an output of a research project implemented as part of the Basic Research Program at the National Research University Higher School of Economics (HSE)

Conflict of interests: The authors reported no potential conflict of interest.

INTRODUCTION

Russia is the largest country in the world and has the highest number of subjects among federative states (85 against 51 in the USA, 27 in Brazil, 16 in Germany, 13 in Canada) (Russian regions, 2011) . In this regard, spatial and socio-economic development policy of the country at a regional level is of particular interest due to diversity of the regions. The Russian school of socio-economic zoning, founded by N. N. Baranskiy in the late 1920s, remains relevant to this day (there are 12 Economic Regions in Russia). The division of the country into 8 Federal Districts has changed the grouping of the regions. These territorial units were created artificially solely for the convenience of management and do not have a deep socio-economic basis, so geographers and economists continue to compare the situation of each region, with the regions within the same Economic region, although State Statistics are often aggregated at the level of Federal districts, which somewhat complicates interregional studies. According to the «Strategy of spatial development of the Russian Federation for the period up to 2025», adopted in February 2019, and developed by the Ministry of economic development of the Russian Federation, the country is again divided into 12 Macro-Regions, but with a different composition of subjects than before.

The Republic of Bashkortostan is a part of the Ural Economic Region, the Volga Federal District and Volga-Ural Macro-Region.

There are other regional classifications as well, that do not take into account the territorial features of the location. L. M. Grigoriev, Y. V. Urazhaeva, D. S. Ivanov proposed classification based on the stage of development and industrial structure of the regions (Russian regions 2011). According to them, the Republic of Bashkortostan along with Krasnoyarsk and Perm kray, Belgorod, Kemerovo, Murmansk and Tomsk oblast were included into the group of developed regions with mainly extractive industry.

Among the indicators that are used to build classifications are GRP and income of the population, characteristics of the sectoral structure of the economy, the situation on the labor market, demographic and infrastructure indicators. However, the output does not necessarily reflect the regional cohesion.

The Republic of Bashkortostan connects the European and Asian parts of Russia through Federal Highways (M5 «Ural» and M7 «Volga») and railroads. Being an ethnic republic it has a high share of Bashkirs (29.5%) and Tatars (25.4%), however, Russians are well integrated as well with their share of 36% in total population. According to Census 2010 data, 83% of people who were born in the Republic of Bashkortostan lived in the region; other 17% lived outside the region. From the perspective of the present population, 87,6% of those who lived the republic were born in the republic, 6,7% were born in other Russian regions and 5,7% had foreign origin. Of those who lived in other Russian regions, 9,8% have moved to their current location within the Republic of Bashkortostan during the last 12 months (Volume 8, 2020). In the interregional migration the republic steadily loses more migrants than gains since the beginning of 2000-s, the migration decline in 2007-2018 has reached 80 thousands persons (Population migration, 2020). In addition, in 2017, the republic was in the top-15 Russian regions with the highest rates of internal labor migration, ranked 3rd place by the number of such migrants and 13th place by the share of migrants in employed population, which were working in other region (Khilazheva 2019). It is estimated that among those who were working out of their communities, 64,5% of men and 38,6% of women used to work outside the republic and the rest – within the republic (Khilazheva 2017).

To date, regional connections have been estimated by measuring physical and economic distances, migration flows and goods turnover. Based on innovative digital data - social media and mobile phone, - researchers are able to introduce and assess social ties. However, we are aware of only few foreign studies that have utilized mobile phone data to measure communicational ties and regional cohesion (Blumenstock 2011; Gao et al. 2013). Indeed, a novel digital source of data may be very useful in the analysis as it becomes increasingly involved in socio-demographical and geographical studies (Inferring, 2016; Makhrova et al 2017; Zamyatina, Yashunskij 2018; Yumaguzin, Vinnik 2019). For example, Yumaguzin (2017) applied mobile phone data in accessing a pendulum migration in Ufa, Republic of Bashkortostan. The research was attempted to follow the migration routes through location-based information of people who made calls regardless of their direction. The current research studies direction and duration of the calls. To the best of our knowledge, this is the first effort to reveal interregional communicational patterns based on cell phone data in Russia.

It is time to say, that in 2018, the number of SIM-cards used in Russia amounted to more than 255 million, the level of penetration of cellular services (the number of SIM-cards per person), according to mobile operators, amounted to 179%. The highest level of penetration was observed in Moscow (249%) and St. Petersburg (248%). In other regions the average level of penetration was 164%[1]. According to this indicator, Russia is among the most developed telecommunication markets in the world. At the same time, the actual level of penetration of cellular services in the mid-2010s was estimated at 75%-79% (Zubarev, Perevoznikova, 2015). For comparison, the level of penetration of social networks in Russia in the same period was only 33% (Inferring, 2016). That is, the results of data analysis of mobile operators are likely to be more reliable due to the lower selectivity of service users.

The aim of the paper is to present social ties of the Republic of Bashkortostan based on voice cell phone data. It is a pilot study of the project intended to explore «The regional cohesion in Russia».

The paper examines three hypotheses:

1. Communicational ties between first-order neighbor regions are higher than with second-order neighbors and so on.
2. Being a Muslim region with a high share of Tatars, the Republic of Bashkortostan has the strongest social connection with the Republic of Tatarstan, which is also more economically developed than the Republic of Bashkortostan and more attractive for migrants.
3. The hypertrophied role of Moscow is manifested not only in economic and demographic interaction with the regions, but also in social communication.

DATA AND METHODS

Our research is based on the fine-grained data of one of the three major companies that covers a third of the whole Russian population. The data includes the number and duration of cellphone calls, which were made or received by the residents of the Republic of Bashkortostan during 1/03-5/03/2020 per 2 hour period. Personal and business accounts are combined. About six millions calls were made in each direction; however, the vast majority of them (96%) belonged to intra-regional calls. We compute the following statistics based on the mobile phone voice transaction history: the amount of inbound and outbound calls, their median and average length, the regional direction of the calls in relation to the Republic of Bashkortostan. We used these parameters in the K-means clustering to build a map and graphs of the social ties of the Republic of Bashkortostan.

Cell phone data has its own limitations. The sample does not represent all the population of the republic, because there may be differences between people who own mobile phones and people who do not own mobile phones. In addition, our sample is restricted by persons who are using the mobile voice call data and do not include those, who communicate exceptionally via SMS, Internet or landline. According to our mobile data, on average 92% of all active SIM-cards are used for making or receiving voice calls (in different combinations with SMS and Internet), ranging from 84% to 95% in Russian regions, the rest of the SIM-cards are used solely for SMS or Internet communication. Furthermore, we are unable to observe and track voice calls that are represented by the other two main operators in the republic.

Though we are exploiting the voice calls made in home regions, i.e. by residents, there is a chance that some proportion of people buy local SIM-cards while travelling in other regions to minimize their communication costs through making local calls and calling to their home region. However, elimination of the interregional roaming in August 2018 in Russia, should have led to the demise of such practices, because communication in a guest region with a person's own SIM-card is not extra charged at a premium anymore.

[1]Kolichestvo abonentov sotovoj svjazi v Rossii sokratilos' v 2018 godu. [The number of mobile subscribers in Russia decreased in 2018]. Rambler. March 27, 2019. URL: https://finance.rambler.ru/realty/41936441/

The cost of interregional calls may depend on tariff plan options, which may encourage or restrain interregional communication between persons. Obviously, we cannot grasp calls made by Skype, WhatsApp and other applications via the Internet, that probably are more common among the youth, and persons for whom the price of mobile calls is expensive.

There are no data on the Republic of Crimea and its capital Sevastopol. Data on Nenets Autonomous Okrug comes with the Arkhangelsk oblast. Data on the Republic of Adygeya is combined with the Krasnodar krai. Data on the Moscow oblast and Moscow are also combined, as well as data on St. Petersburg and the Leningrad oblast. We own data on a total of 79 regions. Maps and graphs are created in GeoDa 1.14.0.24 and Gephi 0.9.2 respectively.

Despite these limitations, it is also important to point out that by using cell phone data, we have been able to depict the regional cohesion.

RESULTS

Based on voice mobile traffic data of the cell phone operator, which covers calls from and to the Republic of Bashkortostan, we built a map of main interlocutors of this region (Fig. 1). The main clusters are – (1) Chelyabinsk oblast, (2) Sverdlovsk, Orenburg oblast and the Republic of Tatarstan, (3) Moscow and Moscow region, (4) the Republic of Bashkortostan itself, (5) Krasnodar kray, Khanty-Mansi Autonomous District (AD) – Yugra, Yamalo-Nenets AD, Samara oblast, St. Petersburg and the Leningrad oblast; and the last cluster (6) is the rest of the regions. Overall, the people of the Republic of Bashkortostan have close connections with those who live in neighboring regions. Comparing the regional composition of the Ural Economic Region, the Volga Federal District and Volga-Ural Macro Region, we can prove that the population of the republic has turned toward Ural regions.

The figure 2 shows inbound and outbound calls in the Republic of Bashkortostan. The highest number of calls are made within the republic; for illustrative purposes, we decreased this number by 80 times. Among other regions, the largest number of calls are received from and made to Chelyabinsk oblast, followed by Moscow and Moscow region, the Republic of Tatarstan, Sverdlovsk oblast and Orenburg oblast. The amount of total talk hours almost corresponds to this ranking; however, the Orenburg oblast is shifted down by Saint-Petersburg and the Leningrad oblast in the ranking of incoming calls; Sverdlovsk oblast and Orenburg oblast switched places in the ranking of outcoming calls. In terms of median duration of the calls, the picture is totally different. The conversation between residents lasts 50 seconds, which is among the smallest values, whereas the longest conversations with people of the Republic of Bashkortostan are induced by residents of the Republic of Khakassia, Magadan oblast, the republics of Sakha and North Ossetia. The median duration of the calls in these cases are more than 5 minutes. In turn, the people of the Republic of Bashkortostan preferred to have long talks with those who live in such republics as Altai, Tyva and Khakassia – the median is 4-5 minutes.

DISCUSSION

In this paper, we provided for the first time (to the best of our knowledge) a snapshot of the social ties between some Russian regions based on voice calls data and identified regional clusters with close social connections. While discussing our findings, we will validate them with both digital and traditional data, such as social media data, migration statistics and economic turnover data. This will allow us to acclaim that cell phone data can be used as a source of social ties data.

E.G. Ravenstein postulated the importance of the first order regions in migration, and now it is a well-known law in regional studies, however widely available means of communication may distort the pattern at different regional scales. That is why it must be tested firstly. As we poses data on the level of Russian regions, we can infer some conclusions at this level, however further work at the community, country and international levels is required in the future. For now, we have found empirical evidence of the importance of the first order neighboring regions in social communication. Chelyabinsk oblast is truly a sister region of the Republic of Bashkortostan. In fact, the Bashkir Far Ural («Zaural'e») territories and towns (Sibay, Uchaly, Baimak and Beloretsk) tend to cooperate with developed

Fig. 1. Clustering of the social ties of the Republic of Bashkortostan

Note: there are six clusters with the number of regions in the brackets.

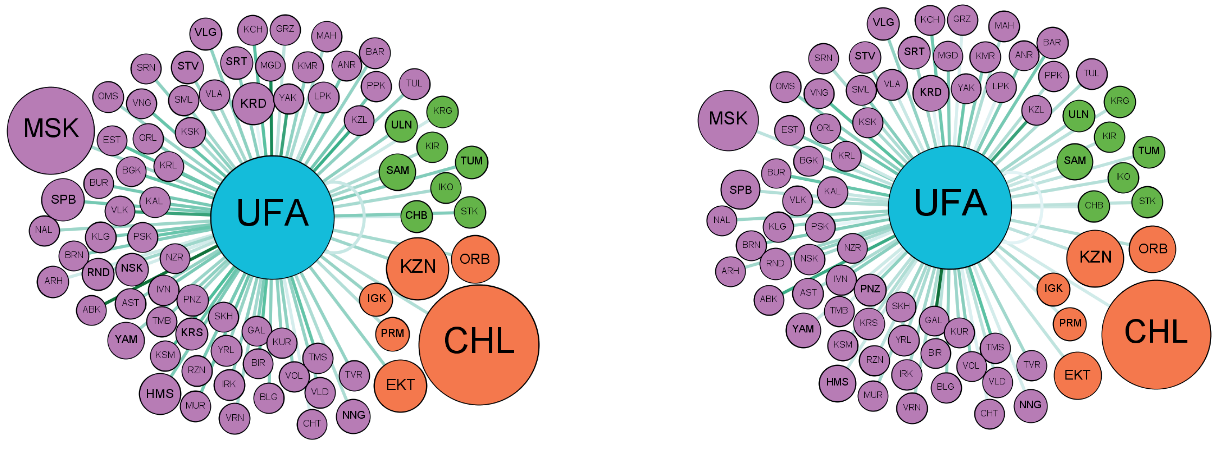

Fig. 2. Inbound (left) and outbound (right) calls in the Republic of Bashkortostan

Note: The size of the nodes corresponds to the number of calls, the color of the nodes represents the border order in relation to the republic (orange – 1st order region, green – 2nd order region, magenta – 3rd order and higher, blue is the Republic of Bashkortostan itself), the color of the edges corresponds to the median duration of the calls. The list of the regions is provided in Appendix.

cities of Magnitogorsk and Chelyabinsk, which are close to the East Bashkir border. On the other hand, the Bashkir capital, Ufa, may attract citizens of Magnitogorsk and Chelyabinsk that forms reverse flows of people. K-means clustering has revealed a huge role of the Moscow region and St. Petersburg as well, depicting the first as a separate cluster (figure 1). Khanty-Mansi AD – Yugra is a second order neighbor region. However, being an oil-producing region it draws in specialists from different regions, especially those that have petroleum technological universities. One of them is located in Ufa; the Ufa State Petroleum Technological University also has three branches, which are in the cities of Oktyabrsky, Salavat and Sterlitamak. The same explanation works for Yamalo-Nenets AD as well.

Both Samara oblast and Krasnodar kray play significant roles in communicational relationships with the republic, they took place in a same cluster with two mentioned autonomous districts, St. Petersburg and the Leningrad oblast. Samara oblast is a second order region neighbor that also has refineries. In addition, the region has leading universities (Ataeva, Ulyaeva 2018), higher wages (Khilazheva et al. 2017) and locates in the European part of Russia so it can serve both as educational center and as a destination point in the «Western drift», including for migrants from Ural regions. Although people of Volga regions themselves started to resettle closer to the Russian capital. Being a regional center of attractiveness for migrants before 2012, Samara oblast has since begun to lose its population showing the negative rates of interregional migration (Population of Russia 2018).

In contrast, Krasnodar kray is a huge region, which along with Moscow and St. Petersburg, belongs to the centers of attraction for migrants throughout the last three decades (Population of Russia 2018), due to the economic development, low unemployment rates and a high level of housing construction. The population of the capital of the region, Krasnodar, has increased by 200 thousands people in the last two decades; now its population is close to 1 million citizens. The city had the highest rate of migration increase among federal cities and regional capitals between 2006-2016 (Population of Russia 2018).

The number of calls from Moscow and Moscow region as well as from Krasnodar kray is 2 times higher than reverse calls. The number of calls from Archangelsk oblast exceeds the number of calls to this region by five times, the same ratio for Novosibirsk oblast equals almost 3. As our data contains both individuals and entities, uneven density of call-centers, marketing and other communication services in the regions may distort the overall picture. Another explanation is that the price of interregional calls is more affordable for these residents; however, it can be captured only on individual-level data.

According to our data, there are 61 thousand people who possessed Bashkir SIM-card and were outside the republic during the research period, which gives roughly 183 (61*3) thousand persons totally with the assumption of equal distribution of other two cell phone operators in the republic (Yumaguzin 2017). The value is very close to the Rosstat data on labour migrants from the republic of Bashkortostan, who were employed outside of the region, which is 161.8 thousand persons in 2018 with the upward trend in the last six years (Distribution 2020). About 26% of cell phone users were in Chelyabinsk oblast, 12% - in Moscow and Moscow region, 10% - in the Republic of Tatarstan, 6% - in the Republic of Chechnya, 5% - in Sverdlovsk oblast. Yamalo-Nenets AD, Orenburg oblast and the Republic of Dagestan each attracted 4% of Bashkir tourists/residents, St. Petersburg and the Leningrad oblast had 3% of Bashkir citizens, Krasnodar kray, Khanty-Mansi AD – Yugra and Samara region each had about 2%. We must highlight here again, that this is actually not the persons themselves, but the distribution of the SIM-cards, which were bought in the republic, and subscribers may own more than one cell phone. On the other hand, as we said earlier, the elimination of the national and interregional roaming have led to the practice when people continue to use their SIM-cards outside their home region and do not buy local ones, even when they plan to stay at the new place for a longer period and probably become residents of that place. Another aspect is that the calls may be made while travelling, so the location does not necessarily coincide with the destination region.

Zamyatina and Yashunskij (2018) presented migration flows and friendship between users' cities and regions based on Russian social network «VK». They found that the regions of the Ural Economic Region have multidirectional migration flows. Huge flows of users interconnect the Republic of Bashkortostan and Chelyabinsk oblast. In addition, there are one-way flows to the Republic of Tatarstan and Khanty-Mansi AD – Yugra from the Republic of Bashkortostan, among the 30 the largest migration flows between Russian regions, excluding Moscow and St. Petersburg. The interregional friendship maps (Virtual 2020) shows that Bashkir users have friends mostly in

Khanty-Mansi AD – Yugra, Yamalo-Nenets AD, Chelyabinsk oblast, the Republic of Tatarstan, Orenburg oblast, Amur oblast, Penza oblast, the Udmurt Republic and Sverdlovsk oblast. Overall, based on social media data, we can confirm that first order border regions of the Republic of Bashkortostan have higher connectivity with it.

While analyzing the conducted research on «Demographic development of the Republic of Bashkortostan», Khilazheva (2015) writes that 3,4% of the sample (n=1000) were intended to move from the Republic of Bashkortostan to other Russian region. In 18-24 age group, this proportion was 2.5 times higher (8,6%). The main reasons for possible relocation were primarily related to the desire to solve socio-economic problems and get an education: the first place took the reason «due to work» (41.6%), which was the most important across all ages, the second most popular reason was «the desire to improve the financial situation» (38.6%), the third one was «due to study» (15.8%). In 2013-2014, among those who actually left the republic, 45% of people were at ages 15-29 (Khilazheva, 2015). In recent years, about 25% of graduates are leaving the republic. However, the situation is worse in periphery, for example, in Uchalinsky district in 2010-2015, from 17.5 to 22% of graduates entered higher education institutions of the republic, while 47% to 55% chose to study in other regions (RBC research 2017). The rural districts in periphery of the republic also demonstrated higher shares of people who were employed in shift work both in Ufa and in other places outside the republic (Khilazheva 2019).

In migration literature (Khilazheva 2017; Khilazheva et al. 2017; Ataeva, Ulyaeva 2018; Valiahmetov et al 2018) we can find that all regions, which we discussed earlier in our analysis, are mentioned among the main destinations of permanent migrants from Bashkortostan. The Bashkortostan's neighbor regions also have huge Bashkir diaspora, which preserve ethnic identity from assimilation and may preserve social ties.

Thus, moving to another region, people retain connections with parents, relatives and friends in their home regions. Being a temporary by the nature, labor migration and holiday trips also fosters family members to stay connected during their separation.

From the economic standpoint, the Republic of Bashkortostan has the highest goods turnover with the Volga Federal District (115.1 billion rubles or 33,7% in 2016), the Central Federal District (92.4 billion rubles, 27,1%) and the Ural Federal District (61.2 billion rubles, 17,9%). Among the regions that have close trade and economic cooperation with the republic, we should mention the Chelyabinsk oblast (36.4 billion rubles, 10,6%), the Republic of Tatarstan (34.3 billion rubles, 10%), Moscow (30.5 billion rubles, 8,9%), the Moscow region (23.4 billion rubles, 6,8%) and the Orenburg oblast (17.5 billion rubles, 5,1%) (Interregional cooperation, 2020). Zakirov (2016) illustrates the cooperation in South Urals, providing the example of pyrometallurgical cycle of non-ferrous metals. First, copper and zinc concentrates are produced in Uchaly, Sibay and Buribay at the mining and processing enterprises with the total capacity of the processing plants of 6.7 million tons of ore per year. Then the production is conveyed to the Chelyabinsk, Orenburg and Sverdlovsk oblast for smelting pure metal at the copper and zinc smelters (Zakirov 2016).

According to different classifications, the Republic of Bashkortostan is part of the Ural Economic Region, the Volga Federal District and the Volga-Ural Macroregion. As we found, communicational ties between the republic and the first-order neighbor regions are much more solid than with higher-order neighbors. Being surrounded by the regions of the Ural Economic Region, the republic tends to be mostly a part of this group, however the republic has close social ties with Moscow, St. Petersburg and Krasnodar regions as well. In this regard, the case of a centrally located region has its own limitations. That is why further research is necessary to build a communication matrix for all regions, and eventually form cultural clusters for a better understanding of the spatial diversity of our country, and propose additional to demographic and economic criteria for regional classification. We would also be able to test the hypothesis that border countries have a bigger impact on Russian border regions, compared to the hinterland. Using individual level data may provide another insight on the migration ties between relatives in further research.

Being an alternative digital source of human behavior, cell phone data demonstrates communicational ties both as a result and a trigger of migration. While social media services allows us to build the friendship network, the cell phone data, besides this, identifies the directions of the conversations and thus may shed light on the economic and social influence and interaction. In our study, we succeed to identify calls between residents of the Republic Bashkortostan and other regions as well as between those who stayed in the republic and moved outside the region for some reason.

CONCLUSION

Overall, the people of the Republic of Bashkortostan have close connections with those who live in neighboring regions that underscores our first hypothesis. Economic relations and moved family members (including those who went to get education or work) are probably the main factors that could explain the pattern. Comparing the regional composition of the Ural Economic Region, the Volga Federal District and Volga-Ural Macro Region, we can prove that the population of the republic has bonded more with Ural regions. We reaffirm the validity of the Soviet economic grid, which considers the republic as part of the Ural Economic Region.

The Republic of Tatarstan is more economically developed than the Republic of Bashkortostan and more attractive for internal migrants. In addition, a quarter of the population of the Republic of Bashkortostan is Tatars. All of this led us to our second hypothesis in which we had supposed that the Republic of Bashkortostan has the closest connection with the Republic of Tatarstan. However, the latter was not emphasized in separate cluster (whereas Chelyabinsk oblast was) but in group with Orenburg and Sverdlovsk oblast. Unfortunately, we cannot split data on Moscow and Moscow region, which combined has stronger tie with the Republic of Bashkortostan than the Republic of Tatarstan solely. All of this makes it difficult to reject the second hypothesis and clearly confirm the third one, which implies the central role of the Russian capital in social communication.

Our paper is intended to stimulate further research at the intersection of international and regional relations, cultural studies, demography and economics. We are going to propose a further assessment of the interconnections and relationships between all Russian regions, to assist with an evidence based socio-economic zoning grid for effective country management, which in turn would lead to balanced spatial development, strengthening the interregional collaboration in infrastructure, investments and social policy. At this stage the results of this study can be utilized by researchers and Bashkir government to explore spatial interaction patterns between regions and may help to guide transportation planning and other potential applications, e.g. infrastructure construction projects.

Our research relied on voice traffic data of the cell phone operator. Increasing the availability of the Internet and widespread of the Social Media will lead to further shift of mobile voice communication into Internet space (for example, voice and text messages, voice and video calls on Skype, WhatsApp, etc.), that cannot give any information about directions of the calls. That is why we think that the current decade may become the last one, when researchers can estimate the social ties according to the voice traffic.

REFERENCES

Ataeva A.G. and Ulyaeva A.G. (2018). Modern trends and factors of inter-regional migration of youth in Russia. Vestnik Tomskogo gosudarstvennogo universiteta. Ekonomika – Tomsk State University Journal of Economics, 44, 38-57 (in Russian).

Distribution of internal Russian labor migrants by the subjects of the Russian Federation from which they leave (2020). Rosstat. Available online at: http://www.gks.ru/free_doc/new_site/population/trud/migrac/tab1_2018.xls [Accessed 22 June 2020] (in Russian).

Duration of residence of the population in the place of permanent residence. Volume 8. (in Russian). Available at: https://www.gks.ru/free_doc/new_site/perepis2010/croc/perepis_itogi1612.htm [Accessed 14 May 2020].

Gao S., Liu Y., Wang Y. and Ma X. (2013). Discovering Spatial Interaction Communities from Mobile Phone Data. Transactions in GIS, 17, 463-481.

Inferring migrations, traditional methods and new approaches based on mobile phone, social media, and other big data. Feasibility study on inferring (labour) mobility and migration in the European Union from big data and social media data (2016). Wi´sniowski, Arkadiusz; Tatem, Andrew J; Abel, Guy J; Zagheni, Emilio; Weber, Ingmar; Sorichetta, Alessandro; Hughes, Christina, 40.

Khilazheva G.F. (2015). Migration behavior of residents of the Republic of Bashkortostan (analysis of sociological data (in Russian). Vestnik Akademii nauk RB, 20, 75-85.

Khilazheva G.F., Shamsutdinova N.K., Utyasheva I.B., Prudnikov V.B., Adigamova O.F. and Yagafarova D.G. (2017). Migration outflow from Bashkortostan in the context of redistribution of the human capital (in Russian). Bulletin USPTU, Science, education, economy, Series Economy, 4 (22), 165-173.

Khilazheva G.F. (2017). Participation of the people of Bashkortostan in the temporary labour migration. Problemy vostokovedeniya, 3 (77), 18-23 (in Russian).

Khilazheva G.F. (2019). The participation of residents of Russian regions in the temporary labor migration (on the example of Republic of Bashkortostan) (in Russian) // Budushchee sfery truda: global'nye vyzovy i regional'noe razvitie: sbornik statej Mezhdunarodnogo foruma «Budushchee sfery truda: dostojnyj trud dlya vsekh» (g. Ufa, 4-5 fevralya 2019 g.) / pod red. G.R. Bajmurzinoj, R.M. Valiahmetova. – Ufa: Mir Pechati, 425-429.

Makhrova A.G., Kirillov P.L. and Bochkarev A.N. (2017). Commuting of the population in the Moscow agglomeration: Estimating commuting flows using mobile operator data // Regional Research of Russia, 7(1), 36-44.

Interregional cooperation of the RB (2020). Gosudarstvennyj komitet Respubliki Bashkortostan po vneshneekonomicheskim svyazyam. Available online at: https://foreign.bashkortostan.ru/activity/419/ [Accessed 17 May 2020] (in Russian).

Population migration by flows (2020). Bashkortostanstat. Available online at: https://bashstat.gks.ru/storage/mediabank/%D0%9C%D0%98%D0%93%D0%A0%D0%90%D0%A6%D0%98%D0%AF%20%D0%9D%D0%90%D0%A1%D0%95%D0%9B%D0%95%D0%9D%D0%98%D0%AF%20%D0%9F%D0%9E%20%D0%9F%D0%9E%D0%A2%D0%9E%D0%9A%D0%90%D0%9C.pdf [Accessed 14 May 2020] (in Russian).

Population of Russia 2016 (2018). Twenty-fourth annual population report. Ed.: S.V. Zakharov. Moscow, HSE Publishing House, 448 (in Russian).

RBC research: what caused migration from Bashkiria (2017). RBC. Available at: https://www.rbc.ru/ufa/27/04/2017/5901b0de9a79474eef6eb833 [Accessed 14 May 2020] (in Russian).

Russian regions: economic crisis and modernization problems (2011). Ed.: Grigoriev L.M., Zubarevich N.V., Khasaev G R. Moscow, Nauka, 349 (in Russian).

Volume 8. Duration of residence of the population in the place of permanent residence (in Russian). Available at: https://www.gks.ru/free_doc/new_site/perepis2010/croc/perepis_itogi1612.htm [Accessed 14 May 2020].

Valiahmetov R.M., Bajmurzina G.R., Turakaev M.S. and Aitov S.G. (2018). Labor Migration as a Factor of Human Development in the Republic of Bashkortostan (in Russian) // Ekonomika i upravlenie: nauchno-prakticheskij zhurnal. 6, 147-156.

Virtual population of Russia (2020). Available at: http://webcensus.ru/ [Accessed 14 March 2020] (in Russian).

Yumaguzin V.V. and Vinnik M. V. (2019). Surnames in modern Russia. Annals of Human Biology, 46 (6), 475-490.

Yumaguzin V. V. (2017). Possibilities of studying pendulum migration based on mobile operators' data (on the example of Ufa) (in Russian) // Demoscope Weekly. № 727 – 728. Available at: http://www.demoscope.ru/weekly/2017/0727/analit01.php [Accessed 15 June 2020].

Zakirov I.V. (2016). Natural Resource Potential as a Factor of Development of Foreign Economic Relations of the Region (on the Example of the Republic of Bashkortostan). Izvestiya Irkutskogo gosudarstvennogo universiteta. Seriya: Nauki o Zemle, 16, 42-54 (in Russian).

Zamyatina N. and Yashunskij A. (2018). Virtual geography of virtual population (in Russian). Monitoring Obshchestvennogo Mneniya: ekonomicheskie i Sotsialnye Peremeny. 143(1), 117–137.

Zubarev A. E. and Perevoznikova M. V. (2015). Review of the market of cellular communication services in Russia (in Russian). Bulletin of the Pacific State University, 3(36), 159-166.

APPENDIX
The list of the used Russian regions

Label	Region
ABK	Republic of Khakassia
ANR	Chukotka AD
ARH	Arkhangelsk oblast, Nenets AD
AST	Astrakhan oblast
BAR	Altai krai
BGK	Amur oblast
BIR	Jewish AO
BLG	Belgorod oblast
BRN	Bryansk oblast
BUR	Republic of Buryatia
CHB	Chuvash Republic
CHL	Chelyabinsk oblast
CHT	Zabaykalsky krai
EKT	Sverdlovsk oblast
EST	Republic of Kalmykia
GAL	Altai Republic
GRZ	Chechen Republic
HMS	Khanty-Mansi AD
IGK	Udmurt Republic
IKO	Mari El Republic
IRK	Irkutsk oblast
IVN	Ivanovo oblast
KAL	Kaliningrad oblast
KCH	Karachay-Cherkess Republic
KIR	Kirov oblast
KLG	Kaluga oblast
KMR	Kemerovo oblast
KRD	Krasnodar krai
KRG	Kurgan oblast
KRL	Republic of Karelia
KRS	Krasnoyarsk krai
KSK	Khabarovsk krai
KSM	Kostroma oblast
KUR	Kursk oblast

Label	Region
KZL	Tyva Republic
KZN	Republic of Tatarstan
LPK	Lipetsk oblast
MAH	Republic of Dagestan
MGD	Magadan oblast
MSK	Moscow, Moscow oblast
MUR	Murmansk oblast
NAL	Kabardino-Balkar Republic
NNG	Nizhni Novgorod oblast
NSK	Novosibirsk oblast
NZR	Republic of Ingushetia
OMS	Omsk oblast
ORB	Orenburg oblast
ORL	Oryol oblast
PNZ	Penza oblast
PPK	Kamchatka krai
PRM	Perm krai
PSK	Pskov oblast
RND	Rostov oblast
RZN	Ryazan oblast
SAM	Samara oblast
SKH	Sakhalin oblast
SML	Smolensk oblast
SPB	St. Petersburg, Leningrad oblast
SRN	Republic of Mordovia
SRT	Saratov oblast
STK	Komi Republic
STV	Stavropol krai
TMB	Tambov oblast
TMS	Tomsk oblast
TUL	Tula oblast
TUM	Tyumen oblast
TVR	Tver oblast
UFA	Republic of Bashkortostan

Label	Region
ULN	Ulyanovsk oblast
VLA	Primorsky krai
VLD	Vladimir oblast
VLG	Volgograd oblast
VLK	Republic of North Ossetia
VNG	Novgorod oblast
VOL	Vologda oblast
VRN	Voronezh oblast
YAK	Republic of Sakha
YAM	Yamalo-Nenets AD
YRL	Yaroslavl oblast

RESEARCH PAPER

CRUCIAL DIFFERENCES BETWEEN PRESENT SERVICE SECTOR STRUCTURES OF RUSSIA AND POLAND: CHANGES AND CONTRIBUTION TO THE ECONOMY

Mikhail E. Savlov
Moscow Innovation Cluster Fund, 22 Voznesensky lane, Moscow, 125009, Russia
*Corresponding author: savlm@yandex.ru
Received: November 30th, 2019 / Accepted: August 9th, 2020 / Published: October 1st, 2020
https://DOI-10.24057/2071-9388-2019-155

ABSTRACT. During the period of planned economies in Russia and Poland, services were underestimated as a sector of economic activity. To some degree, this continues to be the case. In spite of the existence of market economies in Central and Eastern Europe for more than 25 years, Russia and Poland should be categorized differently in terms of economic and social development. Based on D. Bell's and his followers' (M. Castells, A. Toffler, J. Rifkin, P. Drucker) theory of post-industrial society and post-industrial economy, Poland can be classified as a post-industrial country, while Russia is still an industrial country in many aspects. This point of view is based on global statistics and cross-country comparisons. The following statistical data has been used as a source for this research: share of services in GDP by country, contribution (value added) of seven main types of services to the respective GDP of Russia, Poland and other selected countries, value added and governmental expenditures per capita of primary services in aforementioned economies. The main differences between the Russian and Polish service sectors are indicated. The cases of Russia and Poland are presented here to highlight the key common features of Central and Eastern European countries' tertiary sectors.

KEY WORDS: services, tertiary sector, intangible production, Central and Eastern Europe, Poland, Russia

CITATION: Mikhail E. Savlov (2020). Crucial differences between present service sector structures of Russia and Poland: changes and contribution to the economy. Geography, Environment, Sustainability, Vol.13, No 4, p. 140-147
https://DOI-10.24057/2071-9388-2019-155

Conflict of interests: The authors reported no potential conflict of interest.

INTRODUCTION:

There are many ways of defining services as forms of economic activity. It is therefore necessary to set a comprehensive term to describe non-material production. The most popular and significant terms are «services», «tertiary sector of economy», «intangible production», and «non-material production» (Achkasova 2013; Savlov 2018). According to the World Bank methodology, services as an economic activity include, but are not limited to: value added in wholesale and retail trade (including hotels and restaurants), transport, education, health care, and real estate services (The World Bank 2019). If we are looking for a more scientific and methodological definition of services, Cambridge Dictionary applies a system approach and defines services, or service sector, as a business that provides something for people but does not produce goods (Cambridge Dictionary 2019). The Great Russian Encyclopedia defines the service sector as a group of economic activities that provide services to economic actors. The service sector consists of the following economic activities: culture, education, health care, and household services. Often the financial sector is included in the service sector under the heading of financial services, which include tax, budget, monetary, credit, banking and non-banking activities, retirement and insurance systems, and public trading on the stock market. The service sector consists of tertiary economic sector and quaternary economic sector. The quaternary economic sector includes more advanced service economic activities such as IT, education and scientific research (R&D).

However, the term «tertiary economic sector» is basic and widely used to describe all activities in the service sector (The Great Russian Encyclopedia, Electronical edition 2019). In the twentieth century, primary, secondary and tertiary sectors served as a basis for identifying three distinct stages of civilizational development: pre-industrial, industrial and post-industrial. These stages were delineated in works by A. Fisher, C. Clark, J. Fourastié (Fisher 1939; Clark 1940; Fourastié 1949).

The term «service sector» was widely applied in Soviet geographical science. Obviously, the concept of a «service sector» came to Soviet geographers from foreign scientific papers and was interpreted literally (Savlov 2018). As a result, many service activities were excluded. Services were perceived as supporting activities for industry, and only simple services were included in the sector: cleaning, personal services, retail trade, etc. Soviet geographers and their descendants – Russian geographers – considered geography of services as a part of social geography, more specifically, as a part of geography of population (Alekseev, Kovalev and Tkachenko 1991; Sivickij 1998; Savlov 2018).

In Russian economic geography (also known as human geography), the first scientific references to the service sector date back to the 1960s (Savlov 2018). For the first time, the sphere of services became the subject of research in the papers of E. Povitchannaya, which studied the issue of services for the population in cities of the Left Bank of Ukraine (Povitchannaja 1964). The fundamental issues such as theory and research methods in geography of services were noted in the research works of Soviet human geographers S.A. Kovalev and V.V. Pokshishevskij (Kovalev 1966, 1973; Pokshishevskij 1972). Later, in Russian science, geographical research of service sector has been developed by N.V. Zubarevich, V.I. Kruzhalin, A.Y. Aleksandrova, A.P. Gorkin, M.E. Savlov and others (Zubarevich 2013; Kruzhalin 2011; Aleksandrova 2016; Gorkin 2007; Savlov 2013, 2016, 2018).

Over time, recognition and comprehension of services had changed, and the term «tertiary sector» reached Russian geographical science, along with the awareness of an emerging post-industrial society and economy. The shift in perception became more apparent after the market economy had replaced the planned economy, and services became the real driver of the Russian economic system. For example, according to the World Bank, the share of services in Russian GDP in 1991 was 36,7% and it increased to 48,7% in 1992.

As a required remark in this article, the definition of «Eastern Europe» has been taken from the «Standard Country or Area Codes for Statistical Use» by the United Nations and later, it was applied for cross-country comparisons. According to the «Standard Country or Area Codes for Statistical Use» by the United Nations, Eastern Europe consists of 10 countries – Belarus, Bulgaria, Czech Republic, Hungary, Poland, Republic of Moldova, Romania, Russia, Slovakia and Ukraine. The presented article employs the term «Eastern Europe» as something opposed to the designated «Western Europe» and it has the summarizing definition that includes Central and Eastern Europe (CEE).

The development of geography of services as an independent scientific direction in human geography has many common features in Russia and Poland. The same clear underestimation of geography of services as an independent and significant direction of geographical research, as well as services as a crucial economic activity, took place in all formerly socialistic countries, including Poland. As was the case in the USSR, the earliest works in Poland regarding geography of services as an independent geographical direction date back to the 1970s. (Polarczyk 1971; Werwicki 1998; Dominiak 2018). Polish geographers assigned the research of services to the field of settlement research (Dominiak 2018). Perhaps due to this, even 50 years later, there are still many deficiencies in the theory, practice and methodology of geography of services. Polish geographers consider the current state of geography of services to stem from a lack of interest in the subject on the part of primary stakeholders in economics and politics. In Polish science, services as a subject of scientific research has been explored by K. Polarczyk, E. Jakubowicz, A. Werwicki, J. Dominiak and others (Polarczyk 1971; Jakubowicz 1993; Werwicki 1998; Dominiak 2018). The increasing popularity of geographical research of services followed post-industrialisation, or the diminishing share of manufacturing in the world economy in favour of services in the 1970s, connected with the process of tertiarisation (Dominiak and Rachwał 2016).

The economy of Poland after the Second World War, as with the other economies of Central and Eastern Europe, was based on huge industrial plants. As a result, in the 1980's, the share of services in GDP and the share of employment in services were much lower than in Western European countries (Dominiak and Rachwał 2016). For example, according to UNCTAD STAT, the share of services in Polish GDP was 34.0% in 1989 and reached 51.4% in 1992. The current level of service sector development in Poland is a direct consequence of the previous period of socialism and planned economy, and the present socio-economic policy for a more dynamic development of Polish tertiary sector (Dominiak and Hauke 2015).

In foreign scientific research and papers, especially those from Western Europe and the US, the understanding of services as an important part of economy and independent subject of research (economics, social sciences, geography) began with the works of D. Bell (Bell 2004) and his followers: M. Castells, A. Toffler, J. Rifkin, P. Drucker (Castells 2000; Toffler 1980; Rifkin 2011; Drucker 1993, 2002). Now, especially in developed countries, geography of services has the basic role in geographical science – to more faithfully and deeply describe and understand the world, and thus obtain more interesting and useful knowledge (Chojnicki 1991).

MATERIAL AND METHODS

One of the general characteristics of services contribution to the economy is a share of services, value added in a country's GDP. The role of economic sectors can be evaluated in terms of different indicators, basically, in terms of employment and value added. Value added as an indicator better reflects the changes in the economic role of a sector (Dominiak and Rachwał 2016). Otherwise, value added of services as a share of GDP is changeable and it depends on the statistical sources. Taking into account only the general dates of GDP production by main sectors (value added of agriculture, including forestry and fishing; industry, including construction; services) Russia and Poland, as well as the other Central and Eastern European countries have not yet reached the most developed countries' level: Western European Countries, the USA and Canada. Is this an advantage or disadvantage of economic and social development of Eastern European countries? National governments and sciences (economics, sociology, geography) can't give a definite answer to this challenging question. On the one hand, there are ample arguments to be made for the point that countries should keep industries on their national territories and support reindustrialization. On the other hand, some researchers believe that building sustainable economic and social growth depends on «tertiarisation». The term «tertiarisation» means not only an increase in the significance of services in the economy, but also the penetration of service economic activity into the agricultural and industrial sectors (Dominiak and Rachwał 2016). For example, the share of services in German and Japanese GDPs is lower than in other developed countries, but it does not truly mean that services are undeveloped in Germany and Japan (Bolatov and Savlov 2016). This is the case when both industry and services are equally developed. According to the World Bank, services accounted for 56.6% of Russian GDP and 56.3% of Polish GDP in 2016. According to UNCTAD STAT, services accounted for 62.8% and 63.6 % of Russian and Polish GDPs respectively in 2016. In both databases, the shares of services in Russian and Polish GDPs are close and less than the average share in the World GDP (65.1% – The World Bank; 67.5% – UNCTAD STAT in 2016).

Understanding the key features of Russian and Polish tertiary sectors is based on study of cross-country comparisons. Indicators of Russia and Poland were matched with the indicators of the following country groups: the other 8 Eastern European countries, the world's top 10 economies by GDP (the USA, China, Japan, Germany, the United Kingdom, India, France, Brazil,

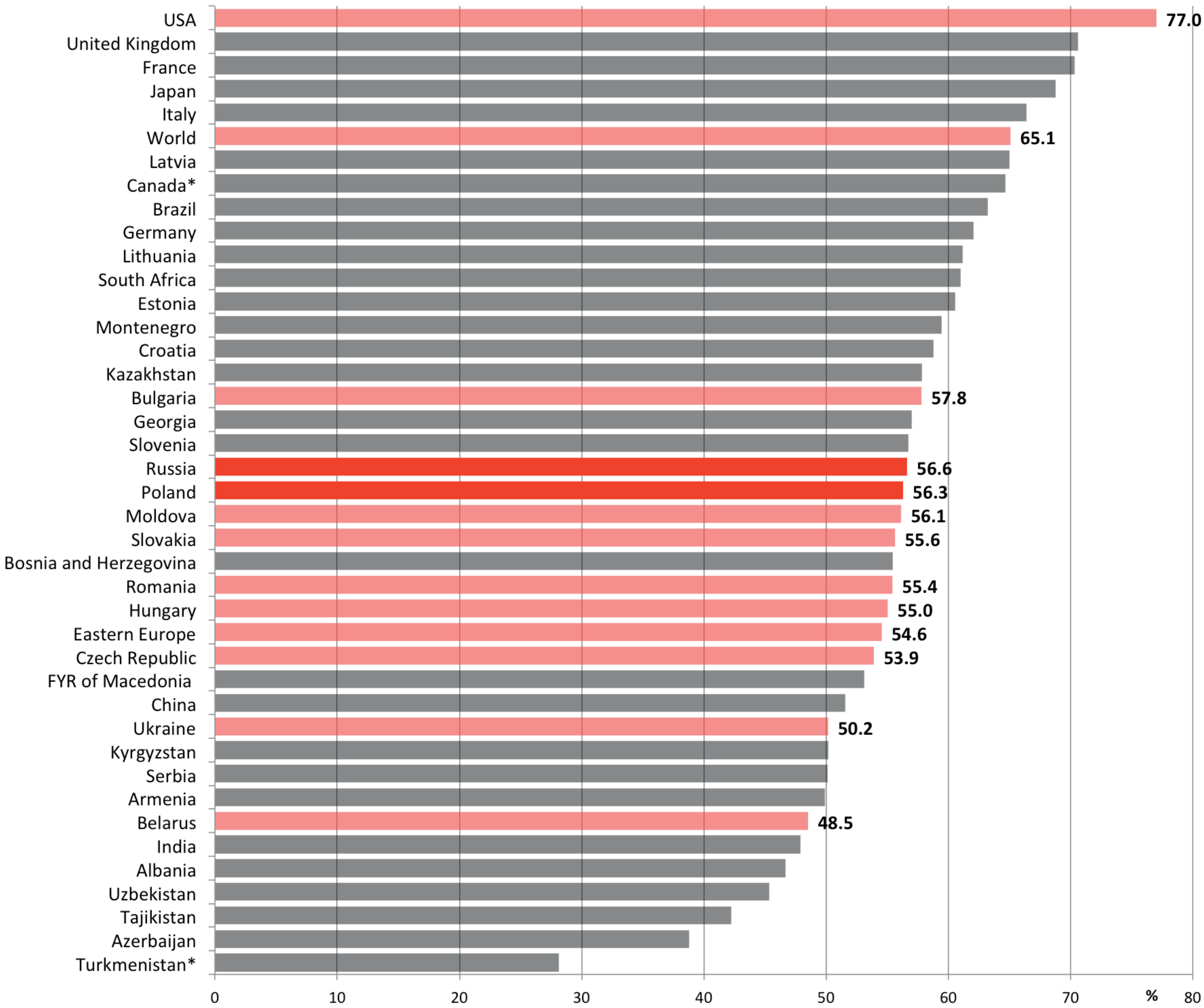

Fig. 1. Services, value added (% of GDP), 2016

*latest available data
Source: The World Bank

Italy, Canada), BRICS, the former USSR republics, Albania and the former republics of Yugoslavia (Fig. 1). A rather average contribution of services to the economy is not the only key feature of Russian and Polish economies. It is common among all Eastern European countries and other post-socialistic economies, including even the German economy. For instance, according to the World Bank, the tertiary sector (services) accounted for 77.0% of the US economy, 70.6% in the United Kingdom, and 70.3% in France in 2016. Besides, Poland could be named one of the most developed Central and Eastern European countries. In addition, in 2018 FTSE Russell (provider of stock market indices) admitted Poland as a country with a developed financial market. A developed Polish financial market is a good point for Poland to be a sustainable post-industrial country. However, in the Central and Eastern European countries and former Soviet republics, services seldom form more than 60% of GDP, therefore Poland and Russia are not exceptions. Only in the three Baltic countries – Latvia, Lithuania and Estonia, do services supply more than 60% of their GDPs.

The challenge of mismatched structures of economies could be solved through the world statistical source, which has the value added of all kinds of economic activity by all countries –a database like the World Bank, OECD, Eurostat, etc. Unfortunately, this source does not yet exist. In this case, the author decided to make an attempt to collect the necessary statistics and to create the comparable estimation structures for the Russian and Polish service sectors. The collection of statistics is based on world sources, which contain data by different types of services. The database was compiled using the World Bank, OECD, UNCTAD STAT, Rosstat, Stockholm International Peace Research Institute (SIPRI) and World Travel & Tourism Council (WTTC). According to the available world statistics sources, the estimation structures of Russian and Polish tertiary sectors include the following services as economic activities: health care; education; research & development (R&D); wholesale, retail trade, restaurants and hotels; tourism; military services; transport, storage and communications.

Comparable formation and estimation of tertiary sectors of Russia and Poland are based on the following indexes (indicators) – value added and governmental or total expenditures. Contribution of three groups of service activities: (wholesale, retail trade, restaurants, hotels); (transport, storage and communications) and tourism were evaluated as a value added, other services were evaluated as governmental expenditures except R&D. The World Bank provides only total expenditures on R&D by countries.

Besides the structure and shares of each service's contribution to GDP, the presented research is considering the indexes (indicators) per capita as crucial insights. Indicators per capita (expenditure or value added) are more representative in cross-country comparisons (Savlov, 2013, 2016). Cross-country comparisons are illustrated through the total or governmental expenditures and value added by 7 main types of services taken per capita.

The latest available dates by groups of services have been compiled in this research and cover the years from 2014 to 2017. The value added of three groups of services (wholesale, retail trade, restaurants, and hotels; transport, storage, and communications; tourism) and current expenditures on health care, education, military services, and R&D were provided by the World Bank, World Travel & Tourism Council (WTTC) and UNCTAD STAT and calculated per capita.

RESULTS AND DISCUSSION

The role of services in the national accounts of Russia and Poland

The structures of national accounts of Russia and Poland include different groups of economic activities. As a result, Russian and Polish structures of economy, and tertiary sector in particular, are mismatched in case of using only national statistical sources (Fig. 2, Fig. 3).

Poland as a part of the European Union uses the Statistical Classification of Economic Activities in the European Community (NACE) as the industry standard classification system to statistically describe the Polish economy. Defining the service sector as all economic activities excluding primary sector (agriculture, forestry, fishing, mining and quarrying) and secondary sector (manufacturing; electricity, gas, steam and air conditioning supply, water supply, sewage, waste management and remediation activities, construction), we can identify the following tertiary sector's economic activities:

- wholesale and retail trade; repair of motor vehicles and motorcycles
- transportation and storage
- accommodation and food service activities
- information and communication
- financial and insurance activities
- real estate activities
- professional, scientific and technical activities
- administrative and support service activities
- public administration and defence; compulsory social security
- education
- human health and social work activities
- arts, entertainment and recreation
- other service activities.

Secondary sector, or industrial sector, and tertiary sector, or services, include economic activities based on the nature of this activity. The tertiary sector is heterogeneous, though at the same time, the services have a common nature (Dominiak and Rachwał 2016).

The same heterogeneity of the service sector is a feature of the tertiary sector of Russia and other countries (Savlov 2018). Estimation of the Russian service sector is based on national accounts by the Federal State Statistics Service of Russian Federation. The internal structure of the Russian tertiary sector is presented by all economic activities aside from agriculture, hunting, forestry, fishing and mining as a primary sector and manufacturing, production and distribution of electricity, gas and water, and construction as a secondary sector (Fig. 3).

The structure of global services has changed significantly from 2005 to 2015 (Fig. 4, Fig. 5). The first conclusion we can make from this analysis is that wholesale, retail trade, restaurants and hotels comprise the largest share of Russian and Polish service sectors. D. Bell identified three types of services accompanied by the level of social development. The pre-industrial society is characterized by the predominance of «simple» services; the industrial society by services for business; the post-industrial society by knowledge-based (advanced) services (Bell 2004; Dominiak and Hauke 2015). «Simple» services still play the main role in the tertiary sectors of Poland and Russia. The same group of service activities comprises the

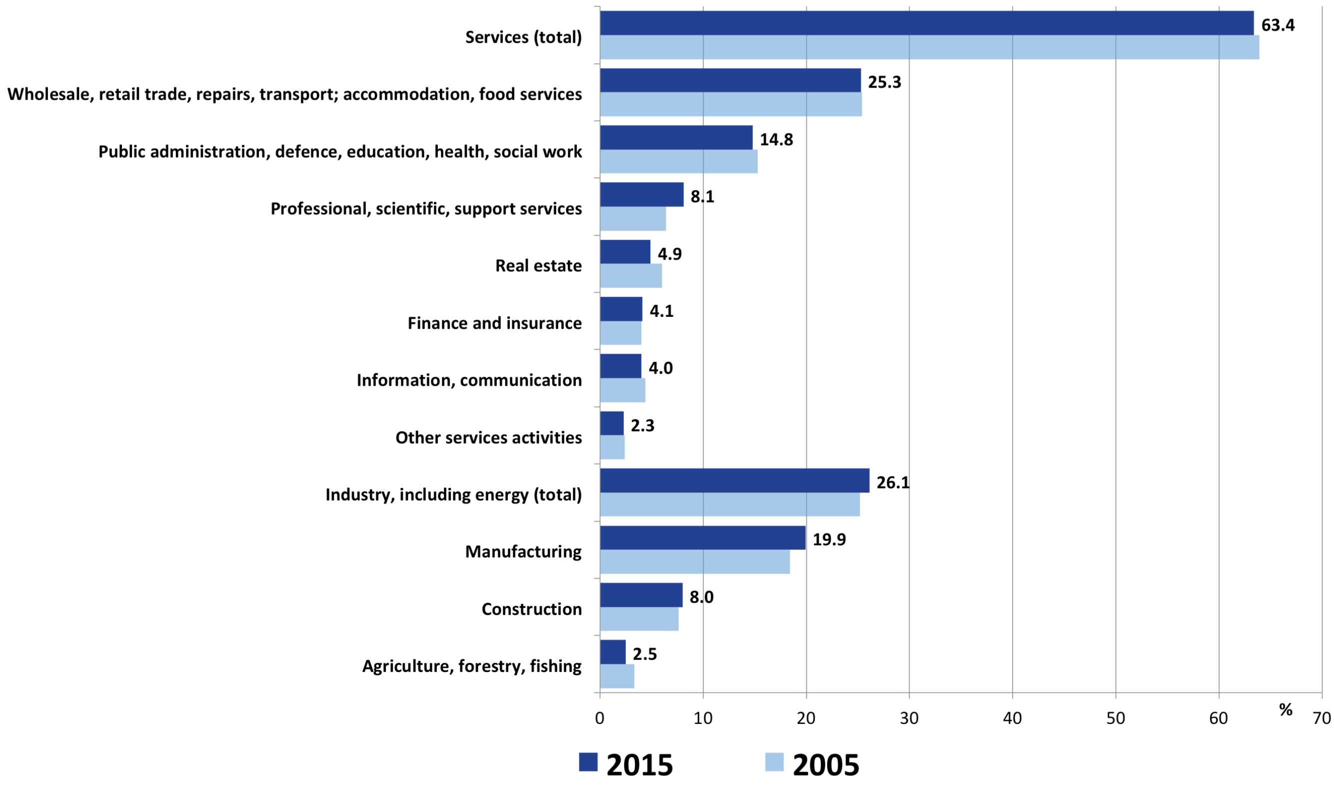

Fig. 2. Gross domestic product of Poland: value added by kinds of economic activity (%) in 2005 and 2015

Source: OECD

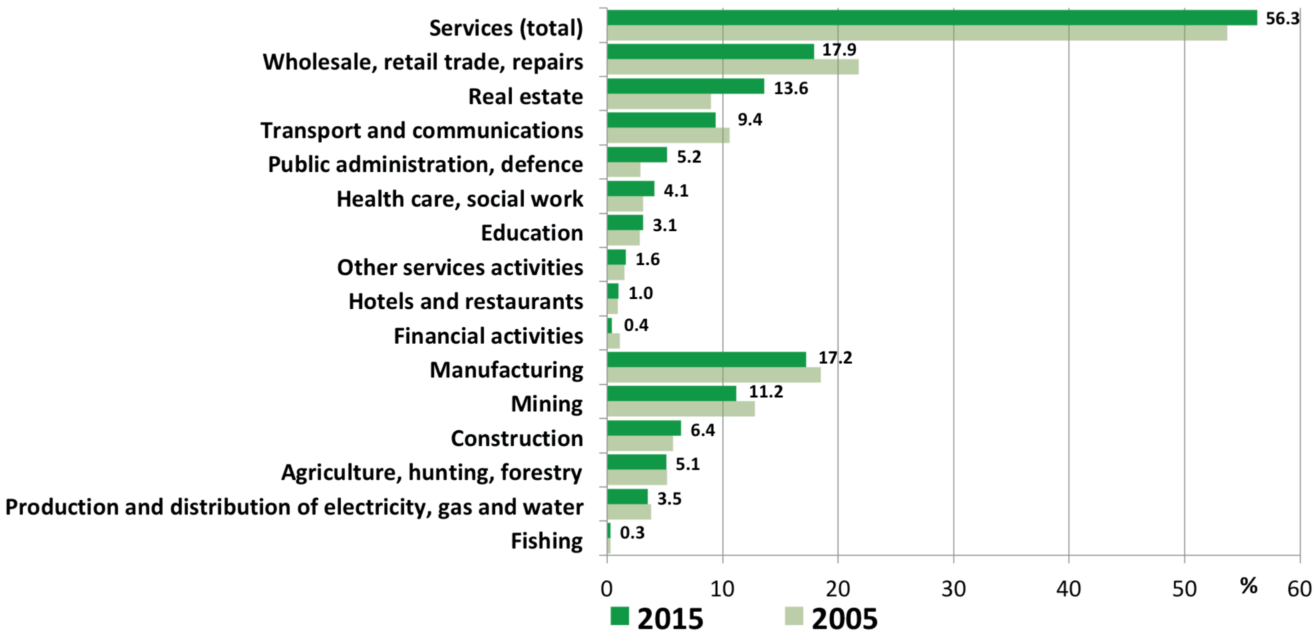

Fig. 3. Gross domestic product of Russia: value added by kinds of economic activity (%) in 2005 and 2015

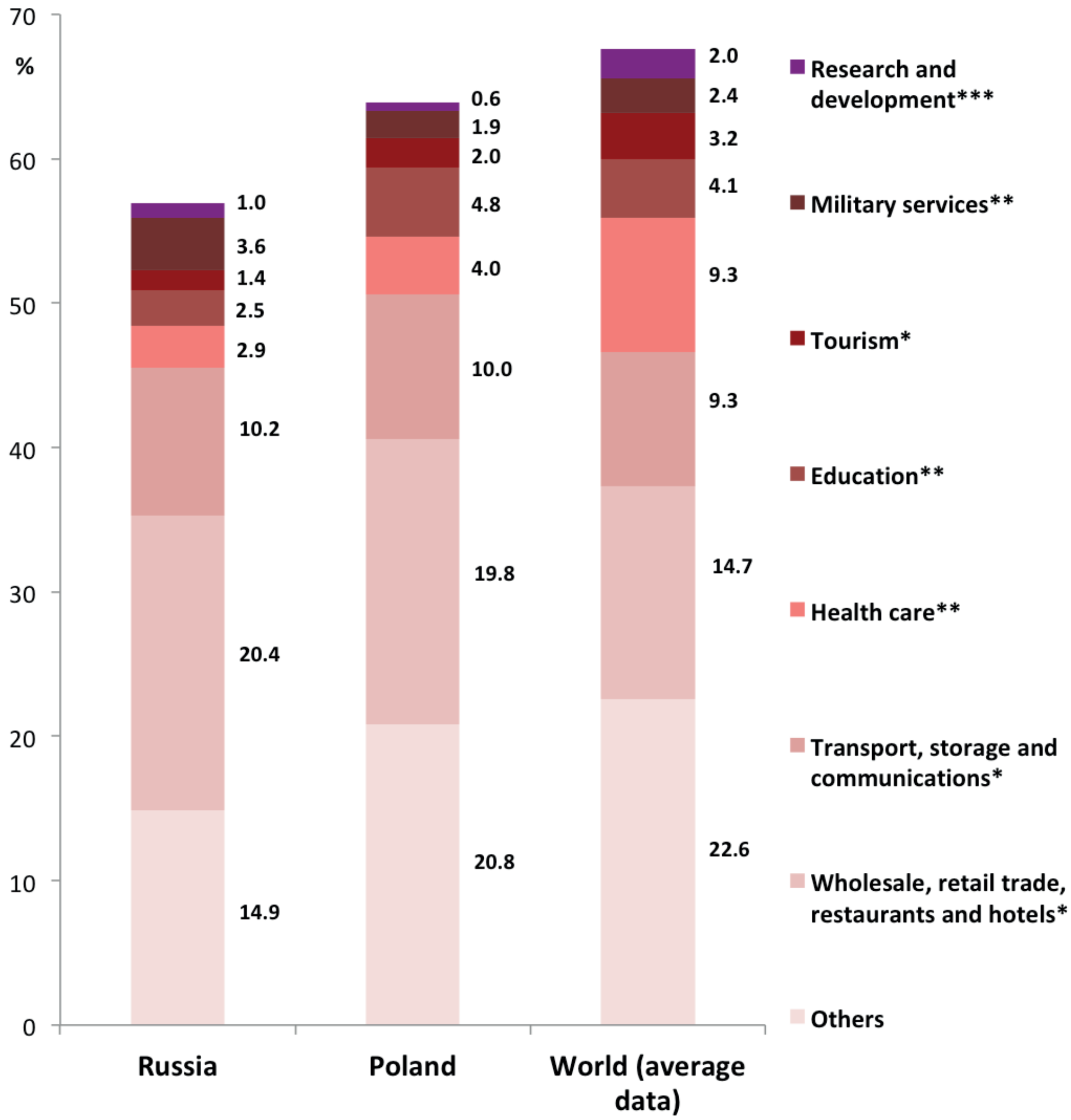

Fig. 4. Services by kinds of economic activity, % of Polish and Russian GDPs in 2005

*value added
**government expenditure
***total expenditure
Source: The World Bank, WTTC, UNCTAD STAT

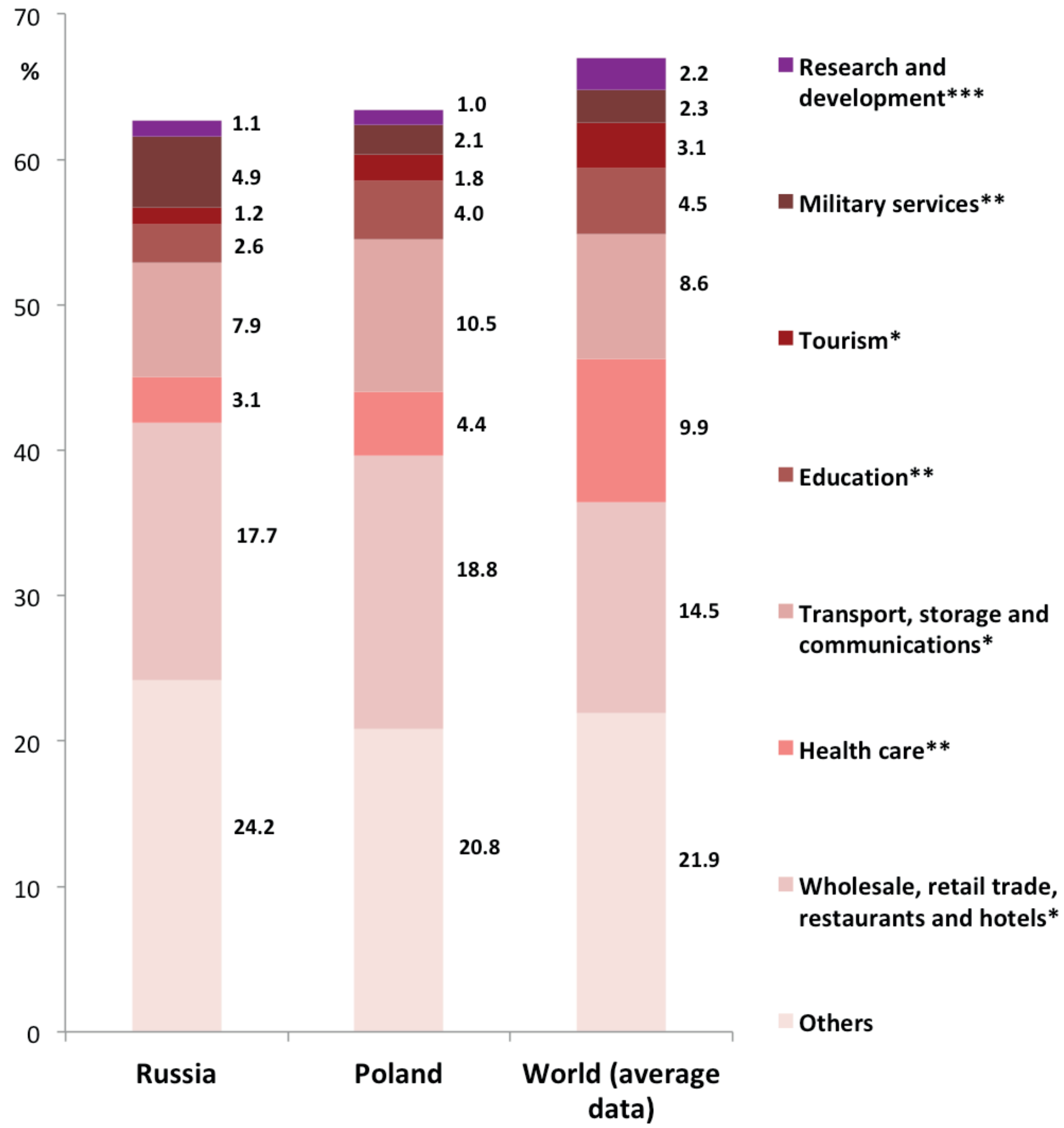

Fig. 5. Services by kinds of economic activity, % of Polish and Russian GDPs in 2015

*value added
**government expenditure
***total expenditure
Source: The World Bank, WTTC, UNCTAD STAT

biggest part of global GDP. At the same time, there is a lack of knowledge-based services in both countries (Fig. 5). The second feature of both Russian and Polish economies is the lower shares of R&D in Russian and Polish GDPs compared with the global average and with developed countries such as the USA, Japan, the UK, France and others. The third key feature is a rather average share of health care and education, which are the main social, human-oriented services in the Russian and Polish economies compared with the world average. The fourth feature is that the contribution of tourism to Russian and Polish GDPs is too small in comparison with the world average. The last but not least – military services share in the Russian service sector is bigger than in Poland and the world average, as well as in many developed countries. In addition, the World Bank and Stockholm International Peace Research Institute (SIPRI) define military services (expenditure) as all current and capital expenditures on the armed forces, including peacekeeping forces, defense ministries and other government agencies engaged in defense projects, as well as paramilitary forces.

Crucial similarities and differences between present state of services as an economic activity in Russia and Poland

According to the conducted research, Central and Eastern European countries have not yet reached the level of global economic leaders in terms of service sector development. For example, according to the World Bank, in 2015, current health care expenditure per capita in the USA was $9503.00, in Germany – $5331.70, in Canada – $4659.20, while meanwhile in Eastern Europe (average data) – $1411.30. Another example – governmental expenditure per capita on education (The World Bank 2014): the USA spent $2729.10, Germany – $2322.20, the United Kingdom – $2317.60, while the average governmental spending on education among 10 Eastern European countries was only $904.50. The strongest differences between «West» and «East» are revealed by matching the total expenditure per capita on R&D. According to the World Bank, the US expenditure per capita on R&D was $1577.00, German was $1375.80, Japanese – $1337.00, while Eastern Europe's – only $234.80 in 2015. According to the World Travel &

Tourism Council (WTTC) data, even if we only analyze tourism as an economic activity, the contribution (value added) of it per capita in Croatia achieved $2760.90, in Italy – $2162.80, in Montenegro – $2065.90 and only $486.50 in Eastern European countries in 2017.

According to the indicators of the service sector, the most developed economies among Central and Eastern European countries are Czech Republic, Hungary, and Slovakia. For instance, in 2015, current health care expenditure per capita in Czech Republic was $2446.00, in Slovakia - $2032.90, in Hungary – $1892.10, and on the contrary, Poland spent $1688.00 per capita and Russia – only $1376.10 per capita. In 2014, the governmental expenditure on education per capita reached $1299.00 in Czech Republic, $1257.70 in Poland, $1223.80 in Slovakia, $1182.30 in Hungary, and in contrast, only $977.20 in Russia. Analyzing total research and development expenditure per capita, the highest-ranking Eastern European country is Czech Republic ($652.20) followed by Hungary ($360.20) and Slovakia ($347.90). Russia and Poland spent just $280.00 and $266.80 per capita on R&D respectively. Otherwise, Russia and Poland hold the top positions among Eastern European economies by military expenditure per capita. In 2017, expenditure per capita on military services amounted to $1088.30 in Russia and $568.00 in Poland. Nevertheless, the military expenditure per capita in the USA was nearly twice the military expenditure per capita in Russia and accounted for $1874.80 in 2017.

Contributions of tourism services to the Russian and Polish economies are rather insignificant. According to the World Travel & Tourism Council (WTTC), in 2017 contribution (value added) per capita of tourism to Polish GDP amounted to $559.80 and only $316.30 in Russian GDP. The Central and Eastern European countries with the biggest contribution of tourism to GDP per capita are Czech Republic ($936.70), Slovakia ($809.30) and Hungary ($622.50).

Thus, Russia and Poland occupy middle positions in the presented rankings. As was mentioned above, Czech Republic, Slovakia and Hungary are the leaders in terms of service indicators. Some Eastern European countries are ranked at the bottom in almost all presented rankings, lower than the majority of former USSR republics and former republics of Yugoslavia. The indicators are especially low in the Republic of Moldova and Ukraine. (Tkachuk 2019) One of the main reasons for the low indicators per capita (value added, expenditure) by crucial kinds of services could be the devaluation of national currency, and economic and political crises in the Republic of Moldova and Ukraine. For instance, among all Central and Eastern European countries, the Republic of Moldova and Ukraine are highlighted for having the lowest rates of current expenditure per capita on health care ($514.40 and $487.60 respectively in 2015), governmental expenditure per capita on education ($374.50 and $509.20 respectively in 2014), total expenditure per capita on research and development ($18.70 and $49.10 respectively in 2015), contribution per capita of tourism to GDP ($54.70 and $133.70 respectively in 2017), value added per capita of wholesale, retail trade, restaurants and hotels ($944.90 and $1414.90 respectively in 2016), value added per capita of transport, storage and communications ($695.30 and $1008.80 respectively in 2016).

CONCLUSIONS

Central and Eastern European countries have the unique experience of economic transformations – from planned economy to market economy, from industrialization to tertiarisation, and to new emerging reindustrialization. Both Russia and Poland still have developed industries. The secondary (industrial) sector developed in the 20th century, including manufacturing activities. As a result, the contribution of the secondary sector to Russian and Polish GDPs is still relatively high. The share of the secondary sector in Poland and Russia is still significant in the economy, unlike in Western European countries. «Traditional» (not advanced) services still hold the main share in the Polish and Russian tertiary sectors. As an assumption, there is a possibility that Russia and Poland can follow the path of development and economic experience of Germany and Japan, which managed to combine developed industries with an excellent level of provided services.

One of the main challenges that both Russia and Poland are facing is the need for an increase in government expenditures on social and basic services such as health care, education and research & development. According to present indicators, Russia and Poland are still behind the most highly developed countries and some Central and Eastern European countries. The most alarming situation in the economy and particularly in the services (especially the social services) can be seen in the Republic of Moldova and Ukraine as a consequence of political and military crises and unsustainable socio-economic development.

The insights of each service and their impacts on economic and social development of Russia, Poland and other countries or macro regions are worth studying in future research projects. In the geography of services, and in the case of Russia and Poland, the issue of unerring tertiarisation or re-industrialization is still open and controversial.

REFERENCES

Achkasova T.A. (2013). Geography of tertiary sector. In: Gorkin A.P. (ed.), Social and economic geography: concepts and terms, Reference book, Smolensk: Ojkumena, 65 (in Russian).

Aleksandrova A.Y. (2016). Typology of countries of the world according to the development level of international tourism. Geography and Natural Resources, 37(1), 18-25.

Alekseev A.I., Kovalev S.A. and Tkachenko A.A. (1991). Geography of services: key concepts and terms. Tver' (in Russian).

Bell D. (2004). The Coming of Post-Industrial Society: A Venture in Social Forecasting. Moscow: Academia (in Russian).

Bolatov M.O. and Savlov M.E. (2016). The Role of Federal States and Cities in Forming the Tertiary Sector of the German Economy. Regional Studies, 1-51, 37-48 (in Russian).

Castells M. (2000). The Information Age: Economy, Society and Culture. Moscow: Higher School of Economics (in Russian).

Clark C. (1940). The conditions of economic progress. London: Macmillan.

Chojnicki Z. (1991). Basic methodological problems of the development of Polish geography. Poznan: Adam Mickiewicz University (in Polish).

Dominiak J. (2018). Contemporary Issues of Services in Light of Polish Geographic Literature. Studies of the Industrial Geography Commission of the Polish Geographical Society, 32(4), 163-175.

Dominiak J. and Hauke J. (2015). The changes of the services sector in Poland and other EU countries. In. Churski P., Kopczewska K., (red.), Regional Studies, 41-42, 37-50.

Dominiak J. and Rachwał T. (2016). Chief Development Tendencies, Structural Changes and Innovativeness of the Industrial and Service Sectors in Poland. Questions Geographic, 35(4), 49-69.

Drucker P. (1993). Post-Capitalist Society. New York: Harper Business.

Drucker P. (2002). Managing in the Next Society. New York: St. Martin's Press.

Fisher A. (1939). Production, primary, secondary and tertiary. Economic Record, 15(1), 24-38.

Fourastié J. (1949). The great hope of the XXth century. Technical progress, economic progress, social progress. Paris: University Press of France (in French).

Giarini O. (1986). Coming of age of the service economy. Science and Public Policy, 13(4), 209-215.

Gierańczyk W. and Rachwał T. (2012). Structural changes in the industry of Poland against the background of Eastern European Union States. Questions Geographic, 31(2), 83-93.

Gorkin A.P. (2007). Postindustriality of the world economy. Bulletin of Moscow University, Ser. 5, Geography, 5, 3-9 (in Russian).

Jakubowicz E. (1993). Methodological Foundations of the Geography of Services. Wroclaw: Wroclaw University (in Polish).

Kenessey Z. (1987). The primary, secondary, tertiary and quaternary sectors of the economy. Review of Income and Wealth, 33, 359-385.

Kovalev S.A. (1966). Geography of consumption and geography of services. Bulletin of Moscow University, Ser. 5, Geography, 2, 3-10 (in Russian).

Kovalev S.A. (1973). On the geographical research of services. Bulletin of Moscow University, Ser. 5, Geography, 6, 3-12 (in Russian).

Kruzhalin V.I. (2011). Tourism and recreation: fundamental and applied research in Russia. GEOGRAPHY, ENVIRONMENT, SUSTAINABILITY, 1(4), 104-107.

Miles I. (2005). Innovation in services. In: Fagerberg J., Mowery R., Nelson R. (ed.): The Oxford Handbook of Innovation (pp. 433–458). Oxford: Oxford University Press, 433-458.

Pokshishevskij V.V. (1972). Geography of services, challenges, content and the place among economic and geographical disciplines. Geography of services / Questions of Geography, 91, 6-26 (in Russian).

Poland in the geographical centre of Europe: political, social and economic consequences (2006). In Miroslawa Czerny (ed.). New York: Nova Science Publishers.

Polarczyk K. (1971). The result of the work as the basis for the definition and classification of services and the sphere of services. Legal, Economic and Sociological Movement, 1, 189-203 (in Polish).

Povitchannaja E.E. (1964). The structure and level of services of large industrial centers of the Left Bank Ukraine. In Donetsk-Pridneprovsky Economic Area: Economic Geography: The Republican Interagency Scientific Book, 1, 42-48 (in Russian).

Rifkin J. (2011). The third industrial revolution: how lateral power is transforming energy, the economy, and the world. New York: St. Martin's Press.

Savlov M.E. (2013). Macro-Geographical features of the tertiary sector of world economy. Bulletin of Moscow University, Ser. 5, Geography, 2, 19-24 (in Russian).

Savlov M.E. (2016). Formation of sectoral structure of tertiary sector of world economy. Dissertation of Cand. Sci. (Geogr.), Moscow: Moscow State University (in Russian).

Savlov M.E. (2018). Methodology for assessment of tertiary sector structure of the world economy. Izvestiya of RAS, Geographic series, 1, 21-30 (in Russian).

Sivickij A.B. (1998). Terminological problems of service sector geography. Bulletin of Moscow University, Ser. 5, Geography, 2, 18-22 (in Russian).

Tkachuk L. (2019). Geopolitical Risks in International Tourism: Methods of Analysis. GEOGRAPHY AND TOURISM, 7(1), 53-62

Toffler A. (1980). The third wave. New York: Morrow.

Voskolovich N.A. (2017). Economics of Paid Services: A Textbook and a Workshop for Bachelor and Master Courses. Moscow: Yurayt Publishing House (in Russian).

Werwicki A. (1998). Changes in the paradigm of the geography of services. Geographic Overview, 70(3-4), 249-267 (in Polish).

Zubarevich N.V. (2013). Geography of services: new challenges. Geography of population and social geography, 483-491 (in Russian).

Ec.Europa.eu, (2019). The European Commission. [online] Available at: https://ec.europa.eu/sfc/sites/sfc2014/files/2007/nace_rev_2.pdf [Accessed 25 July 2019].

Gks.ru (2018). The Federal State Statistics Service of Russian Federation. [online] Available at: http://www.gks.ru/ [Accessed 15 November 2018].

Oecd.org (2018). The Organisation for Economic Co-operation and Development (OECD). [online] Available at: https://www.oecd.org/ [Accessed 15 November 2018].

Sipri.org (2018). The Stockholm International Peace Research Institute (SIPRI). [online] Available at: https://www.sipri.org/ [Accessed 17 November 2018].

Unctadstat.unctad.org (2018). The United Nations Conference on Trade and Development (UNCTAD). [online] Available at: https://unctadstat.unctad.org/EN/ [Accessed 19 November 2018].

Worldbank.org (2018). The World Bank. [online] Available at: https://www.worldbank.org/ [Accessed 15 November 2018].

Wttc.org (2018). The World Travel & Tourism Council (WTTC). [online] Available at: https://www.wttc.org/ [Accessed 19 November 2018].

RESEARCH PAPER

SPATIO-TEMPORAL CHANGE OF DRAINAGE NETWORK AT HUMAN-NATURE INTERFACE AND ITS FUTURE IMPLICATION TO THE ESTUARINE ENVIRONMENT IN GOSABA ISLAND, SUNDARBAN, INDIA

Soumen Ghosh[1*] and Biswaranjan Mistri[1]
[1]Department of Geography, The University of Burdwan, Bardhaman,West Bengal 713104, India.
*Corresponding author: ghoshsoumen864@gmail.com
Received: March 31th, 2020 / Accepted: November 20th, 2020 / Published: December 31st, 2020
https://DOI-10.24057/2071-9388-2020-63

ABSTRACT. Gosaba C.D. Block is an active tidal island of the Indian Sundarban. In this island, human-induced modification of the natural drainage system poses serious threats to the estuarine environment. It was started during the British colonial period through the construction of embankment to protect the reclaimed coastal land from saline water ingression. The rapid growth of population over the last few decades has triggered the changes in the drainage network and also altered the land use land cover of the study area. The human encroachment on the drainage area has hampered the sedimentation process as well as water circulation in the delta. As a result, the island is gradually transforming into saucer-shaped form, which aggravates various coastal threats like flood inundation, waterlogging and embankment breaching during extreme environmental events. To study the spatio-temporal change of the drainage network pattern from 1955 to 2018, different multi-temporal satellite images, US Army Toposheet, Census of India Report (2001 and 2011) and Human Development Report (2014) have been used as a source of secondary data for the analysis in ArcGIS environment. In addition to this, instrumental surveying has been done to measure the slope direction in relation to land use land cover and a questionnaire survey was conducted to understand the livelihood status of people influenced by various coastal threats and risks due to the drainage congestion. The study reveals that population density has gradually increased in recent decades and is negatively correlated with the drainage density on the island. The choking of the surface drainage canals has increased the problem of waterlogging in agricultural fields, which affected their productivity. Therefore, a strategy for management of the drainage network needs to be urgently implemented in order to protect the life and livelihood of rural people from various coastal threats.

KEY WORDS: Drainage system, Human encroachment, Population growth, Drainage congestion, Coastal threats

CITATION: Soumen Ghosh and Biswaranjan Mistri (2020). Spatio-temporal Change of Drainage Network at Human-Nature Interface and Its Future Implication to the Estuarine Environment in Gosaba Island, Sundarban, India. Geography, Environment, Sustainability. Vol.13, No 4, p. 148-158
https://DOI-10.24057/2071-9388-2020-63

ACKNOWLEDGEMENTS: This study is a part of the M. Phil research work submitted to The University of Burdwan, West Bengal, India. The first author wishes to express his sincere gratitude to the University Grants Commission (UGC), New Delhi for providing fellowship assistance to continue the research work. The authors are also thankful to the anonymous reviewers and respected editors for providing valuable suggestions and constructive ideas to improve the standard of the manuscript. The authors would like to acknowledge local villagers of Gosaba Island for their heartfelt support and response during the field survey. **Conflict of interests:** The authors reported no potential conflict of interest.

Conflict of interests: The authors reported no potential conflict of interest.

INTRODUCTION

The Gosaba Island is a tidally active deltaic plain of Indian Sundarban. Topographically, the delta is a flat alluvial plain lying below the high tide level and crisscrossed by several interlinking rivers and creeks. This drainage system plays a significant role in maintaining the morphological balance of the delta (Mistri 2014). The human being, the most dominant species on the earth surface is continuously modifying the natural environment into the world of artifacts (De 2006). This ceaseless transformation of the estuarine environment is more prominent in the modification of the drainage network, which started since the period of land reclamation (from the 1870s onward). The massive deforestation of mangrove forests during the British colonial period (1870–1947) and unsystematic construction of the embankments along the river have disturbed the fluvio-morphological system of the delta over time. However, is this alteration of natural drainage system at the human-nature interface good or bad? This is a matter of serious concern and needs to be critically reviewed from the environmental perspective

(Bandyopadhyay 2000; Danda 2007; Mistri 2014). In the second half of 20th century, the increasing population pressure exerted a serious threat to the natural resources of the delta and the balance between conservation and utilization of natural resources has posed a serious threat to the life and livelihood of the rural people. The haphazard construction of closures, choking of the drainage canals due to human encroachment and obstruction of the free flow of water has hampered the delta formation processes (O'Malley 1914). As a result, the island gradually develops a saucer shape due to uneven supply and distribution of sediment over the entire delta. The intensive waterlogging in the agricultural fields owing to the mismanagement of the drainage system is responsible for declining economic productivity of the agricultural land (Bannerjee 1988). These constraints aggravate the economic crisis and entrap farmers in pervasive poverty (Mandal 1995). Poverty affects different aspects of social livelihood and creates livelihood conflicts. To address these issues, the present research work focuses on three major objectives. Firstly, the study describes the scenario of human interference in the estuarine environment since the period of land reclamation. Secondly, the research highlights the spatio-temporal change of the drainage network at human-nature interfaces and associated changes in land use land cover. Thirdly, it examines the future threats and risks due to mismanagement of the inland drainage system as well as land-use practices.

THE STUDY AREA

The Indian Sundarban delta is a part of the Gangetic delta, which originated from the recent alluvial deposition by the Ganga-Brahmaputra river and their distributaries (Bandyopadhyay 2003). The development of the delta continues for more than 49.5 million years to the present. The initial 'proto delta' experienced a strong regression of the sea and the coastline shifted southward taking almost the present configuration. The rapid deposition took place during the later part of the tertiary period when the 'modern delta' took its present shape (Sanyal 1999). The initial delta building processes are still active but have been interrupted by various human activities. The present study area, Gosaba C.D. Block is one of the major blocks of Indian Sundarban, it lies within Canning Sub- Division of South 24 Parganas district of West Bengal, India. The areal extension of Gosaba is 21º54´N to 22º08´ N and 88º29´E to 88º49´E (Fig. 1). The region is bounded by the River Bidya in the west and the Gomar and Raimangal Rivers in the east. The Gosaba Island consists of 14 Gram Panchayats (Amtali, Bali I, Bali II, Bipradaspur, Chhota Mollakhali, Gosaba, Kachukhali, Kumirmari, Lahiripur, Pathankhali, Radhanagar-Taranagar, Rangabelia, Satjelia and Sambhunagar) and 50 inhabited villages (District Human Development Report 2009). The total area of the block is 296.43 sq. km and the population density is 830 people/sq. km (Census of India 2011). In Gosaba, 44% of the population is living below the poverty level and 87% of people suffer from food shortages (Halder and Dennath 2014).

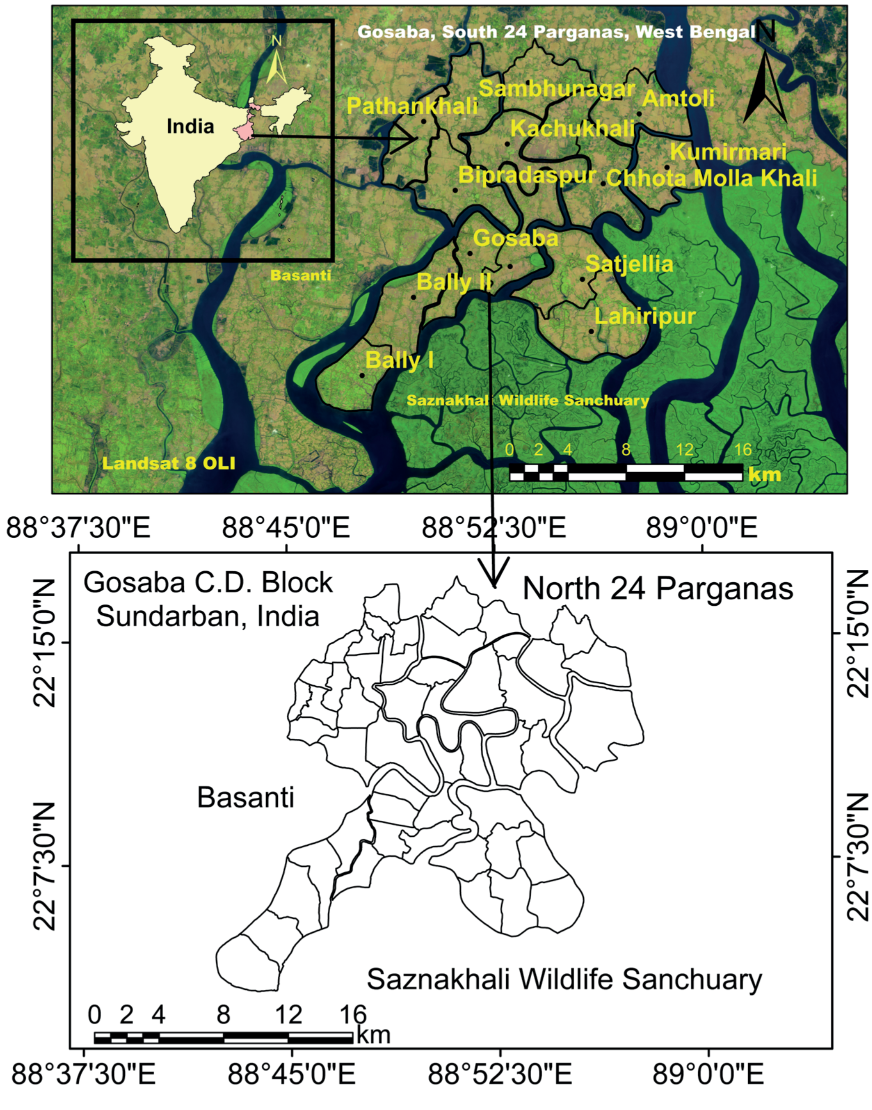

Fig. 1. Location of the study area

Table 1. Details description of data sets for the study

Data Sets	Description	Spatial and Temporal Resolution		Path and Row	Source
		Size of Pixel	Date of Acquisition		
Satellite Data	Landsat MSS	60 m	05-Nov-1972	148 & 45	United States Geological Survey https://earthexplorer.usgs.gov
	Landsat TM	30 m	01 Nov-1997	138 & 45	
	Landsat 8 OLI	30 m	08-Nov-2018	198 & 45	
	LISS III	23.5 m	25-Nov-2017	108 & 56	NRSC, Bhuban http://bhuvan.nrsc.gov.in/data/download/index.php
Population Related Data				Census of India, 2001 and 2011 Human Development Report, 2014	

DATABASE AND METHODOLOGY

The present research work has been done based on both primary and secondary data. Primary data was collected through field surveying along with the questionnaire method. Some field photographs were also collected to show the human intervention on the drainage system. The geo-historical change of Gosaba Island has been studied from various books, journals, and articles. To identify the spatio-temporal change of the drainage network, different multi-temporal satellite images have been used in a GIS environment (Table 1). The on-screen digitization method using polyline feature was adopted for digitizing the drainage network from each satellite image. Thereafter, Image overlay analysis has been done to identify the changing pattern of the drainage network.

Drainage density is an important attribute of the drainage system both from morphological as well as hydrological viewpoints. Drainage density is calculated based on the following formula

$$D_d = \frac{L_u}{A} \quad \text{............. Equation 1............Horton (1945)}$$

Drainage density (D_d) = Stream length (L_u)/Basin area (A)

To understand the population pressure of the study area, population density is calculated based on the following formula

$$D_p = \frac{N}{A} \quad \text{............... Equation 2}$$

Population density (D_p) = Number of people (N)/ Land area (A)

To understand the spatial relationship between population density and drainage density, Pearson correlation is calculated and the statistical significance of this correlation value is also verified using the Student's t-test.

To show the land use land cover changes in the study area, multi-temporal Landsat images of 1972, 1997 and 2018 have been incorporated in the GIS environment. The maximum likelihood classification method has been used for supervised classification of each satellite image. Altogether five LULC classes have been chosen based on the field experience and the author's prior knowledge about the study area.

Gosaba is a flat alluvial island, facing intensive waterlogging problem due to mismanagement of the drainage and land-use system. To understand the minute change of the slope in such a flat alluvial plain, Dumpy level survey has been conducted within a small plot of Gosaba mouza to identify the direction of slope change. The average surface elevation is considered to be 2 meters as collected from the adjacent Gosaba Irrigation Sub-Division Office. The location point data ('X' represents longitude and 'Y' represents latitude) have been collected using GPS receiver. The ground elevation (denoted by Z value) data was surveyed using a Dumpy Level. After getting XY and Z values, the Reduced Level (RL) has been calculated based on collimation method. The DEM is prepared using the spatial analysis tool in the ArcGIS environment incorporating XY and Z values. The contour map is also prepared from DEM to understand the change of the slope direction.

A land-use map has also been prepared using the Georeferenced Google Earth Image (US Dept. of State Geographer, Imagery date 12/8/2018) and cadastral map (Gosaba mouza, Gosaba, Scale-1:2500) in the GIS environment. The horizontal positional accuracy (RMSEr) of Google Earth high-resolution rural imagery is 4.2 meter (Mean-3.4 meter; SD-2.3 meter) from 2008 onward which is reliable for scientific study (Paredes-Hernandez et al. 2013). The following equation was used for the calculation of RMSEr, taken from Federal Geographic Data Committee (FGDC1998).

$$RMSE_x = \sqrt{\frac{\sum_i \left(x_{data,i} - x_{reference.i}\right)^2}{n}} \tag{1}$$

$$RMSE_y = \sqrt{\frac{\sum_i \left(y_{data,i} - y_{reference.i}\right)^2}{n}} \tag{2}$$

$$RMSE_r = RMSE_X^2 + RMSE_y^2 \tag{3}$$

Where, $x_{data,i}$ $y_{data,i}$ are the co-ordinates of the i^{th} point in the evaluated dataset

$x_{reference,i}$ $y_{reference,i}$ are the co-ordinates of the i^{th} point in the independent reference dataset of higher accuracy

'*n*' is the number of checkpoints; '*i*' is an integer that ranges from 1 to n. This land-use map was compared with the previous elevation and slope map to understand the problem of surface slope modification and the extent of human encroachment on abundant channels, locally known as khals, at the human-nature interface.

RESULTS AND DISCUSSION

Evolution of the Drainage and Land Use at the Human-Nature Interface

Rivers act as a lifeline for the sustenance of the daily livelihood in the estuarine Sundarban. The interconnected network of the drainage pattern has been modified and encroached by various human activities for their short-term benefits. This intervention on the drainage system was started during the British colonial period (from the 1870s onward) by the clearing of dense mangrove forests and the land reclamation after the construction of the embankment. (Kanjilal 2000; Bandyopadhyay 2000; Danda 2007). However, large scale land reclamation in Gosaba Island was initiated in the late nineteenth century by Sir Daniel Hamilton, A Scottish businessman who took lease around 9000 acres of land in Sundarban (lots no 143 and 149) (Das 2016). Initially, there were only 900 people (Census of India, 1909) living in this Island, that migrated from neighboring states like Jharkhand, Odisha and surrounding districts. In each phase of the land reclamation, people have neglected the role and importance of the river to the estuarine environment and modified the drainage system according to their own needs. During the early 19th century, frequent flooding was a curse for the sustenance of the livelihood of the people who initially settled in this island. So, an initiative was taken to construct a large-scale embankment along the rivers to prevent saline water intrusion in the agricultural land, which has stopped the natural process of delta building and changed the morphological appearance of the delta (Dhara and Paul 2016). The average elevation (6m from mean sea level) of the island remains below the high tide and storm surge levels, therefore this delta is always prone to several hazards such as saltwater intrusion and coastal flooding because of the embankment breaching and overtopping (Hazra et al. 2002). During the post-colonial period (1955–2018), the characteristics of the land use have rapidly changed due to the fast growth of the decadal population which reaches 10.67 % from 2001 to 2011. During the field survey, it was observed that encroachment of the creek estuary, haphazard construction of closures and transformation of land use characteristics exert huge pressure on land use land cover (Fig. 2). The transformation of land use is more prominent in the conversion of agricultural and fisheries-related land during the last four decades. Numerous creeks of this island have been disconnected from their parent source and transformed by human activities into sweetwater ponds for irrigation as well as fisheries-related activities. These types of changes in land use have altered the morphological as well as hydrological equilibrium of the delta with time.

Spatio-temporal Change in the Drainage Network

The large-scale transformation of the drainage channels into water bodies, that are mainly used for fisheries, and subsequent disappearance of creeks from the delta at the human-nature interface are quite common in entire Sundarban but in the present study, these spatio-temporal changes of the drainage network were analyzed for Gosaba Island over the periods of 1955–1972, 1972–1997 and 1997–2018. Different layers of the drainage network were overlaid to understand the sequential change of the drainage pattern over the last six decades (1955–2018) and these changes are shown in Fig. 3. Before the land reclamation, the island was fully covered by dense mangrove forests but after human footprint on the delta in the late nineteenth century, the pattern of the surface drainage has been immensely modified at the human-nature interface. The haphazard construction of closures and illegal encroachment on the drainage has modified the lateral connectivity of the drainage network. The drainage density has also decreased over time. The total area of the

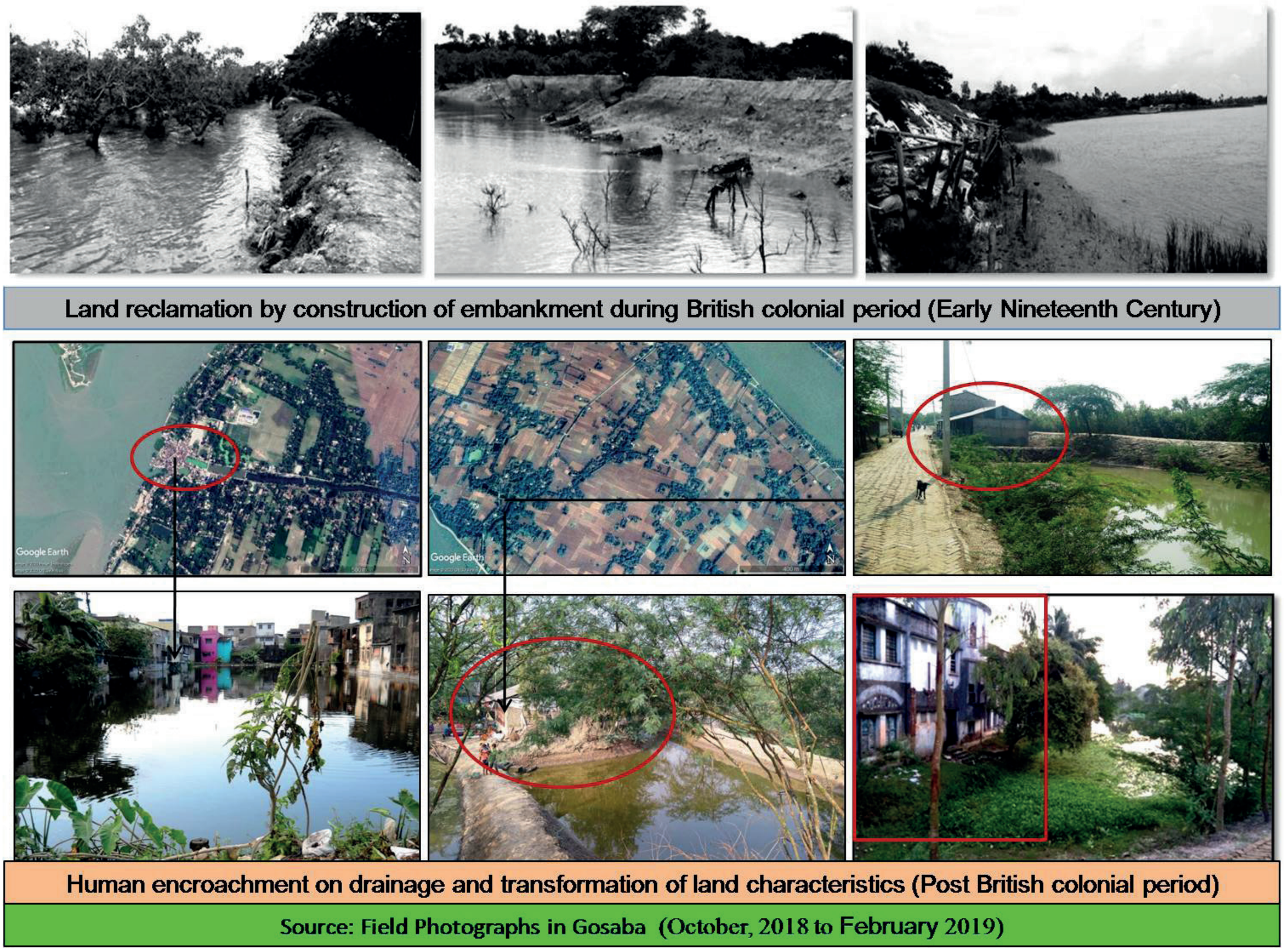

Fig. 2. Human interventions on drainage channel

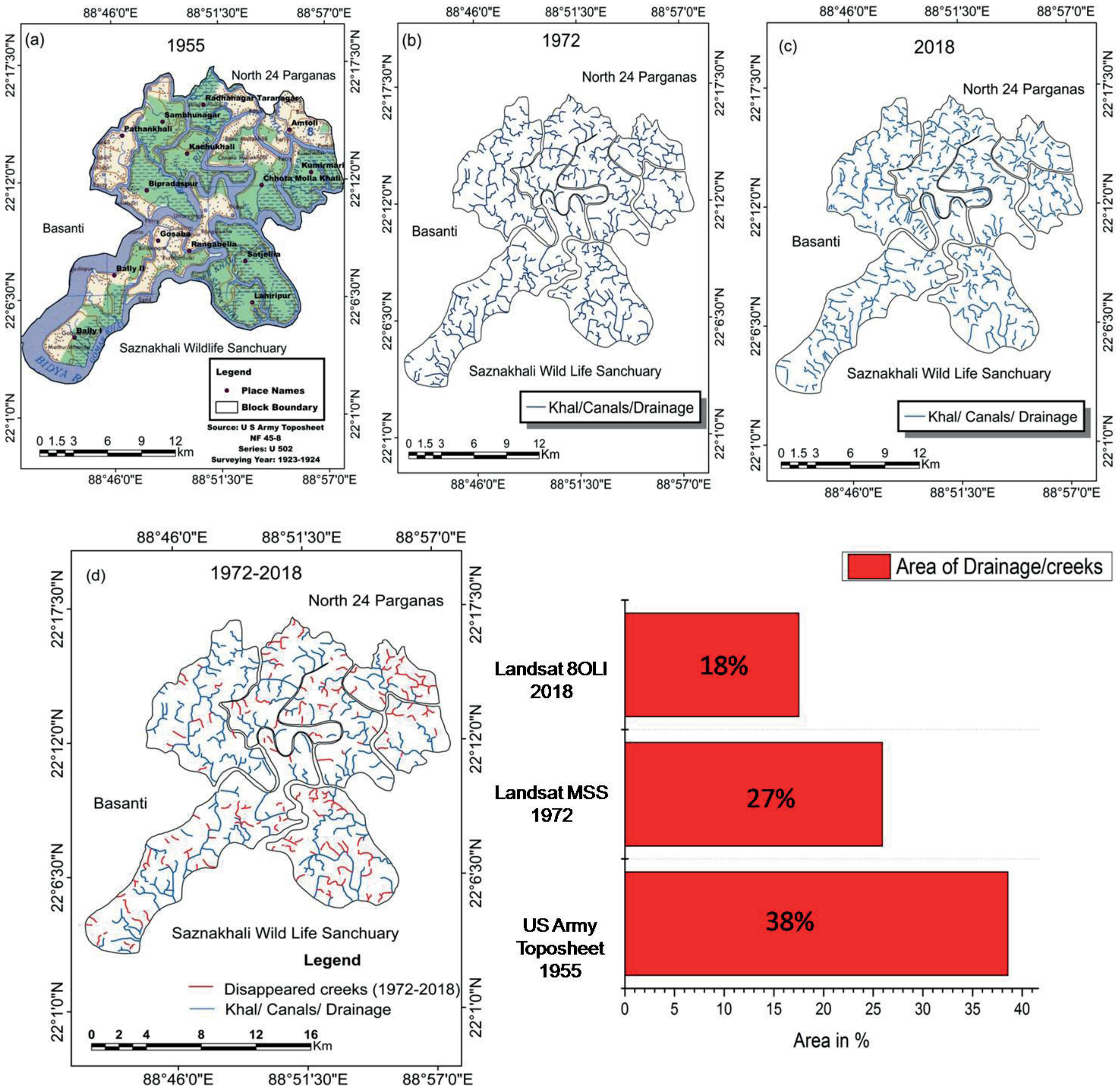

Fig. 3. Spatio-temporal change of the drainage network (1955–2018)

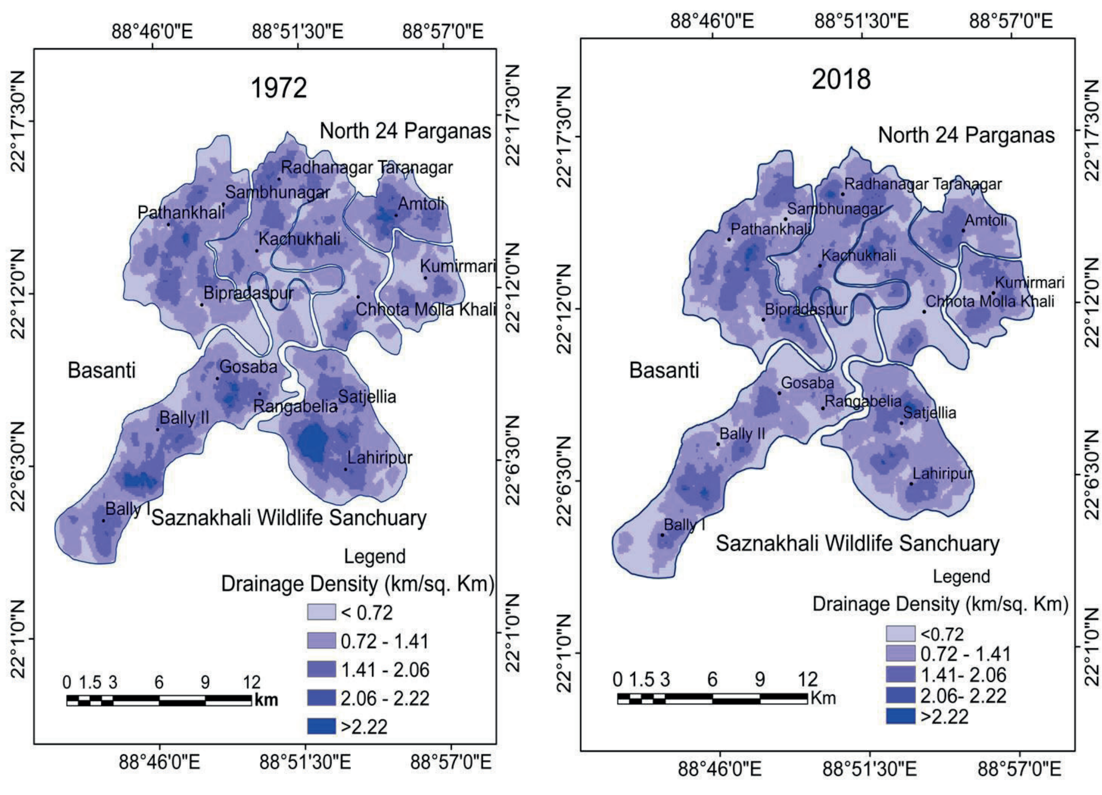

Fig. 4. Spatio-temporal change of drainage density

drainage network in 1955 stood at 38% and has gradually declined to 18% in 2018. The lack of interconnectivity within the drainage network creates drainage congestion, which induces the waterlogging problem in several places within the island.

Spatio-temporal Change in the Drainage Density

Drainage density was first used by Horton (1945) to understand different hydrological parameters. The drainage density depends on the pattern and arrangement of the drainage network and determines the efficiency of the drainage system (Gray 1965). As the spatial arrangement of the drainage network has been continuously modified at the human-nature interface, the drainage density shows a continuously decreasing trend from 1.13 km/sq. km in 1972 to 0.91 km/ sq. km in 2018 (Table 2, Fig. 4). Thus, the drainage density shows a negative change of -0.21 km/sq. km from 1972 to 2018. The change of drainage density was the highest in Gosaba G.P. (-0.29), Lahiripur G.P. (-0.41), Bally I G.P. (-0.34). Chotomollakhali G.P. (-0.30) and Bipradaspur G.P. (-0.29). The medium rate of change was observed

Table 2. Change of the drainage density in different Gram Panchayats of Gosaba C.D. Block

Sl. No.	G.P. Name	Drainage Density (km/sq. km)		Change of Drainage Density (km/ sq. km)
		1972	2018	1972–2018
1	Bipradaspur	1.20	0.91	-0.29
2	Sambhunagar	1.01	1.00	-0.01
3	Pathankhali	1.05	0.90	-0.15
4	Radhanagar Taranagar	1.23	1.00	-0.23
5	Kachukhali	1.26	1.05	-0.21
6	Amtoli	0.91	1.10	0.19
7	Kumirmari	1.19	1.16	0.03
8	Bally I	1.15	0.81	-0.34
9	Bally II	1.27	1.19	-0.08
10	Lahiripur	1.24	0.83	-0.41
11	Satjelia	0.84	0.74	-0.10
12	Chotomollakhali	1.27	0.97	-0.30
13	Gosaba	1.28	0.41	-0.87
14	Rangabelia	0.92	0.78	-0.14
Average		1.13	0.91	-0.21

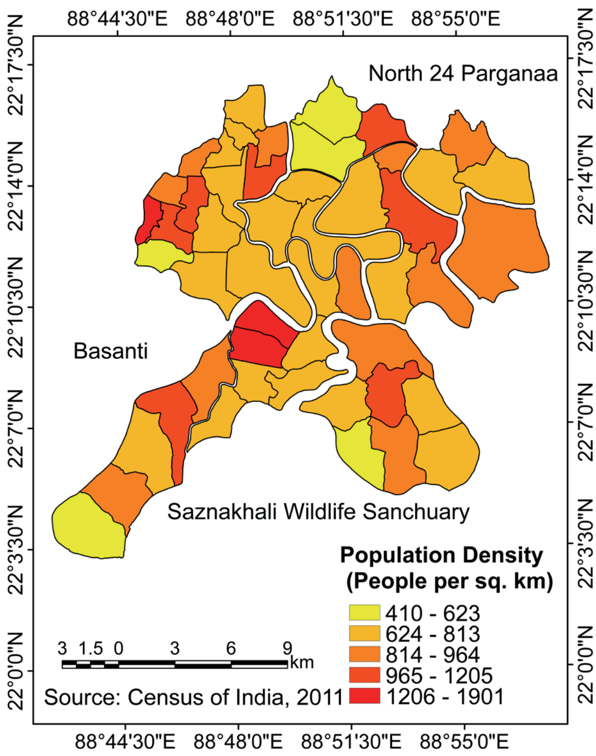

Fig. 5. Population Density in 2011

for Radhanagar Taranagar G.P. (-0.23), Kachukhali G.P. (-0.21), Pathankhali G.P. (-0.15) and Rangabelia G.P. (-0.14). Sambhunagar G.P. (-0.01), Bally II G.P. (-0.08) and Kumirmari G.P. (-0.03) are characterized by the low change of the drainage density. During the field survey, it was observed that different types of human activities, started primarily through land reclamation and embankment construction, were the major cause of the drainage system decay and human encroachment along with unsystematic land-use practices exert massive stress on functioning of the drainage system of the delta in the recent decades.

Impact of Population Density on Drainage Density

The rapid growth of population had an adverse impact on the drainage density in the study area. In the present study, the population density map was prepared based on the latest data of Census of India, 2011 to understand the spatial concentration of the population with relation to the drainage density in various Gram Panchayats (Fig. 5). The study reveals that there is a negative relationship between the population density and drainage density, which means that higher population density corresponds to lower drainage density and vice versa. To understand the relationship between these two variables in quantitative terms, the Pearson Correlation analysis was performed. In the scatter plot, the values of population density are shown on the X-axis as it is considered an independent variable and the values of the drainage density are shown on the Y-axis as it is considered a dependent variable. The position of these paired values shows a graphical correlation between the studied variables. The correlation values were used to draw the best fit line. Here, the type of polynomial regression was used as it better depicts the correlation. The correlation coefficient value here is negative ($r = -0.49$, $r^2 = 0.245$) (Fig. 6). This value indicates that the growth of population has negatively influenced the drainage density of the Gosaba C.D. Block. To test the significance of the 'r' in the present study, the Student's t-test has been performed in MS Excel 2007 platform. The details are presented in Table 3. To perform the Student's t-test, the alpha value was set to 0.05 and the calculated P-value was equal to 0.00, which is less than 0.05 (Table 3). Therefore, this statistical analysis clearly shows that there is a significant difference between the means of the two selected variables.

Dynamics of the Land Use Land Cover Change

To assess the land use land cover change of the study area, different multi-temporal satellite images have been used in the Remote Sensing and GIS environment. Five LU/LC categories were identified i.e. (1) River and Water Bodies (2) Agriculture with Fallow Land (3) Agriculture without Fallow Land (4) Settlement with Vegetation and (5) Mangrove Forest. The LU/LC change was estimated for the years 1972, 1997 and 2018. The study shows that the percentage of area of river and water bodies has rapidly decreased over the years, it was estimated at 14.10% in 1972, 10.11% in 1997 and 7.29% in 2018. This decrease is mainly due to rapid growth of population (10.67% from 2001 to 2011, Census of India), illegal encroachment of khals and conversion of water bodies into the land. The total area of agricultural land has also decreased from 1972 to 2018. The area of agricultural land with fallow stood at 40.54% in 1972, 44.28% in 1997 and 45.87% in 2018 whereas the area of agricultural land without fallow has reduced from 23.97% to 14.69%. Interaction with the farmers during the field survey revealed that extreme weather events in recent years and increasing salinity of the soil after severe cyclone Aila in 2009 has led to a decrease in agricultural production, so much that certain farmers intend to engage in alternative economic activities. Most of the agricultural land remains fallow during Boro season mainly due to lack of irrigation facilities and accumulation of salt in surface soil due to active capillary process. The area of settlements has rapidly increased from 18.42% in 1972 to 28.41% in 2018.

Table 3. Calculation table of the t-test

Variables	Mean	Variance	Pearson Correlation	N	df	Alpha Value	Remarks
Population Density (2011)	855.07	20443.16	-0.44	14	13	0.05	Statistically Significant
Drainage Density (2018)	0.92	0.0406					

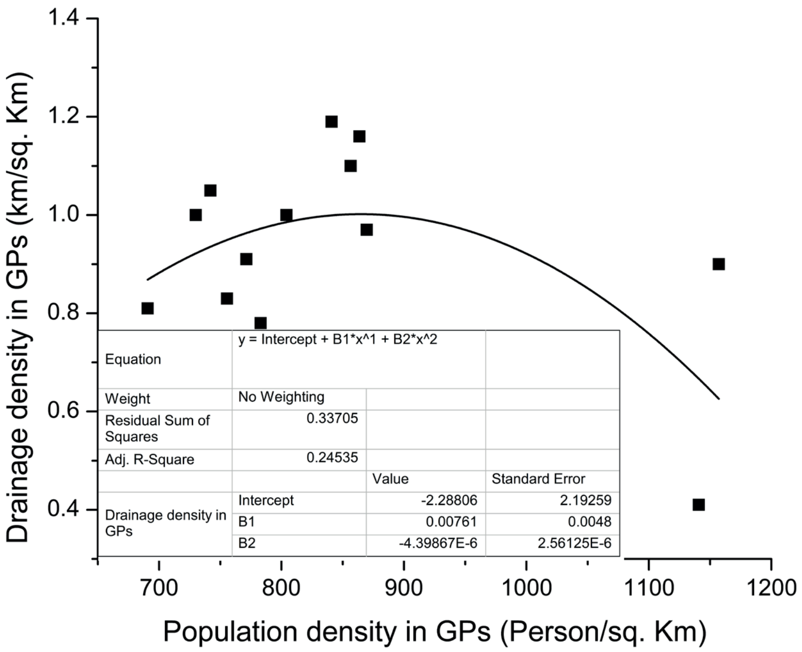

Fig. 6. Relation between population density and drainage density

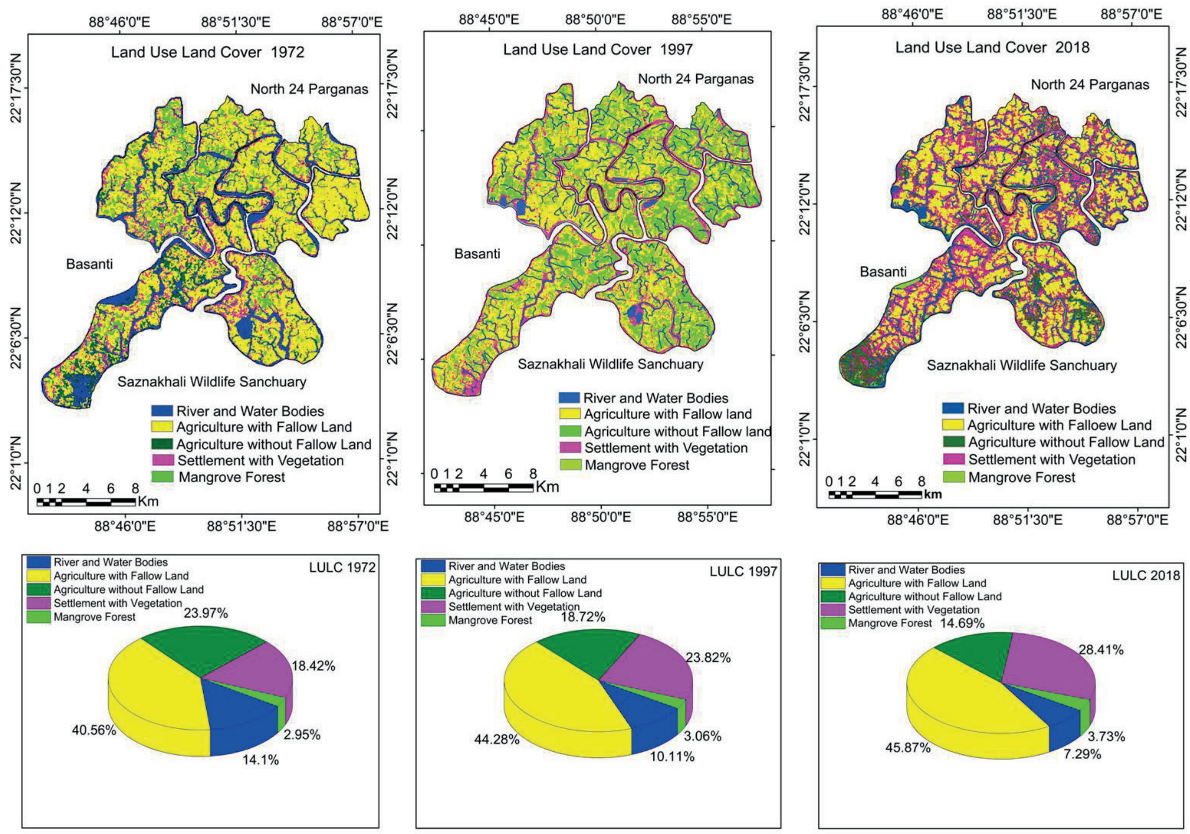

Fig. 7. LU/LC classes in 1972, 1997 and 2018

Table 4. LU/LC classes of the study area in 1972, 1997 and 2018

LU/LC Classes	1972		1997		2018		1972–2018
	Area (sq. km)	Area (%)	Area (sq. km)	Area (%)	Area (sq. km)	Area (%)	Change of area (%)
River and Water Bodies	41.50	14.10	29.75	10.11	21.46	7.29	-6.81
Agriculture with Fallow Land	119.31	40.54	130.32	44.28	135.00	45.87	5.53
Agriculture without Fallow Land	70.56	23.97	55.09	18.72	43.24	14.69	-9.28
Settlement with Vegetation	54.21	18.42	70.13	23.83	83.62	28.41	9.99
Mangrove Forest	8.68	2.95	9.01	3.06	10.98	3.73	0.83

There is a significant growth observed in mangrove forest cover in newly formed river chars and channel bars. The share of mangrove forest cover was 2.95% in 1972, 3.06% in 1997 and has slightly increased up to 3.73% in 2018 (Table 4, Fig. 7).

Future Threats and Risks

Being located in the low-lying coastal region makes the Gosaba Island more vulnerable to various coastal hazards like floods, cyclone, embankment breaching and sea-level rise. The large-scale modification of the natural drainage pattern due to human interference and subsequent disappearance of the drainage network from the delta is a triggering factor of various coastal vulnerabilities and creates potential threats as well as risks for the livelihood of rural people.

Risk of Flood Inundation

Most of the area in Gosaba Island is lying below the high tide level. Since the period of land reclamation, the linear pattern of settlement has been built up primarily along the embankment for easy access to water and transportation facilities. Embankment acts as a coastal safeguard for local inhabitants, despite that coastal region adjacent to rivers and creeks have been frequently inundated due to embankment breaching and resultant overtopping of tidal water. During the field survey, it was observed that height of the embankment is not enough to protect people from water inundation during catastrophic rainfall and cyclones as observed during severe cyclone Aila in May 2009 and more recent Bulbul in November 2019. Some field observations in Rangabelia, Birajnagar and Bagbagan mouzas in Gosaba C.D. Block have shown that there are locations (Fig. 8) where the height of the embankment is less than half a meter above the high tide level. As a result, people who are living adjacent to the coast, are frequently flooded and the risk of inundation as well as the duration of inundation has increased multiple times due to poor drainage condition of the delta. The drainage, haphazard construction of closures and lack of sufficient sluice gates create obstructions in the water circulation system, which increases the risk and vulnerability of the area to coastal flooding during catastrophic events.

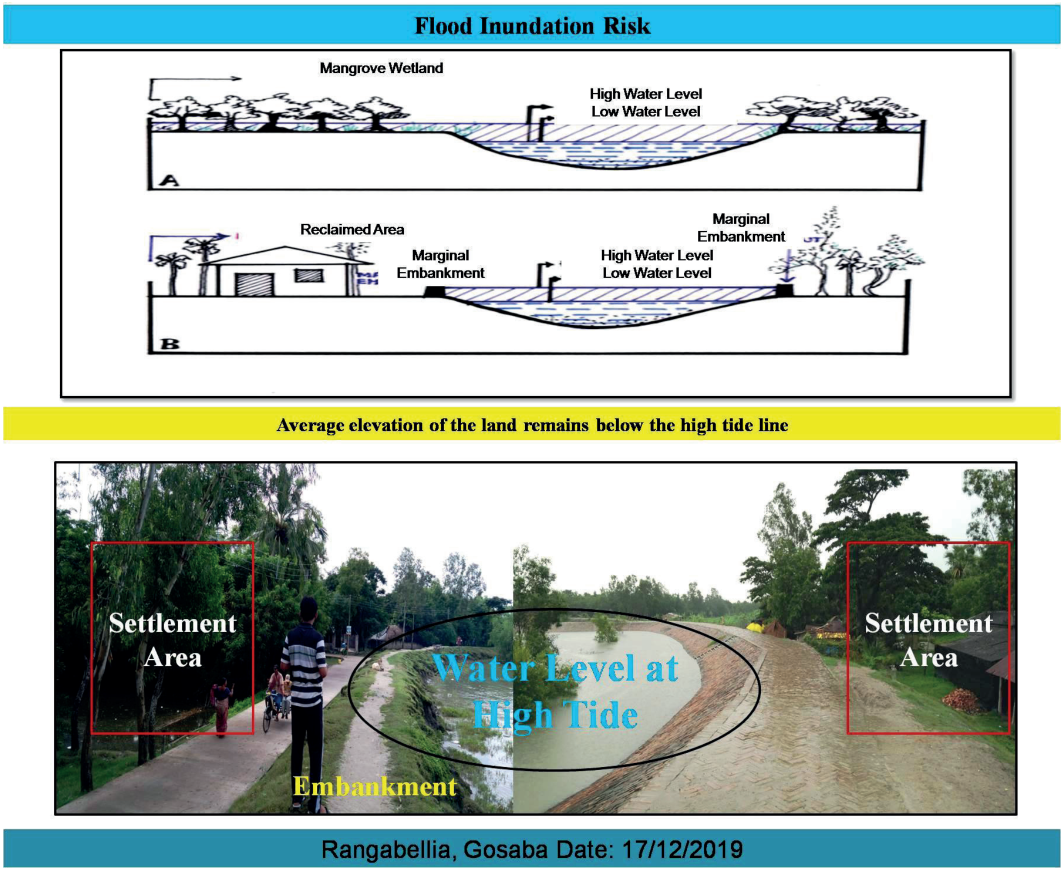

Fig. 8. Risk of flood inundation

The problem of Waterlogging in Agricultural Land

Gosaba is one of the worst suffering blocks in the Indian Sundarban facing acute problem in agriculture because of the poor drainage system. The profound human intervention on the drainage has interrupted the processes of delta building. The gradual human encroachment in various creeks of the estuary has disturbed the sediment as well as water circulation system within the delta. As a result, intensive siltation of the river bed and adjacent floodplains has gradually increased the elevation of the riverine floodplain as compared to the inward land of the island. The inward land is used for agriculture which is extremely prone to waterlogging especially during monsoon season. The change of surface slope direction with relation to land use land cover is presented in Fig. 9. To overview the slope change, a section of Gosaba Mouza was surveyed using dumpy level along with a GPS. The elevation profile shows that there is an inverse relationship between the slope and the distance from the canal within the surveyed section of the interfluve zone. The profile depicts the presence of the saucer shape agricultural land within the delta. Some field photographs have been collected to understand the intensity of the waterlogging problem in agricultural fields caused by the drainage congestion. Almost 68% of the total cultivable land is low lying, mono-cropped and facing acute problem of waterlogging because of excessive rainfall coupled with poor drainage condition (Source: Field Survey in 2018). Management of the drainage system and the land-use practices have received scanty attention and the local people are least concerned about these types of changes despite the fact that disturbing the natural system without any environmental impact assessment may come out as a serious threat to the people's livelihood.

Drainage Congestion and Livelihood Conflicts

Drainage is an important part of the sustainable livelihood of people from the very beginning of human civilization on earth. The role of rivers is unquestionable for human survival and there is no question of conflict at all. However, is the word «conflict» justifiable or not in the context of the present research? It is a matter of debate. The imprudent human intervention on the drainage as well as unsystematic land-use practices has affected the agricultural productivity of the island. There are 75% of people who depend on agriculture for their basic livelihood. It was estimated by the field survey (2018) that production of Aman paddy has decreased by almost 35% to 45% due to waterlogging in agricultural fields. People have very few options for alternative economic activities, which means that they have to rely on agriculture as their mainstay. Agriculture is not profitable at all and does not allow people to secure their minimum needs of a basic livelihood. As per field observations, the low income of farmers especially engaged in monocropping has led to a decline in their standard of livelihood (Table 5). Low literacy rate, early marriage and out-migration are the most common problems of people living on this island, which is also directly or indirectly correlated with their level of income. So, the poor drainage condition has led to a decline in the economic condition of people. The poor economic condition of people has also reinforced other social issues. The human-induced modifications of the natural drainage system will give rise to these conflicts and their future consequences if no management action plan is implemented immediately.

CONCLUSIONS

The life and livelihood of rural people are closely associated with the drainage system of the island. In the

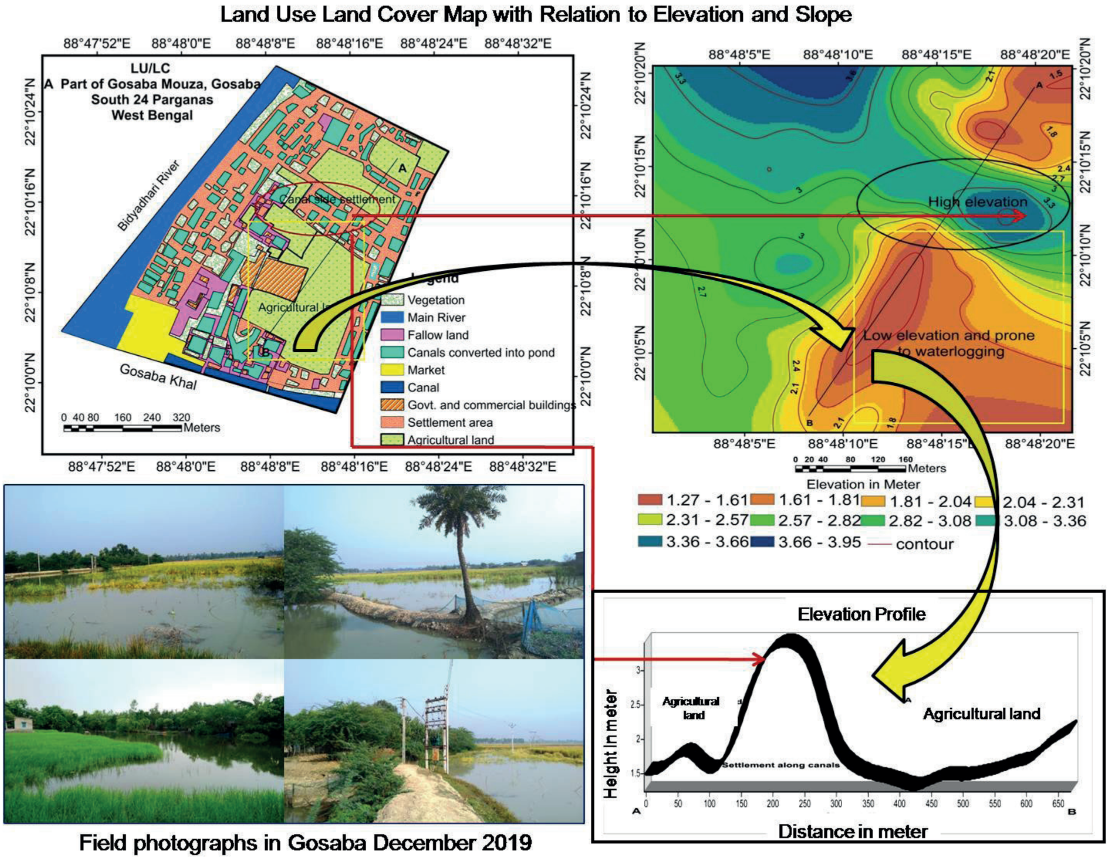

Fig. 9. Problem of waterlogging in agricultural field

Table 5. Livelihood aspects of the people engaged in the farming system

Aspects of Livelihood**	Monocropping (mainly rice farming)			Integrated Farming (Rice+fish or Rice+fish+on dyke horticulture)		
	Sample Size	Response	%	Sample Size	Response	%
Income level (<6,000 Rs./month)	80*	47	58.75	80*	38	47.50
Literacy Rate (able to read write and speak their mother tongue)		33	41.25		44	55.00
Early Marriage (below 18 for female and 21 for male)		32(F)	40.00		24(F)	30.00
		22(M)	27.50		15(M)	18.75
Rate of Migration		42	52.50		30	37.50

**Farmers surveyed (Field Survey: October 2018 - February 2019) those who are affected by waterlogging and engaged in monocropping or integrated farming system to sustain their livelihood.
* Surveying method stratified random sampling in some selected GPs of the Gosaba block.

present study, some issues related to the human-induced drainage congestion and its future consequences are highlighted. Firstly, since the period of land reclamation, the pattern of the surface drainage system has been imprudently modified by various human-induced activities for some short-term benefits without considering its future adverse impact on the delta. The continuous human encroachment on the surface drainage system and subsequent disconnection from the Source River increased the coastal vulnerability during sudden environmental hazards and disasters. Secondly, the interconnectivity of the drainage network and drainage density has been gradually decreasing due to the rapid growth of population in the last few decades. As a consequence, long-duration water inundation caused by poor drainage system became a serious problem for the coastal dwellers, especially during catastrophic events. Thirdly, the saucer shape of the island causes the problem of waterlogging in the agricultural fields, which is directly and indirectly affecting the socio-economic condition of rural people. Therefore, the protection of the natural drainage system is urgently needed in order to improve the livelihood of local people and minimize various threats of drainage congestion. The long-term management strategy for the drainage system is very important although, challenging task due to the conflict between the riot land and common property resources. Therefore, the management of agricultural land through the implementation of land reshaping techniques may emerge as an alternative solution for the farmers to reduce their monetary loss due to the drainage congestion and resultant waterlogging. They can adopt location-specific integrated farming activities like rich-fish-on dyke horticulture system to increase the agricultural productivity and efficiency of land use, which at the same time will increase the relative profitability and ensure better livelihood of the people.

REFERENCES

Central Soil Salinity Research Institute, Regional Research Station, Canning Town, West Bengal, India, Coastal Soils of West Bengal – Their Nature, Distribution and Characteristics, Bulletin No. 1/2003 by B. K. Bandyopadhyay, M. Maji, H. S. Sen, N. K.B. Tyagi, 2003.

Bandyopadhyay S. (2000). Coastal changes in the perspective of long-term evolution of an estuary: Hugli, West Bengal, India. In: V. Rajamanickam and M.J. Tooley (Eds.), Quaternary Sea Level Variation, Shoreline Displacement and Coastal Environments, New Delhi: New Academic Publishers, 103-115.

Banerjee A. (1998). Environment, Population and Human Settlement, New Delhi: Concept Publishing Company, 27-32.

Census of India (2011). Provisional Population Totals. Registrar General and Census Commissioner of India, Ministry of Home Affairs, New Delhi, India. Available at: https://censusindia.gov.in/2011census/dchb/DCHB_A/19/1917_PART_A_DCHB_SOUTH%20TWENTY%20FOUR%20PARGANAS.pdf [Accessed on 15 March 2019].

De K. (2006). Environmental impact of human Interface in the Sundarban Region of West Bengal. Burdwan: The University of Burdwan. Available at http://hdl.handle.net/10603/64002 [Accessed 16 December 2019].

Danda A.A. (2007). Surviving in the Sundarban: Threat and responses- An analytical description of life in an Indian riparian commons. The Netherlands: University of Twente. 1-195. ISBN: 90-365-2566-4.

District Human Development Report South 24 Parganas, 2009. Development & Planning Department, Government of West Bengal. 1-20 Available at: http://www.undp.org/content/dam/india/docs/hdr_south24_parganas_2009_full_report.pdf. [Assessed on 12 November 2019].

Das K. (2016). Sundarban embankments – a study along Suryaberiya River, Sambhunagar Island, Gosaba, West Bengal. International Journal of Current Research, 8(5), 32187-32195.

Dhara S. and Paul A.K. (2016). Status of agriculture -a case study at Patharpratima Block of South 24 Parganas district. International Journal of Innovative Science, Engineering & Technology, 3(2), 239-246.

Federal Geographic Data Committee (1998). Geospatial positioning accuracy standards. Part 3: national standard for spatial data accuracy. USA: U.S. Geological Survey. Available at https://www.fgdc.gov/standards/projects/FGDC-standards-projects/accuracy/part3/chapter3 [Accessed on 16 December 2019].

Gray D.M. (1965). Physiographic Characteristics and the Runoff Patterns: Proc.of Hydrol. Symp. No. 4, Research Watershed, National Research Council of Canada, 147-164.

Halder A. and Debnath A. (2014). Assessment of climate induced soil salinity conditions of Gosaba Island, West Bengal and its influence on local livelihood. In: M. Singh et al. (Ed.), Climate Change and Biodiversity: Proceedings of IGU Rohtak Conference, 1, Advances in Geographical and Environmental Sciences Japan: Springer, 27-44, DOI: 10.1007/978-4-431-54838-6_3.

Hazra S., Ghosh T., Das Gupta R., Sen G. (2002). Sea level and associated changes in the Sundarban. Science and Culture, 68(9), 309-321.

Kanjilal T. (2000). Who killed the Sundarban. Calcutta: Tagore Society for Rural Development.

Mistri B. (2014). Construction of Closure on tidal creeks and its effects: A case study of Patharpratima C.D. Block of Sundarban. Nature and Sustainable Development-Impact of Green Accounting, Published by Academic Staff College, The University of Burdwan. 111-124.

O'Mally L.S.S. (1914). Rivers of Bengal, Bengal District Gazetteers. Calcutta: The Bengal Secretariat Book Depot.

Mandal J. (1995). Implementation of Integrated Rural Development Programme – A Case Study of Sundarban, West Bengal. New Delhi: Jamia Millia University.

Paredes-Hernandez C.U., Salinas-Castillo W. E., Guevara-Cortina F. and Martinez-Becerra X. (2013). Horizontal positional accuracy of Google earth's Imagery over rural areas: a study case in Tamaulipas, Mexico. Boletim de Ciências Geodésicas, 9(4), 588-601, DOI: 10.1590/S1982-21702013000400005 [Accessed on 22 December 2019].

Sanyal P. (1999). Global warming in Sundarban delta and Bengal Coast. In: Guha Bakshi DN, Sanyal P, Naskar KR (eds), Sundarbans Mangal, Kolkata: Naya Prokash, 111–112.

RESEARCH PAPER

NATURAL AND HUMAN-INDUCED LAND DEGRADATION AND ITS IMPACT USING GEOSPATIAL APPROACH IN THE KALLAR WATERSHED OF TAMIL NADU, INDIA

Abdul Rahaman S.[1*], Aruchamy Solavagounder[1]
[1]Department of Geography, School of Earth Science, Bharathidasan University, Tiruchirappalli – 620024 Tamil Nadu, India
***Corresponding author:** abdulatgeo@gmail.com
Received: June 1st, 2020 / Accepted: November 20th, 2020 / Published: December 31st, 2020
https://DOI-10.24057/2071-9388-2020-105

ABSTRACT. Land degradation is human-induced and natural process that adversely affects the land, to function effectively within a complex ecosystem. In recent years, the Kallar watershed has encountered various kinds of multifarious problems on both land and water in the urban and its environs. The upper part of the study area is facing water scarcity problems in the past few years, but which included no such rare occurrences in the past. The mid-portion in the vicinity of foothills are highly affected by soil erosion, whereas the lower portion of the area has faced problems like land degradation, such as an unusual increase of wastelands and conversion of good agriculture lands into construction plots. Apart from these, the study area is frequently affected by nature induced disasters like a landslide, forest fire, flooding, and drought. In this complex situation, the qualitative assessment of human-induced land degradation and its impact is essential. For this, Geospatial-based Multi-Criteria Evaluation (MCE) as a multidisciplinary approach has been adopted. To assess land degradation, six major criterions are preferred such as terrain (slope, elevation), environment (landuse/land cover, NDVI), soil erosion, and demography (population density). Considerable weights and ranks were assigned through an empirical MCE method. Based on the criteria, the land degradation was carefully delineated into five significant categories such as low (38.3%), moderately (23.6%), marginally (15.4%), highly (4.8%), and severely degraded (17.8%). The depletion of vegetation cover on hilly terrain and subsequent cultivation without proper protection measures constitute the possible reason for severe soil erosion and land degradation.

KEY WORDS: Land Degradation, Soil Erosion, Analytical Hierarchy Process, Sustainability

CITATION: Abdul Rahaman S., Aruchamy Solavagounder (2020). Natural And Human-Induced Land Degradation And Its Impact Using Geospatial Approach In The Kallar Watershed Of Tamil Nadu, India. Geography, Environment, Sustainability, Vol.13, No 4, p. 159-175 https://DOI-10.24057/2071-9388-2020-105

ACKNOWLEDGMENT: I would like to acknowledge the UGC – Basic Science Research Fellowship scheme for aiding me to carry out my research work. Also, thank the UGS-SAP-DRS I & II project scheme of Department of Geography, Bharathidasan University for providing high-resolution IRS LISS IV data products for the analysis. I am grateful to SAA, KAR, Meena Gopi, and MJ for their support in the editing of the manuscript.

Conflict of interests: The authors reported no potential conflict of interest.

INTRODUCTION

Globally, land degradation predominantly occurring in the arid, semi-arid, and dry sub-humid regions (UNCCD 1999; IPCC 2001) due to unstable climatic conditions and human activities which invariably causes severe ecological and socio-economic issues in the current scenario (Omar et al. 2013). It critically involves two complex systems: the natural ecosystem and the human social system (Barrow 1994; Scott and Conacher 2008). It implies the loss of productive potential, increasing unsustainability, and potential instability. The land experiences unfavourable impact on agricultural productivity and ecological function which ultimately affects human sustenance and essential quality of life (Taddese 2001; Eliasson et al. 2003; Masoudi 2014; Pan and Li 2013; Barzani and Khairulmaini 2013; Masoudi and Amiri 2015; Masoudi et al. 2018).

The key concept of land degradation «refers to the deterioration or total loss of the productive capacity of the fertile soils for present and future use» (FAO 1980). Such potential losses are due to various forms of soil erosion by different agents, along with chemical and physical deterioration. It involves two physical processes: soil erosivity (tending to cause erosion by the erosive agents such as wind and water) and soil erodability (susceptible to erosion) (Morgan 1983; Rahaman et al. 2015; Nitheshnirmal et al. 2019). Soil degradation is not only the interaction between physiochemical and biological factors but also includes soil properties, climatic factors and topography (Taguas et al. 2015; Brevik et al. 2015; Bhattacharyya 2015). Additionally, it includes human factors and landuse management practices (Khaledian et al. 2017; Camprubi et al. 2015; Cerda et al. 2016).

Sustainability obtains the substance for today's leading global framework for international cooperation. The 2030 Sustainable Development Agenda and it is Sustainable

Development Goals (SDGs), has 17 SDGs. Each of the 17 SDGs includes specific targets to be achieved by 2030. The goals and targets are universal; it denotes, they apply to all countries around the world, not just to underprivileged countries (SDG guideline 2017). Present research broadly focuses on one of the important Sustainable Development Goals (SDGs) that is Life on Land (Goal 15). It refers to protect, restore and promote sustainable use of terrestrial ecosystems, sustainable forest management, combat desertification, and eradicate and minimise land degradation and biodiversity loss (UN 2015). The 15.1, 15.2 and 15.3 targets and global indicators of 15.2.1, and 15.3.1 have been considered and its details are given below.

Under international agreements (15.1) the objective is to ensure the conservation, restoration and sustainable use of forests, wetlands, mountains and drylands by 2020. It also includes effective implementation of sustainable management of all forests; halt deforestation, degraded forests, increase afforestation and reforestation globally (15.2). By 2030, combat desertification, restore degraded land and soil, including land affected by desertification, drought and floods, and strive to achieve a land degradation-neutral world (15.3).

The present study focuses on the above-mentioned SDG main targets of which the following two global indicators were addressed in detail with appropriate case studies such as (1) Progress towards sustainable forest management (15.2.1); (2) Proportion of land that is degraded over the total land area (15.3.1). Globally many organizations and scientific communities have intensively involved and concentrated on land degradation and desertification (UNCCD, IPCC, etc). Numerous independent, academic researchers from around the world are working extensively on monitoring land and environmental degradation (Naseer and Puneeta 2018; Xie 2020; Rahaman and Venkatesh 2020). Those studies were used individually and multi factors were used to assess and monitor land degradation. The assessment of land degradation represents a multifaceted process. It is not a single factor outcome; relatively, an integrated property of interacting human and biophysical factors (Svensson 2005; Masoud 2018; Venkatesh et al. 2020). These works address the role of human activity in land degradation and their influencing factors such as unplanned landuse practices, over utilisation of agricultural lands, conversion of agricultural land into settlement plots, inappropriate conservation methods, planning, land management, and tourism activities. From an ecological and socioeconomic perspective, the selection of appropriate factors such as vegetation, soil, climate, terrain, and demographic layers were evaluated. Within these thematic factors soil erosion, landuse/land cover, NDVI, slope, elevation, and population density were assessed in detail.

Empirical evaluation of soil erosion is one of the key factors in the land degradation assessment. In recent years, as a part of the environment and land degradation assessment policy for sustainable agriculture and development, soil erosion is recognised increasingly as a hazard, which is a serious issue in mountain areas (Millward and Mersey 1999; Angima et al. 2003; Jasrotia and Singh 2006; Dabral et al. 2008; Sharma 2010). Every year around the world 75 billion tons of soil is eroded from the earth's surface, which is about 13-40 times as fast as the natural rate of erosion (Zuazo et al. 2009). Asia has the highest soil erosion rate of 74 tons/acre/year, (El-Swaify 1997). In India, 45% (130 Mha) of the total geographic area is affected by severe soil erosion through ravines, gullies, shifting cultivation, sandy areas, cultivated wastelands, deserts, and waterlogging. The Kallar watershed has a maximum annual soil loss of 398.5 t/ h^{-1}/ y^{-1} and >100 ton/ h^{-1}/ y^{-1} which is about 15 % (200 km^2) of the geographic area (Abdul et al. 2015).

Land degradation eventually leads to enduring and apparent loss of vegetation cover, reduced biomass productivity over time and space (Prince et al. 2009; Jong et al. 2011; Nicholson 1998; Helldén 2008; MEA 2005), it can be detected by comparing actual vegetation levels with potential levels (Haboudane et al. 2002; Eisfelder et al. 2012; D'Odorico et al. 2013; Zhou et al. 2015). Among numerous vegetation indices, the Normalized Difference Vegetation Index (NDVI) (Lin et al. 2016; Wessels et al. 2006, Rahaman et al. 2017a) has demonstrated its reliability in monitoring land degradation. However, the declining NDVI range is associated with various natural factors, i.e. unpredicted rainfall, seasonal variation, and human activity (landuse). Change detection studies of LULC have proven to be effective in assessing the potential adverse impacts on the environment (Leh et al. 2013; Pankaj, et al. 2019; Rahaman et al. 2020). Through LULC Dynamics and simulation models, the extent of land degradation at the landscape level can be evaluated and effective strategies for land management can be developed (Gessesse et al. 2015; Rahaman et al. 2017a).

Abiotic ecological factors like terrain conditions and soil characteristics also influence land degradation in the mountain regions. Terrain conditions determine soil erosion hazards. In mountain areas terrain factors such as elevation and slope play a significant role in land degradation. The steep slope and high elevation mountain/hill lands are more prone to water-related soil erosion, which increases the severity of soil degradation (FAO 1990). Human interventions are highly dominant in low altitude and moderately slope areas, hence being a crucial factor for extensive deforestation in those areas. Increasing population growth combined with other factors causes extensive environmental deterioration on a large scale (FAO/RAPA 1990, p.10).

Currently, the UNCCD has not yet approved any recommended methodology to calculate these indicators mentioned in 15.1 &15.2 (Olena Dubovyk 2017). Few agencies have tried to implement Land Degradation Neutrality based on Soil values and its landuse changes in Germany (Stephanie et al. 2018). The Geospatial based multi-criteria evaluation approach is widely used; it is an accepted model that assesses land degradation at various scales and it supports researchers and policymakers to take appropriate decisions. Remote sensing techniques have emerging technology in spatial information studies. The principles of repetitiveness and consistency, are the prerequisites for land degradation monitoring (Olena 2017). Remote Sensing technology provides significant information for integrated approaches to combining satellite data with specific tools, geographic information system (GIS) analysis, and modelling techniques (Röder et al. 2008). Analytical hierarchy process (AHP) is one of the multi-criteria decision analysis that is popularly utilised to make a decisions related to spatial issues. Several studies were conducted through geospatial techniques coupled with the AHP method i.e. landslides, prioritization of watersheds and many other spatial issues (Feizizadeh and Blaschke 2014; Abdul et al 2014; Rahaman et al. 2015, and 2017b; Ghorbanzadeh et al. 2017). It evaluates various multi-factors and helps to take appropriate decisions to achieve the target objectives.

Over the years, increasing population, growing industrialisation, expanding agricultural activity and rising living standards have increased land degradation and extensive deforestation in mountain areas, especially in the Kallar watershed. Limited studies were attempted in the aspects of desertification, biodiversity loss, etc. Due to this, there is a lack of natural and human-induced land degradation assessment in the mountainous terrain along with the semi-arid region. This research aims to assess natural and human-induced land degradation factors and their impact in the Kallar watershed. To achieve this aim, the following objectives were framed: Determination of land degradation criteria (physical, climatic, environmental and demographic). Integration of various factors to delineate the land degradation vulnerable zones using AHP and GIS within the watershed and to suggest appropriate land resource planning methods, effective management practices and conservation measures in these areas.

DATA AND METHODOLOGY

Study Area

Stretching from west to east, the Kallar watershed is situated in the Eastern part of the Western Ghats. Being a part of the Bhavani River basin, its main river sources are from Moyar and River Bhavani. Spatially located between 11°17´0´´ to 11°31´0´´ N Latitude and 76° 39´ 0´´ to 77° 8´ 45´´ E Longitude it covers an area of 1281.2 km². It comprises of three districts: The Nilgiris, Coimbatore, and Erode, it includes 6 taluks (Coonoor, Kothagiri, Udhagamandalam, Mettupalayam, Coimbatore north, and Sathyamangalam); and 89 Revenue villages (Fig. 1). The maximum and minimum elevation encountered in the watershed is about 177 m and 2615 m above MSL. About 50% of these areas are covered with mountains that have diverse plant communities. These diverse plan communities consist of various types of forest cover and agricultural activities, such as tea, coffee plantation, vegetables, and orchards, which are cultivated in the upper and the lower regions. This region is salubrious experiences a temperate climate for more than half of the year. The average day temperature of the watershed is 20.15° C to 30° C and the average rainfall is about > 1400 mm. The winter is relatively cool. The maximum rainfall is received during October and November. The Kallar streams flow from the Southwest to the north-eastern region of the Western Ghats. Being built-in the north-eastern part of the watershed, the Bhavanisagar dam serves as the primary source of irrigation and hydroelectric power generation. This area is covered by clayey soil, loam soil, and rock outcrop on steep to narrow slope landform. Geomorphologically, the watershed is characterised by steep structural hills, denudational hills, narrow gorges, and intermountain valleys. Geologically, charnockite, and fissile hornblende-biotite gneiss covers a major portion of the study area.

DATA

The assessment of land degradation is influenced by multiple factors that were collected and extracted from different data sources. In this study, baseline layers were generated from the Survey of India (SOI) toposheets 58 A/11, 15, 16 and 58E/3 & 4 at the scale of 1:50,000. The Landsat 8 Operational Land Imager (OLI) data were downloaded from the United States Geological Survey (USGS) Global Visualization Viewer (GloVis) web portal (https://glovis.usgs.gov). Applied pre-processing techniques like atmospheric and radiometric corrections were calibrated for post-processing. Landsat 8 images for the years of 2012 and 2015 with the spatial resolution of 30 m were used to generate two important factors such as NDVI and landuse land cover. IRS – Linear Imaging Self-Scanning Sensor-4 (LISS IV) data product in the year of 2015 with the spatial resolution of 5.8 m was used to classify various landuse classes by manual digitization method and was compared with the existing and present condition of landuse / land cover. Comparisons with the generated

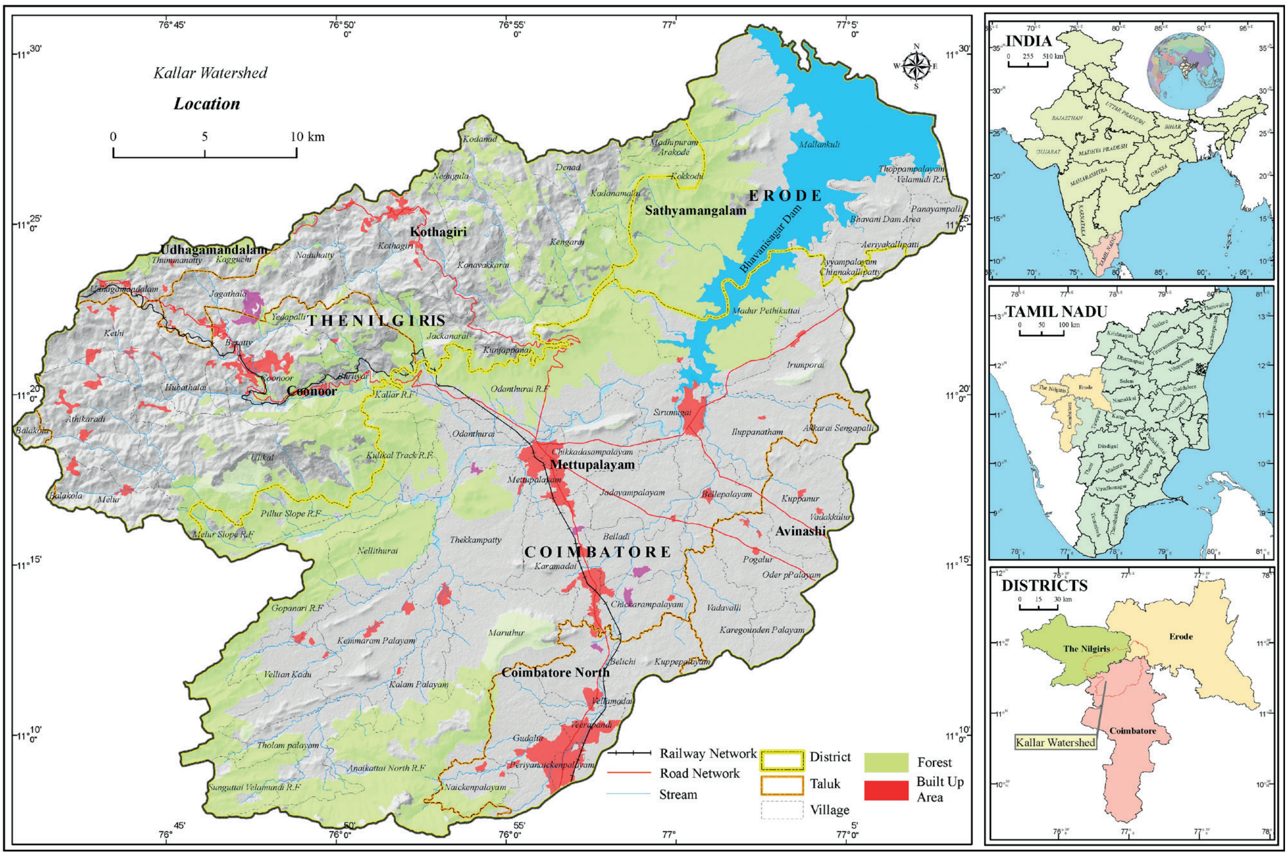

Fig. 1. Study Area

vulnerable land degraded zones were formulated. Advanced Spaceborne Thermal Emission and Reflection Radiometer (ASTER) Global Digital Elevation Model (DEM) data has a spatial resolution of 30 m was used to derive slope and elevation maps. About 30 years of daily precipitation data (1982–2012), from the Indian Meteorological Department (IMD), was used to derive rainfall erosivity and understand the general rainfall pattern of the Kallar watershed. Another important dataset used are soil parameters (physical and chemical properties of the soil) which were collected from Tamil Nadu Agricultural University. The data was used to calculate soil erodibility. The working scale of geographic maps was chosen at 1:50,000. Arc GIS 10.1 and Erdas 9.2 software products were used to prepare thematic maps and layouts.

METHODOLOGY

Revised Universal Soil Loss Equation (RUSLE)

RUSLE is a science-based tool; used to calculate potential average annual soil loss (A) has been improved over the last several years. It is widely used for site evaluation, planning purposes and formulate erosion control measures. It estimates the severity of erosion. Erosion is a function of erosivity and erodibility (Morgan 1983). The power of erosion agent to erode is designated as the erosivity (raindrop impact and surface runoff) and the susceptibility (inverse of resistance) of the soil to erosion is its erodibility. RUSLE factors contain both erosivity and erodibility effect. Erosivity – RKLSCP, Erodibility – RKLS.
The RUSLE model calculates potential average annual soil loss (A) which is given below:

$$A = R \times K \times LS \times C \times P \tag{1}$$

Where A represents computed spatial average annual soil loss, on a yearly basis (t/ ha^{-1} /y^{-1}); R is the rainfall-runoff erosivity factor (MJ mm/ha^{-1}/ h^{-1}/ y^{-1}); K is the soil erodibility factor (t/ ha /h /ha^{-1} / MJ^{-1} mm^{-1}); LS is the slope length-steepness factor (dimensionless); C is the cover management factor (dimensionless); and P is the conservation practices factor (dimensionless).

Rainfall Erosivity (R): The R factor represents the erosivity of the climate at a particular location. Areas with a low slope degree have low erosivity R values; whereas large numbers of R factor indicate more erosive weather conditions. For computing the average R, the recommended time duration which has to be taken is 20–25 years (Wischmeier and Smithl 1978). An alternative formula developed by Wischmeier and Smith (1978) and modified by Arnoldus (1980) involves only annual and monthly precipitation to determine the R factor in equation (2):

$$R = \sum_{i=1}^{12} 1.735 \cdot 10 \left(1.05 \, log_{10} \left(\frac{P_i^2}{P} \right) - 0.08188 \right) \tag{2}$$

Where R = rainfall erosivity factor (MJ mm/ha^{-1}/ h^{-1}/ y^{-1})
Pi = monthly rainfall (mm), P = annual rainfall (mm)

K Factor (Soil Erodibility): Soil erodibility is predicted as a function of soil and soil profile properties like percentage of silt, very fine sand, clay, organic matter (OM) and structure code (s). The regression equation for estimating erodibility factor values from the nomograph, suggested by (Wischmerier 1974) following equation (3):

$$K = \frac{\left[2.1 \times 10^{-4} (12 - OM) M^{1.14} + 3.25(s-2) + 2.5(p-3) \right]}{759.4} \tag{3}$$

where, K= Soil erodibility (ton/yr/MJ/mm), OM = percentage of Organic Matter, 's' = soil structural code, 'p' is permeability code and 'M' is a function of soil primary particle size fractions (Appendices, eq 11). Based on the parameters' characteristics given in the above equation the K factor (soil erodibility) map can be prepared.

LS factor: Slope Length (L) and Steepness (S) accounts for the effects of topography on soil erosion. (L) is determined using the following equation (4 and Appendix: eq14):

$$L = \left(\frac{\lambda}{22.13} \right)^m \tag{4}$$

Where, 22.13= the RUSLE unit plot length (in meters) and m= a variable slope length exponent. Slope length is defined as the horizontal distance from the origin of overload flow to the point where either (1) the slope gradient decreases enough where deposition begins or (2) runoff becomes concentrated in a defined channel.

The slope steepness factor (S) is estimated using the relationships given by McCool et al., (1987,1993). The equations (5 & 6) are as follows,

$$S = 10.8 \sin\theta + 0.03 S < 9\% (i.e. \tan\theta < 0.09) \tag{5}$$

$$S = \left[\sin\theta / \sin 5.143 \right]^{0.6} S < 9\% (i.e. \tan\theta < 0.09) \tag{6}$$

All trigonometric operations like angles have been converted into radians in ArcGIS and detailed equation expressions are given in appendix 1(eq.12 to 17). By multiplying the L factor and S factor, the LS factor map can be generated in the raster format.

Cover Management Factor (C): The Cover Management factor is used to determine the relative effectiveness of soil and crop management systems in terms of preventing or reducing soil loss. Normalized Difference Vegetation Index (NDVI)- based assessment of C factor is carried out by equation 7. It is used effectively to compute the spatial distribution of the C factor (Kouli et al. 2009; Prasannakumar et al. 2012).

$$C = \exp\left[-\alpha \frac{NDVI}{(\beta - NDVI)} \right] \tag{7}$$

Where α and β are units less parameters that determine the shape of the curve relating to NDVI and the C factor (Van der Knijff et al. 2000)

Conservation Practice Factor (P): The P factor represents the ratio of soil loss with a specific support practice to the corresponding soil loss with up and downslope (Contour) tillage (Wischmeier and Smith 1978; Renard et al. 1997; Dabral et al. 2008). It reflects the effects of practices that reduce the quantity and rate of water runoff, consequently reducing erosion levels. Using landuse and land cover, the P factor value can be generated which is 0-1; P-value of 1 indicates that there are no conservation practices in that region.

Rating the factors through AHP

Evaluation of land degradation factors, AHP based weights and scores are assigned through the nature of influence towards degradation. Analytical Hierarchy Process (AHP) is a semi-qualitative method which involves a matrix-based pair-wise comparison of the contribution of different factors for land degradation. It was developed by Saaty (1980) to get factors weightage in AHP. Two-step procedures to assign the scores and weights are calculated using the geometric mean and normalization of weights. In the first step of AHP analysis, the factors are rate based on a well-defined score from a scale of 0-9 to calculate the geometric mean (Table 2). The geometric mean is calculated by dividing the total scale of weights (total score of specific factors) by the total number of parameters given in equation (8) (after Rhoad et al. 1991):

$$Geometric\ mean = \frac{Total\ scale\ of\ weight}{Total\ number\ of\ parameters} \tag{8}$$

The normalized weights are an indicator of multifactor analysis for land degradation assessment. The normalized weights are calculated by dividing the assigned weights of factors subclass with the corresponding geometric mean (Table 3). The formula which is represented in eq.9 (after Yu et al. 2002):

$$Normalised\ weight = \frac{Assigned\ weight\ of\ parameter\ feature\ class}{Geometric\ mean} \quad (9)$$

The normalized weighted map is an indicator of land degradation vulnerability zone which is classified into five classes such as very high, high, moderate, slight and low degraded zones. The class range with the maximum weight is considered as a very high vulnerable zone and the least weighted class is a less vulnerable zone for land degradation (Table 4).

Land Degradation Classification Scheme

FAO based land evaluation methodology is a prime method for assessing land degradation in the arid and semi-arid regions (FAO 1976). The structure of the land degradation system can be broadly classified into three types of decreasing level: i.e. degradation type, degradation class (degree) and degradation unit. Four different forms of land degradation are recognised as degradation types: Soil Erosion (E), Desertification (D), Salinisation (S) and Wasteland (W). Its detailed descriptions are given in Table 1.

The classes/degrees of degradation are assessed based on the severity of degradation. The classes are numbered with increasing degrees of degradation i.e. D1, D2, E1, E2….E5. Herewith, *Class1*: potential degradation, but no substantiation or enriched. *Class 2:* Slight degradation, – (mostly vegetation degradation, affects qualitatively so its consumption rate is reduced). *Class 3:* moderate degradation, which is mostly influenced by vegetation and/or soil. *Class 4:* severe degradation, it is strongly influenced by soil, vegetation and landforms that causes to change the existing landuse practices. *Class 5:* very severe degradation, where land has lost its productivity and is a challenge to reclaim. The present study accomplice above said two FAO methods (i.e., degradation type and class) for the assessment of land degradation.

Land Degradation Vulnerability Index

In order to calculate the vulnerability index, the assigned AHP based sub factors weightages are divided by factors geometric mean and its normalised cumulative values are observed. Finally, all the factors normalised values are overlaid altogether and the land degradation vulnerability index (LDVI) is determined, which is given in equation 10:

$$LDVI = (LUi/LUj) + (SLi/SLj) + (Eli/ELj) + (SEi/SEj) + (NVi/NVj) + (PDi/PDj) \quad (10)$$

Where: Lu – Landuse; SL – Slope; EL – Elevation; SE – Soil Erosion; NV – NDVI; PD – Population Density. Representation of i – Assigned Weight (AW) to individual subfactors, j – Geometric mean (G).

The graphical representation of land degradation assessment methodological workflow is given in figure 2.

Table 1. Land Degradation forms and types

Type	Forms of land degradation	Description
C1	No degradation	The area is not/ somewhat degraded
D	Desertification	The land has been triggered by drought, wind erosion, irregular pattern of farming, overgrazing and over cutting in arid or semiarid areas.
E	Soil Erosion	Land degradation is instigated by water and wind erosion.
S	Salinization	The land has been affected by salinization, due to poor irrigation management.
V	Vegetation Degradation	It affects the land both quantitatively and qualitatively owing by overstocking / fuel cutting.
W	Wasteland	Unsuitable land for any activity i.e. unreclaimed mining spots and polluted areas leads to land degradation.

(FAO 1976 & Chen Guangwei)

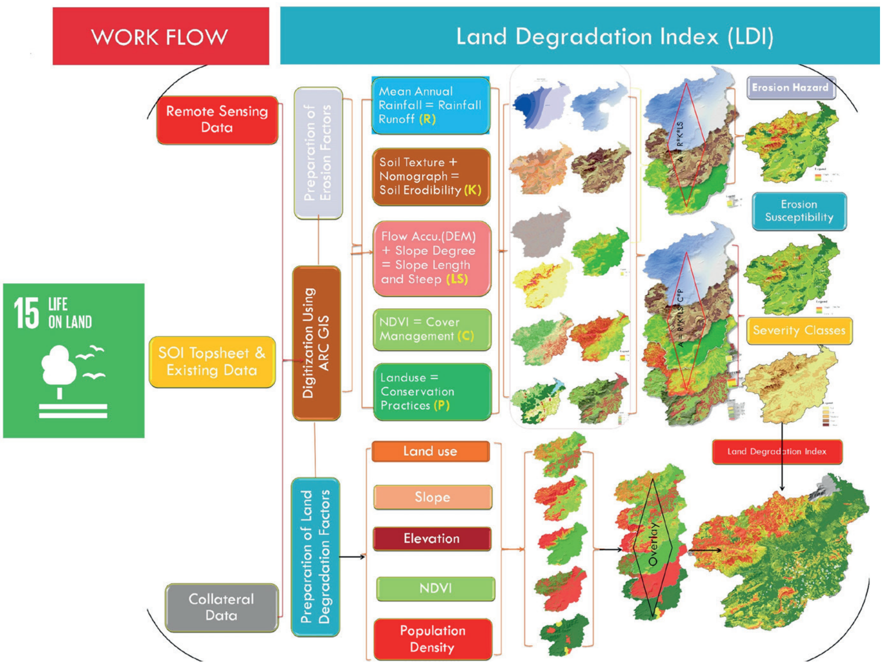

Fig. 2. Land degradation methodological workflow Results

Results

Land degradation is a natural process or human-induced. It affects the land's ability, to function effectively within an ecosystem. It is linked to sustainability in terms of productivity. Over the years, due to population explosion, growing industrialisation, agriculture expansion and rising living standards have increased land degradation and deforestation. In this scenario the present study was conducted after conceding the above-given factors.

Land Degradation Factors and Ranking

To study land degradation in the Kallar watershed the following six thematic factors are selected: soil erosion, elevation, slope, landuse, NDVI, and population density (Figure. 4, 5, 6, & 7). The factors and sub-factors weightages were assigned based on the impact on land degradation. Their areal extents are given in Tables (2, 3 and 4). The detailed interpretation of individual factors results are given in the following sections.

Table 2. Pair-Wise Matrix for LDI Factors

Parameters	Landuse	Slope	Elevation	NDVI	Soil Erosion	Population Density
Landuse	5.5/5.5	5.5/5	5.5/4	5.5/4.5	5.5/5	5.5/3.5
Slope	5/5.5	5/5	5/4	5/4.5	5/5	5/3.5
Elevation	4/5.5	4/5	4/4	4/4.5	4/5	4/3.5
NDVI	4.5/5.5	4.5/5	4.5/4	4.5/4.5	4.5/5	4.5/3.5
Soil Erosion	5/5.5	5/5	5/4	5/4.5	5/5	5/3.5
Population Density	3.5/5.5	3.5/5	3.5/4	3.5/4.5	3.5/5	3.5/3.5

Source: Compiled by Author

Table 3. Normalised Geometric Mean

Parameters	Landuse	Slope	Elevation	NDVI	Soil Erosion	Population Density	Normalized Weight
Landuse	1.00	1.10	1.38	1.22	1.10	1.57	1.23
Slope	0.91	1.00	1.25	1.11	1.00	1.43	1.12
Elevation	0.73	0.80	1.00	0.89	0.80	1.14	0.89
NDVI	0.82	0.90	1.13	1.00	0.90	1.29	1.00
Soil Erosion	0.91	1.00	1.25	1.11	1.00	1.43	1.12
Population Density	0.64	0.70	0.88	0.78	0.70	1.00	0.78

Source: Compiled by Author

Table 4. LDI Sub-Factors Weight and Normalised Weights

Factors	Sub Factors	Assigned weight (AW)	Geometric mean (G)	Normalized weight (N=AW/G)
Landuse	Barren Rock	0	1.23	0.0
	Built-Up Rural	1		0.8
	Built-Up Urban	0		0.0
	Crop Land	1.5		1.2
	Current Fallow	8.5		6.9
	Deciduous Forest	7.5		6.1
	Dense Scrub	6		4.8
	Evergreen Dense	1		0.8
	Evergreen Open	3.5		2.8
	Forest Plantation	4.5		3.6
	Industry	1.5		1.2
	Mine	7.5		6.1
	Open Scrub	9.5		7.7
	Plantation	6.5		5.2
	Reservoirs/Tank	1		0.8
	River	1		0.8
	Scrub Forest	2.5		2.0

Slope (in%)	Nearly Level	1	1.12	0.8
	Very Gently Slope	1.5		1.3
	Gently Slope	2.5		2.2
	Moderately Slope	4.5		4.0
	Strongly Slope	5		4.4
	Moderately Steep to Steep	6.5		5.8
	Steep Slope	7.5		6.7
	Very Steep	8.5		7.5
Elevation (Metre)	< 500	3.5	0.89	3.9
	500- 800	4.5		5.0
	800-1100	5.5		6.1
	1100-1500	6.5		7.3
	1500-1800	7.5		8.4
	>1800	8.5		9.5
Soil Erosion (Ton/Ha/Y)	<25	2.5	1.12	2.2
	25-50	4		3.5
	50-75	5.5		4.9
	75-100	7		6.2
	> 100	8.5		7.5
NDVI	<0.06	0	1	0
	0.06-0.2	7.5		7.5
	0.2-0.4	6.5		6.5
	0.4-0.6	4.5		4.5
Population Density	<500	3.5	0.78	4.4
	500-1000	4.5		5.7
	1000-1500	5.5		7.0
	1500-2000	6.5		8.3
	>2000	7.5		9.6

Soil Erosion Aspect

Estimation of soil erosion is calculated by using RUSLE based empirical model with multi factors such as rainfall erosivity, soil erodibility, slope length and steepness, cover management, and conservation practices. The following section describes the influences and their relationship between other factors in detail.

Rainfall Erosivity (R): The annual and monthly precipitation data of twelve weather stations for a time duration of 30 years (1980–2012) were collected and the average annual rainfall was calculated. Further, it is interpolated using the geostatistical model (spline) over the whole watershed. The average annual R factor values ranges from 251.5 to 798.5 MJ mm/ha^{-1}/ h^{-1}/y^{-1} (Figure.3a). The high-altitude regions such as Coonoor and Gurrency have the highest range of rainfall erosivity and a decreasing trend towards northwest to southeast direction. *Soil Erodibility (K):* depends on soil or geological characteristics, such as parent material, texture, structure, organic matter content, porosity, catena and many more. This factor is influenced by the soil composition and soil texture. The major soil textural classes found in these areas are clay loam, clayey, loamy sand, loamy, sandy clay, sandy clay loam, and sandy loam (Figure.3b). By applying the above-said equation (3) the K factor values were generated and mapped. The results helped to quantitative estimation of soil erosion and express the capability or vulnerability to erode.

Slope length and Steepness (LS): This factor expresses the effect of local topography on soil erosion rate by combining the effects of slope length (L) and slope steepness (S) which is calculated using the equation (4-6). The longer the slope length, the greater the amount of cumulative runoff. Steeper the slope of land, higher the velocities of the runoff which contributes to erosion. By multiplying L and S factors, the LS factor map was generated in raster form, which ranges from 0 to 9.06 (Figure.3c). The range was higher in hilly regions with steeper slopes and lower in the plain surface.

Cover Management (C): It determines the relative effectiveness of soil and crop management systems and sinking soil loss. Normalized Difference Vegetation Index (NDVI) is used to calculate the C factor (equation 7). The highest C factor values indicate a high vulnerability to soil erosion, as they are considered to be unprotected barren land. The C factor ranges from 0.076–1

(Figure.3d). Higher values appear in the lower regions of the study area whereas the least values are noticed in hilly areas, which is occupied by forest cover. ***Conservation Practice (P):*** It is the ratio of soil loss in normal conditions to the soil loss due to plowing. The P factor map was derived from the landuse / land cover and support factors. The values of P factor ranges from 0 to 1 (Fig. 3e). Open areas and grasslands are more prone to soil erosion since they have the highest values with no conservation practices. Minimum values were recorded in built-up land and plantation areas with contour cropping practices that are less prone to erosion. Common support practices such as cross slope cultivation, contour farming, strip cropping, terracing, and grassed waterways are adopted in these regions.

Soil erosion: By integrating all the five thematic layers, the severity of soil erosion and loss is calculated through equation (1). Due to the erosion of more fertile soil, the land quality and its nutrients will be lost. These lands become useless and are instantly converted to cultural wastelands. Finally, it leads to land degradation. By effective utilisation of the RUSLE model, soil loss due to erosion has been carefully estimated at the pixel level. The soil loss rate is classified into five erosion severity classes (Figure.4). Potential annual soil loss is carefully estimated from the desired product of contributing factors (R, K, LS, C, and P) in the Kallar watershed ranges from 0 – > 20 $t/h^{-1}/y^{-1}$. The classified soil loss map shows that about 50.6 % of the total area has very less erosion with a tolerable rate of < 2 $t/h^{-1}/y^{-1}$, followed by 7.6% have less soil loss with the rate of soil erosion 2-4 $t/h^{-1}/y^{-1}$. About 8.5% of the considered area is under moderate erosion with the soil loss of 4-8 $t/h^{-1}/y^{-1}$. The high rate of 8-20 $t/h^{-1}/y^{-1}$ typically covers a sensitive area of 20.3% and 13% is prone to very high erosion with the soil loss of >20 $t/h^{-1}/y^{-1}$ on very steep slopes which is covered with deciduous forest. Estimated soil erosion severity classes were compared with other alternative factors related to the possible vulnerability of land degradation; which incurred the second-highest geometric mean of 1.12. The soil erosion sub-factors were further assigned weights individually that are shown in table (4). By multiplying both erosions factor geometric means with its sub-factors individual weights, the normalised weightage was computed.

After estimating the soil erosion severity classes, the computed values of R, K, LS, C and P were further classified into two categories: (1) Soil erosion susceptibility A=RKLS (2) Soil erosion hazard A=RKLSCP (Fig. 5 a & b). These categories provide insights into real variations of these values. However, RKLS values indicate soil loss, if crop management and erosion control practices are absent. The lowest values of RKLS represent figures for plains (flat to gentle) and the highest for those of hills. On the other hand, RKLSCP values indicate soil loss in the plains (lowest values) where crop management and erosion control practices are persistent. To reduce the loss of soil in the hills which has the highest values, conservation practices are implemented. When measuring the rate of soil erosion, it is found that the RKLS values are comparatively higher than RKLSCP values.

An intriguing inference has been drawn from the two values concerning the highest values (RKLS and RKLSCP). For instance, in the absence of crop management, the watershed has a soil loss of 447.3 $t/h^{-1}/y^{-1}$ but a glance at the RKLSCP value corresponding to this high value indicates > 20 $t/h^{-1}/y^{-1}$ of soil which is mainly attributable to the forest cover.

Terrain Aspect

While assessing land degradation slope and elevation (relief) factors are dominant. They were extracted from ASTER DEM. To understand the stability of the terrain, slope maps were generated and categorised into eight classes: nearly level, very gentle, gentle, moderate, strong, moderately steep, steep, and very steep (Fig. 6a, b). Of which 44.5 % of the geographic area is covered by moderately steep to very steep, 26.2 % of the area is occupied by very steep slope. An overall weightage of 1.12 is allotted to the slope factor. Among the slope class, the steep to very steep slope class is more prone to land degradation due to irregular cropping patterns. This class has been assigned the highest rank of 8.5 and 7.5, respectively. The least rank (1)

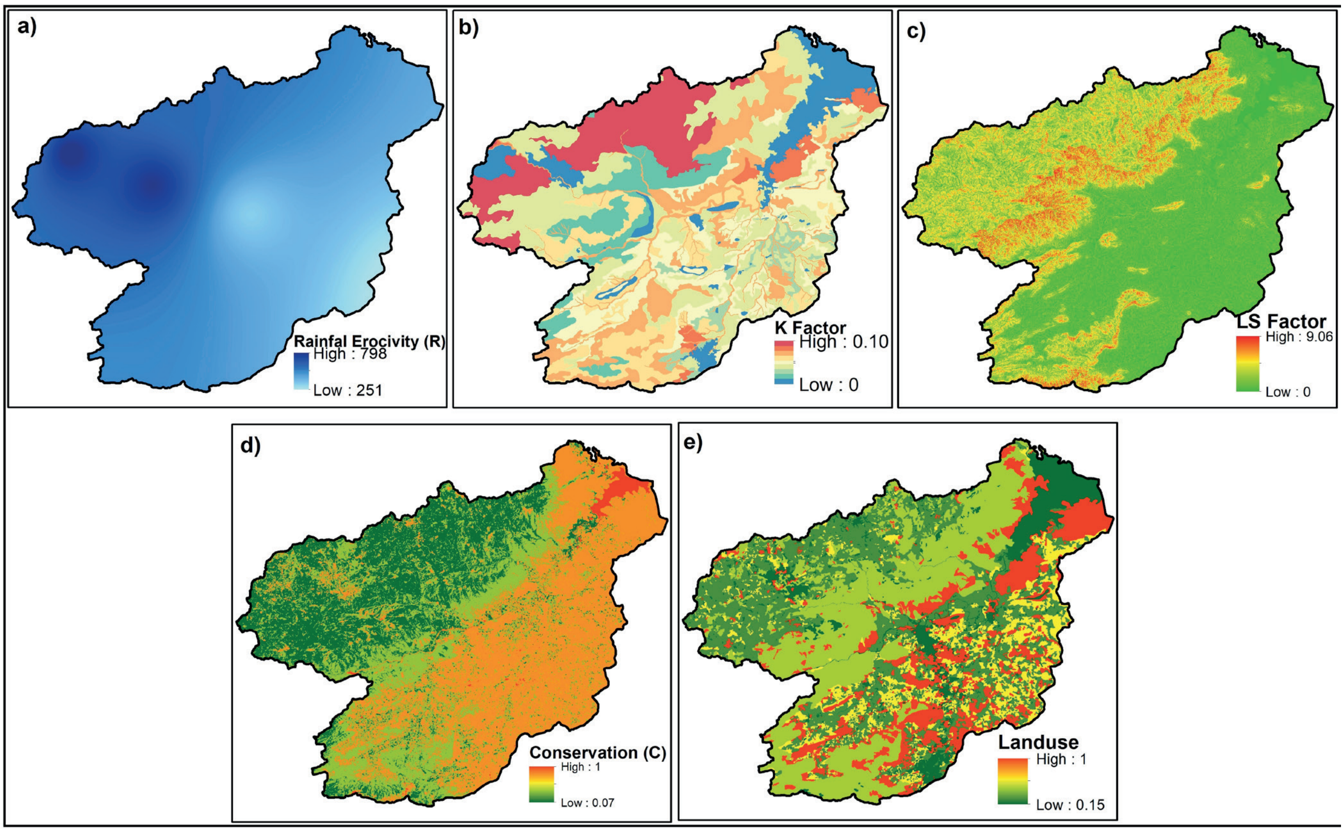

Fig. 3. a) Rainfall Erosivity, b) Soil Erodibility c) Slope length and steepness d) Conservation Practices e) Cover Management

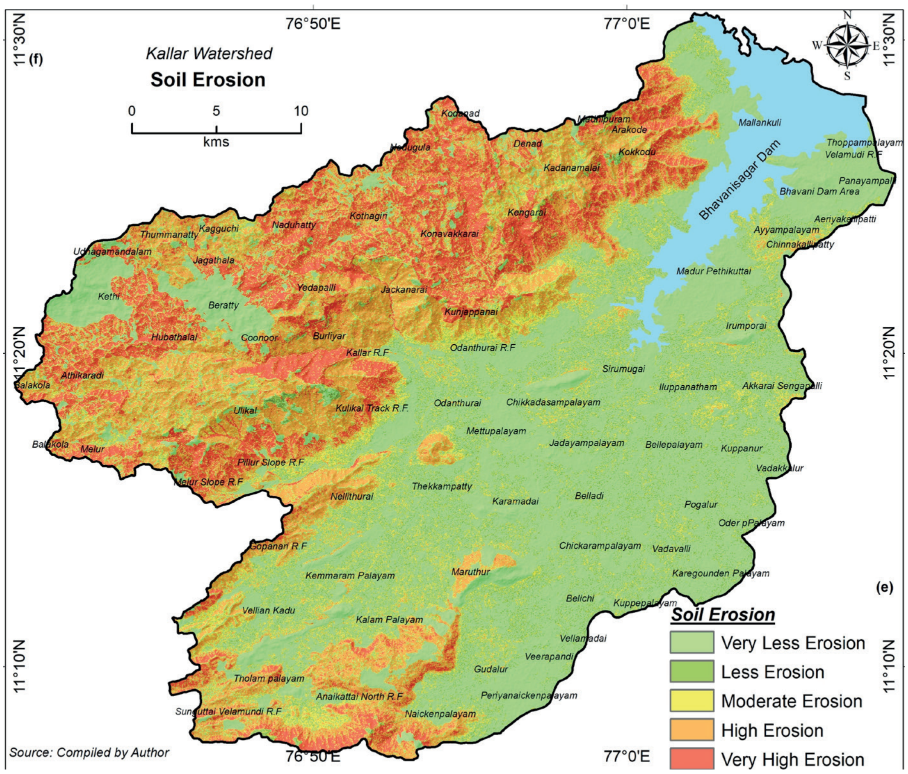

Fig. 4. Soil Erosion Loss

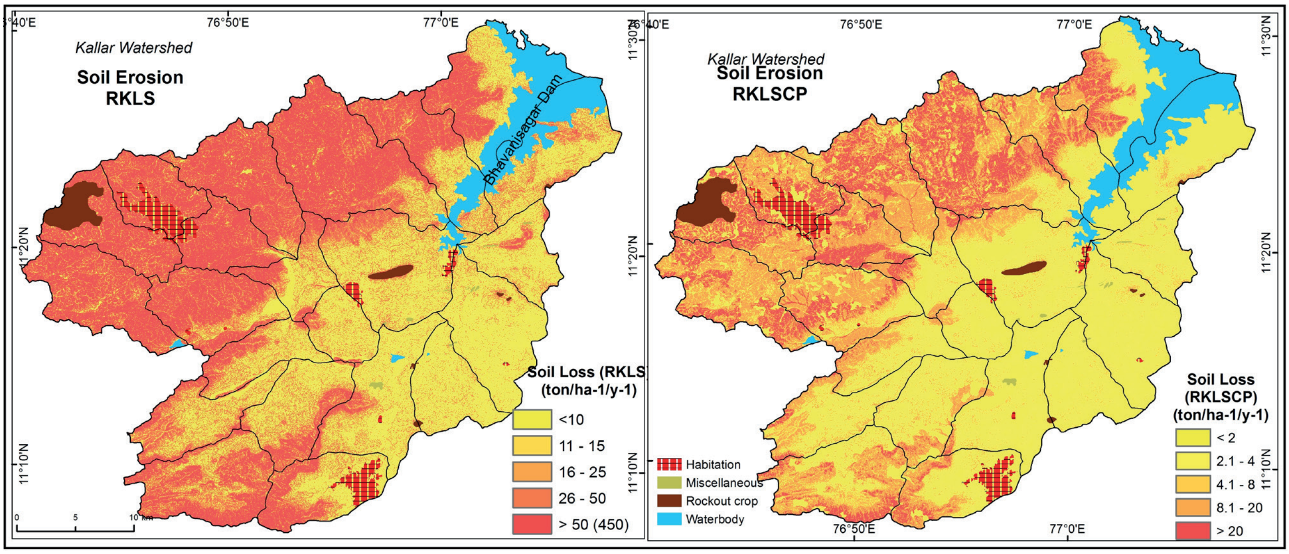

Fig. 5. a) Soil erosion susceptibility (RKLS) b) Soil erosion hazard (RKLSCP)

was assigned to the nearly level slope which represents less possibilities of degradation. Relatively, the role of elevation in the land degradation process is similar to the slope of the land. Higher the altitude, greater the degradation. These land areas have less slope stability and high erosion. Further these elevations are classified into >1800 m, 1500-1800, 1100-1500, 800-1100, 500- 800 and < 500 m (Fig. 6c & d). The present study area shares two various topographies such as mountains with upland plateaus and plains. A weightage of 0.89 was allotted to terrain factor and its sub-classes were assigned weights which is given in (Table 4).

Environmental Aspect

Among all the selected land degradation vulnerability factors, **landuse** secured the highest score of 1.28 from both aspects naturally induced process and human activities. In the present study area, landuse classes are broadly categorised into five classes i.e., 1) Built-up *(urban and rural)*; 2) Agricultural (*cropland, plantation and current fallow land)* and 3) Forest *(evergreen dense, evergreen open, deciduous and forest plantation)*. 4) Wasteland *(barren rock, dense scrub, open scrub, scrub forest, mining)* and 5) Waterbody *(reservoirs/tank and river)* (Fig. 7a). Stretching from north-west to east, the Nilgiri reserve forest dominates the forest cover in this region. Outer sloping and foothill areas comprised of deciduous forests, dense and open scrub forests, which are vulnerable to land and forest degradation. Within this landuse class, open scrub, current fallow, mining and the deciduous forest have been given the highest ranking of 9.5, 8.5 & 7.5 respectively (Fig. 7b). Due to this, these classes are more prone to land degradation when compared with other landuse classes and the least rank is given to built-up areas. NDVI represents vegetation and non-vegetation areas (Fig. 8a). They have been assigned an intermediate weight of 1 and the subclass of NDVI range < 0.4 has been given the highest rank of 7.5. The least rank of 4.5 has been allotted to a range of > 0.4 (Fig. 8b). The range less than 0.4 signifies non-vegetative areas which are mostly covered by barren land and scrubland.

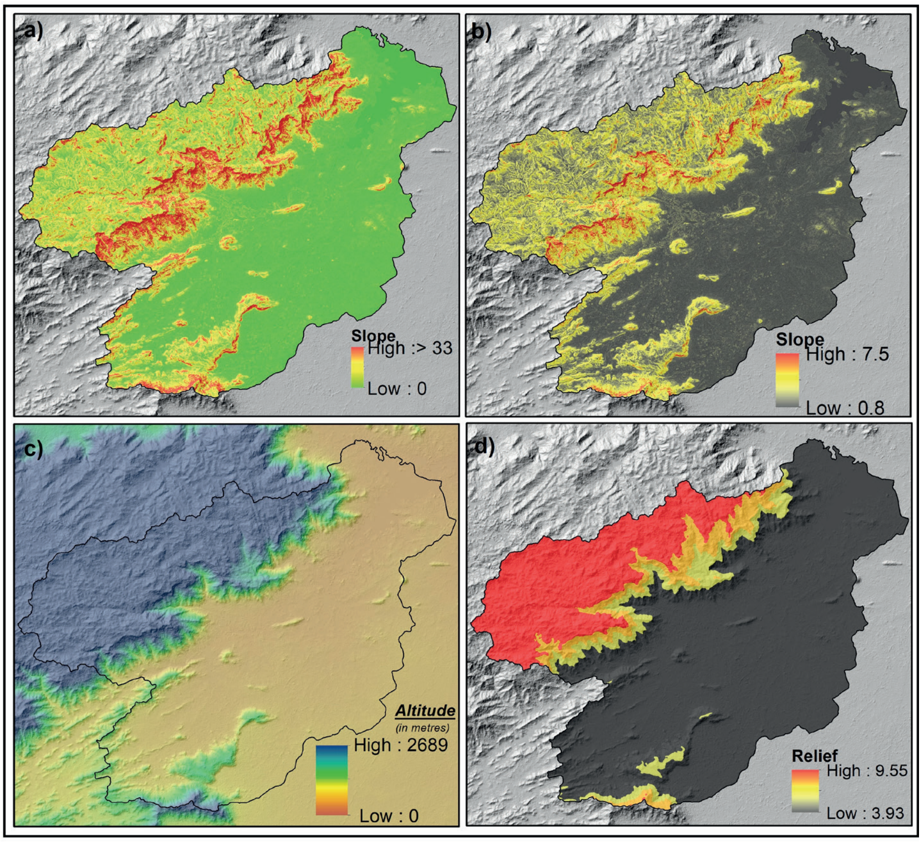

Fig. 6. a) Slope b) Weighted Slope c) Relief d) Weighted Relief

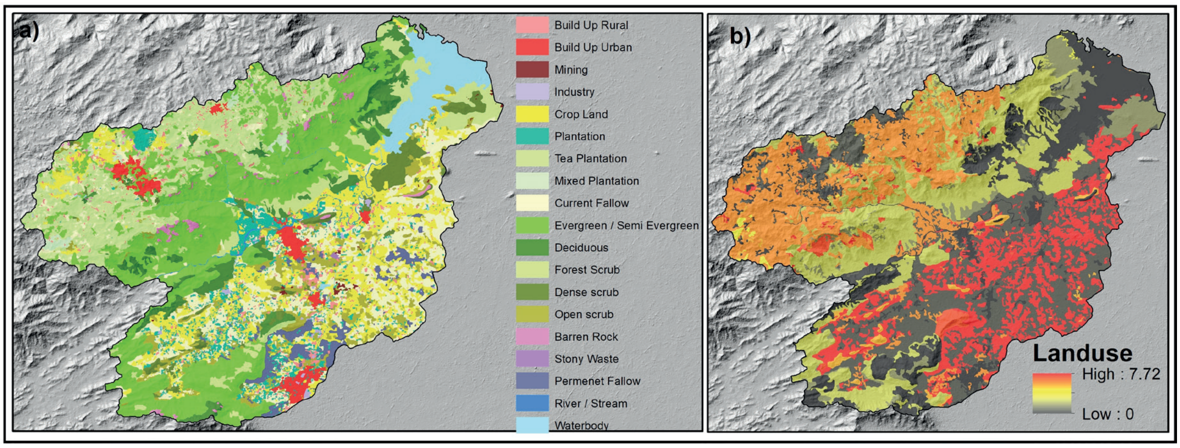

Fig. 7. a) Landuse b) Weighted Landuse

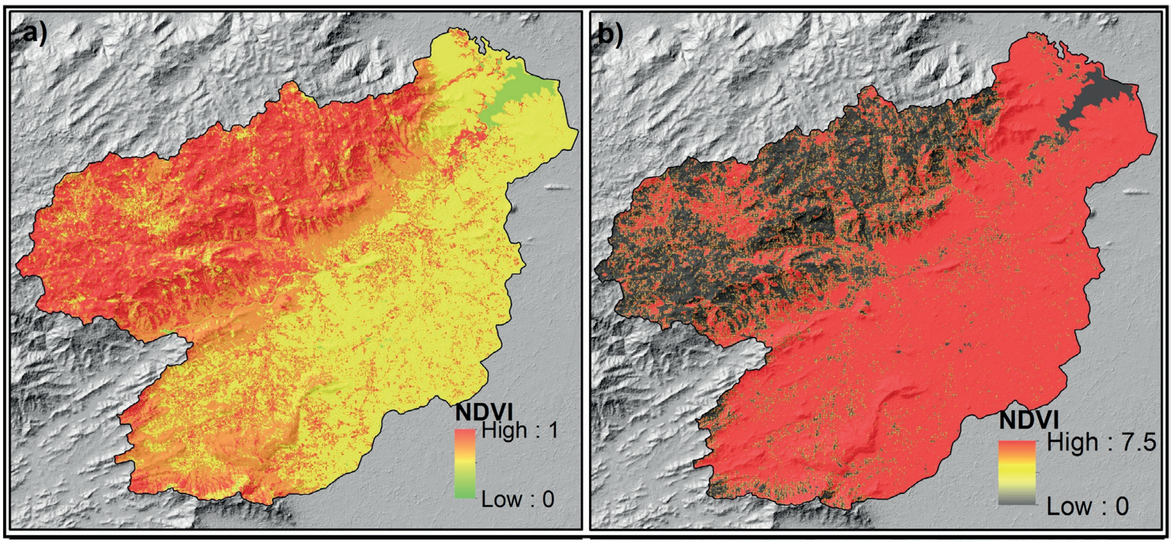

Fig. 8. a) NDVI b) Weighted NDVI

From a human perspective of land degradation, various demographic factors are influenced directly and indirectly i.e., population growth, density, households, literacy and sex ratio. Population density has been chosen as the common demographic factor. Population density has been given the least weight (0.78), even though it is an important hidden factor for land degradation. A high population density pressurises to more land degradation in various aspects, i.e., solid waste disposal, improper wastewater management, rapid urbanization and the need for more food production. The population density sub classes > 2000 persons/sq.km are noticed in Coonoor, Mettupalayam and Periyanayakanpalayam, which has been allotted the highest rank of 7.5. Followed by intermediate ranks (6.5, 5.5, and 4.5) assigned to 1500-2000, 1000-1500, 500-1000 persons/sq.km respectively. < 500 persons/sq.km has been assigned to the least rank of 3.5. Spatial distribution and weighted map of population density are shown in Figures 9a &b.

Land Degradation Vulnerability Index

The six thematic layers (landuse, slope, elevation, soil erosion, NDVI, and population density) were used for the assessment of land degradation. The final cumulative land degradation vulnerability index map was generated by using equation (10). Further, it was classified into five classes such as Severely Degraded, Highly Degraded, Marginally Degraded, Moderately Degraded, and Less Degraded. The spatial distribution and their areal extent are given in Figure. 10 and Table 5.

Low Degraded (D1): This class includes agricultural lands consisting of moderate -to- gentle slopes, very slight erosion and intact topsoil layer. Low degraded class is mostly found in the lower region of the Kallar watershed and occupies an area of 38.3% (49177 ha).

Moderately (D2): Moderately dense forests, grazed and disturbed grasslands and agriculture in moderate to steep slopes with rills and small gullies, and signs of root exposure fall under this class. These classes are mostly seen in the foothill areas and are adjacent to high-degraded areas. This region occupies an area of 39% (50059.7 ha), which require moderate conservation practices to control land degradation.

Marginally Degraded (D3): Sparse forests (vegetation), modified natural grasslands, tea plantation and pastures, moderate – to – steep slopes, absence of large gullies and tree uprooting fall under this category which covers 15.4% of the area.

Severely & Highly Degraded (D4 & D5): These classes occupy an area of about 22.6 % of the total geographic area. These areas consist of moderate-to-open forests, poor cultivation, steep to very steep slopes, severely eroded areas with or without gullies and tree cover uprooting. Mostly D5 and D4 classes are noticed in the northwest part of the Kallar watershed. These regions are dominated by tea plantations and deciduous forests, with less tree crown cover density; this leads to soil erosion. Further, in the upland plateau regions, irregular agricultural activity is practiced.

In recent years, several parcels of the fertile agricultural lands are converted into settlement plots (Fig. 10 – highlighted in white color). For many years, these land areas are either laying wasted without any productivity and waiting for construction or re-sale. Hence, an appropriate landuse policy should be promulgated.

DISCUSSION

Numerous factors on environments cause direct or indirect changes in the process of the system such as LULC transformation, climate change, socio-economic factors, cultural and demographic factors (Uzun and Somuncu 2013; Temiz et al. 2017; Olena 2017; Abhijeet et al. 2020). This study utilised multifaceted factors like climatic, environmental, terrain and demographic factors to assess land degradation along with its strength and weakness of the watershed. An absence of global agreement on the definition of land degradation and a standardised methodology for its assessment at different spatial scales (Metternicht et al. 2010; Higginbottom and Symeonakis 2014) are major limitations of the study. There is not an approved or recommended methodology to evaluate the selected SDG targets and indicators with limited input parameters. Hence, this study has framed a new methodology of integrating physical and empirical model-based, physio-climatic, and socio-environmental inputs to address the issues through geospatial techniques and multicriteria decision making. This research will be an ideal solution to assess land and forest degradation. It is a combination of multi-facet parameters such as physical, environmental and socio-economic aspects. The study evaluates and helps policymakers to take decisions with appropriate conservation measures to fulfil sustainability goals at local and global levels.

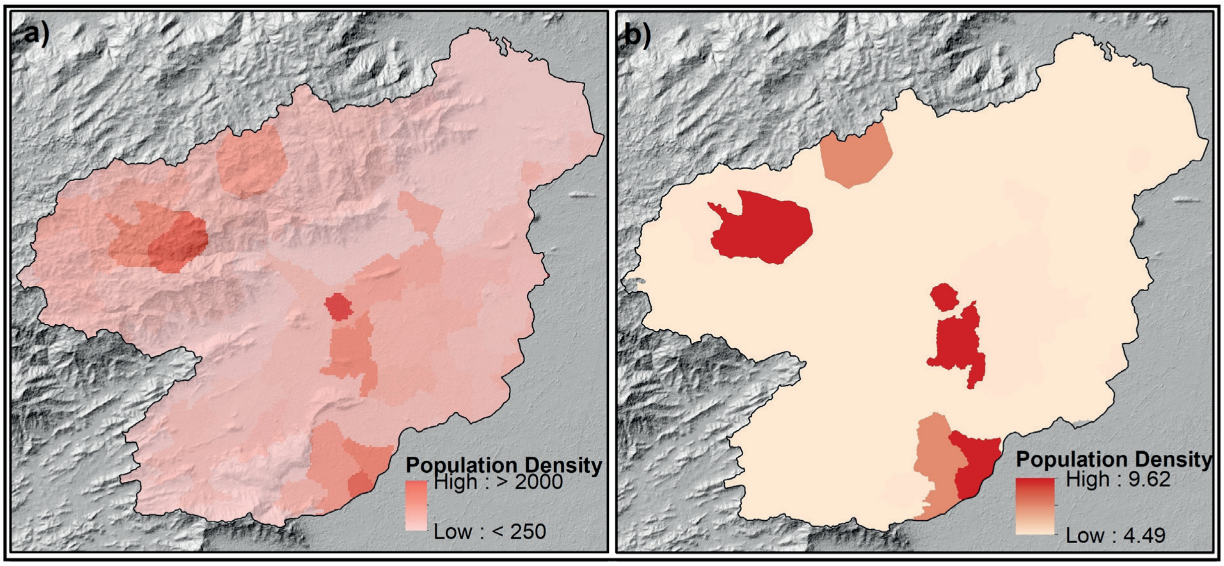

Fig. 9. a) Population Density b) Weighted Population Density

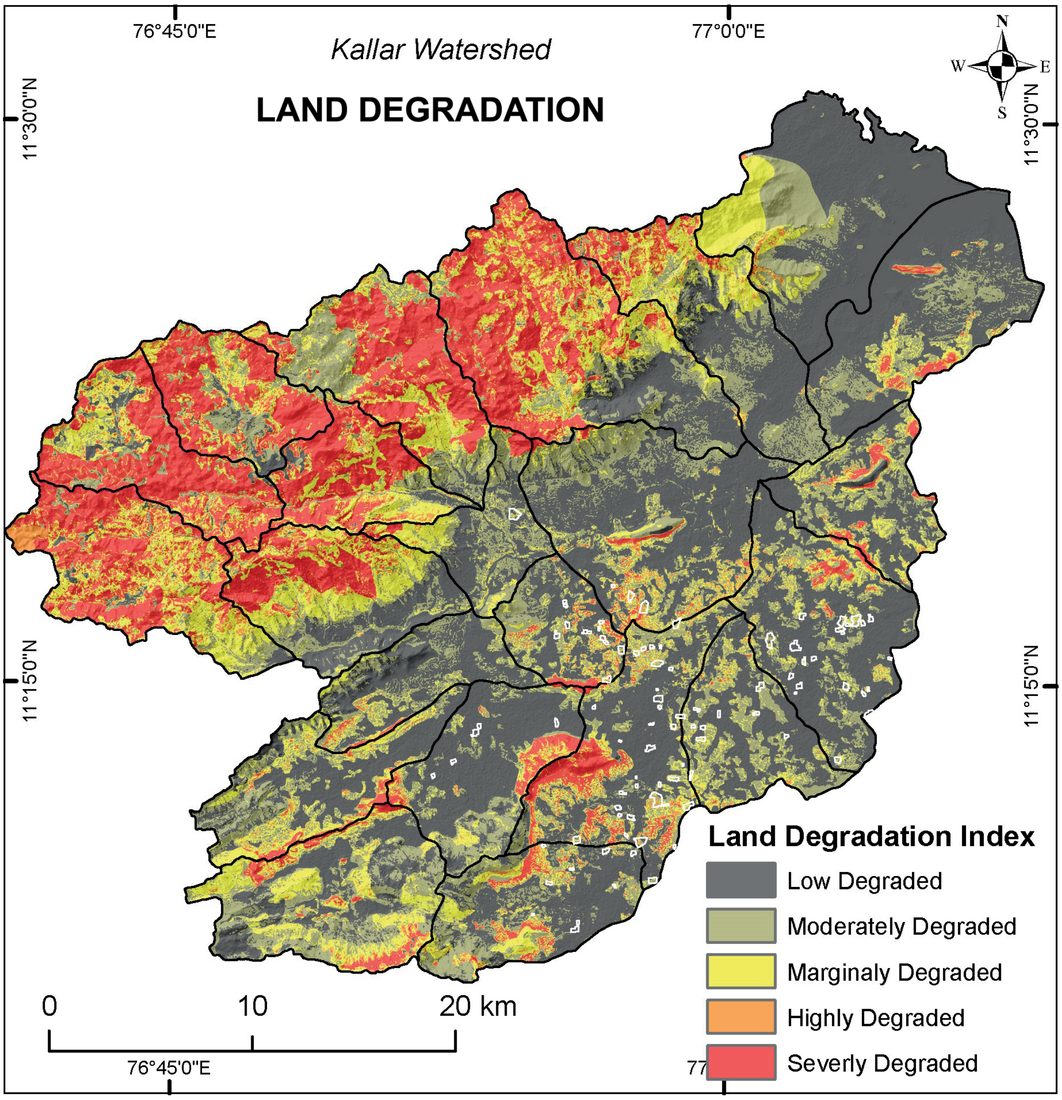

Fig. 10. Land Degradation Index

Table 5. Land degradation class and spatial extend

Land Degradation Class	Area (in Ha)	Area (%)
Low Degraded	49,177.4	38.3
Moderately Degraded	30,258.6	23.6
Marginally Degraded	19,801.0	15.4
Highly Degraded	6,199.5	4.8
Severely Degraded	22,809.1	17.8
Total Area	128,245.6	100

Source: Compiled by Author

From the natural perspective of land degradation, terrain with moderate to steep slope areas are highly prone to soil degradation, which leads to soil erosion during heavy rainfall. It reduces the infiltration rate. This can be seen in the foothill regions which are covered by deciduous forests (sparse trees) and less density of tree crown cover. Due to its nature of topography which consists of hilly terrains, steep slopes and dense forests, the Kallar watershed has a higher possibility of soil erosion. About 30% of the area is covered by various types of forest cover i.e., evergreen, deciduous, and open scrub forest, which is located in the middle of the watershed. Due to this, human and natural forces in this area result in deforestation and land degradation. During the summer monsoon, these deciduous forest areas are frequently affected by severe drought and forest fires. Human activity is higher in moderate slope regions than mountainous terrains and foothills. Human activities in this forest land includes cultivable land and other social activities. It creates forest degradation; the extension of the mentioned processes finally leads to deforestation. The previous studies of Rahaman and Venkatesh (2020), stated that deciduous forest and forest scrub areas are under the degradation stage, which causes environmental degradation in the Nilgiri Biosphere Revere of Western Ghats.

The Kallar watershed has a maximum annual soil loss of 398.5 t/ h^{-1}/ y^{-1} and >100 ton/ h^{-1}/ y^{-1} is about 15 % (200 km^2) of the geographic area (Abdul et al. 2015). Similarly, soil and water losses are serious issues in the western Liaoning low mountains and hills of China, which has erosion rates of up to 3000-5000 t/km^{-1}/year^{-1} are observed (Zhao et al. 1992). Due to severe soil erosion, removal of top layer soil, and declining soil fertility, which causes decreasing land productivity. Through soil erosion susceptibility (RKLS) and soil erosion hazard (RKLSCP), it is understood that the functions of C and P factors can be controlled and thus can greatly reduce soil loss through proper management and conservational measures. The terrain of a region largely determines its suitability for human settlement. Flatter alluvial plains tend to have better farming soils than steeper and rocky uplands. In the present study region, half of the area is covered by forest which is reserved and open type. There are more possibilities of land degradation in the outer fringe of evergreen forests due to human activity. This leads to deforestation and loss of biodiversity richness in this region (Abdul 2016).

Due to the favourable climatic and topographic conditions found in the upper portion of the watershed, this natural land cover (forest) is converted to tea plantations and is used for grazing. The southern regions of the study area can be categorised into agricultural land, current fallow land and other wastelands. In this area, productive agricultural lands are converted into settlement plots due to water scarcity and less quantity of soil nutrients. If this situation persists, the entire area will be affected and will result in agricultural drought and severe land degradation. A detailed qualitative, quantitative analysis and a comparative study has been conducted in the Kallar watershed. The analysed resultant values are classified into five classes based on FAO land evaluation approaches such as: Severely, highly, moderately, marginally, and low degraded.

Further, the outcome of the study was compared and validated with existing results published by the SAC, ISRO; Google Earth Image and IRS LISS IV image along with field verification. 92 settlement plots were identified and mapped (Figure 8a). Under the guidance of the Indian Space Research Organisation (ISRO) and with the help of Space Application Centre (SAC), national-level Desertification and Land Degradation Atlas of India was prepared, using Indian Remote sensing Satellite (IRS), Advanced Wide Field Sensor (A WiFS) data of 2011–13 and 2003-05 (SAC, ISRO, 2016). The analysis depicts that 96.4 million hectares (mha) of land area in the country have undergone land degradation i.e., 29.3% of the total geographic area of the country during 2011–13. According to a sensitive assessment by the Indian Council of Agricultural Research (ICAR 2010), about 120.4 mha (out of 328.7 mha) of land area in the country was affected by land degradation during 2009-10.

By examining the biophysical and demographic factors, they can be distinguished to provide optimal solutions for selected SDG's (15.3) and their targets (15.3.1 & 3) like sustainable forest management and land that is degraded over the total land area. FAO serves as a contributing agency for some of the indicators including 15.3.1. It suggests the following sub-indicators: 1) Land cover and land-cover change; 2) Land productivity; and 3) Carbon stocks above and below ground (UNCCD 2015 and FAO 2018) for «good practice guidence» in the measurement and evaluation of changes. SDG goals, targets, indicators, and sub-indicators have to be addressed and implemented. They require substantial strategies like defining land and forest degradation, measuring its extent, and evaluating spatial dimensions at the local, regional, and global scale. To assess degradation, appropriate indicators like land use, climate, and population have to be determined. Reducing anthropogenic influences on the degraded areas ensures rejuvenation of the natural state of the land areas. User-driven and participatory approaches at the rural level should be encouraged to achieve sustainability.

The study reveals that the Kallar watershed is under severe threat of soil erosion and degradation of forest and land. Continuation of these practices in the current scenario will make this area to the most vulnerable hotspot for land degradation. In this situation, proper conservation management like changing agricultural practices in the plain areas; contour bunds, terrace cultivation on high-altitude regions, construction of check dams, and percolation ponds to control the water scarcity is extremely essential. Strict landuse policies have to be implemented to control and stop the conversion of fertile agricultural lands for other activities. Protection of forest areas, minimizing deforestation and practicing afforestation is highly recommended. The extension of this work should be carried forward to estimate land productivity, land cover changes and biomass at the regional and national levels. Public awareness has to be created and appropriate conservation measures to protect land sustainability have to be taken.

CONCLUSION

The study utilises various modern techniques of geospatial technology coupled with multi-criteria evaluation methods to assess the vulnerability of land degradation by natural and anthropogenic activity. Hence standardized methodology for land degradation assessment at different spatial scales is the major limitation of this study. However, soil erosion, overpopulation, reduction in forest density, overgrazing and inadequate conservation measures are the main causes of land degradation in the Kallar watershed. Both natural and human-induced multi influential factors were chosen to evaluate the degree of land degradation. Soil erosion plays a major role in the land degradation processes at the foothill areas which has the least agricultural activity. Further, the resultant classes were cross-validated with the field and Google earth images. In many places, cultivable land areas are converted to construction plots or permanent fallow lands (wasteland). By replacing land exploitation with land conservation practices, cautious utilization of the land resource can be adopted. Based on the analysis, it is observed that the Kallar watershed is prone to very high to high degradation stage. The land area has to be controlled and monitored regularly with the aid of advanced technologies.

A strategic measure to prevent loss of soil and water and minimize ecological disturbances, the development of forestry can be accelerated. Practicing afforestation in degraded forest areas to enrich soil nutrition, increases the availability of water. To reduce soil erosion, implementing various engineering and biological conservation measures such as conversion of land on slopes to fallow and gully engineering techniques can be adopted. Modern agricultural practices that includes farming between ridges across the slope and inter-cropping along the contour belt should be encouraged. Planting fruit trees and growing herbals can be enriching the ecosystem. This is an important strategic measure for developing the economy which helps in ecological conditions in mountain areas and maintaining ecological balance. Further, the implementation of efficient land system management and landuse policies to protect the natural environment through sustainable approaches in the Kallar watershed is crucial for future generations. The imminent scope of the present study pursued through advanced machine learning algorithms is used to monitor the environment, assess biomass estimation, and evaluate ecological assessment for a sustainable environment.

REFERENCES

Abdul Rahaman S., Aruchamy S. and Jegankumar R. (2014). Geospatial approach on landslide hazard zonation mapping using multi-criteria decision analysis: a study on Coonoor and Ooty, part of Kallar watershed, The Nilgiris, Tamil Nadu, Int. Arch. Photo. Remot Sens. Spatial Inf. Sci., XL-8, 1417-1422, DOI: 10.5194/isprsarchives-XL-8-1417-2014.

Abdul Rahaman S., Aruchamy S., Jegankumar R. and Abdul Ajeez S. (2015). Estimation of annual average soil loss, based on rusle model in Kallar watershed, Bhavani basin, Tamil Nadu, India, ISPRS Ann. Photogramm. Remote Sens. Spatial Inf. Sci., II-2/W2, 207–214, DOI: 10.5194/isprsannals-II-2-W2-207-2015.

Abhijeet Ghadge, Sjoerd van der Werf, Merve Er Kara, Mohit Goswami, Pankaj Kumar, Michael Bourlakis (2020). Modelling the impact of climate change risk on bioethanol supply chains, Technological Forecasting & Social Change 160, DOI: 10.1016/j.techfore.2020.120227.

Arnoldus H.M.J. (1980). An approximation of the rainfall factor in the Universal Soil Loss Equation.

Angima S.D., Stott D.E., O'Neill M.K., Ong C.K. and Weesies G.A. (2003). Soil erosion prediction using RUSLE for central Kenyan highland conditions agriculture. Ecosystems and Environment, 97(1-3), 295-308.

Barzani and Khairulmaini (2013). Desertification risk mapping of the Zayandeh Rood Basin in Iran. Journal of Earth System Science 122(5), 1269-1282, DOI: 10.1007/s12040-013-0348-1.

Bhattacharyya R., Ghosh B.N., Mishra P.K., Mandal B., Rao C.S. and Sarkar D. (2015). Soil degradation in India: challenges and potential solutions. Sustainability 7, 3528-3570.

Barrow C. (1994). Land degradation development and breakdown of terrestrial environments. Cambridge University Press, New York.

Brevik E.C., Cerda A., Mataix-Solera J., Pereg L., Quinton J.N. Six, J. and Van Oost K. (2015). The interdisciplinary nature of soil, Soil, 1, 117-129, DOI: 10.5194/soil-1-117-2015.

Camprubi A., Zarate I.A., Adholeya A., Lovato P.E. and Calvet C. (2015). Field performance and essential oil production of mycorrhizal rosemary in restoration low-nutrient soils, Land Degrad. Dev., 26, 793-799, DOI: 10.1002/ldr.2229.

Cerda A., Gonzalez-Pelayo O., Gimenez-Morera A., Jordan A., Pereira P., Novara A., Brevik E.C., Prosdocimi M., Mahmoodabadi M., Keesstra S., Garcia Orenes F. and Ritsema C. (2016). The use of barley straw residues to avoid high erosion and runoff rates on persimmon plantations in Eastern Spain under low frequency – high magnitude simulated rainfall events, Soil Res., 54, 154-165, DOI: 10.1071/SR15092.

Christopher Morgan (1983). The non-independence of rainfall erosivity and soil erodibility, Earth Surface Processes and Landforms, 8, 323-338.

Chen Guangwei (1994). Land Degradation Approach – Methodology and Practice, CISNAR, China.

Dabral P.P., Baithuri N. and Pandey A. (2008). Soil erosion assessment in a hilly catchment of North Eastern India using USLE, GIS and remote sensing. Water Resources Management, 22, 1783-1798.

De Boodt M. and Gabriels D. (Eds.) (1980). Assessment of Erosion, Wiley, Chichester, UK, 127-132.

Desertification and Land Degradation Atlas of India (2016). (Based on IRS AWiFS data of 2011–13 and 2003-05), Space Applications Centre, ISRO, Ahmedabad, India.

D'Odorico P.; Bhattachan A., Davis K.F., Ravi S. and Runyan C.W. (2013). Global desertification: Drivers and feedbacks. Adv. Water Resour., 51, 326-344.

Eisfelder C., Kuenzer C. and Dech S. (2012). Derivation of biomass information for semi-arid areas using remote-sensing data. Int. J. Remote Sens., 33, 2937-2984.

Eliasson K., Lindgren U. and Westerlund O. (2003). Geographical labour mobility: Migration or commuting. Regional Studies 37, 827-37.

El-Swaify S.A. (1997). Factors affecting soil erosion hazards and conservation needs for tropical steeplands. Soil Technology 11, 3-6.

FAO (1976). A Framework for Land Evaluation. FAO Soil Bulletin No. 32. ILRI Publication No. 22. Rome, Italy.

FAO (1980). Natural resources and the human environment for food and agriculture. Environment Paper No 1. Rome.

FAO (1990). Rural area development planning; A review and synthesis of approaches. FAO training materials for agricultural planning. Rome.

FAO (2018). LDN – Restoring degraded lands. http://www.fao.org/land-water/land/ldn/en/

Feizizadeh B. and Blaschke T. (2014). An uncertainty and sensitivity analysis approach for GIS-based multicriteria landslide susceptibility mapping, International Journal of Geographical Information Science, 28:3, 610-638, DOI: 10.1080/13658816.2013.869821.

Gessesse B., Bewket W. and Brauning A. (2015). Model-based characterization and monitoring of runoff and soil erosion in response to landuse/land cover changes in the Modjo Watershed, Ethiopia, Land Degrad. Dev., 26, 711-724, DOI: 10.1002/ldr.2276.

Higginbottom T.P. and Symeonakis E. (2014). Assessing land degradation and desertification using vegetation index data: Current frameworks and future directions. Remote Sensing, 6(10), 9552-9575, DOI: 10.3390/rs6109552

Helldén U. (2008). Tottrup C. Regional desertification: A global synthesis. Glob. Planet. Chang. 64, 169-176.

Haboudane D., Bonn F., Royer A., Sommer S. and Mehl W. (2002). Land degradation and erosion risk mapping by fusion of spectrally-based information and digital geomorphometric attributes. Int. J. Remote Sens., 23, 3795-3820.

ICAR (Indian Council of Agricultural Research) (2010). State of Indian Agriculture, 2012–2013, A report of Department of Agriculture and Cooperation, New Delhi, 9.

IPCC (2001). Intergovernmental Panel on Climatic Change, «Impacts, Adaptation and Vulnerability».

Jong R.D., Bruin S.D. and Dent M.S.D. (2011). Quantitative mapping of global land degradation using earth observations. Int. J. Remote Sens., 32, 6823-6853.

Jasrotia A.S. and Singh R. (2006). Modeling runoff and soil erosion in a catchment area, using the GIS, in the Himalayan region, India. Environ Geol 51, 29-37, DOI: 10.1007/s00254-006-0301-6.

Khaledian Y., Kiani F., Ebrahimi S., Brevik E.C. and Aitkenhead-Peterson J. (2017). Assessment and monitoring of soil degradation during landuse change using multivariate analysis, Land Degrad. Dev., 28, 128-141, DOI: 10.1002/ldr.2541.

Kouli M., Soupios P. and Vallianatos F. (2009). Soil erosion prediction using the Revised Universal Soil Loss Equation (RUSLE) in a GIS framework, Chania, Northwestern Crete, Greece Environmental Geology, 57, 483-497.

Leh M., Bajwa S. and Chaubey I. (2013). Impact of landuse change on erosion risk: an integrated remote sensing, geographic information system and modelling methodology, Land Degrad. Dev., 24, 409-421, DOI: 10.1002/ldr.1137.

Lin D.G., Yu H., Lian F., Wang J.A., Zhu A.X. and Yue Y.J. (2016). Quantifying the hazardous impacts of human-induced land degradation on terrestrial ecosystems: A case study of karst areas of south China. Environ. Earth Sci., 75, 1127.

Masoudi M. (2010). Risk Assessment and Remedial Measures of Land Degradation, in Parts of Southern Iran, Lambert Academic Publishing (LAP), Germany, 220.

Masoudi M. (2014). Risk assessment of vegetation degradation using GIS J. Agr. Sci. Tech.-Iran, 16, 1711-1722.

Masoudi M. and Amiri E. (2015). A new model for hazard evaluation of vegetation degradation using DPSIR framework, a case study: Sadra region, Iran, Pol. J. Ecol., 63, 1-9, DOI: 10.3161/15052249PJE2015.63.1.001.

Masoud Masoudi, Parviz Jokar, and Biswajeet Pradhan (2018). A new approach for land degradation and desertification assessment using geospatial techniques. Nat. Hazards Earth Syst. Sci., 18, 1133-1140.

Mendoza G.A., Martins H. (2006). Multi-criteria decision analysis in natural resource management: A critical review of methods and new modelling paradigms. Forest Ecology and Management 230, 1-22.

McCool D.K., Brown L.C., Foster G.R., Mutchler C.K. and Meyer L.D. (1987). Revised slope steepness factor for the Universal Soil Loss Equation. TRANSACTIONS of the ASAE 30(5), 1387-1396.

McCool D.K., George G.O., Freckleton M., Douglas C.L., Jr. and Papendick R.I. (1993). Topographic effect on erosion from crop land in the northwestern wheat region. TRANSACTIONS of the ASAE 36(4), 1067-1071.

Metternicht G., Zinck J.A., Blanco P.D. & Del Valle H.F. (2010). Remote sensing of land degradation: Experiences from Latin America and the Caribbean. Journal of Environmental Quality, 39(1), 42-61, DOI: 10.2134/jeq2009.0127.

Morgan R.P.C. (1983). The impact of recreation on mountain soils: towards a predictive model for soil erosion. Conference on the ecological impacts of outdoor recreation on mountain areas in Europe and North America, Recreation Ecology Research Group, Ambleside, Cumbria.

Millennium Ecosystem Assessment (MEA 2005). Ecosystems and Human-Being: Desertification Synthesis; World Resources Institute: Washington, DC, USA.

Millward A.A. and Mersey J.E. (1999). Adapting the RUSLE to model soil erosion potential in a mountainous tropical watershed. Catena, 38(2), 109-129.

Nicholson S.E. Tucker C.J., Ba M.B. (1998). Desertification, drought, and surface vegetation: An example from the West African Sahel. Bull. Am. Meteorol. Soc., 79, 815-830.

Naseer Ahmad and Puneeta Pandey (2018). Assessment and monitoring of land degradation using geospatial technology in Bathinda district, Punjab, India. Solid Earth, 9, 75-90, DOI: 10.5194/se-9-75-2018.

Nitheshnirmal S. Ashutosh Bhardwaj, Dineshkumar C. and Abdul Rahaman S. (2019). Prioritization of Erosion Prone Micro-watersheds using Morphometric Analysis coupled with Multi-Criteria Decision Making. Proceedings MDPI, 2nd International Electronic Conference on Geosciences (IECG 2019).

Abdi O.A.,. Glover E.K. and Luukkanen O. (2013). Causes and Impacts of Land Degradation and Desertification: Case Study of the Sudan. International Journal of Agriculture and Forestry 2013, 3(2), 40-51.

Ghorbanzadeh O., Feizizadeh B. and Blaschke T. (2017). Multi-criteria risk evaluation by integrating an analytical network process approach into GIS based sensitivity and uncertainty analyses, Geomatics, Natural Hazards and Risk, DOI: 10.1080/19475705.2017.1413012.

Olena D. (2017). The role of Remote Sensing in land degradation assessments: opportunities and challenges, European Journal of Remote Sensing, 50(1), 601-613, DOI: 10.1080/22797254.2017.1378926.

Pan J.H. and Li T.Y. (2013). Extracting desertification from LANDSAT imagery based on spectral mixture analysis and Albedo- Vegetation feature space, Nat. Hazards, 25, 915-927, DOI: 10.1007/s11069-013-0665-3.

Pankaj K., Wei Liu, Xi Chu, Yue Zhang, Zhihui Li (2019). Integrated water resources management for an inland river basin in China. Watershed Ecology and the Environment 1, 33-38, DOI: 10.1016/j.wsee.2019.10.002.

Prasannakumar V., Vijith H., Abinod S. and Geetha N. (2012). Estimation of soil erosion risk within a small mountainous sub-watershed in Kerala, India, using Revised Universal Soil Loss Equation (RUSLE) and geo-information technology. Geoscience Frontiers, 3(2), 209-215.

Prince S., Becker-Reshef I. and Rishmawi K. (2009). Detection and mapping of long-term land degradation using local net production scaling: Application to Zimbabwe. Remote Sens. Environ., 113, 1046-1057.

Rahaman S.A., Ajeez S.A., Aruchamy S. and Jegankumar R. (2015). Prioritization of Sub Watershed based on morphometric characteristics using fuzzy analytical hierarchy process and geographical information system — a study of Kallar watershed, Tamil Nadu. International conference on water resources, coastal and ocean. Aquatic Proc. 4, 1322-1330, DOI: 10.1016/j.aqpro.2015.02.172.

Rahaman S.A., Aruchamy S., Balasubramani K. and Jegankumar R. (2017a). Landuse / land cover changes in semi-arid mountain landscape in southern India: a geoinformatics based markov chain approach. Int. Arch. Photo. Remote Sens. Spatial Inf. Sci., Vol XLII-1/W1. 231-237, DOI: 10.5194/isprs-archives-XLII-1-W1-231-2017.

Rahaman S.A. and Aruchamy S. (2017b). Geoinformatics based landslide vulnerable zonation mapping using analytical hierarchy process (AHP), a study of Kallar river sub watershed, Kallar watershed, Bhavani basin, Tamil Nadu. Model. Earth Syst. Environ., 3(41), 13, DOI: 10.1007/s40808-017-0298-8.

Rahaman S., Aruchamy S. and Jegankumar R. (2016). Geospatial Approach for forest cover change and vulnerability analysis through MCE in Kallar watershed, Part of Nilgiri Biosphere Reserve. Geo Eye, 5(2), 40-50.

Rahaman S., Kumar P., Chen R., Meadows M.E. and Singh R.B. (2020). Remote Sensing Assessment of the Impact of Land Use and Land Cover Change on the Environment of Barddhaman District, West Bengal, India. Front. Environ. Sci. 8:127, DOI: 10.3389/fenvs.2020.00127.

Rahaman S.A. and Venkatesh R. (2020). Application of remote sensing and google earth engine for monitoring environmental degradation in the Nilgiri biosphere reserve and its ecosystem of Western Ghats, India. Int. Arch. Photo. Remote Sens. Spatial Inf. Sci., Volume XLIII-B3, 933-940, DOI: 10.5194/isprs-archives-XLIII-B3-2020-933-2020.

Renard K.G and Ferreira V.A. (1993). RUSLE model description and database sensitivity. Journal of Environmental Quality 22(3), 458-466.

Rhoad R., Milauskas G. and Whipple R. (1991). Geometry for enjoyment and challenge. McDougal Littell, Evanston, IL.

Röder A., Udelhoven T., Hill J., del Barrio G. and Tsiourlis G. (2008). Trend analysis of landsat-tm and -etm+ imagery to monitor grazing impact in a rangeland ecosystem in northern greece. Remote Sensing of Environment 112(6), 2863-2875.

Saaty T.L. (1980). The Analytic Hierarchy Process. McGraw-Hill, New York.

Scott S. and Conacher A. (2008). Land degradation and poverty. Geographical Research 46, 1-3.

Sharma A. (2010). Integrating terrain and vegetation indices for identifying potential soil erosion risk area Geo-Spatial Information Science, 13 (3), 201-209.

Stephanie W., Timo K., Ana Frelih-Larsen., Keighley M F. and Stefanie A. (2018). Report on Implementing SDG target 15.3 on «Land Degradation Neutrality» Ecologic Institut, Berlin. Umweltbundesamt, Germany.

Svenson L. (2005). Socio-economic Indicators for Causes and Consequences of Land degradation. LADA Technical paper, FAO, Rome.

Taddese Y. (2001). Land degradation: a challenge to Ethiopia, Environ. Manage., 27, 815-824, DOI: 10.1007/s002670010190.

Temiz F., Bozdag A., Durduran S.S, Gumus M.G. (2017). Monitoring Coastline Change Using Remote Sensing and Gis Technology: A Case Study of Burdur Lake, Turkey. Fresen. Environ. Bull. 26, 7235-7242.

Taguas E.V., Arroyo C., Lora A., Guzmán G., Vanderlinden K. and Gómez J.A. (2015). Exploring the linkage between spontaneous grass cover biodiversity and soil degradation in two olive orchard microcatchments with contrasting environmental and management conditions, SOIL, 1, 651-664, DOI: 10.5194/soil-1-651-2015.

UNCCD (1999). United Nations Convention to Combat Desertification in Those Countries Experiencing Serious Drought and/or Desertification, Particularly in Africa. Text with Annexes. Secretariat of the Convention to Combat Desertification, Bonn.

United Nations General Assembly (2015). Transforming our world: The 2030 agenda for sustainable development. Retrieved from http://www.un.org/ga/search/view_doc.asp?symbol=A/RES/70/1&Lang=E

Uzun A., Somuncu M. (2013). Using Remote Sensing Method to Evaluate the Change of the Land Cover/Land Use in Time in Madra Mountain. Balikesir University Journal of Social Sciences Institute.16(30), 1-21.

Van der Knijff J.M., Jones R.J.A. and Montanarella L. (2000). Soil Erosion Risk Assessment in Europe. EUR 19044 EN Office for Official Publications of the European Communities, Luxembourg 34.

Venkatesh R., Abdul Rahaman S., Jegankumar R. and Masilamani P. (2020). Eco-environmental vulnerability zonation in essence of environmental monitoring and management, Int. Arch. Photogramm. Remote Sens. Spatial Inf. Sci., XLIII-B5-2020, 149-155, DOI: 10.5194/isprs-archives-XLIII-B5-2020-149-2020.

Wessels K., Prince S., Zambatis N., MacFadyen S., Frost P. and van Zyl D. (2006). Relationship between herbaceous biomass and 1 km2 Advanced Very High Resolution Radiometer (AVHRR) NDVI in Kruger National Park, South Africa. Int. J. Remote Sens., 27, 951-973.

Wischmeier W.H. (1974). New developments in estimating water erosion. 29e Meeting Soil Cons. Soc. Amer. Syracuse, New York. 179-186.

Wischmeier W.H. and Smith D.D. (1978). Predicting Rainfall Erosion Losses: A Guide to Conservation Planning, Agricultural Handbook No. 537, US Department of Agriculture, Washington DC.

Xie H., Zhang Y., Wu Z. and Lv T. (2020). A Bibliometric Analysis on Land Degradation: Current Status, Development, and Future Directions. Land, 9, 28.

Yu C., Liu K., Meng W., Wu Z. and Rishe N. (2002). A methodology for retrieving text documents from multiple databases. IEEE TKDE 14(6), 1347-1361.

Zhou W., Gang C., Zhou F., Li J., Dong X. and Zhao C. (2015). Quantitative assessment of the individual contribution of climate and human factors to desertification in northwest China using net primary productivity as an indicator. Ecol. Indic., 48, 560-569.

Zuazo V.H.D. and Pleguezuelo C.R.R. (2009). Soil-erosion and runoff prevention by plant covers: a review. In Lichtfouse, Eric; et al. Sustainable agriculture. Springer. 785.

APPENDICES 1

K Factor (Soil Erodibility): soil erodibility is predicted as a function of soil and soil profile properties like per cent of silt, very fine sand, clay, organic matter (OM) and structure code (s). The regression equation for estimating erodibility factor values from nomograph as suggested by Wischmerier (1974) is equation (4 and 5):

$$K = \frac{\left[2.1\times10^{-4}(12-OM)M^{1.14}+3.25(s-2)+2.5(p-3)\right]}{759.4} \quad ...(4)$$

where, K= Soil erodibility (ton/yr/MJ/mm), OM = percentage Organic Matter, 's' = soil structural code, 'p' is permeability code and 'M' is a function of soil primary particle size fractions calculated as follows:

$$M = (\%silt + \%Veryfindsand)\times(100-\%clay) \quad ...(11)$$

Soil structure codes (s): very fine granular (1), fine granular (2), medium or coarse granular (3), blocky, platy, prism (4). *Soil permeability codes (p):* 1- rapid (> 150mm/hr), 2- moderate to rapid (50-150mm/hr), 3- moderate (15-50 mm/hr), 4- slow to moderate (5-15 mm/hr), 5 – slow (1-5 mm/hr), and 6- very slow (<1 mm/hr).

Slope length Cont

The slope length factor has often been expressed as (Zingg, 1940):

$$L' = \alpha\lambda^{m}$$

where *L'* is soil loss (mass per unit area per unit time), \ (m) is slope length, and a and m are empirical coefficients. Normalizing to a unit plot of length 22.13 m, both the USLE and RUSLE use the equation

The slope length exponent m can be calculated as following equation (12 & 13)

$$m = \beta/(1+\beta) \quad (12)$$

$$\beta = (\sin\theta/0.0896)/\left[3.0(\sin\theta)^{0.8}+0.56\right] \quad (13)$$

Were, Ø is the slope angle

To generate LS factor, the following methods were adopted. DEM is used as the primary input data sources by which flow direction and flow accumulation can be prepared. This flow accumulation raster is used for the generation of L factor by using following equation (14).

$$L = (Flowaccumulation * cellsize/22.13)^{m} \quad (14)$$

The stream network is created by determining a threshold value. Normally for plain areas 2000 is taken as the threshold value. In hilly areas it will be much less and is assigned 750. The following expressions (15) are used in the raster calculator to estimate L factor

$$Con(("Flow\_Acc" < 500), (Power(("Flow\_Acc" * 12.5/22.13), 0.14)), (Power((500 * 12.5/22.13), 0.14))) \quad (15)$$

For a generation of S factor, slope map is required, both in radians and in percentage. To convert the slope map in degree to radians the following expressions (16) in raster calculator is used.

$$Slopedegree * 22/(7 * 180) \quad (16)$$

S factor can be calculated according to equation (17) by using the following expression in raster calculator

$$\begin{gathered} Con(("Slope\_per" < 9), ((10.8 * \mathrm{Sin}("Slope\_rad")) + 0.03), \\ Power((\mathrm{Sin}("Slope\_rad")/\mathrm{Sin}(5.143 * 22/(7 * 180))), 06)) \end{gathered} \quad (17)$$